Micro-analytical studies of the petrogenesis of silicic arc magmas in the Taupo Volcanic Zone and southern Kermadec Arc, New Zealand

By

Katharine Emma Saunders

A thesis submitted to the Victoria University of Wellington in fulfilment of the requirements for the degree of Doctor of Philosophy in Geology

Victoria University of Wellington
2009

Abstract

The petrogenesis of silicic arc magmas is controversial with end-member models of fractional crystallisation and crustal anatexis having been invoked. A prime example of this is the archetypical continental Taupo Volcanic Zone and the adjacent oceanic Kermadec Arc. Insights into the genesis and timescales of magmatic processes of four continental rhyolitic magmas (Whakamaru, Oruanui, Taupo and Rotorua eruptives) and an oceanic (Healy seamount) rhyodacitic magma are documented through micro-analytical chemical studies of melt inclusions and crystal zonation of plagioclase and quartz. Electron probe microanalysis, laser ablation inductively coupled plasma mass spectrometry and Fourier transform infrared spectroscopy have been used to measure major, trace and volatile element concentrations, respectively, of melt inclusions and crystals.

Melt inclusions are high silica (e.g. 74 - 79 wt%) irrespective of arc setting and display a wide range of trace element compositions (e.g. Sr = 17 - 180 ppm). Taupo Volcanic Zone melt inclusions exhibit higher K_2O and Ce/Yb relative to Healy melt inclusions reflecting the assimilation of continental lithosphere. Quantitative trace element modelling of melt inclusion compositions: (a) demonstrates that magma genesis occurred through 62 - 76% fractional crystallisation at Healy whereas assimilation of continental lithosphere (greywacke) in addition to 60 - 80% fractional crystallisation is required for the Taupo Volcanic Zone magmas; and (b) suggests the presence of crystal mush bodies beneath silicic magma chambers in both continental and oceanic arc environments. Water concentrations of melt inclusions ranged between 1.4 - 5.1 wt% for the Whakamaru, Taupo and Healy samples. However, the

inconsistency in the measured molecular water to hydroxyl concentrations of melt inclusions relative to those determined experimentally for groundmass rhyolitic glasses provide evidence for the degassing of inclusions prior to quenching, by diffusion of hydroxyl groups through the crystal host. Thus, partial pressures of water estimated from the inclusions and inferred depths of the crystallising magma bodies are underestimated.

Chemical profiles of mineral zonation, however, indicate a more complex origin of silicic melts than simple fractionation and assimilation. For example, trace element modelling of Whakamaru plagioclase suggests that the three distinct textural plagioclase populations present in Whakamaru samples crystallised from four physiochemically discrete silicic melts. This modelling indicates a strong petrogenetic link between andesitic and silicic magmas from the chemical variation of selected Whakamaru plagioclase crystals possessing high anorthite (45-60 mol %) cores and low anorthite (~ 30 mol %) rim compositions and the interaction of greywacke partial melts. Furthermore, Sr diffusion modelling of core-rim interfaces of the same plagioclase crystals indicate the amalgamation of the magma chamber occurred continuously over the 15,000 years preceding the climactic eruption. Conversely, the major element zonation of Taupo plagioclases implies magma genesis occurred solely through assimilation and fractional crystallisation without the incorporation of evolved crystal mush magmas, indicating a spectrum of magmatic processes are occurring beneath the Taupo Volcanic Zone with each eruption providing only a snapshot of the petrogenesis of the Taupo Volcanic Zone.

Acknowledgements

First and foremost I must thank my supervisors Joel Baker and Richard Wysoczanski, for their encouragement, advice and especially their unwavering support over the last three years. Furthermore, I would like to thank Joel for initially inspiring me, being there to point out the obvious when required and for providing such a challenging and stimulating research environment. I would like to thank Dan Morgan for his patient (e-mail) tuition, advice and many insightful discussions on the principals of diffusion modelling of minerals and Alex Nichols for the many thought provoking discussions and his hospitality during my visit to the FTIR laboratory at JAMSTEC, Japan. This input will ultimately lead to submission of Chapters 3 and 4 as manuscripts with Alex Nichols and Dan Morgan as co-authors respectively.

Special thanks go to: Ian Wright for his provision of Healy samples and discussions on the nature of magma genesis in oceanic arcs; John Gamble for his support and many discussions on the Taupo Volcanic Zone; Julie Vry for her continuing support, advice and baking; John Patterson for his technical expertise in the running of the electron microprobe; Stewart Bush for his help with sample preparation; Susanne Grigull and Leonie Short for field assistance; Aidan Allan, Sophie Barton and Martin Schiller for help in the initial establishment of the analytical techniques of volcanic glasses in the Geochemistry Laboratory; Rebecca Fisher, Zoe Laing, Hannu Seebeck and Srimathy Sriskantharajah for their discussions and support; Chris Webster for his time proof reading.

A huge thanks goes to Monica Handler and Yvette Baker for countless cups of tea and for keeping me sane for the last three years. Many thanks go to my various office mates; Ruth, Susanne, Aidan, Alex, Matt, Chelsea, Sophie, Sarah, Elodie and also Evelien, Jess, Annette, Kim, John, Katie, Caell, Matt, John, Cliff, Warren, Mike, Trish, Norbert, Nuala, John, Kay, Chris, Sophia, Lydia, Aratahi Rangers and anyone else I may have forgotten for the adventures, fun and support. Many thanks go to the fantastic general staff both past and present, but especially to Susan Cayless and Gill Ruthven.

Furthermore, I would like to thank Geoff Batt, Martin Menzies, Euan Nisbet and Matthew Thirlwall for providing the early inspiration and for sending me on this journey.

A Commonwealth Scholarship to New Zealand and smaller grants from Victoria University of Wellington Science Faculty Small Research Grants, The Daniel Pidgeon Fund of The Geological Society of London, a Postgraduate bursary from The Mineralogical Society of Great Britain and a Goldschmidt travel award funded this project and for these I am eternally grateful.

Finally, I would like to thank my parents Wendy and Tony and brother Tim (and dogs, Bruno and Nell) for their amazing support, even when I announced I was moving to the antipodes again for a further three years, for without it none of this would have been possible.

Table of Contents

List of Figures

Chapter 1: Introduction

Chapter 2: Petrogenesis of large-volume silicic magmas in continental arcs: melt inclusions in Taupo Volcanic Zone and Kermadec Arc rhyolites, South West Pacific

Chapter 3: Water speciation and the degassing of unruptured rhyolitic melt inclusions: case studies from the Taupo Volcanic Zone, New Zealand

Chapter 4: The magmatic evolution of the Whakamaru supereruption from crystal specific studies of plagioclase and quartz crystals

Chapter 5: Crystal specific studies of Healy and Taupo eruptives: insights into the petrogenesis of silicic arc magmas

Chapter 6: Synthesis and Conclusions

Appendix 1: Samples and Analytical Methods

Appendix 2: Diffusion

Appendix 4: Backscattered and Cathodoluminescence images

List of Tables

Chapter 5: Crystal specific studies of Healy and Taupo eruptives: insights into the petrogenesis of silicic arc magmas

Appendix 1: Samples and Analytical Methods

Appendix 2: Diffusion

Appendix 3: Data tables

Chapter 1

Introduction

Oceanic lithosphere is created at mid-ocean ridges and recycled back into the Earth at convergent margins. This subduction of material back into the Earth's mantle is pivotal to the large-scale recycling of elements between the crust, mantle, hydrosphere and atmosphere. The addition of subducted material (i.e. oceanic lithosphere and associated sediment) results in the overriding mantle becoming enriched in fluid and melt mobile elements such as large ion lithophile elements and water. It is this addition of water to the mantle that ultimately drives arc volcanism and the catastrophic eruptions that are common along many continental margins (McCulloch and Gamble, 1991; Lowenstern et al., 2006). The most devastating of these eruptions and perhaps the least well understood are large-volume silicic eruptions. The largest of these eruptions (> 450 km^3) are termed supereruptions and are a magnitude greater than any volcanic eruption witnessed within recent history (Lowenstern et al., 2006; Miller and Wark, 2008). Of the eighteen known supereruptions to have occurred in the last 2 million years, seventeen of these are derived from arc volcanism (Lowenstern et al., 2006). The most recent and well-documented supereruption is the 26.5 ka Oruanui eruption from the hyper-productive Taupo Volcanic Zone, New Zealand (Wilson, 2001; Mason et al., 2004; Miller and Wark, 2008).

1.1 Global rhyolitic volcanism

Large-volume silicic eruptions and supereruptions are not constrained to a single tectonic setting but have been documented globally from continental margins

such as New Zealand and South America (e.g. Wilson, 2001; Wilson et al., 2006; Lindsey et al., 2001); continental rifts, e.g. Yemen-Ethiopia (e.g. Baker et al., 2000; Ukstins Peate et al., 2003; 2007); and intra-continental plume related volcanism such as Yellowstone, USA (e.g. Christensen, 2001) (Figure 1.1).

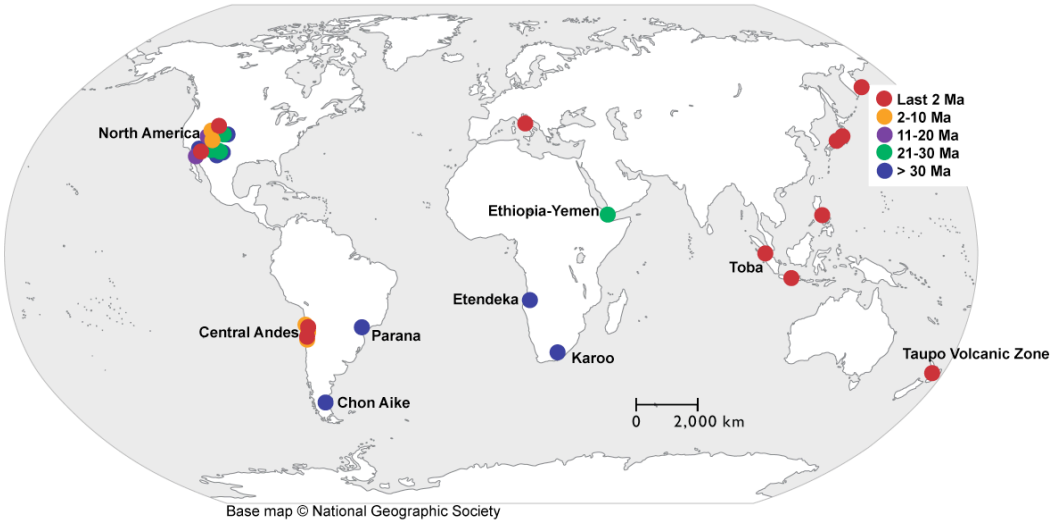

Figure 1.1. Global map of silicic volcanism after Bryan et al. (2002), Mason et al. (2004) and Sparks et al. (2005) illustrating the location of the largest identified and studied rhyolitic eruptions.

Models for the generation of rhyolitic magmatism are ultimately driven by mantle-derived mafic magmas, resident at deeper crustal levels providing thermal energy and supplying at least the initial melt (e.g. Hildreth, 1981; Bachmann and Bergantz, 2004; Miller and Wark, 2008). Extreme fractional crystallisation from this mantle-derived mafic magma ensues and/or the presence of this mafic magma promotes crustal anatexis generating large volumes of silicic magmas (e.g. Hildreth, 1981; Bachmann and Bergantz, 2004; 2008; Annen et al., 2006; Brophy, 2008). These silicic magmas accumulate in the upper crust, forming crystal mush zones, which are magmatic bodies composed of interconnecting semi-solidified crystals and interstitial liquid that are potentially preserved as silicic plutons (e.g. Bachmann and Bergantz, 2004; Glazner et al., 2004; Hildreth

and Wilson, 2007, Wilson et al., 2006; Lipman, 2007; Bachmann and Bergantz, 2008). The interstitial liquid is extracted from the crystal mush and ponds in an overlying magma chamber (Figure 1.2) providing the large volumes of eruptible magma evacuated during supereruptions (e.g. Bachmann and Bergantz, 2004; Hildreth and Wilson, 2007, Wilson et al., 2006; Bachmann and Bergantz, 2008).

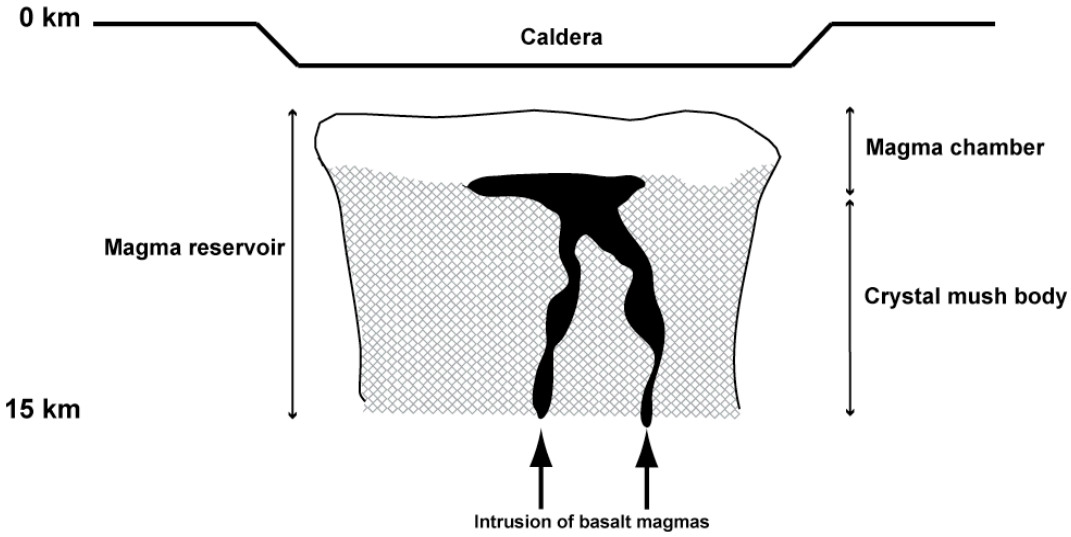

Figure 1.2 Schematic cross section of a rhyolitic magma reservoir after Bachmann and Bergantz (2004, 2008).

This model explains the occurrence of both crystal-poor (5-10 % volume crystals) rhyolites sourced from the magma chamber and crystal-rich (40-50 % volume crystals, often termed 'monotonous intermediates') dacite/rhyolite magmas originating from semi-formed or rejuvenated crystal mush bodies (e.g. Hildreth, 1981; Lindsey et al., 2001; Bachmann et al., 2002; Bachmann and Bergantz, 2004; Hildreth, 2004; Christensen, 2005; Wilson et al., 2006). The storage of large volumes of silicic melts in crystal mush bodies provides a viable explanation for the failure of geophysical surveys to detect large-volumes of partial melt in shallow (< 6 km) upper crustal magma chambers, underlying

volcanically active regions of the world (e.g. Bachmann and Bergantz, 2003; Glazner et al., 2004).

Recent studies have indicated that the crystal mush model is applicable for both intra-continental and subduction related rhyolites (e.g. Hildreth and Wilson, 2007; Wilson et al., 2006; Shane et al., 2008). However, many intra-continental rhyolite deposits such as the Bishop Tuff, USA possess strong geochemical fractional crystallisation signatures and systematically zoned deposits (Hildreth, 1981; Hildreth and Wilson, 2007). In comparison, and although similar in chemical composition, Taupo Volcanic Zone rhyolites display only limited chemical variation that lacks any systematic zonation or is chemically 'reversed' (e.g. Hildreth, 1981; Briggs et al., 1993; Brown et al., 1998a; Wilson et al., 2006), implying that a single petrogenetic model may not adequately explain the formation of silicic magmas in all tectonic settings.

One possible mechanism that may account for the disparity in chemical stratification of silicic magmas is the geometry of magma chambers. Slab shaped magma chambers may prevent the separation of crystals from liquid melt, inhibiting the chemical zonation of the chamber (Christensen, 2005). Whereas, cylindrical magma chambers readily promote crystallisation on the wall of the chamber resulting in the migration of more chemically evolved buoyant melt to the top of the magma chamber generating chemical zonation (Christensen, 2005).

Volcanic rock nomenclature in this study is based on the SiO_2 (wt%) and total alkali contents ($Na_2O + K_2O$, wt%) of samples using the Total Alkali Silica

diagram of Le Bas et al. (1986) (Figure 1.3). Rhyolites are typically characterised by high SiO_2 (> 69 wt%) (Figure 1.3), low MgO and Sr concentrations, enriched light rare earth elements concentrations, generally enriched $^{87}Sr/^{86}Sr$ and depleted ε_{Nd} isotopes (Figure 1.4), high water contents (1-6 wt%) and are highly viscous compared to mid ocean ridge basalts (e.g. Bowen, 1928; Hildreth, 1981; McCulloch et al., 1994; Graham et al., 1995; Anderson et al., 2000; Ukstins Peate et al., 2005; Wallace, 2005; Wilson et al., 2006). Mineral assemblages are typically a combination of plagioclase, orthopyroxene, quartz, ilmenite, magnetite, K-feldspar, biotite, hornblende, apatite, zircon, clinopyroxene and cummingtonite (e.g. Graham et al., 1995; Anderson et al., 2000; Schmitz and Smith, 2004; Wilson et al., 2006).

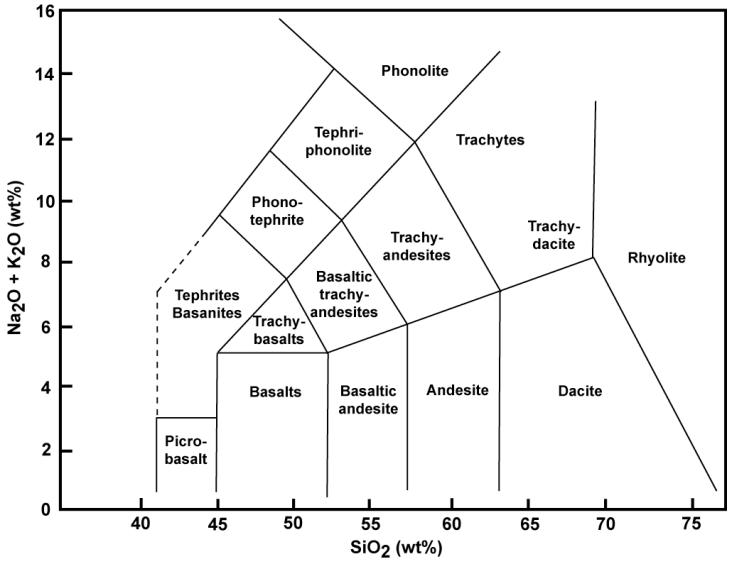

Figure 1.3. Total alkali silica diagram after Le Bas et al. (1986) illustrating the nomenclature of volcanic rock classification used in this study.

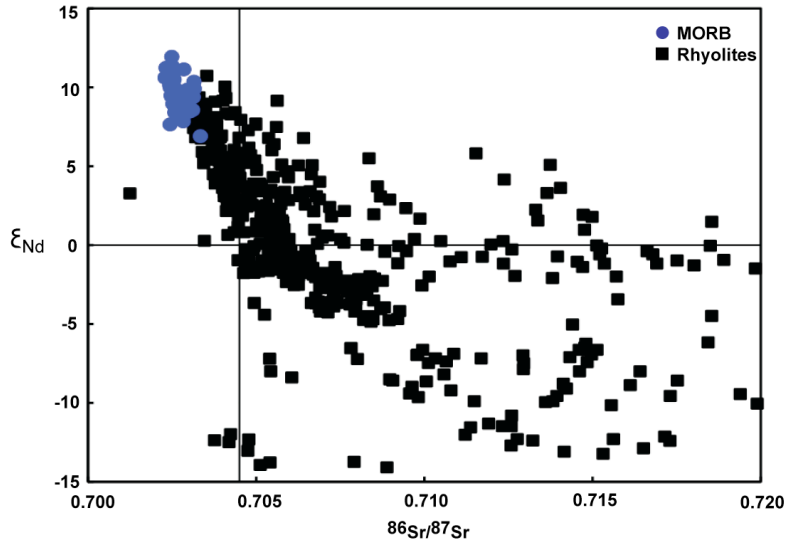

Figure 1.4. $^{86}Sr/^{87}Sr$ versus ε_{Nd} ratios of global rhyolites compared to mid-ocean ridge basalts (MORB). Data sources: MORB - Ito et al. (1987); Rhyolites: Africa - Ayalew et al. (2002); China - Zhang et al. (2008); Iceland - Martin and Sigmarsson (2007); Italy - Gioncada et al. (2003); Japan - Takagai et al. (1999); Mexico - Albrecht and Goldstein (2000); New Zealand – Beresford et al. (2000); Schmidtz and Smith (2004); Sutton et al. (1995); Wilson et al. (2006); South America - Siebel et al. (2000); USA - Hildreth et al. (1991); Heuman et al. (1997); Borg and Clynne (1998); Hammersely and DePaolo (2006). Black lines represent the Bulk Earth isotopic compositions from Zindler and Hart (1986).

1.2 Subduction magmatism

Subduction generated mafic magmas are widely recognised to originate from the partial melting of the mantle wedge (e.g. McCulloch and Gamble, 1991; Davis and Stevenson, 1992; Schmidt and Poli, 1998; Annen et al., 2006). The dehydration of the subducting plate and associated sediment package causes the solidus temperature of the overlying mantle to be lowered and allows partial melts to form (e.g. McCulloch and Gamble, 1991). The higher buoyancy of partial melts relative to the surrounding mantle instigates the ascent of these melts towards the surface. As mafic melts ascend crustal processes such as density filtering causes these mafic magmas to stagnate, becoming lodged in the

crust, and preventing substantial quantities of primary mantle-derived magmas from reaching the surface (e.g. Hildreth, 1981; Annen et al., 2006). In contrast, the ultimate origin of silicic arc magmas is still equivocal. Two widely cited end-member models are fractional crystallisation from primary mantle-derived magmas and crustal anatexis (Ewart and Stipp, 1968; Pearce et al., 1995; Borg and Clynne, 1998; Kawate and Arima, 1998; Brophy et al., 1999; Grove et al., 2003; Smith et al., 2003a,b; Shukuno et al., 2006; Wysoczanski and Tani, 2006). Distinguishing between these two models is difficult, as silicic magmas generated by either model could possess similar chemical signatures (Haase et al., 2006; Brophy, 2008). Furthermore, fractional crystallisation of a primary magma has the potential to trigger crustal melting or assimilation of crustal material, thereby obscuring the original geochemical signature of the source (DePaolo, 1981; Annen et al., 2006). Increasingly, evidence is emerging of multiple crystal populations within magmas that cannot be derived solely from a single source but provide evidence for the recycling of crystals from progenitor melts and the remobilization of crystal mushes (Davidson et al., 2001; Bachmann and Bergantz, 2004; Charlier et al., 2005; Davidson et al., 2007; Jerram and Martin, 2008).

Many of the largest known silicic volcanoes are associated with continental subduction and in areas that are also characterised by regional extension (Jellinek and DePaolo, 2003; Lowenstern et al., 2006). In these settings, intra-crustal magmatism responsible for large-volume silicic eruptions is often expressed at the surface as caldera structures (Houghton et al., 1995). Silicic eruptions range from small volume, (< 1 km^3 dense rock equivalent [DRE]) local eruptions to

potentially devastating supereruptions (> 450 km^3 DRE) (Newhall and Self, 1982; Houghton et al., 1995; Mason et al., 2004; Miller and Wark, 2008; Wilson et al., in press). The growth of large inter-crustal magma chambers is favoured in regions with elevated geothermal gradients that heat country rocks, allowing for the expansion of magma chambers with increasing magma volumes (Jellinek and DePaolo, 2003).

The continental Taupo Volcanic Zone in the southwest Pacific with its elevated geothermal gradient and rift setting (Stern, 1987; Wilson et al., 1995) is a prime location for the production of large-volume silicic arc magmas. The region is characterised by thin (15-25 km), extending (~8-10 mm/yr) continental crust resulting in a graben packed structure of volcanic infill with high heat flow of ~700 mW/m^2 (Cole, 1981; Stern, 1987; Houghton et al., 1995; Darby et al., 2000; Harrison and White, 2004). Moreover, in the last 1.6 Ma, eight active caldera centres have been recognised that have produced > 15,000 km^3 of rhyolite designating this as the most active silicic magmatic system on Earth (Wilson et al., 1995). Volcanic activity is not continuous, but is characterised by short 25-35 kyr bursts of activity interspersed with 100 kyr periods of quiescence (Allan et al., 2008), although the oceanic record that this is based on could be biased and may not reflect the complete eruptive history of the Taupo Volcanic Zone.

Silicic magmatism is not confined to the continental Taupo Volcanic Zone, but continues to the north of New Zealand along the concomitant oceanic Kermadec Arc (Figure 1.5), where eleven of the eighteen sampled frontal arc Kermadec

volcanoes in the southern Kermadec arc have been identified as having silicic deposits (Smith et al., 2003a; Wright and Gamble, 1999; Wright et al., 2003, 2006; Hasse et al., 2006).

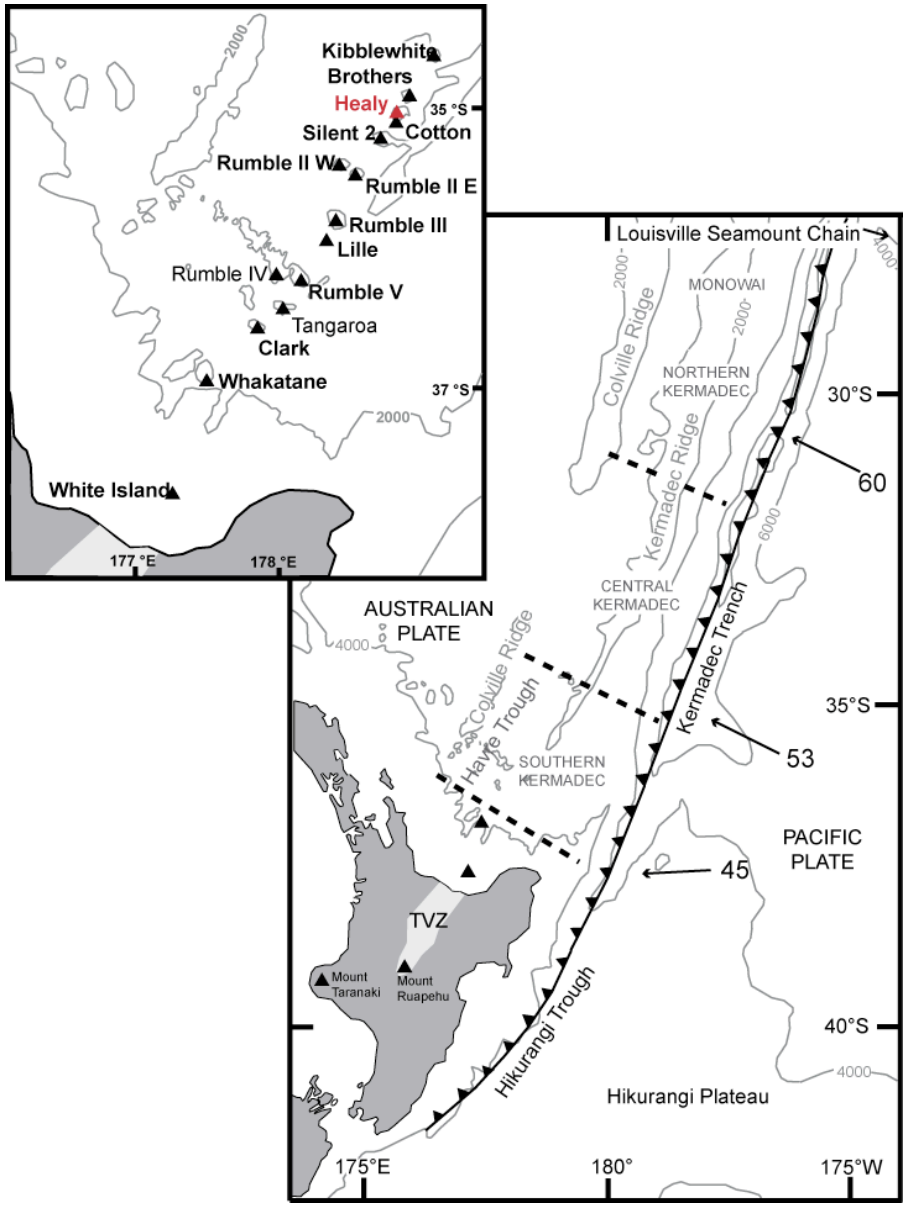

Figure 1.5 Regional setting of the Taupo-Kermadec subduction system. Inset shows the southern Kermadec Arc and location of volcanic centres. Bathymetry is shown for 2000 m from de Ronde et al. (2001). Plate motions are in mm/yr and taken from Wright et al. (2006).

The presence of continental lithosphere has been proposed as a key component in the production of large volumes of silicic magmas, potentially inhibiting the rise

of dense mafic melts and thereby promoting the accumulation of crustal magma reservoirs (Jellinek and DePaolo, 2003; Bachmann and Bergantz, 2008). Whilst continental lithosphere may increase the number of potential melt sources and processes that can affect an ascending melt, the abundance of silicic volcanism in oceanic arcs (e.g. Kermadec Arc, South Sandwich Islands, New Britain Island Arc, Izu-Bonin Arc) implies continental lithosphere is not always required to produce silicic arc magmas. However, to generate large-volume eruptions the presence of continental or over- thickened oceanic crust appears to be required in order to insulate the ascending melts at elevated magmatic temperatures for extended periods of time. This allows extensive fractional crystallisation and/or promotes the assimilation or melting of country rock to take place, thereby generating additional melt to feed the magma bodies that are the source of large-volume silicic eruptions.

1.3 Melt inclusions: a window into magmatic evolution

Given the complexity of silicic arc volcanism and the presence of potentially multiple crystal populations derived from polygenetic sources (e.g. Davidson et al., 2005), a single liquid line of descent of magmas is improbable. Crushing of bulk rock samples provides an average rock compositions and the analysis of groundmass glass compositions provides information of the final liquid compositions. Any information on the former melt compositions is either erased or obscured providing little evidence of the early magmatic evolution (Sobolev, 1996). An alternative is to analyse melt inclusions (Figure 1.6), which are small bubbles of melt that become trapped during crystal growth (Roedder, 1979; Sobolev, 1996; Danyushevsky et al., 2002). This allows direct analysis of the

melt compositions at the time the inclusions were sealed from the external melt, which may not be expressed in the final eruptives due to subsequent magmatic processes (e.g. Roedder, 1979; Kent and Elliot, 2002; Blundy et al., in press). Thus, the chemistry of multiple magma batches is potentially sampled as inclusions in different crystal hosts and this may permit the evolution of the melt to be deciphered (Roedder, 1979; Danyushevsky et al., 2002).

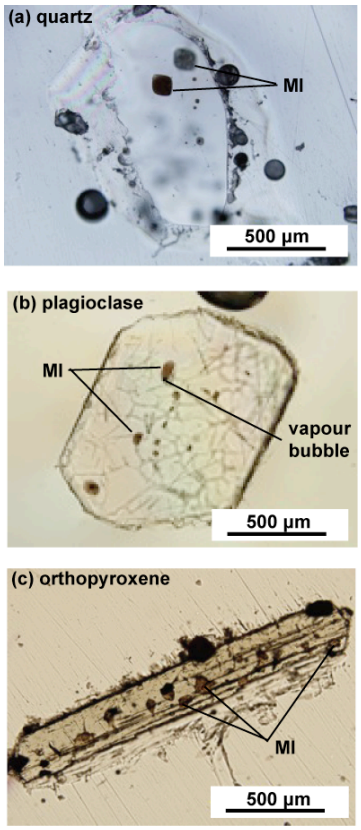

Figure 1.6 Transmitted light photographs of Taupo Volcanic Zone melt inclusions in: (a) quartz; (b) plagioclase and; (c) orthopyroxene hosts. Note the small vapour bubble at the base of the melt inclusion in (b). Melt inclusions are ubiquitous throughout the orthopyroxene crystal. MI = melt inclusion.

A major assumption in melt inclusion studies is that inclusions remain isolated post entrapment, retaining their original compositions and are not modified by subsequent magmatic processes (Sobolev, 1996; Frezzotti et al., 2001). While

this may be valid for major and trace element concentrations in low temperature silicic magmas, increasingly experimental evidence is questioning this assumption and proposing that crystal hosts are in fact semi-closed systems that permit the diffusive exchange of volatiles and potentially other elements (Spandler et al., 2007; Portnyagin et al., 2008). Therefore, anomalous melt inclusion compositions may in fact reflect diffusive exchange of elements and not the original melt compositions (Spandler et al., 2007). Consequently, but with careful consideration of diffusive processes, melt inclusions can provide fundamental insights into the magmatic evolution that would otherwise be erased or obscured by later magmatic processes.

1.4 The role of water in silicic magmatism

Water is the most abundant volatile species in terrestrial magmas and controls the eruptive power and dynamics of a volcanic eruption (Wilson, 1980; Blake, 1984; Zhang, 1999). Melt properties such as viscosity, density, liquidus and solidus temperatures and the crystallising mineral assemblage are also affected by the water content of a melt (e.g. Yoder, 1957; Tuttle and Bowen, 1958; Shaw, 1972; Blake, 1984; Johannes, 1989; Jaupart and Tait, 1990; Ochs and Lange, 1997; Zhang, 1999; Wallace, 2005). Unless magmas are erupted under pressure, as is the case for submarine eruptions, they degas on eruption, erasing all evidence of the pre-eruptive volatile content (e.g., Delaney et al., 1978; Gerlach, 1986; Dixon et al., 1995; Dixon, 1997; Newman and Lowenstern, 2002; Nichols and Wysoczanski, 2007). An exception to this is the volatile concentration of melt inclusions (e.g. Wallace, 2005). Consequently, melt inclusions are routinely analysed in order to determine the pre-eruptive dissolved water content of

magmas. These studies for example reveal that water concentrations of basaltic arc magmas span a range from below detection limits to ≥ 6 wt% (e.g. Wallace, 2005).

Stalling and differentiation of mafic magmas within the crust could potentially generate intermediate and evolved magmas with extremely high H_2O (e.g. > 6 wt%) concentrations (Sparks, 2003). However, measured H_2O concentrations of melt inclusions from dacitic and rhyolitic arc magmas range between 1-6 wt% coinciding with H_2O concentrations of basaltic magmas (Wallace, 2005). This overlapping range of water concentrations of melt inclusions can be attributed to: (1) open system magmatic processes allowing significant amounts of volatiles to be degassed; (2) the generation of arc magmas from crustal fusion resulting in lower observed H_2O concentrations (Wallace, 2005) or; (3) the diffusive exchange of volatiles with the external melt (e.g. Portnyagin et al., 2008). Given laboratory based experimental evidence indicates (Severs et al., 2007; Portnyagin et al., 2008) diffusive exchange of volatiles occurs between melt inclusions and the external magma post sealing of the inclusion, this process must be recognised and identified to allow the correct pre-magmatic water concentrations to be constrained. This is important to our understanding of volcanic processes, as determination of accurate water concentrations of magmas is fundamental for the application of geobarometry models and the estimation of depths of crystallising magma bodies and the crustal location of magma chambers (e.g. Bacon et al., 1992; Atlas et al., 2005; Gurenko et al., 2005; Nishimura et al., 2005; Lui et al., 2006; Fulignati and Marianelli, 2007; Shane et al., 2007).

1.5 Timescales of silicic magmatic processes

One of the fundamental questions that remain unanswered in relation to large-volume silicic eruptions is the timescale for the petrogenesis and accumulation of large volumes of magma. Differentiation processes in silicic magmas are speculated to occur over a range of timescales. For example, Oligocene supereruption deposits derived from Yemen and Ethiopia post-date the flood basalts that they are derived from by < 1 Myr, indicating that the volumes of silicic magma required to feed supereruptions can be generated in < 10^6 years (Baker et al., 1996, 2000; Ukstins Peate et al., 2005, 2007). In contrast, processes such as gravity settling of crystals and the formation of crystal mush bodies occur over timescales of 10^4-10^5 years (Bachmann and Bergantz, 2004) and the modelling of fractional crystallisation of both basaltic and rhyolitic magmas in a 10 km^3 magma chamber indicate 50 % crystallisation could be achieved in < 3000 years (Hawkesworth et al., 2000). In comparison, crustal anatexis instigated and driven by mantle-derived mafic melts occurs rapidly with the potential of forming large volumes of melts in relatively short time periods (e.g. 10^2-10^3 years) (Bergantz, 1989; Huppert and Sparks. 1988). Thus, detailing the timescales of magmatic processes is fundamental to our understanding of the dynamics of magmatic systems and the prediction of future eruptions.

Some of the earliest investigations into the timescales of the formation of large-volume silicic magmas focused on the residence time of the 760 ka intra-continental Bishop Tuff eruption (Halliday et al., 1989; Christensen and DePaolo, 1993; Christensen and Halliday, 1996). ^{87}Rb-^{87}Sr dating of mineral and glasses from the Bishop Tuff provided evidence for the gradual accumulation of

a large magma body over a period of 1.7 Myr (Christensen and DePaolo, 1993). However, processes such as mixing could compromise these isochrons (e.g. Hawkesworth et al., 2003). With the advancement in micro-analytical techniques, geochemical analyses of samples could be conducted at even higher spatial resolutions. This allows individual growth zones of zircons to be dated and the longevity of magmas inferred (e.g. Reid et al., 1997; Brown and Fletcher, 1999; Bindeman et al., 2001; Charlier et al., 2005; Reid, 2008). Moreover, this improvement in analytical techniques allows elemental concentrations of zoned crystals to be documented at sufficient precision to allow chemical diffusion gradients between adjacent zones to be modelled, thus constraining the timescales of magmatic processes (Zellmer et al., 1999; Costa et al., 2003; Morgan et al., 2004; Reid, 2008).

If a crystal resides in a magma at a significantly high temperature then diffusion smoothes the compositional gradient between two adjacent crystal zones, homogenising the crystal composition (Figure 1.7). On eruption, the final diffusion profile is quenched into the crystal and if equilibrium has not been attained, the length of time the crystal resided at magmatic temperature can be modelled from Fick's second law, using the appropriate partition coefficients and diffusivities of elements (e.g. Crank, 1976; Blundy and Wood, 1991; Zellmer et al., 1999; Costa et al., 2003; Morgan et al., 2004; Turner and Costa, 2007). The rate of diffusion of elements can vary by over seven orders of magnitude at a given set of conditions (Costa et al., 2003). As a result, modelling of specific elements can provide insights into a range of magmatic processes over different timescales. For example Sr diffusion permits the residence times of plagioclase

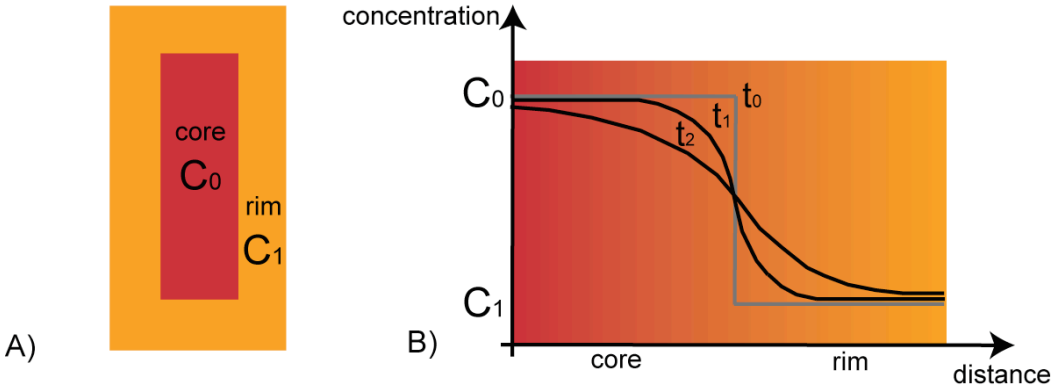

Figure 1.7. A) Cartoon of crystal zonation with an initial core concentration, C_0, and initial rim concentration, C_1. B) Evolution of the compositional gradient of the core-rim interface over time. Initially a step function is assumed at the rim (t_0) that is progressively smoothed through diffusion with time (t_1 and t_2).

crystals in a magma chamber to be calculated whilst Li diffusion in plagioclase crystals can be used to infer the rate of vapour transfer (Zellmer et al., 1999; Kent et al., 2007). Diffusion studies are not restricted to a single crystal phase but can be used to detail magmatic processes in numerous crystals, potentially preserving a record of numerous magmatic processes and therefore, allowing a comprehensive history of the magmatic evolution from a single eruption to be deciphered.

1.6 Geologic background

1.6.1 Taupo Volcanic Zone, North Island, New Zealand

Arc volcanism is observed along the entire length of the Tonga-Kermadec-Hikurangi convergent margin (Smith and Price, 2006). The hyper-productive Taupo Volcanic Zone is a 300 km long section of continental arc volcanism generated from the oblique westward subduction of the Pacific plate beneath the overlying Australian plate east of New Zealand (e.g. Stern, 1987; Wilson et al., 1995).

Rhyolitic volcanism in the Taupo Volcanic Zone commenced at ca. 1.6 Ma in the Mangakino volcanic centre and continues to the present day at the active caldera centres of Taupo and Okataina (Figure 1.8; Houghton et al., 1995; Wilson et al., 1995). Currently, 20 to 30 known caldera-forming eruptions have been recognised originating from eight caldera centres (Figure 1.8), which have been identified through the presence of negative gravity anomalies (Wilson et al., 1984; Houghton et al., 1995; Wilson et al., 1995; Davy and Caldwell, 1998; Cole

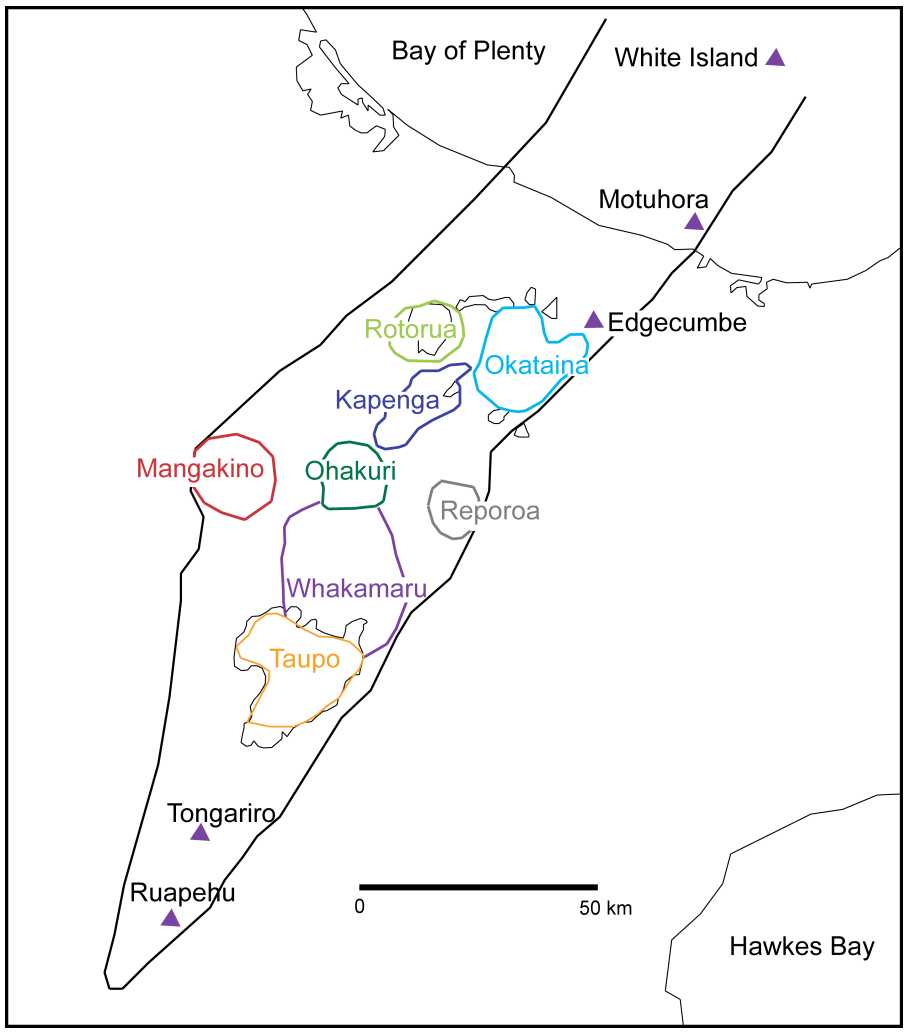

Figure 1.8 Caldera centres of the Taupo Volcanic Zone and major andesitic (purple triangles) centres after Cole et al. (1998) and Wilson et al. (in press).

et al., 2001; Allan et al., 2008; Wilson et al., in press). Rhyolitic deposits in the Taupo Volcanic Zone are predominantly welded and non-welded ignimbrite and air fall deposits with only minor occurrences of lava flows.

There is a paucity of basaltic volcanic rock (< 1%) exposed at the surface in the Taupo Volcanic Zone compared to the copious quantities of rhyolite (ca. 94 %) (Gamble et al., 1990; Graham et al., 1995). Basalt outcrops as small monogenetic scoria cones typically aligned along fault zones (e.g. Rotokawau and Tarawera basalts) (Gamble et al., 1990; Graham et al., 1995). The basalts are porphyritic containing olivine, plagioclase ± clinopyroxene and orthopyroxene phenocrysts, with groundmass glasses extending to rhyolitic compositions in the most evolved clinopyroxene-bearing basalts (Gamble et al., 1990). Chemical and isotopic signatures of the basalts indicate that they are derived from a subduction modified mantle source (Gamble et al., 1990, 1993; Graham et al., 1995).

Andesitic rocks form a relatively small component (5%) of the exposed surface magmatism of the Taupo Volcanic Zone (Graham et al., 1995). Exposures are confined to the northern (White Island) and southern extremes (Mt. Ruapehu, Tongariro volcanic centre) of the region, but are also observed as lithics within ignimbrites (Brown et al., 1998b; Cole et al., 1998). Nine distinct crystal-rich andesite types have been petrologically defined from the Taupo Volcanic Zone, from rare low-silica (ca. 52 wt % SiO_2) olivine-rich lavas to high silica (ca. 64 wt % SiO_2), almost dacitic plagioclase dominated samples (Graham et al., 1995). However, recent in-situ elemental and isotopic studies have demonstrated chemical disequilibrium between the crystal cargo and high-Si groundmass

glasses of andesites (e.g. Price et al., 2005; Davidson et al., 2007) indicating a more complex magmatic evolution.

The extent and nature of the basement rock of the Taupo Volcanic Zone is equivocal but is of importance as the interaction of, in particular, basement greywacke with the magmatic systems can influence the composition of the magmas. The North Island of New Zealand is underlain by Mesozoic basement comprising a range of deposits from massive turbidites to interbedded sandstones, mudstones and argillites (hereafter termed greywacke), deposited in a deep-water environment (Reid, 1982; Mortimer, 2004). However, several previous studies have argued for the replacement of the greywacke basement with the intrusion of igneous compositions of andesite/diorite (e.g. Cole, 1981; Stern, 1987; Soengkono, 1995). This is partly due to the inability of seismic and gravity surveys to distinguish between greywacke basement and intermediate igneous compositions of andesite/diorite due to the similar densities of both lithologies (Ewart and Stipp, 1968; Stern, 1985, 1987). Recent magnetotelluric studies (Heise et al., 2007) and isotopic studies of zircon and plagioclase crystals (Charlier et al., 2005, 2008) have provided compelling evidence for the presence of underlying greywacke basement throughout the Taupo Volcanic Zone. This is further confirmed by the presence of greywacke in drill holes and the ubiquitous occurrence of greywacke xenoliths within ignimbrites throughout the region (Reid, 1982; Browne et al., 1992; Graham et al., 1992; Cole et al., 1998; Brown et al., 1998a) although the extent and nature of this greywacke basement beneath the Taupo Volcanic Zone remains equivocal.

1.6.2 Kermadec Arc, South West Pacific

The 760 km long Kermadec Arc (25°-36°30' S) extends northwards from the northern boundary of the Taupo Volcanic Zone to the Tonga Arc (ca. 26°S) in the north, and represents the oceanic section of the Tonga-Kermadec-Hikurangi subduction system (Wright et al., 2006). The predominantly submarine volcanic frontal arc is confined to a 40 km wide zone consistently located at 100 km above the subducting slab (Smith and Price, 2006) although arc volcanoes are also present in the back arc Havre Trough (Wysoczanski et al., in press). The Kermadec Arc has been sub-divided into three regions (southern, central, northern) based on changes in arc elevation and lava chemistry (Smith and Price, 2006; Wright et al., 2006) (Figure 1.5). The central Kermadec Arc is characterised by relatively simple stratovolcanoes at water depths > 3.2 km (Wright et al., 2006). In contrast, the southern and northern Kermadec Arc possess multi-vent volcanic edifices that include submarine calderas at water depths < 2.5 km (Wright et al., 2006). Volcanic centres are primarily composed of basalt and basaltic andesite (~61%), and andesite (~9%) (Smith and Price, 2006). However, recent multibeam mapping and dredging along the Kermadec Arc has revealed the presence of substantial proportions of silicic volcanism (~30%) and submarine caldera structures (Wright and Gamble, 1999; Wright et al., 2002, 2006; Smith and Price, 2006).

1.7 Objectives of this thesis

The objectives of this study are to investigate the petrogenesis of large-volume silicic arc magmas, contrasting the different mechanisms operating in both continental and oceanic arc margins. This is achieved through the application of *in-situ* micro-analytical techniques i.e. electron probe microanalysis (EPMA), laser ablation inductively coupled plasma mass spectrometry (LA-ICPMS) and Fourier transform infrared (FTIR) spectrometry applied to individual magma components of crystal-hosted melt inclusions, groundmass glass and crystals.

Melt inclusions are examined from a range of continental Taupo Volcanic Zone rhyolitic eruptions (330 ka Whakamaru supereruption, 26.5 ka Oruanui supereruption, 15.8 ka Rotorua eruptive and 1800 BP Taupo eruption) representing various age and eruptions sizes (0.4 to > 1000 km^3 DRE) and are compared to the chemical composition of the rhyodacite eruption from the Healy seamount, sourced from the adjacent oceanic Kermadec Arc (Frogatt, 1981; Wilson and Walker, 1985; Brown et al., 1998a; Smith et al., 2004; Wilson et al., 2006). The major and trace element compositions of melt inclusions can be used to: (1) investigate the heterogeneity of the magma during the fractionation of the various crystal phases within individual eruptions; (2) to distinguish source components of the eruptions and whether these change through time; (3) to discriminate between petrogenetic models of fractional crystallisation and crustal anatexis, and (4) to examine the contribution of continental crust in the Taupo Volcanic Zone rhyolites by taking the composition of the Healy melt inclusions as a baseline for silicic petrogenesis due to the absence of continental lithosphere along the Kermadec Arc.

As water plays such a fundamental role in the genesis of silicic magmas and the subsequent eruption dynamics, dissolved H_2O and CO_2 concentrations of Whakamaru, Taupo and Healy melt inclusions were characterised. The objectives of this are to: (1) constrain the pre-eruptive H_2O and CO_2 concentrations directly prior to eruption, to establish the volatile content required to drive supereruptions; (2) document any heterogeneities in volatile concentrations of individual eruptions, between eruptions and particularly between continental and oceanic silicic eruptions; (3) estimate the depth of the magma immediately prior to eruption through the calculation of saturation pressures; and (4) examine the H_2O speciation of silicic melt inclusions and contrast this to the known behaviour of water speciation in groundmass rhyolitic glasses.

The chemical composition of melt inclusions whilst providing important constraints on the magmatic evolution, provides only limited information on the timescales of magmatic processes. Therefore the chemical and textural zonation of plagioclase crystals from the Whakamaru, Taupo and Healy eruptions and quartz crystals from the Whakamaru eruption are investigated to: (1) document the changing magmatic conditions derived from the textural observations; (2) identify whether multiple crystal populations are present within each eruption; (3) fingerprint the chemical source of each individual zone of plagioclase crystals; (4) characterise the magmatic processes responsible for the chemical zonation of crystals; and (5) establish the timescales of magmatic processes from the diffusional relaxation of elements across major compositional interfaces.

1.8 Structure of this thesis

Melt inclusions from both continental and oceanic silicic eruptions are firstly examined for major and trace element concentrations to contrast the petrogenesis of silicic magmas in each of these settings. The results of this study are presented in Chapter 2, which is a manuscript that has been submitted for consideration for publication to the Journal of Volcanology and Geothermal Research.

The majority of rhyolitic deposits observed in the Taupo Volcanic Zone are produced by highly explosive eruptions. Hence, the pre-eruptive volatile concentrations of magmas are explored through the investigation of water speciation of melt inclusions from the Whakamaru and Taupo ignimbrites and associated crystal lag deposits from the Taupo Volcanic Zone. The results of this study are presented in Chapter 3 as a draft manuscript to be submitted to Chemical Geology.

Chapter 4 addresses one of the fundamental questions remaining on the timescales of accumulation of large-volumes of eruptible magma and focuses on the 330 ka Whakamaru supereruption (Wilson et al., in press). A study of chemical zonation and diffusion modelling of plagioclase and quartz crystals attempts to constrain the timescales of magmatic processes prior to eruption. This chapter is presented as a draft manuscript to be submitted to Journal of Petrology.

Chapter 5 examines the major element zonation of Healy and Taupo plagioclase crystals and volatile concentrations of Healy melt inclusions. This data is allied with the chemical composition of melt inclusions (Chapter 2) and the insights

this provides into the petrogenesis of silicic continental and oceanic arc magmas is discussed.

A synthesis of the findings of this thesis and major conclusions are presented and discussed in Chapter 6. Details of analytical methods not included in the chapters of this thesis, the theory behind diffusion modelling, data tables and backscattered and cathodoluminescence images can be found in Appendices 1 - 4.

Chapter 2

Petrogenesis of large-volume silicic magma in continental arcs: melt inclusions in Taupo Volcanic Zone and Kermadec Arc rhyolites, South West Pacific.

Abstract

Petrogenesis of large volume silicic magmas at continental arc margins is investigated through microanalysis of four major eruptives of variable size from the archetypical continental Taupo Volcanic Zone to determine if they are produced from assimilation and fractional crystallisation of mafic magmas or by crustal anatexis. We report major and trace element concentrations of melt inclusions from four continental (Whakamaru, Oruanui, Taupo and Rotorua) eruptive units, as well as one oceanic (Healy) eruptive unit from the contiguous Kermadec arc, which provides a baseline to evaluate the contribution of evolved crust to silicic magma petrogenesis in a continental arc setting. Orthopyroxene, plagioclase and quartz hosted melt inclusions and groundmass glass display a range in major element (e.g. SiO_2 = 74 - 79 wt %, CaO = 0.2 - 2.5 wt % and FeO = 0 - 3 wt %) and trace element compositions (e.g. Sr = 17 - 180 ppm and Ba = 140 - 1500 ppm). Healy melt inclusions are lower in K_2O and Ce/Yb relative to Taupo Volcanic Zone melt inclusions reflecting the lack of continental lithosphere in the oceanic setting. Quantitative trace element modelling of Healy melt inclusions demonstrates that extensive fractional crystallisation (62 - 76%) is responsible for the magma genesis of the rhyodacitic magma. However, assimilation is required in addition to extensive fractional crystallisation (60 - 80%) to attain the compositions of Taupo Volcanic Zone melt inclusions. High

Rb/Sr ratios of melt inclusions compared to published pumice compositions from the same eruptions indicate some crystals were inherited from a more evolved rhyolitic melt that subsequently mixed with a local basement (greywacke) partial melt. These models indicate that assimilation and fractional crystallisation of mafic magmas with variable amounts of mixing with crustal partial melts are able to produce silicic magmas of all sizes in the Taupo Volcanic Zone and that models of pure crustal anatexis are not required.

2.1. Introduction

Continental arc margins are a dominant setting for silicic magmatism on Earth, with a growing recognition of the role of oceanic arcs in producing silicic magmas. Nonetheless the petrogenesis of silicic magmas in continental and oceanic arcs is controversial with two end-member models invoked: (1) fractional crystallisation from a basaltic parent (e.g. Graham et al., 1995; Pearce et al., 1995; Grove et al., 2003; Hasse et al., 2006); and (2) crustal anatexis of amphibolitic or tonalitic lower crust, and/or continental or oceanic crust where present (e.g. Borg and Clynne, 1998; Kawate and Arima, 1998; Tamura and Tatsumi, 2002; Smith et al., 2003a and b; Shukuno et al., 2006; Smith et al., 2006; Wysoczanski and Tani, 2006). At continental margins magma storage is commonly characterised by complex plumbing systems allowing for polybaric crystal fractionation and ample opportunity for the recycling of crystals, magma mixing and assimilation of continental crust. This has led to diverse models of silicic magma genesis that include assimilation and fractional crystallisation (AFC) and magma mixing in addition to the end-member fractionation and crustal anatexis models proposed above (Ewart and Stipp, 1968; Graham et al.,

1992; McCulloch et al., 1994; Price et al., 2005; Davidson et al., 2007; Price et al., 2007). Differences in compositions of magmas in oceanic and continental arcs suggest that different magma genesis processes dominate in each of these settings, as large-volume silicic eruptions are a characteristic feature of continental subduction zones whereas basaltic and basaltic andesitic volcanism dominates in oceanic subduction settings (Gamble et al., 1996; Tamura and Wysoczanski, 2006; Wright et al., 2006). There is, however, increasing evidence for voluminous silicic volcanoes and caldera-forming eruptions in oceanic arcs such as New Britain Island Arc, Kermadec Arc, South Sandwich Arc and Izu-Bonin Arc (e.g. Woodhead et al., 1998; Wright and Gamble, 1999; Tamura and Tatsumi, 2002; Leat et al., 2003; Shukuno et al., 2006; Wright et al., 2006) suggesting that magma petrogenesis may not be substantially different in oceanic and continental arcs.

The Taupo Volcanic Zone of New Zealand and the Kermadec Arc (Figure 2.1) are archetypal examples of continental and oceanic arcs that typify the contentious nature of silicic magma petrogenesis. In the Kermadec arc, both fractional crystallisation and crustal anatexis have recently been proposed as mechanisms for the generation of silicic volcanoes (e.g. Haase et al., (2006) for Brothers Volcano and Smith et al. (2006) for Raoul Volcano, respectively), whilst a host of AFC and crustal melting models have been invoked for the origin of continental Taupo Volcanic Zone silicic magmas (McCulloch et al., 1994; Graham et al., 1995; Charlier et al., 2005: Wilson et al., 2006; Price et al., 2007). Geophysical studies are unable to distinguish between fractionation and anatexis

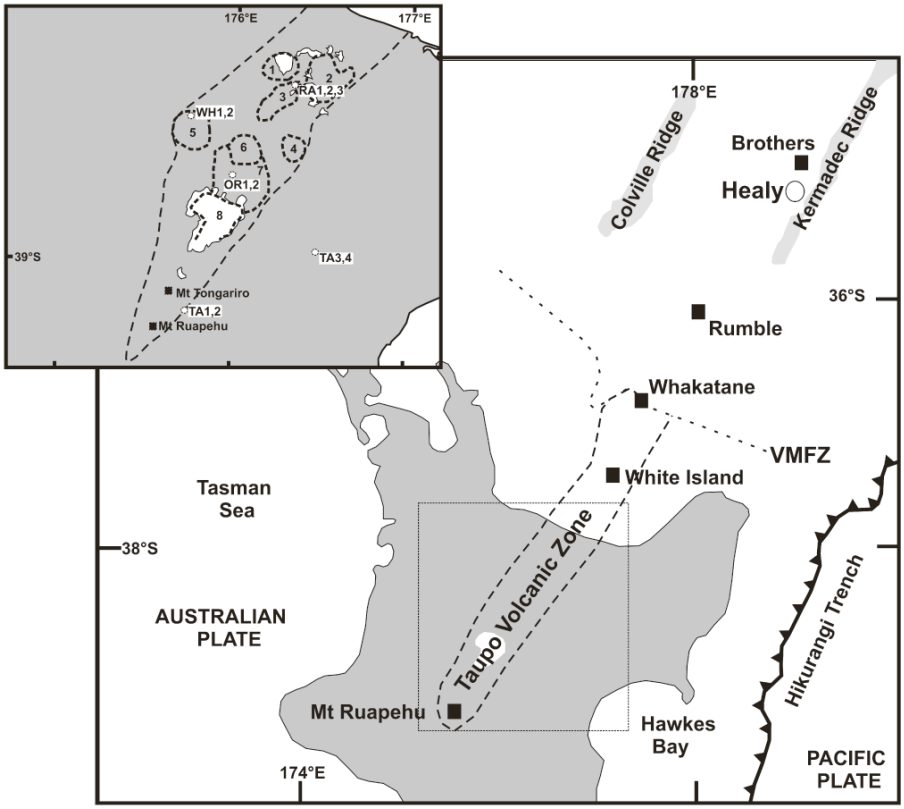

Figure 2.1. Map of Taupo Volcanic Zone and southern Kermadec arc with sample locations (white circles) shown in relation to the known caldera complexes of the Taupo Volcanic Zone. Outline of the Taupo Volcanic Zone - thick dashed line; continental-oceanic crust transition - thin dotted line, from Macpherson et al. (1998). Caldera complexes from Cole et al. (2001): 1 = Rotorua; 2 = Okataina; 3 = Kapenga; 4 = Reporoa; 5 = Mangakino; 6 = Maroa; 7 = Whakamaru; 8 = Taupo.

models. Until recently, limited geophysical evidence for the crustal structure of the Taupo Volcanic Zone has provided little evidence for mafic cumulates in the mid-lower crust fuelling the arguments for crustal anatexis models. However, melting experiments have shown that complete melting of lower crustal rocks would not occur and that crustal anatexis models also require an extensive restite to be present within the crust (Beard and Lofgren, 1991; Wolf and Wyllie, 1994; Rapp and Watson, 1995). Recent seismic surveys of the Taupo Volcanic Zone (Harrison and White, 2006; Stratford and Stern 2006) appear to image a layer of

intruded or underplated material at the base of the crust beneath the Taupo Volcanic Zone that may be sufficient to account for the cumulative or restite component required by either petrogenetic model.

Distinguishing between the models is complicated as both fractional crystallisation and crustal anatexis produce similar major element compositions (Haase et al., 2006). In continental arcs, assimilation of even small quantities of evolved crust will mask any primary geochemical signature of the melt. This is further complicated by whole rock analysis of silicic pyroclastic rocks, which are composed of a mixture of juvenile, lithic and inherited material (e.g. Brown et al., 1998b; Cole et al., 1998), resulting in average rock compositions rather than liquid compositions of the magma, making source contributions difficult to unravel.

An alternative to analysing bulk rock compositions is to analyse direct samples of trapped melts. As crystals grow during the life cycle of magmatic bodies they incorporate small (typically <100 μm) pockets of melt that remain trapped within the crystal, and which on eruption are quenched to glass (Roedder, 1979; Sobolev, 1996; Danyushevsky et al., 2002). As these melt inclusions reflect direct samples of the crystallising magma they allow the chemistry of multiple magma sources to be constrained. This has the potential to distinguish between the various models for the origin of silicic magmas in both oceanic and continental arc settings. Published studies of melt inclusions in silicic rocks, however, are limited, with very few studies on Kermadec Arc – Taupo Volcanic

Zone samples (Dunbar and Kyle, 1993; Schmitz and Smith, 2004; Liu et al., 2006; Shane et al., 2008).

Here we present *in situ* microanalyses of major and trace elements in melt inclusions from four Taupo Volcanic Zone silicic eruptives of varying size and age (Whakamaru, Oruanui, Rotorua and Taupo) to distinguish source components in large-scale silicic eruptives and distinguish between varying petrogenetic models. We also present data from melt inclusions from one rhyodacitic caldera from the Kermadec Arc (Healy caldera) as oceanic silicic magmas are generated without the potential for contributions from continental crust, allowing a baseline from which to examine the contribution of continental crust in magma genesis in continental arcs. Trace element modelling of the results requires only extensive fractional crystallisation from a basaltic parent to produce the oceanic arc rhyodacite at Healy caldera, whereas the presence of silicic crust in the continental Taupo Volcanic Zone has resulted in both assimilation and partial melting of continental crust in addition to extensive fractional crystallisation. None of the sampled eruptive products can be produced purely by crustal anatexis.

2.2. Regional background and samples

Taupo Volcanic Zone is the most active site of silicic magmatism on Earth, having produced more than 15 000 km^3 of material in the last 1.6 million years (Wilson et al., 1995). Volcanism is dominantly rhyolitic (>97%), with small volumes of andesitic (2-3%) and minor dacitic and basaltic volcanism (Cole, 1979; Wilson et al., 1984). Andesitic and basaltic lithics are present in many

ignimbrite deposits (e.g. Cole et al., 1998; Wilson et al., 2006) suggesting that andesite volcanics underlie and predate the main silicic deposits throughout the Taupo Volcanic Zone. Silicic volcanism in the Taupo Volcanic Zone commenced from the Mangakino caldera (Figure 2.1) and has continued to the present day from eight recognised caldera centres (Wilson et al., 1995), although the large Whakamaru Group ignimbrite sheets erupted since ca. 340 ka cover much of the evidence of earlier eruptive periods (Graham et al., 1995; Wilson et al., 1995; Brown et al., 1998a). Only two of the eight calderas (Taupo and Okataina) are considered to be active. Samples were chosen to represent eruptions of varying volumes (0.4 to >1000 km^3 dense rock equivalent (DRE)) and age (Table 2.1).

Whakamaru Group ignimbrites are the most voluminous known ignimbrites of the Taupo Volcanic Zone; with volumes exceeding 1000 km^3 of magma erupted following a ca. 350 ka lull in caldera-forming activity in the Taupo Volcanic Zone (Wilson et al., 1986; Brown et al., 1998a). The Whakamaru ignimbrite, which is the largest ignimbrite of the Whakamaru Group, has a mineral assemblage consisting of large, resorbed quartz, plagioclase, orthopyroxene and amphibole with smaller amounts of ilmenite, magnetite, K-feldspar and biotite (Brown et al., 1998a). A characteristic, but discontinuous crystal lag at the base of the ignimbrite (Brown, 1994) was sampled as part of this study (WH1), with a second sample (WH2) collected midway through the ignimbrite (from ‘layer E’ of Briggs, 1976).

Eruption	Latitude (°S)	Longitude (°E)	Age (ka)	Volume DRE (km^3)	Magma Temperature (°C)	Crystal content	Mineral phases
Whakamaru			340	>1000	750-850		
WH1 – crystal lag	38°21.005’	175°42.037’			(Fe-Ti oxides)	50%	plag>qtz>opx>amp>bt>oxides
WH2	38°20.849’	175°44.026’				30%	plag>qtz>opx>oxides
Oruanui			26.5	530	760		
OR1 (pumice)	38°35.840’	175°58.685’			(Fe-Ti oxides)	3%	plag>qtz>opx>oxides
OR2 (matrix)	38°35.840’	175°58.685’				10%	plag>qtz>opx>oxides
Rotorua Eruptive			15.8	1	750-870		
RA1	38°10.338’	176°19.765’			(Fe-Ti oxides)	5%	plag>opx>amp>qtz>bt>oxides
RA2	38°10.327’	176°19.716’				5%	plag>qtz>opx>amp>bt>oxides
RA3	38°10.338’	176°19.765’				15%	plag>qtz>opx>bt
Taupo			1.8	35	850-870		
TA1 – crystal lag	39°13.092’	175°44.115’			(Fe-Ti oxides)	50%	plag>opx>qtz>oxides
TA2 – Taupo ignimbrite	39°13.092’	175°44.115’				2%	plag>opx>qtz>oxides
TA3 – Taupo Plinian	38°55.772’	176°29.255’				1%	plag>opx>oxides
TA4 – Hatepe Plinian	38°55.772’	176°29.255’				5%	plag>oxides>opx>qtz
Healy			0.59	5	950		
X590 – caldera floor	34°59.249’	178°59.573’			(2-pyroxene)	3%	plag>opx>oxides
X590/B – caldera floor	34°59.249’	178°59.573’				3%	plag>opx>oxides>amp
X609 – north flank	34°57.490’	179°00.522’				5%	plag>opx>oxides>amp

Table 2.1. Details of samples analysed in this study. Abbreviations used are: plag = plagioclase; opx = orthopyroxene; oxides = Fe-Ti oxides; qtz = quartz; amp = amphibole; bt = biotite; and DRE = dense rock equivalent. Whakamaru data from Brown et al. (1998a); Oruanui from Charlier et al. (2005) and Wilson et al. (2006); Rotorua eruption from Smith et al. (2004); Taupo from Wilson and Walker (1985), Wilson et al. (2006); and Healy from Wright and Gamble (1999) and Wright et al. (2003).

The youngest caldera forming eruption of the Taupo Volcanic Zone was the 26.5 ka Oruanui eruption (~ 530 km^3), which formed the caldera of Taupo volcano. The eruption occurred in ten phases over several months (Wilson, 2001; Wilson et al., 2006), with each phase consisting of both pyroclastic fall and flow deposits. The volume of eruptives increased with each successive phase, with the final phase producing half of the total volume. Rhyolite erupted during the initial and final stages of the eruption are indistinguishable in composition suggesting the presence of a large volume (> 100 km^3) weakly zoned magma body prior to eruption (Sutton et al., 1995). Most of the erupted material was rhyolitic pumice, although a small amount (<1 %) of juvenile basalt-andesitic material was also involved (Wilson, 2001). The pumices contain 3-13 % crystals consisting of the assemblage plagioclase + orthopyroxene + quartz + hornblende + magnetite + ilmenite, with apatite and zircon as accessory minerals (Wilson et al., 2006). Pumice clasts (OR1) and the ash matrix (OR2) from poorly sorted Oruanui Ignimbrite were collected and analysed separately.

Numerous small silicic eruptions followed the Oruanui eruption, reflecting the rapid reorganisation of the magmatic system beneath Taupo volcano (Sutton et al., 1995; Wilson et al., 2006; Charlier et al., 2008). Post-Oruanui magmatism included initial dacitic volcanism followed by the eruption of three distinct rhyolitic magmas (Sutton et al., 1995). The largest of these, and the largest eruption in historic times, is the ca. 1800 BP (Wilson and Walker, 1985) Taupo eruption.

The Taupo eruption occurred in six distinctive episodes, which in stratigraphic order are: Initial ash (0.015 km^3); Hatepe Plinian (6 km^3); Hatepe Ash (2.5 km^3); Rotongaio Ash (1.3 km^3); Taupo Plinian (24.5 km^3); and the youngest and most voluminous unit, Taupo Ignimbrite (31 km^3) (Froggatt, 1981; Wilson and Walker, 1985). The total erupted volume, which includes re-worked material and primary material beneath Lake Taupo, is estimated at > 105 km^3 covering an area of ca. 20 000 km^2 (Wilson and Walker, 1985). Samples analysed here were collected from crystal rich lenses at the base of the Taupo Ignimbrite (TA1), and pumice from the Taupo Ignimbrite (TA2), Taupo Plinian (TA3) and Hatepe Plinian (TA4). The crystal assemblage consists of plagioclase + orthopyroxene + quartz + ilmenite + magnetite.

Okataina Caldera is the only caldera other than Taupo volcano to produce extensive silicic magmatism since the 26.5 ka Oruanui eruption (Wilson et al., 1995). The smallest (but well preserved) of the nine post-Oruanui eruptive episodes from the Okataina Volcanic centre is the Rotorua eruption at 15.8 ka (Froggatt and Lowe, 1990). The eruption consisted of plinian pumice fall deposits with a minimum volume of > 0.4 km^3 DRE (Kilgour, 2002) and late-stage lava domes (Nairn, 1980; Smith et al., 2004). The plinian fall deposits consist of interlayered pumice and fine ash layers (typically 5-10 cm) interpreted to reflect rain-washing or phreatomagmatic activity (Smith et al., 2004). The crystal assemblage is diverse, consisting of plagioclase, quartz, orthopyroxene, hornblende, clinopyroxene, biotite and oxides. Three samples of the Rotorua eruption were collected from Okareka

Quarry: RA5 and RA6 are pumice from two different beds within the sequence and RA7 is from a crystal rich lens.

Subduction volcanism continues north of the Taupo Volcanic Zone along the length of the Kermadec Arc – Havre Trough where oceanic lithosphere overlies the subducting slab (Smith and Price, 2006). The transition from continental to oceanic arc occurs to the north of the Whakatane and Colville Knolls (Figure 2.1) where an abrupt NW-SE trending deep indenter, the Vening Meinesz Fracture Zone, cuts perpendicular to the arc (Wright, 1994; Smith and Price, 2006). Rates of subduction in the southern Kermadec Arc are approximately 6 cm/yr, increasing to 10 cm/yr in the north towards Tonga (Parson and Wright, 1996; Smith and Price, 2006). Magmatism in both the arc and backarc is dominantly basaltic-andesite although silicic calderas have recently been discovered, mapped and sampled along the frontal arc (e.g. Gamble et al., 1996; Wright et al., 2006; Wysoczanski et al., 2006).

Healy volcano is a recently discovered young composite volcanic complex consisting of a basaltic-andesitic stratovolcano and silicic caldera complex located on over-thicken oceanic crust (Wright et al., 2006). The volcano is approximately 15 km long and 7 km wide with a water depth of 1150 m at the summit. A flat ca. 2.5 km wide caldera floor is flanked by 200 - 400 m high, shallowly inclined walls covered in well-sorted blocks and lapilli. A large proportion of samples recovered from this site, including two samples analysed here (X590 and X609) are rhyodacitic pumiceous clasts that

represent some of the most silicic compositions recovered from the southern Kermadec Arc (Wright and Gamble, 1999; Wright et al., 2003).

2.3. Methods

2.3.1 Sample preparation

Blocks of pumice were coarsely crushed using a mortar and pestle, then dry sieved to extract material finer than 1 mm. Fine glass was floated off in water and the remaining material was dried for 12 - 24 hours at 40 °C. Crystal lag deposits were sieved, washed and dried. All samples were further sieved into 1 mm - 710 μm, 710 - 500 μm and <500 μm fractions. For the majority of samples, the 1 mm - 710 μm fraction was further processed, and for crystal poor samples (e.g. OR1) the 710 - 500 μm fraction was also further processed. Quartz and feldspar were magnetically separated and quartz, plagioclase and orthopyroxene crystals were hand picked under a binocular microscope to obtain crystals containing the largest and least crystallised melt inclusions (melt inclusions with few if any daughter crystals).

Melt inclusions were present in quartz, plagioclase and/or orthopyroxene crystals from the analysed samples. The inclusions are spherical to ellipsoidal in shape and range in size from 10 μm to > 300 μm, the majority being 30 - 100 μm in size (Figure 2.2). Orthopyroxene crystals contain multiple small melt (10 - 50 μm), ilmenite, magnetite and apatite inclusions hosted throughout the crystal (Figure 2.2). Plagioclase and quartz hosted

melt inclusions are generally larger (50 - 100 µm) and, in some instances, contain a vapour bubble. Plagioclase hosted melt inclusions sometimes occur in an inner rim around the crystal and may represent a period of resorbtion or a slow growth period of the crystal (Figure 2.2). The melt inclusions are brown in colour except for the Whakamaru samples where the majority of melt inclusions are light green, similar to those observed in quartz and feldspars crystals from peralkaline rhyolites from Mayor Island in the northern Taupo Volcanic Zone (Barclay et al., 1996). Matrix glass adhered to the exterior of crystals was also analysed where present.

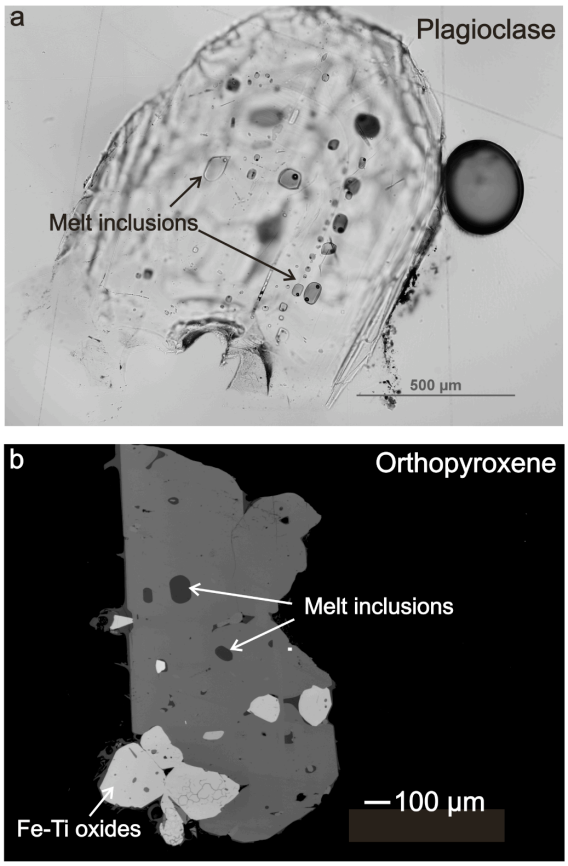

Figure 2.2. a) Transmitted light photomicrograph of melt inclusions in a plagioclase crystal from Taupo Ignimbrite. Small vapour bubbles are observed in some melt inclusions. b) Backscattered electron image of melt inclusions in an orthopyroxene crystal from Taupo Ignimbrite.

Melt inclusions were exposed for analysis by placing a single crystal in crystal bond cement on a glass slide and then grinding using 600 and 2400 grit SiC paper, until the inclusion became exposed. Multiple crystals containing exposed melt inclusions were then removed and washed in acetone to remove crystal bond, mounted in epoxy blocks and finely polished using 3 micron and ¼ micron diamond paste.

2.3.2 Electron microprobe analyses

Most major element analyses were determined on a JEOL 733 SuperProbe electron probe microanalyser (EPMA) at Victoria University of Wellington. A subset of Healy inclusions were analysed at the Institute for Research on Earth Evolution, Japan Agency for Marine-Earth Science and Technology. Operating conditions were 15 kV and 8 nA, with a 10 µm defocused beam. Na and K were analysed first with a short count time to minimise volatile loss and ZAF corrections were applied.

	Average n = 5	2 S D	% 2 S D	% difference	Reference values
SiO_2	50.91	0.45	0.9	0.2	50.81
TiO_2	1.83	0.14	7.6	-0.9	1.85
Al_2O_3	14.02	0.17	1.2	-0.3	14.06
FeO	11.71	0.48	4.1	-1.1	11.84
MnO	0.25	0.12	42	12	0.22
MgO	7.20	0.17	2.3	7.3	6.71
CaO	10.85	0.27	2.5	-2.5	11.12
Na_2O	2.69	0.33	12.3	2.5	2.62
K_2O	0.21	0.05	24.7	8.5	0.19
$Cl^{\#}$	1.22	0.04	3.5	-15	1.43
$SO_3{}^{\#}$	1.32	0.41	31	-0.04	1.32
Total [1]	99.67				

Table 2.2. Standard calibrations and reference values for VG2 and scapolite for electron probe microanalysis. Reference values taken from Jarosewich et al. (1980). [1]Total for VG2 only, [#] Values are for scapolite

Primary calibrations used a mixture of natural and synthetic standards, and VG2 glass and scapolite (Jarosewich et al., 1980) were analysed as secondary standards at the beginning and end of each session to monitor instrumental drift (Table 2.2). Normalisation of data to VG2 and scapolite allows comparison of the data from the two laboratories.

2.3.3 Laser ablation inductively coupled plasma mass spectrometry

Trace element concentrations were determined by laser ablation inductively coupled plasma mass spectrometry (LA-ICP-MS) in the Geochemistry Laboratory of Victoria University of Wellington using a NewWave deep UV laser (193 nm solid state) coupled to an Agilent 7500cs ICP-MS with helium as the ablation gas. Samples were analysed using 35 μm or 20 μm laser spot diameters, a laser repetition rate of 5 Hz and 60% power. CaO was determined by EPMA prior to LA-ICP-MS analysis enabling ^{43}Ca to be used as an internal calibration. NIST 612 glass was used as the primary standard as it provides an excellent matrix match for rhyolitic samples (Baker and Wysoczanski, unpublished data). Prior to each run the MPI-DING rhyolitic glass ATHO-G was analysed. Average trace element data obtained for ATHO-G is shown in Table 2.3 along with the reproducibly and recommended reference values (Jochum et al., 2006; GeoRem http://georem.mpch-mainz.gwdg.de/). Full LA-ICP-MS analytical procedures are documented by Allan et al. (2008).

Sample ID	WH1_ 24-1.1	WH1_ 39-1.1	OR1_ 12-1.1	OR1_ 17-1	OR1_ 16.1	TA1_ 41-4	TA1_ 29-1	RA1_ 5-1.1
Host Phase	opx	qtz	opx	plag	qtz	opx	plag	opx
SiO_2 (wt%)	77.96	76.51	78.62	78.52	78.15	75.76	76.39	77.24
TiO_2	0.10	0.08	0.21	0.12	0.19	0.29	0.23	0.29
Al_2O_3	12.45	13.18	12.25	12.56	12.74	13.37	13.55	13.91
FeO	0.51	0.24	1.67	1.39	1.21	2.62	1.95	1.89
MnO	0.15	0.20	0.07	0.03	0.11	0.13	0.18	0.13
MgO	0.04	0.04	0.17	0.15	0.16	0.28	0.25	0.25
CaO	0.37	0.61	0.86	1.27	1.17	1.57	1.59	1.38
Na_2O	3.42	3.84	2.50	2.92	2.88	3.11	2.84	2.51
K_2O	3.77	4.98	3.29	2.59	2.77	2.48	2.82	2.20
Cl	0.18	0.20	0.21	0.23	0.22	0.17	0.17	0.16
SO_3	0.06	0.10	0.05	0.19	0.13	0.21	0.04	0.04
Total	100.00	100.00	100.00	100.00	100.00	100.00	100.00	100.00
Sc (ppm)	5.64	8.35	9.06	10.0	11.3	31.8	17.2	11.2
V	3.65	2.28	2.62	1.96	1.81	2.09	0.987	6.28
Cr	4.34	11.4	14.9	4.44	6.09	11.2	5.0	11.5
Mn	188	552	314	445	424	2221	792	432
Co	0.436	1.86	0.572	0.605	0.853	1.81	0.616	0.62
Ni	b.d.	3.08	b.d.	0.912	1.07	1.80	1.31	2.45
Cu	9.74	2.86	1.95	1.99	2.73	0.00	1.97	2.09
Zn	9.82	50.4	27.1	48.8	44.9	183	97.0	44.7
Ga	16.1	16.2	14.1	13.9	14.5	15.4	18.1	14.9
Rb	223	221	182	112	129	113	125	118
Sr	62.2	45.8	56.5	95.1	92.3	141	156	102
Y	21.5	17.9	17.8	24.4	24.8	38.1	34.8	21.7
Zr	170	91.4	90.7	147	133	243	221	150
Nb	10.8	9.59	8.13	7.91	8.59	9.96	9.50	8.65
Mo	3.66	3.39	2.06	1.53	1.64	1.23	1.50	1.55
Cs	13.8	10.6	8.97	5.70	6.56	5.67	5.90	4.49
Ba	1228	709	766	674	721	722	672	895
La	28.9	24.5	26.1	22.1	24.3	28.0	27.3	24.9
Ce	64.6	52.9	48.3	47.1	50.1	63.9	67.2	46.8
Pr	5.28	4.48	4.36	5.09	5.35	6.76	7.12	4.74
Nd	21.5	15.6	17.7	19.7	19.7	29.8	28.0	21.1
Sm	3.50	3.17	3.88	3.92	4.06	5.37	6.28	3.36
Eu	0.137	0.363	0.440	0.709	0.715	1.36	1.33	0.61
Gd	3.82	2.38	2.81	3.93	3.64	5.46	6.07	3.51
Tb		0.483		0.677	0.630			
Dy	1.74	2.81	3.07	4.08	3.96	5.46	6.37	3.93
Ho		0.695		0.861	0.908			
Er	2.53	1.87	1.71	2.75	2.47	3.85	3.84	2.33
Tm		0.474		0.418	0.456			
Yb	2.25	3.86	2.36	3.06	3.04	3.98	3.65	2.75
Lu	0.354	0.738	0.291	0.485	0.502	0.649	0.556	0.42
Hf	4.10	3.19	3.37	4.54	4.26	6.90	5.75	4.1
Ta	2.02	1.28	1.14	0.763	0.715	0.574	0.802	0.7
W	3.56	3.86	2.19	1.41	1.94	1.99	1.80	1.51
Pb	23.8	24.8	19.2	15.5	16.5	21.7	23.0	15.1
Th	21.6	17.7	18.9	11.8	13.4	11.2	11.1	11.0
U	5.79	4.82	4.54	2.62	3.37	2.39	3.14	2.77

Table 2.3. (continued overleaf). Representative major and trace element data for Taupo Volcanic Zone and Healy melt inclusions.

Sample ID	RA2_13 -3.1	X590_3 -2	X609_1 7-1	ATHO-G	% 2SD	ref values
Host Phase	plag	opx	plag	n=5		
SiO_2	77.41	75.79	76.21			
TiO_2	0.19	0.39	0.40			
Al_2O_3	13.51	13.12	13.56			
FeO	1.39	2.65	2.49			
MnO	0.12	0.27	0.04			
MgO	0.24	0.16	0.42			
CaO	1.33	1.66	2.01			
Na_2O	2.81	3.61	2.51			
K_2O	2.74	1.89	1.70			
Cl	0.19	0.37	0.56			
SO_3	0.07	0.09	0.09			
Total	100.00	100.00	100.00			
Sc	9.5	19.4	11.6	8.83	19.6	7.00
V	4.55	9.9	5.5	3.84	12.6	3.91
Cr	7.5	2.9	10.8	9.07	21.9	6.1
Mn	443	2434	809	859	5.84	798
Co	0.599	6.20	1.12	1.32	36.3	2.13
Ni	1.86	0.99	0.962	6.51	37.0	13.0
Cu	2.21	8.80	4.00	15.2	5.54	18.6
Zn	40.1	159	65.0	154	3.34	141
Ga	16.0	13.6	10.9	21.5	3.06	25.3
Rb	97	25.4	31.0	70.1	12.0	65
Sr	140	113	156	92.7	5.94	94.1
Y	19.9	37.5	45.8	94.7	6.20	94.5
Zr	153	142	254	522	4.47	512
Nb	7.84	3.24	4.82	67.5	2.84	62.4
Mo	1.59	2.13	1.89	3.63	11.1	4.8
Cs	4.47	0.77	1.11	0.904	17.9	1.1
Ba	802	811	892	535	1.95	547
La	19.2	11.3	12.9	54.8	5.78	55.6
Ce	44.4	31.0	30.0	132	6.03	121
Pr	4.36	3.89	4.27	14.8	3.00	14.6
Nd	15.3	16.4	21.5	61.6	5.76	60.9
Sm	2.74	4.42	6.17	14.6	10.4	14.2
Eu	0.770	1.06	1.18	2.50	6.28	2.76
Gd	2.68	4.86	6.89	14.8	6.21	15.3
Tb				2.61	3.11	2.51
Dy	2.72	6.13	7.40	16.5	3.54	16.2
Ho				3.74	6.41	3.43
Er	1.81	4.07	4.79	10.3	1.78	10.3
Tm				1.70	4.40	1.52
Yb	2.05	4.39	6.12	10.1	5.70	10.5
Lu	0.43	0.74	0.878	1.52	12.0	1.54
Hf	4.2	3.24	6.70	12.9	3.59	13.7
Ta	0.4	0.26	0.268	4.15	8.84	3.90
W	1.07	0.29	0.263	9.70	9.51	9.30
Pb	14.5	4.45	5.00	5.52	6.95	5.67
Th	8.00	2.17	3.69	7.74	7.84	7.40
U	2.21	0.831	1.01	2.38	11.79	2.37

All sample data are recalculated on an anhydrous basis. Trace element data for repeat analyses of the standard ATHO-G (n = 5) and reference values of Jochum et al. (2006) are also shown. b.d. = below detection limits, spaces indicate element was not analysed.

2.4. Results

A brief petrographic overview and details of the samples studied are summarised in Table 1. Representative major and trace element compositions are presented in Table 2.3 and groundmass glass compositions in Table 2.4.

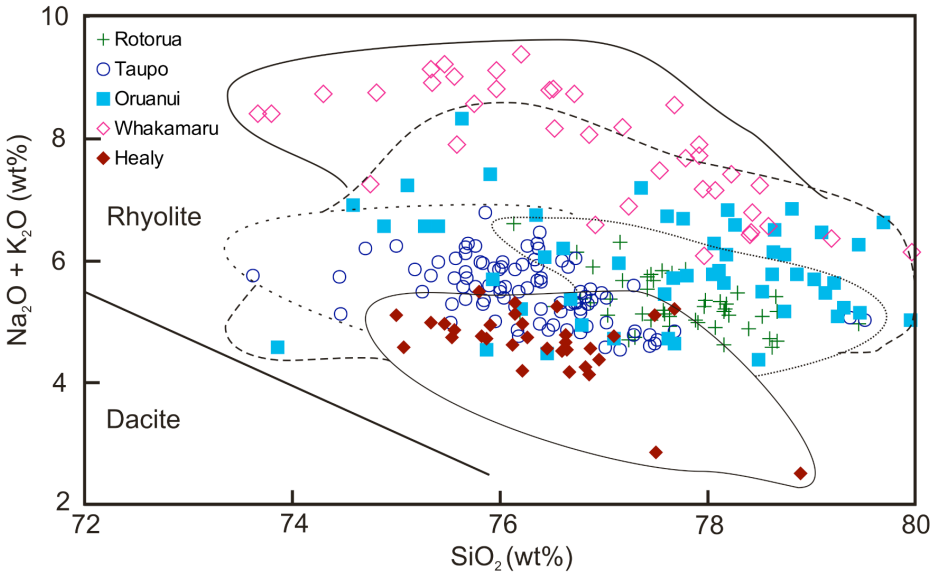

Figure 2.3. Total alkali silica diagram of Taupo Volcanic Zone and Healy melt inclusions. Dacite and rhyolite fields are after Le Bas et al. (1986).

Melt inclusions from all five silicic eruptions are rhyolitic in composition irrespective of setting (Figures 2.3 and 2.4). Where inclusions occur in both plagioclase and orthopyroxene crystals from the same sample, they overlap in composition (Figure 2.5). However, quartz hosted melt inclusions in the Whakamaru and Oruanui samples range to higher SiO_2 and K_2O, consistent with quartz crystallising at a different stage of magma formation compared to orthopyroxene and plagioclase. The large difference in K_2O concentration observed between quartz and orthopyroxene hosted melt inclusions in the Whakamaru ignimbrite is not evident in other major element concentrations.

Sample ID	OR2_23g	OR1_31g	OR1_26g	OR1_24g	X590/B_6g	X590/B_5g
n	2	2	2	2	1	1
SiO_2	78.25	78.07	78.54	77.75	75.61	74.95
TiO_2	0.18	0.16	0.15	0.14	0.28	0.50
Al_2O_3	12.43	12.35	12.29	12.95	13.50	13.56
FeO	1.73	1.80	1.46	1.38	2.20	2.08
MnO	0.04	0.14	0.06	0.11	0.15	0.09
MgO	0.13	0.11	0.10	0.12	0.39	0.39
CaO	1.04	1.13	1.14	1.22	2.04	2.45
Na_2O	3.10	3.34	3.28	3.34	3.56	3.67
K_2O	2.76	2.62	2.67	2.68	1.57	1.71
Cl	0.24	0.27	0.23	0.23	0.53	0.49
SO_3	0.10	0.01	0.08	0.08	0.18	0.05
Total	100.00	100.00	100.00	100.00	100.00	100.00
Sc	3.22	9.28	8.45	7.83	24.0	20.7
Ti	335	1020	976	972	0.136	0.445
V	0.566	1.58	1.49	1.14	12.2	8.98
Cr	1.46	6.91	6.98	5.95	33.8	45.7
Mn	148	528	420	398	721	856
Co	0.337	1.13	0.790	0.897	3.31	2.12
Ni	0.215	1.59	1.45	1.96	11.0	14.6
Cu	0.463	3.00	2.37	2.37	13.8	38.4
Zn	15.5	59.1	49.2	41.1	52.2	56.0
Ga	6.46	16.4	15.4	14.8	11.2	11.1
Rb	44.0	135	132	127	27.9	28.8
Sr	33.0	80.3	86.7	88.5	99.2	115.7
Y	18.4	19.4	22.3	22.9	28.3	28.8
Zr	38.9	105	123	127	122	129
Nb	2.26	8.51	7.86	7.16	2.47	3.05
Mo	0.391	1.63	1.66	1.75	5.90	3.62
Cs	2.13	7.15	6.61	6.06	0.747	0.864
Ba	224	677	672	696	533	861
La	17.6	20.0	21.8	21.8	8.19	11.29
Ce	44.5	48.5	49.1	46.9	26.3	26.0
Pr	5.30	4.40	5.18	4.72	3.10	2.61
Nd	23.7	17.9	19.1	19.3	15.0	15.5
Sm	5.24	3.12	4.25	3.41	4.46	3.08
Eu	0.607	0.610	0.611	0.524	0.766	0.979
Gd	4.66	2.83	3.37	3.48	4.42	3.35
Tb	0.661	0.492	0.533	0.536		
Dy	4.07	3.27	3.67	3.94	9.27	5.03
Ho	0.721	0.610	0.836	0.751		
Er	1.94	2.11	2.44	2.37	3.41	2.24
Tm	0.279	0.344	0.366	0.388		
Yb	1.51	2.43	2.45	2.69	1.86	3.72
Lu	0.177	0.373	0.393	0.518	0.487	0.809
Hf	1.10	3.15	3.63	3.51	2.56	2.49
Ta	0.303	0.615	0.776	0.663	0.561	0.444
W	0.410	2.15	1.68	2.08	1.96	2.49
Pb	5.13	17.6	15.1	15.5	2.43	4.61
Th	3.77	10.5	11.5	12.3	1.76	1.66
U	1.07	3.30	3.03	2.86	0.977	1.05

Table 2.4. Representative major and trace element concentrations of groundmass glass adhered to the exterior of crystals from the Oruanui and Healy samples. All data are recalculated on an anhydrous basis.

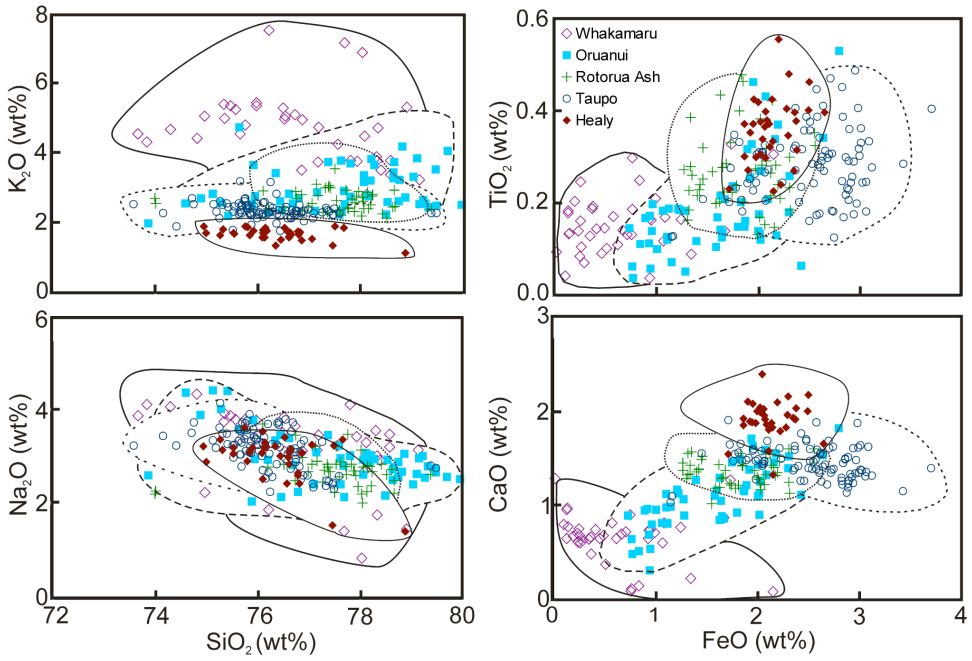

Figure 2.4. Major element bivariate diagrams for Taupo Volcanic Zone and Healy volcano melt inclusions.

Due to the small size (<25 μm) of the majority of orthopyroxene hosted melt inclusions there are insufficient data to distinguish any difference in trace element chemistry. Matrix glass compositions are often distinct from the melt inclusion compositions (Figure 2.5). For example plagioclase-hosted melt inclusions in the Rotorua eruptive display K_2O contents of 2.6-3.1 wt% in comparison to groundmass glass with K_2O of 2.2-2.4 wt% (Figure 2.5). However, Taupo melt inclusions and groundmass glasses compositions coincide (Figure 2.5).

Whakamaru melt inclusion compositions are distinct from those of the smaller volume Taupo and Rotorua eruptions, with higher large ion lithophile element (LILE), light rare earth element (LREE) and Nb and Ta contents, and lower CaO, FeO, Zr, Hf and varying heavy rare earth element (HREE) contents, with little or no overlap in composition (Figures 2.4 and

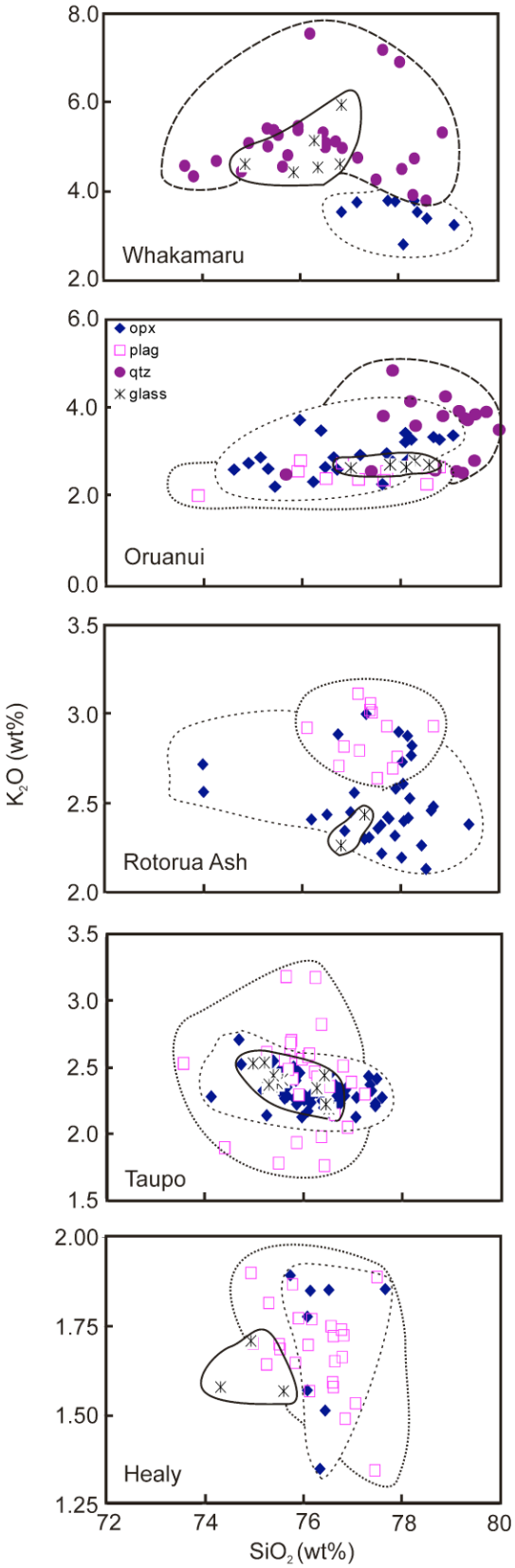

Figure 2.5. SiO_2 versus K_2O plots with melt inclusions distinguished by host crystals and groundmass glass compositions.

2.6). Whakamaru melt inclusions are also particularly notable for their high K_2O (4 - 6 wt %) content.

Rotorua and Taupo melt inclusions are similar, although the latter are less silicic. Oruanui compositions span the range between Whakamaru and Rotorua and Taupo compositions, with some overlap. Healy melt inclusions are distinct from Taupo Volcanic Zone inclusions, with lower K_2O, LILE (except Ba), actinides, Nb, Ta and LREE, and higher CaO and HREE contents (Figures 2.4 and 2.6).

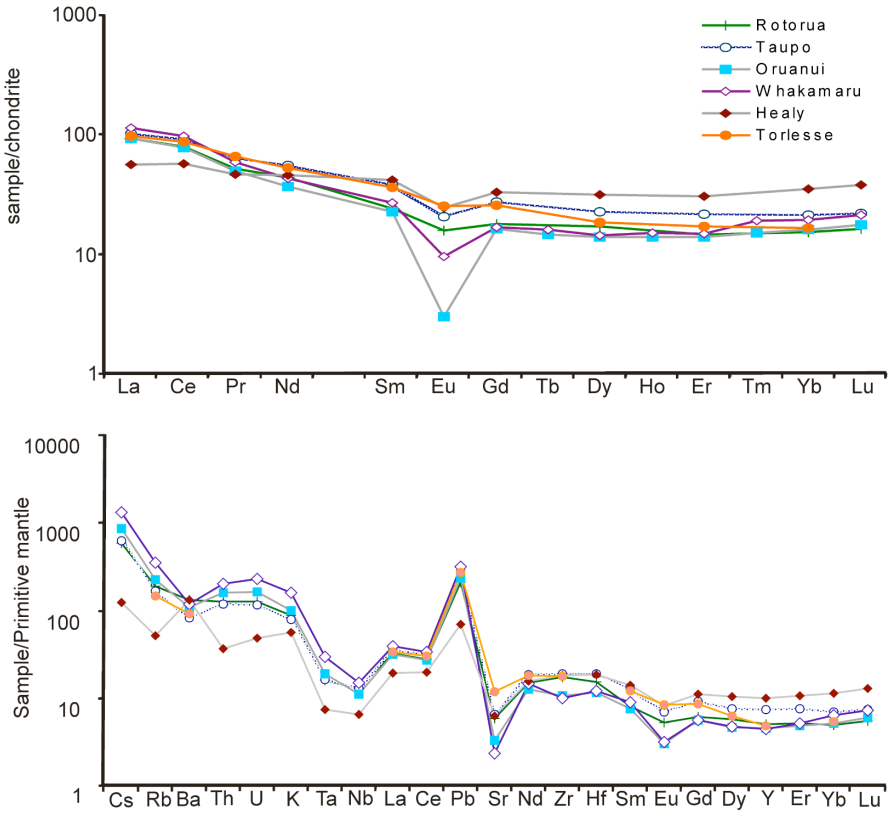

Figure 2.6. Chondrite-normalised rare earth element plot and primitive mantle-normalised multi-element diagram for mean melt inclusion compositions for each studied eruption. Chondrite values are taken from McDonough and Sun (1995) and those for primitive mantle are taken from Sun and McDonough (1989). REE concentrations of Torlesse greywacke are from Reid (1982).

Positive Pb anomalies and negative Sr and Eu anomalies are observed in all melt inclusions, with Whakamaru inclusions showing the largest anomalies, and Healy the smallest (Figure 2.6). All Taupo Volcanic Zone melt inclusions show a negative Ba anomaly, whereas Healy inclusions have a distinctive positive Ba anomaly.

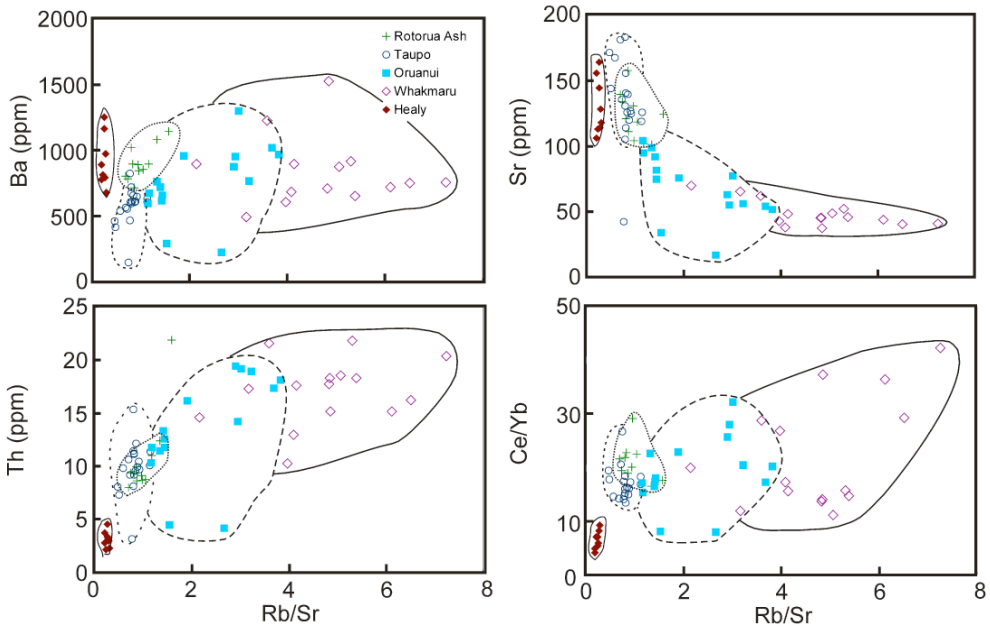

Figure 2.7. Trace element diagrams for Taupo Volcanic Zone and Healy melt inclusions using Rb/Sr as a fractionation index.

Selected trace element abundances and ratios are plotted against Rb/Sr as an index of fractionation in Figure 2.7, as Sr shows a general decrease with increasing Rb/Sr due to fractionation of plagioclase. Whakamaru inclusions have the highest Rb/Sr, suggesting that they are the most fractionated melts. Taupo and Rotorua melt inclusions have the lowest and least fractionated Rb/Sr ratios of the Taupo Volcanic Zone rhyolites and Oruanui melt inclusions span the range between Whakamaru and Taupo/Rotorua compositions. The enrichment in LREE and depletion of HREE of Taupo

Volcanic Zone melt inclusions compared to Healy inclusions is reflected in lower Ce/Yb ratios (mean of 6.4 for Healy compared to 19.2 for Taupo Volcanic Zone melt inclusions). Absolute Ba concentrations of Healy melt inclusions are similar to those of the Taupo Volcanic Zone melt inclusions but Th contents of Healy melt inclusions are 2.5 times lower than Taupo Volcanic Zone inclusions (Figure 2.7), resulting in a large variation in Ba/Th and Ba/Nb between Healy and Taupo Volcanic Zone inclusions (Figure 2.8).

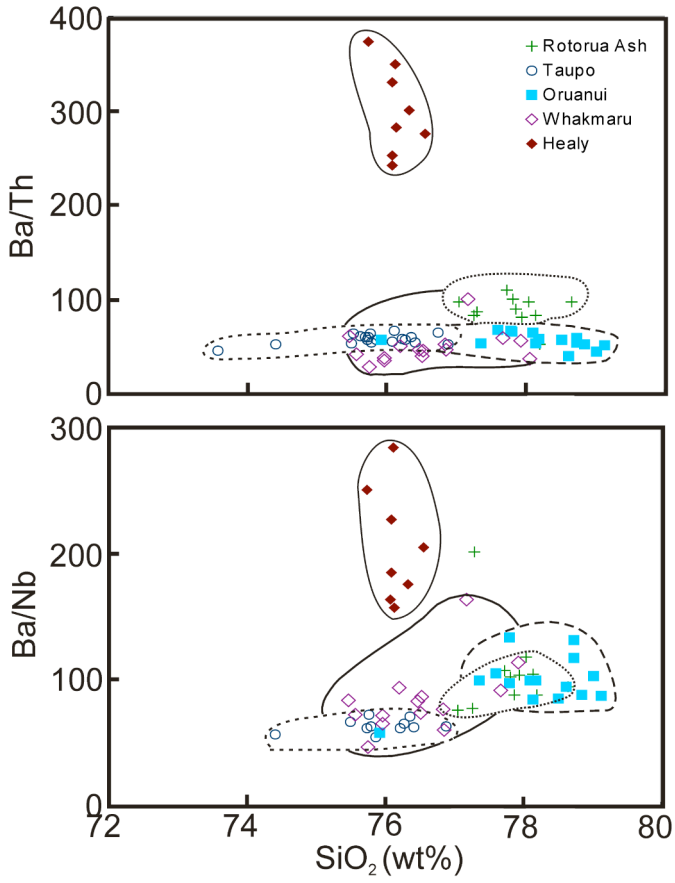

Figure 2.8. Ba/Nb and Ba/Th plotted against SiO_2 for Taupo Volcanic Zone and Healy volcano melt inclusions.

The Rb/Sr ratios of Whakamaru melt inclusions are two to three times higher than reported Rb/Sr ratios of the host pumice (mean Rb/Sr of 4.8 and

1.4, respectively) (Figure 2.9) (Brown, 1994). This trend is also evident in Oruanui melt inclusions where Rb/Sr ratios are approximately four times higher than in reported pumice compositions (Sutton et al., 1995; Wilson et al., 2006), as previously noted for quartz-hosted Oruanui melt inclusions (Liu et al., 2006). The Rb/Sr ratios of Taupo and Rotorua melt inclusions overlap and are slightly higher (up to 1.5 times) than pumice compositions (Figure 2.9) (Sutton et al., 1995; Smith et al., 2004).

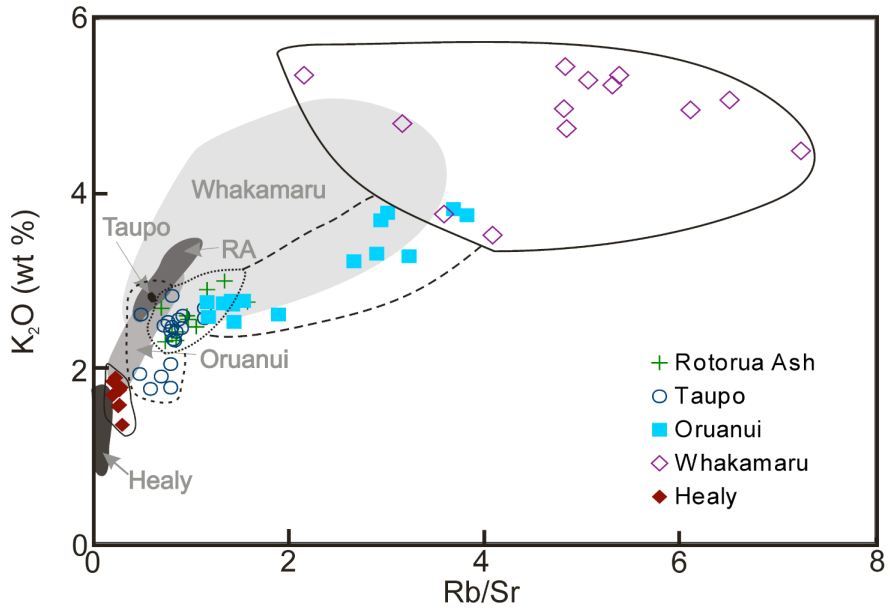

Figure 2.9. Rb/Sr plotted against K_2O comparing melt inclusions and pumice (shaded regions) from the same eruptive units. Pumice data are taken from Sutton et al. (1995), Brown et al. (1998a), Smith et al. (2004) and Wilson et al. (2006).

2.5. Discussion

2.5.1 Comparison of Healy and Taupo Volcanic Zone melt inclusion compositions

There are several important differences between the oceanic Healy and continental Taupo Volcanic Zone melt inclusions: (1) Healy REE patterns

have Ce/Yb ratios of ca. 6.4 compared to 19.2 for Taupo Volcanic Zone melt inclusions; (2) HREE concentrations in Healy melt inclusions are 1.8 to 2.5 times higher than Taupo Volcanic Zone melt inclusions; (3) Taupo Volcanic Zone melt inclusions have significantly higher K_2O (1.4 to 3 times), LILE such as Cs, Rb, and Pb (3 to 10 times), and LREE (1.8 times); and (4) Ba shows a positive anomaly in Healy melt inclusions but a negative anomaly in the Taupo Volcanic Zone inclusions (Figure 2.6).

The depletion of elements including Cs, Rb, Pb and LREE and enrichment of Zr, Hf and HREE in Healy samples compared to Taupo Volcanic Zone samples cannot be caused by varying degrees of partial melting or fractional crystallisation. If the relatively high Zr, Hf and HREE concentrations of the Healy samples were produced by lower degrees of partial melting than Taupo Volcanic Zone inclusions, Healy inclusions should also be relatively enriched, not depleted, in LILE and LREE concentrations. Similarly, crystal fractionation increases incompatible trace element abundances but will not strongly fractionate LILE and LREE from HFSE and HREE as observed in Taupo Volcanic Zone inclusions (Figure 2.6). The higher Zr, Hf and HREE contents of Healy inclusions could indicate a less depleted source beneath the Kermadec arc, although this is not complemented by higher Ta, Nb, LILE and LREE. Furthermore, Gamble et al. (1993) used HFSE modelling of basalts to argue that the mantle source beneath the Kermadec Arc is more depleted than the mantle beneath the Taupo Volcanic Zone. It should be noted, however, that depleted sources are more susceptible to secondary enrichment processes such as from fluids or melts from the descending slab

(Woodhead et al., 1993), so the greater depletion in Zr, Hf and HREE of Taupo Volcanic Zone magmas may be due to high degrees of partial melting with subsequent enrichment of LILE and LREE by a secondary process. It is likely that the disparity in composition between Healy and Taupo Volcanic Zone melt inclusion compositions is due to the difference in their geological settings, i.e. the lack of continental lithosphere in the oceanic Kermadec Arc. This raises the possibility of crustal assimilation and/or melting.

2.5.2 Petrogenesis of silicic magma at Healy caldera

Models of both fractional crystallisation (Haase et al., 2006) and crustal anatexis of oceanic crust (Smith et al., 2003a and b) have been invoked for the generation of Kermadec arc silicic magmas. The lithology of the [overlying] lithosphere beneath Healy precludes assimilation of continental lithosphere, making it an ideal location to investigate the viability of fractional crystallisation in producing rhyodacite from basaltic magmas.

Haase et al. (2006) used major element modelling to demonstrate that the rhyolitic glass from Brothers seamount adjacent to Healy caldera (Figure 2.1) could be produced through extensive fractional crystallisation of plagioclase, olivine, clinopyroxene, amphibole, Fe-Ti oxides and minor amounts of orthopyroxene. Rare earth element modelling of Healy inclusions is shown in Figure 2.10 using a Healy basalt (Wright and Worthington, unpublished data) as the starting composition, mineral proportions similar to those used by Haase et al. (2006), and basaltic

distribution coefficients from the literature (Table 2.5). The REE modelling indicates that the Healy silicic melts can be produced from basaltic magma through 62-76% fractional crystallisation of 43.5% plagioclase, 29% clinopyroxene, 7.2% orthopyroxene, 7.2% magnetite, 7.2% olivine, 4.4% amphibole and 1.5% ilmenite. These results, together with the model of Haase et al. (2006), indicate that at least some of the silicic magmas in the Kermadec arc can be produced from near perfect fractional crystallisation of basaltic magma.

Basalt	Plag	Opx	Cpx	Amp	Ilm	Mag	Ol
La	0.14	0.002	0.05	0.17	0.005	0.22	0.012
Ce	0.09	0.003	0.098	0.26	0.006	0.26	0.009
Pr	0.17	0.0048	0.15	0.35			0.005
Nd	0.04	0.0068	0.4	0.44	0.008	0.3	0.004
Sm	0.036	0.01	0.26	0.76	0.01	0.335	0.0013
Eu	0.73	0.013	0.6	0.88	0.007	0.36	0.0016
Gd	0.04	0.016	0.6	0.86	0.017	0.32	0.004
Dy	0.055	0.022	0.7	0.78	0.028	0.28	0.014
Er	0.041	0.03	0.6	0.68	0.046	0.22	0.008
Yb	0.016	0.049	0.28	0.59	0.077	0.18	0.0015
Lu	0.025	0.06	0.1	0.51	0.1	0.18	0.0018

Table 2.5. Rare earth element distribution coefficients for basaltic magmas used in the modelling of the trace element concentrations of Healy melt inclusions. Sources: Higuchi and Nagasawa (1969); Frey (1969); Irving and Frey (1984); Martin (1987); McKenzie and O'Nions (1991); and Dunn and Sen (1994).

The sparsely porphyritic nature of the Healy samples suggests that: (1) crystals efficiently settled out of the melt in the magma chamber; or (2) rhyodacitic melt was separated from fractionated material into a secondary magma chamber where only limited fractional crystallisation occurred prior to eruption.

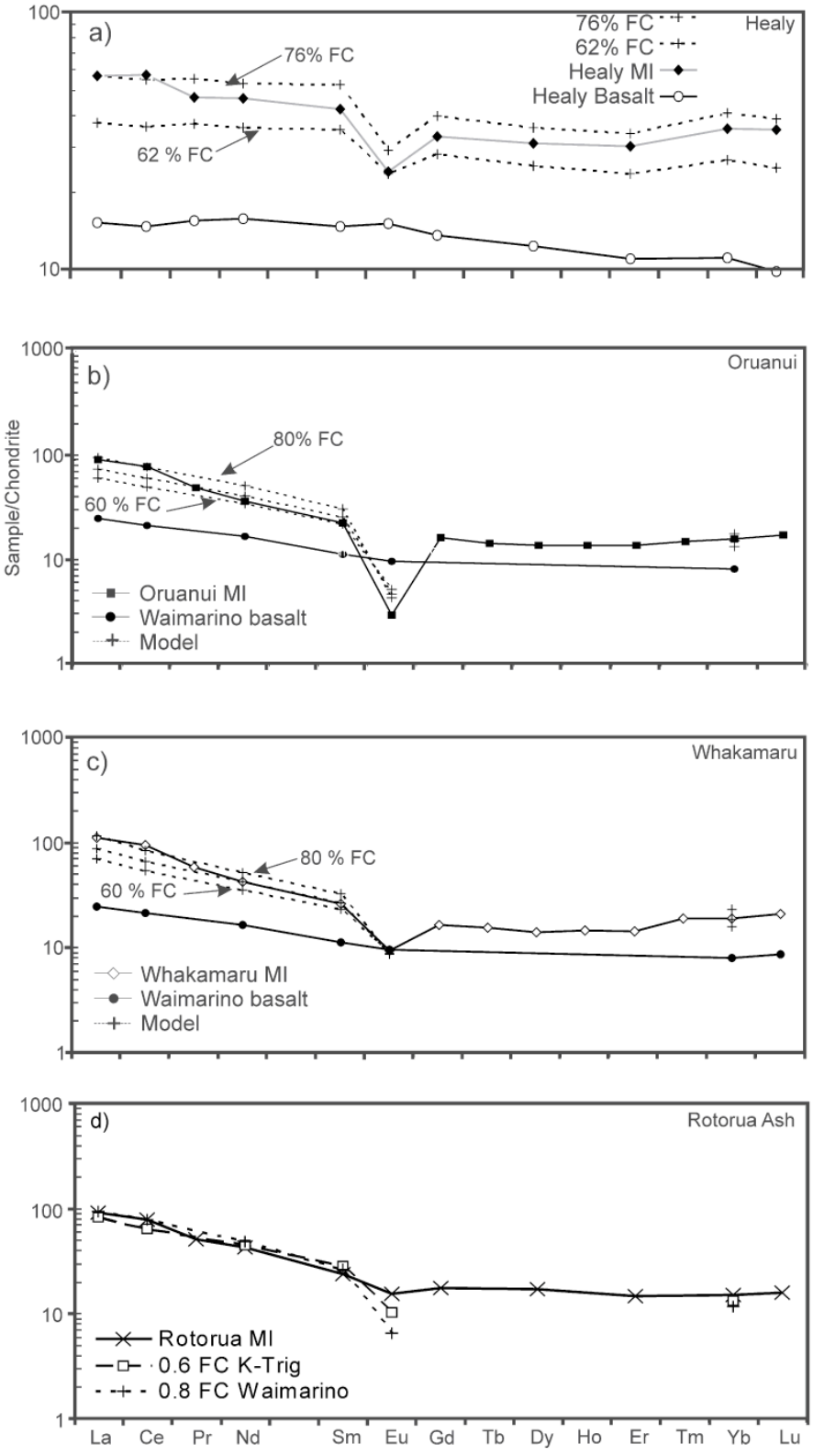

Figure 2.10. Caption overleaf

Figure 2.10. (Figure overleaf) Chondrite-normalised rare earth element diagrams showing models for producing rhyolitic melt inclusion compositions from a basaltic melt. (a) Healy inclusions by perfect fractional crystallisation from Healy basalt. Proportions of crystallising phases are: 43.5% plagioclase, 29% clinopyroxene, 7.2% orthopyroxene, 7.2% magnetite, 7.2% olivine, 4.4% amphibole and 1.5% ilmenite. (b) Oruanui ignimbrite by AFC from a Waimarino basalt parent. Proportions of crystallising phases are: plagioclase 70%; orthopyroxene 7%; quartz 9%; ilmenite 4.5%; magnetite 4.5%; amphibole 4.5%; and apatite 0.5%. (c) Whakamaru ignimbrite by AFC from a Waimarino basalt parent. Proportions of crystallising phases are: plagioclase 23.8%; orthopyroxene 9.5%; quartz 28.5%; ilmenite 2.38%; magnetite 2.38%; K-feldspar 9.5%; amphibole 14.3%; and biotite 9.5%. (d) Rotorua eruption by AFC from a Waimarino basalt parent. Proportions of crystallising phases are: plagioclase 44%; orthopyroxene 15%; quartz 22%; ilmenite 4.1%; magnetite 4.1%; amphibole 6.5%; biotite 3%; and clinopyroxene 1.6%. Also shown is modelling from K-Trig basalt under the same conditions (see text for discussion). Healy basalt composition from Wright and Worthington (unpublished data), Waimarino and K-Trig basalts from Gamble et al. (1993).

2.5.3 Petrogenesis of silicic magma in the Taupo Volcanic Zone

The predominant country rock in the Taupo Volcanic Zone is greywacke of the Torlesse Supergroup and Waipapa Group (Reid, 1982). Greywacke xenoliths occur in Taupo Volcanic Zone ignimbrites (Brown et al., 1998b; Cole et al., 1998) and the widespread presence of basement greywacke is confirmed by magnetotelluric surveying (Heise et al., 2007) and geophysical modelling (e.g. Stratford and Stern, 2008). Numerous lithologies are present in the greywacke providing a range of possible sedimentary assimilants and partial melts (Reid, 1982).

Assimilation of Torlesse greywacke in Taupo Volcanic Zone magmas is evident even in the most primitive basaltic compositions (Kakuki and Waimarino Basalts: Gamble et al., 1990), resulting in enriched LREE relative to the HREE concentrations (Gamble et al., 1993). The contribution

of greywacke assimilation or partial melting to silicic magma petrogenesis in the Taupo Volcanic Zone has been suggested from radiogenic and stable isotopic studies. Rhyolites have Sr-Nd isotopic compositions (e.g. $^{87}Sr/^{86}Sr$ = 0.705236 – 0.705660) that are intermediate between basalt ($^{87}Sr/^{86}Sr$ = 0.703875 – 0.704364) and greywacke basement (mean $^{87}Sr/^{86}Sr$ = 0.71029) compositions (McCulloch et al., 1994; Graham et al., 1995), which are inconsistent with either a pure fractional crystallisation or greywacke partial melting model. Oxygen isotope studies further confirm that rhyolites (mean $\delta^{18}O$ ~ 8 ‰; Reid, 1982) cannot be attained through progressive fractional crystallisation from a basaltic parent ($\delta^{18}O$ ~ 6.5 ‰; Reid, 1982) without the assimilation of greywacke ($\delta^{18}O$ ~ 10 - 14 ‰; Reid, 1982) or through pure partial melting of Waipapa or Torlesse greywacke (Reid, 1982; McCulloch et al., 1994; Blattner et al., 1996; Macpherson et al., 1998), suggesting that a hybrid model is required.

Contamination of silicic magmas with basement greywacke can be tested through the simple binary mixing of a mean Healy melt inclusion composition, representing an uncontaminated rhyolite, and greywacke of the Torlesse Supergroup (Reid, 1982). Such models suggest that the concentrations of LILE and LREE increase and HREE decrease(s) with progressive addition of greywacke with only 10-20% greywacke required to obtain similar REE concentrations to measured REE in Taupo melt inclusions. Barium concentrations also decrease relative to LILE, resulting in negative Ba anomalies. A positive Ba anomaly, which has been attributed to a slab fluid component in Kermadec arc lavas (Wysoczanski et al., 2006),

is observed in rhyolitic glasses of the Brothers seamount and is a feature of basalts from the Kermadec arc and Taupo Volcanic Zone (Gamble et al., 1993; Haase et al., 2006; Wysoczanski et al., 2006). The positive Ba anomaly of Taupo Volcanic Zone basalts (Gamble et al., 1993) indicates that the mechanism responsible for the negative Ba anomalies observed in the Taupo Volcanic Zone rhyolitic magmas is most likely a crustal process as it occurred after the formation of the basaltic magma, but prior to eruption of the rhyolitic magma. This process could occur through either assimilation of greywacke or magma mixing with greywacke partial melts.

Assimilation and fractional crystallisation (AFC) modelling of Taupo Volcanic Zone rhyolitic inclusions, applying the equations of DePaolo (1981) and using the observed crystal assemblages (Table 2.6) and distribution coefficients listed in Table 2.7, demonstrates that REE compositions of Whakamaru and Oruanui ignimbrites can be attained by AFC processes from a basaltic parental magma, with Torlesse greywacke (Reid, 1982; 1983) as the assimilant (Figure 2.10b; 2.10c). The ratio of assimilant to melt fraction (r) is 0.2, which is consistent with isotopic modelling of Graham et al. (1992) and Price et al. (2007). Modelling of Waimarino basalt as the starting composition produces a good fit for the Whakamaru melt inclusion compositions with 70-80% fractional crystallisation (Figure 2.10b; 2.10c), and the proportion of phases required to be fractionated (Table 2.6) changes slightly if Kakuki basalt is used as the parental magma.

Oruanui melt inclusion compositions are also better modelled when the Waimarino basalt is used as the parental magma, requiring 70 - 80% fractional crystallisation. Compositions of mafic clasts entrained within the Oruanui ignimbrite (Wilson et al., 2006) produced poor fits for AFC modelling, providing further evidence that these mafic magmas were

Eruption	plag	opx	qtz	ilm	mag	amp	bt	k-feld	cpx	ap
Whakamaru										
Waimarino	23.8	9.5	28.5	2.4	2.4	14.4	9.5	9.5		
Kakuki	24	17.3	20.6	1.7	1.7	20.7	7	7		
Oruanui [1]	70	7	9	4.5	4.5	4.5				0.5
Taupo	62.5	25		6.3	6.2					
Rotorua Ash [2]	44	15	22	4.1	4.1	6.5	3		1.6	

Table 2.6. Crystal assemblages recalculated to 100% for use with fractional crystallisation models. Additional data are: [1] Wilson et al. (2006); and [2] Smith et al. (2004), assuming T1 assemblage. Abbreviations used are: plag = plagioclase; opx = orthopyroxene; qtz = quartz; ilm = ilmenite; mag = magnetite; amp = amphibole; bt = biotite; k-feld = k-feldspar; cpx = clinopyroxene; and ap = apatite.

injected into the magma body at a later stage in the evolution of the magma and did not play a significant role in genesis of the magma, although they may have been important in triggering the eruption (Wilson et al., 2006). Similar AFC models can be calculated for Rotorua and Taupo melt inclusions producing comparable results indicating that 70 - 80% fractional crystallisation is required for the generation of rhyolitic melt. However, modelling using a more evolved Taupo Volcanic Zone basalt such as K-Trig (Gamble et al., 1993) as the parental magma produces a better fit for Rotorua and Taupo melt inclusions after 60% fractional crystallisation and better reproduces the Eu concentrations (Figure 2.10d).

Progressive AFC of basaltic magma alone cannot, however, explain the observed chemical variation of melt inclusions from within individual suites. Furthermore, Rb/Sr ratios of Whakamaru, Oruanui and Rotorua melt inclusions are more enriched than whole rock pumice Rb/Sr ratios from the same eruption (Figure 2.9). This suggests that the magma from which the crystals fractionated was more evolved than the magma in which they were erupted, as previously noted for Oruanui melt inclusion compositions (Liu et al., 2006; Wilson et al., 2006).

Rhyolite	Oruanui		Healy		Literature					
	plag	opx	plag	opx	amp	ilm	mag	K-feld	bt	ap
La	0.17	0.01	0.29	0.002	0.36	7.1	0.66	0.1	2	8
Ce	0.12	0.03	0.20	0.01	0.68	7.8	0.71	0.06	2.82	16.6
Pr	0.11	0.02	0.16	0.03						
Nd	0.06	0.02	0.11	0.02	1.6	7.6	0.93	0.04	2	21
Sm	0.14	0.13	0.15	0.09	2.3	6.9	1.2	0.04	1.4	20.7
Eu	2.46	0.14	2.28	0.09	3.2	2.5	0.91	3.3	0.85	14.5
Gd	0.15	0.16	0.17	0.14						
Dy	0.09	0.28	0.05	0.19	4.92	4.9	2.4	0.9	0.76	16.9
Er	0.15	0.57	0.09	0.55	7.28					
Yb	0.4	1.01	0.13	0.98	1.8	4.1	0.44	0.03	0.6	9.4
Lu	0.54	1.19	0.00	0.78	1.8	3.6	0.3	0.02	0.6	7.9

Table 2.7. Rare earth element distribution coefficients for rhyolitic magmas used in the modelling of the trace element concentrations of Taupo Volcanic Zone melt inclusions. Plagioclase and orthopyroxene distribution coefficients from the Oruanui and Healy samples are determined from this study. Additional sources: Mysen and Virgo (1980); Watson and Green (1981); Nash and Crecraft (1985); and Bacon and Druitt (1988).

Melt inclusion compositions for individual eruptions lie on a mixing line between a parental rhyolitic magma generated by the AFC model described above (hereafter termed 'rhyolitic melt fraction') and a greywacke partial melt. This can be modelled using a greywacke partial melt calculated using

the greywacke melting model of Reid (1982, 1983), and the least evolved melt inclusion composition as the parental composition.

Whakamaru melt inclusion trends (Figure 2.11) can be obtained by mixing of the end-member rhyolitic melt fraction generated by AFC processes and

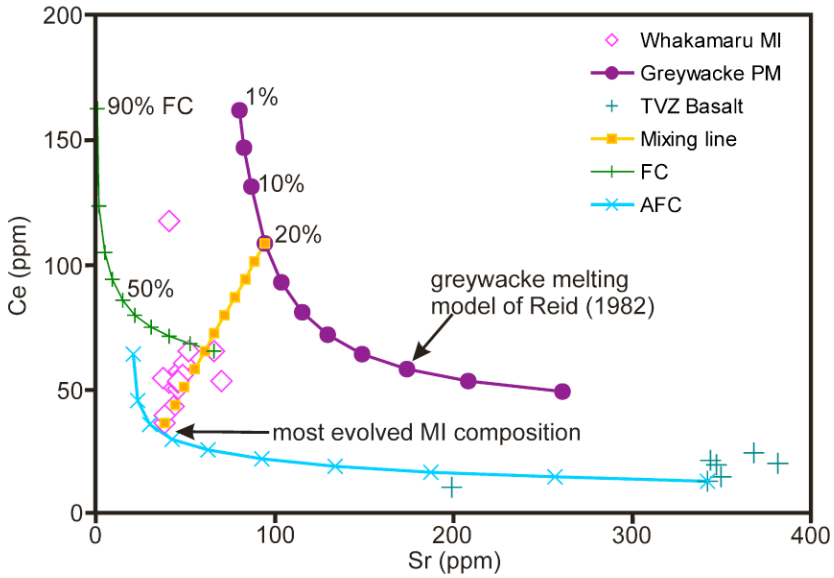

Figure 2.11. Sr versus Ce trace element diagram showing a magma mixing model to produce Whakamaru melt inclusion variation. Mixing of between 10 and 50 % of a 20% greywacke partial melt with an evolved rhyolitic melt explains the observed trace element trends (see text for discussion). Compositions of greywacke melts were calculated using the Shaw equation and a Torlesse greywacke composition (Reid, 1982) and perfect fractional crystallisation modelling of melt inclusions was conducted using the observed crystal assemblages (Table 2.6) and distribution coefficients from the literature (Table 2.7).

a 20% greywacke partial melt. The proportion of partial melt required ranges from 10% for the most evolved rhyolitic composition (highest Rb/Sr) to 50% for the least evolved composition (Figure 2.11). Similar mixing trends can be obtained for the Oruanui melt inclusions, with up to 70% of a 50% greywacke partial melt required to be added to the rhyolitic melt

fraction for the most extreme melt inclusion compositions, but the majority of melt inclusions require mixing with only 30-40% greywacke melts. Rotorua and Taupo melt inclusions show only a minimal contribution from greywacke partial melts.

2.5.4 Silicic magma generation model for the Taupo Volcanic Zone

Taupo Volcanic Zone silicic magmas are envisaged here to form through a two-stage process of fractional crystallisation from a basaltic parental magma (≥ 80%) with coupled assimilation (20%) of greywacke country rock, followed by mixing with up to 40% greywacke partial melt(s) prior to eruption. Any model for silicic magma petrogenesis must provide a mechanism for these processes to occur, for the predominance of silicic magma generation over other compositions, and account for more evolved compositions being the most crystal poor.

Large scale silicic magma bodies evolve over a significant period of time, as evidenced by the > 40 ka life span of the Oruanui magma (Charlier et al., 2005; Wilson et al., 2006). This allows multiple processes to occur, including AFC, mixing with partial melts of greywacke, and allowing crystal mush zones to develop from which evolved melts are ultimately extracted. Crystal mush zones are bodies of semi-solidified magmas consisting of a 'rigid' framework of 40 - 50% interlocking crystals that allow percolation of melts through the crystal network and accumulation of less dense melt above the mush zone (Bachman and Bergantz, 2004, 2008). The framework nature of the crystal mush zone prohibits the migration of

large proportions of crystals into the upper crustal magma chamber; instead only small (e.g. zircon) and semi-formed crystals are entrained (Bachman and Bergantz, 2004). This process could explain the crystal-poor nature of many silicic eruptives in the Taupo Volcanic Zone and other arcs worldwide, such as the Izu-Bonin arc (Shukuno et al., 2006; Wysoczanski and Tani, 2006). The more crystal rich eruptions (e.g. Whakamaru) may have resulted from a longer residence time in secondary magma chambers where crystal fractionation continued, but without sufficient time for a crystal mush zone to develop.

Geophysical data indicate the presence of solidified/semi-solidified magma bodies at 10-25 km depth beneath known caldera structures in the Taupo Volcanic Zone interpreted to represent crystal mush bodies and partial melts (Heise et al., 2007). Static crystal mush resident in the crust cools more slowly than crystal poor magma (Bachmann and Bergantz, 2004) providing a long term heat source, maintaining the elevated heat flow observed in the Taupo Volcanic Zone (Stern, 1987) and promoting the melting of greywacke country rock. Partial melting of greywacke provides space in the crust to accommodate upper crustal magma chambers and allows mixing of individual melt batches within the crust.

Crystal mush can also be mobilised and erupted to produce andesitic bulk rock compositions, as may be the case for Taupo Volcanic Zone andesites, which have intense disequilibrium textures between the crystal cargo and the rhyolitic groundmass (Gamble et al., 1990; Gamble et al., 2003; Price et

al., 2005). It should be noted that Taupo melt inclusion compositions overlap with Ruapehu groundmass glass (Price et al., 2005) and both overlap with Torlesse greywacke (Figure 2.12). Applying the same AFC model used previously, Taupo ignimbrite melt inclusions can be modelled from 0 - 50% fractional crystallisation of Ruapehu groundmass glass (Figure 2.12), providing evidence for a strong petrogenetic link between Taupo Volcanic Zone silicic magmas and andesites.

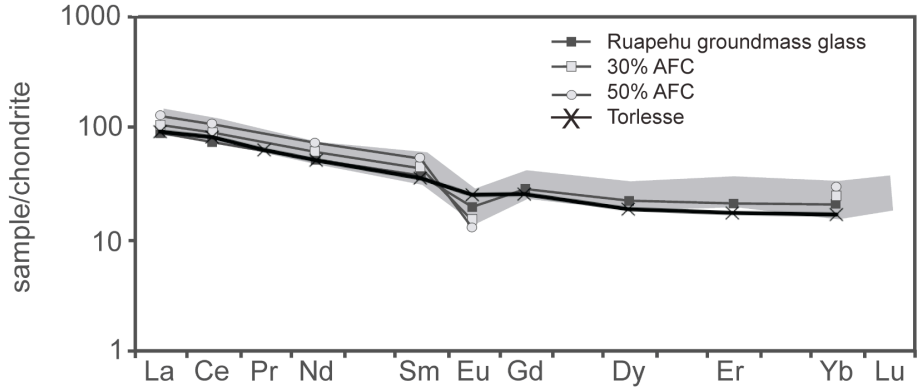

Figure 2.12. Chondrite-normalised rare earth element diagram for 30% and 50% AFC modelling to obtain the Taupo Ignimbrite melt inclusion composition using Ruapehu groundmass glass (Price et al., 2005) as the parental composition and assimilating Torlesse greywacke (Reid, 1982). Shaded region represents the range of Taupo Ignimbrite melt inclusion compositions. Proportions of crystallising phases are: plagioclase 62%; orthopyroxene 25%; ilmenite 6.5%; and magnetite 6.5%.

If these crystal rich magmas of andesitic composition with rhyolitic groundmass (e.g. Price et al., 2005; Humphreys et al., 2006) continued to fractionate, the rhyolitic upper part of the crystal mush zone would co-exist with more highly evolved interstitial liquids (high Rb/Sr ratios). Crystals that form in this part of the crystal mush would entrap melt inclusions with a highly evolved rhyolitic composition that would subsequently be entrained

and transported into a secondary upper crustal magma chamber where the magma could mix with greywacke partial melts (lower Rb/Sr ratios). This mechanism would also account for melt inclusions having more evolved Rb/Sr ratios than pumice from the same eruptions, as observed in Taupo Volcanic Zone silicic deposits.

2.6. Conclusions

A combination of new melt inclusion major and trace element data and previously reported data for eruptives from the Taupo Volcanic Zone and Kermadec arc allow the following conclusions to be made on silicic magma genesis in continental and oceanic arcs:

1. The generation of silicic magmas from the oceanic Healy Volcano can be modelled by (62-76%) fractional crystallisation of a basaltic parental melt.
2. In contrast, quantitative modelling of REE concentrations of Taupo Volcanic Zone melt inclusions indicates a two-stage magma petrogenetic model. Basaltic melts undergo extreme fractionation and assimilation of greywacke country rock at depth (10-25 km) to form crystal mush zones and rhyolitic magmas. The magma separates from the crystal mush to migrate to secondary magma chambers, where little or no fractionation occurs. Here the magma mixes with varying proportions (10-70%) of greywacke partial melt(s) prior to eruption. The result is a crystal-poor silicic magma with melt inclusion compositions

that represent the fractionated rhyolitic melts formed in a mush zone, and whole rock pumice compositions that are a mix of the fractionated melt and greywacke partial melt.

3. The addition of greywacke partial melt provides the volume of material required to feed the large-volume eruptions typical of the last 1.6 Ma of the Taupo Volcanic Zone and to create the larger volume eruptions than those observed in the southern Kermadec Arc where no continental lithosphere is present.
4. The range in parental mafic magma compositions, varying ratios of greywacke assimilant, proportions of fractionation and of phases crystallised, and the degree of mixing of magmas and greywacke partial melts has the ability to produce the entire spectrum of silicic volcanism observed in the Taupo Volcanic Zone. This suggests that pure crustal anatexis does not play a significant part in the generation of large-scale silicic volcanism in continental arcs.

Chapter 3

The speciation and degassing of water in rhyolitic melt inclusions: case studies from the Taupo Volcanic Zone, New Zealand.

Abstract

Water speciation and concentration data have been determined for melt inclusions in crystals from rhyolitic magmas erupted from the Taupo Volcanic Zone, New Zealand. Quartz and plagioclase hosted rhyolitic melt inclusions from the Whakamaru and Taupo ignimbrites, respectively, were analysed for water and carbon dioxide by Fourier transform infrared spectroscopy. Total measured water concentrations range between 1.4-4.4 wt% for Whakamaru and 1.9-5.1 wt% for Taupo melt inclusions, respectively. The melt inclusions have molecular water to hydroxyl concentrations that are inconsistent with the speciation models determined for groundmass rhyolitic glasses. This is interpreted as evidence for a secondary process that alters the water speciation of rhyolitic melt inclusions, but not groundmass glasses. Spectroscopic Fourier transform infrared imaging shows the inclusions are not ruptured during eruption and could provide evidence to indicate water is degassed from inclusions through the crystalline diffusion of hydroxyl groups prior to quenching. This results in a significant underestimation of the partial pressure of water of melt inclusions and thus the inferred depths of the crystallising magma bodies. Revised depths of the crystallising magma bodies based on maximum initial magmatic water concentrations of ca. 8.3 and 8.4 wt% derived from plagioclase-melt equilibria reconciles geochemical and geophysical evidence that indicate such magmas reside at depths > 6 km.

3.1 Introduction

Continental silicic arc margins, specifically those surrounding the Pacific Rim, have been the major source of explosive eruptions in the last 2 Myr (Lowenstern, 2006), particularly the hyper-productive Taupo Volcanic Zone of New Zealand. It is the volatile content of these magmas that causes their explosivity and the resulting eruption dynamics. Water is the dominant volatile species in rhyolites and fundamental in the magma generation, influencing the magmatic viscosity, density and composition (e.g. Tuttle and Bowen, 1958; Shaw, 1972; Ochs and Lange, 1997). On eruption volatile species are degassed into the atmosphere erasing any evidence of the initial magmatic water concentrations (e.g. Delaney et al., 1978; Gerlach, 1986; Dixon et al., 1995; Newman and Lowenstern, 2002). An exception may occur in the form of melt inclusions that remain pressurised during eruption, potentially preserving a record of the magmatic water concentration (e.g. Sobolev and Chaussidon, 1996; Wallace, 2005). With the advances in microbeam techniques in the last few decades, melt inclusions as small as 20-30 μm can now be characterised for elemental and volatile concentrations (e.g. Bacon et al., 1992; Barclay et al., 1996, 1998; Sobolev and Chaussidon, 1996; Kamenetsky, 1996; Danyushevsky et al., 2002; Hauri et al., 2002; Liu et al., 2006; Nichols and Wysoczanski, 2007). The two most commonly utilised techniques for the characterisation of H_2O and CO_2 in melt inclusions are Fourier transform infrared (FTIR) spectroscopy and secondary ion mass spectrometry (SIMS). The advantage of FTIR spectroscopy is the ability to directly determine the speciation of volatiles, such as the proportion of molecular water (hereafter H_2O_m) and hydroxyl groups (hereafter, OH^-) in a sample. The speciation of water is significant as it controls the diffusion of water through

rhyolitic melts and hence dictates the magmatic behaviour and subsequent magmatic dynamics (Zhang et al., 1991).

A number of previous studies have focussed on the characterisation of H_2O_m and OH^- interaction and behaviour in groundmass rhyolitic glasses (e.g. Stolper, 1982; Silver et al., 1990; Zhang et al., 1991; Zhang, 1994; Zhang et al., 1995, 1997a, 2000; Behrens and Nowark, 1997; Ihinger et al., 1999). However, there has been little consideration on whether the behaviour of H_2O_m and OH^- in rhyolitic melt inclusions is consistent with that determined for groundmass glasses or whether the presence of a crystal host causes secondary effects on the final measured concentrations of H_2O_m and OH^- groups. This is significant as much of our knowledge of pre-eruptive magmatic water concentrations are achieved through melt inclusion studies and it is imperative to our understanding of volcanic processes to accurately constrain not only the total water concentrations (hereafter H_2O_t) but also the proportions of H_2O_m and OH^- in the melt prior to eruption (Zhang et al., 1997b).

Many large-volume silicic eruptions, including four of the youngest known supereruptions worldwide, have originated from the hyper-productive Taupo Volcanic Zone during the Quaternary (Wilson et al., in press). Here we examine the water speciation of 8 quartz-hosted melt inclusions from the ~ 330 ka Whakamaru ignimbrite, currently the largest supereruption recognised from the region with estimated volumes > 1500 km^3 (Wilson et al., in press), and 31 plagioclase- and orthopyroxene-hosted melt inclusions from the smaller volume (35 km^3) 1800 years BP Taupo eruption (Wilson and Walker, 1985). The

measured speciation of melt inclusions are compared to the hypothetical concentrations derived from experimental studies of water speciation in groundmass rhyolitic glasses. We show that there are significant discrepancies and discuss the possible reasons for these, and the implications that this has for our understanding of rhyolitic magma chambers and the depth of the crystallising magma body.

3.2 Water speciation

Water occurs as two species in silicate melts, H_2O_m and OH^- groups, with the interaction of these species described by the following equilibrium reaction:

$$H_2O_m + O \Leftrightarrow 2OH^- \qquad [3.1]$$

where H_2O_m represents molecular water, O is an anhydrous oxygen and OH^- is a hydroxyl group bonded to a silicate polymer (Stolper, 1982). The corresponding equilibrium constant, K, is defined as;

$$K = \frac{[OH^-]^2}{[H_2O_m][OH^-]} \qquad [3.2]$$

where brackets indicate activities and can be approximated by mole fractions on a single oxygen basis (Stolper, 1982; Zhang et al., 1991; Zhang, 1999). At low total water concentrations (H_2O_t) contents, water is predominantly dissolved as OH^-, whereas at higher H_2O_t contents, H_2O_m becomes dominant (Stolper, 1982; Silver et al., 1990). The concentration at which H_2O_m becomes the principal water species varies with bulk composition and cooling rate (Stolper, 1982; Silver et al., 1990; Zhang, 1999; Zhang et al., 1995, 1997a, 2000; Wallace, 2003). As the cooling reaction is a continuous process, the rate of the reaction decreases with decreasing temperature and equilibrium between H_2O_m and OH^-

is not always attained prior to quenching (Zhang et al., 1995, 1997a, 2000; 2007 Zhang, 1999). Instead Q, (K at some temperature: Zhang et al., 1991) is substituted for K (Equation 3.2) when reactions do not attain equilibrium (Zhang et al., 1991). This temperature is defined as the apparent equilibrium temperature (T_{ae}) of the reaction recorded by the measured water speciation of glasses and does not represent the magmatic temperature (Zhang et al., 1991; Zhang, 1994; Ihinger et al., 1999).

Experimental studies have demonstrated that H_2O_m is the primary diffusing water species at low temperatures (400-500°C) and OH^- groups may be produced as a result of the reaction of the diffusing H_2O_m and the silicate structure (Stolper, 1982; Zhang et al., 1991; 2000). The rate at which water diffuses through a melt is critical as: (1) it controls the formation of bubbles during degassing, thus influencing the subsequent eruption dynamics; and (2) at low temperatures it governs the availability of water for hydration reactions (Zhang et al., 1991).

3.3 Samples and methods

The Whakamaru supereruption deposited four ignimbrite sheets (Brown et al., 1998). The most voluminous is the Whakamaru ignimbrite possessing a mineral assemblage of quartz, plagioclase, orthopyroxene, amphibole, ilmenite, magnetite, K-feldspar and biotite (Brown et al., 1998; Chapter 2). Importantly, large (> 50 μm) melt inclusions are present in quartz crystals. These inclusions are green to brown in colour and frequently host numerous micro-phenocrysts. Water analyses were conducted on non-homogenised melt inclusions (inclusions that have not been homogenised prior to analysis to create inclusions composed

of 100% glass) composed of > 90 % glass sampled from the discontinuous crystal lag layer at the base of the ignimbrite.

One of the largest rhyolitic eruptions in historic times from the Taupo Volcanic Zone is the 1800 years BP Taupo eruption (Wilson and Walker, 1985). Samples were taken from the youngest and most voluminous unit, the Taupo ignimbrite, (sample TA2) and associated crystal lag layer (sample TA1). The mineral assemblage consists of plagioclase, orthopyroxene, and Fe-Ti oxides with both plagioclase- and orthopyroxene-hosted melt inclusions analysed for volatile concentrations. Melt inclusions are brown in colour and often include a small vapour bubble.

Whakamaru and Taupo melt inclusions are of rhyolitic composition (Table 3.1) (Chapter 2). Speciation curves are calculated throughout this study using the regular solution model of Ihinger et al. (1999), as experimental studies have shown these models described the experimental data more adequately at high H_2O_t (> 2.5 wt%) than an ideal solution model (Ihinger et al., 1999). A mean molecular weight of anhydrous melt inclusions on a single oxygen basis (Silver et al., 1990) of 31.81 g/mol was calculated from melt inclusion compositions.

Full details of sample preparation are given in Chapter 2 with only those specific to FTIR spectroscopy analyses described here. Crystals were adhered to a glass slide using crystal bond cement and polished with 600, 2400 and 4000 SiC grit paper to expose the melt inclusion. The resulting crystal wafer was then turned

and the opposite side of the inclusion polished to create a doubly exposed inclusion.

(wt%)	Whakamaru	Taupo
SiO_2	76.56	75.96
TiO_2	0.15	0.29
Al_2O_3	13.1	13.5
FeO	0.51	2.17
MnO	0.10	0.19
MgO	0.05	0.30
CaO	0.67	1.55
Na_2O	3.24	3.28
K_2O	5.20	2.38
Cl	0.38	0.30
SO_3	0.04	0.05
Total	100.00	100.00

Table 3.1. Mean anhydrous major element composition of Whakamaru and Taupo melt inclusions.

Water analyses were conducted by FTIR spectroscopy at IFREE, Japan Agency for Marine-Earth Science and Technology (JAMSTEC), Japan. Analytical sessions were conducted over a period of approximately two years. Both conventional FTIR and spectroscopic imaging FTIR analyses of melt inclusions were conducted on a Varian FTS Stingray 7000 spectrometer with a KBr beamsplitter following the method of Wysoczanski and Tani (2006). The aperture ranged between 10-30 μm square with the majority of analyses conducted at 20 μm square. The concentrations of water species in melt inclusions were calculated by a modified Beer-Lambert law (Newman et al., 1986; Ihinger et al., 1994).

Total water concentrations were determined using the height above background of the overtone of the bending vibration of the H_2O_m group at 5200 cm^{-1} and molar absorptivity of 1.86 l mol^{-1} cm and OH^- concentrations were calculated using the overtone of the stretching and bending of Si-OH^- groups at 4500 cm^{-1} and molar absorptivity of 1.5 l mol^{-1} cm (Ihinger et al., 1994). Total H_2O was calculated summing the H_2O_m concentration from the peak at 5200 cm^{-1} and OH^- concentration from the peak at 4500 cm^{-1}. When the absorbance was low, the fundamental OH^- stretching vibration at 3535 cm^{-1} and molar absorptivity of 90 ± 2 l mol^{-1} cm (Hauri et al., 2002) and the height of the HOH bending vibration at 1630 cm^{-1} and molar absorptivity of 56 ±2 l mol^{-1} cm (Newman et al., 1986) were used to calculate H_2O_t and H_2O_m contents, respectively. OH^- concentrations were calculated from the difference in H_2O_t (3535 cm^{-1}) and H_2O_m (1630 cm^{-1}). In each case peak heights were determined using a linear baseline; applying a flexicurve baseline produced results consistent with the linear baseline. The molecular CO_2 peaks at 2350 cm^{-1} and the carbonate doublet peaks of CO_3^{2-} at 1515 cm^{-1} and 1435 cm^{-1} were analysed (Fine and Stolper, 1985; Ihinger et al., 1994), but were found to be below detection limits. Glass densities were calculated using the method of R. Lange described by Luhr (2001) from electron microprobe analyses of melt inclusion compositions (Chapter 2). These ranged between 2303 g/l and 2361 g/l and a value of 2350 g/l was used for all Beer-Lambert law calculations, which equates to a maximum of 0.06 wt% error on the calculated water concentrations. Sample thicknesses of doubly exposed inclusions were determined at the analytical point using interference fringes on reflection spectra (Wysoczanski and Tani, 2006; Nichols and Wysoczanski, 2007). Thicknesses of melt inclusions suspected to retain a thin wafer of the host

crystal were determined by placing the crystals side-on in crystal bond on a glass slide and then examining them under the microscope. Uncertainties of calculated water concentrations are estimated to be 10 % (e.g. Wysoczanski and Tani, 2006).

3.4. Results

Water concentrations range from 1.43-4.43 wt% for the Whakamaru melt inclusions and 1.91-5.14 wt% for the Taupo melt inclusions (Table 3.2). Water concentrations of the Taupo inclusions show no variation between the two different samples TA1 and TA2 and overlap with water concentrations determined by Dunbar and Kyle (1993) using SIMS. CO_2 was not detected in any of the analysed melt inclusions. Detection limits for CO_2 were calculated for individual inclusions by taking the minimum possible detectable absorbance peak as 0.01 (ca. three times background) and the specific melt inclusion thickness. This resulted in average CO_2 detection limits of 36 ppm and 53 ppm for Whakamaru and Taupo melt inclusions respectively (Table 3.2).

Variations in the measured speciation of Whakamaru and Taupo melt inclusions are shown in Figure 3.1 and are evaluated against experimentally constrained speciation curves (Ihinger et al., 1999). Natural rhyolitic glasses exhibit measured speciation trends that run parallel to the experimentally determined speciation curves (Newman et al., 1988). However, the measured speciation of Whakamaru and Taupo melt inclusions do not form linear arrays but display a

Sample	Host	H_2O_m (wt%)	OH (wt%)	H_2O_t (wt%)	A5200 mm^{-1}	A4500 mm^{-1}	Thickness (μm)	CO_2 detection limits (ppm)
TA1_18-1.1	opx	2.27	0.30	2.57	0.547	0.063	32	54
TA1_18-1.1	opx	1.84	0.68	2.52	0.442	0.139	33	53
TA1_13	opx			2.16				
TA1_40	opx	1.80	0.00	1.80			31	56
TA1_41-1.1	opx	2.52	0.92	3.44	0.611	0.191	35	50
TA1_41-2.1	opx	2.88	0.87	3.75	0.719	0.185	27	64
TA1_41-3.1	opx	2.02	0.97	2.99	0.490	0.200	20	87
TA1_29-1.1	plag	2.92	1.14	4.06	0.705	0.236	59	29
TA1_29-2.1	plag	2.79	0.70	3.49	0.682	0.227	22	79
TA1_30-1.1	plag	3.32	0.00	3.32			35	50
TA1_43-1.1	plag	2.35	0.71	3.06	0.570	0.147	30	58
TA1_43-2.1	plag	1.92	0.72	2.64	0.465	0.150	40	43
TA1_43-3.1	plag	1.90	0.69	2.59	0.460	0.143	40	43
TA1_44-1.1	plag	2.08	0.23	2.31			39	45
TA1_44-2.1	plag	1.78	0.32	2.10			15	116
TA1_50.1	plag	2.12	1.26	3.38	0.514	0.246	50	35
TA1_51.1	plag	1.81	1.21	3.01	0.438	0.236	57	30
TA1_52.1	plag	3.51	1.63	5.14	0.852	0.318	30	58
TA1_53.1	plag	1.20	1.13	2.33	0.259	0.196	35	50
TA1_55.1	plag	1.83	0.58	2.42	0.443	0.115	117	15
TA1_61.1	plag	3.57	1.00	4.57	0.955	0.216	118	15
TA1_76.1	plag	2.90	1.61	4.50	0.703	0.314	95	18
TA1_77.1	plag	2.10	0.78	2.88	0.495	0.149	55	32
TA1a_8-1.1	plag	1.72	1.06	2.78	0.412	0.218	17	102
TA1a_8-2.1	plag	2.37	0.82	3.19			25	70
TA2_22-2.1	plag	3.45	0.32	3.77			64	27
TA2_22-3.1	plag	2.03	0.12	2.15			22	79
TA2_31-1.1	opx	3.08	0.00	3.08			30	58
TA2_31-2.1	opx	2.64	0.92	3.56	0.640	0.190	30	58
TA2_32-1.1	opx	3.16	1.86	5.02	0.766	0.386	35	50
TA2_32-2.1	opx	4.75	0.23	4.98			20	87
WH1_4-1.1	qtz	3.18	0.74	3.92	0.759	0.208	66	26
WH1_19-1.1	qtz	1.02	0.40	1.43	0.241	0.099	80	22
WH1_19-3.1	qtz	3.06	0.03	3.07			30	58
WH1_50-1	qtz	3.50	0.78	4.28	0.847	0.154	37	47
WH1_51-1	qtz	3.07	1.36	4.43	0.745	0.265	75	23
WH1_52-1	qtz	2.67	0.72	3.40	0.648	0.142	48	36
WH1_52-2	qtz	2.71	0.65	3.36	0.657	0.128	61	28
WH1_53-1	qtz	2.57	0.89	3.46	0.623	0.174	38	46

Table 3.2. Measured speciation of melt inclusions from the Taupo eruption (TA1 – crystal lag; TA2 – Taupo ignimbrite) and Whakamaru ignimbrite (WH1). Water concentrations are calculated using the Beer-Lambert law as discussed in the text from the 5200 cm^{-1} and 4500 cm^{-1} peaks where shown and using the 3500 cm^{-1} and 1630 cm^{-1} for all others. See text for calculation of CO_2 detection limits. Abbreviations: H_2O_t = total water concentrations; A5200 = peak height at 5200 cm^{-1} per mm; A4500 = peak height at 4500 cm^{-1} per mm.

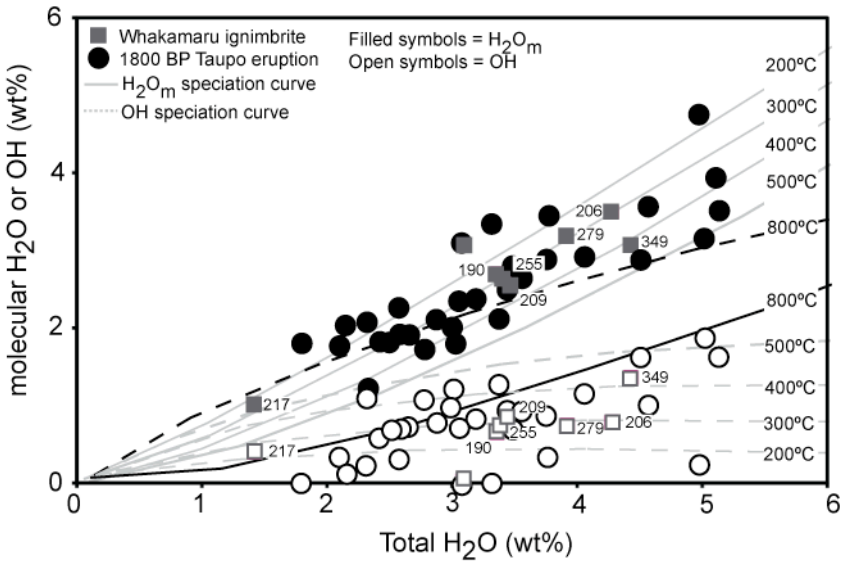

Figure 3.1. Measured water speciation of Whakamaru (squares) and Taupo (circles) melt inclusions. H_2O_m concentrations are shown by filled symbols and OH^- concentrations by open symbols. Speciation curves for H_2O_m (solid lines) and OH^- (dashed lines) are plotted for 200°C, 300°C, 400°C, 500°C (thin lines) and 800°C (thick line) using the regular solution model of Ihinger et al. (1999). T_{ae} of Whakamaru melt inclusions are shown calculated from the method of Ihinger et al. (1999).

range of speciation spread across a region corresponding to T_{ae} of ≤ 500°C with no systematic variation (Figure 3.1), consistent with heterogeneous cooling of individual inclusions. Application of the hydrous species geospeedometer (Zhang et al., 2000; Xu and Zhang, 2002) to the measured speciation results in only 28% of Whakamaru inclusions producing realistic cooling rates (e.g. WH1_51-1 = 0.001 years and WH1_4-1.1 = 1580 years) and 40% of Taupo inclusions indicate extremely slow and unrealistic cooling rates (e.g. TA1_41-1.1 = 57,000 years) (Table 3.3). Furthermore, T_{ae} of Whakamaru melt inclusions calculated directly from the measured absorbances of the 4500 cm^{-1} and 5200 cm^{-1} peaks of melt inclusions using the method described of Ihinger et al. (1999) (Table 3.3) are

Sample	T_{ae} (°C)	Q (K/s)	log q	Pressure (M Pa)	Depth (km)
TA1_18-1.1	101	cc		43.3	1.63
TA1_18-1.1	235	2.45E-21	-20.610	41.8	1.58
TA1_13				31.7	1.20
TA1_40				22.7	0.86
TA1_41-1.1	278	3.18E-10	-9.498	73.1	2.76
TA1_41-2.1	256	5.37E-13	-12.270	85.3	3.22
TA1_41-3.1	312	2.10E-07	-6.679	56.9	2.15
TA1_29-1.1	320	5.53E-05	-4.257	98.4	3.72
TA1_29-2.1	313	1.02E-05	-4.991	75	2.83
TA1_30-1.1				68.6	2.59
TA1_43-1.1	225	2.24E-30	-29.650	59.3	2.24
TA1_43-2.1	247	6.10E-18	-17.215	45.5	1.72
TA1_43-3.1	237	6.35E-21	-20.197	43.9	1.66
TA1_44-1.1				35.8	1.35
TA1_44-2.1				30.1	1.14
TA1_50.1	370	5.02E-03	-2.300	70.8	2.67
TA1_51.1	377	3.70E-03	-2.432	57.5	2.17
TA1_52.1	395	4.35E+00	0.638	148.9	5.62
TA1_53.1	386	3.20E-04	-3.495	36.3	1.37
TA1_55.1	198	cc		38.9	1.47
TA1_61.1	268	4.02E-08	-7.395	121.4	4.58
TA1_76.1	416	5.29E+00	0.724	118.1	4.46
TA1_77.1	239	5.93E-20	-19.227	53.2	2.01
TA1a_8-1.1	358	1.73E-04	-3.761	49.9	1.88
TA1a_8-2.1				63.9	2.41
TA2_22-2.1				86.2	3.25
TA2_22-3.1				31.4	1.19
TA2_31-1.1				60	2.27
TA2_31-2.1	272	7.49E-11	-10.126	77.7	2.93
TA2_32-1.1	490	7.92E+02	2.899	143	5.40
TA2_32-2.1				141.1	5.33
WH1_4-1.1	279	1.05E-08	-7.981	89.7	3.39
WH1_19-1.1	217	3.20E-24	-23.494	14	0.53
WH1_19-3.1				58.2	2.20
WH1_50-1	206	cc		105.2	3.97
WH1_51-1	349	1.01E-02	-1.996	111.9	4.22
WH1_52-1	209	cc		69.2	2.61
WH1_52-2	190	cc		67.8	2.56
WH1_53-1	255	1.67E-14	-13.778	71.5	2.70

Table 3.3. Calculated T_{ae} and cooling rates of Whakamaru and Taupo melt inclusions. T_{ae} is calculated from the method of Ihinger et al. (1999). Cooling rates (Q and log q) are calculated using the spreadsheet supplied from Xu and Zhang (2002). cc in the Q and log q columns indicate the supplied spreadsheet could not calculate a cooling rate. Pressures were calculated using VolatileCalc and magmatic temperatures of 760 °C and 780 °C for the Whakamaru and Taupo melt inclusions respectively. Depths are calculated assuming a bulk crustal density of 2700 Kg/m^3. Abbreviations: opx = orthopyroxene; plag = plagioclase; qtz = quartz.

inconsistent by ≥ 100 °C with the T_{ae} derived from the location of the same measured speciation in relation to the calculated speciation curves in Figure 3.1.

3.5. Discussion

The samples studied here were collected from a limited stratigraphic section for both eruptions. Consequently, the wide scatter in measured speciation and cooling rates are hard to reconcile without invoking a secondary process(es) that alters the H_2O_m/OH^- speciation of rhyolitic melt inclusions. Similar scatter has not been reported from natural rhyolitic groundmass glasses, but has been noted for a selection of quartz-hosted rhyolitic melt inclusions from the Bishop Tuff (Wallace et al., 2003). This modification of H_2O_m/OH^- could potentially have an impact on H_2O_t and our understanding on the role water plays within the melt, as many calculations (e.g. geospeedometry and saturation pressures) rely on the accurate measurement or determination of speciation from solution models (Zhang et al., 1997b; Zhang et al., 2000; Newman and Lowenstern, 2002; Xu and Zhang, 2002). Measured water speciation of rhyolitic melt inclusions are inconsistent with models that calculate the proportions of H_2O_m and OH^- from the measured H_2O_t water concentration of natural rhyolitic glasses, for example VolatileCalc (Figure 3.2). This could lead to erroneous saturation pressures, the extent of which is not discussed here.

3.5.1 Secondary alteration of water speciation in rhyolitic melt inclusions

Several possible mechanisms could alter the water speciation of rhyolitic melt inclusions from the original glass compositions, including those suggested by Wallace et al. (2003). These mechanisms are: (1) the formation of hydrous

mineral reservoirs within inclusions; (2) hydration of melt inclusions (Wallace et al., 2003); (3) the calibration method used for the calculation of water concentrations; (4) the time of sealing of melt inclusions; (5) rupturing and/or degassing of melt inclusions; and (6) diffusion of water in or out of inclusions.

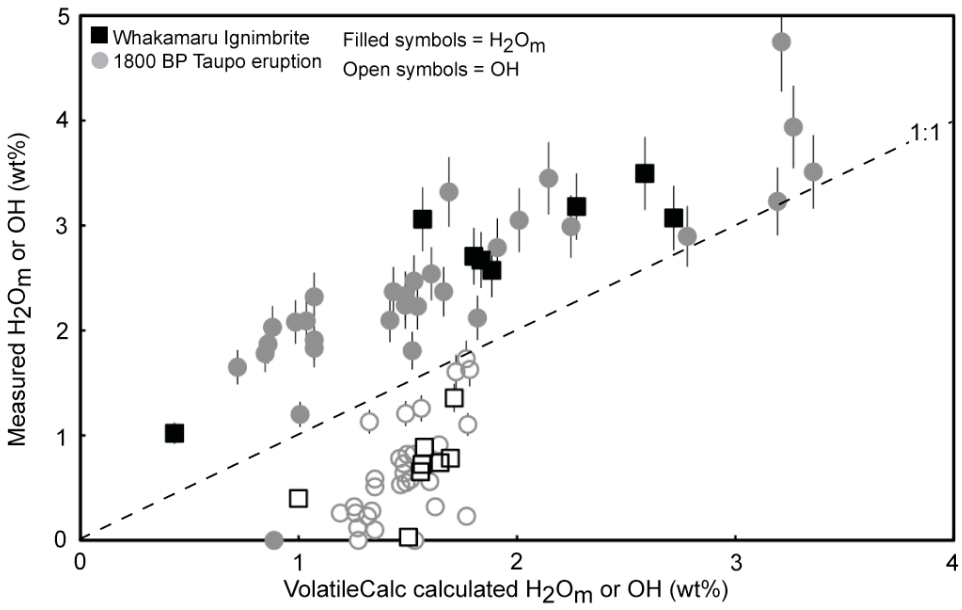

Figure 3.2. Comparison of measured H_2O_m and OH^- concentrations of Taupo melt inclusions (circles) and Whakamaru melt inclusions (squares) and those calculated from H_2O_t by VolatileCalc (Newman and Lowenstern, 2002) at a magmatic temperature 760 °C and 780 °C for the Whakamaru and Taupo magmas, respectively. Error bars of 10 % are shown on the measured water concentrations and the 1:1 line is shown (dashed line).

The discrepancy in measured water speciation of melt inclusions is observed in both Whakamaru melt inclusions that possess micro-crystals and Taupo melt inclusions that display no evidence of micro-crystals. This absence of micro-crystals in Taupo melt inclusions eliminates the formation of hydrous minerals reservoirs within inclusions as the primary mechanism for altering the water speciation of melt inclusions.

Hydration of melt inclusions post-eruption may have affected both Whakamaru and Taupo melt inclusions. This is characterised in groundmass basaltic and rhyolitic glasses by anomalously high H_2O_m concentrations at constant OH^- concentrations (Pandya et al., 1992; Yokoyama et al., 2007). Although hydration of melt inclusions could explain the relative elevated H_2O_m concentrations, it cannot account for the associated relative depletion in OH^- concentrations (Figure 3.1), precluding the hydration of melt inclusions as a possible mechanism for changing water speciation.

Two main calibration methods are used to calculate the water concentrations of glasses in FTIR spectroscopy: (1) Beer-Lambert calibration (Newman et al., 1986; Ihinger et al., 1994) and; (2) the Zhang et al. (1997b) calibration. The different methods could potentially affect the calculated proportions of H_2O_m and OH^-. Total H_2O, H_2O_m and OH^- concentrations of Taupo melt inclusions were calculated using both of these calibrations from the 5200 cm^{-1} and 4500 cm^{-1} peaks (Figure 3.3). Below 3 wt% the calculated concentrations agree well, but the agreement is not as good at higher total H_2O (Figure 3.3). This can be attributed to the uncertainty in the extrapolations of the calibration of Zhang et al. (1997b) to high total H_2O (> 2.7 wt%) (Zhang et al., 1997b; Zhang, 1999). Moreover, irrespective of the calibration used, the same scatter in measured water speciation of Taupo melt inclusions is observed (Figure 3.3), eliminating the calibration method as the source of the discrepancies in H_2O_m/OH^- ratios.

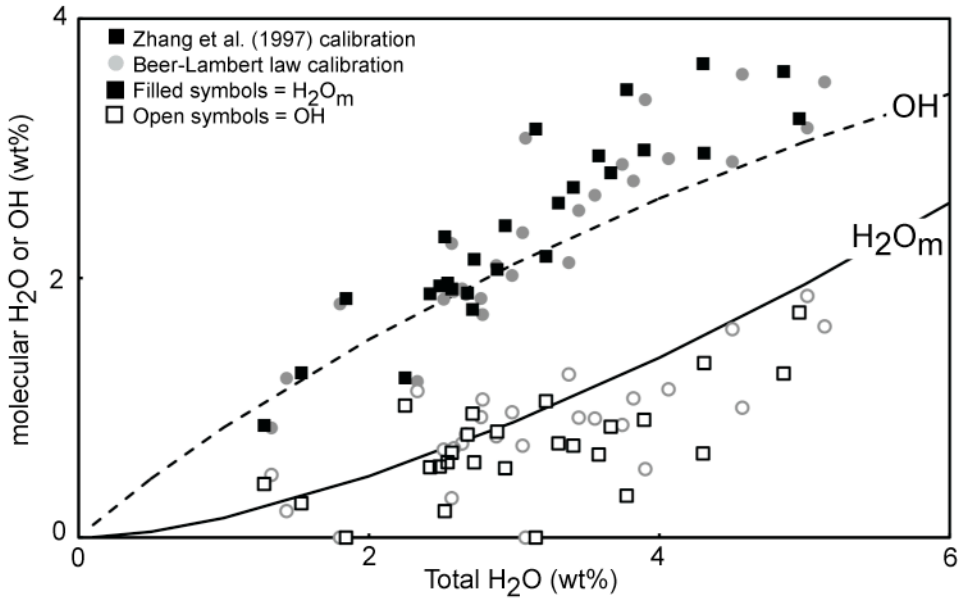

Figure 3.3 Measured speciation of Taupo melt inclusions using the Beer-Lambert law (circles) (Newman et al., 1986; Ihinger et al., 1994) and the Zhang et al. (1997a) (squares) calibration. H_2O_m are filled symbols and OH groups are open symbols. The speciation curve for 500°C is shown using the regular solution model of Ihinger et al. (1999).

Melt inclusions are not simultaneously isolated from the external magma and could potentially record changing magmatic conditions. However, the major element composition of Whakamaru and Taupo melt inclusions (Chapter 2) within individual eruptions are relatively homogeneous, indicating sealing from the external magma occurred at similar magmatic conditions. Therefore, such a wide range in measured water speciation is hard to reconcile, unless rapid degassing of the melt occurred as the inclusions became sealed and the quenching of inclusions ensued before sufficient time had occurred for the re-equilibrium of H_2O_m and OH^- of melt inclusions. The lower relative OH^- concentrations of melt inclusions compared to the modelled OH^- speciation curve would suggest that it was the OH^- groups that degassed from the melt first. This is inconsistent with the bonded nature of OH^- groups to the silicate network implying OH^- groups are the least mobile water species and H_2O_m would

preferentially degassed, contradictory to the observed water speciation of inclusions.

Previous studies have implied that the rupturing of inclusions prior to quenching has resulted in the recorded degassed signatures (e.g. Cervantes and Wallace, 2003; Wallace et al., 2003; Blundy and Cashman, 2005). Whakamaru and Taupo melt inclusions were examined for evidence of rupturing through spectroscopic FTIR imaging. This technique allows images of the water peak absorbance height (3550 cm^{-1}) to be obtained over an area of 350 μm^2 encompassing both the inclusion and surrounding crystal, allowing water species to be determined at 5 μm resolution (Wysoczanski and Tani, 2006). Consequently, the location of dissolved water within the sample can be identified. Ruptured melt inclusions form cracks that radiate out from the inclusion through which volatiles can be lost (e.g. Danyushevsky et al., 2002; Wallace, 2005). Although cracks are present in several of our samples they formed during sample preparation. Inclusions that were ruptured during eruption and not during sample preparation should display evidence of water along these cracks on FTIR images (Figure 3.4), though no evidence of this is observed in any of our FTIR images. Therefore, it is possible to conclude that the analysed melt inclusions from the Whakamaru and Taupo eruptions did not rupture during eruption. As none of the previously discussed mechanisms can adequately explain the observed water speciation of Whakamaru and Taupo melt inclusions, it is proposed that water is loss by diffusion through the crystal host altering the original H_2O_m/OH ratio of melt inclusions.

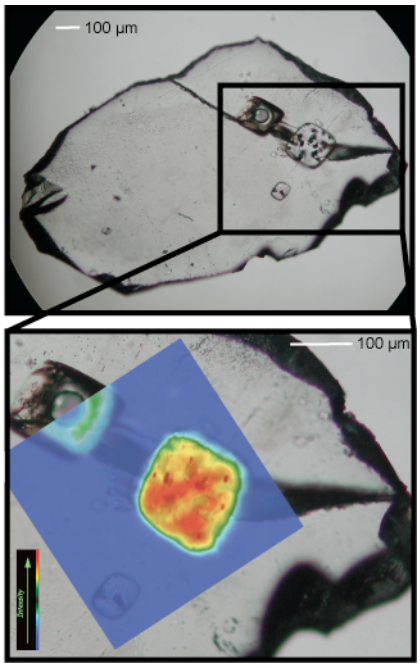

Figure 3.4. Representative spectroscopic image of a quartz crystal and hosted melt inclusions from the Whakamaru ignimbrite. Relative peak height for the 3535 cm^{-1} band is shown and is a proxy for total water concentrations. Colour intensity reflects the intensity of the peak and the thickness of the sample. Low peak heights (approximating low H_2O concentrations) are blue and high peak heights (high H_2O) are shown in red.

3.5.2 Water diffusion and degassing of rhyolitic melt inclusions

Experimental studies examining the diffusion of water from rhyolitic melt inclusions are limited, as the majority of research has focused on olivine-hosted inclusions in basaltic magmas (e.g. Danyushevsky et al., 2002; Hauri, 2002; Massare et al., 2002; Portnyagin et al., 2008). This has shown that small amounts of water (< 1 wt%) can be lost from olivine melt inclusions from the dissolution of water molecules and the diffusion of H_2 though the crystal host in extremely short timescales (e.g. hours) (Danyushevsky et al., 2002; Hauri, 2002). Diffusion of H_2 requires a gradient in fH_2 to be sustained but this only occurs if a reducing agent is present (Qin et al., 1992). As rhyolitic magmas contain relatively large

amounts of H_2O and low FeO_t concentrations this prevents significant reduction of H_2O to H_2 resulting in the negligible diffusion of H_2 in rhyolitic magmas (Qin et al., 1992). Consequently, this indicates that diffusion of H_2 cannot account for the large water losses or gains observed in the experiments of Massare et al. (2002) or of Portnyagin et al. (2008) on olivine-hosted melt inclusions and Severs et al. (2007) on quartz-hosted, melt inclusions. The study of Severs et al. (2007) demonstrated that water is lost from quartz-hosted rhyolitic melt inclusions from the Bishop Tuff after just 12-14 hours of heating, and after 63 days an average of only 25 % of the original water concentration remained. This indicates there is a mechanism that transports H_2O_m and/or OH^- between the melt inclusions and the external melt and it seems logical if water molecules can move in one direction, in favourable circumstances, the reverse process could occur increasing the water concentrations of melt inclusions. The addition of water to melt inclusions was observed in the experiments of Portnyagin et al. (2008) of olivine hosted melt inclusions indicating that this is the case. Consequently, it appears that rhyolitic melt inclusions preserve a record of the magmatic water conditions immediately prior to eruption but can provide little evidence for earlier magmatic water concentrations such as at the time the melt inclusion was sealed from the external melt.

FTIR spectroscopy studies have measured structural OH^- groups in quartz and orthopyroxene crystals but the presence of structural H_2O_m is ambiguous (Cordier and Doukhan, 1991; Dobson et al., 1995). Furthermore, OH^- is the only structural water species detected in volcanic plagioclase crystals (Johnson and Rossman, 2004; Johnson, 2006). Johnson (2003) measured the OH^- diffusion in

plagioclase crystals and showed that it occurred on a timescale of hours to weeks in a 1 mm size plagioclase at 800 – 900 °C with similar results reported for water diffusion in quartz crystals (Qin et al., 1992). These results suggests that H_2O_m may not be easily accommodated within the crystal structures, which would prohibit the diffusion of H_2O_m between the melt inclusion and the external melt without reacting to form OH^- groups.

It is therefore proposed that OH^- is the dominant diffusing species, transporting water between rhyolitic melt inclusions and the external melt after the sealing of inclusions. The water speciation of Whakamaru and Taupo melt inclusions may reflect the diffusion of OH^- groups out of inclusions and through the crystal host prior to quenching rather than through the rupturing of melt inclusions. The assorted crystal sizes and variation in the position of melt inclusions in the crystal alters the path length of the OH^- groups and could account for the variable range of H_2O_m and OH^- concentrations measured.

Evidence for degassing of melt inclusions can also be gained from the textural appearance of inclusions. The crystallisation of micro-crystals and the formation of shrinkage bubbles inside inclusions can result from the substantial diffusive loss of H_2O (Johnson et al., 2008) and not from slow cooling as previously attributed (e.g. Danyushevsky, et al., 2002; Wallace, 2005). The prevalent vapour bubbles observed in the Taupo melt inclusions and the micro-crystals in the Whakamaru melt inclusions are interpreted to reflect degassing and do not merely result from the slow cooling of inclusions. During crystallisation, latent heat is released to the surroundings, increasing the melt temperature (Blundy et

al., 2006). The crystallisation of micro-crystals in the Whakamaru melt inclusions could result in the heating of the entrapped melt, potentially explaining the observed deviations between calculated T_{ae} of inclusions and the modelled speciation curves that are not observed in the Taupo melt inclusions.

3.5.3 Initial water concentrations of melt inclusions

The extent of degassing cannot be established from FTIR spectroscopy analyses alone, but requires an estimate of the initial melt inclusion water concentration. One possible method to do this is through the application of plagioclase-melt thermometry. Two commonly utilised plagioclase thermometers are those of Housh and Luhr (1991) and Putrika (2005), which are also calibrated to calculate water contents of the melt in equilibrium with the plagioclase crystal. It is noted that neither of these thermometers are highly accurate when predicting water concentrations of natural melts (Putirka, 2005), although the Putirka model produced more realistic estimates of water concentrations compared to reported H_2O concentrations of hydrous experiments than the Housh and Luhr model (Putrika, 2005 their Figure 6). In addition, the thermometer of Housh and Luhr was calibrated for basaltic and andesitic compositions while the Putirka model was calibrated for basaltic to rhyolitic compositions, and is more suitable for this study.

Initial maximum magmatic water concentrations of Whakamaru and Taupo melt inclusions were tentatively estimated using the Putirka model from the major element composition of plagioclase crystals and mean groundmass glass compositions. Magmatic temperature was determined using the plagioclase-melt

equilibria and directly substituted back in to calculate the magmatic water concentrations. These results indicate mean magmatic water concentrations of 8.2 wt% and 8.4 wt % at the time the plagioclase crystals fractionated for the Whakamaru and Taupo magmas respectively (Table A3.5).

Blundy and Cashman (2005) illustrated that the chemical variation of melt inclusions (e.g. SiO_2 concentration) combined with the H_2O_t content can be used to discriminate between different crystallisation processes. Whakamaru and Taupo melt inclusions display a syn-eruptive degassing trend when the measured water concentrations are plotted against anhydrous SiO_2 concentrations (Chapter 2) of inclusions and the calculated initial water estimates (Figure 3.5, after Blundy and Cashman, 2005). Utilising more conservative initial water estimates of 4.4 wt% and 5.1 wt%, the maximum measured water concentrations of inclusions for the Whakamaru and Taupo inclusions respectively; a degassing trend is still observed (Figure 3.5). This suggests the degassing of inclusions was rapid (e.g. during eruption) with little or no contemporaneous crystallisation (Blundy and Cashman, 2005). Assuming these initial water estimates are realistic, a substantial amount of water has been degassed from the melt inclusion prior to quenching.

3.5.4 Geobarometry and crystallisation depths of magmas

One of the most common applications of measured water concentrations of rhyolitic melt inclusions is the application of geobarometry models and inferred depths of the crystallising magma body. If melt inclusions are degassed, the estimated pressures and depths will be underestimated and will only reflect the

magmatic conditions directly prior to eruption. The depths of earlier episodes of magmatic evolution, such as periods of residence within deeper crystal mush bodies (e.g. Whakamaru melt inclusions, Chapter 4), cannot be determined from the saturation pressures of melt inclusions.

The partial pressures of H_2O (pH_2O) of Whakamaru and Taupo melt inclusions (Table 3.3) have been calculated using VolatileCalc (Newman and Lowenstern, 2002) and a magmatic temperature of 760 °C and 780 °C for the Whakamaru and Taupo magmas respectively (Table A3.5). This results in pH_2O of 14 - 112 MPa for the Whakamaru melt inclusions and 22 - 149 MPa for the Taupo melt inclusions (Table 3.3). This constrains the minimum lithospheric depths of the crystallising magma body (assuming a crustal density of 2700 kg/m^3 from Ellis et al., 2007) to a mean depth of 2.7 km (0.5 - 4.2 km) for the Whakamaru magma and 2.6 km (0.9 - 5.6 km) for the Taupo magma (Figure 3.6). As CO_2 is below detection limit any estimates of partial pressures are only minimum estimates (e.g. Bacon et al., 1992) and do not take into account the partial pressures of other volatile species such as Cl and SO_3. Assuming that CO_2 concentrations of melt inclusions equates to the estimated detection limits (Table 3.2), this would increase the pressure estimates on average by 40 MPa and 90 MPa (equating to an additional 200 m and 300 m depth) for the Whakamaru and Taupo melt inclusions, respectively. However, increasing the CO_2 concentration to 100 ppm, the approximate average measured CO_2 concentrations of Oruanui melt inclusions (Liu et al. 2006) increases the inferred depths by ca. 1 km.

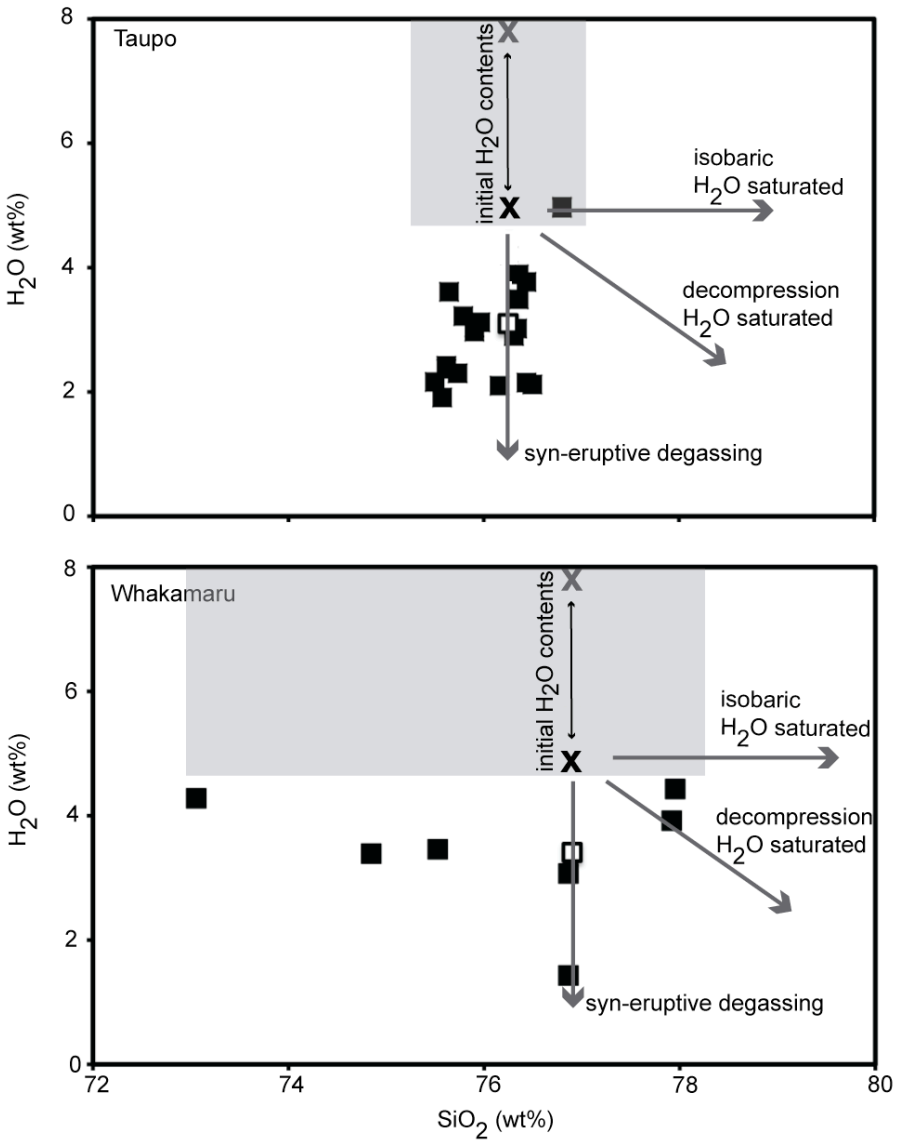

Figure 3.5. Syn-eruptive degassing of melt inclusions after Blundy and Cashman (2005). (a) Taupo melt inclusions and (b) Whakamaru melt inclusions. Grey shaded region indicates estimated initial water concentrations calculated from a combination plagioclase-melt thermometry (grey X) and the maximum measured water content of melt inclusions (black, X) as discussed in the text. White open squares denote the mean melt inclusion compositions.

The geochemically inferred depths of the crystallising Whakamaru and Taupo magma bodies are inconsistent with geophysical studies, which do not detect the presence of partial melt bodies above 6 km in the Taupo Volcanic Zone (e.g. Ogawa et al., 1999; Sherburn et al., 2003; Heise et al., 2007). A similar inconsistency is noted for the Oruanui eruption by Ellis et al. (2007). The

chemical composition of Whakamaru melt inclusions suggests inclusions are trapped and sealed at the top of a crystal mush body (Chapters 2 and 4). However, the calculated depths of melt inclusions indicate a mean depth of 2.7 km and a range of between 0.5 - 4.2 km. This range of calculated depths centred at 2.7 km depth would provide insufficient space in which to accommodate the volume of eruptible magma required to feed the Whakamaru eruption in the crust prior to eruption. Similar doubts are also raised for the geochemically inferred depths of the Taupo magma body, which would place the crystallising magma body in a layer of permeable volcanic infill generated by earlier eruptions (e.g. Ogawa et al., 1999; Sherburn et al., 2003; Heise et al., 2007). This would allow for the passive degassing of the magma prior to eruption, preventing the accumulation of sufficient volatiles to drive such an explosive eruption (Sparks, 2003).

However, if the estimated initial water concentrations predicted from plagioclase-melt equilibria and maximum measured water concentrations of melt inclusion are used to calculate the pH_2O of the crystallising magma body, the crustal depths of the crystallising magma bodies are estimated at 4.2-11.1 km for Whakamaru magma and 5.6-11.9 km for the Taupo magma. This is consistent with the depths estimated from geophysical studies (Figure 3.6) suggesting this is the location for the bulk of magma petrogenesis in the continental Taupo Volcanic Zone.

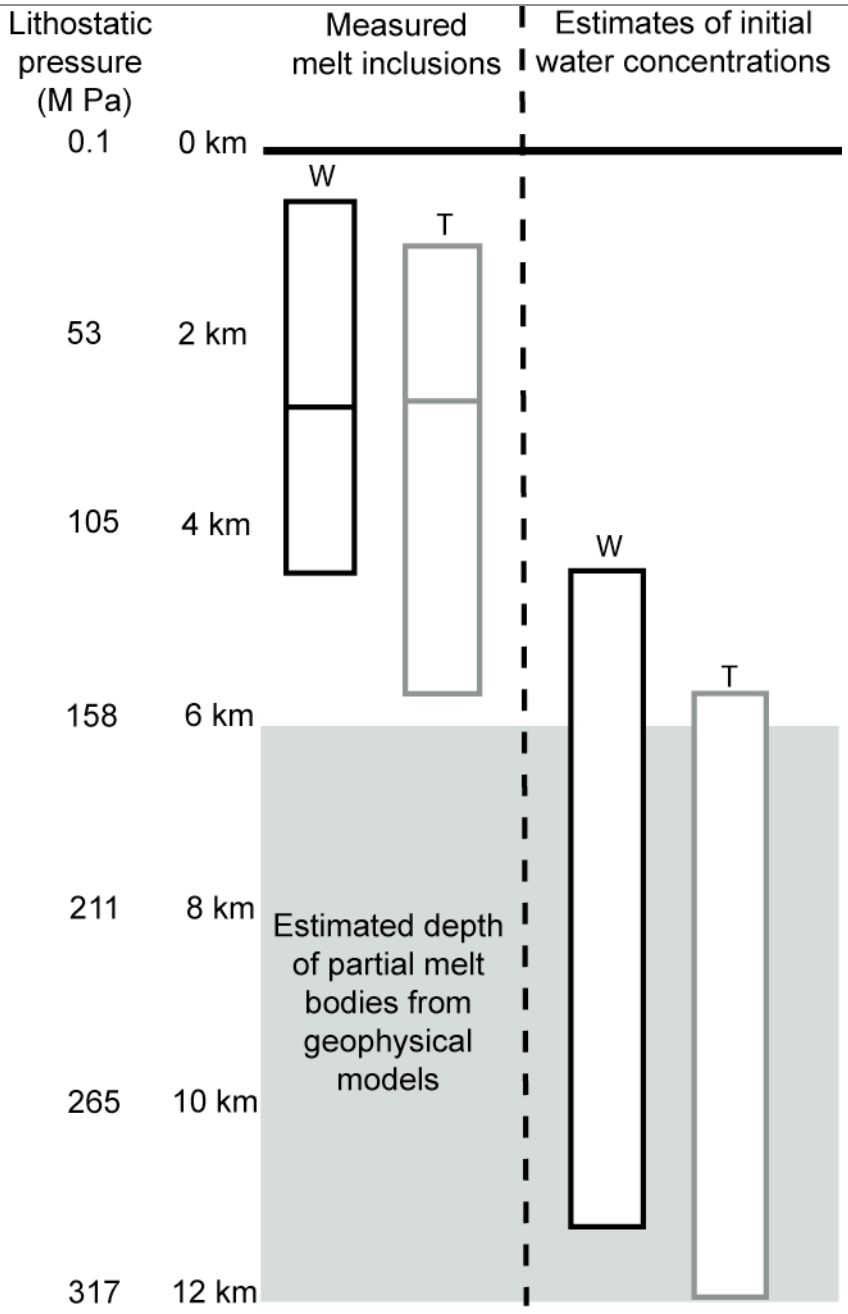

Figure 3.6. Comparison of pH_2O and inferred crustal depths to magma chamber from the measured water concentrations of Whakamaru (W) and Taupo (T) melt inclusions and initial water concentration estimates as discussed in the text. Depth of partial melt bodies estimated from geophysical studies are taken from Ogawa et al. (1999), Sherburn et al. (2003), Heise et al. (2007). The outline of the boxes indicates the range of observed or calculated concentrations. A horizontal line denotes the mean measured concentrations. A bulk crustal density of 2700 kg/m^3 is used to calculate the crustal depths.

3.6. Conclusions

Whakamaru and Taupo melt inclusions are unruptured yet degassed. The degassing occurs by the diffusion of OH^- groups out of the melt inclusion and through the crystal host. This process can be identified by measured H_2O_m and OH^- concentrations inconsistent with those predicted from experimental studies and results in an underestimation of calculated pH_2O of melt inclusions. Therefore any inferred crystallisation depths of magmas will represent the depth of the magma body immediately prior to eruption. This is not necessary where the bulk of the magma petrogenesis occurred. Tentative initial magmatic water concentrations estimated from plagioclase-melt equilibria, however, reconciles the differences in geochemical and geophysical studies. Further work is required to establish why some melt inclusions appear degassed and others do not and the mechanism(s) that permits degassing to occur.

The degassing of rhyolitic melt inclusions may not occur in all rhyolitic magmas. However, investigation of water speciation from the scientific literature indicates the wide scatter described from the Whakamaru and Taupo melt inclusions are present in other melt inclusions derived from silicic arc magmas (Lowenstern, 1993; Barclay et al., 1996; 1998). Degassing of unruptured rhyolitic arc melt inclusions may thus explain the lack of any obvious relationship between H_2O concentrations and melt compositions that are observed in intercontinental rhyolitic magmas (Wallace, 2005).

Chapter 4

The magmatic evolution of the Whakamaru supereruption constrained by microanalytical study of plagioclase and quartz.

Abstract

The Whakamaru eruption is the largest known eruption to have originated from the hyper-productive Taupo Volcanic Zone, New Zealand. Major, minor and trace element concentrations of plagioclase crystals and cathodoluminescence images allied with Ti concentrations of quartz crystals, have been used to determine the chemical zonation of these phases. Three plagioclase populations have been identified: Group 1 crystals with inherited cores of An_{45-60}, Ba (115 - 650 ppm) and La (3 - 9 ppm) and rims of ca. An_{30}, Ba (450 - 800 ppm) and La (7 - 10 ppm); Group 2 crystals are oscillatory zoned plagioclases of An_{30-40}, Ba (450 - 730 ppm) and La (8.5 - 9.5 ppm) and; rare Group 3 plagioclase crystals with low Sr (280 - 480 ppm), cores of An_{25-35} and rims of An_{20-25}. From the chemical composition of these plagioclase crystals, four physiochemically distinct rhyolitic melts are identified: (1) an andesitic progenitor melt (a more mafic melt of andesitic composition) in which crystallised the cores of Group 1 crystals; (2) a greywacke melt or greywacke protolith melt responsible for overgrowth rims of Group 1 crystal cores; (3) melt derived from the rejuvenation of a mature crystal mush body evidenced from Group 3 plagioclase crystals; and (4) a final rhyolitic melt created by amalgamation from the varying proportions of the first three melts and subsequent fractional crystallisation of a plagioclase-dominant crystal assemblage in an open-system. Sr diffusion modelling of core-rim interfaces of

Group 1 crystals implies magma chamber formation in the 15,000 years preceding the climatic eruption, showing that the chamber was potentially an ephemeral feature that formed shortly prior to eruption and which was therefore not present for the entire history of the magma reservoir. Cathodoluminescence imaging of quartz crystals reveals complex zonation, implying a complex evolution of quartz crystals from potentially polygenetic sources. Diffusion modelling of the greyscale intensity of cathodoluminescence images (as a proxy for Ti content) for a selection of bright core-rim interfaces of quartz crystals, suggests that renewed quartz growth occurred < 80 yrs prior to eruption and continued towards the climatic eruption.

4.1 Introduction

A contemporary view of sub-volcanic magmatic systems is a complex one of interlinked sills, dykes and multi-level storage areas that in a rhyolitic system culminates in a magma reservoir composed of a crystal mush zone and overlying melt-rich magma chamber (Bachmann and Bergantz, 2004; Davidson et al., 2007; Hildreth and Wilson, 2007; Jerram and Davidson, 2007). The magmatic evolution of an eruptive unit is therefore not simple, but may result from the mixing and mingling of discrete magma batches prior to eruption (Davidson et al., 2007; Pabst et al., 2008). Increasingly, upper crustal magma chambers are being considered as ephemeral bodies that can be replenished on much shorter timescales than the actual formation and growth of the magmatic system (e.g. Glazner et al., 2004) or from the rejuvenation of pre-existing crystal mush bodies (e.g. Charlier et al., 2007). These magma chambers are fed from below by large crystal mush bodies that have become stalled within the upper crustal lithosphere

in a near solid state, and which may represent the early stages of batholith formation (Bachmann and Bergantz, 2003; Glazner et al., 2004; Hildreth and Wilson, 2007; Wiebe et al., 2007). The storage of such large-volumes of silicic magma in the crust in a semi-solid state may explain the scarcity of detected melt bodies through geophysical techniques in active volcanic regions (Bachmann and Bergantz, 2003; 2008; Glazner et al., 2004; Bachmann et al., 2007).

Crystals hosted within volcanic rocks have the ability to record the magmatic evolution within their crystal structure; each magmatic process (e.g. fractional crystallisation, magma mixing, assimilation) depositing a chemical or textural signature within the crystal creating highly zoned crystals (Ginibre et al., 2002a and b; 2004; 2007 Davidson et al., 2007). Identification of these magmatic process(es) responsible for the chemical zonation permits the deciphering and piecing together of processes affecting the evolving magmatic system (Ginibre et al., 2002b and 2007; Jerram and Davidson, 2007). Furthermore, the chemical gradient between two adjacent crystal zones may allow the timescales of these processes to be determined (e.g. Zellmer et al., 1999; Costa et al., 2003; Costa and Chakraborty, 2004; Morgan et al., 2004; 2006; Morgan and Blake, 2006). The longevity of rhyolitic magmatic systems and the timescales over which large-volumes of eruptible magmas sufficient to feed supereruptions accumulate is controversial but is fundamental to our understanding of the dynamics of magma storage (e.g. Halliday et al., 1989; Christensen and DePaolo, 1993; Brown and Fletcher, 1999; Reid, 2003; Charlier et al., 2005; Morgan and Blake, 2006). Diffusion modelling has the advantage over other timescale techniques (e.g. radiometric dating such as U-Pb of zircons) in its ability to determine the

relative timing of a range of magmatic processes from magma degassing to the residence times of crystals prior to eruption (Zellmer et al., 1999; Costa et al., 2003; Kent et al., 2007).

Plagioclase crystallises over the entire igneous compositional spectrum from basalt to rhyolite (Bowen, 1913) and its ubiquitous zonation renders it an ideal candidate to investigate and infer the magmatic evolution of silicic magmas (e.g. Ginibre et al., 2002a; Berlo et al., 2007; Charlier et al., 2008). Recent studies have documented Ti zonation in quartz crystals, illustrating the potential of quartz crystals to record aspects of the magmatic evolution within their crystal structure (Liu et al., 2006; Wark et al., 2007; Shane et al., 2008).

Here we present major, minor and trace element data for plagioclase and Ti concentrations of quartz crystals from the ~330 ka Whakamaru supereruption. We show that both plagioclase and quartz crystals are composed of assorted crystal populations amalgamated from polygenetic sources prior to eruption. Modelling of Sr profiles in a selection of plagioclase crystals and Ti diffusion (using cathodoluminescence intensity as a proxy (e.g. Wark et al., 2007)) in quartz crystals provide insights into the timescales of magmatic processes in the lead up to eruption.

4.2 Whakamaru supereruption and samples

The Taupo Volcanic Zone is currently the most productive region of silicic volcanism on Earth (Houghton et al., 1995; Wilson et al., in press). The largest eruption known to originate from this region is the 320-340 ka Whakamaru

supereruption that occurred in two eruptive periods following a 350 ka hiatus in large-volume explosive rhyolitic volcanism (Houghton et al., 1995; Brown et al., 1998a; Wilson et al., in press). The earlier of these two eruptive periods (ca. 325 ka) deposited the Whakamaru Group ignimbrites, a large-scale crystal-rich, and in places highly welded, group of ignimbrites blanketing a large extent of the central North Island of New Zealand with estimated volumes exceeding 1500 km^3 of magma (Briggs, 1976; Brown et al., 1998a; Wilson et al., in press). The largest of these is the Whakamaru ignimbrite, which is the focus of this study (Figure 4.1).

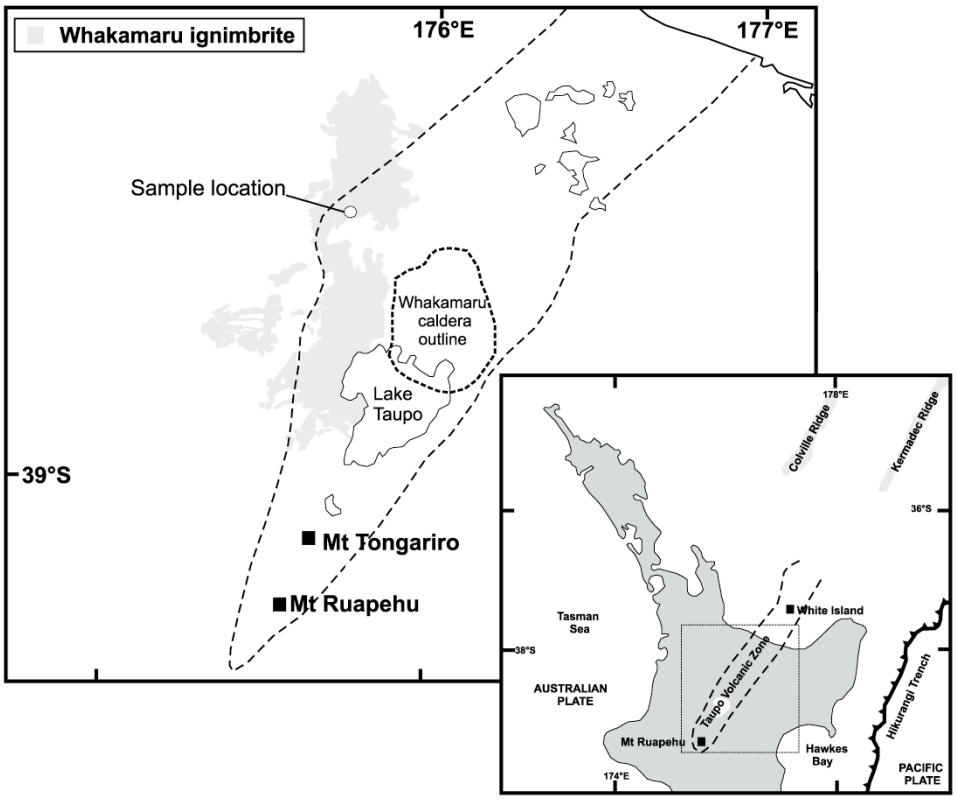

Figure 4.1. Map of the Taupo Volcanic Zone showing the location of the Whakamaru caldera, the extent of the Whakamaru ignimbrite and sample location (white circle) of this study. The extent of the Whakamaru ignimbrite is taken from Brown et al. (1998a). Inset shows the regional setting of the Taupo Volcanic Zone with the outline of the Taupo Volcanic Zone shown by a thick dashed line.

A previous whole rock study of the Whakamaru group ignimbrites indicate at least four distinct rhyolitic magmas and a high-alumina basalt were involved in the generation of the magma body (Brown et al., 1998a). Zircon geochronology has potentially indicated that the Whakamaru magmatic system was active for at least 250 ka preceding the final catastrophic eruption (Brown and Fletcher, 1999; Charlier et al., 2005).

The mineral assemblage fluctuates through the Whakamaru ignimbrite consisting of quartz, plagioclase, orthopyroxene ± amphibole, ilmenite, magnetite, K-feldspar, biotite (Table 4.1) and zircon. A previous study of quartz-hosted melt inclusions indicated at least a proportion of quartz crystals are antecrysts derived from an evolved crystal mush body (Chapter 2). Plagioclase and quartz crystals studied in this work were sampled from the discontinuous crystal lag at the base of the ignimbrite (WH1) and samples (WH2, WH3, WH4, WH5, WH6) were obtained intermittently throughout a ca.100 m section of the ignimbrite at Maraetai Dam (Figure 4.1; Table 4.1).

Sample No.	Latitude	Longitude	Altitude (m)	Mineralogy
WH1	S 38°21.016’	E 175°31.020’		plag; qtz; opx; amp; bt; K- spar Fe-Ti oxides
WH2	S 38°20.849’	E 175°44.206’	170	plag; qtz; opx; Fe-Ti oxides
WH3	S 38°20.953’	E 175°44.034’	250	plag; opx; qtz; amp; bt; Fe-Ti oxides
WH4	S 38°20.782’	E 175°44.033’	246	plag; qtz; opx; amp; Fe-Ti oxides;
WH5	S 38°20.782’	E 175°44.033’	246	plag; qtz; opx; amp; Fe-Ti oxides
WH6	S 38°20.737’	E 175°44.110’	211	plag; qtz; opx; amp; K-spar; Fe-Ti oxides
WH7	S 38°20.799’	E 175°44.144’	196	plag; qtz; opx; amp; Fe-Ti oxides;

Table 4.1. Sample locations and mineralogy of samples used in this study. Mineral phases of listed in order of decreasing abundance. Abbreviations: plag = plagioclase, qtz = quartz, opx = orthopyroxene, amp = amphibole, bt = biotite, K-spar = K-feldspar.

4.3. Analytical methods

4.3.1 Sample preparation

Samples were lightly crushed and sieved and plagioclase, quartz and orthopyroxene crystals were extracted from the 500-1000 μm size fraction for analysis, mounted and polished in epoxy blocks (see Chapter 2). In addition, thick (100 μm) polished sections of Whakamaru pumices were also prepared and used for plagioclase analyses by microprobe and LA-ICPMS.

4.3.2 Electron microprobe analyses

Major elements of plagioclase, quartz and Fe-Ti oxides were determined on the JEOL 733 SuperProbe Electron probe microanalyser (EPMA) at Victoria University of Wellington (VUW). All crystals were analysed at 15 kV accelerating voltage and 12 nA beam current. Plagioclase crystals were analysed with a 10 μm spot size at 10 μm intervals. Fe-Ti oxides were analysed at the same conditions with a focused beam. Quartz crystals were analysed with long count times of 240 seconds on peak and 120 seconds on background with a focused beam. ZAF corrections (Bence and Albee, 1968) were used for data reduction. Primary calibrations used a mixture of natural and synthetic standards. Secondary standards of basaltic glass A99 (USNM 113498/1) for plagioclase analyses, ilmenite standard USNM 96189 for Fe-Ti oxides analyses (Jaroeswich et al., 1980) and KN18 obsidian glass (S. Malik and D.A. Bungard, reported in Devine et al., 1995) for Ti analyses in quartz were analysed at the beginning and end of each analytical session (Table 4.2). Quality control was applied to the plagioclase data and only analyses with totals between 97-102 wt% are reported.

Cathodoluminescence (CL) images of quartz crystals were obtained using a photomultiplier attached to the electron microprobe at the same analytical conditions as described above. Excitation of Ti due to long emission times while collecting CL images can lead to blurry images. However, examination of the images reveals distinct, sharp boundaries are visible, suggesting that this effect is not significant.

4.3.3 Laser ablation inductively coupled plasma mass spectrometry

Laser ablation inductively coupled plasma mass spectrometry (LA-ICPMS) analyses of plagioclase crystals were performed in the Geochemical Laboratory at VUW with a NewWave deep UV laser (193 nm solid state) coupled to an Agilent 7500cs ICP-MS using helium as the carrier gas. CaO was determined prior to LA-ICPMS analysis by EPMA, enabling ^{43}Ca to be used as the internal standard. Samples were analysed for Sr, Ba and Mg with 20 μm laser spot diameters at 20 μm intervals along the EPMA profile. Core and rim analyses of rare earth elements (REE), Y and Pb were also carried out at 35 or 50 μm laser spot diameters, a repetition rate of 5 Hz and power of ~ 5.6-6.7 J/cm^2. The NIST SRM 610 glass standard is used as the primary standard and for signal optimisation at the start and throughout each analytical session. NIST SRM 610 reference values are taken as the GeoRem preferred reference values (http:///georem.mpch-mainz.gwdg.de/). Repeat analyses of MPI-DING glass STH-G at 20 μm laser spot diameters at the same analytical conditions as described above are given in Table 4.3. This indicates an elemental uncertainty (2σ) of ± 6.5% for Sr, Ba and Mg at 20 μm laser spot diameters. We estimate an elemental uncertainty of (2σ) < 10 % for rare earth elements and Y and < 20%

	A99 – Basalt glass					Ilmenite standard USNM 96189					KN18 – obsidian glass				
	Mean n = 19 (wt%)	2 SD	% 2SD	% diff	ref values (wt%)	Mean n = 6 (wt%)	2 SD	% 2SD	% diff	ref values (wt%)	Mean, n = 9 (wt%)	2 SD	% 2SD	% diff	ref values (wt%)
SiO_2	50.9	1.44	2.8	0.1	50.9						73.2	2.67	3.6	-1.8	74.6
TiO_2						47.6	1.55	3.2	4.3	45.7	0.18	0.03	14	1.4	0.18
Al_2O_3	12.4	0.57	4.6	-0.4	12.4					46.5					
FeO	13.3	0.63	4.7	0.5	13.3	46.1	2.32	5.0	-0.9						
MgO	5.16	0.11	2.1	1.6	5.08	0.32	0.07	22	3.1	0.31					
MnO						4.61	0.22	4.7	-3.4	4.77					
CaO	9.15	0.38	4.2	-1.6	9.30										
Na_2O	2.60	0.19	7.2	-2.2	2.66										
K_2O	0.84	0.07	8.2	2.7	0.82										
Total	94.5				94.5					92.5	73.4				74.7

Table 4.2. Standard calibrations and reference values of basaltic glass A99, ilmenite standard USNM 96189 (Jaroeswich et al., 1980) and obsidian standard KN15 (S. Malik and D.A. Bungard reported in Devine et al., 1995) for electron microprobe analyses. n = number of analyses averaged.

Pb when analysed at 35 and 50 μm laser spot diameters from repeat analysis of STH-G at 35 μm laser spot diameters with NIST SRM 612 as the primary standard at the analytical conditions described above (Table 4.3). Correlation between EPMA and LA-ICPMS analytical areas was achieved through detailed backscattered electron images taken before and after both EPMA and LA-ICPMS analyses.

Isotope	Element	Spot size	Mean n = 5	2 SD	% 2SD	% diff	Ref values
24	Mg	20	12643	155	1.23	6.43	11879
25	Mg	20	11234	393	3.50	-5.43	11879
88	Sr	20	486	15.6	3.21	0.773	482
137	Ba	20	306	22.6	7.37	2.74	298
89	Y*	35	10.9	0.289	2.65	-4.51	11.4
139	La*	35	11.8	0.560	4.74	-1.45	12.0
140	Ce*	35	25.5	0.540	2.12	-2.37	26.1
141	Pr*	35	2.97	0.132	4.45	-7.08	3.20
146	Nd*	35	13.1	1.00	7.65	0.90	13.0
147	Sm*	35	2.76	0.388	2.78	-0.57	2.78
153	Eu*	35	0.917	0.069	7.54	0.953	0.950
157	Gd*	35	2.26	0.292	12.9	-12.58	2.59
163	Dy*	35	2.16	0.286	13.2	-2.79	2.22
166	Er*	35	1.10	0.082	7.44	-7.00	1.18
172	Yb*	35	1.02	0.105	10.3	-9.80	1.13
175	Lu*	35	0.157	0.027	17.4	0.168	0.170
208	Pb*	35	8.29	0.424	5.12	-19.49	10.3

Table 4.3. Repetitive analyses of STH-G at 20 μm and 35 μm laser spot diameters. Reference values are taken from GeoRem preferred values (http:///georem.mpch-mainz.gwdg.de/). * indicates Baker, unpublished data at 35 μm laser spot diameters and NIST SRM 612 as primary standard.

4.4. Results

4.4.1 Plagioclase

Backscattered electron images of > 100 plagioclase crystals from 7 samples of the Whakamaru ignimbrite were obtained and revealed subtle yet ubiquitous zoning of crystals (Appendix A4.1 and A4.2). Of these, 61 were analysed for core and rim compositions and major element profiles across 22 crystals (Appendix A3.6 and A3.7) were measured with representative compositions

given in Table 4.4. Sr, Ba and Mg profiles were obtained for 8 of the crystals and spot analyses of REE, Y and Pb were obtained for a representative selection of crystals (Appendix A3.8 and A3.9).

Sample (wt%)	WH1 h_8	WH1 h_38	WH6 da_2	WH6 da_38	WH2 a_3	WH3 e_4	WH2 g_x2	WH3 b_4
Group	1 rim	1 core	1 rim	1 core	2	2	3	3
SiO_2	60.8	53.3	59.9	56.4	60.6	60.5	61.4	60.5
Al_2O_3	25.4	29.9	24.8	28.8	24.2	24.7	24.0	24.5
FeO	0.31	0.24	0.21	0.20	0.30	0.28	0.24	0.17
CaO	6.67	10.8	6.68	10.46	6.37	6.65	5.74	6.06
Na_2O	7.82	5.16	7.29	5.59	7.49	7.35	8.33	7.98
K_2O	0.72	0.30	0.64	0.25	0.71	0.65	0.71	0.67
Total	101.8	99.7	99.6	101.7	99.7	100.2	100.4	99.9
X An	0.31	0.54	0.32	0.50	0.31	0.32	0.27	0.28

Table 4.4. Representative major element analyses of plagioclase crystals. *X An* calculated on a mole fraction basis.

Plagioclase crystals are generally euhedral to sub-euhedral and in some instances are fragmented and broken. On the basis of textural observations and anorthite (*An*) composition (Figure 4.2), plagioclase crystals fall into three Groups, denoted 1, 2, and 3 (Figure 4.3). The most abundant type of plagioclase crystals

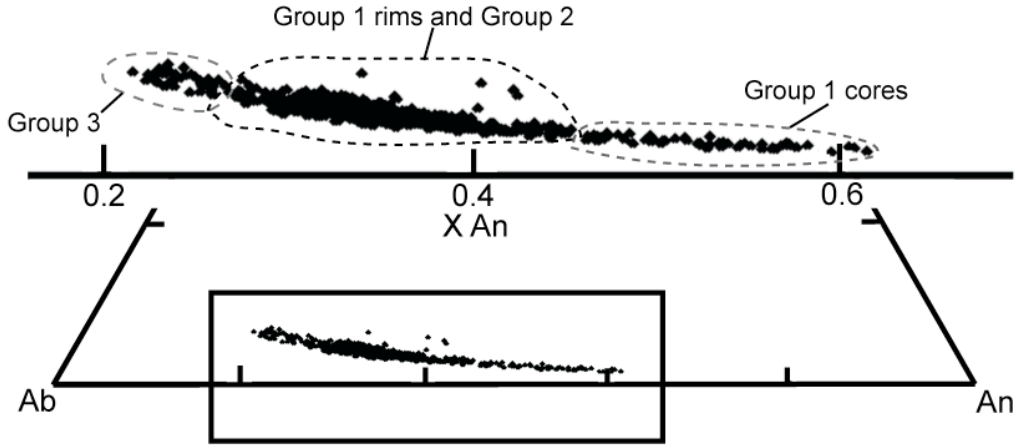

Figure 4.2. Partial ternary diagram of Whakamaru plagioclase crystals and the anorthite composition of the three plagioclase groups are illustrated. Number of analyses = 1246.

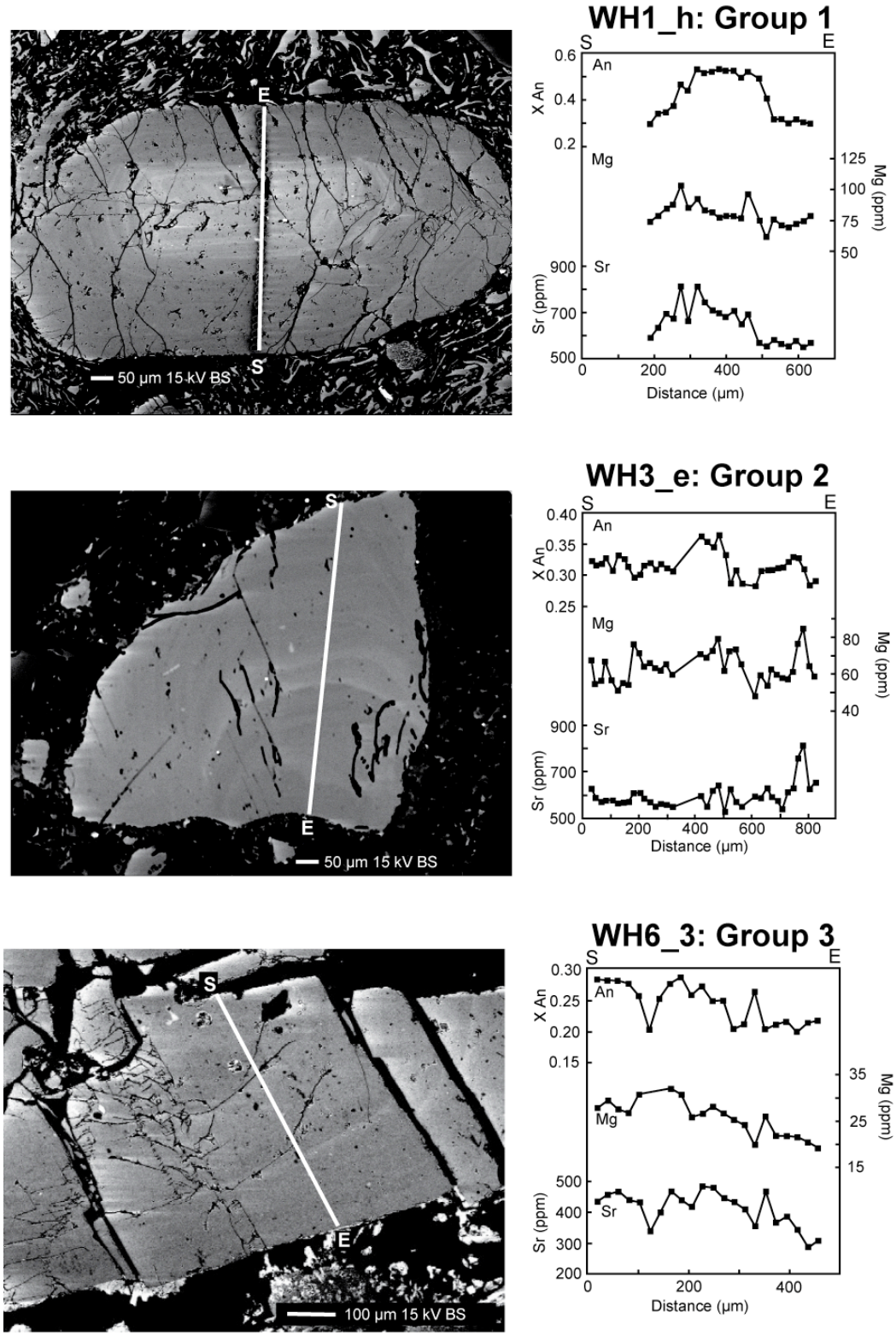

Figure 4.3. Representative backscattered images and *X An*, Sr and Mg concentrations of each of the plagioclase populations. The start (S) and end (E) of EPMA and LA-ICPMS profiles are shown.

observed are Group 2 crystals (77%) with only relatively minor quantities of Group 1 (11%) and Group 3 (12%) crystals, although the abundance of Group 1 crystals may be biased if the sectioning of crystals was off-centre (Appendix A3.6 and A3.7; Appendix A4.1 and A4.2). There is no observed systematic variation in the abundance of plagioclase populations with stratigraphic height.

4.4.1.1 Group 1

Group 1 crystals are characterised by cores of $An_{45\text{-}60}$ mantled by concentric relatively homogeneous oscillatory-zoned rims of ca. An_{30} (Figure 4.3). Trace element concentrations of cores and rims are distinct with elevated Ba (ca. 400-800 ppm), La (7-10 ppm) and Ce (9-13 ppm) concentrations of rims compared to cores at similar Sr concentrations (Figure 4.4). Texturally, two distinct core types are observed: (1) crystals with a gradual diffuse core-rim interface such as WH1_h and WH2_b; and (2) crystals with partially resorbed cores and a sharp core-rim interface, for example WH2_d (Appendix A4.1 and A4.2).

4.4.1.2 Group 2

Group 2 plagioclase crystals exhibit pronounced oscillatory zoning with a limited $An_{30\text{-}40}$ composition (Figure 4.3). High *An* spikes (ca. $An_{36\text{-}40}$) are observed and these correspond to micro-inclusion trails within the crystal. Sr (dominantly 550-630 ppm), Ba (dominantly 450-730 ppm), Pb and REE concentrations from a single representative Group 2 plagioclase crystal overlap those of Group 1 rims with the exception of four analyses from the region surrounding the core of the crystal that possess anomalously high Sr (625-815 ppm) and Ba (1010-1325

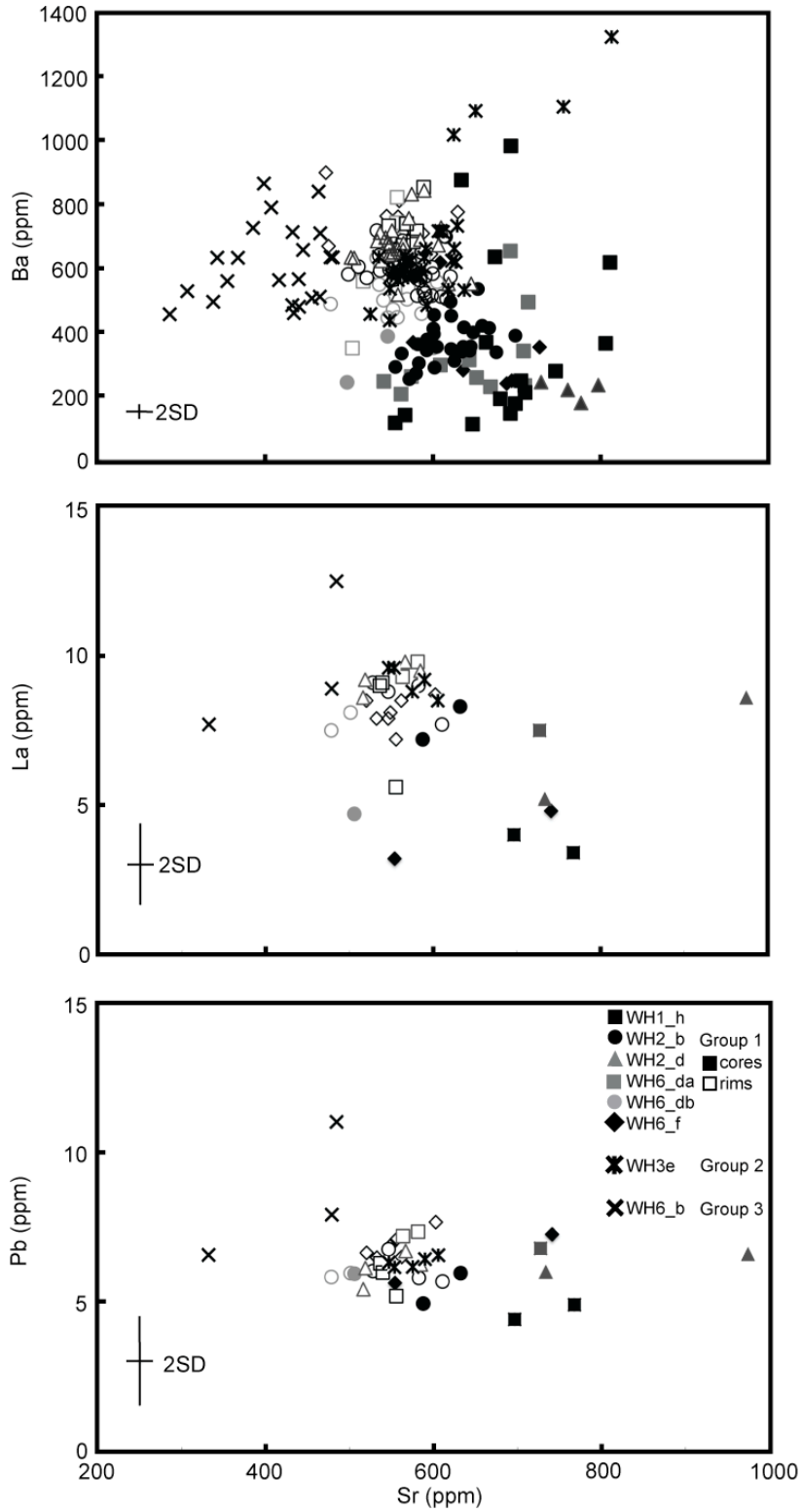

Figure 4.4. Measured Sr, Ba, La and Pb concentrations of plagioclase crystals. Note only a single representative plagioclase crystal was analysed for trace elements for Group 2 and 3 crystals.

ppm) concentrations that are not reflected in the Pb and REE analyses (Figure 4.4).

4.4.1.3 Group 3

These crystals are characterised by cores of An_{25-35} and rims of An_{20-25}, and low Sr (280 - 480 ppm) and Mg (19 - 32 ppm) concentrations compared to Group 1 and 2 plagioclase crystals (Figure 4.4). In addition, Sr and Ba are more compatible in Group 3 plagioclases compared to Group 1 and Group 2 crystals. REE concentrations indicate the most extreme concentrations are observed in the crystal core with elevated Pb, Eu, and La concentrations relative to Group 1, Group 2 and Group 3 rim concentrations (Figure 4.4).

4.4.2 Quartz crystals

CL images reveal complex zonation within Whakamaru quartz crystals (Figure 4.5; Appendix A4.3), demonstrating a growth history just as complex as that of the plagioclase crystals and the presence of multiple populations. Oscillatory zoning is ubiquitous and in some cases is truncated by later overgrowths (e.g. WH1_39), demonstrating the presence of distinct core regions and multiple resorption events. Several quartz crystals (e.g. WH1_37, WH2_3, WH2_6) display a bright CL rim implying these crystals experienced a common final stage of magmatic evolution; however, the bright CL core of WH1_37 in comparison with those of WH2_3 and WH2_6 indicates the early period of magmatic evolution is unique to each crystal. In contrast, crystals WH1_40,

WH2_4, WH2_5 and WH2_8 exhibit strong oscillatory-zoned rims indicative of fluctuating magmatic conditions during the final stages of quartz growth.

The intensity of CL zoning can be used as a proxy for Ti concentrations with darker regions indicating lower Ti concentrations that result from either a change in magmatic temperature or the Ti activity of the melt (Wark and Spear, 2005). Core and rim concentrations of 14 quartz crystals were analysed for TiO_2 concentrations from samples WH1 and WH2 (Table 4.5) and ranged between 0.002 – 0.049 wt. %.

Sample	TiO_2 (wt%)	Position
WH1_4_Q1	0.002	core
WH1_4_Q2	0.011	rim
WH1_35_Q1	0.009	core
WH1_35_Q2	0.029	rim
WH1_36_Q1	0.016	core
WH1_36_Q2	0.025	rim
WH1_37_Q1	0.050	core
WH1_37_Q2	0.039	rim
WH1_38_Q1	0.027	core
WH1_38_Q2	0.049	rim
WH1_39_Q1	0.022	rim
WH1_39_Q3	0.021	core
WH1_40_Q1	0.033	rim
WH1_40_Q2	0.029	core
WH2_2_Q1	0.022	core
WH2_2_Q2	0.034	rim
WH2_3_Q1	0.015	core
WH2_3_Q2	0.005	rim
WH2_4_Q1	0.009	core
WH2_4_Q2	0.024	rim
WH2_5_Q1	0.021	core
WH2_5_Q2	0.013	rim
WH2_6_Q1	0.012	core
WH2_6_Q2	0.046	rim
WH2_7_Q1	0.026	core
WH2_7_Q2	0.005	rim
WH2_8_Q1	0.007	core
WH2_8_Q2	0.013	rim

Table 4.5. TiO_2 concentrations of quartz crystals.

4.4.3 Fe-Ti oxides

Fe-Ti oxides are present as both free crystals and hosted within orthopyroxene phenocrysts. Free Fe-Ti oxides were not analysed, as it is impossible to determine the relationship of these crystals prior to the crushing of pumices and separation of crystals. Fourteen-orthopyroxene hosted Fe-Ti oxide pairs were analysed from sample WH1 (Table 4.6), with only six of these pairs being fully enclosed in the orthopyroxene crystal allowing homogenisation for the majority of Fe-Ti oxides with the external melt prior to eruption. Equilibrium between oxides was tested using the method of Bacon and Hirschmann (1988) with temperatures and oxygen fugacity (-log fO_2) calculated using the ILMAT spreadsheet of Lepage (1998) (Table 4.6).

4.4.4 Geothermometry

Fe-Ti oxides are useful probes of magmatic temperature with the ability to record heating events on the timescales of hours to days prior to eruption (Venezky et al., 1999). Therefore, Fe-Ti oxides from WH1 are used to infer a final mean magmatic temperature of 789 ± 40 °C (2SD) (Table 4.6). A longer record of magmatic temperature is potentially preserved in plagioclase and quartz crystals, as these crystallise earlier in the magmatic evolution and major element diffusion is much slower than in Fe-Ti oxides (Grove et al., 1994; Morse et al., 1994; Venezky et al., 1999; Cherniak et al., 2007). Application of plagioclase-melt equilibria of Putirka (2005) permits magmatic temperatures at the time of plagioclase fractionation to be detailed. The presence of three distinct plagioclase populations indicates the existence of multiple magma batches.

Ilmenite (wt%)	WH1 O12-1	*WH1 O18-1	*WH1 O21-2	*WH1 O23-2	*WH1 O24-1	*WH1 O26-2	WH1 21-O1	WH1 24-O2	WH1 26-O2	WH1 27-O2	*WH1 30-O2	WH1 31a-2	*WH1 32-O2	*WH1 32-O3
SiO_2	0.049	0.051	0.000	0.042	0.042	0.052	0.073	0.004	0.047	0.072	0.000	0.046	0.012	0.000
TiO_2	47.93	48.75	49.03	49.02	49.23	49.37	48.30	45.30	48.65	45.59	45.44	45.20	45.73	45.31
Al_2O_3	0.109	0.127	0.103	0.185	0.137	0.073	0.16	0.111	0.08	0.121	0.1	0.164	0.111	0.135
FeO	49.88	48.79	50.53	49.57	49.13	48.61	48.26	49.96	49.38	50.09	49.86	50.19	50.02	50.80
MnO	0.848	0.772	0.825	0.866	0.927	0.889	0.834	0.863	0.943	0.818	0.801	0.870	0.972	0.842
MgO	1.85	1.97	1.76	1.81	1.78	1.83	1.73	1.75	1.89	1.80	1.68	1.76	1.69	1.65
Total	100.61	100.42	102.26	101.45	101.20	100.77	99.28	97.98	100.94	98.48	97.88	98.23	98.53	98.74
Fe_2O_3	12.10	10.20	11.60	10.60	9.90	9.20	9.60	14.70	11.00	14.50	14.20	15.00	14.30	15.40
FeO	39.00	39.60	40.10	40.00	30.20	40.30	39.60	36.80	39.50	37.10	37.10	36.70	37.20	37.00
Magnetite (wt%)	WH1 O12-2	WH1 O18-2	WH1 O21-1	WH1 O23-1	WH1 O24-2	WH1 O26-1	WH1 21-O2	WH1 24-O3	WH1 26-O3	WH1 27-O1	WH1 30-O1	WH1 31a-1	WH1 32-O1	WH1 32-O4
SiO_2	0.064	0.144	0.082	0.076	0.071	0.143	0.087	0.018	0.079	0.048	0.009	0.044	0.059	0.074
TiO_2	8.80	9.31	9.30	9.57	9.32	9.47	9.22	8.63	9.23	8.68	8.50	8.80	8.43	8.69
Al_2O_3	1.41	1.55	1.44	1.45	1.43	1.50	1.50	1.40	1.50	1.49	1.38	1.50	1.51	1.43
FeO	81.52	81.22	81.72	82.28	82.08	81.49	81.93	82.82	81.53	83.45	83.49	84.33	83.42	83.61
MnO	0.487	0.517	0.624	0.522	0.576	0.524	0.627	0.532	0.559	0.444	0.563	0.596	0.667	0.505
MgO	0.75	0.95	0.88	0.89	0.91	0.82	0.86	0.76	0.87	0.86	0.83	0.87	0.85	0.87
Total	92.96	93.54	93.96	94.72	94.32	93.79	94.13	94.16	93.69	94.98	94.77	96.14	94.93	95.17
Fe_2O_3	49.20	48.30	48.90	48.90	49.20	48.20	49.10	50.50	48.70	50.90	51.30	51.50	51.30	51.00
FeO	37.30	37.70	37.70	38.30	37.90	38.10	37.80	37.40	37.70	37.70	37.30	38.00	37.30	37.70
Temp (°C)	793	768	787	779	766	763	764	820	786	814	808	819	807	821
Oxygen fugacity (log $10fO_2$)	-13.5	-14.4	-13.8	-14.1	-14.5	-14.7	-14.5	-12.6	-13.8	-12.71	-12.83	-12.56	-12.8	-12.50

Table 4.6. Fe-Ti oxides major element compositions and calculated temperature and oxygen fugacity. * denotes Fe-Ti oxide pairs exposed to the external melt.

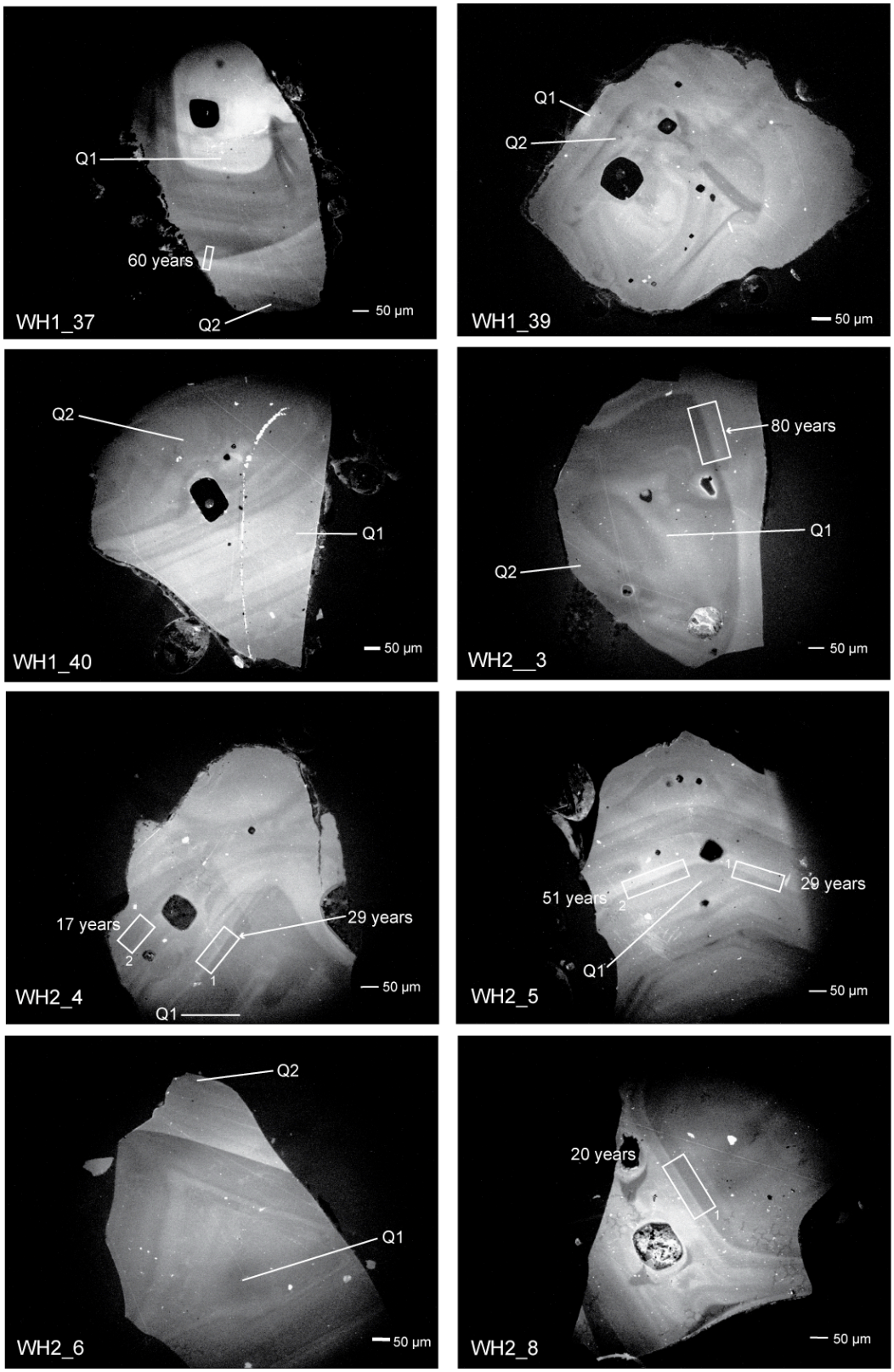

Figure 4.5. CL images for a selection of quartz crystals from WH1 and WH2. White boxes denote areas modelled by diffusion with the respective timescales displayed in years. Locations of point analyses are denoted by Q and relate to Table 4.5.

Therefore, to employ a single constant melt composition in association with the plagioclase-melt equilibria may provide erroneous temperature estimates. As Group 1 rims and Group 2 plagioclase crystals appear to be in equilibrium with the groundmass glass (see Section 4.6.1 and 4.6.2) and comprise the majority of crystals, a mean groundmass glass composition (Brown, 1994) is taken as the melt composition and used to calculate magmatic temperatures. A summary of calculated magmatic temperatures is given in Table 4.7 and indicates a mean temperature of 760 °C for Group 1 rims and Group 2 crystals. Furthermore, this would indicate Group 1 cores fractionated from magma with a temperature of ca. 830 °C or 950 °C if, as discussed below, the cores of Group 1 crystals fractionated from an andesitic progenitor melt of dacitic composition. Magmatic temperatures of Group 3 plagioclase crystals are more equivocal. A groundmass glass melt composition yields magmatic temperatures ca. 30 °C lower than the melt in equilibrium with the Group 1 rims and Group 2 crystals, whilst utilising a melt inclusion composition (see Section 4.6.3) indicates a temperature of ca. 770 °C.

Magmatic temperatures can be calculated using the Ti-in-quartz geothermometer (Wark and Watson, 2006). However, it relies on the Ti activity of the melt being accurately constrained. Ti activity was calculated for the Whakamaru magma using the method of Hayden et al. (2007) from the major element composition of melt inclusions (Chapter 2) and groundmass glasses (Brown, 1994). This produced varying and inconsistent estimates of Ti activity of 1.48 for WH1 melt

Group	Sample	n	Minimum temperature (°C)	Maximum temperature (°C)	Average temperature (°C)
Rims					
1	WH1_h	33	724	775	751
1	WH2_b	59	718	776	754
1	WH2_d	52	734	793	758
1	WH6_da	36	739	772	758
1	WH6_db	29	713	807	772
1	WH6_f	52	731	790	761
Cores					
1	WH1_h	28	780	849	830
1	WH2_b	49	767	835	812
1	WH2_d	22	781	848	828
1	WH6_da	21	789	844	828
1	WH6_db	7	789	846	828
1	WH6_f	10	790	848	832
2	WH1_b	98	729	796	752
2	WH2_a	151	723	798	756
2	WH2_f	69	741	803	763
2	WH3_c	57	744	790	764
2	WH3_d	58	724	805	778
2	WH3_e	88	728	795	757
2	WH5_d	66	749	835	784
2	WH5_f	61	728	792	760
2	WH6_e	47	748	791	762
2	WH6_g	65	735	813	758
3	WH2_g	42	694	812	747
3	WH3_b	51	663	744	707
3	WH6_b	42	701	813	748
3	WH6_c	90	673	785	732

Table 4.7. Summary of magmatic temperatures estimated from the plagioclase-melt equilibria of Putirka (2005). n = number of plagioclase analyses from each crystal used to calculate average. Full temperature determinations are given in Appendix A3.6.

inclusions, 0.98 for WH2 melt inclusions and 1.35 for groundmass glasses; indicating that Ti activity fluctuated either temporally or spatially within the magma chamber. Consequently, TiO_2 was not sufficiently buffered to permit the thermal evolution of quartz crystals to be determined.

This range of calculated magmatic temperatures is interpreted to reflect the changing thermal regime of a cooling magma. Cores of Group 1 plagioclase

crystals are inferred to fractionate from an initial, hotter (ca. 950 °C) andesitic progenitor melt that with time cooled and differentiates into a cooler (ca. 760 °C) rhyolitic magma, represented by the calculated magmatic temperatures of Group 1 rim and Group 2 plagioclase crystals. Heating of the magma immediately prior to eruption is speculated to have occurred from the slightly elevated mean magmatic temperature of 789 °C determined from the Fe-Ti oxides.

4.5. Diffusion modelling

4.5.1. Plagioclase crystals

As plagioclase crystallises, the crystal rim maintains local equilibrium with surrounding melt. Due to the slow, coupled inter-diffusion of NaSi - CaAl, the original anorthite composition of Whakamaru plagioclase crystals is retained at length scales > 5μm (Blundy and Shimizu, 1991; Grove et al., 1984; Morse et al., 1984). The incorporation of trace elements into plagioclase crystals is governed by well-constrained partitioning relationships (Blundy and Wood, 1991; 1994; Bindeman et al., 1998) that are dependent on temperature melt composition and crystal composition. Disequilibrium can arise between adjacent crystal zones as the result of changing melt temperature or chemistry (leading to net uptake or loss of trace elements from the melt) or changes in major element composition caused by other factors such as pressure or water content. Such changes in the magma conditions (be they pressure, temperature, H_2O budget or melt composition) result in subsequent plagioclase growth at different anorthite concentrations (e.g. Bowen, 1913; Johannes, 1989; Putirka, 2005; Ginibre et al., 2007) with concomitant step changes in trace element concentrations. The induced disequilibrium of this step change between two adjacent zones is erased

by a subsequent homogenisation of the trace element concentrations via a diffusion-governed process that will only cease on eruption when the compositional profile is "frozen" into the crystal by the rapid drop in diffusion rates. The chemical potential of elements is the driving force for diffusion, and can be approximated by using standard partition coefficients to translate element abundance into a melt equivalent. The partition coefficients of adjacent crystal zones govern the relative equilibrium concentrations of trace elements between the two regions of the crystal. Therefore, two adjacent zones of plagioclase with differing *An* contents will not necessarily possess the same trace element concentrations when fully equilibrated (e.g. Zellmer et al., 1999; Costa et al., 2003), although locally, the chemical potential will be in equilibrium. If equilibrium has not been attained, the length of time a crystal interface resided at magmatic temperature can be modelled with the appropriate solution to Fick's second law and calculated partition coefficients (K) (e.g. Crank, 1976; Zellmer et al., 1999; Costa et al., 2003; Morgan et al., 2004).

Partition coefficients of Sr and Ba in plagioclase crystals can be calculated from the relationships determined by Blundy and Wood (1991) and relate the trace element concentration of the plagioclase to the melt they fractionated from:

$$RT\ln K_{Sr} = 26{,}800 - 26{,}700X_{An} \quad (4.1a)$$

$$RT\ln K_{Ba} = 10{,}200 - 38{,}200X_{An} \quad (4.1b)$$

where R is the gas constant (8.3145 J $mol^{-1}K^{-1}$), T is the temperature in Kelvin and X_{An} is the *An* content on a mole fraction basis. These partition coefficients can then be used to calculate equilibrium melt concentrations of Sr and Ba that would be in instantaneous equilibrium with that crystal zone, following the

method described by Costa et al. (2003) and the co-existing melt compositions at the time the plagioclase crystallised

4.5.2. Diffusion modelling based on Sr profiles

Timescales for the length of time the core-rim interface in Group 1 crystals resided at magmatic temperatures can then be estimated through analysis of Sr diffusion profiles. Sr diffusion modelling is conducted as the diffusivity of Sr is well constrained for plagioclase and process appropriate diffusion rates (Zellmer et al. 1999). A simple spherical diffusion model (Crank, 1976) (Equation 4.2) is applied with a radius, *a*, assuming an initially uniform core composition (C_1) buffered by a constant rim composition (C_0), with a measured concentration (C) at a distance, *r* from the centre. As equilibrium is governed by the chemical potential of elements and not concentration, a calculated fictional melt equivalent for Sr is determined (calculated by dividing measured/equilibrium elemental concentrations) (Zellmer et al., 2003) and substituted for concentration in Equation 4.2.

$$\frac{C - C_1}{C_0 - C_1} = 1 + \frac{2a}{\pi r}\sum_{n=1}^{\infty}\frac{(-1)^n}{n}\sin\frac{n\pi r}{a}e^{-Dn^2\pi^2 t/a^2} \qquad (4.2)$$

Diffusivity of Sr (D) is assumed to be isotropic within analytical error (Giletti and Casserly, 1994; Zellmer et al., 1999) and calculated following the method described in Zellmer et al. (1999), where the pre-exponential factor, $D_0 = 10^{-(4.1XAn+4.08)}$, activation energy of 276 kJ mol^{-1} and a magmatic temperature of 760 °C (Section 4.4.4).

Of the six Group 1 crystals analysed for Sr diffusion profiles, the core-rim interface in WH2_d and WH6_f decreases in *An* by 0.26 mol % over 30 μm and 20 μm, respectively, and therefore sufficient resolution could not be attained to fully constrain residence times. However, maximum residence times of < 2300 yrs have been estimated for these two crystals (Table 4.8). The residence times of the other four crystals yield a range of ages from 13.5 ka to 3 ka (Table 4.8). The longest times of ca. 13.5 ka were recorded in crystals WH1_h and WH2_b that possess diffuse boundaries. In comparison, crystals WH6_da and WH6_db possess semi-resorbed cores and return much shorter times in the region of 3000 - 6500 years. This continuum of plagioclase residence times may hint at the frequent mixing of magmas and implies that not all Group 1 cores were incorporated simultaneously into the final magma body.

Sample	Maximum X An	Initial Sr fictional melt	Measured Sr fictional melt	a (μm)	r (μm)	Age (yrs)
WH1_h	0.53	2.5	1.81	200	122	13500
WH2_b	0.48	1.8	1.61	488	280	13500
			1.31		300	10000
WH2_d	0.57	2.73	ca. 1.50	170	145	< 2300
WH6_da	0.52	2.09	1.28	140	112	6400
WH6_db	0.55	2.16	1.28	64	42	3400
			1.59		20	3000
WH6_f	0.58	2.74	ca. 1.64	55	40	< 2000

Table 4.8. Calculated residence times of Group 1 plagioclase crystals from Sr diffusion. Diffusivity of Sr is calculated at 760 °C at the highest observed *X An*. Initial calculated fictional Sr melt equivalent is determined from the core of the crystals and measured calculated fictional Sr melt equivalent is taken at a distance (*r*) from the centre of the sphere with a radius (*a*).

Errors are estimated by propagating the 2σ temperature uncertainty on the calculated temperatures onto the calculated diffusivities and these are illustrated in Figure 4.6 as probability distributions for each interface modelled.

Propagating the measured analytical errors of the pre-exponential factor and activation energy onto the calculated diffusivities results in errors that are negligible (e.g. 0.05 $\log_{10}$ units for 1σ) compared to the determined errors due to the temperature uncertainties (e.g. 0.209 $\log_{10}$ units for 1σ) and gives a combined calculated uncertainty of 0.214 $\log_{10}$ units for 1σ. The probability density function of the entire plagioclase population suggests there is a bimodal distribution in diffusional timescales providing further evidence for the incorporation of plagioclase cores over a period of time or from multiple mixing events.

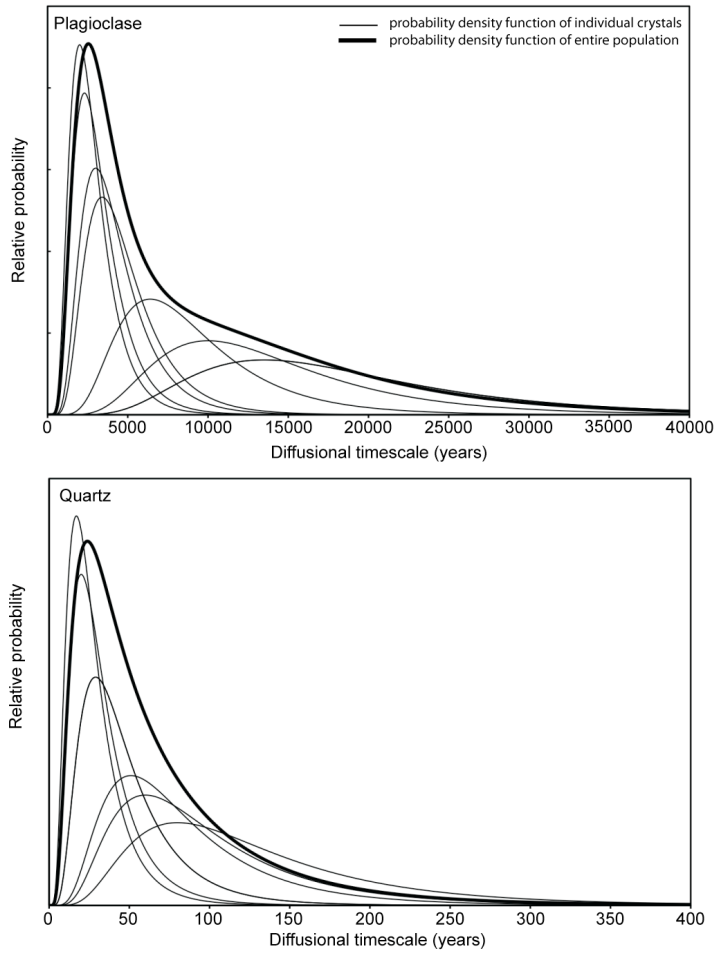

Figure 4.6. Probability distributions of each diffusional timescale calculated in this study as a function of 2σ temperature uncertainty of plagioclase and quartz crystals. Thin lines denote the probability distribution for each individual timescale and the thick line denotes the entire population.

4.5.3 Quartz crystals

Several of the imaged quartz crystals display a pronounced zone of high CL intensity at or near the rim of crystals (Figure 4.5). Irrespective of whether the higher-Ti growth zones result from an increase in magmatic temperature or a change in the Ti activity of the melt, the interfaces between low and high Ti zones are distinct. Using the CL intensity as a proxy for Ti concentration, Ti diffusion across this interface can be modelled, allowing the timescale between the renewed growth of the quartz crystal and eruption to be estimated (Wark et al., 2007). The rounded nature of the inner crystal cores indicates a period of resorption occurred pre-dating the final growth and therefore the timing of the final recharge event cannot be dated (Wark et al., 2007).

As diffusion only spans a small fraction of the two adjacent regions, a simple, one-dimensional diffusion model is sufficient. A refinement to the diffusion model presented by Morgan et al. (2004) is applied. Ti diffusivity in quartz is calculated using a D_0 of 7.01×10^{-8} m^2s^{-1} ($\log D_0 = -7.154 \pm 0.525$), an activation energy of 273 ± 12 kJ mol^{-1} (Cherniak et al., 2007) and a temperature of 789°C derived from Fe-Ti oxides as this best represents the magmatic temperature immediately prior to eruption when this final growth would have occurred. Calculated timescales using a diffusivity of 2.63×10^{-21} m^2s^{-1} indicate that the initiation of renewed quartz growth occurred < 80 years prior to eruption (Figure 4.5; Table 4.9). Errors are calculated in the same manner as described above for Sr diffusion in plagioclase crystals by combining the 2σ of our Fe-Ti oxide temperature determinations of ± 40 K onto the calculated diffusivities giving a combined error of 0.25 $\log_{10}$ unit for 1σ. The results are illustrated as probability

distributions due to the temperature uncertainty in Figure 4.6, which suggests renewed quartz growth, occurred ca. 30-35 years prior to eruption.

Sample		Diffusional half-width (μm)	Residence time (years)
WH1_37		4.60	60
WH2_3		5.92	80
WH2_4	1	2.97	29
	2	2.38	17
WH2_5	1	2.97	29
	2	4.16	51
WH2_8		2.97	20

Table 4.9. Summary of the diffusional timescales calculated from the smoothing of bright CL rims on quartz crystals. Boundaries modelled are highlighted in Figure 4.5.

4.6. Discussion

None of the examined plagioclase or quartz crystals yield identical values for the timescale, indicating that each of these crystals experienced an unique history. However, each crystal population possesses common features that allow the successive magmatic evolution to be unravelled. The compositional variability of the melt bodies from which the plagioclase crystals fractionated is explored by determining the Sr and Ba melt compositions in equilibrium with the crystal throughout its growth and comparing these to known melt compositions (Figure 4.7). However, caution must be applied as diffusion does modify the Sr and Ba concentrations of plagioclase after crystallisation. Nevertheless, this work exposes the presence of at least four, compositionally-distinct rhyolitic melts during the formation of the Whakamaru magma (Figure 4.7).

4.6.1 Origins of Group 1 plagioclase crystals

The documented compositional variability of Group 1 cores and rims points to at least two distinct periods of crystallisation. Importantly, the change in

composition from core to rim can be used to trace the successive magmatic evolution. The relatively wide variability and high Sr and Eu, and low Ba, La and Ce core concentrations compared to the rims suggests the cores fractionated from a more mafic magma (Figure 4.4). Further evidence for this is gained from the calculated Sr and Ba concentrations in the melt, which intersect with the defined composition of andesitic groundmass glasses (Price et al., 2005) at 760 °C. However, the calculated range of Sr and Ba melt compositions would encompass the andesitic groundmass glass compositions if the core of the plagioclase crystals fractionated from the magma at an earlier stage of the petrogenetic evolution when the magma was hotter (e.g. ca. 950 °C) prior to the cooling of magma (hereafter denoted at Melt 1); the estimated magmatic temperature calculated from plagioclase-melt equilibria (Putirka, 2005) when the andesitic groundmass glass composition is taken as the melt composition. Unfortunately, the limited data for the measured Sr and Ba concentrations of andesitic melts from the Taupo Volcanic Zone restricts our evaluation of whether the wide variability of Sr and Ba melt concentrations observed in the cores characterises that of the natural melt composition or is instead the result of diffusional modification of the crystal core Sr and Ba concentrations.

In contrast, Group 1 rims possess a restricted Sr (465 -630 ppm), Ba (450-575 ppm), La, Ce and Eu composition and the calculated Sr and Ba melt compositions span the known compositional range of Whakamaru group ignimbrite groundmass glasses (Brown, 1994). This therefore, provides compelling evidence for the crystallisation of Group 1 rims from the final host

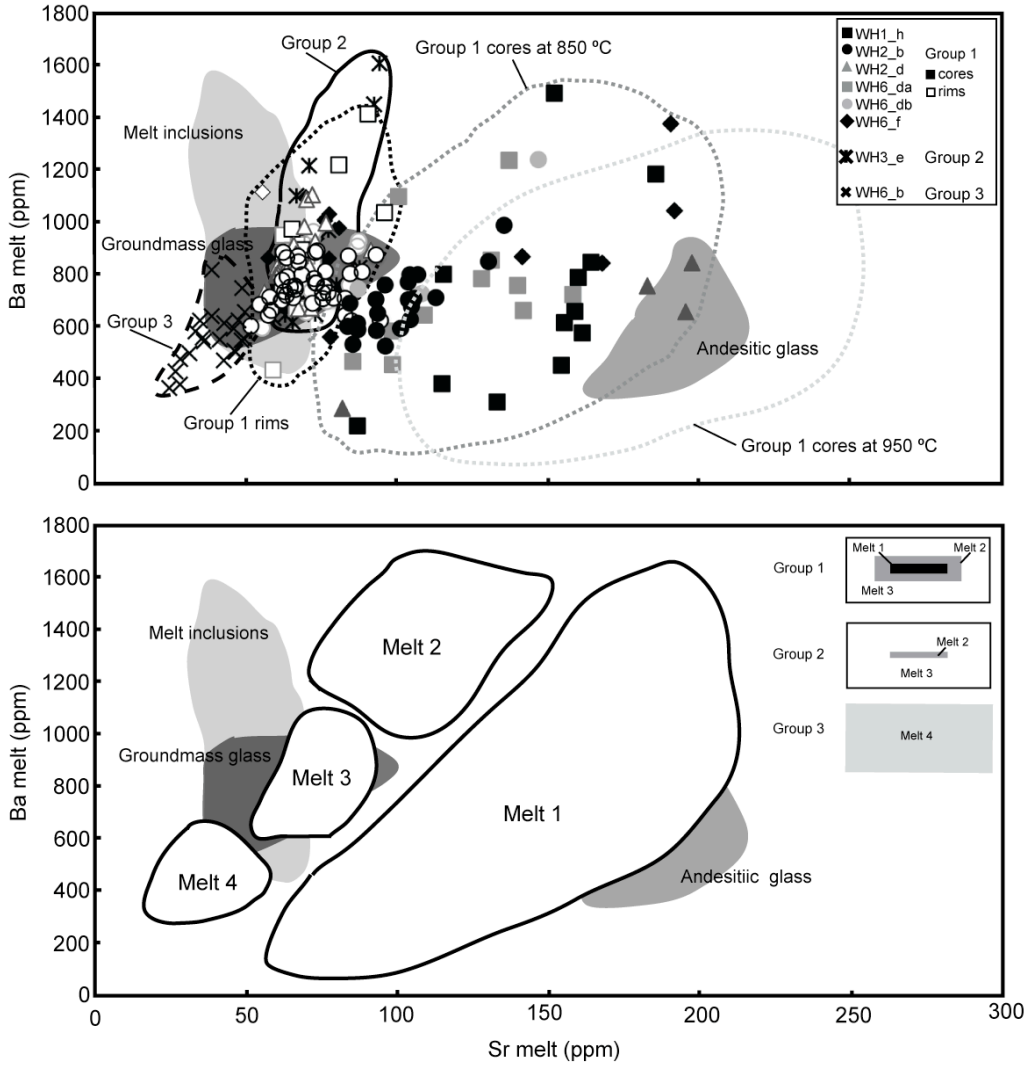

Figure 4.7. (a) Calculated co-existing Sr and Ba melt compositions for the three defined plagioclase populations calculated at 760 °C, with the partitioning relationships (Equation 3.1a and 3.1b) of Blundy and Wood (1991) and the measured Sr and Ba concentrations of the plagioclase crystals (Appendix A3.8). The melt composition of Group 1 cores at 950 °C is denoted by a thin grey dashed line. (b) Cartoon of the Sr and Ba concentrations of the four Melt compositions discussed in the text. The grey shaded regions represent melts of known compositions: dark grey – Whakamaru groundmass glasses (Brown, 1994); medium grey – andesitic glasses (Price et al., 2005); and light grey – quartz-hosted melt inclusions (Chapter 2). Insert represents the location of melt compositions in relation to the three plagioclase populations.

melt (hereafter termed Melt 3) prior to eruption. Furthermore, a third minor melt composition (hereafter denoted Melt 2) is present in some Group 1 crystals. It is most readily distinguished on the basis of calculated Sr and Ba melt compositions and the calculated melt equivalent concentration of measured Sr and Mg (Figure 4.8) and is located as a thin overgrowth surrounding the core (Figure 4.5).

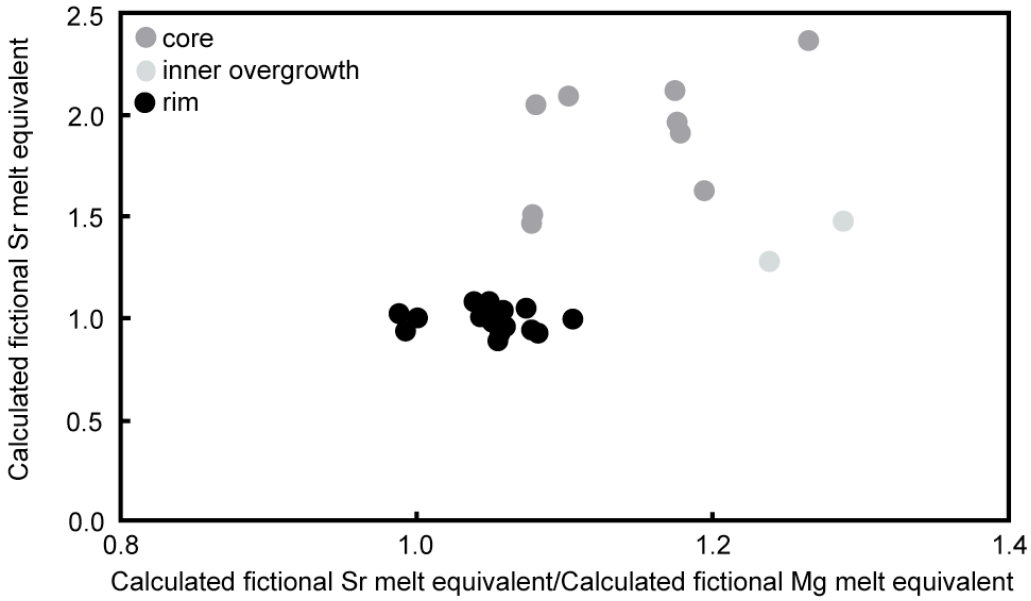

Figure 4.8. Calculated equilibrium melt composition of Sr, normalised to the groundmass glass, versus the ratio of the same value to its Mg equivalent. Equilibrium of elements with groundmass glass is attained when the value is equal to 1 on each axis. Consequently, the rim analyses that form a group at (1,1) are showing full equilibrium. This then trends to the right, showing that the Mg in this region is more equilibrated than Sr, whilst the absolute value for Sr has not changed. In subsequent analyses towards the core, it becomes clear that the normalised, calculated equilibrium melt composition of Sr is significantly higher, whilst retaining a high ratio to Mg. This implies that the core is significantly less equilibrated for both elements, however markedly more so for Sr.

The core and the rim melts of Group 1 crystals are petrologically linked by the fractional crystallisation of the observed crystal assemblage, similar to patterns described by Berlo et al. (2007) for Mount St. Helens. The crystal assemblage is

dominated by plagioclase but contains smaller proportions of K-feldspar, biotite, amphibole, and Fe-Ti oxides that may influence the behaviour of Sr and Ba in the melt. Conversely, the presence of quartz and orthopyroxene, with K_{Sr} and $K_{Ba} \sim 0$ will cause an increase in the Sr and Ba compositions of the melt. Beginning with a parental melt composition of 160 ppm and 780 ppm of Sr and Ba respectively, calculated from the core region with the highest *An* content, and therefore slowest Sr diffusion (Giletti and Casserly, 1994; Giletti and Shanahan, 1997; Zellmer et al., 1999), combined with a magmatic temperature of 760 °C, the fractionation trend of a crystal assemblage consisting of purely plagioclase with *X An* of 0.3 and 0.4 is modelled (Figure 4.9). Fractional crystallisation modelling of the observed crystal assemblage of plagioclase, quartz, orthopyroxene, K-feldspar, biotite, amphibole, and Fe-Ti oxides (Table 4.10) results in a trend parallel to that of the pure plagioclase assemblage, but requires greater degrees of fractional crystallisation (30 - 40%) compared to 10 - 20 % fractional crystallisation of a pure plagioclase assemblage to attain a Melt 3 composition (Figure 4.9). Thus, all of the calculated fractionation trends project through the calculated rim melt composition providing strong evidence for the formation of Melt 3 by fractional crystallisation of the observed crystal assemblage from a progenitor andesitic melt (Melt 1) (Figure 4.9). Furthermore, the modelled decrease in Ba concentrations at low Sr concentrations (< 50 ppm) of the observed crystal assemblage hints at a possible origin of Melt 4 from extreme fractional crystallisation of progenitor andesitic melts from either: (1) the observed crystal assemblage as modelled; or (2) crystallisation of a dominantly plagioclase, quartz and orthopyroxene ± Fe-Ti oxides assemblage generating Melt 3, with late stage crystallisation of K-feldspar, amphibole and

biotite significantly reducing the Sr and Ba concentrations of the residual melt, to produce Melt 4.

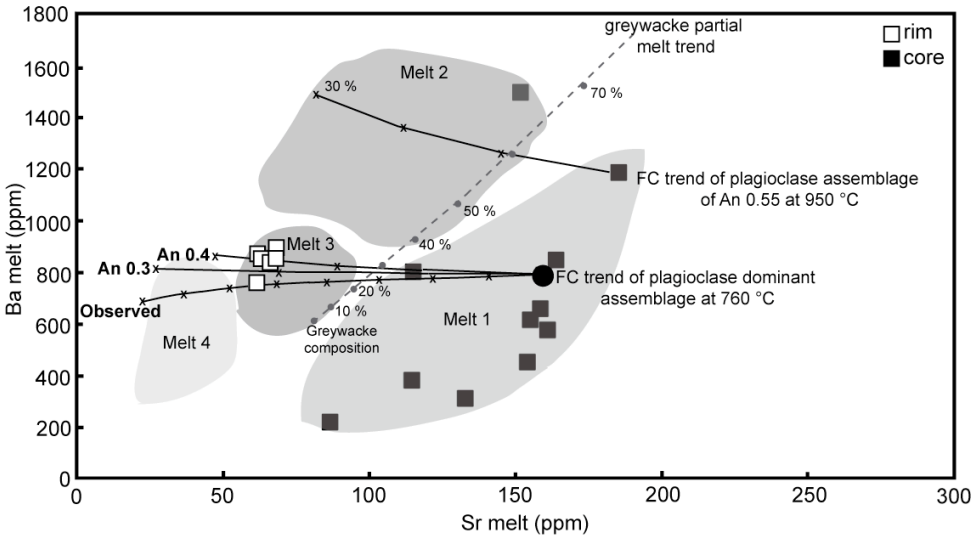

Figure 4.9. Fractional crystallisation model for the generation of Group 1 rim Sr and Ba melt compositions (Melt 3) from the calculated Sr and Ba melt composition of Group 1 cores (Melt 1) using WH1_h as an example. A crystal assemblage consisting of pure An_{30} or An_{40} plagioclase is modelled and the observed phenocryst assemblage (Table 4.10). Partition coefficients for Sr and Ba are calculated from the relationships of Blundy and Wood, (1991) and a magmatic temperature of 760°C for An_{30} and An_{40} assemblage. Partition coefficients for the observed assemblage are given in Table 4.10. Crosses mark every 10% of fractional crystallisation from the parental composition (black circle) of 160 ppm Sr and 783 ppm Ba and shows that a plagioclase dominate crystal assemblage of $An_{30\text{-}40}$ could generate the Group 1 rim compositions after only 10-20 % crystallisation, in comparison to the observed crystal assemblage which requires 40-55 % crystallisation. Also shown is a possible fractional crystallisation trend illustrating the generation of Melt 2 compositions from a parental Group 1 core melt composition of 185 ppm and 1179 ppm of Sr and Ba respectively at high magmatic temperatures of 950 °C. The crystal assemblage is dominated by plagioclase with a composition of An_{55} (as observed in Group 1 cores) and partition coefficients are calculated from the relationships of Blundy and Wood (1991). A greywacke partial melt model (dark grey dashed line) from Reid (1982) is also shown and suggests Melt 2 could be produce by a 40-65 % greywacke partial melt.

The source of Melt 2 is somewhat ambiguous, but lies on a vector parallel to a possible greywacke partial melt, calculated from the greywacke partial melt model from Reid, (1982) or at least a melt generated from a progenitor greywacke partial melt (Figure 4.9). An alternative origin for this melt is through the fractional crystallisation of a crystal assemblage dominated by plagioclase at high (950 °C) magmatic temperatures from a progenitor core melt (Figure 4.9).

Irrespective of the source of Melt 2, the presence of this melt as a thin overgrowth mantling the core in several crystals suggests a magma mixing event, that may not necessarily have been chamber wide occurred prior to the substantial crystallisation of Group 1 rims.

Modal %	plag	opx	qtz	ilm	mag	k-feld	amp	bt	Bulk K_i
	24	17.3	20.6	1.7	1.7	7	20.7	7	
Sr	8.46	0.00		0.1	0.01	1.2	0.4	0.3	2.23
Ba	0.86	0.00			0.1	4.9	0.3	7	1.09

Table 4.10. Crystal assemblage of WH1 recalculated to 100% for use with the fractional crystallisation model of Group 1 plagioclase crystals. K_{Sr} and K_{Ba} of plagioclase and orthopyroxene crystals are calculated from the measured Sr and Ba concentrations of Oruanui crystals and glass compositions (Chapter 2). Sr and Ba are assumed perfectly incompatible where no partition coefficients are shown. K_{Sr} and K_{Ba} of amphibole and biotite are from Nash and Crecraft (1985), amphibole and magnetite are from Bacon and Druitt (1988) and ilmenite from Ewart and Griffin (1994). Abbreviations used are: plag = plagioclase; opx = orthopyroxene; qtz = quartz; ilm = ilmenite; mag = magnetite; k-feld = K-feldspar; amp = amphibole; bt = biotite.

4.6.2 Origins of Group 2 plagioclase crystals

The limited compositional variability of Group 2 crystals implies crystallisation from a relatively homogeneous melt. The small oscillations in *An* can be accounted for through either thermal perturbations and/or fluctuations in the

water content of the magma (Ginibre et al., 2002a; Putirka, 2005). Furthermore, the consistency between the composition of the majority of Group 2 crystals and Group 1 rims (Figure 4.4, 4.6) signifies crystallisation from the same or a similar melt body; that is the final melt composition as represented by groundmass glass compositions (Brown, 1994), Melt 3, and denotes Group 2 plagioclases as 'true' phenocrysts (Jerram and Martin, 2008). The only exception being the four analyses at the core of WH3_e, which result in calculated Sr and Ba melt compositions that corresponds with a Melt 2 composition (Figure 4.7). Conversely, as WH3_e is the only Group 2 plagioclase for which trace element data has been obtained for, it is unclear whether it is common for Group 2 crystals to have a core composition of Melt 2 or not.

4.6.3 Origin of Group 3 plagioclase crystals

Group 3 crystals are distinctive with extremely low Sr (280-480 ppm), Mg (19-32 ppm) and *X An* concentrations but similar REE and Pb concentrations to Group 1 and Group 2 crystals (Figure 4.4). The core analysis of crystal WH6_b exhibits elevated La, Eu and Pb concentrations compared to the rim, consistent with either a highly evolved igneous or greywacke protolith. Reported *An* compositions of greywacke plagioclase crystals indicate two plagioclase populations of An_{40-50} and An_{0-10} in the Waipapa terrain and a single plagioclase population of An_{0-10} in the Torlesse terrain (Reid, 1982), precluding a greywacke protolith origin. Furthermore, an igneous origin is probable as the calculated Sr and Ba melt compositions of Group 3 crystals partially overlap the Sr and Ba concentrations of quartz-hosted melt inclusions that are interpreted to originate from a mature crystal mush body (Chapter 2) and the calculated melt trend

overlap and trends towards granitic compositions (e.g. Walker et al., 2007; Wiebe et al., 2007). Therefore it is interpreted that Group 3 crystals are antecrysts derived from a mature and highly evolved crystal mush body, possible formed through the extreme fractional crystallisation of progenitor andesitic melts (see above discussion on fractional crystallisation of Group 1 core and rim melts). It is also noted that there is an increase in compatibility of Sr and Ba in Group 3 plagioclase crystals compared to Group 1 and 2 plagioclases and this change in compatibility of elements could contribute to the low Sr and Ba melt concentrations recorded by Group 3 plagioclase crystals. Due to the low abundance of K-feldspar and biotite crystals observed in the Whakamaru magma, it is speculated that these crystals may also be potentially inherited from this crystal mush body. The timing and growth of crystals from the various melts in summarised in Figure 4.10.

4.6.4 *Origin of quartz crystals*

The origin of quartz crystals is more difficult to decipher. We can infer the existence of at least two populations or two discrete evolutional pathways for quartz crystals from the presence of bright CL rims and those crystals with oscillatory-zoned rims. However, little can be interpreted about the early history of these crystals. The observed bright CL rims (e.g. WH1_37, WH2_3) mantling dissolution surfaces indicates mixing into a hotter magma prior to the renewed growth. One possible source for the ‘cores’ of these crystals is a mature crystal mush body as indicated from the melt inclusion compositions (Chapter 2). In contrast, the second group of quartz crystals with dominantly oscillatory-zoned

rims may indicate growth from a magma that experienced multiply small recharge events leading to renewed quartz growth.

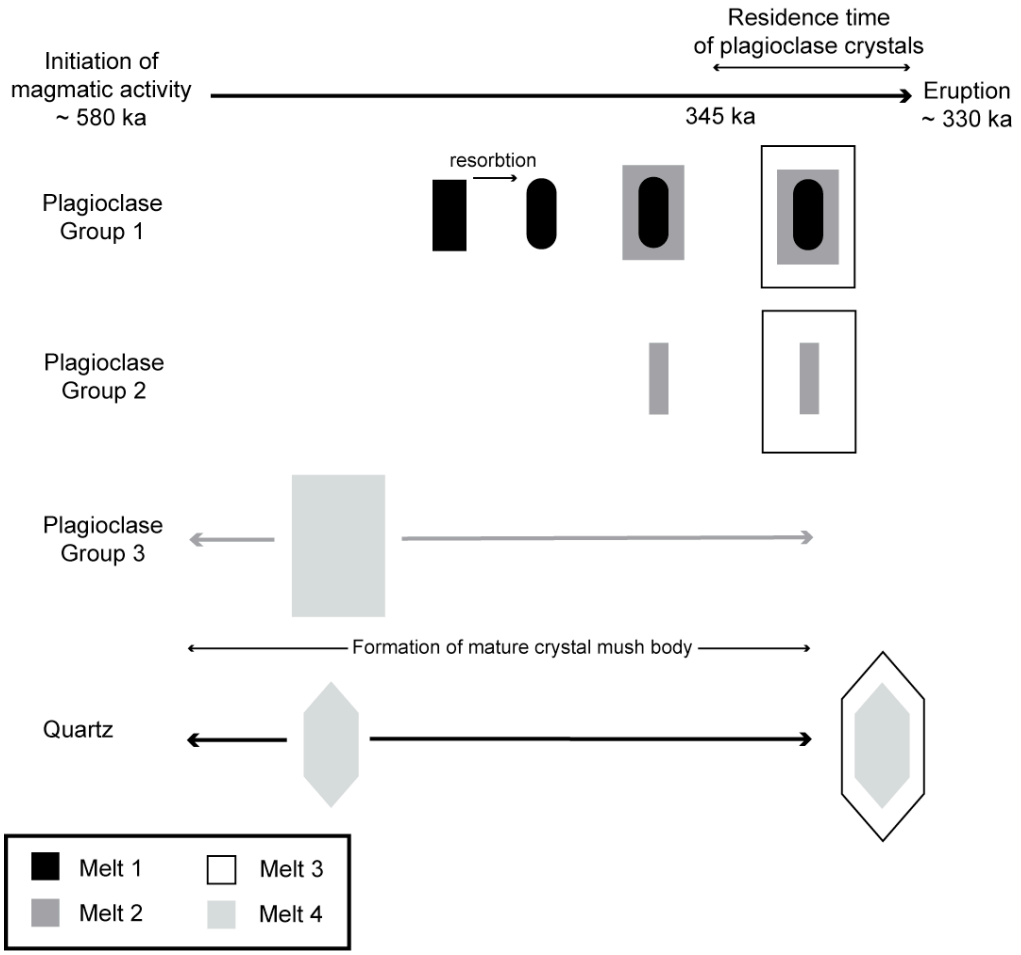

Figure 4.10. A cartoon summarising the timing and growth of Whakamaru plagioclase and quartz crystals studied. Initiation of the magmatic system is assumed to occur 250 ka prior to the eruption from zircon chronology (Brown and Fletcher, 1999). The timing for the growth of Group 3 plagioclase crystals and the quartz cores is unknown, but is speculated to occur during the earlier stages of the magmatic evolution. The timing of the growth of plagioclase and quartz rims are constrained through Sr diffusion and greyscale intensity of CL images, respectively.

4.7. Petrogenesis of the Whakamaru magma

The formation of the Whakamaru magma system commenced at least 250 ka prior to the catastrophic eruption (Brown and Fletcher, 1999). However, evidence indicates the assembly of the magma chamber only occurred in the

15,000 years (Table 4.8) preceding the 330 ka eruption. The assembly of the final Whakamaru magma body was not simple but entailed the mixing and mingling of magmas from multiple sources that varied temporally and spatially within the magmatic system. It is perceived that the earliest history of the magmatic system involved fractional crystallisation of, and assimilation of greywacke country rock by, mantle-derived magmas that eventually formed mature, highly-evolved crystal mush bodies that would later supply Melt 4 compositions to the Whakamaru magma. However, it is speculated that with continued magma supply, further generation of crystal-rich magmas transpired, generating proto-mush bodies (Melt 1) that are witnessed at the surface as high-Si crystal rich andesites (e.g. Price et al., 2005). It is such magma bodies that provide a 'crystal nursery', generating the cores observed in Group 1 plagioclase crystals (Figure 4.11).

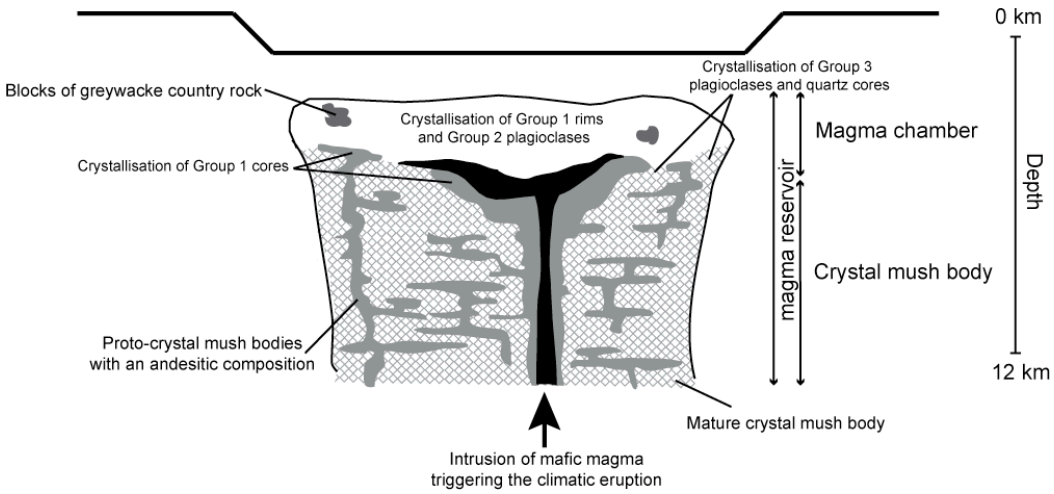

Figure 4.11 Cartoon of the sub-volcanic Whakamaru magma chamber summarising the petrogenetic model discussed in the text. Depths of magma reservoir are estimated from Harrison and White (2004) and are consistent with estimated depths from the initial H_2O contents of quartz-hosted melt inclusions (Chapter 3).

At the magmatic conditions observed in the Whakamaru magma (low temperature, high Si), pressure exerts little control over the *An* composition of plagioclase crystals (Putirka, 2005). During ascent, however, the change in pressure can explain the resorbed and/or rounded texture of Group 1 cores (e.g. Nelson and Montana, 1992; Berlo et al., 2007). It is, therefore, unlikely that the ascent of the magma body can account for change in *An* composition between Group 1 plagioclase cores and rims. Plagioclase stability is controlled by the water saturation of the melt and the degree of plagioclase crystallisation increases at low partial pressures of water at shallow levels (Blundy et al., 2006; Berlo et al., 2007). We interpret the overwhelming dominance of Group 2 crystals combined with the coherent Group 1 rim compositions as evidence for a dramatic increase in the amount of plagioclase crystallisation (Berlo et al., 2007). This increase in plagioclase fractionation is driven by the intersecting of the plagioclase liquidus at shallower levels (Berlo et al., 2007) due to the degassing of water previously dissolved in the interstitial liquid, as this liquid is expelled from the andesitic proto-mush body into the overlying magma chamber. Further crystallisation of plagioclase follows but in insufficient proportions to generate a new crystal mush zone. Prior to this, the crystallisation of plagioclase is suppressed due to the high H_2O concentrations of the andesitic proto-mush body generated from the extreme fractional crystallisation required to generate this magma body. Concurrently, the crystal mush body provide heat to the surrounding greywacke country rock assimilating rocks and generating the third melt composition (Melt 2).

It is the amalgamation of these melts in varying proportions combined with fractionation crystallisation that generates the final Whakamaru melt compositions. The relative abundance of greywacke melts (Melt 2) observed in plagioclase crystals and Group 3 plagioclases derived from mature crystal mushes (Melt 4) indicate these melts contribute in much smaller proportions than the andesitic progenitor melt (Melt 1) (Figure 4.11). This can be further investigated by considering the oxygen isotope composition of each of these proposed melts and a hypothetical oxygen isotope composition of the mature crystal mush body (Melt 4). Oxygen isotopic studies indicate that rhyolites have a mean $\delta^{18}O \sim 7.9\text{-}8.0$ ‰ compared to basalts of $\delta^{18}O \sim 6.4$ ‰, andesites of $\delta^{18}O \sim 7.7$ ‰, and greywacke with $\delta^{18}O$ of ~ 12 ‰ (Blattner and Reid, 1982; Reid, 1982). If, as postulated, the mature crystal mush body (Melt 4) was generated through fractional crystallisation from mantled-derived mafic magmas and assimilation of greywacke country rock without further petrogenetic modification, it is reasonable to assume this melt would have a $\delta^{18}O$ similar to the Taupo Volcanic Zone rhyolites. Therefore, assuming the observed proportions of plagioclase crystals represent the quantity of melt incorporated from each source, a simple mass balance calculation mixing 88 % andesite melt estimated from the abundance of Group 1 and 2 crystals with a 3 % greywacke melt as evident from the high Sr overgrowths on some Group 1 cores and 9 % mature crystal mush melt results in a final $\delta^{18}O$ melt composition of 7.9 ‰ consistent with the measured $\delta^{18}O$ of 7.8 ‰ of the Whakamaru ignimbrite (Blattner and Reid, 1982).

The zonation of plagioclase and quartz crystals and residence times of Group 1 plagioclases imply that the mixing of these magmas occurred continually until the final eruption. Moreover, diffusion modelling of CL intensity of quartz crystals provides evidence that the final quartz growth occurred < 80 years prior to the catastrophic eruption. We speculate that this is likely to be due to the intrusion of a hot mafic magma into the base of the magma chamber as evidenced by the elevated magmatic temperatures calculated from Fe-Ti oxide thermometry and the rounded nature of plagioclase crystals indicating they are actively resorbing as the eruption commenced. Additionally, Brown et al. (1998a) observed high-alumina basalt, as both mixed pumices and as basaltic scoria indicating the presence of such a magmatic composition existed in the Whakamaru magma prior to eruption. Hornblende crystals present within the mixed pumices are euhedral, indicating the mixing of basaltic and rhyolitic magmas transpired immediately prior or during eruption (Brown et al., 1998a). Intrusion of mafic magmas into silicic magma bodies is commonly implied to trigger volcanic eruptions (e.g. Pallister et al., 1992; Synder, 2000; Ginibre et al., 2007; Martin et al., 2008). In small magmatic systems that cannot buffer the incoming magma volume this recharge can cause almost immediate eruption (e.g. Ginibre et al., 2007; Martin et al., 2008) while in larger systems there may be a response delay or no eruption at all. Large density contrasts exist between the mafic and silicic magmas and this prevents the substantial mixing of these melt bodies, but promotes the exsolution of volatiles that are then free to diffuse through the overlying magma, heating as it goes (Synder, 2000; Bachmann and Bergantz, 2003; Wark et al., 2007). Therefore, it is conceivable that the time elapsed since the renewed quartz growth preserves a record of the time delay

required for sufficient secondary processes to transpire in order to trigger the Whakamaru eruption.

4.8. Conclusions

Chemical and textural zonation of plagioclase and quartz crystals provides evidence of four distinct rhyolitic melt bodies fuelling the generation of the final Whakamaru supereruption. The magmatic evolution occurred over a period exceeding 250 ka (Brown and Fletcher, 1999), however, Sr diffusion modelling of core-rim interfaces of Group 1 plagioclase crystals indicate that melt-dominant magma chambers bodies may be an ephemeral feature or at the least form relatively shortly prior to eruption in timeframes of < 15,000 years. In contrast, diffusion modelling of bright CL rims of quartz crystals details the initiation of renewed quartz growth < 80 years prior to eruption implying mixing of magmas continued until the climatic eruption.

Chapter 5

Crystal specific studies of Healy and Taupo eruptives: insights into the petrogenesis of silicic arc magmas

Abstract

The petrogenesis of silicic arc magmas from the oceanic Kermadec Arc (Healy seamount) and continental Taupo Volcanic Zone (1800 BP Taupo eruption) is examined here through the major element zonation of plagioclase crystals. Healy plagioclase crystals display limited fluctuating anorthite concentrations of 40 - 50 mol %, dissolution interfaces and rare high anorthite cores. In contrast, Taupo plagioclase crystals possess both low (35 - 38 mol %) and high (48 - 50 mol %) anorthite cores mantled by rims with 35 - 40 mol % anorthite. Application of plagioclase-melt equilibria illustrates that anorthite variability in both Healy and Taupo plagioclase crystals can be achieved through a combination of fractional crystallisation and the cryptic mixing of chemically similar magmas, indicating the same petrogenetic processes occur in both oceanic and continental arc magmas. In addition, water and chlorine concentrations of plagioclase-hosted Healy melt inclusions provide evidence for the degassing of the Healy magma prior to eruption.

5.1 Introduction

Healy seamount is the most silicic submarine caldera yet documented in the southern Kermadec Arc, and is characterised by pumices of dominantly rhyodacitic compositions (Wright and Gamble, 1999). The ubiquitous occurrence of these highly vesiculated pumices mantling the topography of the volcanic edifice, allied with the presence of a ~ 3 km wide, flat-floored, caldera has

provided compelling evidence for a single subaqueously quenched pyroclastic eruption (Wright and Gamble, 1999; Wright et al., 2003).

In contrast, Taupo Volcano in the continental Taupo Volcanic Zone has been active for > 40 kyr with numerous silicic eruptions recognised prior to and after the 26.5 ka Oruanui supereruption (Wilson and Walker, 1985; Sutton et al., 1995; 2000; Wilson et al., 2006; Charlier et al., 2005, 2008). Since the Oruanui supereruption, 28 eruptions have occurred from the Taupo volcano, in three distinct periods (11.8 - 9.5 ka; 7.05 - 2.75 ka; 2.15 - 1.74 ka) with the 1800 BP Taupo eruption being the largest of these (Sutton et al., 2000). Whole rock and mineralogical studies have detailed compositional and isotopic variability between these three eruptive periods and the Oruanui eruption, providing evidence for short repose intervals and the complete reorganisation of the magmatic system beneath Taupo volcano (Sutton et al., 2000; Wilson et al., 2006).

The petrogenesis of Healy and Taupo silicic magmas was examined through a chemical study of plagioclase- and orthopyroxene- hosted melt inclusions (Chapter 2). These geochemical data demonstrate that Healy silicic melt was generated through extensive fractional crystallisation from a mantle-derived basalt parent consistent with a study of volcanic glasses from the neighbouring Brothers volcano (Haase et al., 2006). In comparison, the major, trace and volatile element concentrations of orthopyroxene- and plagioclase- hosted Taupo melt inclusions demonstrates an origin through extensive fractional crystallisation and assimilation of greywacke country rock (Chapter 2).

Here, additional geochemical evidence in the form of major element zonation of Healy and Taupo plagioclase crystals are presented together with the water concentrations of Healy melt inclusions. These data provide further insight into the petrogenesis of silicic magmas in continental and oceanic silicic arc magmas. Analytical methods and samples are described fully in the previous chapters and are only summarised here.

5.2 Results

5.2.1 Volatile concentrations of Healy melt inclusions

Orthopyroxene- and plagioclase- hosted melt inclusions were previously analysed for Cl and SO_3 by electron probe microanalysis (EPMA) (Chapter 2). In addition, H_2O and CO_2 contents for a selection of plagioclase-hosted melt inclusions were analysed by Fourier Transform Infrared Mass Spectrometry (FTIR) using the methods described in Appendix A.1.5 (Table 5.1).

Chlorine ranges between 0.33 - 0.66 wt%, displaying a negative trend with increasing SiO_2 (Figure 5.1; Appendix 3, Table A3.1; A3.2), and Cl concentrations in plagioclase and orthopyroxene hosts overlap. This is consistent with either fractionation of a Cl-rich mineral such as apatite or the degassing of Cl from a continuously cooling melt. Apatite is observed as inclusions in all crystal phases (Wright et al., 2003), however, rare earth elements compatible in apatite display positive trends with SiO_2 (e.g. Figure 5.1) suggesting apatite crystallisation was not the central process controlling the evolution of Cl in the

Sample	MI thickness (μm)	H_2O_m (wt%)	OH^- (wt%)	H_2O_t (wt%)	A5200 mm^{-1}	A4500 mm^{-1}	pH_2O (M Pa)	Depth (km)	CO_2 detection limits (ppm)
X590-15.1	71	2.41	1.69	4.10	0.585	0.329	92.5	3.08	24
X590-16.1	55	3.02	0.91	3.93	0.721	0.184	85.4	2.81	32
X590-16.2	44	3.81	0.91	4.72	0.933	0.171	120	4.13	40
X590B-15.1	27	3.35	1.22	4.56	0.813	0.238	112	3.85	64
X590B-15.2	21	3.20	1.30	4.50	0.776	0.255	110	3.74	83
X590B-15.3	18	2.77	1.35	4.12	0.672	0.264	93.3	3.11	97
X590B-15.4	18	2.38	1.31	3.69	0.578	0.256	75.9	2.45	97
X590B-16.1	69	2.00	0.83	2.83	0.485	0.163	46.5	1.34	25
X590B-16.2	24	3.35	1.73	5.07	0.813	0.338	137	4.77	72
X609-1 1.1	48	1.38	0.17	1.56	0.323	0.104	15.6	0.17	36
X609-1 2.1	31	0.00	0.00	2.82	0.929	0.161	46.2	1.33	56
X690-20 1.1	31	3.15	0.93	4.08	0.758	0.252	91.6	3.04	56
X609-25.1	35	2.74	0.64	3.38	0.662	0.126	64.5	2.02	50
X609-25.2	20	2.66	0.79	3.45	0.645	0.155	67.0	2.11	87

Table 5.1. Measured water speciation of plagioclase hosted Healy melt inclusions. Analytical methods, methods for calculation of H_2O concentrations and CO_2 detection limits are given in Chapter 3. pH_2O (partial pressure of water) is calculated using VolatileCalc (Newman and Lowenstern, 2002) and a magmatic temperature of 726 °C (see text). Depths are calculated assuming a bulk crustal density of 2700 Kg/m^3 (Case et al., 1973) and assuming an overlying water pressure of 11 MPa. A5200 mm^{-1} and A4500 mm^{-1} are the absorbance peak per mm for the 5200 cm^{-1} and 4500 cm^{-1} peaks respectively. Abbreviations: MI = melt inclusions H_2O_m = molecular water; OH^- = hydroxyl; H_2O_t = total water.

melt. Experiments have shown that Cl is partitioned into co-existing hydrous fluids only after H_2O saturation is attained (Cline and Bodnar, 1991; Sun et al., 2007), thus providing evidence for H_2O saturation of the magma and indicating that Cl is degassed from Healy melts.

Total H_2O concentrations of Healy melt inclusions range from 1.56 - 5.07 wt% (Figure 5.2) and CO_2 is below detection limits (Table 5.1). Similar trends in measured water speciation are observed in Healy melt inclusions (Figure 5.2) as are displayed in Whakamaru and Taupo melt inclusions (Chapter 3). Thus, as the speciation does not form coherent linear trends parallel to the experimentally determined speciation curves (e.g. Ihinger et al., 1999) it is highly probable that

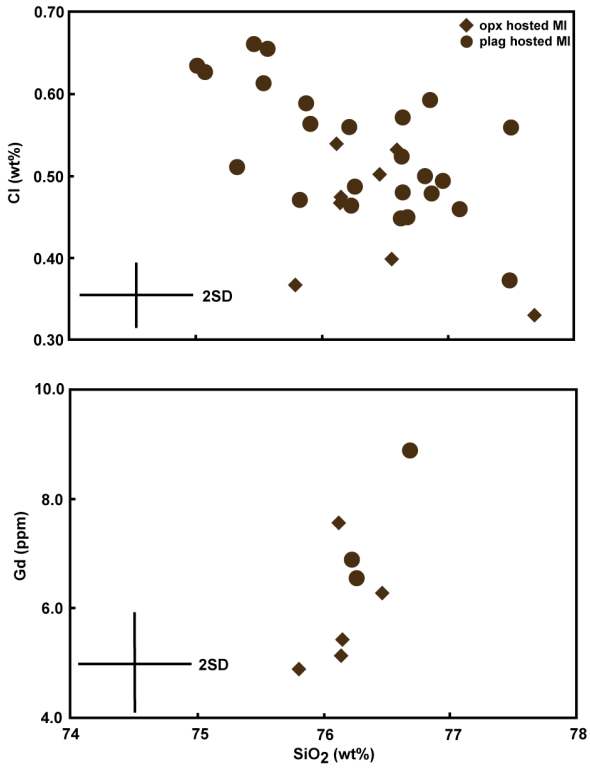

Figure 5.1. Cl and Gd concentrations of Healy melt inclusions plotted against SiO_2 as a fractionation index. Orthopyroxene hosted inclusions are shown as diamonds and plagioclase hosted inclusions as circles. opx = orthopyroxene; plag = plagioclase.

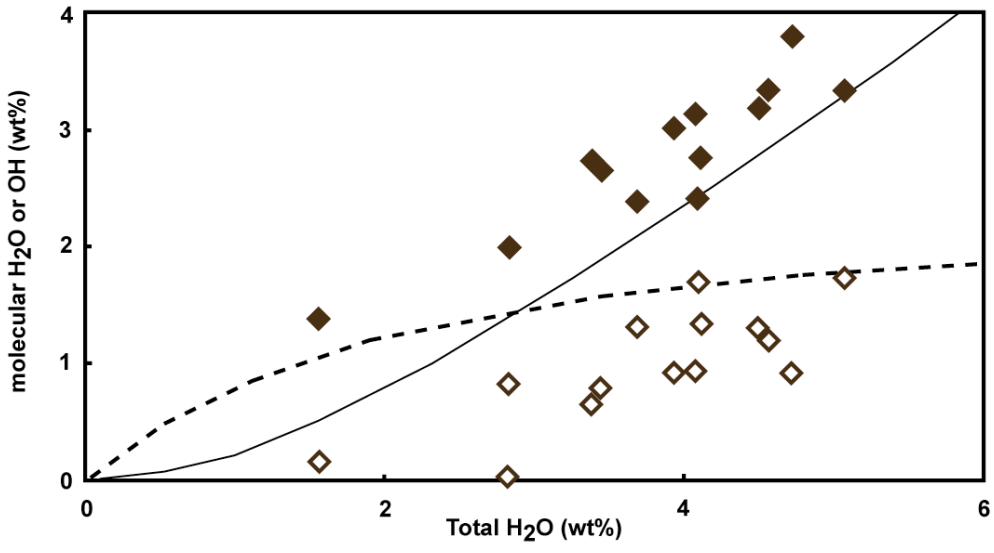

Figure 5.2. Measured water speciation of Healy melt inclusions. Filled symbols are molecular H_2O and open symbols OH^- concentrations. Speciation curves for molecular H_2O (solid line) and OH^- (dashed line) are shown for magmatic temperature calculated using VolatileCalc (Newman and Lowenstern, 2002).

Healy melt inclusions have degassed through diffusion of H_2O with the external melt prior to quenching and preserve only a record of magmatic water concentrations directly prior to eruption (see Chapter 3 for a full discussion on the water speciation and degassing of rhyolitic melt inclusions). The partial pressure of water (pH_2O) from melt inclusions was calculated using the VolatileCalc algorithm of Newman and Lowenstern (2002) and an inferred minimum depth of crystallising magma attained assuming H_2O saturation (Table 5.1).

5.2.2. Major element composition of plagioclase crystals

Despite the evidence from melt inclusions for the generation of the Healy and Taupo magmas through extreme fractional crystallisation (and assimilation) processes (Chapter 2), phenocrysts are sparse and rarely exceed 5 percent volume (Sutton et al., 1995; Wright et al., 2003). The most prolific phenocryst phase is plagioclase, which forms euhedral grains approximately 0.5 - 1.0 mm in size.

Backscattered electron images of 28 Healy and 37 Taupo plagioclase crystals were acquired. Major element profiles across 12 Healy plagioclases from three samples (X590, X590B and X609; Table 2.1; Figure 5.3; Table A3.9; Figure A4.4) and 14 Taupo plagioclases from the Taupo ignimbrite (TA2) and associated crystal lag (TA1), Taupo Plinian (TA3) and Hatepe Plinian (TA4) were performed by EPMA using the methods described in Chapter 4 (Figure 5.4; Table A3.10; Figure A4.5).

Symmetrical oscillatory zoning ca. 5 - 50 μm in width is observed in all Healy plagioclase crystals and dissolution interfaces are common (Figure 5.3). However, anorthite (*An*) variations are limited and oscillate between An_{40} and An_{50} with only one example of a high-*An* core (X590Ba) observed. In contrast, Taupo plagioclase crystals display subtle zoning ranging from 5 - 100 μm in width of $An_{35\text{-}40}$ and notable cores in numerous crystals. However, with the exception of TA3_q, resorption textures are rare (Figure 5.4). Two core types are identified: (1) rounded low $An_{35\text{-}38}$ cores mantled by an abrupt interface followed by high $An_{38\text{-}40}$ rims (e.g. TA1_a and TA1_d); (2) sub-euhedral high $An_{ca.\ 48\text{-}50}$ cores surrounded by normal zoning (denoted by FC in Figure 5.4) and low $An_{35\text{-}40}$ rims (e.g. TA1_c).

5.3 Discussion

5.3.1. Pre-eruptive magmatic water concentrations of the Healy magma

The minimum depth of the crystallising magma body prior to eruption can be assessed from the pH_2O of measured water concentrations of melt inclusions (see Chapter 3). This denotes a mean depth of 2.5 km for the Healy magma chamber. However, the initial H_2O concentrations most likely exceed some of the measured values due to: (1) the presence of amphibole in pumices that indicates an initial H_2O content > 4 wt% (Eggler, 1972; Annen et al., 2006), and; (2) the spread in measured water speciation (see Chapter 3). Water estimates determined through plagioclase-melt equilibria (Appendix 3, Table A3.9) (Putirka, 2005) and conservative initial estimates taken as the maximum measured water content indicate magmatic water estimates of 5.1 - 8.8 wt% for the time plagioclase and orthopyroxene crystals fractionated from the melt (see Chapter 3 for full

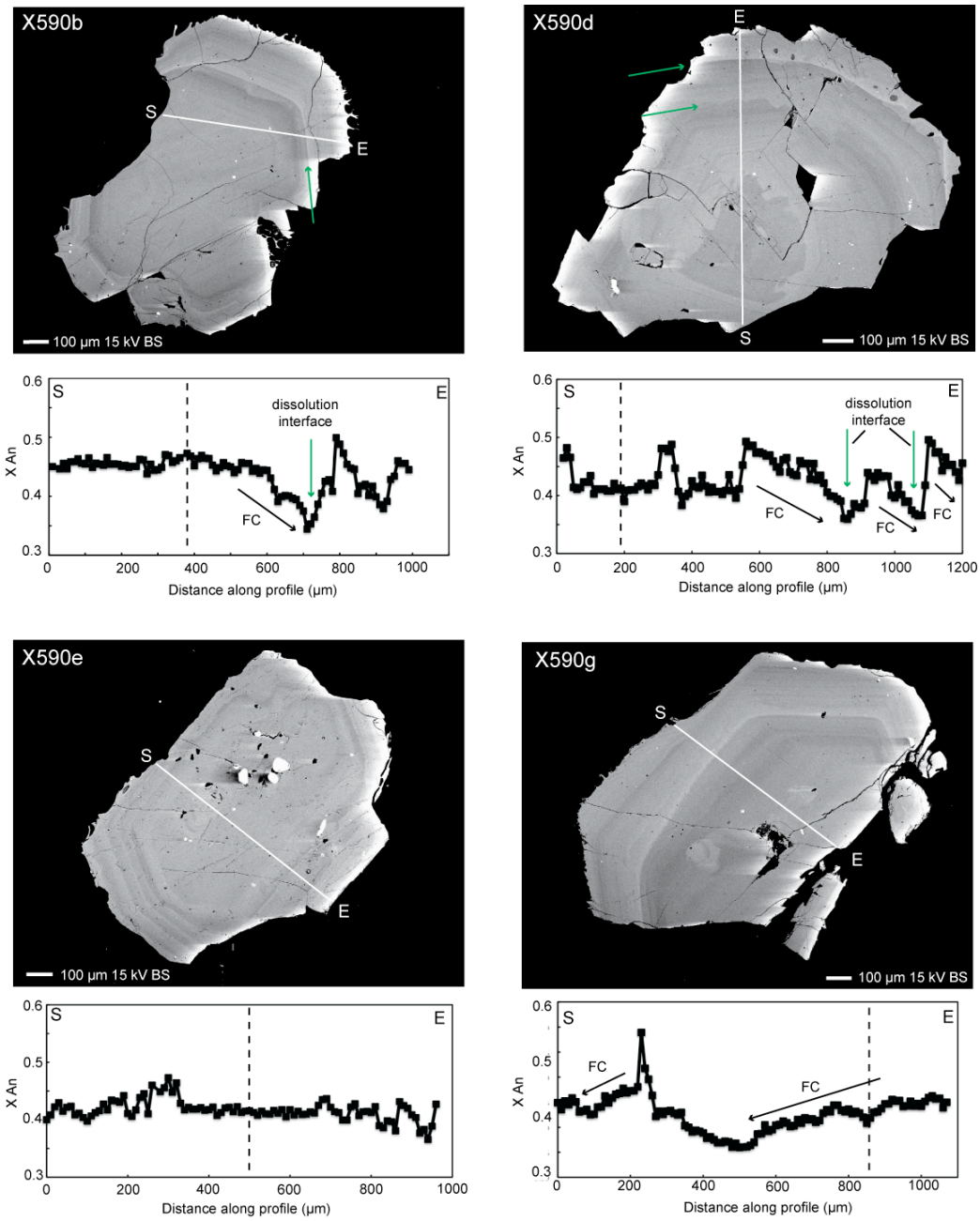

Figure 5.3. Backscattered electron images of Healy plagioclase crystals and anorthite (X_{An}) profiles. Start (S) and end (E) of profiles are shown and correspond to the start and end of anorthite profiles and dashed vertical lines, the core of the crystals. Several examples of dissolution surfaces are highlighted by green arrows. FC denotes zones of normal *An* zoning.

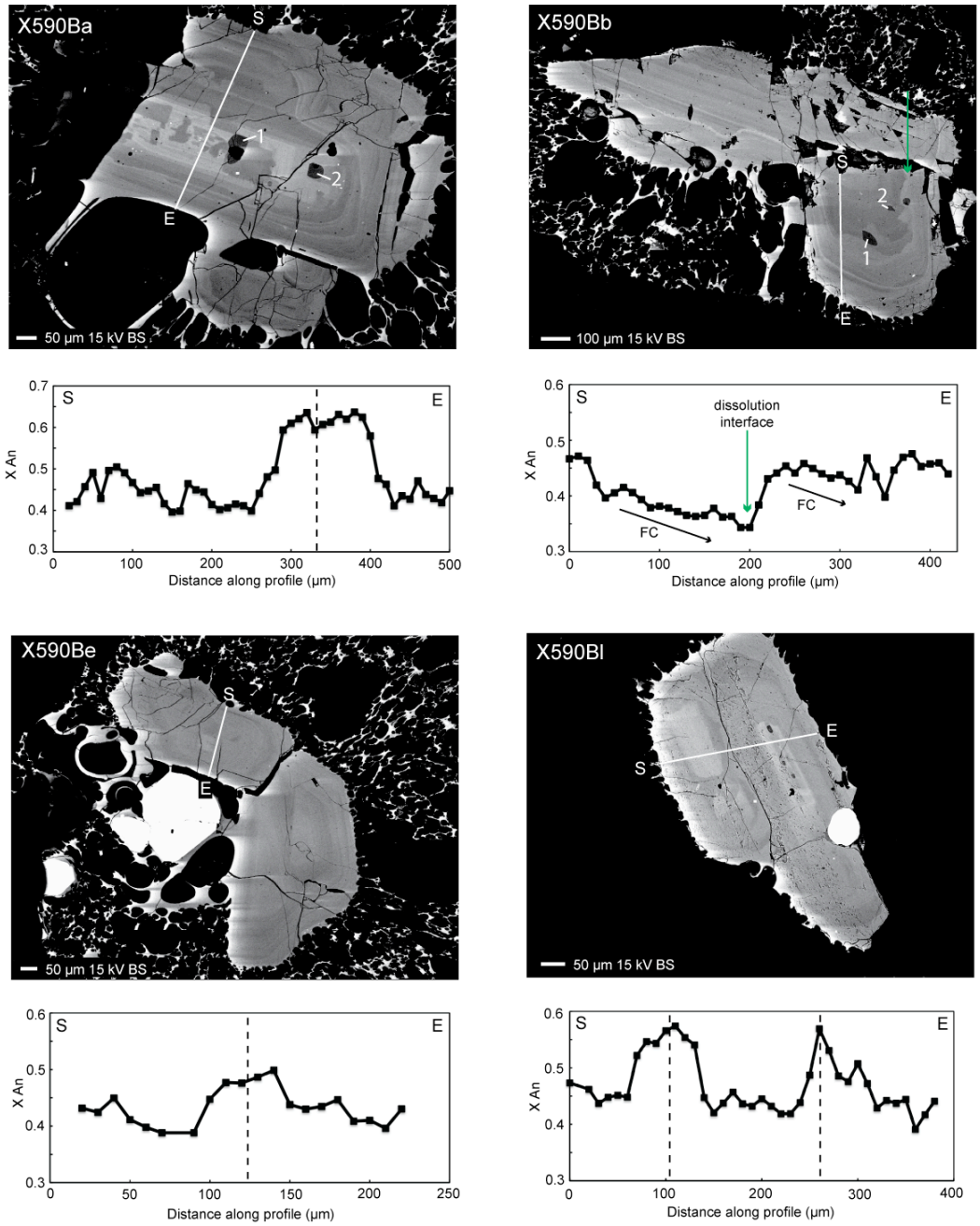

Figure 5.3 continued.

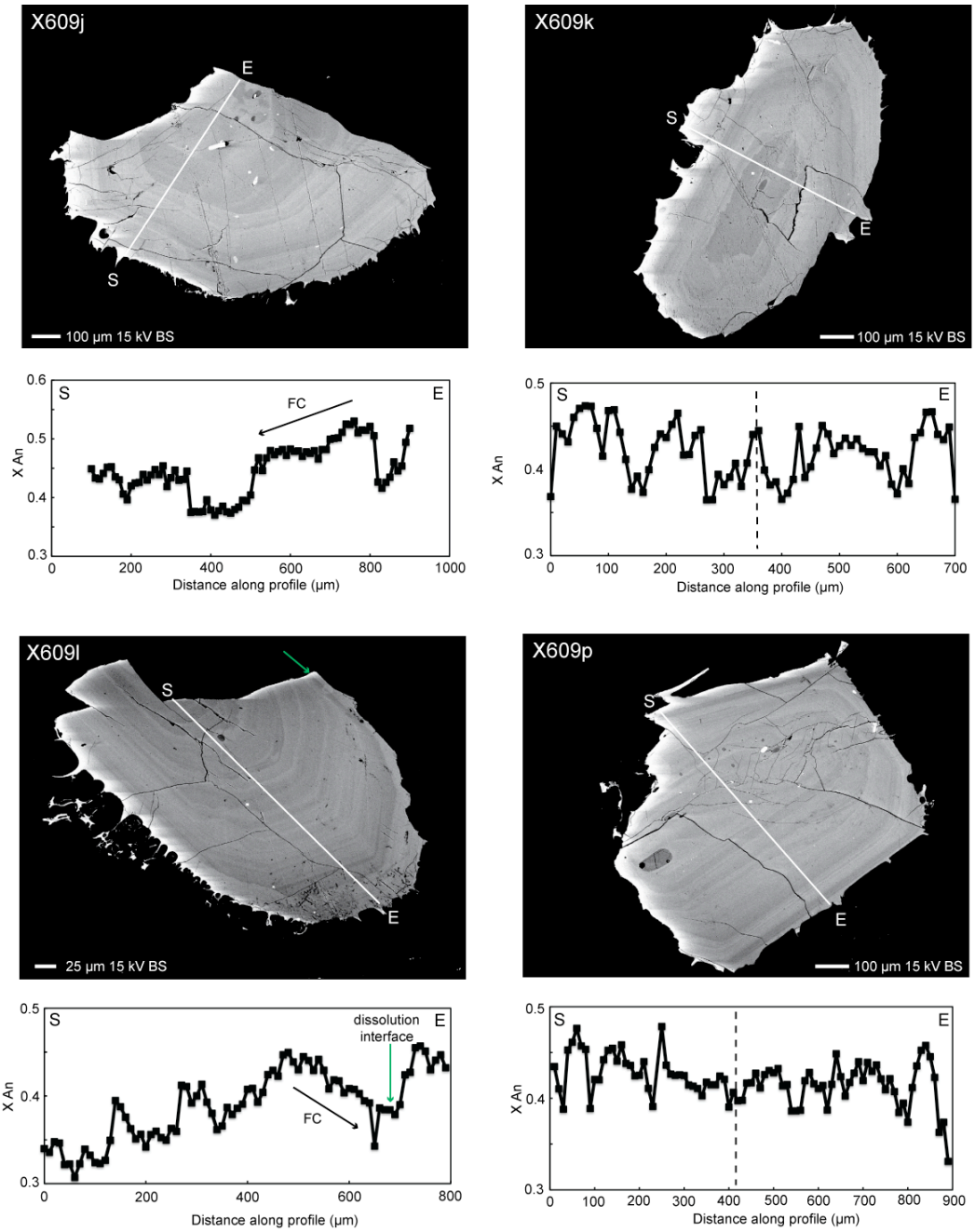

Figure 5.3 continued.

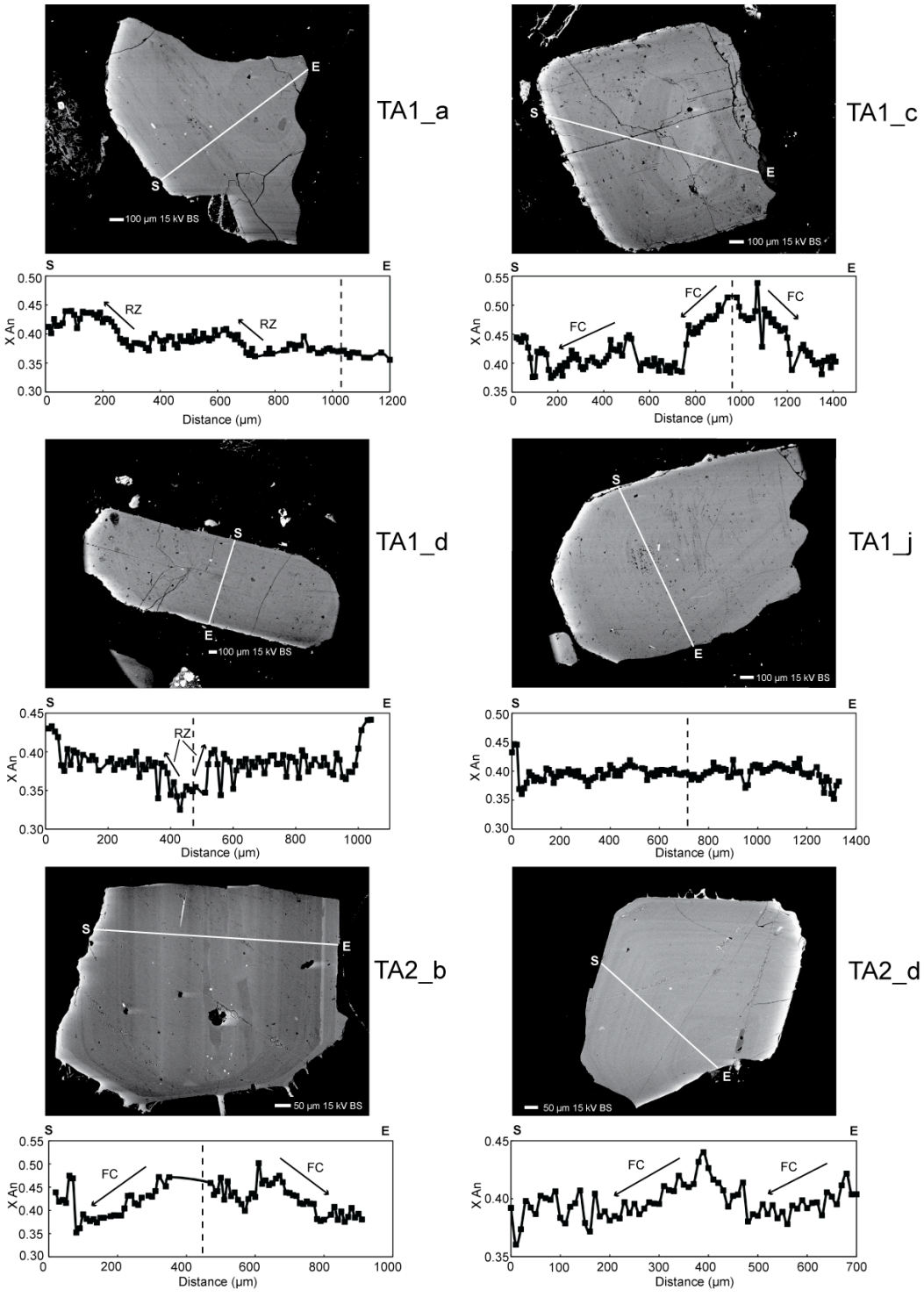

Figure 5.4. Backscattered electron images of Taupo plagioclase crystals and X_{An} profiles. Start (S) and end (E) of profiles correspond to the start and end of anorthite profiles. Dashed vertical lines represent the core of the crystal. Normal *An* zonation is denoted by FC and reverse *An* zoning by RZ.

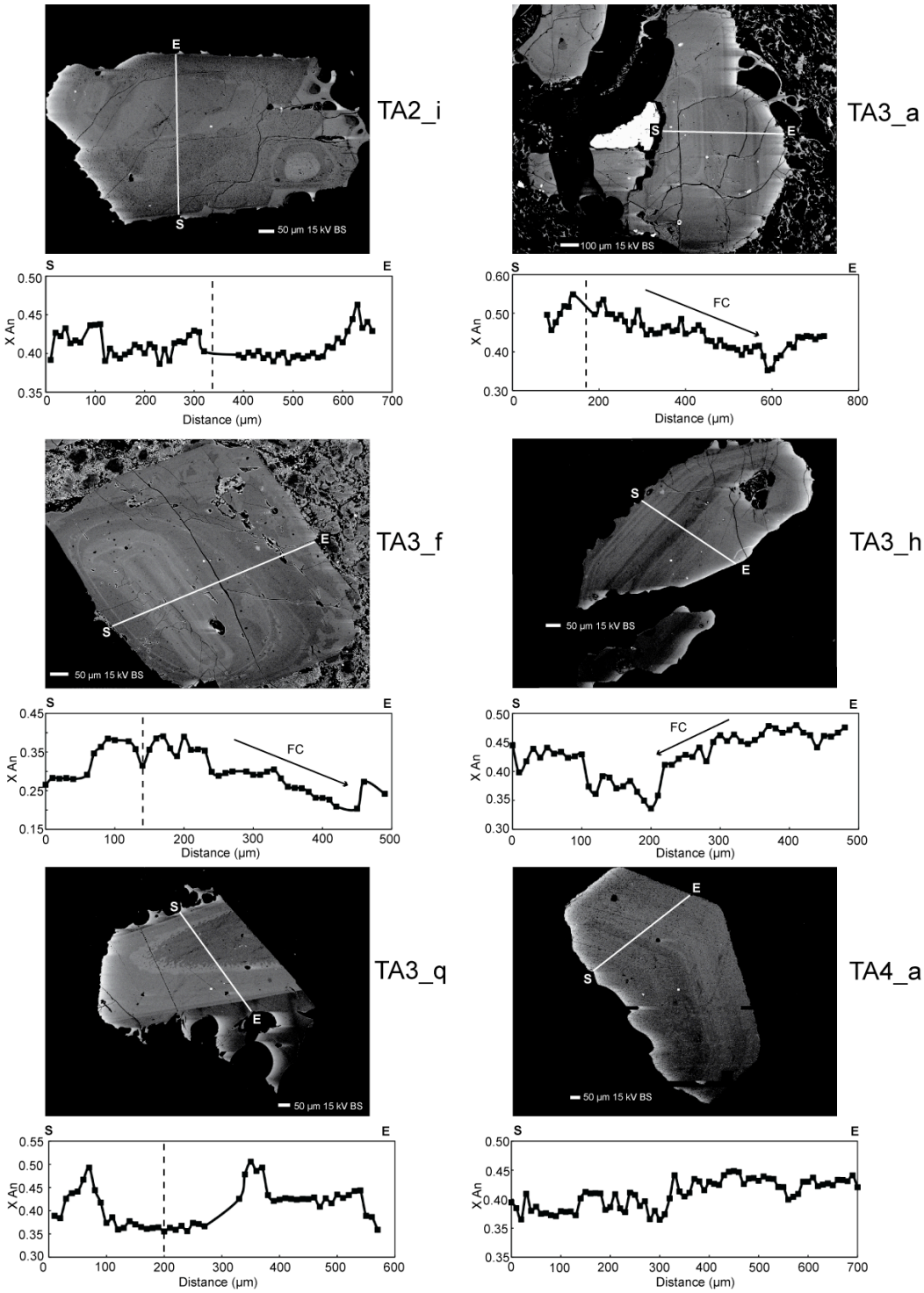

Figure 5.4 continued.

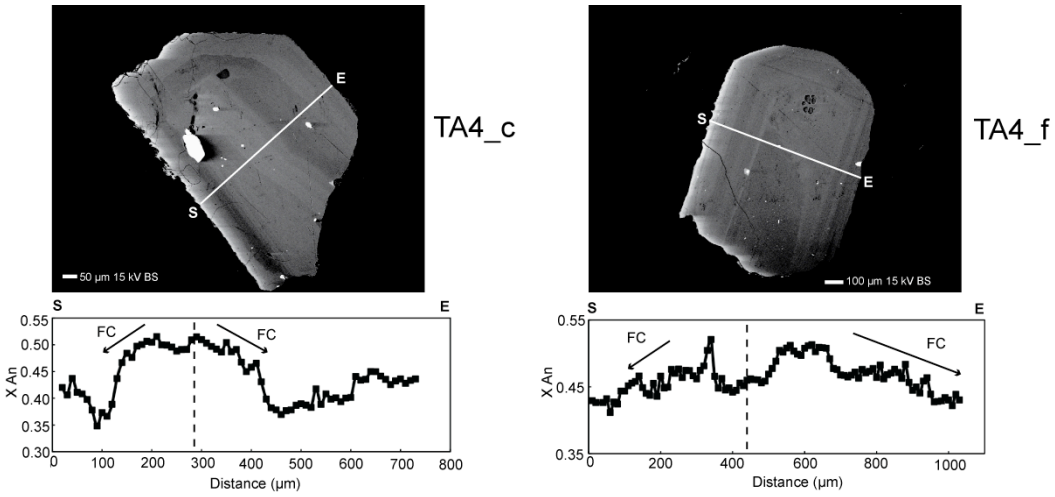

Figure 5.4 continued.

discussion) and infer a former depth of ca. 5.2 - 12.3 km for the crystallising magma. This is consistent with the estimated crustal thickness of 16 km as cited by Haase et al. (2006) from Shor et al. (1971).

5.3.2 Magmatic temperature and thermal evolution of Healy and Taupo melts

Magmatic temperatures in this study were determined by plagioclase-melt equilibria (Putirka, 2005) using a melt composition obtained from the mean melt inclusion compositions and pressures of 60 and 100 MPa for the Healy and Taupo magmas respectively (Chapters 2 and 3; Table 5.2).

Temperature estimates range between 670 - 750 °C with an average temperature of 725 °C for Healy plagioclases (Appendix 3, Table A3.9) and 655 - 798 °C and a mean temperature of 760 °C for Taupo plagioclase crystals (Appendix 3, Table A3.10).

An average plagioclase-melt temperature of 725 °C for Healy is inconsistent with the magmatic temperature of 950 °C for Healy pumices calculated by two-pyroxene thermometry (Wright et al., 2003). This discrepancy is interpreted to reflect the cooling of the magma body, as it is unlikely these clinopyroxene crystals were in equilibrium with such a high-silica melt. Thus, clinopyroxene crystals could be interpreted as antecrysts (e.g., after Hildreth, 2001 as cited by Charlier et al., 2005 and Jerram and Martin, 2008), fractionated from a progenitor magma that preceded the formation and cooling of the ultimate rhyodacitic magma. Moreover, the prominent rhyolitic compositions of plagioclase- and orthopyroxene- hosted melt inclusions (Chapter 2) are consistent with the lower magmatic temperatures derived from plagioclase-melt equilibria.

In contrast, Sutton et al. (2000) reported Fe-Ti oxides temperatures of 850-860 °C, for the Taupo ignimbrite, which represents the magmatic temperature immediately prior to eruption (Venezky et al., 1999; Couch et al., 2003). This is 90 - 100 °C higher than the mean plagioclase-melt temperature of 760 °C, providing evidence for the heating of the Taupo magma shortly prior to eruption. This would be most readily achieved through the intrusion of mafic magma into the base of the magma chamber, which would trigger the eruption (e.g. Pallister et al., 1992; Sydner, 2000).

5.3.3 Plagioclase zonation

Changes in pressure, temperature, H_2O content or mixing of magmas modify the magmatic composition and result in new plagioclase growth of different *An*

contents. Healy and Taupo plagioclase crystals exhibit regions of normal *An* zoning (illustrated by FC in Figure 5.3 and 5.4). This is where initially Ca-rich plagioclase (high *An*) is crystallised from the melt followed immediately by more Na-rich plagioclase (lower *An*) as the magma differentiates and cools (e.g. Pearce and Kolisnk, 1990; Ginibre et al., 2007). These *An* patterns thus indicates periods of crystal growth during the cooling of the magma and reverse *An* zoning is indicative of changing magmatic conditions, for example magma mixing. The magmatic process(es) responsible for this change in *An* can be deciphered by considering the relative concentrations of minor and trace elements (e.g. K, Fe, Mg, Sr and Ba) that partition into plagioclase crystals during growth, according to well-known partitioning relationships that are not dependent on the melt composition (Longhi et al., 1976; Blundy and Wood, 1994; Bindeman et al., 1998; Ginibre et al., 2002).

Fe concentrations do not vary systematically with *An* content in plagioclases from either the Healy or Taupo eruptions (Figure 5.5; Table A3.9; A3.10). This could provide evidence for a change in pressure, temperature, or H_2O content of the melt rather than magma mixing (Ginibre and Wörner, 2007; Ginibre et al., 2007) but may also reflect an analytical artefact, as the low Fe concentrations of the plagioclase crystals are close to the detection limits of the EPMA. Partitioning of Fe into plagioclase is, however, strongly dependent on the oxygen fugacity of the melt (Longhi et al., 1976; Wilkes and Behren, 1999), and may also be modified further by diffusion after crystal growth. Therefore, Fe concentrations may not provide an accurate representation of the melt composition without further analyses of minor and trace elements to constrain

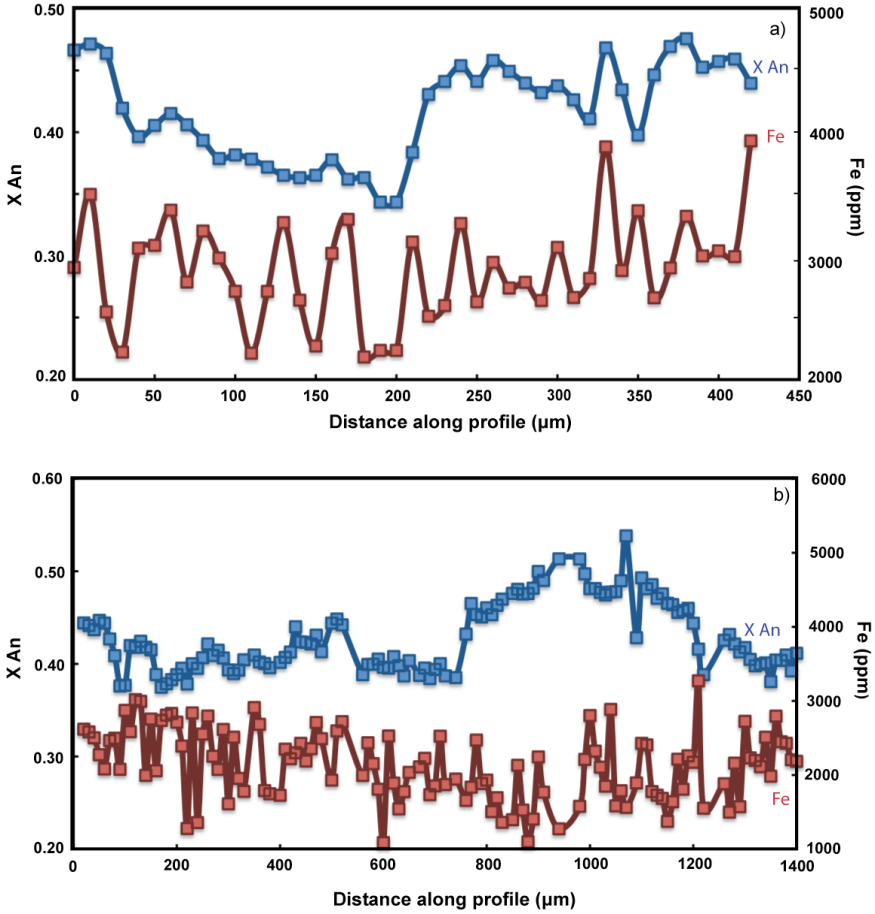

Figure 5.5. Measured *An* and Fe concentrations versus the distance along (a) Healy plagioclase X590Bb and (b) Taupo plagioclase TA1c. Note that Fe concentrations do not vary systematically with *An* content.

the behaviour of Fe in the Healy and Taupo plagioclases. Nonetheless, changes in *An* can be examined through the application of plagioclase-melt equilibria (Putirka, 2005; Humphreys et al., 2006).

The largest changes in *An* in Healy plagioclase crystals are observed at dissolution interfaces and core-rim boundaries (Figure 5.3) and at core-rim interfaces in Taupo plagioclase crystals (Figure 5.4). Melt inclusion compositions on either side of the interface (Figure 5.3; Table 5.2) are indistinguishable providing further evidence for a constant melt chemistry

throughout the crystallisation of this plagioclase crystal. Homogenisation of melt inclusions within the plagioclase crystal is considered unlikely as the major element composition of both plagioclase- and orthopyroxene- hosted Healy melt inclusions are similar (Figure 2.5) indicating the composition of inclusions is not controlled through host-inclusion exchange (Blundy et al., in press). Pressure variations provide negligible change (i.e. <0.02 mol%) in *An* content at these magmatic compositions and temperatures (Putirka, 2005) and indicates that variations in both temperature and H_2O content of the melt are required to account for the observed *An* gradient in Healy and Taupo plagioclase crystals. This is illustrated schematically by taking the dissolution interface in X590Bb as an example. Anorthite increases by 11 mol% across this interface, from An_{34} to An_{45} over 40 μm (Figure 5.3, crystal X590Bb). Both an isothermal melt (at 726 °C), and a melt at a constant water composition (3.7 wt%), are considered but neither could account for the 11 mol% increase in *An* alone (Figure 5.6). In addition, an isothermal melt is inconsistent with the calculated temperatures from plagioclase-melt equilibria that indicates a 42 °C rise across this interface (Appendix 3, Table A3.9) implying changes in both temperature and magmatic H_2O concentrations are required to account for the *An* gradient.

The abundance of normal *An* zoning displayed in Taupo plagioclase crystals (Figure 5.4) implies fractional crystallisation plays a fundamental role in the petrogenesis of the Taupo magma consistent with the modelling of the melt inclusion chemistry (Chapter 2). The presence of both high $An_{48\text{-}50}$ and low $An_{35\text{-}38}$ cores suggests cores are incorporated into the Taupo magma from

	X590Bb_1	X590Bb_2	X590Ba_1	X590Ba_2
SiO_2	80.48	79.12	77.58	77.29
TiO_2	0.26	0.30	0.38	0.36
Al_2O_3	12.43	13.00	13.53	13.34
FeO	1.21	1.70	2.23	2.20
MnO	0.06	0.14	0.20	0.22
MgO			0.42	0.42
CaO	1.37	1.67	1.81	2.00
Na_2O	2.59	2.50	1.53	2.52
K_2O	1.60	1.57	2.17	1.65
Total	100.00	100.00	100.00	100.00

Table 5.2. Measured anhydrous major element composition of melt inclusions in X590Ba and X590Ba. Melt inclusions numbers correspond to the labelled melt inclusions in Figure 5.3. MgO was not analysed for X590Bb.

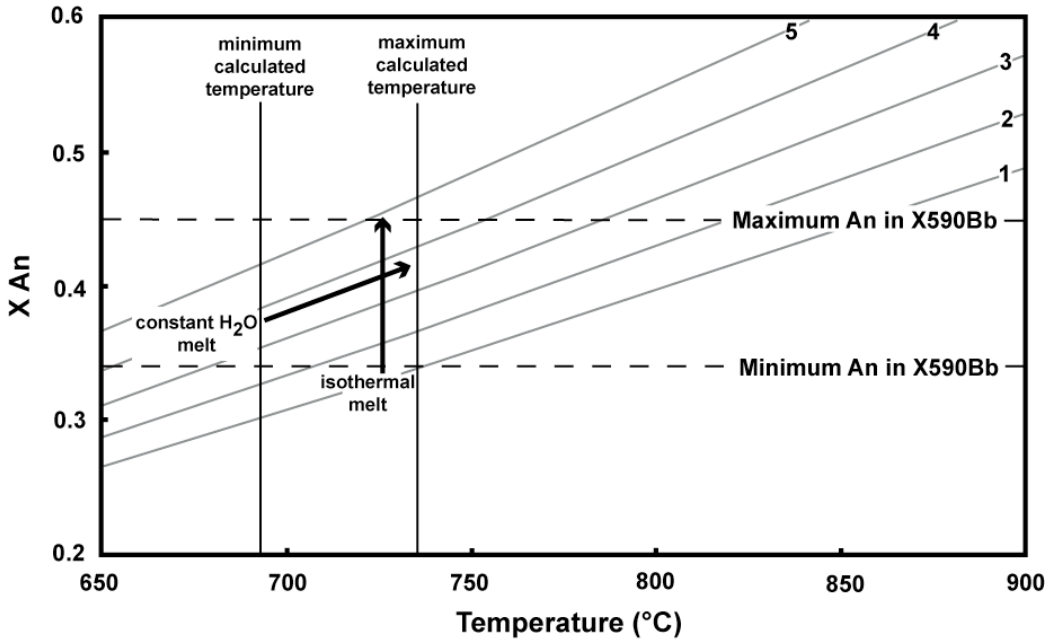

Figure 5.6. Calculated *An* variation of Taupo and Healy plagioclases as a function of temperature and H_2O content, at a pressure of 80 MPa of the melt, using plagioclase-melt equilibria of Putirka (2005). Water content of melt is contoured for 1, 2, 3, 4 and 5 wt%. Illustrated, as an example is the dissolution interface in X590Bb discussed in the text. Dashed lines are the minimum and maximum measured *An* content at either side of the interface. Black lines are the magmatic temperature as calculated by plagioclase-melt equilibria (Putirka, 2005) (Table A3.9). Arrows represent an isothermal melt and a melt with a constant H_2O concentration.

multiple sources. Without further geochemical evidence the origin of these cores remain equivocal as the high An_{48-50} cores overlap the known compositions of Waipapa greywacke plagioclase crystals (Reid, 1982) and the composition of Oruanui plagioclase crystals (Charlier et al., 2008). The paucity of other detritus (e.g. quartz, zircon) from the disaggregation of a greywacke protolith in the same quantities as the plagioclase cores in the Taupo magma suggests cores are incorporated from igneous progenitor melts (Charlier et al., 2005 and 2008). Therefore, it is hypothesised that the high An_{48-50} cores of Taupo plagioclase crystals are derived from a more mafic progenitor melt and the low An_{35-38} cores are recycled or rejuvenated from a semi-formed more evolved (e.g. higher silica) crystal mush body.

5.3.4 Petrogenesis and accumulation of silicic magma at Healy caldera

Quantitative trace element modelling of Healy melt inclusions demonstrated the formation of Healy rhyodacitic magma through 62-76% fractional crystallisation originating from a basaltic parental magma (Chapter 2). This process would, however, generate a large quantity of crystals that are not observed in the pumices at the surface. Further evidence for a large crystal residue is gained from calculated crystallinities of the melt, derived from the measured concentrations of highly incompatible elements such as Rb or Zr where the minimum partition coefficient of Rb or Zr are assumed to be zero, and Rb and Zr concentrations of the parental melt are known (Blundy et al., 2006; Blundy et al., in press). For Healy, Rb and Zr concentrations of the basaltic parental magma are 6.14 ppm and 44.05 ppm, respectively (Wright and Worthington, unpublished data), yielding calculated crystallinities of 0.71 -0.85 from Rb concentrations and 0.64 -

0.87 from Zr concentrations (Table 5.3). This is consistent with the estimated proportion of crystals required for fractional crystallisation to generate this rhyodacitic melt.

Sample	Rb	Zr
X590-2.1	0.76	0.69
X590-3.2	0.80	0.73
X590B-6.1	0.82	0.64
X609-5.1	0.83	0.79
X609-8.1	0.71	0.72
X609-17.1	0.80	0.83
X609-17.2	0.83	0.80
X609-17.3	0.85	0.87

Table 5.3. Calculated crystallinity of Healy melt inclusions from Rb and Zr concentrations, see text for full details.

These calculated quantities of crystals far exceed the requisite 50% for the creation of crystal mush bodies (Bachman and Bergantz, 2004, 2008). Therefore, allied with the phenocryst sparse nature of pumices and the occurrence of inherited plagioclase cores, the presence of a mature crystal mush body is perceived at Healy, with the generation of high-silica rhyodacitic melts following large degrees of fractional crystallisation from mantle-derived basalt magmas. These silicic melts pond in an overlying magma chamber above the crystal mush body and provide the eruptible magma feeding subsequent eruptions (e.g., Bachmann and Bergantz, 2004; Miller and Wark, 2008).

Elemental concentrations of melt inclusions and plagioclase zonation indicate the Healy silicic magma possessed a relatively stable melt composition that experienced periodic thermal and volatile perturbations. Therefore a petrogenetic model is proposed whereby the accumulation of large-volumes of rhyodacitic magma at Healy was characterised by small multiple ‘cryptic’ magma mixing events. This process is where melts of similar compositions but of differing

oxygen fugacity or volatile compositions are mixed together in small pulses (Humphreys et al., 2006). In the case of Healy, these melt pulses are conceived to be small volumes of interstitial melt that infiltrate the silicic magma chamber from the underlying crystal mush. Additionally, mafic magmas have the potential to intrude into the base of the magma chamber resulting in thermal perturbations and the mass transfer of volatiles with little change in the chemical composition of the overlying silicic magma due to the density and viscosity contrasts of the melt (e.g., Koyaguchi and Kaneko, 1999; Couch et al., 2001; Ruprecht and Wörner, 2007). This could provide a viable mechanism producing the *An* gradients within plagioclase crystals without a significant change in melt composition, with the intrusion of a larger than normal quantity of mafic magma into the magma chamber to trigger the eventual eruption of Healy (e.g., Pallister et al., 1992; Ginibre et al., 2007).

In contrast, several previous studies have argued for a crustal anatexis origin of Kermadec Arc silicic magmas, specifically silicic magmas from Raoul and Macaulay Island in the northern Kermadec's (Smith et al., 2003 a and b; Smith et al., 2006; Wright et al., 2006). This was on the basis of: (1) the chemical heterogeneity of silicic magmas between adjacent volcanic centres; (2) the aphyric nature of samples; (3) that substantial volumes of silicic magma cannot be generated through fractional crystallisation processes alone and; (4) the delay in occurrence of silicic eruptions after the initiation of basaltic volcanism. Yet all of these points can be justified through the generation and presence of a crystal mush body by fractional crystallisation processes. Crystal mush bodies resident beneath each volcanic edifice have an unique magmatic evolution, crystallising

similar mineral assemblages, but with differing proportions of minerals that would result in distinct melt compositions. This provides a possible explanation for the geochemical heterogeneities between neighbouring silicic volcanoes such as the Healy and Brothers seamounts (southern Kermadec Arc). In addition, the framework nature of the crystal mush model permits a significant proportion of the fractionated crystals to remain in the crust with only high-silica interstitial melt, percolating through and accumulating in the overlying magma chamber where crystallisation is limited prior to eruption; thus justifying the aphyric nature of some silicic eruptives. Furthermore, large-volumes of rhyolitic magmas (> 850 km^3) produced by fractional crystallisation from mantle-derived basalt magmas occurred < 1 Ma after extensive basaltic flood volcanism from the Oligocene Afro-Arabian flood volcanics (Baker et al., 2000; Ukstins Peate et al., 2005, 2007). This shows that considerable volumes of silicic magmas can be generated in relatively short timescales by fractional crystallisation. The time lapse of 10^6 years proposed by Smith et al. (2003b) as evidence for the preconditioning of the ocean crust for anatexis could represent the time required for fractional crystallisation processes to generate the observed silicic magmas. Brophy (2008) also demonstrated through covariations of La and Yb concentrations with SiO_2, that the generation of Raoul Island and Macaulay Island silicic magmas was by fractional crystallisation processes and not crustal anatexis of amphibolite lower crust as proposed by Smith et al. (2003 a and b, 2006), providing further evidence for the genesis of silicic arc magmas in the Kermadec Arc through dominantly fractional crystallisation processes.

5.3.5 Petrogenesis and accumulation of 1800 BP Taupo magma

Taupo melt inclusion compositions overlap the Ruapehu groundmass glass compositions (Price et al., 2005) and rare earth element modelling showed these melts can be petrogenetically related through assimilation of greywacke and fractional crystallisation processes (Chapter 2). The abundance of normal *An* zoning in Taupo plagioclase crystals indicates fractional crystallisation processes are fundamental during the magmatic evolution. However, not all *An* variations result from fractional crystallisation, with plagioclase-melt equilibria indicating that changes in both the magmatic temperature and water concentrations are periodically required to account for these. The relatively consistent melt inclusion and groundmass glass compositions suggest any mixing of magmas is likely to be cryptic (Humphreys et al., 2006) and the aphyric nature of the Taupo pumices (Sutton et al., 1995) may suggest large quantities of crystals are retained within the crust during eruption providing evidence for the presence of a juvenile crystal mush body of similar composition as the final melt. However, it must be noted that the Taupo Ignimbrite possesses a discontinuous crystal lag deposit that could potentially account for the crystal poor nature of Taupo pumices. Additionally, there is evidence from the discrepancies in the calculated magmatic temperatures of plagioclase-melt equilibria and Fe-Ti oxides for the heating of the Taupo magma prior shortly prior to eruption. This most probably reflects the intrusion of a mafic magma into the base of the magma chamber, which would have triggered the eruption (e.g. Pallister et al., 1992; Sydner, 2000).

5.7 Conclusions

Elemental concentrations of melt inclusions and plagioclase zonation indicates fractional crystallisation is fundamental in the generation of both Healy and Taupo silicic magmas. The limited compositional variability of melt inclusions and plagioclase crystals within individual eruptions from both Healy and Taupo suggests a petrogenetic model whereby the accumulation of large volumes of silicic magma in upper crustal magma chambers occurs through the cryptic mixing of multiple small melt batches derived from underlying crystal mush zones. This suggests that, irrespective of the continental or oceanic arc setting, fractional crystallisation is potentially the dominant mechanism responsible for the genesis of silicic arc magmas and that the compositional differences observed between Healy and Taupo magmas are due to the assimilation of continental lithosphere in the Taupo Volcanic Zone (Chapter 2).

Chapter 6

Synthesis and Conclusions

6.1 Synthesis

The petrogenesis of large-volume silicic magmas from the hyper-productive continental Taupo Volcanic Zone and the oceanic Kermadec Arc were examined in this study though the chemical composition of rhyolitic melt inclusions (Chapters 2 and 3) and the chemical and textural zonation of plagioclase and quartz crystals (Chapters 4 and 5).

Major element composition of melt inclusions from the five rhyolitic eruptions studied (Whakamaru, Oruanui, Rotorua, Taupo and Healy) typically overlap (Figure 2.4) and cannot be used to discriminate between the individual eruptions or the end-member petrogenetic models of fractional crystallisation and crustal anatexis. Trace element concentrations of melt inclusions, however, can distinguish between the individual eruptions and indicate that the Whakamaru magma, the oldest and largest eruption studied, was the most evolved at the time of eruption (Figure 2.7). Furthermore, the chemical diversity observed between the continental Taupo Volcanic Zone melt inclusions and oceanic Healy melt inclusions, for example the lower K_2O and Ce/Yb concentrations of Healy melt inclusions, can be explained through the absence of continental lithosphere overlying the subducting slab in the Kermadec Arc. The generation of the silicic magma at Healy can be quantitatively modelled through 62 - 76 % fractional crystallisation from a basaltic parent melt (Chapter 2). Allied with this is the high

calculated crystallinities of Healy melt inclusion compositions and the abundance of normal *An* zoning of Healy plagioclase crystals (Chapter 5). This provides compelling evidence for the presence of a juvenile crystal mush body and the magmatic evolution of the rhyodacitic magma at Healy through fractional crystallisation processes (Chapter 5).

There is a close resemblance between middle to heavy rare earth element trends of Healy and Taupo melt inclusions (Figure 2.6), signifying a common origin for these continental and oceanic silicic arc magmas. However, quantitative trace element modelling of continental melt inclusion compositions using a simple fractional crystallisation model cannot explain both the LREE (e.g. La = 7 - 53 ppm) and HREE (e.g. Yb = 1.5 - 5.5 ppm) concentrations. The modelling is consistent with assimilation of continental lithosphere (greywacke country rock) in addition to extreme fractional crystallisation (60 – 80 %) from basaltic parental magmas is required to attain the Taupo Volcanic Zone melt inclusion compositions. Although Taupo melt inclusion compositions can be attained by using this model, a better reproducibility of calculated and observed trace element concentrations is achieved when the Ruapehu groundmass glass composition (Price et al., 2005) is substituted as the parental composition (Figure 2.12). Coupled with the overlapping calculated Sr and Ba melt compositions of Whakamaru Group 1 plagioclase cores and Ruapehu groundmass glass compositions (Chapter 4) this provides strong evidence of a petrogenetic link between Taupo Volcanic Zone rhyolites and andesites, dominantly through fractional crystallisation (and assimilation) processes (Chapters 2 and 5).

A more complex origin for the Whakamaru, Oruanui and Rotorua rhyolitic magmas than exclusively fractional crystallisation and assimilation of greywacke country rock is implied from the enriched Rb/Sr ratios of melt inclusions in comparison to whole rock pumice compositions (Figure 2.9). For these eruptions, melt inclusions and crystal hosts are interpreted to be derived from a more evolved melt and incorporated into the final magma prior to eruption (Chapter 2). A mature crystal mush origin of these crystals is inferred due to the crystal sparse nature of erupted pumices and the strong fractional crystallisation signatures of melt inclusions that reflect and preserve a record of the interstitial melt composition. Trace element modelling of the compositional variation of melt inclusions within individual eruptions indicate that this interstitial liquid was mixed with greywacke partial melts prior to eruption, resulting in the entire compositional spectrum of melt inclusions (Chapter 2).

Crystal zonation supports the amalgamation of crystals in magmas from multiple sources (Chapters 4 and 5). For example, CL imaging of Whakamaru quartz crystals (Figure 4.5 and A4.3) revealed distinct cores and rims that allowed the location of melt inclusions in relation to these zones to be identified. This exposes distinct compositional variation between melt inclusions located in the cores of the crystal and those in the rims (Figure 6.1). With the exception of the melt inclusion located in the core of the crystal WH1_37, the most evolved melt inclusions are located in the core of the quartz crystals and the least evolved at the rims.

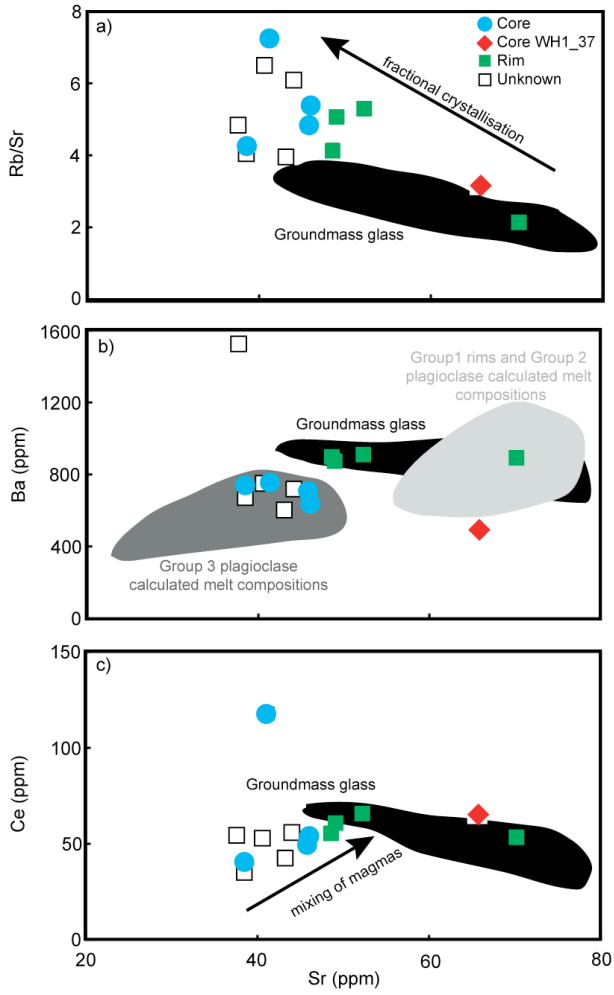

Figure 6.1. Compositional variation of quartz-hosted Whakamaru melt inclusions. Location of melt inclusions is based on the presence of core (blue circles and red diamond) and rim (green squares) regions identified by CL imaging of crystals (Figure 4.5 and A4.3). Melt inclusions hosted in crystals where CL images were not obtained are shown by open black squares. Note that melt inclusions in the core of crystals are more evolved (with the exception of WH1_37) than melt inclusions in the rim. Shaded regions denote groundmass glass compositions (black) (Brown, 1994), calculated melt compositions in equilibrium with Group 3 plagioclases (dark grey) and Group 1 rims and Group 2 plagioclase crystals (light grey).

Melt inclusions hosted in the rim of quartz crystals display compositions similar to groundmass glass compositions (Brown, 1994), demonstrating that the most recent quartz growth occurred while resident in the host magma. The timing of the final quartz growth is constrained from the greyscale intensity of CL images. This growth occurred < 80 years prior to eruption (Chapter 4) suggesting that the

incorporation of the quartz cores and thus crystal mush, into the magma transpired only a short time prior to eruption.

Chemical and textural zonation of Whakamaru plagioclase crystals reveals the presence of three distinct plagioclase populations. Calculation of co-existing Sr and Ba melt compositions of the low *An* plagioclase population (Group 3) indicates these plagioclase crystals fractionated from a low Sr (25 - 50 ppm) melt whose composition is consistent with the melt inclusions located in the core of quartz crystals (Figure 6.1). These crystals are inferred to originate from a crystal mush body (Chapter 4). Furthermore, similar trace element modelling of Group 1 plagioclase crystals (possessing inherited cores of An_{45-60}) demonstrate the crystallisation of cores occurred from progenitor andesitic melts, whereas the rims and Group 2 plagioclase crystals fractionated from the final host melt contemporaneously with the rims of quartz crystals.

These observations provide a second possible source for the origin of the less evolved melt that mixed with the interstitial crystal mush melt to generate the chemical heterogeneity of melt inclusions observed within individual eruptions (Chapter 2). Instead of the interstitial melt mixing with a greywacke partial melt, the interstitial melt could have combined with a less evolved rhyolitic melt (e.g. Sr = 58 - 93 ppm Group 3 melt composition with a consistent melt composition to the groundmass glass) generated through fractional crystallisation of a plagioclase dominant crystal assemblage (Chapter 4) (Figure 6.1). This would indicate that the majority of greywacke assimilation occurred prior to the generation of the initial rhyolitic magmas, during the petrogenesis of basaltic and

andesitic magmas and the growth of the crystal mush body. This model is consistent with the Pb isotopic compositions of Taupo Volcanic Zone glass tephra shards that indicate assimilation of greywacke basement occurred during the early stages of magmatic evolution (Allan, 2008). Sr and Pb isotopic analyses of Whakamaru melt inclusions and specific zones of plagioclase crystals were unable to be conducted in this current study and so the origin of the melt that combined with the interstitial crystal mush melt to create the compositional heterogeneity of the Whakamaru melt inclusions remains ambiguous. However, several Group 1 plagioclase crystals provide evidence for an overgrowth rim surrounding the core that is characterised by high Ba (e.g. 1200 - 1590 ppm) potentially representing a greywacke partial melt (Chapter 4). As demonstrated for the overgrowth rims of Oruanui plagioclase crystals that possess extremely radiogenetic $^{86}Sr/^{87}Sr$ (e.g. maximum $^{86}Sr/^{87}Sr = 0.70764$ compared to whole rock pumice of $^{86}Sr/^{87}Sr = 0.7055$) (Charlier et al., 2008), the timing of the input of greywacke melts and incorporation of crystal mush magmas varies from eruption to eruption.

Major element compositions of Taupo plagioclase- and orthopyroxene- hosted melt inclusions and groundmass glasses overlap (Figure 2.5) indicating all three phases are co-genetic and crystallised from the same magma body. As discussed above, quantitative modelling of melt inclusion compositions indicates the Taupo magma is derived through assimilation of greywacke country rock and fractional crystallisation from an andesitic progenitor melt (Chapter 2). However, the absence of a low *An* plagioclase population in the Taupo magma (Chapter 5), allied with the relatively homogenous melt inclusion compositions, indicate

magma genesis did not involve the incorporation of a crystal mush magma. Consequently, it is interpreted that the genesis of the 1800 BP Taupo magma (the least evolved continental melt inclusion composition) occurred through dominantly fractional crystallisation and assimilation of greywacke country rock from a precursor parental andesitic melt at approximately 5-12 km depth (Chapters 2, 3 and 5).

A similar petrogenetic evolution is inferred for the Rotorua eruptive. However, the slightly enriched Rb/Sr ratios of Rotorua melt inclusions relative to whole rock pumices allied with the lower Sr (102 - 158 ppm) and higher Ba (717 - 1086 ppm) concentrations of melt inclusions (Figure 6.2) suggest magma genesis also required the amalgamation of small degrees of crystal mush magmas (Chapter 2).

The larger-volume Whakamaru and Oruanui magmas contain polygenetic crystal populations derived from multiple sources of: (1) andesitic progenitor melts; (2) greywacke partial melts and; (3) mature crystal mush (plutonic) bodies, amalgamated together in differing proportions prior to eruption (Chapter 4; Charlier et al., 2008). These three melt sources are reflected in the Sr and Ba concentrations of Oruanui melt inclusions that fall into three discrete groups: (1) high Sr (75 - 105 ppm) melts that are potentially generated from the fractional crystallisation of andesitic parental melts, as discussed for the Taupo magma; (2) high Ba (710 - 1218 ppm) melts that may represent a greywacke melt but, as discussed above, without Sr or Pb isotopic compositions this remains equivocal, and; (3) low Sr (<40 ppm) and Ba (< 290 ppm) concentrations, similar to the Whakamaru Melt 4 compositions inferred to reflect fractionation of crystal hosts in a crystal mush body (Figure 6.2).

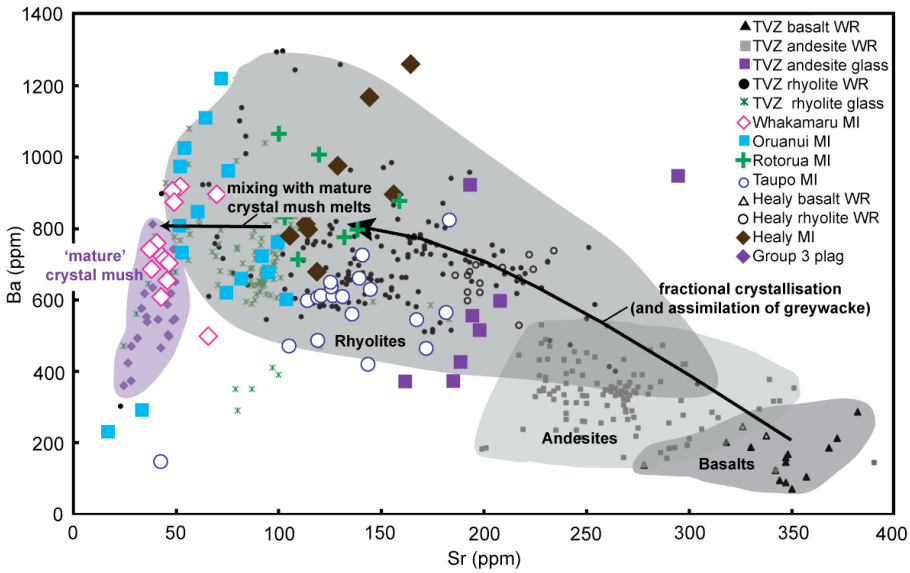

Figure 6.2. Sr versus Ba concentrations of Taupo Volcanic Zone and Healy magmas. Shaded regions represent whole rock compositions of basalts (dark grey), andesites (light grey) and rhyolites (medium grey). Groundmass and melt inclusion glass compositions are shown in colour. Whakamaru Group 3 calculated Sr and Ba melt compositions are in purple (Chapter 4). Data sources: Graham and Hackett (1987); Graham and Worthington (1988); Patterson and Graham (1988); Gamble et al. (1993 and 1999); Nairn (1992); Briggs et al. (1993); Cole et al. (1998); Donoghue et al. (1995); Sutton et al. (1995 and 2000); Brown et al. (1998); Krippner et al. (1998); Waight et al. (1999); Nakagawa et al. (1998 and 2002); Smith et al. (2002; 2004 and 2006); Price et al. (2005); Shane et al. (2005); Wilson et al. (2006).

Measured water concentrations of Whakamaru, Taupo and Healy melt inclusions allied with the fluctuating *An* contents of Taupo and Healy plagioclase crystals require both a change in magmatic water concentration and temperature to account for the *An* variation, suggesting that the magmatic water concentration was not constant but changed during evolution of the magma body (Chapters 3 and 5). The measured H_2O_m and OH^- concentrations of melt inclusions provide evidence for the degassing of the magma prior to eruption and indicate that the magma was resident at shallow (e.g. < 4 km) crustal depths for at least a short period of time prior to eruption (Chapters 3 and 5). However, estimation of the initial magmatic water concentrations for the Whakamaru, Taupo and Healy

eruptions range between 4.4 - 8.8 wt%, implying a significant proportion of the petrogenesis of these silicic magmas occurred at a depth of 4 - 12 km.

The assembly of the eruptible magma body required to feed the Whakamaru supereruption is estimated to have occurred continuously over the 15,000 years preceding the final climatic eruption (Chapter 4). This period is significantly shorter than that proposed by zircon chronology for the formation of the Whakamaru magmatic system (Brown and Fletcher, 1999; Charlier et al., 2005), providing evidence that magma chambers are ephemeral features of magma reservoirs and are only formed shortly prior to eruption. This timescale is, however, significantly longer than the maximum residence times of 1010-2750 years for the Taupo eruption, estimated from the repose intervals between volcanic eruptions from Taupo Volcano (Sutton et al., 2000). It is therefore speculated that the larger volume eruptions, for example the Whakamaru and Oruanui supereruptions, assembled over extended time periods, which increased the probability for the injection and mixing of magmas from secondary sources such as crystal mush magmas and greywacke partial melts. However, it remains equivocal as to why eruptions are triggered at certain times.

Evaluation of magmatic temperatures obtained from plagioclase-melt equilibria and Fe-Ti oxides implies that Whakamaru and Taupo magmas temperatures rose prior to eruption (Chapters 4 and 5), most likely due to the intrusion of a hotter (and more mafic) magma into the base of the magma chamber. This is further illustrated by the presence of high Ti rims (bright CL intensity) on a selection of Whakamaru quartz crystals that can indicate either a rise in magmatic

temperature or a change in the Ti activity of the melt (Wark and Watson, 2006). The absence of late-stage growth of high *An* rims on plagioclase crystals (Chapter 4 and 5) indicates that the substantial mixing of magmas prior to eruption did not occur and that it was the mass transfer of volatiles that heated the overlying magma (e.g. Koyaguchi and Kaneko, 1999; Couch et al., 2001; Ruprecht and Wörner, 2007). It was only when an anomalous volume of hotter magma was intruded into the magma chamber that an eruption was triggered.

It is thus concluded that the rhyolitic magmas in the continental Taupo Volcanic Zone are generated through fractional crystallisation (and assimilation of greywacke country rock) of a plagioclase dominant crystal assemblage from andesitic progenitor melts (Figure 6.3). Furthermore, the heterogeneity of rhyolitic magmas is produced from the mixing of greywacke partial melts and the incorporation of crystal mush magmas generating the most evolved compositions (Figure 6.2 and 6.3). Thus, it is the presence and assimilation of continental lithosphere within the Taupo Volcanic Zone that generates the observed compositional heterogeneity of silicic magmas between the continental Taupo Volcanic Zone and oceanic Kermadec Arc (Figure 6.3).

Figure 6.3. (Figure overleaf) Cartoon cross section of the petrogenesis of silicic magmas in the continental Taupo Volcanic Zone and oceanic Kermadec Arc. Crystal mush bodies (grey diamonds) are generated through extreme fractional crystallisation in the Kermadec Arc (Chapters 2 and 5) and through assimilation of greywacke country rock and fractional crystallisation in the Taupo Volcanic Zone. These crystal mush bodies are envisaged to the zoned from mafic compositions at deeper crustal levels to silicic compositions at shallow crustal depths. Magma chambers are considered to be ephemeral features generated in the lead up to eruption and may not be present for the entire history of the magma reservoir.

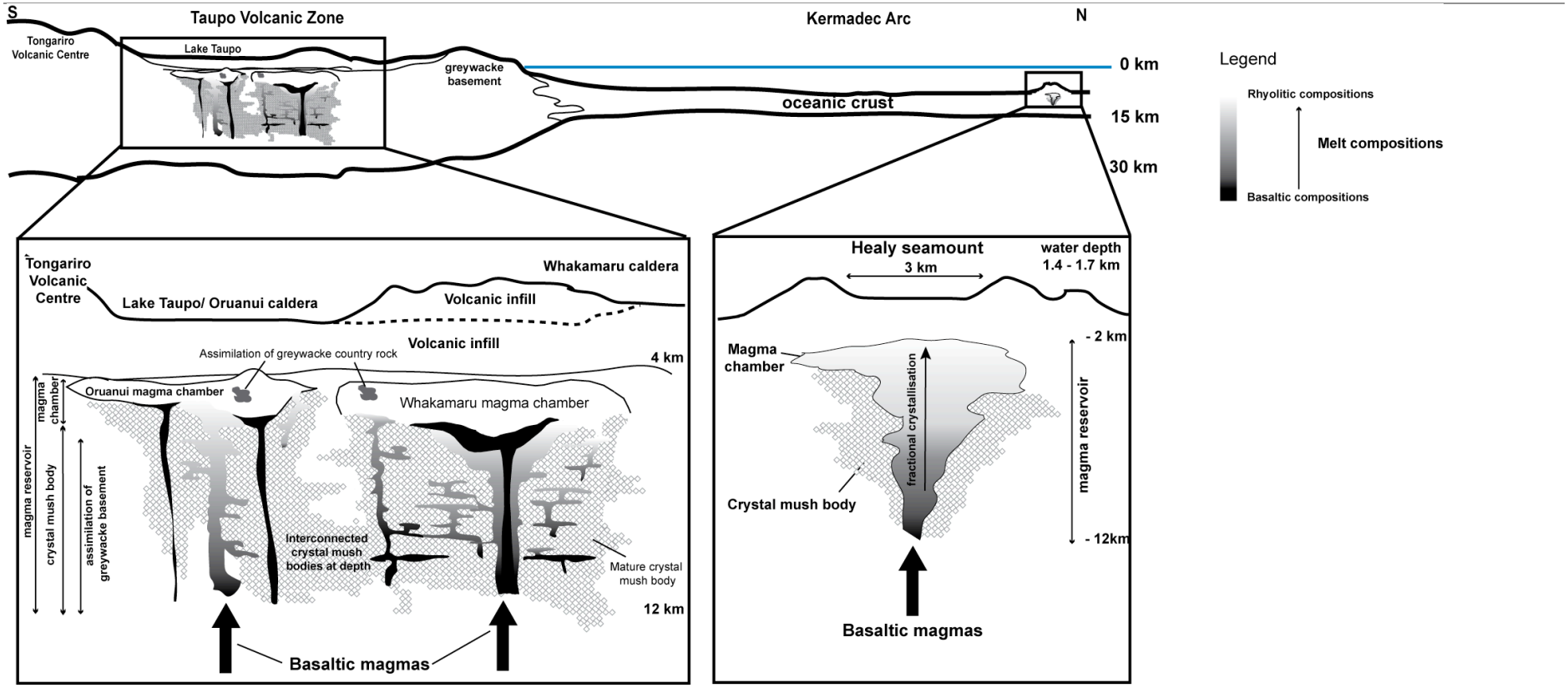

Figure 6.3 (Caption overleaf).

6.2 Conclusions

A combination of elemental concentrations of melt inclusions and crystal specific studies of plagioclase and quartz crystals have shown that:

1. Fractional crystallisation is the dominant magmatic process responsible for the formation of silicic magmas in both the continental Taupo Volcanic Zone and neighbouring oceanic Kermadec Arc (Chapters 2, 3 and 5). Quantitative modelling of trace element compositions of melt inclusions demonstrates the generation of the silicic magma from the oceanic Healy seamount occurred by 62 - 76 % fractional crystallisation from a basaltic parental melt. In contrast, assimilation of greywacke country rock (r = 0.2 in AFC modelling, Chapter 2) combined with extensive fractional crystallisation (60 - 80 %) is required to produce the compositions of Taupo Volcanic Zone melt inclusions (Chapter 2).
2. Continental silicic magmas in the Taupo Volcanic Zone have more complex histories than silicic magmas in the Kermadec Arc and are generated from the amalgamation of discrete magma batches from polygenetic sources. This is most evident in the largest volume evolved magmas such as the Whakamaru Ignimbrite (Chapters 2, 4 and 5).
3. It is the presence of continental lithosphere that provides the additional melt sources required to generate large-volume silicic eruptions in the Taupo Volcanic Zone compared to the relatively small volume silicic eruptions observed in the Kermadec Arc (Chapters 2 and 5).
4. The magma reservoir model for the generation of silicic magmas (e.g. Bachman and Bergantz, 2004; 2008) is applicable to oceanic as well as continental silicic arc magmas and can provide a viable explanation for

many of the geochemical features observed in the Taupo Volcanic Zone and Kermadec Arc silicic magmas.

5. The relatively homogenous compositions of the studied magmas conceals the presence of polygenetic magma sources in whole rock studies, requiring *in-situ* crystal specific studies to discriminate between various sources (Chapters 2, 4 and 5).
6. The measured water speciation of Whakamaru, Taupo and Healy melt inclusions are inconsistent with the speciation trends derived experimentally for groundmass rhyolitic glasses. Investigation into this inconsistency was interpreted to represent the degassing of melt inclusions prior to quenching. It is concluded that the measured water speciation of melt inclusions records the dissolved water concentration of the respective magmas immediately prior to eruption but provides no information about the dissolved magmatic water content at the time the melt inclusions were sealed from the external magma (Chapter 3).

6.3 Future work

Many questions still remain unanswered about the petrogenesis of silicic arc magmas in the continental Taupo Volcanic Zone and oceanic Kermadec Arc. In particular:

1. What are the timescales for the formation of magma reservoirs, especially the timing of the creation of the final magma chamber that feeds the eruption? Does the timescale change with eruption volume or geologic setting.

2. What was the timing of the input of greywacke partial melts and/or the bulk assimilation of country rock (e.g. greywacke) in the continental Taupo Volcanic Zone magmas?
3. What were the proportions of crystal mush magmas incorporated into silicic magmas in both continental and oceanic subduction environments?
4. What was the extent of crystal mush bodies beneath the Taupo Volcanic Zone and Kermadec Arc?
5. What is the petrogenetic relationship between the Taupo Volcanic Zone andesites and rhyolites?

These problems could be investigated through further *in-situ* crystal specific studies detailing the trace element and isotopic studies of crystal zonation. In particular studies on:

1. Sr, and Pb isotopic compositions of melt inclusions and specific zones of crystals, to detail the source of multiple melt components of rhyolite, andesite and basalt magmas. This would for example reduce the ambiguity of the Melt 2 plagioclase composition (Chapter 4).
2. The major and trace element composition of melt inclusions and groundmass glasses of both Taupo Volcanic Zone and Kermadec Arc andesites and basalts. However, these mafic melt inclusions would first have to be examined carefully for signs of diffusive homogenisation of inclusions with the external melt. This would permit detailed examination of magmatic processes linking basaltic and andesitic magmas and andesitic and rhyolitic magmas in arc environments.

3. Examination of textural and chemical zonation of plagioclase crystals from rhyolite, andesite and basalt magmas. This would decipher the magmatic evolution of the entire compositional spectrum observed in the Taupo Volcanic Zone and Kermadec Arc and unravel the timing of the input of greywacke country rock to silicic magmas.
4. Diffusional timescales for the zoning of crystals (e.g. olivine, pyroxene, plagioclase and quartz) allowing timescales of magmatic processes to be constrained and providing information on whether this changes between eruptions.
5. Crystal specific study of the Kaingaroa Ignimbrite, known to contain significant proportions of andesitic as well as rhyolitic components (e.g. Nairn et al., 1994). This would allow the relationship between andesitic and rhyolitic magmas in the Taupo Volcanic Zone to be examined in detail, deciphering the petrogenetic processes involved.

Finally, water speciation of rhyolitic melt inclusions was found to be inconsistent with the predicted speciation trends of groundmass rhyolitic glasses (Chapter 3). However, it remains equivocal as to whether or not this inconsistency in water speciation is confined to high-silica melt inclusions and what triggers the degassing of some melt inclusions and not others. To investigate this further, water speciation in a range of samples from basalt to rhyolite melt inclusions and co-genetic groundmass glasses, from a range of geological environments, would need to be examined to establish how widespread this phenomenon is.

References

Albrecht, A., and Goldstein, S.L., 2000. Effects of basement composition and age on silicic magmas across an accreted Terrane-Precambrian crust boundary, Sierra Madre Occidental, Mexico. Journal of South American Earth Sciences, 13: 255-273.

Allan, A.S.R., 2008. An elemental and isotopic investigation of Quaternary silicic Taupo Volcanic Zone tephras from ODP Site 1123: chronostratigraphic and petrogenetic applications. MSc thesis, Victoria University of Wellington, Wellington, New Zealand.

Allan, A.S.R., Baker, J.A., Carter, L., and Wysoczanski, R.J., 2008. Reconstructing the Quaternary evolution of the world's most active rhyolitic system: insights from a ~ 1.65 Myr deep ocean tephra record sourced from Taupo Volcanic Zone, New Zealand. Quaternary Science Reviews, 27: 2341-2360.

Anderson, A.T., Swihart, G.H., Artioli, G. and Geiger, C.A., 1984. Segregation vesicles, gas filtering-pressing, and igneous differentiation. Journal of Geology, 92: 55-72.

Anderson, A.T., Davis, A.M. and Lu, F., 2000. Evolution of Bishop Tuff rhyolitic magma based on melt and magnetite inclusions and zoned phenocrysts. Journal of Petrology, 41(3): 449-473.

Annen, C., Blundy, J.D. and Sparks, R.S.J., 2006. The genesis of intermediate and silicic magmas in deep crustal hot zones. Journal of Petrology, 47(3): 505-539.

Atlas, Z.D., Dixon, J.E., Sen, G., Finny, M., and Martin-Del Pozzo, A., L., 2005. Melt inclusions from Volcán Popocatépetl and Volcán de Colima,

Mexico: Melt evolution due to vapor-saturated crystallization during ascent. Journal of Volcanology and Geothermal Research, 153:221-240.

Ayalew, D., Barbey, P., Marty, B., Reisberg, L., Yirgu, G., and Pik, R., 2002. Source, genesis and timing of giant ignimbrite deposits associated with Ethiopian continental flood basalts. Geochimica et Cosmochimica Acta, 66: 1429-1448.

Bachmann, O., and Bergantz, G.W., 2003. Rejuvenation of the Fish Canyon magma body: A window into the evolution of large-volume silicic magma systems. Geology, 31(9): 789-792.

Bachmann, O., and Bergantz, G.W., 2004. On the origin of crystal-poor rhyolites: extracted from batholithic crystal mushes. Journal of Petrology 45(8): 1565-1582.

Bachmann, O. and Bergantz, G., 2008. The Magma Reservoirs That Feed Supereruptions. Elements, 4(1): 17-21.

Bachmann, O., Dungan, M.A., and Lipman, P.W., 2002. The Fish Canyon magma body, San Juan Volcanic Field, Colorado: Rejuvenation and eruption of an upper-crustal batholith. Journal of Petrology, 43(8): 1469-1503.

Bachmann, O., Miller, C.F., and de Silva, S.L., 2007. The volcanic-plutonic connection as a stage for understanding crustal magmatism. Journal of Volcanology and Geothermal Research, 167: 1-23.

Bacon, C.R.I., and Druitt, T.H., 1988. Compositional evolution of the zoned calc-alkaline magma chamber of Mount Mazama Crater Lake, Oregon. Contributions to Mineralogy and Petrology 98(2): 224-256.

Bacon., C.R., and Hirschmann, M.M., 1988. Mg/Mn partitioning as a test for equilibrium between coexisting Fe-Ti oxides. American Mineralogist, 73: 57-61.

Bacon, C.R., Newman, S. and Stolper, E., 1992. Water, CO_2, Cl, and F in melt inclusions in phenocrysts from three Holocene explosive eruptions, Crater Lake, Oregon. American Mineralogist, 77: 1021-1030.

Baker, J.A., Snee, L., and Menzies, M., 1996. A brief Oligocene period of flood volcanism: implications for the duration and rate of continental flood volcanics at the Afro-Arabian triple junction. Earth and Planetary Science Letters, 138: 39-55.

Baker, J.A., MacPherson, C.G., Menzies, M.A., Thirlwall, M.F., Al-Kadasi, M., and Mattey, D.P., 2000. Resolving crustal and mantle contributions to continental flood volcanism, Yemen; Constraints from mineral oxygen isotope data. Journal of Petrology, 41:1805-1820.

Barclay, J., Carroll, M.R., Houghton, B.F., and Wilson, C.J.N., 1996. Pre-eruptive volatile content and degassing history of an evolving peralkaline volcano. Journal of Volcanology and Geothermal Research, 74: 75-87.

Barclay, J., Rutherford, M.J., Carroll, M.R., Murphy, M.D., Devine, J.D., Gardner, J., and Sparks, R.S.J., 1998. Experimental phase equilibria constraints on pre-eruptive storage conditions of the Soufriere Hills magma. Geophysical Research Letter, 25: 3437-3440.

Beard, J.S., and Lofgren, G.E., 1991. Dehydration melting and water-saturated melting of basaltic and andesitic greenstones and amphibolites at 1, 3, and 6.9 kb. Journal of Petrology, 32(2): 365-401.

Behrens, H., and Nowak, M., 1997. The mechanisms of water diffusion in polymerized silicate melts. Contributions to Mineralogy and Petrology, 126: 377-385.

Bence, A.E., and Albee, A.L., 1968. Empirical correction factors for the electron microprobe analysis of silicates and oxides. Journal of Geology, 76: 382-403.

Beresford, S.W., Cole, J.W., and Weaver, S.D., 2000. Weak chemical and mineralogical zonation in the Kaingaroa Ignimbrite, Taupo Volcanic Zone, New Zealand. New Zealand Journal of Geology and Geophysics, 43: 639-650.

Bergantz, G.W., 1989. Underplating and Partial Melting: Implications for Melt Generation and Extraction. Science, 245(4922): 1093-1095.

Berlo, K., Blundy, J., Turner, S., and Hawkesworth, C., 2007. Textural and chemical variation in plagioclase phenocrysts from the 1980 eruptions of Mount St. Helens, USA. Contributions to Mineralogy and Petrology, 154: 291-308.

Bindeman, I.N., Davis, A.M. and Drake, M.J., 1998. Ion microprobe study of plagioclase-basalt partition experiments at natural concentration levels of trace elements. Geochimica et Cosmochimica Acta, 62(7): 1175-1193.

Bindeman, I.N., Valley, J.W., Wooden, J.L. and Persing, H.M., 2001. Post-caldera volcanism: in situ measurement of U-Pb age and oxygen isotope ratio in Pleistocene zircons from Yellowstone caldera. Earth and Planetary Science Letters, 189(3-4): 197-206.

Blank, J.G., Stolper, E.M., and Carroll, M.R., 1993. Solubilities of carbon dioxide and water in rhyolitic melt at 850°C and 750 bars. Earth and Planetary Science Letters, 1993: 27-36.

Blake, S., 1984. Volatile oversaturation during the evolution of silicic magma chambers as an eruption trigger. Journal of Geophysical Research, 89: 8237-8244.

Blattner, P., and Reid, F., 1982. The origin of lavas and ignimbrites of the Taupo Volcanic Zone, New Zealand in the light of oxygen isotope data. Geochimica et Cosmochimica Acta, 46: 1417-1429.

Blattner, P., RuiZhong, H., Graham, I.J., Houston-Eleftheriadis, C., 1996. Temperatures and isotopic evolution of silicic magmas, Taupo Volcanic Zone and Coromandel, New Zealand. New Zealand Journal of Geology and Geophysics 39(3): 353-362.

Blundy, J.D. and Shimizu, N., 1991. Trace-element evidence for plagioclase recycling in calc-alkaline magmas. Earth and Planetary Science Letters, 102(2): 178-197.

Blundy, J.D. and Wood, B.J., 1991. Crystal-chemical controls on the partitioning of Sr and Ba between plagioclase feldspar, silicate melts, and hydrothermal solutions. Geochimica et Cosmochimica Acta, 55(1): 193-209.

Blundy, J.D., and Wood, B.J., 1994. Prediction of crystal-melt partition coefficients from elastic moduli. Nature, 372: 452-454.

Blundy, J. and Cashman, K., 2005. Rapid decompression-driven crystallization recorded by melt inclusions from Mount St. Helens volcano. Geology, 33(10): 793-796.

Blundy, J., Cashman, K., and Humphreys, M., 2006. Magma heating by decompression-driven crystallization beneath andesite volcanoes. Nature, 443: 76-80.

Blundy, J., Cashman, K., and Berlo, K., in press. Evolving magma storage conditions beneath Mount St. Helens inferred from chemical variations in melt inclusions from the 1980-1986 and current eruptions. In Sherrod, D.R., et al., eds., A volcano rekindled: The first year of renewed eruption

at Mount St. Helens, 2004-2006: U.S. Geological Survey Professional Paper (in press).

Borg, L.E., Clynne, M.A., 1998. The petrogenesis of felsic calc-alkaline magmas from the southernmost Cascades, California: origin by partial melting of basaltic lower crust. Journal of Petrology, 39(6): 1197-1222.

Bowen, N.L., 1913. The melting phenomena of plagioclase feldspars. American Journal of Science, 35: 577-599.

Bowen, N.L., 1928. The evolution of igneous rocks. Princeton University Press. pp 332.

Briggs, N.D., 1976. Recognition and correlation of subdivisions within the Whakamaru ignimbrite, central North Island, New Zealand. New Zealand Journal of Geology and Geophysics, 19: 463-501.

Briggs, R.M., Gifford, M.G., Moyle, A.R., Taylor, S.R., Norman, M.D., Houghton, B.F., and Wilson, C.J.N., 1993. Geochemical zoning and eruptive mixing in ignimbrites from Mangakino volcano, Taupo Volcanic Zone, New Zealand. Journal of Volcanology and Geothermal Research, 56: 175-203.

Brophy, J.G., Whittington, C.S. and Park, Y.R., 1999. Sector-zoned augite megacrysts in Aleutian high alumina basalts: implications for the conditions of basalt crystallization and the generation of calc-alkaline series magmas. Contributions to Mineralogy and Petrology, 135(2-3): 277-290.

Brophy, J.G., 2008. A study of rare earth element (REE)-SiO_2 variations in felsic liquids generated by basalt fractionation and amphibolite melting: a potential test for discriminating between two different processes. Contributions to Mineralogy and Petrology, 156: 337-357.

Brown, S.J.A., 1994. Geology and geochemistry of the Whakamaru group ignimbrites, and associated rhyolite domes, Taupo Volcanic Zone, New Zealand. PhD thesis, University of Canterbury, Christchurch, 288 pp.

Brown, S.J.A., and Fletcher, I.R., 1999. SHRIMP U-PB dating of the preeruption growth history of zircons from the 340 ka Whakamaru Ignimbrite, New Zealand: Evidence for >250 k.y. magma residence times. Geology, 27: 1035-1038.

Brown, S.J.A., Wilson, C.J.N., Cole, J.W., and Wooden, J., 1998a. The Whakamaru group ignimbrites, Taupo Volcanic Zone, New Zealand: evidence for reverse tapping of a zoned silicic magmatic system. Journal of Volcanology and Geothermal Research, 84(1-2): 1-37.

Brown, S.J.A., Burt, R.M., Cole, J.W., Krippner, S.J.P., Price, R.C., and Cartwright, I., 1998b. Plutonic lithics in ignimbrites of Taupo Volcanic Zone, New Zealand; sources and conditions of crystallisation. Chemical Geology 148: 21-41.

Browne, P.R.L., Graham, I.J., Parker, R.J. and Wood, C.P., 1992. Subsurface andesite lavas and plutonic rocks in the Rotokawa and Ngatamariki geothermal systems, Taupo Volcanic Zone, New Zealand. Journal of Volcanology and Geothermal Research, 51: 199-215.

Bryan, S.E., Riley, T.R., Jerram, D.A., Stephens, C.J., and Leat, P.T., 2002. Silicic volcanism: An undervalued component of large igneous provinces and volcanic rifted margins. In Menzies, M.A., Klemperer, S.L., Ebinger, C.J., and Baker, J (Editors). Volcanic rifted margins. Geological Society of America Special Paper, 362: 97-118.

Case, J.E., Ryland, S.L., Simkin, T., and Howard, K.A., 1973. Gravitational evidence for a low-density mass beneath the Galápagos Islands. Science, 181: 1040-1042.

Cervantes, P., and Wallace, P., 2003. Magma degassing and basaltic eruption styles: a case study of ~ 2000 year BP Xitle volcano in central Mexico. Journal of Volcanology and Geothermal, 120: 249-270.

Charlier, B.L.A., Wilson, C.J.N., Lowenstern, J.B., Blake, S., Van Calsteren, P.W., and Davidson, J.P., 2005. Magma generation at a large, hyperactive silicic volcano (Taupo, New Zealand) revealed by U-Th and U-Pb systematics in zircons. Journal of Petrology, 46(1): 3-32.

Charlier, B.L.A., Bachmann, O., Davidson, J.P., Dungan, M.A., and Morgan, D.J., 2007. The upper crustal evolution of a large silicic magma body: Evidence from crystal-scale Rb-Sr isotopic heterogeneities in the Fish Canyon magmatic system, Colorado. Journal of Petrology, 48: 1875-1894.

Charlier, B.L.A., Wilson, C.J.N., and Davidson, J.P., 2008. Rapid open-system assembly of a large silicic magma body: time-resolved from cored plagioclase crystals in the Oruanui eruption deposits, New Zealand. Contributions to Mineralogy and Petrology, 156: 799-813.

Cherniak, D.J., Watson, E.B., and Wark., D.A., 2007. Ti diffusion in quartz. Chemical Geology, 236: 65-74.

Christensen, J.N. and DePaolo, D.J., 1993. Time scales of large volume silicic magma systems - Sr isotopic systematics of phenocrysts and glass from the Bishop Tuff, Long Valley, California. Contributions to Mineralogy and Petrology, 113(1): 100-114.

Christensen, J.N. and Halliday, A.N., 1996. Rb-Sr ages and Nd isotopic compositions of melt inclusions from the Bishop Tuff and the generation of silicic magma. Earth and Planetary Science Letters, 144(3-4): 547-561.

Christiansen, R.L., 2001. The Quaternary and Pliocene Yellowstone Plateau volcanic field of Wyoming, Idaho and Montana. USGS Professional Paper, 729: 1-146.

Christiansen, E.H., 2005. Contrasting processes in silicic magma chambers: evidence from very large volume ignimbrites. Geological Magazine, 142: 669-681.

Cline, J.S., and Bodnar, R.J., 1991. Can economic porphyry copper mineralization be generated by a typical calc-alkaline melt. Journal of Geophysical Research – Solid Earth and Planets, 96: 8113-8126.

Cole, J.W., 1979. Structure, petrology, and genesis of Cenozoic volcanism, Taupo Volcanic Zone, New Zealand – a review. New Zealand Journal of Geology and Geophysics, 22: 631-657.

Cole, J.W., 1981. Genesis of Lavas of the Taupo Volcanic Zone, North Island, New Zealand. Journal of Volcanology and Geothermal Research, 10: 317-337.

Cole, J.W., Brown, S.J.A., Burt, R.M., Beresford, S.W., and Wilson, C.J.N., 1998. Lithic types in ignimbrites as a guide to the evolution of a caldera complex, Taupo volcanic centre, New Zealand. Journal of Volcanology and Geothermal Research, 80(3-4): 217-237.

Cole, J.W., Gamble, J.A., Burt, R.M., Carroll, L.D., and Shelley, D., 2001. Mixing and mingling in the evolution of andesite-dacite magmas; evidence from co-magmatic plutonic enclaves, Taupo Volcanic Zone, New Zealand. Lithos, 59: 25-46.

Cordier, P., and Doukhan, J.C., 1991. Water speciation in quartz: A near infrared study. American Mineralogist, 76: 361-369.

Costa, F., and Chakraborty, S., 2004. Decadel time gaps between mafic intrusion and silicic eruption obtained from chemical zoning patterns in olivine. Earth and Planetary Science Letters, 227: 517-530.

Costa, F., Chakraborty, S. and Dohmen, R., 2003. Diffusion coupling between trace and major elements and a model for calculation of magma residence times using plagioclase. Geochimica et Cosmochimica Acta, 67(12): 2189-2200.

Couch, S., Sparks, R.S.J., and Carroll, M.R., 2001. Mineral disequilibrium in lavas explained by convective self-mixing in open magma chambers. Nature, 411: 1037-1039.

Couch, S., Sparks, R.S.J., and Carroll, M.R., 2003. The kinetics of degassing-induced crystallization at Soufrière Hills Volcano, Montserrat. Journal of Petrology, 44: 1477-1502.

Crank, J., 1976. The mathematics of diffusion. Oxford University Press, 414pp.

Danyushevsky, L.V., McNeill, A.W., and Sobolev, A.V., 2002. Experimental and petrological studies of melt inclusions in phenocrysts from mantle-derived magmas: an overview of techniques, advantages and complications. Chemical Geology, 183: 5-24.

Darby, D.J., Hodgkinson, K.H. and Blick, G.H., 2000. Geodetic measurement of deformation in the Taupo Volcanic Zone, New Zealand: the North Taupo Network revisited. New Zealand Journal of Geology and Geophysics, 43(2): 157-170.

Davidson, J., Tepley, F., Palacz, Z. and Meffan-Main, S., 2001. Magma recharge, contamination and residence times revealed by in situ laser ablation isotopic analysis of feldspar in volcanic rocks. Earth and Planetary Science Letters, 184(2): 427-442.

Davidson, J.P. Hora, J.H. Garrison, J.M., and Dungan, M.A., 2005. Crustal forensics in arc magmas. Journal of Volcanology and Geothermal Research, 140: 157-170.

Davidson, J.P., Morgan, D.J., Charlier, B.L.A., Harlou, R., and Hora, J.M., 2007. Microsampling and isotopic analysis of igneous rocks: implications for the study of magmatic systems. Annual Review of Earth and Planetary Sciences, 35(1): 273-311.

Davis, J.H., and Stevenson, D.J., 1992. Physical model of source region of subduction zone volcanics. Journal of Geophysical Research, 97:2037-2070.

Davy, B.W. and Caldwell, T.G., 1998. Gravity, magnetic and seismic surveys of the caldera complex, Lake Taupo, North Island, New Zealand. Journal of Volcanology and Geothermal Research, 81(1-2): 69-89.

Delaney, J.R., Muenow, D.W. and Graham, D.G., 1978. Abundance and distribution of water, carbon and sulfur in the glassy rims of submarine pillow basalts. Geochimica et Cosmochimica Acta, 42: 581-584.

DePaolo, D.J., 1981. Trace-element and isotopic effects of combined wallrock assimilation and fractional crystallization. Earth and Planetary Science Letters, 53(2): 189-202.

DeRonde, C.E.J., Baker, E.T., Massoth, G.J., Lupton, J.E., Wright, I.C., Feely, R.A., and Greene, R.R., 2001. Intra-oceanic subduction-related hydrothermal venting, Kermadec volcanic arc, New Zealand. Earth and Planetary Science Letters, 193: 359-369.

Devine., J.D., Gardner, J.E., Brack, H.P., Layne, G.D., and Rutherford, M.J., 1995. Comparison of microanalytical methods fro estimating H_2O contents of silicic volcanic glasses. American Mineralogist, 80:319-328.

Dixon, J.E., 1997. Degassing of alkalic basalts. American Mineralogist, 82: 368-378.

Dixon, J.E., Stolper, E.M., and Delaney, J.R., 1988. Infrared spectroscopic measurements of CO_2 and H_2O in Juan de Fuca ridge basaltic glasses. Earth and Planetary Science Letters, 90: 87-104.

Dixon, J.E., Stolper, E.M. and Holloway, J.R., 1995. An experimental study of water and carbon dioxide solubilities in mid-ocean ridge basaltic liquids. Part I: Calibration and solubility models. Journal of Petrology, 36: 1607-1631.

Dobson, P.F., Skogby, H. and Rossman, G.R., 1995. Water in boninite glass and coexisting orthopyroxene: concentration and partitioning. Contributions to Mineralogy and Petrology, 118(4): 414-419.

Donoghue, S.L., Gamble, J.A., Palmer, A.S., Stewart, R.B., 1995. Magma mingling in an andesite pyroclastic flow of the Pourahu member, Ruapehu Volcano, New Zealand. Journal of Volcanology and Geothermal Research, 68: 177-191.

Dunbar, N.W., and Kyle, P.R., 1993. Lack of volatile gradient in the Taupo plinian-ignimbrite transition: evidence from melt inclusion analysis. American Mineralogist, 78: 612-618.

Dunn, T., and Sen, C., 1994. Mineral/matrix partition coefficients for orthopyroxene, plagioclase, and olivine in basaltic to andesitic systems: a combined analytical and experimental study. Geochimica et Cosmochimica Acta, 58(2): 717-733.

Eggler, D.H., 1972. Amphibole stability in H_2O-undersaturated calc-alkaline melts. Earth and Planetary Science Letters, 15: 38-44.

Ellis, S.M., Wilson, C.J.N., Bannister, S., Bibby, H.M., Heise, W., Wallace, L., and Patterson, N., 2007. A future magma inflation event under the rhyolitic Taupo volcano, New Zealand: Numerical models based on constraints from geochemical, geological, and geophysical data. Journal of Volcanology and Geothermal Research, 168(1-4): 1-27.

Ewart, A., and Stipp, J.J., 1968. Petrogenesis of the volcanic rocks of the Central North Island, New Zealand, as indicated by a study of $^{87}Sr/^{86}Sr$ ratios, and St, Rb, K, U and Th abundances. Geochimica et Cosmochimica Acta, 32: 699-736.

Ewart, A., and Griffin, W.L., 1994. Application of Proton-Microprobe data to trace element partitioning in volcanic-rocks. Chemical Geology, 117: 251-284.

Fine, G., and Stolper, E., 1985. The speciation of carbon dioxide in sodium aluminosilicate glasses. Contributions to Mineralogy and Petrology, 91: 105-121.

Fogel, R.A. and Rutherford, M.J., 1990. The solubility of carbon dioxide in rhyolitic melts: A quantitative FTIR study. American Mineralogist, 75: 1311-1326.

Frey, F.A., 1969. Rare earth abundances in a high-temperature peridotite intrusion. Geochimica et Cosmochimica Acta, 33(11): 1429-1447.

Frezzotti, M.-L., 2001. Silicate-melt inclusions in magmatic rocks: applications to petrology. Lithos, 55(1-4): 273-299.

Froggatt, P.C., 1981. Stratigraphy and nature of Taupo Pumice Formation. New Zealand Journal of Geology and Geophysics, 24: 231-248.

Froggat, P.C., and Lowe, D.J., 1990. A review of late Quaternary silicic and some other tephra formation from New Zealand – their stratigraphy,

nomenclature, distribution, volume and age. New Zealand Journal of Geology and Geophysics, 33 (1): 89-109.

Fulignati, P., and Marianelli, P., 2007. Tracing volatile exsolution within the 472 AD "Pollena" magma chamber of Vesuvius (Italy) from melt inclusion investigation. Journal of Volcanology and Geothermal Research, 161: 289-302.

Gamble, J.A., Smith, I.E.M., Graham, I.J., Kokelaar, B.P., Cole, J.W., Houghton, B.F., and Wilson, C.J.N., 1990. The petrology, phase relations and tectonic setting of basalts from Taupo Volcanic Zone, New Zealand and the Kermadec Island Arc - Havre Trough, SW Pacific. Journal of Volcanology and Geothermal Research, 43: 235-270.

Gamble, J.A., Smith, I.E.M., McCulloch, M.T., Graham, I.J., and Kokelaar, B.P., 1993. The Geochemistry and petrogenesis of basalts from the Taupo Volcanic Zone and Kermadec Island-Arc, SW Pacific. Journal of Volcanology and Geothermal Research, 54(3-4): 265-290.

Gamble, J., Woodhead, J., Wright, I., and Smith, I., 1996. Basalt and sediment geochemistry and magma petrogenesis in a transect from oceanic island arc to rifted continental margin arc: The Kermadec Hikurangi Margin, SW Pacific. Journal of Petrology, 37(6): 1523-1546.

Gamble, J.A., Wood, C.P., Price, R.C., Smith, I.E.M., Stewart, R.B., and Waight, T., 1999. A fifty year perspective of magmatic evolution on Ruapehu Volcano, New Zealand: Verification of open system behaviour in an arc volcano. Earth and Planetary Science Letters, 170: 301-314.

Gamble, J.A., Price, R.C., Smith, I.E.M., McIntosh, W.C., and Dunbar, N.W., 2003. Ar^{40}/Ar^{39} geochronology of magmatic activity, magma flux and hazards at Ruapehu volcano, Taupo Volcanic Zone, New Zealand. Journal of Volcanology and Geothermal Research, 120(3-4): 15-29.

Gerlach, T.M., 1986. Exsolution of H_2O, CO_2 and S during eruptive episodes at Kilauea volcano, Hawaii. Journal of Geophysical Research, 91: 12177-12185.

Giletti, B.J. and Casserly, J.E.D., 1994. Strontium diffusion kinetics in plagioclase feldspars. Geochimica et Cosmochimica Acta, 58(18): 3785-3793.

Giletti, B.J., and Shanahan T.M., 1997. Alkali diffusion in plagioclase feldspar. Chemical Geology, 139: 3-20.

Ginibre, C., and Wörner, G., 2007. Variable parent magmas and recharge regimes of the Parinacota magma system (N. Chile) revealed by Fe, Mg and Sr zoning in plagioclase. Lithos, 98: 118-140.

Ginibre, C., Kronz, A. and Wörner, G., 2002a. High-resolution quantitative imaging of plagioclase composition using accumulated backscattered electron images: new constraints on oscillatory zoning. Contributions to Mineralogy and Petrology, 142(4): 436-448.

Ginibre, C., Wörner, G., and Kronz, A., 2002b. Minor- and trace-element zoning in plagioclase: implications for magma chamber processes at Parinacota volcano, northern Chile. Contributions to Mineralogy and Petrology, 143: 300-315.

Ginibre, C., Wörner, G. and Kronz, A., 2004. Structure and dynamics of the Laacher See magma chamber (Eifel, Germany) from major and trace element zoning in sanidine: a cathodoluminescence and electron microprobe study. Journal of Petrology, 45: 2197-2223.

Ginibre, C., Wörner, G. and Kronz, A., 2007. Crystal Zoning as an Archive for Magma Evolution. Elements, 3(4): 261-266.

Gioncada, A., Mazzuoli, R., Bisson M., and Pareschi, M.T., 2003. Petrology of volcanic products younger than 42 ka on the Lipari-Vulcano complex (Aeolian Islands, Italy): An example of volcanism controlled by tectonics: Journal of Volcanology and Geothermal Research, 122: 191-220.

Glazner, A.F., Bartley, J.M., Coleman, D.S., Gray, W., and Taylor, R.Z., 2004. Are plutons assembled over millions of years by amalgamation from small magma chambers? GSA Today, 14: 4-11.

Graham, I.J., and Hackett, W.R., 1987. Petrology of Calc-alkaline lavas from Ruapehu Volcano and related vents, Taupo Volcanic Zone, New Zealand. Journal of Petrology, 28: 531-567.

Graham, I.J., and Worthington, T.J., 1988. Petrogenesis of Tauhara dacite (Taupo Volcanic Zone, New Zealand) – Evidence for magma mixing between high-alumina andesite and rhyolite. Journal of Volcanology and Geothermal Research, 35: 279-294.

Graham, I.J., Gulson, B.L., Hedenquist, J.W., and Mizon, K., 1992. Petrogenesis of late Cenozoic volcanic rocks from the Taupo Volcanic Zone, New-Zealand, in the light of new lead isotope data. Geochimica et Cosmochimica Acta, 56(7): 2797-2819.

Graham, I.J., Cole, J.W., Briggs, R.M., Gamble, J.A., and Smith, I.E.M., 1995. Petrology and petrogenesis of volcanic rocks from the Taupo Volcanic Zone - a review. Journal of Volcanology and Geothermal Research, 68(1-3): 59-87.

Grove, T.L., Baker, M.B. and Kinzler, R.J., 1984. Coupled CaAl-NaSi diffusion in plagioclase feldspar: Experiments and applications to cooling rate speedometry. Geochimica et Cosmochimica Acta, 48(10): 2113-2121.

Grove, T.L., Elkins-Tanton, L.T., Parman, S.W., Chatterjee, N., Muntener, O., and Gaetani, G.A., 2003. Fractional crystallization and mantle melting controls on calc-alkaline differentiation trends. Contributions to Mineralogy and Petrology, 145(5): 515-533.

Gurenko, A.A., Trumbull, R.B., Thomas, R., and Lindsay, J.M., 2005. A melt inclusion record of volatiles, trace elements and Li-B isotope variations in a single magma system from the Plat Pays Volcanic Complex, Dominica, Lesser Antilles. Journal of Petrology, 46: 2495-2526.

Haase, K.M., Stroncik, N., Garbe-Schonberg, D., and Stoffers, P., 2006. Formation of island arc dacite magmas by extreme crystal fractionation: an example from Brothers Seamount, Kermadec Island arc (SW Pacific). Journal of Volcanology and Geothermal Research, 152(3-4): 316-330.

Halliday, A.N., Mahood, G.A., Holden, P., Metz, J.M., Dempster, T.J., and Davidson, J.P., 1989. Evidence for long residence times of rhyolitic magma in the Long Valley magmatic system: the isotopic record in precaldera lavas of Glass Mountain. Earth and Planetary Science Letters, 94(3-4): 274-290.

Hammersley, L., and DePaolo, D.J., 2006. Isotopic and geophysical constraints on the structure and evolution of the Clear Lake volcanic system. Journal of Volcanology and Geothermal Research, 153: 331-356.

Harrison, A.J. and White, R.S., 2004. Crustal structure of the Taupo Volcanic Zone, New Zealand: Stretching and igneous intrusion. Geophysical Research Letters, 31: L13615.

Harrison, A., and White, R.S., 2006. Lithospheric structure of an active backarc basin: The Taupo Volcanic Zone, New Zealand. Geophysical Journal International, 167(2): 968-990.

Hauri, E., 2002. SIMS analysis of volatiles in silicate glasses, 2: isotopes and abundances in Hawaiian melt inclusions. Chemical Geology, 183: 115-141.

Hauri, E., Wang, J., Dixon, J.E., King, P.L., Mandeville, C., and Newman, S., 2002. SIMS analysis of volatiles in silicate glasses 1. Calibration, matrix effects and comparisons with FTIR. Chemical Geology, 183: 99-114.

Hawkesworth, C.J., Blake, S., Evans, P., Hughes, R., MacDonald, R., Thomas, L.E., Turner, S.P., and Zellmer, G., 2000. Time scales of crystal fractionation in magma chambers – Integrating physical, isotopic and geochemical perspectives. Journal of Petrology, 41(7): 991-1006.

Hawkesworth, C., George, R., Turner, S., and Zellmer, G., 2003. Estimating the times scales of magmatic processes. In DeVivo, B., and Bodnar, R.J., (Editors) Melt inclusions in volcanic systems: Methods, applications and problems. Developments in Volcanology, 5: 23-43.

Hayden, L.A., and Watson, E.B., 2007. Rutile saturation in hydrous siliceous melts and its bearing on Ti-thermometry of quartz and zircon. Earth and Planetary Science Letters, 258: 561-568.

Heise, W., Bibby, H.M., Caldwell, G., Bannister, S.C., Ogawa, Y., Takakura, S., and Uchida, T., 2007. Melt distribution beneath a young continental rift: The Taupo Volcanic Zone, New Zealand. Geophysical Research Letters, 34: L14313.

Heuman, A., and Davis, G.R., 1997. Isotopic and chemical evolution of the post-caldera rhyolite system at Long Valley, California. Journal of Petrology, 38: 1661-1678.

Higuchi, H., and Nagasawa, H., 1969. Partition of trace elements between rock-forming minerals and the host volcanic rocks. Earth and Planetary Science Letters, 7(3): 281-287.

Hildreth, W., 1981. Gradients in silicic magma chambers: implications for lithospheric magmatism. Journal of Geophysical Research, 86: 10153-10192.

Hildreth, W., 2004. Volcanological perspectives on Long Valley, Mammoth Mountain, and Mono Craters: several contiguous but discrete systems. Journal of Volcanology and Geothermal Research, 136: 169-198.

Hildreth, W., and Wilson, C.J.N., 2007. Compositional zoning of the Bishop Tuff. Journal of Petrology, 48(5): 951-999.

Hildreth, W., Halliday, A.N., and Christiansen, R.L., 1991. Isotopic and chemical evidence concerning the genesis and contamination of basaltic and rhyolitic magma beneath the Yellowstone Plateau volcanic field. Journal of Petrology, 32: 63-138.

Houghton, B.F., Wilson, C.J.N., McWilliams, M.O., Lanphere, M.A., Weaver, S.D., Briggs, R.M., and Pringle, M.S., 1995. Chronology and dynamics of a large silicic magmatic system: Central Taupo Volcanic Zone, New Zealand. Geology, 23(1): 13-16.

Housh, T.B., and Luhr, J.F., Plagioclase-melt equilibria in hydrous systems. American Mineralogist, 76: 477-492.

Humphreys, M.C.S., Blundy, J.D., and Sparks, R.S.J., 2006. Magma Evolution and Open-System Processes at Shiveluch Volcano: insights from Phenocryst Zoning. Journal of Petrology, 47(12): 2303-2334.

Huppert, H.E., and Sparks, S.J., 1988. The generation of granitic magmas by intrusion of basalt into continental crust. Journal of Petrology, 29(3): 599-624.

Ihinger, P.D., Hervig, R.L. and McMillan, P.F., 1994. Analytical methods for volatiles in glasses. In: M.R. Carroll and J.R. Holloway (Editors),

Volatiles in magmas. Mineralogical Society of America, Washington, pp. 517.

Ihinger, P.D., Zhang, Y. and Stolper, E.M., 1999. The speciation of dissolved water in rhyolitic melt. Geochimica et Cosmochimica Acta, 63(21): 3567-3578.

Irving, A.J., and Frey, F.A., 1984. Trace element abundances in megacrysts and their host basalts: constraints on partition coefficients and megacryst genesis. Geochimica et Cosmochimica Acta, 48(6): 1201-1221.

Jarosewich, J.A., Nelen, J.A., and Norberg, J.A., 1980. Reference samples for electron microprobe analysis. Geostandards Newsletter, 4 (1): 43-47.

Jaupart, C. and Tait, S., 1990. Dynamics of eruptive phenomena. In: J. Nicholls and J.K. Russell (Editors), Modern methods of Igneous petrology: understanding magmatic processes. The Mineralogical Society of America, Washington, D.C., pp. 213-236.

Jellinek, A.M. and DePaolo, D.J., 2003. A model for the origin of large silicic magma chambers: precursors of caldera-forming eruptions. Bulletin of Volcanology, 65(5): 363-381.

Jerram, D.A. and Davidson, J.P., 2007. Frontiers in textural and microgeochemical Analysis. Elements, 3(4): 235-238.

Jerram, D.A., and Martin, V.M., 2008. Understanding crystal populations and their significance through the magma plumbing system. In Annen, C., and Zellmer, G.F., (editors). Dynamics of Crustal Magma Transfer, Storage and Differentiation. Geological Society of London Special Publications, 304: 133-148.

Jochum, K. P., Stoll, B., Herwig, K., Willbold, M., Hofmann, A.W., Amini, M., Aarburg, S., Abouchami, W., Hellebrand, E., Mocek, B., Raczek, I.,

Stracke, A., Alard, O., Bouman, C., Becker, S., Dücking, M., Brätz, H., Klemd, R., de Bruin, D., Canil, D., Cornell,D., de Hoog, C-J., Dalpé, C., Danyushevsky, L., Eisenhauer, A., Gao, Y., Snow, J.E., Groschopf, N., Günther, D., Latkoczy, C., Guillong, M., Hauri, E.H., Höfer, H.E., Lahaye, Y., Horz, K., Jacob, D.E., Kasemann, S.A., Kent, A.J.R., Ludwig, T., Zack, T., Mason, P.R.D., Meixner, A., Rosner, M., Misawa, K., Nash, B.P., Pfänder, J., Premo, W.R., Sun, W.D., Tiepolo, M., Vannucci, R., Vennemann, T., Wayne, D., and Woodhead, J., 2006. MPI-DING reference glasses for in situ microanalysis: new reference values for element concentrations and isotope ratios. Geochemistry, Geophysics, Geosystems, 7: Q02008, doi:10.1029/2005GC001060.

Johannes, W., 1989. Melting of plagioclase-quartz assemblages at 2 kbar water pressure. Contributions to Mineralogy and Petrology, 103: 270-276.

Johnson, E.A., 2003. Hydrogen in nominally hydrous crustal minerals. PhD thesis, California Institute of Technology, Pasadena, California.

Johnson, E.A., 2006. Water in Nominally Anhydrous Crustal Minerals: Speciation, Concentration, and Geologic Significance. Reviews in Mineralogy and Geochemistry, 62(1): 117-154.

Johnson, E.A. and Rossman, G.R., 2004. A survey of hydrous species and concentrations in igneous feldspars. American Mineralogist, 89(4): 586-600.

Johnson, E.R., Wallace, P.J., Cashman, K.V., Granados, H.D. and Kent, A.J.R., 2008. Magmatic volatile contents and degassing-induced crystallization at Volcán Jorullo, Mexico: Implications for melt evolution and the plumbing systems of monogenetic volcanoes. Earth and Planetary Science Letters, 269(3-4): 477-486.

Kamenetsky, V., 1996. Methodology for the study of melt inclusions in Cr-spinel, and implications for parental melts of MORB from FAMOUS area. Earth and Planetary Science Letters, 142(3-4): 479-486.

Kawate, S., and Arima, M., 1998. Petrogenesis of the Tanzawa plutonic complex, central Japan: exposed felsic middle crust of the Izu-Bonin-Mariana arc. Island Arc, 7(3): 342-358.

Kent, A.J.R. and Elliot, T.R., 2002. Melt inclusions from Marianas arc lavas: implications for the composition and formation of island arc magmas. Chemical Geology, 183: 263-286.

Kent, A.J.R., Blundy, J., Cashman, K.V., Cooper, K.M., Donnelly, C., Pallister, J.S., Reagan, M., Rowe, M.C., and Thornber, C.R., 2007. Vapor transfer prior to the October 2004 eruption of Mount St. Helens, Washington. Geology, 35(3): 231-234.

Kilgour, G.N., 2002. The nature and dynamics of the Rotorua Eruptive Episode, Okataina Volcanic Centre, Taupo Volcanic Zone. MSc thesis, University of Waikato, Hamilton, New Zealand.

Koyaguchi, T., and Kaneko, K., 1999. A two-stage thermal evolution model of magmas in continental crust. Journal of Petrology, 40: 241-254.

Krippner, S.J.P., Briggs, R.M., Wilson, C.J.N., and Cole, J.W., 1998. Petrography and geochemistry of lithic fragments in ignimbrites from the Mangakino Volcanic Center: Implications for the composition of the subvolcanic crust in western Taupo Volcanic Zone, New Zealand. New Zealand Journal of Geology and Geophysics, 41: 187-199.

Leat, P.T., Smellie, J.L., Millar, I.L., and Larter, R.D., 2003. Magmatism in the South Sandwich arc. In: R.D. Larter, P.T. Leat (Editors), Intra-Oceanic subduction systems: tectonic and Magmatic Processes. Geological Society of London Special Publication 219, London, pp. 285-313.

Le Bas, M.J., Le Maitre, R.W., Streckeisen, A., and Zanettin, B., 1986. A chemical classification of volcanic rocks based on the total alkali-silica diagram. Journal of Petrology, 27: 745-750.

LePage, L.D., 2003. ILMAT: an Excel worksheet for ilmenite-magnetite geothermometry and geobarometry. Computers and Geosciences, 29:673-678.

Lindsey, J.M., Schmitt, A.K., Trumbull, R.B., de Silva, S.L., Siebel, W., and Emmermann, R., (2001). Magmatic evolution of the La Pacana caldera system, Central Andes, Chile: compositional variation of two cogenetic large-volume felsic ignimbrites. Journal of Petrology, 42: 459-486.

Lipman, P.W., 2007. Incremental assembly and prolonged consolidation of Cordilleran magma chambers: Evidence from the Southern Rocky Mountain volcanic field. Geosphere, 3(1):42-70.

Liu, Y., Anderson, A.T., Wilson, C.J.N., Davis, A.M., and Steele, I.M., 2006. Mixing and differentiation in the Oruanui rhyolitic magma, Taupo, New Zealand: evidence from volatiles and trace elements in melt inclusions. Contributions to Mineralogy and Petrology, 151(1): 71-87.

Longhi, J., Walker, D., and Hays, J.F., 1976. Fe and Mg in plagioclase. Proceedings of the 7th Lunar Science Conference, Geochimica et Cosmochimica Acta supplement, 1281-1300.

Lowenstern, J.B., 1993. Evidence for a copper-bearing fluid in magma erupted at the Valley of Ten Thousand Smokes, Alaska. Contributions to Mineralogy and Petrology, 114: 409-421.

Lowenstern, J.B., 2003. Melt Inclusions Come of Age: Volatiles, Volcanoes, and Sorby's Legacy. In: B. De Vivo and R.J. Bodnar (Editors), Melt inclusions in volcanic systems: Methods, applications and problems Developments in Volcanology, 5: 1-21.

Lowenstern, J.B., Smith, R.B. and Hill, D.P., 2006. Monitoring super-volcanoes: geophysical and geochemical signals at Yellowstone and other large caldera systems. Philosophical Transactions of the Royal Society A: Mathematical, Physical and Engineering Sciences, 364(1845): 2055-2072.

Luhr, J., 2001. Glass inclusions and melt volatile contents at Parícutin Volcano, Mexico. Contributions to Mineralogy and Petrology, 142(3): 261-283.

Macpherson, C.G., Gamble, J.A., and Mattey, D.P., 1998. Oxygen isotope geochemistry of lavas from an oceanic to continental arc transition, Kermadec-Hikurangi margin, SW Pacific. Earth and Planetary Science Letters, 160(3-4): 609-621.

Martin, E., and Sigmarsson, O., 2007. Crustal thermal state and origin of silicic magma in Iceland: The case of Torfajökull, Ljosufjökull and Snaefellsjökull volcanoes. Contributions to Mineralogy and Petrology, 153: 593-605.

Martin, H., 1987. Petrogenesis of Archaean trondhjemites, tonalites, and granodiorites from eastern Finland: major and trace element geochemistry. Journal of Petrology, 28: 921-953.

Martin, V.M., Morgan, D.J., Jerram, D.A., Caddick, M.J., Prior, D.J., and Davidson, J.P., 2007. Bang! Month-scale eruption triggering at Santorini volcano. Science, 321: 1178.

Mason, B.G., Pyle, D.M., and Oppenheimer, C., 2004. The size and frequency of the largest explosive eruptions on Earth. Bulletin of Volcanology, 66:735-748.

Massare, D., Metrich, N. and Clocchiatti, R., 2002. High-temperature experiments on silicate melt inclusions in olivine at 1 atm: inference on

temperatures of homogenization and H_2O concentrations. Chemical Geology, 183: 87-98.

McCulloch, M.T. and Gamble, J.A., 1991. Geochemical and geodynamical constraints on subduction zone magmatism. Earth and Planetary Science Letters, 102: 358-374.

McCulloch, M.T., Kyser, T.K., Woodhead, J.D., and Kinsley, L., 1994. Pb-Sr-Nd-O isotopic constraints on the origin of rhyolites from the Taupo Volcanic Zone of New Zealand - Evidence for assimilation followed by fractionation from basalt. Contributions to Mineralogy and Petrology, 115(3): 303-312.

McDonough, W.F., and Sun, S.S., 1995. The Composition of the Earth. Chemical Geology, 120(3-4): 223-253.

McKenzie. D., and O'Nions, R.K., 1991. Partial melt distributions from inversion of rare earth element concentrations. Journal of Petrology, 32(5): 1021-1091.

Miller, C.F. and Wark, D.A., 2008. Supervolcanoes and their explosive supereruptions. Elements, 4(1): 11-15.

Morgan, D.J., and Blake, S., 2006. Magmatic residence times of zoned phenocrysts: introduction and application of the binary element diffusion modelling (BEDM) technique. Contributions to Mineralogy and Petrology, 151: 58-70.

Morgan, D.J., Blake, S., Rogers, N.W., DeVivo, B., Rolandi, G., Macdonald, R., and Hawkesworth, C.J., 2004. Time scales of crystal residence and magma chamber volume from modelling of diffusion profiles in phenocrysts: Vesuvius 1944. Earth and Planetary Science Letters, 222: 933-946.

Morgan, D.J., Blake, S., Rogers, N.W., DeVivo, B., Rolandi, G., and Davidson, J.P., 2006. Magma chamber recharge at Vesuvius in the century prior to eruption of A.D. 79. Geology, 34: 845-848.

Morse, S.A., 1984. Cation Diffusion in Plagioclase Feldspar. Science, 225(4661): 504-505.

Mortimer, N., 2004. New Zealand's Geological Foundations. Gondwana Research, 7: 261-272.

Mysen, B.O., and Virgo, D., 1980. Trace element partitioning and melt structure: An experimental study at 1 atm pressure. Geochimica et Cosmochimica Acta, 44(12): 1917-1930.

Nakagawa, M., Wada, K., Thordarson, T., Wood, C.P., and Gamble, J.A., 1999. Petrologic investigations of the 1995 and 1996 eruptions of Ruapehu Volcano, New Zealand: Formation of discrete and small magma pockets and their intermittent discharge. Bulletin of Volcanology, 61: 15-31.

Nakagawa, M., Wada, K., and Wood, C.P., 2002. Mixed magmas, mush chambers and eruption triggers: Evidence from zoned clinopyroxene phenocrysts in andesitic scoria from the 1995 eruptions of Ruapehu Volcano, New Zealand. Journal of Petrology, 43: 2279-2303.

Nash, W.P., and Crecraft, H.R., 1985. Partition coefficients for trace elements in silicic magmas. Geochimica et Cosmochimica Acta, 49(11): 2309-2322.

Nairn, I.A., 1980. Source, age, and eruptive mechanisms of Rotorua Ash. New Zealand Journal of Geology and Geophysics 23: 193-207.

Nairn, I.A., 1992. The Te Rere and Okareka eruptive episodes – Okataina Volcanic Centre, Taupo Volcanic Zone, New Zealand. New Zealand Journal of Geology and Geophysics, 35: 93-108.

Nairn, I.A., Wood, C.P., and Bailey, R.A., 1994. The Reporoa Caldera, Taupo Volcanic Zone: source of the Kaingaroa Ignimbrite. Bulletin of Volcanology, 56: 529-537.

Nelson, S.T., and Montana, A., 1992. Sieve-textured plagioclase in volcanic rocks produced by rapid decompression. American Mineralogist, 77:1242-1249.

Newhall, C.G. and Self, S., 1982. The volcanic explosivity index (VEI): An estimate of explosive magnitude for historical volcanism. Journal of Geophysical Research, 87: 1231-1238.

Newman, S., Stolper, E.M. and Epstein, S., 1986. Measurement of water in rhyolitic glasses: calibration of an infrared spectroscopic technique. American Mineralogist, 71: 1527-1541.

Newman, S., Epstein, S. and Stolper, E., 1988. Water, carbon dioxide, and hydrogen isotopes in glasses from the ca. 1340 A.D. eruption of the Mono Craters, California: Constraints on degassing phenomena and initial volatile content. Journal of Volcanology and Geothermal Research, 35(1-2): 75-96.

Newman, S. and Lowenstern, J.B., 2002. VOLATILECALC: a silicate melt-H_2O-CO_2 solution model written in Visual Basic for excel. Computers & Geosciences, 28: 597-604.

Nichols, A.R.L. and Wysoczanski, R.J., 2007. Using micro-FTIR spectroscopy to measure volatile contents in small and unexposed inclusions hosted in olivine crystals. Chemical Geology, 242(3-4): 371-384.

Nishimura, K., Kawamoto, T., Kobayashi, T., Sugimoto, T., and Yamashita, S., 2005. Melt inclusion analysis of the Unzen 1991-1995 dacite: implications for crystallization processes of dacite magma. Bulletin of Volcanology, 67: 648-662.

Ochs III, F.A., and Lange, R., 1997. The density of hydrous magmatic liquids. Science, 283: 1314-1317.

Ogawa. Y., Bibby, H.M., Caldwell, T.G., Takakura, S., Uchida, T., Matsushima, N., Bennie, S.L., Tosha, T., and Nishi, Y., 1999. Wide-band magnetotelluric measurements across the Taupo volcanic zone: preliminary results. Geophysical Research Letters, 26: 3673-3676.

Pabst, S., Wörner, G., Civetta, L., and Tesoro, R., 2008. Magma chamber evolution prior to the Campanian Ignimbrite and Neapolitan Yellow Tuff eruptions (Campi Flegrei, Italy). Bulletin of Volcanology, 70: 961-976.

Pallister, J.S., Hoblitt, R.P., and Reyes, A.G., 1992. A basalt trigger for the 1991 eruption of Pinatubo volcano? Nature, 356: 426-428.

Pandya, N., Muenow, D.W. and Sharma, S.K., 1992. The effect of bulk composition on the speciation of water in submarine volcanic glasses. Geochimica et Cosmochimica Acta, 56(5): 1875-1883.

Patterson, D.S., and Graham, I.J., 1988. Petrogenesis of andesitic lavas from Mangatepopo Valley and Upper Tama Lake, Tongariro Volcanic Centre, New Zealand. Journal of Volcanology and Geothermal Research, 35: 17-29.

Parson, L.M., and Wright, I.C., 1996. The Lau-Havre-Taupo back-arc basin: a southward-propagating, multi-stage evolution from rifting to spreading. Tectonophysics, 263(1-4): 1-22.

Pearce, J.A., Baker, P.E., Harvey, P.K., and Luff, I.W., 1995. Geochemical evidence for subduction fluxes, mantle melting and fractional crystallization beneath the South Sandwich-Island Arc. Journal of Petrology, 36(4): 1073-1109.

Pearce, T.H., and Kolisnik, A.M., 1990. Observation of plagioclase zoning using interference imaging. Earth Science Reviews, 29: 9-26.

Portnyagin, M., Almeev, R., Matveev, S. and Holtz, F., 2008. Experimental evidence for rapid water exchange between melt inclusions in olivine and host magma. Earth and Planetary Science Letters, 272: 541-552.

Price, R.C., Gamble, J.A., Smith, I.E.M., Stewart, R.B., Eggins, S., and Wright, I.C., 2005. An integrated model for the temporal evolution of andesites and rhyolites and crustal development in New Zealand's North Island. Journal of Volcanology and Geothermal Research, 140(1-3): 1-24.

Price, R.C., George, R., Gamble, J.A., Turner, S., Smith, I.E.M., Cook, C., Hobden, B., and Dosseto, A., 2007. U-Th-Ra fractionation during crustal-level andesite formation at Ruapehu volcano, New Zealand. Chemical Geology, 244 (3-4): 437-451.

Putirka, K.D., 2005. Igneous thermometers and barometers based on plagioclase + liquid equilibria: Tests of some existing models and new calibrations. American Mineralogist, 90(2-3): 336-346.

Qin, Z., Lu, F. and Anderson, A.T., 1992. Diffusive reequilibration of melt and fluid inclusions. American Mineralogist, 77: 565-576.

Rapp, R.P., and Watson, E.B., 1995. Dehydration melting of metabasalt at 8-32-Kbar - implications for continental growth and crust-mantle recycling. Journal of Petrology, 36(4): 891-931.

Reid, F.E., 1982. Geochemistry of Central North Island greywackes and genesis of silicic magmas. PhD thesis, Victoria University of Wellington, Wellington, 329 pp.

Reid, F., 1983. Origin of the rhyolitic rocks of the Taupo Volcanic Zone, New Zealand. Journal of Volcanology and Geothermal Research, 15(4): 315-338.

Reid, M.R., 2003. Timescales of magma transfer and storage in the crust. In Rudnick, R.L., (editors) The Crust, Treatise on Geochemistry 3, Elsevier, Oxford, pp 167-193.

Reid, M.R., 2008. How Long Does It Take to Supersize an Eruption? Elements, 4(1): 23-28.

Reid, M.R., Coath, C.D., Mark Harrison, T. and McKeegan, K.D., 1997. Prolonged residence times for the youngest rhyolites associated with Long Valley Caldera: ^{230}Th-^{238}U ion microprobe dating of young zircons. Earth and Planetary Science Letters, 150(1-2): 27-39.

Roedder, E., 1979. Origin and significance of magmatic inclusions. Bulletin of Mineralogy, 102: 487-510.

Ruprecht, P., and Wörner, G., 2007. Variable regimes in magma systems documented in plagioclase zoning patterns: El Misti stratovolcano and Andahua monogenetic cones. Journal of Volcanology and Geothermal Research, 165: 142-162.

Schmitz, M.D., and Smith, I.E.M., 2004. The petrology of the Rotoiti eruption sequence, Taupo Volcanic Zone: an example of fractionation and mixing in a rhyolitic system. Journal of Petrology, 45(10): 2045-2066.

Schmidt, M.W., and Poli, S., 1998. Experimentally based water budgets for dehydrating slabs and consequences for arc magma generation. Earth and Planetary Science Letters, 163: 361-379.

Severs, M.J., Azbej, T., Thomas, J.B., Mandeville, C.W. and Bodnar, R.J., 2007. Experimental determination of H_2O loss from melt inclusions during

laboratory heating: Evidence from Raman spectroscopy. Chemical Geology, 237(3-4): 358-371.

Shane, P., Smith, V.C., and Nairn, I.A., 2005. High temperature rhyodacites of the 36 ka Hauparu pyroclastic eruption, Okataina Volcanic Centre, New Zealand: Change in a silicic magmatic system following caldera collapse. Journal of Volcanology and Geothermal Research, 147: 357-376.

Shane, P., Martin, S.B., Smith, V.C., Beggs, K.F., Darragh, M.B., Cole, J.W., and Nairn, I.A., 2007. Multiple rhyolite magmas and basalt injection in the 17.7 ka Rerewhakaaitu eruption episode from Tarawera volcanic complex, New Zealand. Journal of Volcanology and Geothermal Research, 164: 1-26.

Shane, P., Smith, V.C., and Nairn, I., 2008. Millennial timescale resolution of rhyolite magma recharge at Tarawera volcano: insights from quartz chemistry and melt inclusions. Contributions to Mineralogy and Petrology, 156(3): 397-411.

Shaw, H.R., 1972. Viscosities of magmatic silicate liquids; an empirical method of prediction. American Journal of Science, 272(9): 870-893.

Sherburn, S., Bannister, S. and Bibby, H., 2003. Seismic velocity structure of the central Taupo Volcanic Zone, New Zealand, from local earthquake tomography. Journal of Volcanology and Geothermal Research, 122(1-2): 69-88.

Shukuno, H., Tamura, Y., Tani, K., Chang, Q., Suzuki, T., and Fiske, R.S., 2006. Origin of silicic magmas and the compositional gap at Sumisu submarine caldera, Izu-Bonin arc, Japan. Journal of Volcanology and Geothermal Research, 156: 187-216.

Shor, G.G., Kirk, H.K., and Menard, H.W., 1971. Crustal structure of the Melanesian Area. Journal of Geophysical Research, 76: 2562-2586.

Siebel, W., Schnurr, W.B., Hahne, K., Kraemer, B., Trumbull, R., Van den Bogaard, P., and Emmermann, R., 2000. Geochemistry and isotope systematics of small to medium volume Neogene-Quaternary ignimbrites in the southern central Andes: Evidence for derivation from andesitic magma source. Chemical Geology, 171: 213-237.

Silver, L.A. and Stolper, E., 1985. A thermodynamic model for hydrous silicate melts. Journal of Geology, 93: 161-178.

Silver, L.A., Ihinger, P.D. and Stolper, E., 1990. The influence of bulk composition on the speciation of water in silicate glasses. Contributions to Mineralogy and Petrology, 104: 142-162.

Singer, B.S., Dungan, M.A. and Layne, G.D., 1995. Textures and Sr, Ba, Mg, Fe, K and Ti compositional profiles in volcanic plagioclase -clues to the dynamics of calc-alkaline magma chambers. American Mineralogist, 80(7-8): 776-798.

Sisson, T.W. and Bacon, C.R., 1999. Gas-driven filter pressing in magmas. Geology, 27(7): 613-616.

Smith, I.E.M., and Price, R.C., 2006. Tonga-Kermadec arc and Havre-Lau back-arc system: their role in the development of tectonic and magmatic models for the western Pacific. Journal of Volcanology and Geothermal Research, 156(3-4): 315-331.

Smith, I.E.M., Worthington, T.J., Stewart, R.B., Price, R.C., and Gamble, J.A., 2003a. Felsic volcanism in the Kermadec Arc, SW Pacific: crustal recycling in an oceanic setting. In: R.D. Larter, P.T. Leat (Editors), Intra-Oceanic Subduction Systems: Tectonic and Magmatic Processes. Geological Society of London Special Publication 219: 99-118.

Smith, I.E.M., Stewart, R.B., and Price, R.C., 2003b. The petrology of a large intra-oceanic silicic eruption: the Sandy Bay Tephra, Kermadec Arc, Southwest Pacific. Journal of Volcanology and Geothermal Research, 124: 173-194.

Smith, I.E.M., Worthington, T.J., Price, R.C., Stewart, R.B., and Maas, R., 2006. Petrogenesis of dacite in an oceanic subduction environment: Raoul Island, Kermadec arc. Journal of Volcanology and Geothermal Research, 156(3-4): 252-265.

Smith, R.L., 1979. Ash-flow magmatism. In Chapin, C.E., and Elston, W.E., (Editors), Ash-flow Tuffs. Geological Society of America Special Publication, 180:5-17.

Smith, V.C., Shane, P., and Smith, I.E.M., 2002. Tephrostratigraphy and geochemical fingerprints of the Mangaone subgroup tephra beds, Okataina Volcanic Centre, New Zealand. New Zealand Journal of Geology and Geophysics, 45: 207-219.

Smith, V.C., Shane, P., and Nairn, I.A., 2004. Reactivation of a rhyolitic magma body by new rhyolite intrusion before the 15.8ka Rotorua eruptive episode: implications for magma storage in the Okataina Volcanic Centre, New Zealand. Journal of the Geological Society of London, 161: 757-772.

Smith, V.C., Shane, P., Nairn, I.A., and Williams, C.M., 2006. Geochemistry and magmatic properties of eruption episodes from Haroharo linear vent zone, Okataina Volcanic Centre, New Zealand during the last 10 Kyr. Bulletin of Volcanology, 69: 57-88.

Sobolev, A.V., 1996. Melt inclusions in minerals as a source of principle petrological information. Petrology, 4(3): 209-220.

Sobolev, A.V. and Chaussidon, M., 1996. H2O concentrations in primary melts from supra-subduction zones and mid-ocean ridges: Implications for H2O

storage and recycling in the mantle. Earth and Planetary Science Letters, 137(1-4): 45-55.

Soengkono, S., 1995. A magnetic model for deep plutonic bodies beneath the central Taupo Volcanic Zone, North Island, New Zealand. Journal of Volcanology and Geothermal Research, 68: 193-207.

Spandler, C., O'Neill, H.St C., Kamenetsky, V.S., 2007. Survival times of anomalous melt inclusions from element diffusion in olivine and chromite. Nature, 447: 303-306.

Sparks, R.S.J., 2003. Dynamics of magma degassing. In, Oppenheimer, C., Pyle, D.M., and Barclay, J. (eds). Volcanic degassing. Geological Society, London, Special Publications, 213(1): 5-22.

Sparks, R.S.J., Self, S., Grattan, J.P., Oppenheimer, C., Pyle, D.M. and Rymer, H., 2005. Supereruptions: global effects and future threats. Report of a Geological Society of London Working Group, The Geological Society of London, 24pp.

Stern, T.A., 1985. A back-arc basin formed within continental lithosphere: the Central Volcanic Region of New Zealand. Tectonophysics, 122: 385-409.

Stern, T.A., 1987. Asymmetric back-arc spreading, heat flux and structure beneath the Central Volcanic Region of New Zealand. Earth and Planetary Science Letters, 85: 265-267.

Stolper, E., 1982. The speciation of water in silicate melts. Geochimica et Cosmochimica Acta, 46(12): 2609-2620.

Stratford, W.R., and Stern, T.A., 2006. Crust and upper mantle structure of a continental backarc: central North Island, New Zealand. Geophysical Journal International, 166(1): 469-484.

Stratford, W.R., and Stern, T.A., 2008. Geophysical imaging of buried volcanic structures within a continental back-arc basin: the Central Volcanic Region, North Island, New Zealand. Journal of Volcanology and Geothermal Research, 174: 257-268.

Sun, S.S., and McDonough, W.F., 1989. Chemical and isotopic systematics of oceanic basalts: implications for mantle composition and processes. In: A.D. Saunders, M.J. Norry (Editors), Magmatism in Ocean Basins. Geological Society of London Special Publication, 42: 313-345.

Sun, W.D., Binns, R.A., Fan, A.C., Kamenetsky, V.S., Wysoczanski, R., Wei, G.J., Hu, Y.H., and Arculus, R.J., 2007. Chlorine in submarine volcanic glasses from the eastern Manus basin. Geochimica et Cosmochimica Acta, 71: 1542-1552.

Sutton, A.N., Blake, S., and Wilson, C.J.N., 1995. An outline geochemistry of rhyolite eruptives from Taupo Volcanic Centre, New-Zealand. Journal of Volcanology and Geothermal Research, 68(1-3): 153-175.

Sutton, A.N., Blake, S., Wilson, C.J.N., and Charlier, B.L.A., 2000. Late Quaternary evolution of a hyperactive rhyolite magmatic system: Taupo volcanic centre, New Zealand. Journal of the Geological Society, London, 157: 537-552.

Synder, D., 2000. Thermal effects of the intrusion of basaltic magma into a more silicic magmas chamber and implications for eruption triggering. Earth and Planetary Sciences, 175: 257-273.

Takagai, T., Orihashi, Y., Naito, K., and Watanabe, Y. 1999. Petrology of a mantle-derived rhyolite, Hokkaido, Japan. Chemical Geology, 160: 425-445.

Tamura, Y., and Tatsumi, Y., 2002. Remelting of an andesitic crust as a possible origin for rhyolitic magma in oceanic arcs: an example from the Izu-Bonin Arc. Journal of Petrology, 43(6): 1029-1047.

Tamura, Y., and Wysoczanski, R., 2006. Silicic volcanism and crustal evolution in oceanic arcs: Introduction. Journal of Volcanology and Geothermal Research, 156(3-4): v-vii.

Turner, S. and Costa, F., 2007. Measuring Timescales of Magmatic Evolution. Elements, 3(4): 267-272.

Tuttle, O.F. and Bowen, N.L., 1958. Origin of granite in the light of experimental studies in the system $NaAlSi_3O_8$ -$KASi_3O_8$ – SiO_2-H_2O. Geological Society America Memoir, 74.

Ukstins Peate, I., Baker, J.A., Kent, A.J.R., Al-Kadasi, M., Al-Subbary, A., Ayalew, D., and Menzies, M., 2003. Correlation of Indian Ocean tephra to individual Oligocene silicic eruptions from Afro-Arabian flood volcanism. Earth and Planetary Science Letters, 211: 311-327.

Ukstins Peate, I., Baker, J.A., Al-Kadasi, M., Al-Subbary, A., Knight, K.B., Riisager, P., Thirlwall, M.F., Peate, DW., Renne, P.R., and Menzies, M.A., 2005. Volcanic Stratigraphy of large-volume silicic pyroclastic eruptions during Oligocene Afro-Arabian flood volcanism in Yemen. Bulletin of Volcanology, 68: 135-156.

Ukstins Peate, I., Kent, A.J.R., Baker, J.A., and Menzies, M.A., 2007. Extreme geochemical heterogeneity in Afro-Arabian Oligocene tephras: Preserving fractional crystallization and mafic recharge processes in silicic magma chambers. Lithos, 102: 260-278.

Venezky, D.Y., and Rutherford, M.J., 1999. Petrology and Fe-Ti oxide reequilibration of the 1991 Mount Unzen mixed magma. Journal of Volcanology and Geothermal Research, 89:213-230.

Waight, T.E., Price, R.C., Stewart, R.B., Smith, I.E.M. and Gamble, J.A., 1999. Stratigraphy and geochemistry of the Turoa area, with implications for andesite petrogenesis at Mt. Ruapheu, Taupo Volcanic Zone, New Zealand. New Zealand Journal of Geology and Geophysics, 42: 513-532.

Wallace, P.J., 2005. Volatiles in subduction zone magmas: concentrations and fluxes based on melt inclusion and volcanic gas data. Journal of Volcanology and Geothermal Research, 140(1-3): 217-240.

Wallace, P.J., Dufek, J., Anderson, A.T. and Zhang, Y., 2003. Cooling rates of Plinian-fall and pyroclastic-flow deposits in the Bishop Tuff: inferences from water speciation in quartz-hosted glass inclusions. Bulletin of Volcanology, 65: 105-123.

Walker Jr., B.A., Miller, C.F., Lowery Claiborne, L., Wooden, J.L., and Miller, J.S., 2007. Geology and geochronology of the Spirit Mountain batholith southern Nevada: Implications for timescales and physical processes of batholith construction. Journal of Volcanology and Geothermal Research, 167: 239-262.

Wark, D.A. and Spear, F.S., 2005. Ti in quartz: Cathodoluminescence and thermometry. Geochimica et Cosmochimica Acta, 69: A592.

Wark, D.A., and Watson, E.B., 2006. TitaniQ: A titanium-in-quartz geothermometer. Contributions to Mineralogy and Petrology, 152: 743-754.

Wark, D.A., Hildreth, W., Spear, F.S., Cherniak, D.J., and Watson, E.B., 2007. Pre-eruption recharge of the Bishop magma system. Geology, 35(3): 235-238.

Watson, E.B., and Green, T.H., 1981. Apatite/liquid partition coefficients for the rare earth elements and strontium. Earth and Planetary Science Letters, 56: 405-421.

Wiebe, R.A., Wark, D.A., and Hawkins, D.P., 2007. Insights from quartz cathodoluminescence zoning into crystallisation of the Vinalhaven granite, coastal Maine. Contributions to Mineralogy and Petrology, 154: 439-453.

Wilke, M., and Behrens, H., 1999. The dependence of the partitioning of iron and europium between plagioclase and hydrous tonalitic melt on oxygen fugacity. Contributions to Mineralogy and Petrology, 137: 102-114.

Wilson, C.J.N., 2001. The 26.5 ka Oruanui eruption, New Zealand: an introduction and overview. Journal of Volcanology and Geothermal Research, 112: 133-174.

Wilson, C.J.N., and Walker, G.P.L., 1985. The Taupo Eruption, New Zealand: 1. General aspects. Philosophical Transactions of the Royal Society of London Series A: Mathematical, Physical and Engineering Sciences, 134(1529): 199-228.

Wilson, C.J.N., Rogan, A.M., Smith, I.E.M., Northey, D.J., Nairn, I.A., and Houghton, B.F., 1984. Caldera volcanoes of the Taupo Volcanic Zone, New Zealand. Journal of Geophysical Research, 89 (B10): 8463-8484.

Wilson, C.J.N., Houghton, B.F., and Lloyd, E.F., 1986. Volcanic history and evolution of the Maroa-Taupo area central North Island. In: I.E.M. Smith (Editor), Late Cenozoic volcanism in New Zealand. Royal Society of New Zealand Bulletin, pp. 194-223.

Wilson, C.J.N., Houghton, B.F., McWilliams, M.O., Lanphere, M.A., Weaver, S.D., and Briggs, R.M., 1995. Volcanic and structural evolution of Taupo Volcanic Zone, New Zealand: a review. Journal of Volcanology and Geothermal Research, 68: 1-28.

Wilson, C.J.N., Blake, S., Charlier, B.L.A., and Sutton, A.N., 2006. The 26.5 ka Oruanui eruption, Taupo volcano, New Zealand: development, characteristics and evacuation of a large rhyolitic magma body. Journal of Petrology, 47(1): 34-69.

Wilson, C.J.N., Gravley, D.M., Leonard, G.S. and Rowland, J.V., in press. Volcanism in the central Taupo Volcanic Zone, New Zealand: tempo, styles and controls, Studies in Volcanology: The Legacy of George Walker. The Geological Society of London, London.

Wilson, L., 1980. Relationships between pressure, volatile content and ejecta velocity in three types of volcanic explosion. Journal of Volcanology and Geothermal Research, 8(2-4): 297-313.

Wolf, M.B., and Wyllie, P.J., 1994. Dehydration-melting of amphibolite at 10 Kbar - the effects of temperature and time. Contributions to Mineralogy and Petrology, 115(4): 369-383.

Woodhead, J., Eggins, S.M., and Gamble, J., 1993. High-field strength and transition element systematics in island-arc and back-arc basin basalts: evidence for multiphase melt extraction and depleted mantle wedge. Earth and Planetary Science Letters, 144(4): 491-504.

Woodhead, J.D., Eggins, S.M., and Johnson, R.W., 1998. Magma genesis in the New Britain island arc: further insights into melting and mass transfer processes. Journal of Petrology, 39(9): 1641-1668.

Wright, I.C., 1994. Nature and tectonic setting of the southern Kermadec submarine arc volcanoes: an overview. Marine Geology, 118(3-4): 217-236.

Wright, I.C., and Gamble, J.A., 1999. Southern Kermadec submarine caldera arc volcanoes (SW Pacific): caldera formation by effusive and pyroclastic eruption. Marine Geology, 161: 207-227.

Wright, I.C., Stoffers, P., Hannington, M., de Ronde, C.E.J., Herzig, P., Smith, I.E.M., and Browne, P.R.L., 2002. Towed-camera investigations of shallow-intermediate water-depth submarine stratovolcanoes of the southern Kermadec arc, New Zealand. Marine Geology, 185(3-4): 207-218.

Wright, I.C., Gamble, J.A., and Shane, P.A.R., 2003. Submarine silicic volcanism of the Healy caldera, southern Kermadec arc (SW Pacific): I - volcanology and eruption mechanisms. Bulletin of Volcanology, 65(1): 15-29.

Wright, I.C., Worthington, T.J., and Gamble, J.A., 2006. New multibeam mapping and geochemistry of the 30°-35°S sector, and overview, of southern Kermadec arc volcanism. Journal of Volcanology and Geothermal Research, 149: 263-296.

Wysoczanski, R.J., and Tani, K., 2006. Spectroscopic FTIR imaging of water species in silicic volcanic glasses and melt inclusions: an example from the Izu-Bonin arc. Journal of Volcanology and Geothermal Research, 156(3-4): 302-314.

Wysoczanski, R.J., Wright, I.C., Gamble, J.A., Hauri, E.H., Luhr, J.F., Eggins, S.M., and Handler, M.R., 2006. Volatile contents of Kermadec Arc-Havre Trough pillow glasses: fingerprinting slab-derived aqueous fluids in the mantle sources of arc and back-arc lavas. Journal of Volcanology and Geothermal Research, 152(1-2): 51-73.

Wysoczanski, R.J., Todd, E., Wright, I.C., Leybourne, M., Hergt, J.M., Adam, C., and Mackay, K., in press. Backarc rifting, constructional volcanism

and possible nascent spreading in the southern Havre Trough backarc rifts (SW Pacific). Journal of Volcanology and Geothermal Research.

Xu, Z. and Zhang, Y., 2002. Quench rates in air, water, and liquid nitrogen, and inference of temperature in volcanic eruption columns. Earth and Planetary Science Letters, 200(3-4): 315-330.

Yoder, H., S., Jr, Stewart, D., B., and Smith, J., R.. 1957. Ab-An-H_2O, An-Or-H_2O, and Ab-Or-H_2O at 5000 bars. Geological Society of American Bulletin, 68(12): 1815.

Yokoyama, T., Okumura, S. and Nakashima, S., 2007. Hydration of rhyolitic glass during weathering as characterised by IR microscpectroscopy. Geochimica et Cosmochimica Acta, 72: 117-125.

Zellmer, G.F., Blake, S., Vance, D., Hawkesworth, C. and Turner, S., 1999. Plagioclase residence times at two island arc volcanoes (Kameni Islands, Santorini, and Soufriere, St. Vincent) determined by Sr diffusion systematics. Contributions to Mineralogy and Petrology, 136(4): 345-357.

Zellmer, G.F., Sparks, R.S.J., Hawkesworth, C.J. and Wiedenbeck, M., 2003. Magma emplacement and remobilization timescales beneath Montserrat: Insights from Sr and Ba zonation in plagioclase phenocrysts. Journal of Petrology, 44(8): 1413-1431.

Zhang, X., Zhang, H-F., Tang, Y-J., Wilde, S.A., and Hu, Z., 2008. Geochemistry of Permian bimodal volcanic rocks from central Inner Mongolia, North China: Implications for tectonic setting and Phanerozoic continental growth in central Asian Orogenic Belt. Chemical Geology, 249: 262-283.

Zhang, Y., 1994. Reaction kinetics, geospeedometry, and relaxation theory. Earth and Planetary Science Letters, 122: 373-391.

Zhang, Y., 1999. H_2O in rhyolitic glasses and melts: measurement, speciation, solubility and diffusion. Reviews of Geophysics, 37: 493-516.

Zhang, Y., 2007. Silicate melt properties and volcanic eruptions. Reviews of Geophysics, 45: RG4004

Zhang, Y., Stolper, E.M. and Wasserburg, G.J., 1991. Diffusion of water in rhyolitic glasses. Geochimica et Cosmochimica Acta, 55(2): 441-456.

Zhang, Y., Stolper, E.M. and Ihinger, P.D., 1995. Kinetics of the reaction H_2O + O = 2OH in rhyolitic and albitic glasses: Preliminary results. American Mineralogist, 80: 593-612.

Zhang, Y., Jenkins, J. and Xu, Z., 1997a. Kinetics of the reaction H_2O + O -->2 2OH in rhyolitic glasses upon cooling: Geospeedometry and comparison with glass transition. Geochimica et Cosmochimica Acta, 61(11): 2167-2173.

Zhang, Y., Belcher, R., Ihinger, P.D., Wang, L., Xu, Z., and Newman, S., 1997b. New calibration of infrared measurement of dissolved water in rhyolitic glasses. Geochimica et Cosmochimica Acta, 61(15): 3089-3100.

Zhang, Y., Xu, Z. and Behrens, H., 2000. Hydrous species geospeedometer in rhyolite: improved calibration and application. Geochimica et Cosmochimica Acta, 64(19): 3347-3355.

Zhang, Y., Xu, Z. and Wang, H., 2007. Silicate melt properties and volcanic eruptions. Reviews of Geophysics, 45: RG4004.

Zindler, A., and Hart, S., 1986. Chemical geodynamics. Annual Reviews of Earth and Planetary Sciences, 14: 493-571.

Appendix 1

Samples and Analytical Methods

This appendix documents all information pertaining to analysed samples and analytical methods.

A1.1 Fieldwork and Samples

Samples were collected from the Taupo Volcanic Zone in April 2006. Whole rock ignimbrite, pumice and lavas samples were collected (Table A1.1). A thorough thin section examination revealed the presence or absence of suitable crystals hosting melt inclusions and zoned crystals permitting the samples used in this study to be selected. Individual pumice samples were preferred as syn- and post- eruptive processes can alter the groundmass, obscuring the original magmatic processes (e.g. Hildreth, 1981; Brown et al., 1998). However, in the more highly welded ignimbrite units (e.g. Whakamaru), separation of pumices could not be achieved for all samples and whole rock ignimbrite samples were obtained and analysed. As this study focused on mineral specific processes it was not as critical to sample individual pumices, but this was preferred where possible.

Dr. Ian Wright from the National Institute of Water and Atmospheric Research (NIWA), presently at the University of Southampton, UK generously provided offshore samples from Healy seamount (Table A1.1). These samples were dredged during a cruise in February 1996 by the RV *Tangaroa* (Wright and Gamble 1999).

Field Number	Sample Number	Unit	Latitude	Longitude	Elevation (m)	Brief Description	Collection date	Volcanic Centre
KS 1	TA1	Taupo Ignimbrite	S 39°13.092'	E 175°44.115'	922	crystal lag from base of ignimbrite	08/04/2006	Taupo
KS 2	TA2	Taupo Ignimbrite	S 39°13.092'	E 175°44.115'	922	pumice from ignimbrite	08/04/2006	Taupo
KS 3		Mamaku Ignimbrite	S 38°03.343'	E 176°25.729'		welded ignimbrite	09/04/2006	Rotorua
KS 5	RA1	Rotorua Ash	S 38°10.338'	E 176°19.765'		pumice and lapilli	09/04/2006	Rotorua
KS 6	RA2	Rotorua Ash	S 38°10.327'	E 176°19.716'		pumice and lapilli above KS 5 in sequence	09/04/2006	Rotorua
KS 7	RA3	Rotorua Ash	S 38°10.338'	E 176°19.765'		crystal rich layer within airfall deposits	09/04/2006	Rotorua
KS 8		Rhyolite dome, Okataina caldera	S 38°10.338'	E 176°19.765'		rhyolite	09/04/2006	Okataina
KS 9	WH3	Whakamaru Ignimbrite	S 38°20.953'	E 175°44.034'	250	crystal rich ignimbrite (top)	09/04/2006	Whakamaru
KS 10		Whakamaru Ignimbrite	S 38°20.911'	E 175°43.955'	237	crystal rich ignimbrite	09/04/2006	Whakamaru
KS 11	WH4	Whakamaru Ignimbrite	S 38°20.782'	E 175°44.033'	246	crystal rich ignimbrite	09/04/2006	Whakamaru
KS 12	WH5	Whakamaru Ignimbrite	S 38°20.782'	E 175°44.033'	246	crystal rich ignimbrite	09/04/2006	Whakamaru
KS 13	WH6	Whakamaru Ignimbrite	S 38°20.737'	E 175°44.110'	211	crystal rich ignimbrite	09/04/2006	Whakamaru
KS 14	WH7	Whakamaru Ignimbrite	S 38°20.799'	E 175°44.144'	198	crystal rich ignimbrite	09/04/2006	Whakamaru
KS 15		Whakamaru Ignimbrite	S 38°20.813'	E 175°44.151'	183	crystal rich ignimbrite (welded)	09/04/2006	Whakamaru
KS 16	WH2	Whakamaru Ignimbrite	S 38°20.849'	E 175°44.206'	170	crystal rich ignimbrite (highly welded) (base)	09/04/2006	Whakamaru
KS 17		Poihipi Rd Obsidian	S 38°35.154'	E 175°57.286'	658	obsidian	10/04/2006	
KS 21a	OR1	Oruanui Ignimbrite	S 38°35.840'	E 175°58.685'	611	pumice	10/04/2006	Taupo
KS 21b	OR2	Oruanui Ignimbrite	S 38°35.840'	E 175°58.685'	611	ash matrix	10/04/2006	Taupo
KS 24		Tauhara Dacite	S 38°40.790'	E 176°10.865'	591	dacite	10/04/2006	
KS 25		Taupo Plinian	S 38°42.520'	E 176°07.330'	412	pumice	11/04/2006	Taupo
KS 26		Taupo Plinian	S 38°43.026'	E 176°09.820'	584	pumice	11/04/2006	Taupo
KS 27	TA3	Taupo Plinian	S 38°55.772'	E 176°29.255'	711	airfall deposit	11/04/2006	Taupo
KS 28		Taupo Plinian (crystal lag)	S 38°55.772'	E 176°29.255'	711	crystal lag	11/04/2006	Taupo
KS 29	TA4	Hatepe Plinian	S 38°55.772'	E 176°29.255'	711	airfall deposit	11/04/2006	Taupo
KS 30		Rangitaiki Ignimbrite	S 38°57.016'	E 176°31.020'	692	welded ignimbrite	11/04/2006	Whakamaru
WH	WH1	Whakamaru Ignimbrite	S 38°21.005'	E 175°42.037'		crystal lag from basal layer	04/2005	Whakamaru
X590	X590	Healy Volcano	S 34°59.249'	E 178°59.573'	1638-1658	pumice	05/02/1996	Healy
X590/B	X590/B	Healy Volcano	S 34°59.249'	E 178°59.573'	1638-1658	pumice	05/02/1996	Healy
X609	X609	Healy Volcano	S 34°57.490'	E 179°00.522'	1719-1724	pumice with mafics	07/02/1996	Healy
X612/B		Healy Volcano	S 34°58.288'	E 179°02.549'	1480-1551	grey pumice with flatten fiamme	07/02/1996	Healy
X612/C		Healy Volcano	S 35°01.172'	E 178°57.509'	1480-1551	grey pumice	07/021996	Healy

Table A1.1. Summary of samples collected for this study. Elevation for Healy samples represents the water depths at the beginning and end of each sample dredge.

A1.2 Sample preparation

Blocks of pumice were coarsely crushed using a mortar and pestle and dry sieved to extract material finer than 1mm. Pumice was floated off by washing with water and the remaining material dried for 12 - 24 hours at 40 °C. Crystal lag, matrix material and crushed samples were further sieved into 1mm – 710 μm, 710 – 500 μm and <500 μm fractions and magnetically separated on a Frantz magnetic separator.

A1.2.1 Melt inclusions

Of the initial six Taupo Volcanic Zone rhyolitic eruptions (Mamaku ignimbrite; Rotorua eruptive; Whakamaru ignimbrite; Rangitaiki ignimbrite; Oruanui ignimbrite; Taupo ignimbrite) sampled and processed for melt inclusions only the Rotorua eruptive, Whakamaru and Oruanui ignimbrites and Taupo samples contained melt inclusions suitable for analysis.

Quartz, plagioclase and orthopyroxene crystals containing the largest melt inclusions were hand picked under a binocular microscope from the 1 mm - 710 μm size fraction and the 710 - 500 μm size fraction in the extremely crystal sparse samples. Melt inclusions were exposed by placing a single phenocryst in crystal bond cement on a glass slide and then grinding using 600, 2400 and 4000 grit silicon carbide paper, until the inclusion became exposed. Crystals containing exposed melt inclusions were then removed and washed in acetone to eliminate any excess crystal bond, mounted in epoxy blocks and finely polished using 3 μm and ¼ μm diamond paste. Melt inclusions that were analysed for H_2O and CO_2 after major element analysis and were removed from the epoxy

mounts with a fine tip soldering iron. Crystals were washed in acetone, remounted in crystal bond and the parallel surface polished as above. This obtained parallel polished exposed surfaces of the melt inclusions allowing for analysis for H_2O and CO_2 by Fourier transform infrared (FTIR) spectrometry. Transmitted and reflected light photos of each crystal were obtained prior to chemical analysis and used for identification purposes throughout.

A1.2.2 Crystals

Quartz, plagioclase, orthopyroxene and Fe-Ti oxides were hand picked from the 1 mm - 710 μm size fraction under a binocular microscope. Approximately 15 - 25 crystals were mounted in semi-circular epoxy mounts from each sample. Centres of the crystals were exposed by grinding the epoxy blocks with 600, 2400 and 4000 grit silicon carbide paper and polished using 3 μm and ¼ μm diamond paste. Thick polished sections (100 μm) of Whakamaru samples were also prepared for plagioclase analyses. These thick sections were examined under a petrographic microscope to identify the most suitable plagioclase crystals and to determine whether the crystals appear in equilibrium with the surrounding phases and groundmass. Crystals were marked with Indian ink for easy identification during electron microprobe analysis. Transmitted light photos and backscattered images of crystals were obtained prior to analysis.

A1.3 Electron microprobe microanalysis

Major elements were determined on the JEOL 733 SuperProbe Electron Probe Microanalyser (EPMA) using three wavelength dispersive spectrometers at the Analytical Facility, Victoria University of Wellington. Thallium acid phthalate

(TAP), Pentaerythritol (PET) and Lithium fluoride (LIF) crystals were utilised in spectrometers 1, 2 and 3, respectively. Prior to analysis samples were coated with a 25 nm thick layer of carbon. The carbon coat was removed from the epoxy mounts by ethanol post EPMA analyses and then dried in air prior to laser ablation inductively coupled plasma mass spectrometry analyses. Operating conditions were 15 kV, 8 nA, and a 10 μm defocused beam for melt inclusions and glass adhered to the exterior of crystals, 15 kV, 12 nA and a focused beam for quartz and Fe-Ti oxide analyses and 15 kV, 12 nA and a 10 μm defocused beam for plagioclase analyses. Primary calibrations were performed daily to optimise operating conditions using a mixture of natural and synthetic standards prior to analysis (Table A1.2). Counting times were optimised for each element for each sample analysed. ZAF corrections were applied to all data (Bence and Albee, 1968).

Oxide	Internal calibration standard	Counting time (s)		Crystal
		BG (+/-)	Peak	
SiO_2	Wollastonite	10	30	TAP
TiO_2	Synthetic TiO_2	10	30	PET
Al_2O_3	Synthetic Al_2O_3	10	30	TAP
FeO	Synthetic Fe_2O_3	10	30	LIF
MnO	Synthetic MnO	10	30	LIF
MgO	Synthetic MgO	10	30	TAP
CaO	Wollastonite	10	30	PET
Na_2O	Jadeite	5	10	TAP
K_2O	Orthoclase	5	10	PET
P_2O_5	Apatite	10	30	PET
SO_3	Celestine	10	30	PET
Cl	Sodalite	10	30	PET

Table A1.2. Typical operating conditions for EPMA analysis of melt inclusions indicating counting times, internal standard and crystal each element was analysed with. BG = background count times.

Na and K had a short count time of 5 seconds and were run first to minimised volatile lost during glass analyses. For Ti analyses of quartz, Ti was analysed with count times of 120 seconds on background and 240 seconds on peak.

Secondary standards were run at the beginning and end of each session to monitor for instrumental drift and to normalize results between each analytical session. Secondary standards used were the Smithsonian standards basaltic glass VG2 (USNM 111240/52) for major elements and scapolite (USNM R-600-1) for Cl and SO_3 analyses of melt inclusions, basaltic glass VG-A99 (USNM 113498/1) for plagioclase analyses, ilmenite (USNM 96189) for Fe-Ti oxide analyses (Jarosewich et al., 1980), and comenditic glass (obsidian, KN18) for Ti analyses of quartz (S. Malik and D.A. Bungard as reported in Devine et al., 1995) (Table A1.3).

Oxide (wt%)	VG2	Scapolite	VG-A99	KN18	Ilmenite
SiO_2	50.81*	49.78	50.9*	74.6*	
TiO_2	1.85*		4.06	0.18*	45.7*
Al_2O_3	14.06*	25.05	12.4*	10.53	
FeO	11.84*	0.17	13.3*	3.45	46.5*
MgO	0.22*		5.08*	0.01	0.31*
MnO	6.71*		0.15	0.06	4.77*
CaO	11.12*	13.58	9.3*	0.15	
Na_2O	2.62*	5.20	2.66*	5.68	
K_2O	0.19*	0.94	0.82*	4.39	
SO_3		1.32*			
Cl		1.43*		0.37	
Total	99.42	97.47	98.71	99.42	92.5

Table A1.3. Reference values of secondary standards used in EPMA analyses. Elements used for normalisation are denoted by *. Sources: VG-A99, VG2, scapolite, ilmenite standard from Jarosewich et al. (1980) and KN18 obsidian glass from S. Malik and D.A. Bungard as reported in Devine et al. (1995).

A typical example of the precision and accuracy of EPMA data is shown in Table A1.4 for the analysis of the basalt glass standard A99 prior to the analysis of Whakamaru plagioclase.

wt%	A99 1	A99 2	A99 3	A99 4	A99 5	Mean	2 SD	% 2SD (precision)	% difference (accuracy)	Ref Values
SiO_2	50.42	51.08	50.05	49.77	49.60	50.18	1.18	2.34	-1.49	50.94
Al_2O_3	12.18	12.38	12.90	13.18	12.58	12.64	0.80	6.33	1.24	12.49
FeO	13.56	13.66	13.32	12.64	13.52	13.34	0.82	6.16	0.29	13.30
CaO	9.10	9.51	8.91	9.00	9.21	9.14	0.47	5.11	-1.67	9.30
Na_2O	2.68	2.71	2.49	2.52	2.57	2.59	0.20	7.53	-2.49	2.66
K_2O	0.84	0.85	0.84	0.81	0.82	0.83	0.03	4.04	1.46	0.82
Total	88.78	90.19	88.49	87.92	88.30	88.74				89.51

Table A1.4. Precision and accuracy of basalt glass A99 standard. Calculation of %2SD (precision) = (2SD/mean)*100; % difference (accuracy) = [(mean/reference values)/reference values]*100. Reference values from Jarosewich et al. (1980). Note only elements analysed in the plagioclase are shown for VG-A99.

Backscattered electron images of crystals and melt inclusions as appropriate were obtained prior to analysis at the same analytical conditions with a focus beam. Cathodoluminescence (CL) images of quartz crystals were obtained using a photomultiplier attached to the electron microprobe at 12 nA and 15 kV. This setup to obtain CL images is a homemade addition to the VUW EPMA by John Patterson. It consists of a tubular adaptor with a perspex light pipe mounted in place of the optical microscope. This connects the optical window on the column directly to the photomultiplier of the secondary electron detector, which allows light emitted from the sample to be detected and a CL image obtained.

A1.4 Laser ablation inductively coupled plasma mass spectrometry

A1.4.1 Introduction

The Geochemical Laboratory at Victoria University of Wellington (VUW), was newly established in 2006 and houses an Agilent 7500cs inductively coupled plasma mass spectrometry (ICPMS) coupled to a NewWave deep UV laser (193 nm solid state) permitting the laser ablation inductively coupled plasma mass spectrometry (LA-ICPMS) analyses of samples. Prior to analysis of samples it was essential to establish a technique suitable for the analysis of basaltic and rhyolitic glasses in this new laboratory. This consisted of running analyses of well-characterised reference materials until the elemental concentrations were reproduced to a high degree of accuracy and precision. The initial part of the technique development is presented here and was conducted together with Joel Baker, Martin Schiller, Aidan Allan and Sophie Barton.

A1.4.2 Operating conditions, setup and problems of LA-ICPMS analyses

Several important analytical factors may influence the quality of the data attained by LA-ICPMS analyses and these are highlighted below. For an in-depth review of LA-ICPMS the reader is referred to Durrant (1999), Sylvester (2001), Heinrich et al. (2003) and Günther and Hattendorf (2005).

A1.4.2.1 Carrier gas

An important factor controlling the amount of ablated material removed from the ablation cell and transported to the ICPMS during analysis is the composition of the carrier gas, as this influences the amount and size of particles removed and

the path flow through the ablation cell (e.g. Horn and Günther, 2003). For example, ablation in He generates more small particles resulting in an increase in sensitivity recorded by ICPMS analyses compared to when Ar is used solely as the carrier gas (Horn and Günther, 2003). Consequently, a He-Ar mixture was utilised during ablation and for transportation of ablated material to the ICPMS during this study.

A1.4.2.2 Ablation cell volume

Previous studies have noted that a reduction in volume of the ablation cell is beneficial as it minimises the available area over which ablated material can be dispersed, increasing the chances of material being transported to the ICPMS and also reducing the time required for the flushing of cells between analyses (e.g. Košler and Sylvester, 2003).

A1.4.2.3 Elemental fractionation during transport

Refractory and volatile elements behave differently during ablation and transport and may become fractionated (Outridge et al., 1997). Decreasing the spot size affects the diameter/depth ratio of the resulting laser pit. At smaller spot sizes the ablation pit becomes deeper compared to its width limiting the amount of ablated material that can escape and subsequently be transported to the ICPMS. This effect is most pronounced when ablating refractory elements such as Sr and U compared to more volatile elements such as Rb or Pb (Günther and Hattendorf, 2005). The proportion of elemental fractionation can be monitored by observing volatile/refractory element ratios such as Rb/Sr or Pb/U during ablation (Günther and Hattendorf, 2005).

A1.4.2.4 Interferences

Interferences which occur when the analytical signal of an isotope is either enhanced or suppressed due to the occurrence of another element having the same isotopic mass, are one of the greatest limitations of LA-ICPMS analyses (Mason, 2001; Kent and Ungerer, 2005). With a quadruple ICPMS only a single unit mass can be analysed at a time, so all ions or molecules that are present with the same mass/charge ratio are measured simultaneously (Mason, 2001). This can lead to inaccurate determinations of the elemental concentrations of a sample. Interferences are caused by: (1) the overlap of two elements having naturally occurring isotopes of the same mass; (2) isobaric interferences caused by the ionization of molecular species such as oxygen and argon; and (3) doubly charged ions (Mason, 2001; Kent and Ungerer, 2005). Potential interferences that may affect each element analysed are shown in Table A1.5 and the justification for each isotope analysed in this study are given in Table A1.6.

Oxygen is a major constituent of the studied samples and isobaric interferences arise when the ablated ions combine with molecular species, (e.g. oxygen and argon) derived from the sample matrix, plasma or entrainment of atmospheric gases through the system to form polyatomic ion species (Kent and Ungerer, 2005). The maximum oxide production rate at a given plasma condition can be determined by monitoring the strongest known bond for oxides, the Th-O bond (Kent and Ungerer, 2005). The affect of oxide interferences can be determined by monitoring mass 248, which has no naturally occurring elements but is the mass of the molecule ThO^+ (Kent and Ungerer, 2005). The ThO^+/Th^+ ratio was kept to < 2-3% during analysis.

Isotope	Element	Notes	Natural Abundance (%)	Direct Interferences	Oxide Interferences	Ar-based Interferences	Doubly Charged
6	Li		7.5		22 Na	46 Ca	3 H
7	Li		92.5	7 Be	23 Na	47 Ti	
7	Be	C		7 Li	23 Na	47 Ti	
9	Be	S	100%		27 Al	49 Ti	
10	Be			10 B	26 Mg, 26 Al	50 Ti, 50 V, 50 Cr	
10	B		19.9	10 Be	26 Mg, 26 Al	50 Ti, 50 V, 50 Cr	
11	B		80.1		27 Al	51 V, 51 Cr	
24	Mg		78.99		40 K, 40 Ar, 40 Ca	64 Zn	12 C
25	Mg		10		41 K, 41 Ca	65 Cu, 65 Zn	
26	Mg		11.01	26 Al	42 Ca	66 Zn	13 C
40	Ca		96.941	40 Ar, 40 K	56 Fe	80 Kr	20 Ne
41	Ca	H		41 K	57 Fe	81 Br, 81 Kr	
42	Ca		0.647		58 Ni	82 Kr	21 Ne
43	Ca		0.135		59 Ni (C)	83 Kr	
44	Ca		2.086		60 Ni, 60 Co, 60 Fe	84 Kr, 84 Sr	22 Ne, 22 Na
46	Ca		0.004	46 Ti	62 Ni	86 Sr	23 Na
48	Ca		0.187	48 Ti	64 Zn	88 Sr	24 Mg
45	Sc	S	100			85 Rb	
46	Ti		8	46 Ca	62 Ni	86 Sr	23 Na
47	Ti		7.3		63 Cu	87 Sr	
48	Ti		73.8	48 Ca	64 Zn	88 Sr	24 Mg
49	Ti		5.5		65 Zn	89 Y	
50	Ti		5.4	50 Cr, 50 V	66 Zn	90 Sr, 90 Zr	25 Mg
50	V	H	0.25	50 Ti, 50 Cr	66 Zn	90 Sr, 90 Zr	25 Mg
51	V	S	99.75	51 Cr	67 Zn	91 Zr	
50	Cr		4.345	50 Ti, 50 V	66 Zn	90 Sr, 90 Zr	25 Mg
51	Cr	H		51 V	67 Zn	91 Zr	
52	Cr		83.789		68 Zn	92 Zr, 92 Mo	26 Mg, 26 Al
53	Cr		9.501	53 Mn	69 Ga	93 Nb	
54	Cr		2.365	54 Mn	70 Ge	94 Zr, 94 Mo	27 Al
53	Mn	C		53 Cr	69 Ga	93 Zr, 93 Nb	
54	Mn	B,R		54 Cr, 54 Fe		94 Zr	27 Al
55	Mn		100		71 Ga	95 Mo	
59	Co	S	100	59 Ni	75 As	99 Tc, 99 Ru	
60	Co	H		60 Fe, 60 Ni	76 Ge, 76 Se	100 Mo, 100 Ru	30 Si
58	Ni		68.077	58 Fe	74 Ge, 74 Se	98 Mo, 98 Ru	29 Si
59	Ni	H		59 Ni, 59 Co	75 As	99 Ru	
60	Ni		26.233	60 Fe (extinct), 60 Co (B,R)	76 Ge, 76 Se	100 Mo, 100 Ru	30 Si
61	Ni		1.14		77 Se	101 Ru	
62	Ni		3.634		78 Se	102 Ru, 102 Pd	31 P
63	Cu		69.17		79 Br	103 Rh	
65	Cu		30.83		81 Br	105 Pd	
64	Zn		48.6		80 Kr	104 Ru, 104 Pd	32 Si, 32 P, 32 S
65	Zn	H			81 Br, 81 Kr	105 Pd	
66	Zn		27.9		82 Kr	106 Pd, 106 Cd	33 P, 33 S
67	Zn		4.1		83 Kr	107 Pd, 107 Ag	
68	Zn		18.8		84 Kr, 84 Sr	108 Pd, 108 Cd	34 S
69	Ga		60.108		85 Rb,	109 Ag	
71	Ga		39.892		87 Rb	111 Cd	
85	Rb	S	72.165	85 Kr	101 Ru	125 Te	
87	Rb		27.835	87 Sr	103 Rh	127 I	
84	Sr		0.56	84 Kr	100 Ru	124 Xe, 124 Te, 124 Sn	42 Ca
86	Sr		9.86		102 Ru	126 Xe, 126 Te	43 Ca
87	Sr		7	87 Rb	103 Rh	127 I	
88	Sr		82.58		104 Ru, 104 Pd	128 Te	44 Ca
90	Sr	H		90 Zr	106 Pd	130 Xe, 130 Te	45 Sc
89	Y	S	100		105 Pd	129 I	
90	Zr		51.45	90 Sr (H)	106 Pd, 106 Cd	130 Xe, 130 Te	Sc

Table A1.5

Isotope	Element	Notes	Abundance (%)	Direct Interferences	Oxide Interferences	Ar-based Interferences	Doubly Charged
91	Zr		11.22		107 Pd, 107 Ag	131 Xe	
92	Zr		17.15	92 Mo	108 Pd, 108 Cd	132 Ba, 132 Xe	Ca, 46 Ti
93	Zr	H		93 Nb	109 Ag	133 Cs	
94	Zr		17.38	94 Mo	110 Pd, 110 Cd	134 Cs, 134 Xe	47 Ti
95	Zr				111 Cd	135 Ba	
96	Zr	H	2	96 Mo	112 Cd	136 Ba, 136 Xe	48 Ca, 48 Ti
93	Nb	S	100	93 Zr	109 Ag	133 Cs	
92	Mo		14.84	92 Zr	108 Cd	132 Xe	46 Ti, 46 Ca
94	Mo		9.25	94 Zr	110 Pd, 110 Cd	134 Xe, 134 Cs	47 Ti
95	Mo		15.92		111 Cd	135 Ba	
96	Mo		16.68	96 Zr	112 Cd, 112 Sn	136 Xe, 136 Ba	48 Ca
97	Mo		9.55		113 Cd, 113 In	137 Ba	
98	Mo		21.13		114 Sn	138 Ba, 138 Ce	49 Ti
100	Mo		9.63	100 Ru	116 Sn	140 Ce	50 V, 50 Cr
133	Cs	S	100		149 Sm	173 Yb	
134	Cs	H		134 Ba, 134 Xe	150 Nd, 150 Sm	174 Hf, 174 Yb	67 Zn
137	Cs	H		137 Ba	153 Eu	177 Hf	
130	Ba		0.106	130 Xe, 130 Te	146 Sm, 146 Nd	170 Er	65 Cu
132	Ba		0.101	132 Xe	148 Nd, 148 Sm	172 Yb	66 Zn
134	Ba		2.417	134 Xe, 134 Cs	150 Nd, 150 Sm	174 Yb, 175 Hf	67 Zn
135	Ba		6.592		151 Eu	175 Lu	
136	Ba		7.854	136 Xe	152 Sm, 152 Gd	176 Hf	68 Zn
137	Ba		11.23	137 Cs (B, M)	153 Eu	177 Hf	
138	Ba		71.7	138 La, 138 Ce	154 Sm, 154 Gd	178 Hf	69 Ga
138	La	H	0.0902	138 Ba, 138 Ce	154 Sm, 154Gd	178 Hf	69 Ga
139	La	S	99.9098		155 Gd	179 Hf	
138	Ce		0.25	138 Ba, 138 La	154 Sm, 154 Gd	178 Hf	69 Ga
140	Ce		88.48		156 Gd, 156 Gd	180 W, 180 Hf	70 Ge
142	Ce		11.08	142 Nd	158 Gd, 158 Dy	182 W	71 Ga
141	Pr	S	100		157 Gd	181 Ta	
142	Nd		27.13	142 Ce	158 Gd, 158 Dy	182 W	71 Ga
143	Nd		12.18		159 Tb	183 W	
144	Nd		23.8	144 Sm	160 Gd, 160 Dy	184 W, 184 Os	72 Ge
145	Nd		8.3		161 Dy	185 Re	
146	Nd		17.19	146 Sm	162 Dy, 162 Er	186 W	73 Ge
148	Nd		5.76	148 Sm	164 Dy, 164 Er	188 Os	74 Ge
150	Nd		5.64	150 Sm	166 Er	190 Pt	75 As
144	Sm		3.1	144 Nd	160 Dy	184 W, 184 Os	72 Ge
146	Sm	H		146 Nd	162 Dy, 162 Er	186 W, 186 Os	73 Ge
147	Sm		15		163 Dy	187 Re, 187 Os	
148	Sm	H	11.3	148 Nd	164 Dy, 164 Er	188 Os	74 Ge
149	Sm	H	13.8		165 Ho	189 Os	
150	Sm		7.4	150 Nd	166 Er	190 Pt, 190 Os	75 As
152	Sm		26.7		168 Er	192 Os, 192 Pt	76 Se
154	Sm		22.7	154 Gd	170 Er	194 Pt	77 Se
151	Eu		47.8		167 Er	191 Ir	
153	Eu		52.2		169 Tm	193 Ir	
152	Gd		0.2	152 Sm	168 Er, 168 Yb	192 Pt	76 Se
154	Gd		2.18	154 Sm	170 Er	194 Pt	77 Se
155	Gd		14.8		171 Yb	195 Pt	
156	Gd		20.47	156 Dy	172 Yb	196 Pt, 196 Hg	78 Se, 78 Kr
157	Gd		15.65		173 Yb	197 Au	

Table A1.5 continued

Isotope	Element	Notes	Abundance (%)	Direct Interferences	Oxide Interferences	Ar-based Interferences	Doubly Charged
158	Gd		24.84	158 Dy	174 Yb, 174 Hf	198 Hg, 198 Pt	79 Br
160	Gd	H	21.86	160 Dy	176 Yb, 176 Lu, 176 Hf	200 Hg	80 Kr
156	Dy		0.06	156 Gd	172 Yb	196 Pt, 196 Hg	78 Se, 78 Kr
158	Dy		0.1	158 Gd	174 Yb, 174 Hf	198 Hg, 198 Pt	79 Br
160	Dy		2.34	160 Gd	176 Yb, 176 Lu, 176 Hf	200 Hg	80 Kr
161	Dy		18.9		177 Hf	201 Hg	
162	Dy		25.5	162 Er	178 Hf	202 Hg	81 Br
163	Dy		24.9		179 Hf	203 Tl	
164	Dy		28.2	164 Er	180 Hf, 180 Ta	204 Pb, 204 Hg	82 Kr
162	Er		0.14	162 Dy	178 Hf	202 Hg	81 Br
164	Er		1.61	164 Er	180 Hf, 180 Ta, 180 W	204 Pb, 204 Hg	82 Kr
166	Er		33.6		182 W	206 Pb, 206 Tl	83 Kr
167	Er		22.95		183 W	207Pb, 207Tl	
168	Er		26.8	168 Yb	184 W, 184 Os	208 Pb, 208 Tl	84 Kr, 84 Sr
170	Er		14.9		186 W	210 Tl, 210 Pb, 210 Bi, 210 Po	85 Kr, 85 Rb
168	Yb		3.05	168 Er	184 W, 184 Os	208 Pb, 208 Tl	84 Kr, 84 Sr
171	Yb		14.3		187 Re, 187 Os	211 Pb, 211 Bi, 211 Po	
172	Yb		21.9		188 Os	212 Pb, 212 Bi, 212 Po	86 Sr
173	Yb		16.12		189 Os		
174	Yb		31.8	174 Hf	190 Os, 190 Pt	214 Pb, 214 Po, 214 Bi	87 Rb, 87 Sr
176	Yb		12.7	176 Lu, 176 Hf	192 Os, 192 Pt	216 Po	88 Sr
175	Lu	S	97.41		191 Ir	215 Bi, 215 At, 215 Po	
176	Lu		2.59	176 Yb, 176 Hf	192 Os, 192 Pt		88 Sr
174	Hf		0.162	174 Yb	190 Os, 190 Pt	214 Po	87 Rb, 87 Sr
176	Hf		5.206	176 Yb, 176 Lu	192 Os, 192 Pt	216 Po	88 Sr
177	Hf		18.606		193 Ir		
178	Hf		27.279		194 Pt	218 At, 218 Po	89 Y
179	Hf		13.629		195 Pt	219 Rn	
180	Hf		35.1	180 W, 180 Ta	196 Pt, 196 Hg	220 Rn	90 Sr, 90 Zr
180	Ta	H	0.0012	180 W, 180 Hf	196 Pt, 196 Hg		90 Sr, 90 Zr
181	Ta	S	99.988		197 Au		
180	W		0.13	180 Ta	196 Pt	220 Rn	90 Zr
182	W		26.3		198 Pt, 198 Hg	222 Rn	91 Zr
183	W		14.3		199 Hg	223 Fr	
184	W		30.67	184 Os	200 Hg	224 Ra	92 Zr, 92 Mo
186	W		28.6		202 Hg	226 Ra	93 Nb, 93 Zr,
204	Pb	H	1.4	204 Hg,	220 Rn		102 Ru, 102 Pd
206	Pb						
207	Pb		22.1	207 Tl	223 Fr, 223 Ra		
208	Pb		52.4	208 Tl	224 Ra		104 Ru, 104 Pd
228	Th	H		228 Ac			114 Cd
230	Th	H					115 In
232	Th		100				116 Sn
234	Th			234 U			117 Sn
234	U		0.0055	234 Th			117 Sn
235	U		0.72				
238	U		99.2745				119 Sn

Table A1.5. Potential interferences for each element and isotope analysed by LA-ICPMS. Isotopes, abundances and notes are taken from Appendix 2, Treatise on Geochemistry (Turekian and Holland, 2003). Isotopes highlighted in yellow indicate the analysed isotope. Abbreviations: C = cosmogenetic source; S = only stable isotope; B = produced in bombs; R = produced in nuclear reactors; H = half-life < 10,000 years.

Element	Isotope analysed	Justification for analysed isotope
Ca	43	The least abundant of the three Ca isotopes (^{42}Ca, ^{43}Ca, ^{44}Ca) without a direct interference and only a minor oxide interference.
Sc	45	The only stable isotope, but possible Ar-based interference due to ^{85}Rb.
Ti	47	Most abundant isotope without a direct interference.
V	51	The only stable isotope, but possible direct interference from ^{51}Cr, oxide interference from ^{60}Zn and Ar-based interference due to ^{91}Zr.
Cr	53	Second most abundant isotope with no major direct interferences.
Co	59	The only stable isotope but with possible oxide interference from ^{75}As.
Ni	60	The second most abundant isotope and not affected by direct interferences from long live isotopes.
Cu	63	Is the smaller of the two Cu isotopes but is more than twice as abundant than ^{65}Cu and both isotopes suffer from oxide interference from Br.
Zn	66	Zn isotopes do not suffer from direct interferences. ^{66}Zn is larger and more abundant than ^{64}Zn and as both of these isotopes could suffer from oxide interferences from Kr, ^{66}Zn is analysed.
Ga	71	Gd isotopes have no direct interferences, but ^{71}Ga is the larger isotope of the two isotopes. Both Ga isotopes can be affect by oxide interferences from Rb from, but ^{71}Ga is affected by ^{87}Rb which is less abundant than ^{85}Rb, which causes oxide inference on ^{69}Ga.
Rb	85	The only stable isotope with no major direct interferences.
Sr	88	The most abundant and largest Sr isotope with no direct interferences.
Y	89	The only isotope with no direct interferences, but a possible oxide interference from ^{105}Pd.
Zr	90	The most abundant and smallest isotope with direct interferences only occurring from ^{90}Sr; a very short-lived ½ life and not produced in nature.
Nb	93	The only isotope. May suffer from a direct interference from ^{93}Zr, but this is a minor isotope with a short ½ life. Possible oxide interference from ^{109}Ag and Ar-based interference from ^{133}Ca.
Cs	133	The only naturally occurring isotope and no direct interferences.
Ba	137	The largest and most abundant Ba isotope not affected by a direct interference from a naturally occurring isotope.
La	139	The only stable isotope with no direct interferences.
Ce	140	Most abundant isotope with no direct interferences.
Pr	141	The only stable isotope with no direct interferences.
Nd	146	Is one of the larger more abundant Nd isotopes with a possible direct interference from ^{146}Sm.
Sm	147	One of the three Sm isotopes (^{147}Sm, ^{149}Sm, ^{152}Sm) without direct interferences. All three isotopes have possible oxide and Ar-based interference, but ^{147}Sm is slightly more abundant, although it is smaller than ^{149}Sm.
Eu	153	Neither Eu isotopes have direct interferences, but both have possible oxide and Ar-based interferences. ^{153}Eu is the more abundant and larger of the two isotopes.
Gd	157	One of the two Gd isotopes (^{155}Gd, ^{157}Gd) without direct interference. ^{157}Gd is the more abundant and larger isotope.
Dy	163	One of the two Dy isotopes (^{161}Dy, ^{163}Dy) without direct interference, but both could suffer oxide interference, although ^{163}Dy is more abundant than ^{161}Dy.
Er	166	Most abundant of the two Er (^{166}Er, ^{167}Er) isotopes without direct interferences.
Yb	172	Most abundant of the three Yb isotopes (^{171}Yb, ^{172}Yb, ^{173}Yb) without direct interference.
Lu	175	The only stable isotope with no direct interferences.
Hf	178	One of the three Hf isotopes (^{177}Hf, ^{178}Hf, ^{179}Hf) without direct interferences and the most abundant isotope of the three.
Ta	181	The only stable isotope with no direct interferences.
Pb	208	The most abundant long-lived isotope with no major direct isotopic interferences.
Th	232	The only major isotope with no direct interferences.
U	238	The major isotope with no direct interferences.

Table A1.6. Justification for the isotopes analysed in this study. Isotope data and relative abundance of isotopes are taken from Appendix 2, Treatise of Geochemistry (Turekian and Holland, 2003).

A1.4.2.5 Analytical conditions

Prior to each analytical session, tuning of the LA-ICPMS was conducted on a standard to maximise the operating conditions. Typical conditions for optimisation of BCR-2G resulted in: ca. 20,000 cps on Ce; 2000-3000 cps Pb (Pb background ca. 50 cps); ThO^+/Th^+ <2.5 %; and relative standard deviations (RSD) of the monitored isotopes < 5%. Thirty-three trace elements were routinely analysed and are given in Table A1.6. Typical analytical conditions are shown in Table A1.7.

Typical Analytical Conditions	
Laser	New Wave deep UV
Wavelength (nm)	193 nm solid state
Spot size (μm)	35 μm (unless stated)
Repetition rate (Hz)	5
Energy	~ 5.6-6.7 J/cm^2
Carrier Gas	He-Ar mixture
Mass spectrometer	Agilent 7500cs
Internal standard	^{43}Ca
Calibration standard	BCR-2G
Integration time	10 ms except for ^{95}Mo, ^{133}Cs and ^{141}Pr to ^{238}U = 20 ms

Table A1.7. Typical analytical conditions for LA-ICPMS analyses for basalt glasses

A1.4.2.6 Elemental concentrations

The sensitivity of an element, S_i, at the mass spectrometer is dependant on instrumental conditions that can vary over an analytical session (Longerich et al., 1996; Heinrich et al., 2003). Therefore, quantification of elemental concentrations of an unknown sample (SAMP) by LA-ICPMS requires both an external standard (STD) and an internal reference element (r), both of known composition that has been established independently (Longerich et al., 1996;

Heinrich et al., 2003). The external standard is measured throughout an analytical session bracketing the analyses of the unknown. Therefore, the measured count rates of the analysed element for both the external standard and unknown sample together with the internal standard can be used to quantify the elemental concentrations of the unknown sample through the following relationship (Longerich et al., 1996);

$$\frac{C_i^{SAMP}}{C_r^{SAMP}} = \frac{C_i^{STD}}{C_r^{STD}} \times \frac{I_i^{SAMP} I_r^{STD}}{I_r^{SAMP} I_i^{STD}} \times \frac{S_i^{SAMP} S_r^{STD}}{S_r^{SAMP} S_i^{STD}} \qquad [A1.1]$$

where: C is the concentration of an element, *i,* or internal standard element, r of the sample (SAMP) or external standard (STD); I is the background-corrected signal intensity in counts per second of the sample or external standard of an element, *i*, or internal standard, r (Longerich et al., 1996). The final term in the equation is equal to 1 as the sensitivity ratios are identical for all elements (Longerich et al., 1996; Heinrich et al., 2003). In this study, the internal reference element, r, is taken as the CaO content of either the reference material (see below) or the measured CaO concentration of the volcanic glass or mineral determined by EPMA prior to LA-ICPMS analysis (Jackson et al., 1992).

A1.4.2.7 Reference materials

Well-characterised reference materials are indispensable in LA-ICPMS as they allow for the calculation of trace element concentrations of unknown samples (e.g. Longerich et al., 1996). During ablation, the location of cations and type of chemical bonds within the crystal structure dictates the amount of energy required to free cations from the crystal lattice. Hence, reference materials should be as near as possible to the composition of your unknown to prevent the occurrence of matrix affects.

Published elemental concentrations of materials vary between analytical techniques and laboratories. Reference materials and values used in this research are listed in Table A1.8 and are the GeoRem preferred values at the time of analyses (Jochum et al., 2006; GeoRem: http://georem.mpch-mainz.gwdg.de). These values have been determined at a number of different institutions and using analytical techniques including LA-ICPMS, secondary ion microprobe spectrometry (SIMS), isotope dilution analysis by thermal ionisation mass spectrometry (TIMS) and multi-collector inductively coupled mass spectrometry (MC-ICPMS).

A1.4.3 LA-ICPMS analysis of volcanic glasses

A1.4.3.1. Basaltic glasses

A series of experiments were performed to determine the optimal conditions for LA-ICPMS analyses of basaltic and rhyolitic glass. Basaltic glasses were focussed on first and initially the USGS basaltic reference glasses BCR-2G and BHVO-2G were taken as the standard and "unknown" respectively using the analytical conditions described above. These early LA-ICPMS analyses of volcanic glass consisted of 100 counts that included ca. 45 counts of instrumental background and then 50 counts of ablation. In general, analytical sessions during this period of technique development consisted of analysis of five 'unknowns' with each unknown bracketed by analysis of the external standard.

The initial results of BHVO-2G (Table A1.9) as the unknown indicated better than 10% precision for the majority of elements. Some of the least precise results were obtained for the rare earth elements (e.g. Nd and Gd).

Isotope	Element	NIST 610	NIST 612	BCR-2G	BHVO-2G	STH-G (StHs6/80)	ATHO-G
7	Li	485	41.5	10.5	4.7	20.7	28.6
9	B	356	34.7	7.3	5.4	11.8	5.7
11	Be	466	37.7	1.3	0.79	1.2	3.2
25	Mg	465	77	21466	42992	11879	621
43	Ca	11.5	11.9	7.06	11.4	5.28	1.7
45	Sc	441	41	33	33	11.5	7
47	Ti	434	44	14100	16300	421	1527
51	V	442	39	425	308	90.3	3.91
53	Cr	405	36	17	293	16.9	6.1
55	Mn	485	38	1472	1317	589	821
59	Co	405	35	38	44	13.2	2.13
60	Ni	459	38.8	13	116	23.7	13
63	Cu	430	37	21	127	41.5	18.6
66	Zn	456	38	125	102	67	141
71	Ga	438	36	23	22	20.9	25.3
85	Rb	426	31.4	47	9.2	30.7	65.3
88	Sr	516	78.4	342	396	482	94.1
89	Y	450	38.2	35	26	11.4	94.5
90	Zr	440	38	184	170	118	512
93	Nb	149	40	12.5	18.3	6.94	62.4
95	Mo	410	38	270	3.8	2	4.8
133	Cs	361	42	1.16	0.1	1.75	1.08
137	Ba	435	39.7	683	131	298	559
139	La	457	35.8	24.7	15.2	12	55.6
140	Ce	448	38.7	53.3	37.6	26.1	121
141	Pr	430	37.2	6.7	5.35	3.2	14.6
146	Nd	431	35.9	28.9	24.5	13	60.9
147	Sm	451	38.1	6.59	6.1	2.78	14.2
153	Eu	461	35	1.97	2.07	0.953	2.76
157	Gd	444	36.7	6.71	6.16	2.59	15.3
159	Tb	443	36	1.02	0.92	0.371	2.51
163	Dy	427	36	6.44	5.28	2.22	16.2
165	Ho	449	38	1.27	0.98	0.42	3.43
166	Er	426	38	3.7	2.56	1.18	10.3
169	Tm	420	38	0.51	0.34	0.172	1.52
172	Yb	445	38	3.39	2.01	1.13	10.5
175	Lu	435	36.9	0.503	0.279	0.168	1.54
178	Hf	432	35	4.84	4.32	3.07	13.7
181	Ta	452	40	0.78	1.15	0.42	3.9
182	W	445	40	0.5	0.23	0.47	9.3
208	Pb	426	38.6	11	1.7	10.3	5.67
232	Th	457	37.8	5.9	1.22	2.28	7.4
238	U	462	37.4	1.69	0.403	1.01	2.37

Table A1.8 Trace element concentrations in ppm and CaO in wt% of reference glasses used in this study (GeoRem: http://georem.mpch-mainz.gwdg.de and Jochum et al., 2006).

In an effort to increase the precision of the obtained data BCR-2G and BHVO-2G were polished with 600, 2400 and 4000 grit silicon carbide paper and ¼ µm diamond paste to create a level surface for ablation. Isobaric interferences are known to occur on the middle rare earths due to oxide interferences from the light rare earths (Kent and Ungerer, 2005) and therefore the oxides production rate was closely monitored by analysis of four gadolinium isotopes (^{155}Gd, ^{156}Gd, ^{157}Gd, ^{158}Gd). Results from this set of analyses (Table A1.10) indicate the polishing of the sample and standard improved the quality of data with an increase in precision and accuracy, however, the rare earth elements still displayed only ca. 10% precision and no significant interferences were observed to occur on the middle rare earth elements, indicating that another factor was controlling the precision of rare earth elements.

Initially samples were mounted in a circular epoxy block and the standard in a rectangular epoxy block and positioned in the ablation chamber as shown in Figure A1.1a. The position of the standard off centre, out of the direct flow of the carrier gas, resulted in inconsistent proportions of ablated sample and standard material being transported to the ICPMS. To eliminate this discrepancy, and to position both the sample and standard as centrally as possible in the direct flow of the carrier gas, both the sample and standard were remounted into semi-circular epoxy mounts of 5 mm thickness (Figure A1.1b). This had the additional benefit that both mounts could now be dropped flush with the top of the ablation cell (Figure A1.1c) allowing for the unhindered flow of gas through the chamber. BHVO-2G was reanalysed with the new configuration of mounts in the ablation

chamber resulting in an increase in both precision and accuracy for the majority of trace elements, including the rare earth elements (Table A1.11).

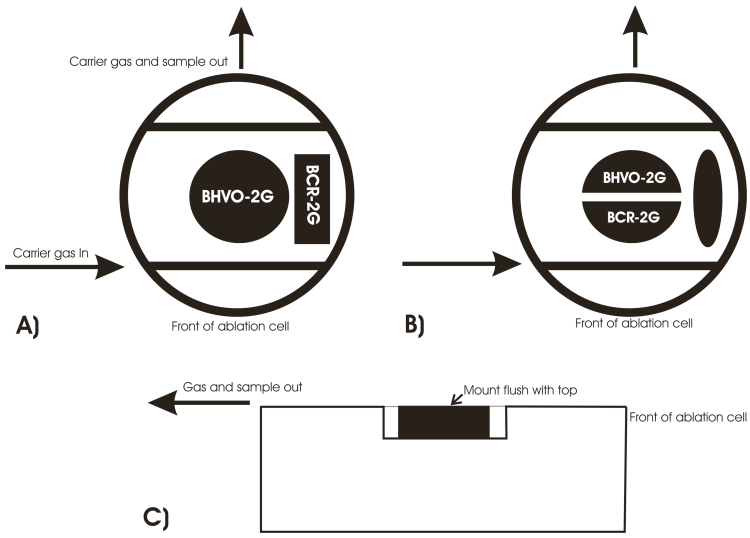

Figure A1.1. Position of the sample and standard in the ablation cell for analysis. A) Initial configuration and shape of epoxy mounts of BHVO-2G and BCR-2G. B) Revised configuration and shapes of mounts with location of block on down flow side of cell reducing the cell volume. C) Profile of ablation cell showing mount flush with top of cell.

It should be noted though, that if the two mounts are rotated 90° from that shown in Figure A1.1b the precision of the data is greatly reduced (Table A1.12), most probably as a result of the channelling of a proportion of the carrier gas between the epoxy mounts instead of flowing over them. The channel between the two epoxy mounts, had the unfortunate affect of allowing gas to escape into the lower proportion of the ablation chamber that had previously been inaccessible in the earlier experiments and this greatly increased the Pb background. This was solved simply by placing a piece of tape beneath the mounts preventing access to the lower proportion of the ablation chamber.

The volume of the ablation cell was reduced by positioning an epoxy block off to one side where previously the standard (BCR-2G) had been located (Figure A1.1) with the result of containing the gas flow within the central portion of the ablation chamber. BHVO-2G was reanalysed with this new arrangement and again results showed a further increase in the precision and accuracy of the obtained elemental concentrations (Table A1.13) indicating the importance of sample configuration within the sample cell.

All the previous experiments were conducted with a spot size of 35μm, however, melt inclusions vary in size from >200μm to <10μm diameter and therefore it would be advantageous to analyse samples at smaller spot sizes. Conversely, a series of analyses of BHVO-2G were performed with spot sizes spanning between 10 μm to 50 μm (Table A1.14). These results indicate that a spot size down to 15 μm could be implemented and still retain a 10% accuracy for the majority of elements, with only elements with low concentrations such as Cs requiring a larger spot size in order to acquire sufficient material for analysis (Table A1.14). However, analysis of BHVO-2G at 10, 35 and 50 μm spot diameters shows elemental fractionation of volatile/refractory elements increases at smaller spot sizes (Figure A1.2) indicating the largest possible spot size viable should be utilised when analysing samples.

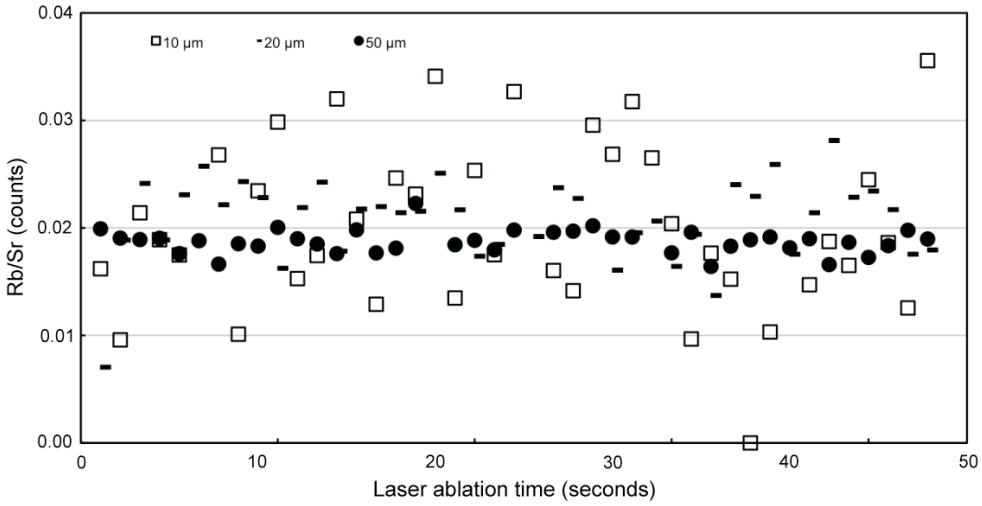

Figure A1.2. Elemental fractionation of refractory/volatile elements at 10 µm, 20 µm and 50 µm spot sizes displayed by measured Rb/Sr ratio (calculated from the analysed counts) of BHVO-2G with increasing ablation time (seconds).

A1.4.3.2. Rhyolitic glasses

Melt inclusions in this study are sourced from large-volume rhyolites that are characterised by high SiO_2 (e.g. > 70 wt% anhydrous, Chapter 2) and low CaO (e.g. < 2.5 wt%, Chapter 2) concentrations. Therefore, it was imperative that the same precision and accuracy was attained for LA-ICPMS analyses of rhyolitic glass standards as was achieved for basaltic glass standards to ensure no secondary affects such as elemental fractionation occurred at high-silica compositions that were not previously observed for basaltic compositions. To this end the rhyolitic glass ATHO-G (Jochum et al., 2006) was analysed as the unknown with BCR-2G as the calibration standard.

At the outset, due to the low CaO concentrations of ATHO-G, analyses were conducted in reaction cell mode (Table A1.15). This reduced the Ca background to compensate for the low Ca compositions of rhyolitic material (Mason, 2001).

This resulted in a loss of both precision and accuracy of ATHO-G analyses compared to BHVO-2G (Table A1.13). Repeating these analyses without the reaction cell increased the accuracy of the ATHO-G analyses (Table A1.16), however, measured concentrations still lacked the precision and accuracy achieved for BHVO-2G analyses (Table A1.13). Discrepancies were observed between reported Ba, La and Eu concentrations of ATHO-G from LA-ICPMS and isotope dilution values (Jochum et al., 2006) indicating that a matrix affect could have occurred between the rhyolitic sample (ATHO-G) and the basaltic reference material (BCR-2G). Consequently, the synthetic glass standard NIST SRM 612 was substituted for BCR-2G and ATHO-G was reanalysed, first with a 35 µm spot (Table A1.17) and second with a range of spot sizes (20-50 µm) (Table A1.18). Both sets of analyses displayed a significant improvement in both precision and accuracy comparative to those achieved for basaltic glasses (Table A1.13; A1.14).

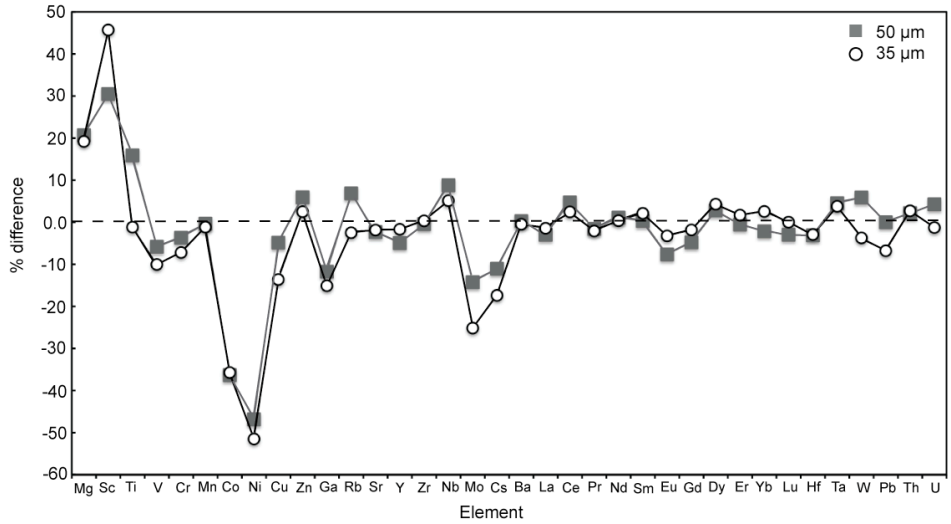

Figure A1.3. Reproducibility of trace element concentrations in ATHO-G at 50 and 35 µm spot size.

The elements that show the least reproducibility (e.g. Cr, Co, Ni) are those that are present in low concentrations and hence have low count rates (Figure A1.3). Therefore, the analysed concentrations of these elements in 'unknown' samples should be treated with caution.

A1.4.3.3. Analysis of rhyolitic melt inclusions by LA-ICPMS

As a result of the above experiments, rhyolitic melt inclusions in this study were analysed by LA-ICPMS utilising: NIST SRM 612 as the external standard; ^{43}Ca as the internal standard determined prior to LA-ICPMS analysis by EPMA; and background correcting samples to Ca. Melt inclusions were analysed with 35 μm spot size decreasing to 20μm spot size only when it was absolutely essential. Since the original development of this methodology, the technique has been further refined and run conditions for volcanic glasses may differ to those presented here (e.g. Baker et al., 2008).

A1.4.4. LA-ICPMS of plagioclase crystals

The difference in atomic structure of crystals and glasses means the optimal conditions for the ablation of volcanic glasses may not be the same for plagioclase crystals. Unfortunately, the lack of a plagioclase specific standard resulted in the use of glass standards as the external standard during LA-ICPMS analyses for plagioclase crystals, which is not ideal.

Plagioclase was analysed for Sr, Ba and Mg with 20 μm spot diameters and REE, Y, Sr and Pb spot analyses were conducted at 35 and 50 μm spot diameters. Backscattered electron images taken before and after LA-ICPMS, permitted the

EPMA and LA-ICPMS profiles to be correlated and the determination of CaO values for the internal standard (r) resolved.

A series of experiments were performed in order to determine the optimal spot size with which to analyse plagioclase crystals. The reference glass closest in composition to plagioclase is MPI-DING glass STHs6/80-G (hereafter referred to as STH-80G) was taken as the unknown in these experiments. STH-80G has Sr (482 ppm) and Ba (298 ppm) concentrations that are expected to be in the region of the Sr and Ba concentrations of the plagioclase crystals of interest (Jochum et al., 2006). NIST SRM 610 was chosen as the external standard as Sr (515.5 ppm) and Ba (435 ppm) concentrations are nearer to STH-80G and expected plagioclase concentrations than NIST 612 (Sr = 76.8 ppm; Ba = 39.7 ppm) (Table A1.8). As plagioclase zonation occurs on scales < 20 μm, it was desirable to analyse plagioclase crystals at the smallest possible spot size. Analyses of STH-80G were conducted at 10 μm and 20 μm spot diameters for Mg, Ca, Sr, Ba and REE, at the same operating conditions as for volcanic glasses, with NIST SRM 610 as the external standard and STH-80G as the 'unknown' (Table A1.19; A1.20). This demonstrated that Mg, Ca, Sr and Ba could be analysed at 20 μm spot diameters whereas it would be preferable to analyse REE at 35 or 50 μm spot diameters.

A1.5 Fourier transform infrared spectroscopy

Water and carbon dioxide analyses of melt inclusions were conducted by both conventional Fourier Transform Infrared (FTIR) spectroscopy and spectroscopic imaging FTIR (Wysoczanski and Tani, 2006). FTIR spectroscopy is a non-

destructive technique and H_2O and CO_2 analyses can be obtained from the same analytical point as major and trace element compositions. FTIR spectroscopy also has the advantage over other techniques such as SIMS of being able to determine speciation of H_2O and CO_2.

Analyses were conducted on a Varian FTS Stingray 7000 Micro Image Analyser spectrometer with a KBr beamsplitter at the Institute for Research on Earth Evolution (IFREE), Japan Agency for Marine Earth Science and Technology (JAMSTEC). N_2 gas continuously purged the beam path in an attempt to minimise the affect of atmospheric water on the measured spectra (Wysoczanski and Tani, 2006). A background analysis taken through a KBr plate was conducted prior to each sample at the same analytical conditions as for sample analysis. Samples were placed onto the KBr plate and both transmission and reflection spectra were acquired (Figure A1.4) with the background spectra subtracted from the sample spectra.

Concentrations of water species were calculated from absorbance bands in the FTIR transmission spectra using the Beer- Lambert Law;

$$c_i = \frac{M_i A}{\rho d \varepsilon} \qquad [A1.2]$$

where c_i is the concentration of species i in weight %, M_i is the molecular weight of species i (g/mol), A is the absorbance (peak height) of the relevant vibration band, ρ is the sample density (g/l), d is the thickness of sample (cm) and ε is the molar absorptivity (l/mol-cm). Total water concentrations were determined using the height above background of the overtone of the bending vibration of the H_2O_m group at 5200 cm^{-1} and molar absorptivity of 1.86 l mol^{-1} cm and OH^-

concentrations were calculated using the overtone of the stretching and bending of Si-OH^- groups at 4500 cm^{-1} and molar absorptivity of 1.5 l mol^{-1} cm (Ihinger et al., 1994). Total H_2O was calculated summing the H_2O_m concentration from the peak at 5200 cm^{-1} and OH^- concentration from the peak at 4500 cm^{-1}. When the absorbance was low, the fundamental OH^- stretching vibration at 3535 cm^{-1} and molar absorptivity of 90 ± 2 l mol^{-1} cm (Hauri et al., 2002) and the height of the HOH bending vibration at 1630 cm^{-1} and molar absorptivity of 56 ±2 l mol^{-1} cm (Newman et al., 1986) were used to calculate H_2O_m and H_2O_t contents, respectively. OH^- concentrations were calculated from the difference in H_2O_t (3535 cm^{-1}) and H_2O_m (1630 cm^{-1}). In each case peak heights were determined using a linear baseline; applying a flexicurve baseline produced results consistent with the linear baseline. The molecular CO_2 peaks at 2350 cm^{-1} and the carbonate doublet peaks of CO_3^{2-} at 1515 cm^{-1} and 1435 cm^{-1} were analysed (Fine and Stolper, 1985; Ihinger et al., 1994), but were found to be below detection limits.

In addition, the calibration of Zhang et al. (1997) can be used to calculate molecular H_2O (H_2O_m) concentrations and hydroxyl (OH^-) concentrations from the following relationships;

$$H_2O_m = \delta_{5230} A_{5230} \qquad [A1.3]$$

$$OH^- = \delta_{4520} A_{4520} \qquad [A1.4]$$

where,

$$\delta_{5230} = (\rho/18.015)(a_0) \qquad [A1.5]$$

$$\delta_{4520} = (\rho/18.015)(b_0 - b_1 A_{5230} + b_2 A_{4520}) \qquad [A1.6]$$

where A_{4520} is the 4520 cm^{-1} absorbance (peak height), A_{5230} is the 5230 cm^{-1} absorbance (peak height), ρ is the glass density (g/l), a_0 = 0.04217, b_0 = 0.04024, b_1 = 0.02011 and b_2 = 0.0522 (Zhang et al., 1997; Ihinger et al., 1999). However, this is only accurate for species concentrations for samples with total H_2O concentrations below 2.7 wt % (Zhang et al., 1997; Ihinger et al., 1999; Chapter 3).

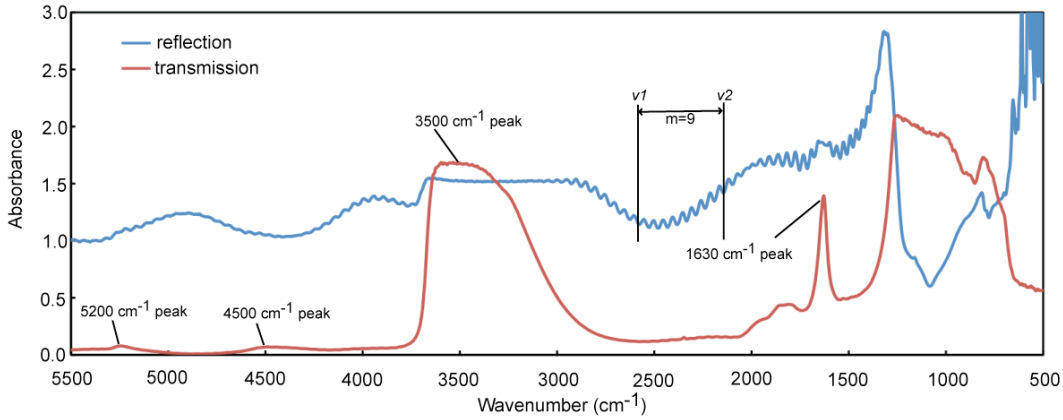

Figure A1.4. Transmission and reflected spectra of a Whakamaru melt inclusion. The four peaks used for the determination of water concentrations are shown and the reflection spectra used for thickness calculations (see text).

Glass density was calculated using the method of R. Lange as described by Luhr (2001) from electron microprobe analyses of melt inclusion compositions (Chapter 2). These ranged between 2303 g/l and 2361 g/l. A value of 2350 g/l was used with the Beer-Lambert law for all analyses, which equates to a maximum of 0.06 wt% error on the calculated water concentrations. Sample thicknesses of doubly exposed inclusions were determined at the analytical point using spacing of interference fringes on reflection spectra (Wysoczanski and Tani, 2006; Nichols and Wysoczanski, 2007). The refractive index (*n*) and

sample thickness (∂) are related to the number of waves (m) over a selected wave number interval ($v1$-$v2$) by the following relationship (Figure A1.4);

$$\partial = m/2n(v1 - v2) \qquad [A1.7]$$

A refractive index of 1.5 was used for all melt inclusions in this study (Lui et al., 2005). Thicknesses of melt inclusions suspected to retain a thin wafer of the host crystal were determined by placing the crystals side-on in crystal bond on a glass slide and then examining them under the microscope. Uncertainties of calculated water concentrations are estimated to be 10 % (e.g. Dixon et al., 1988).

		BHVO-2G ref values	BHVO-2G_A	BHVO-2G_B	BHVO-2G_C	BHVO-2G_D	BHVO-2G_E	Mean	2 SD	% 2 SD	% Difference
43	CaO	11.4	11.4	11.4	11.4	11.4	11.4	11.4			
45	Sc	33.0	34.7	34.7	32.5	32.5	32.5	33.4	2.42	7.23	1.27
47	TiO_2	2.79	2.70	2.70	2.64	2.66	2.66	2.67	0.06	2.17	-4.25
51	V	308	307	307	298	294	303	302	11.05	3.66	-2.10
53	Cr	293	317	317	296	287	296	303	27.55	9.10	3.36
59	Co	44	45.0	45.0	42.3	42.2	42.3	43.4	2.99	6.89	-1.39
60	Ni	116	125	125	116	113	115	119	10.91	9.19	2.32
63	Cu	127	126	126	120	119	118	122	7.38	6.07	-4.23
66	Zn	102	101	101	97.3	96.3	103	99.7	5.58	5.59	-2.24
71	Ga	22	22.6	22.6	21.7	20.7	20.6	21.6	1.91	8.82	-1.64
85	Rb	9.2	8.79	8.79	8.75	8.63	8.90	8.77	0.19	2.20	-4.63
88	Sr	396	440	440	432	407	394	423	41.92	9.92	6.76
89	Y	26	31.2	31.2	30.5	29.8	28.6	30.3	2.18	7.19	16.5
90	Zr	170	191	191	191	186	183	189	7.35	3.90	10.9
93	Nb	18.3	18.8	18.8	18.3	17.8	17.6	18.3	1.08	5.90	-0.07
133	Cs	0.1	0.10	0.10	0.10	0.10	0.10	0.101	0.01	5.79	0.72
137	Ba	131	129	129	127	125	125.	127	3.77	2.96	-2.82
139	La	15.2	16.9	16.9	16.3	16.1	15.6	16.4	1.05	6.43	7.60
140	Ce	37.6	37.2	37.2	36.2	36.3	36.1	36.6	1.12	3.05	-2.62
141	Pr	5.35	5.46	5.46	5.39	5.41	5.54	5.45	0.12	2.12	1.96
146	Nd	24.5	27.0	27.0	24.6	25.1	24.6	25.7	2.44	9.53	4.75
147	Sm	6.1	6.77	6.77	6.27	6.73	6.56	6.62	0.43	6.50	8.54
153	Eu	2.07	2.08	2.08	1.96	2.10	1.99	2.04	0.13	6.18	-1.21
157	Gd	6.16	7.01	7.01	6.19	6.53	7.35	6.82	0.91	13.3	10.7
163	Dy	5.28	6.04	6.04	6.10	5.91	6.34	6.09	0.32	5.24	15.3
166	Er	2.56	2.80	2.80	2.80	2.61	2.79	2.76	0.17	6.04	7.78
172	Yb	2.01	2.20	2.20	2.12	2.03	2.05	2.12	0.16	7.36	5.42
175	Lu	0.279	0.294	0.294	0.300	0.252	0.282	0.284	0.04	13.6	1.96
178	Hf	4.32	4.99	4.99	4.99	4.48	4.99	4.89	0.45	9.28	13.2
181	Ta	1.15	1.16	1.16	1.08	1.19	1.13	1.14	0.08	6.92	-0.542
208	Pb	1.7	1.97	1.97	1.95	1.92	1.95	1.95	0.05	2.40	14.9
232	Th	1.22	1.27	1.27	1.29	1.23	1.30	1.27	0.05	3.95	4.10
238	U	0.403	0.345	0.349	0.371	0.390	0.395	0.370	0.05	12.4	-8.22

Table A1.9. Initial LA-ICPMS results for BHVO-2G and BCR-2G as the unknown and standard respectively. Elemental concentrations in ppm except CaO and TiO_2 in wt%.

		BHVO-2G ref values	BHVO-2G_G	BHVO-2G_H	BHVO-2G_I	BHVO-2G_J	BHVO-2G_K	Mean	2 SD	% 2 SD	% Difference
43	CaO	11.4	11.4	11.4	11.4	11.4	11.4	11.4			
45	Sc	33.0	32.0	32.4	32.2	31.8	32.6	32.2	0.60	1.87	-2.41
47	TiO_2	2.79	2.70	2.60	2.64	2.68	2.71	2.67	0.09	3.33	-4.42
51	V	308	283	283	282	285	287	284	4.13	1.45	-7.75
53	Cr	293	311	303	283	288	275	292	29.7	10.2	-0.43
59	Co	44	40.2	40.7	40.7	40.6	40.7	40.6	0.49	1.21	-7.75
60	Ni	116	111	109	112	111	114	111	3.33	2.99	-3.95
63	Cu	127	112	111	110	109	118	112	6.40	5.71	-11.8
66	Zn	102	90.7	86.5	88.5	89.9	94.7	90.1	6.09	6.76	-11.7
71	Ga	22	20.1	19.5	18.2	19.2	20.6	19.5	1.78	9.13	-11.2
85	Rb	9.2	8.20	7.93	8.32	8.25	8.59	8.26	0.48	5.78	-10.2
88	Sr	396	395	394	392	393	406	396	11.5	2.91	0.03
89	Y	26	29.5	29.1	29.1	28.9	30.3	29.4	1.13	3.85	13.0
90	Zr	170	185	182	181	181	187	183	5.31	2.90	7.73
93	Nb	18.3	17.5	17.4	17.4	17.1	18.1	17.5	0.76	4.32	-4.28
133	Cs	0.1	0.094	0.087	0.091	0.089	0.099	0.092	0.01	9.97	-8.19
137	Ba	131	125	125	126	127	125	125	1.38	1.10	-4.24
139	La	15.2	16.5	16.1	16.1	15.9	16.8	16.3	0.71	4.38	6.95
140	Ce	37.6	36.0	35.0	35.1	35.5	36.1	35.5	1.03	2.90	-5.51
141	Pr	5.35	5.39	5.25	5.46	5.51	5.57	5.44	0.25	4.57	1.62
146	Nd	24.5	25.1	24.8	25.0	25.4	25.6	25.2	0.61	2.43	2.74
147	Sm	6.1	6.33	6.50	6.54	6.36	6.88	6.52	0.44	6.68	6.94
153	Eu	2.07	1.96	2.07	1.97	2.07	2.14	2.04	0.15	7.50	-1.30
155	Gd	6.16	5.37	5.34	5.57	5.16	5.80	5.45	0.49	8.90	-11.5
156	Gd	6.16	5.73	5.57	5.73	6.16	6.10	5.86	0.52	8.87	-4.92
157	Gd	6.16	6.42	6.75	7.03	6.70	7.41	6.86	0.75	10.9	11.4
158	Gd	6.16	6.91	6.86	6.81	6.56	6.83	6.79	0.27	3.98	10.3
163	Dy	5.28	5.86	5.77	5.81	5.63	5.99	5.81	0.26	4.51	10.1
166	Er	2.56	2.74	2.76	2.70	2.74	2.98	2.78	0.22	8.00	8.72
172	Yb	2.01	2.17	2.07	2.05	2.00	2.17	2.09	0.15	7.25	4.13
175	Lu	0.279	0.314	0.301	0.315	0.309	0.318	0.311	0.01	4.09	11.6
178	Hf	4.32	4.74	4.54	4.71	4.84	5.01	4.77	0.35	7.35	10.4
181	Ta	1.15	1.05	1.11	1.18	1.08	1.11	1.11	0.10	9.01	-3.85
208	Pb	1.7	1.59	1.61	1.64	1.72	1.80	1.67	0.17	10.5	-1.56
232	Th	1.22	1.23	1.22	1.26	1.27	1.26	1.25	0.05	3.83	2.17
238	U	0.403	0.371	0.383	0.366	0.357	0.380	0.371	0.02	5.73	-7.85

Table A1.10. Analysis of polished BHVO-2G and BCR-2G as the unknown and standard respectively. Elemental concentrations in ppm except CaO and TiO_2 in wt%.

		BHVO-2G ref values	BHVO-2G_L	BHVO-2G_M	BHVO-2G_N	BHVO-2G_O	BHVO-2G_P	Mean	2 SD	% 2 SD	% Difference
43	CaO	11.4	11.4	11.4	11.4	11.4	11.4	11.4			
45	Sc	33.0	32.3	34.1	34.1	34.7	36.1	34.3	2.70	7.87	3.88
47	TiO_2	2.79	2.61	2.66	2.66	2.67	2.72	2.67	0.08	2.97	-4.44
51	V	308	293	300	300	304	309	301	11.2	3.71	-2.14
53	Cr	293	305	336	336	312	330	324	29.0	8.95	10.6
59	Co	44	41.4	41.9	41.9	44.1	45.1	42.9	3.23	7.53	-2.52
60	Ni	116	118	122	122	119	127	121	7.07	5.82	4.67
63	Cu	127	116	113	113	116	122	116	7.50	6.45	-8.46
66	Zn	102	93.4	95.4	95.4	88.5	94.8	93.5	5.83	6.23	-8.30
71	Ga	22	21.0	21.7	21.7	20.2	20.9	21.1	1.27	6.01	-3.97
85	Rb	9.2	8.72	9.10	9.10	9.01	8.90	8.97	0.33	3.64	-2.54
88	Sr	396	389	396	396	397	399	395	7.46	1.89	-0.189
89	Y	26	31.0	31.1	31.1	31.2	30.7	31.0	0.34	1.10	19.3
90	Zr	170	189	196	196	192	192	193	5.95	3.08	13.5
93	Nb	18.3	17.7	17.8	17.8	17.7	17.2	17.7	0.52	2.92	-3.54
133	Cs	0.1	0.110	0.109	0.109	0.099	0.085	0.103	0.02	21.4	2.61
137	Ba	131	126	127	127	123	127	126	3.22	2.55	-3.76
139	La	15.2	16.3	16.8	16.8	16.1	16.2	16.5	0.73	4.43	8.27
140	Ce	37.6	36.3	36.6	36.6	35.7	36.0	36.3	0.77	2.11	-3.56
141	Pr	5.35	5.24	5.36	5.36	5.59	5.54	5.42	0.28	5.24	1.31
146	Nd	24.5	25.2	25.2	25.2	26.6	26.3	25.7	1.36	5.28	5.00
147	Sm	6.1	6.44	6.22	6.22	6.54	7.06	6.50	0.69	10.6	6.52
153	Eu	2.07	2.06	1.99	1.99	2.15	2.05	2.05	0.13	6.37	-0.97
155	Gd	6.16	6.02	5.64	5.64	5.73	6.20	5.85	0.50	8.60	-5.11
156	Gd	6.16	6.80	6.59	6.59	6.85	6.98	6.76	0.34	4.98	9.76
157	Gd	6.16	6.91	6.77	6.77	6.70	6.99	6.83	0.24	3.50	10.8
158	Gd	6.16	6.96	6.88	6.88	6.83	7.54	7.02	0.59	8.38	13.9
163	Dy	5.28	5.89	6.40	6.40	5.80	6.03	6.10	0.57	9.28	15.6
166	Er	2.56	2.93	3.15	3.15	3.02	3.06	3.06	0.19	6.08	19.7
172	Yb	2.01	2.18	2.15	2.15	2.20	2.38	2.22	0.19	8.60	10.2
175	Lu	0.279	0.277	0.315	0.315	0.317	0.363	0.317	0.06	19.3	13.8
178	Hf	4.32	4.99	5.19	5.19	5.41	5.17	5.19	0.30	5.69	20.1
181	Ta	1.15	1.15	1.17	1.17	1.23	1.19	1.18	0.06	5.50	2.70
208	Pb	1.7	1.76	1.78	1.78	1.71	1.71	1.75	0.07	3.94	2.69
232	Th	1.22	1.28	1.33	1.33	1.29	1.33	1.31	0.05	3.68	7.64
238	U	0.403	0.380	0.381	0.381	0.370	0.388	0.380	0.01	3.37	-5.71

Table A1.10 continued

		BHVO-2G ref values	BHVO-2G_Q	BHVO-2G_R	BHVO-2G_S	BHVO-2G_T	BHVO-2G_U	Mean	2 SD	% 2 SD	% Difference
43	CaO	11.4	11.4	11.4	11.4	11.4	11.4	11.4			
45	Sc	33.0	31.1	30.8	31.9	30.9	31.7	31.3	1.00	3.20	-5.19
47	TiO_2	2.79	2.68	2.69	2.74	2.74	2.73	2.72	0.06	2.28	-2.64
51	V	308	312	309	315	315	311	312	5.63	1.80	1.46
53	Cr	293	349	329	315	325	308	325	31.3	9.62	11.0
59	Co	44.0	44.1	44.6	43.6	43.4	44.2	44.0	0.938	2.13	-0.08
60	Ni	116	117	127	113	125	120	120	10.9	9.06	3.81
63	Cu	127	123	124	114	123	125	122	8.65	7.09	-3.94
66	Zn	102	102	104	96.4	100	98	100	6.37	6.36	-1.83
71	Ga	22.0	21.3	21.9	19.4	21.6	21.5	21.1	1.99	9.42	-3.97
85	Rb	9.20	8.98	9.07	8.48	8.91	8.75	8.84	0.463	5.24	-3.93
88	Sr	396	395	399	372	391	395	390	21.8	5.58	-1.39
89	Y	26.0	26.2	26.6	25.3	26.3	25.8	26.0	1.02	3.90	0.121
90	Zr	170	166	164	155	169	164	163	10.2	6.24	-3.87
93	Nb	18.3	17.7	17.9	17.5	18.6	17.5	17.9	0.904	5.06	-2.42
133	Cs	0.10	0.099	0.090	0.087	0.077	0.103	0.091	0.020	22.4	-8.92
137	Ba	131	131	128	131	130	131	130	2.78	2.13	-0.430
139	La	15.2	15.6	14.9	14.4	15.5	15.4	15.1	1.00	6.63	-0.358
140	Ce	37.6	37.7	38.0	38.0	37.9	39.2	38.2	1.19	3.13	1.47
141	Pr	5.35	5.33	5.10	5.18	5.45	5.52	5.32	0.347	6.53	-0.638
146	Nd	24.5	24.6	24.0	21.6	23.6	24.5	23.6	2.47	10.4	-3.47
147	Sm	6.1	5.98	5.98	5.28	5.98	6.13	5.87	0.674	11.5	-3.76
153	Eu	2.07	1.98	1.98	2.00	2.05	1.99	2.00	0.060	2.99	-3.28
157	Gd	6.16	6.52	6.62	6.15	6.05	6.40	6.35	0.483	7.6	3.02
163	Dy	5.28	5.18	5.00	4.98	5.09	5.10	5.07	0.168	3.31	-4.00
166	Er	2.56	2.63	2.53	2.44	2.64	2.49	2.55	0.173	6.79	-0.523
172	Yb	2.01	1.96	1.77	1.91	2.06	1.92	1.92	0.206	10.7	-4.25
175	Lu	0.279	0.276	0.262	0.254	0.291	0.264	0.269	0.029	10.9	-3.45
178	Hf	4.32	4.59	4.45	4.05	4.33	4.54	4.39	0.431	9.81	1.70
181	Ta	1.15	1.08	1.15	1.15	1.07	1.08	1.11	0.076	6.85	-3.87
208	Pb	1.7	1.88	1.88	2.19	1.76	1.80	1.90	0.340	17.9	11.9
232	Th	1.22	1.25	1.17	1.18	1.22	1.17	1.20	0.073	6.07	-1.85
238	U	0.403	0.419	0.415	0.385	0.440	0.395	0.411	0.043	10.5	1.89

Table A1.11 Analysis of polished BHVO-2G and BCR-2G as the unknown and standard respectively when mounted in half circles. Elemental concentrations in ppm except CaO and TiO_2 in wt%.

		BHVO-2G ref values	BHVO-2G_V1	BHVO-2G_U1	BHVO-2G_W1	BHVO-2G_X1	BHVO-2G_Y1	Mean	2 SD	% 2 SD	% Difference
43	CaO	11.4	11.4	11.4	11.4	11.4	11.4	11.4			
45	Sc	33.0	30.0	30.0	30.0	30.2	30.1	30.0	0.202	0.673	-8.98
47	TiO_2	2.79	2.71	2.71	2.57	2.61	2.60	2.64	0.130	4.93	-5.38
51	V	308	356	356	302	316	331	332	47.8	14.4	7.77
53	Cr	293	358	358	300	307	329	330	54.6	16.5	12.7
59	Co	44.0	47.6	47.6	45.3	47.0	47.2	46.9	1.85	3.93	6.66
60	Ni	116	127	127	132	133	124	128	8.11	6.31	10.8
63	Cu	127	127	127	137	131	133	131	9.01	6.88	3.10
66	Zn	102	111	111	119	114	105	112	9.93	8.87	9.70
71	Ga	22.0	25.2	25.2	25.0	26.2	23.6	25.0	1.86	7.43	13.7
85	Rb	9.20	10.7	10.7	9.94	11.3	9.71	10.5	1.29	12.3	13.8
88	Sr	396	446	446	418	447	393	430	48.2	11.2	8.59
89	Y	26.0	26.5	26.5	25.0	26.7	24.7	25.9	1.89	7.31	-0.466
90	Zr	170	165	165	158	173	154	163	14.3	8.81	-4.19
93	Nb	18.3	17.9	17.9	17.2	19.6	17.8	18.1	1.74	9.64	-1.28
133	Cs	0.10	0.106	0.106	0.098	0.104	0.111	0.105	0.009	8.9	4.94
137	Ba	131	135	135	129	137	130	133	6.96	5.21	1.82
139	La	15.2	15.2	15.2	14.6	15.1	15.2	15.0	0.507	3.37	-1.02
140	Ce	37.6	43.4	43.4	41.2	38.7	41.1	41.6	3.93	9.46	10.57
141	Pr	5.35	6.12	6.12	5.63	5.43	5.80	5.82	0.609	10.5	8.79
146	Nd	24.5	27.2	27.2	26.3	26.4	24.5	26.3	2.17	8.23	7.44
147	Sm	6.1	6.48	6.48	6.55	6.49	5.88	6.38	0.554	8.69	4.55
153	Eu	2.07	2.35	2.35	1.97	2.36	1.99	2.21	0.414	18.8	6.53
157	Gd	6.16	6.34	6.34	5.67	6.38	5.52	6.05	0.841	13.9	-1.81
163	Dy	5.28	4.89	4.89	4.83	5.43	5.02	5.01	0.483	9.64	-5.06
166	Er	2.56	2.35	2.35	2.32	2.57	2.39	2.40	0.201	8.39	-6.426
172	Yb	2.01	1.81	1.81	1.85	1.93	1.75	1.83	0.132	7.21	-8.90
175	Lu	0.279	0.272	0.272	0.266	0.237	0.262	0.262	0.029	10.9	-6.23
178	Hf	4.32	4.57	4.57	4.06	4.51	4.66	4.48	0.475	10.61	3.61
181	Ta	1.15	1.13	1.13	1.07	1.14	1.10	1.11	0.056	5.02	-3.23
208	Pb	1.7	2.21	2.21	1.94	2.06	1.92	2.07	0.278	13.5	21.6
232	Th	1.22	1.18	1.18	1.08	1.22	1.16	1.17	0.106	9.13	-4.47
238	U	0.403	0.425	0.425	0.395	0.432	0.422	0.420	0.028	6.76	4.22

Table A1.12. Analysis of BHVO-2G and BCR-2G mounted in half circles rotated by 90°. Elemental concentrations in ppm except CaO and TiO_2 in wt%.

	BHVO-2G ref values		BHVO-2G_AA	BHVO-2G_AB	BHVO-2G_AC	BHVO-2G_AD	BHVO-2G_AE	Mean	2 SD	% 2 SD
43	CaO	11.4	11.4	11.4	11.4	11.4	11.4	11.4		
45	Sc	33.0	30.1	31.3	31.0	31.1	29.8	30.7	1.31	4.29
47	TiO_2	2.79	2.65	2.74	2.69	2.70	2.65	2.69	0.078	2.89
51	V	308	317	314	305	315	306	312	11.8	3.77
53	Cr	293	311	289	299	316	313	306	22.5	7.36
59	Co	44.0	45.1	44.7	42.4	43.4	43.4	43.8	2.16	4.94
60	Ni	116	124	126	123	121	121	123	3.99	3.24
63	Cu	127	128	125	118	124	126	124	7.95	6.39
66	Zn	102	105	101	95.2	97.1	97.6	99.2	7.98	8.05
71	Ga	22.0	22.4	22.7	21.5	20.8	21.3	21.7	1.58	7.25
85	Rb	9.20	9.05	9.26	9.07	8.57	8.96	8.98	0.508	5.66
88	Sr	396	411	394	384	391	397	396	20.0	5.06
89	Y	26.0	26.0	26.1	26.0	25.4	25.5	25.8	0.626	2.43
90	Zr	170	162	170	157	161	166	163	9.34	5.73
93	Nb	18.3	17.7	18.5	17.3	17.4	18.1	17.8	0.982	5.52
133	Cs	0.10	0.094	0.089	0.095	0.096	0.089	0.092	0.007	7.33
137	Ba	131	133	131	128	125	130	129	6.05	4.68
139	La	15.2	14.8	15.2	14.6	14.7	14.6	14.8	0.481	3.25
140	Ce	37.6	37.3	37.5	36.8	37.8	37.3	37.3	0.721	1.93
141	Pr	5.35	5.43	5.31	5.24	5.28	5.22	5.30	0.168	3.18
146	Nd	24.5	24.9	24.0	24.0	24.2	24.2	24.3	0.686	2.82
147	Sm	6.1	5.97	5.87	5.87	5.66	5.90	5.85	0.236	4.03
153	Eu	2.07	1.94	1.97	1.97	2.02	1.91	1.96	0.085	4.34
157	Gd	6.16	5.71	5.77	5.91	6.08	6.21	5.94	0.413	6.96
163	Dy	5.28	5.23	5.25	5.14	5.14	4.91	5.14	0.270	5.25
166	Er	2.56	2.44	2.51	2.51	2.31	2.19	2.39	0.278	11.6
172	Yb	2.01	1.84	1.83	1.98	1.80	1.92	1.87	0.152	8.09
175	Lu	0.279	0.240	0.266	0.272	0.261	0.257	0.260	0.024	9.39
178	Hf	4.32	4.14	4.58	4.26	3.99	4.15	4.22	0.440	10.4
181	Ta	1.15	1.11	1.15	1.05	1.00	1.11	1.08	0.120	11.1
208	Pb	1.7	1.82	1.77	1.74	1.73	1.73	1.76	0.072	4.07
232	Th	1.22	1.23	1.21	1.11	1.20	1.11	1.17	0.116	9.89
238	U	0.403	0.408	0.392	0.350	0.392	0.398	0.388	0.045	11.6

Table A1.13. Analysis of BHVO-2G and BCR-2G as the unknown and standard respectively, mounted in half circles with reduced cell volume. Elemental concentrations in ppm except CaO and TiO_2 in wt%.

	BHVO-2G ref values		BHVO-2G_AF	% Difference	BHVO-2G_AG	% Difference	BHVO-2G_AH	% Difference	BHVO-2G_AI	% Difference	BHVO-2G_AJ	% Difference
	Spot size		50 µm		35 µm		20 µm		15 µm		10 µm	
43	CaO	11.4	11.4		11.4		11.4		11.4		11.4	
45	Sc	33.0	30.8	-6.53	29.9	-9.29	29.6	-10.4	29.2	-11.4	32.3	-2.01
47	TiO_2	2.79	2.65	-5.01	2.58	-7.56	2.48	-11.0	2.60	-6.90	2.65	-5.01
51	V	308	313	1.67	300	-2.56	315	2.15	300	-2.58	329	6.89
53	Cr	293	300	2.41	271	-7.51	300	2.45	318	8.44	327	11.7
59	Co	44.0	43.9	-0.326	42.3	-3.89	46.1	4.83	45.1	2.49	46.2	5.00
60	Ni	116	120	3.37	118	1.74	127	9.42	122	5.13	139	19.7
63	Cu	127	124	-2.37	127	0.023	144	13.1	127	0.359	138	9.02
66	Zn	102	108	5.65	103	1.36	109	6.38	96	-5.60	102	-0.164
71	Ga	22.0	21.8	-0.917	21.8	-0.689	24.0	9.00	23.9	8.84	26.5	20.6
85	Rb	9.20	8.97	-2.51	9.11	-0.960	8.99	-2.28	9.77	6.17	9.34	1.54
88	Sr	396	434	9.57	388	-2.12	401	1.18	413	4.26	404	1.95
89	Y	26.0	24.7	-4.81	26.4	1.45	25.5	-1.93	26.6	2.15	28.5	9.43
90	Zr	170	162	-4.65	161	-5.39	169	-0.31	178	4.87	188	10.3
93	Nb	18.3	17.4	-4.97	18.0	-1.85	19.3	5.49	18.6	1.38	18.8	2.78
133	Cs	0.10	0.107	6.88	0.095	-5.36	0.168	68.4	0.199	99.5	0.501	401
137	Ba	131	132	0.973	129	-1.82	140	6.53	131	-0.279	130	-0.83
139	La	15.2	14.9	-1.99	14.8	-2.59	14.8	-2.71	15.8	3.89	15.3	0.77
140	Ce	37.6	37.5	-0.273	37.4	-0.555	39.5	5.04	38.3	1.86	36.9	-1.79
141	Pr	5.35	5.16	-3.47	5.20	-2.80	5.35	0.01	5.66	5.87	5.29	-1.14
146	Nd	24.5	22.9	-6.39	23.7	-3.12	25.4	3.63	24.7	0.730	27.3	11.5
147	Sm	6.1	5.56	-8.91	5.82	-4.53	5.68	-6.88	5.88	-3.68	6.30	3.23
153	Eu	2.07	2.14	3.40	2.09	0.889	1.90	-8.18	1.94	-6.23	1.98	-4.21
157	Gd	6.16	6.09	-1.21	5.86	-4.89	5.37	-12.9	5.94	-3.52	7.96	29.3
163	Dy	5.28	5.06	-4.08	4.95	-6.26	4.63	-12.4	5.63	6.56	6.79	28.6
166	Er	2.56	2.56	-0.127	2.46	-3.99	2.23	-12.9	2.48	-2.99	1.86	-27.5
172	Yb	2.01	2.02	0.587	1.96	-2.57	1.81	-9.71	2.15	6.87	3.01	49.9
175	Lu	0.279	0.249	-10.6	0.251	-9.98	0.222	-20.4	0.283	1.41	0.474	69.7
178	Hf	4.32	4.27	-1.26	4.29	-0.809	4.25	-1.71	4.49	3.92	5.52	27.8
181	Ta	1.15	1.03	-10.7	1.01	-12.5	1.13	-2.02	1.33	15.5	1.17	1.40
208	Pb	1.7	1.81	6.73	2.10	23.8	2.39	40.5	1.81	6.71	3.59	111
232	Th	1.22	1.15	-5.82	1.16	-4.62	1.13	-7.09	1.48	21.1	1.44	18.2
238	U	0.403	0.409	1.45	0.447	11.0	0.419	3.85	0.403	0.044	0.524	30.0

Table A1.14 Analysis of BHVO-2G and BCR-2G at 10-50 µm spot sizes. Elemental concentrations in ppm except CaO and TiO_2 in wt%.

	ATHO-G ref values		ATHO-G-K12	ATHO-G-K13	ATHO-G-K14	ATHO-G-K15	ATHO-G-K16	Mean	2 SD	% 2 SD	% Difference
43	CaO	1.70	1.70	1.70	1.70	1.70	1.70	1.7			
45	Sc	7.00	12.0	10.9	11.6	10.7	10.8	11.2	1.20	10.7	60.1
47	TiO_2	0.26	0.263	0.259	0.279	0.249	0.258	0.262	0.023	8.61	2.57
51	V	3.91	3.28	3.49	3.50	3.32	3.24	3.37	0.241	7.17	-13.9
53	Cr	6.10	6.06	5.21	9.83	6.49	6.56	6.83	3.52	51.6	11.9
59	Co	2.13	1.13	1.24	1.20	1.35	1.09	1.20	0.201	16.7	-43.6
60	Ni	13.0	6.79	6.13	6.63	5.68	5.74	6.19	1.01	16.4	-52.4
63	Cu	18.6	18.8	20.6	18.9	18.0	17.1	18.7	2.57	13.8	0.476
66	Zn	141	135	143	137	129	129	135	11.8	8.76	-4.54
71	Ga	25.3	23.9	25.8	24.6	23.2	23.8	24.2	2.00	8.26	-4.20
85	Rb	65.3	65.5	67.9	68.4	62.2	64.8	65.7	5.08	7.72	0.684
88	Sr	94.1	96.7	94.5	97.3	90.6	90.4	93.9	6.55	6.98	-0.195
89	Y	94.5	110	111	120	106	108	111	10.53	9.49	17.4
90	Zr	512	570	561	578	537	546	558	34.5	6.17	9.07
93	Nb	62.4	64.8	64.6	66.1	61.2	62.7	63.9	3.84	6.01	2.37
133	Cs	1.08	0.938	0.964	0.950	0.847	0.851	0.910	0.113	12.4	-15.8
137	Ba	559	547	552	566	506	531	540	46.0	8.51	-3.33
139	La	55.6	57.0	57.9	58.7	55.1	54.3	56.6	3.70	6.55	1.76
140	Ce	121	131	132	133	120	120	127	13.1	10.3	5.00
141	Pr	14.6	15.5	15.9	16.4	15.1	14.5	15.5	1.43	9.25	6.09
146	Nd	60.9	65.1	65.7	65.8	63.6	61.0	64.2	4.06	6.32	5.47
147	Sm	14.2	15.2	14.9	15.7	14.5	14.5	15.0	0.95	6.38	5.36
153	Eu	2.76	2.65	2.75	2.77	2.59	2.61	2.67	0.16	6.07	-3.11
157	Gd	15.3	15.9	16.1	16.6	16.7	16.4	16.3	0.68	4.18	6.70
163	Dy	16.2	17.6	17.2	19.1	17.7	17.3	17.8	1.51	8.48	9.96
166	Er	10.3	11.6	11.3	12.8	12.2	10.6	11.7	1.69	14.5	13.6
172	Yb	10.5	11.2	10.5	11.0	10.4	10.6	10.7	0.677	6.31	2.20
175	Lu	1.54	1.70	1.75	1.80	1.58	1.51	1.67	0.238	14.3	8.46
178	Hf	13.7	15.3	15.4	15.9	14.6	14.7	15.2	1.09	7.20	10.7
181	Ta	3.9	4.00	4.00	4.13	3.80	3.70	3.93	0.349	8.87	0.731
208	Pb	5.67	6.49	6.40	6.63	6.09	6.45	6.41	0.403	6.28	13.1
232	Th	7.4	7.58	7.84	8.21	7.38	7.72	7.75	0.618	7.97	4.67
238	U	2.37	2.28	2.45	2.40	2.27	2.37	2.35	0.153	6.51	-0.777

Table A1.15 Analysis of ATHO-G and BCR-2G as the unknown and standard respectively in reaction cell mode. Elemental concentrations in ppm except CaO and TiO_2 in wt%.

		ATHO-G ref values	ATHO-G3	ATHO-G4	ATHO-G5	ATHO-G6	ATHO-G7	Mean	2 SD	% 2 SD	% Difference
25	Mg	621	573	580	587	623	596	592	38.93	6.58	-4.68
43	CaO	1.70	1.70	1.70	1.70	1.70	1.70	1.70			
45	Sc	7.00	9.65	9.40	9.82	9.84	9.65	9.67	0.351	3.63	38.1
47	TiO_2	0.26	0.262	0.279	0.275	0.287	0.279	0.276	0.018	6.55	8.40
51	V	3.91	3.48	3.58	3.84	3.88	3.96	3.75	0.412	11.0	-4.11
53	Cr	6.10	6.92	5.58	6.14	5.40	7.03	6.21	1.50	24.1	1.84
59	Co	2.13	1.51	1.50	1.49	1.47	1.65	1.52	0.142	9.29	-28.4
60	Ni	13.0	8.76	8.24	7.55	8.44	8.85	8.37	1.04	12.4	-35.6
63	Cu	18.6	18.1	19.5	18.4	18.4	19.9	18.9	1.58	8.35	1.45
66	Zn	141	137	139	141	151	145	143	11.6	8.16	1.14
71	Ga	25.3	23.2	23.6	23.5	26.1	25.1	24.3	2.47	10.2	-3.96
85	Rb	65.3	68.1	69.0	67.8	72.0	75.2	70.4	6.33	8.99	7.83
88	Sr	94.1	88.5	89.5	87.6	94.8	96.8	91.4	8.19	8.96	-2.83
89	Y	94.5	102	104	102	111	108	105	7.64	7.25	11.6
90	Zr	512	529	511	522	555	533	530	33.1	6.24	3.50
93	Nb	62.4	65.0	65.0	63.3	67.6	67.6	65.7	3.72	5.66	5.32
133	Cs	1.08	0.938	0.965	0.925	1.04	1.11	0.995	0.154	15.5	-7.9
137	Ba	559	528	533	530	564	551	541	31.7	5.86	-3.16
139	La	55.6	54.2	56.9	53.9	60.2	58.1	56.7	5.32	9.39	1.91
140	Ce	121	126	133	130	147	137	135	15.6	11.6	11.2
146	Nd	60.9	57.4	63.3	62.2	67.3	64.0	62.8	7.20	11.5	3.18
147	Sm	14.2	13.7	13.5	14.5	15.7	15.5	14.6	1.97	13.5	2.74
153	Eu	2.76	2.54	2.70	2.84	2.95	2.70	2.74	0.312	11.4	-0.58
157	Gd	15.3	16.3	15.3	14.8	17.4	17.0	16.2	2.21	13.6	5.72
163	Dy	16.2	17.3	16.5	15.7	19.0	18.6	17.4	2.82	16.2	7.59
166	Er	10.3	10.9	10.5	10.2	11.4	11.6	10.9	1.14	10.5	6.3
172	Yb	10.5	10.5	10.2	10.0	11.7	11.1	10.7	1.389	13.0	1.75
175	Lu	1.54	1.44	1.46	1.48	1.66	1.59	1.53	0.186	12.2	-0.93
178	Hf	13.7	13.6	14.2	14.1	15.6	14.6	14.4	1.52	10.5	5.4
181	Ta	3.9	3.66	3.65	3.69	3.92	3.93	3.77	0.289	7.65	-3.32
208	Pb	5.67	6.12	5.87	6.02	6.45	6.36	6.16	0.478	7.76	8.7
232	Th	7.4	7.06	7.31	7.17	7.93	7.83	7.46	0.787	10.5	0.80
238	U	2.37	2.29	2.63	2.47	2.57	2.68	2.53	0.307	12.2	6.56

Table A1.16. Analysis of ATHO-G and BCR-2G without the reaction cell. Elemental concentrations in ppm except CaO and TiO_2 in wt%.

		ATHO-G ref values	ATHO-G_A	ATHO-G_B	ATHO-G_C	Mean	2 SD	% 2 SD	% Difference
25	Mg	621	868	997	909	925	131	14.2	48.9
43	CaO	1.70	1.70	1.70	1.70	1.70			
45	Sc	7.00	9.24	11.6	9.73	10.2	2.52	24.7	45.7
47	TiO_2	0.26	0.325	0.320	0.30	0.314	0.029	9.23	23.3
51	V	3.91	4.49	3.90	3.37	3.92	1.12	28.5	0.239
53	Cr	6.10	13.3	18.1	12.34	14.6	6.15	42.2	139
55	Mn	798	855	868	816	846	53.3	6.30	6.05
59	Co	2.13	1.30	1.67	1.90	1.62	0.610	37.6	-23.8
60	Ni	13.0	6.58	7.67	6.15	6.80	1.56	23.0	-47.7
63	Cu	18.6	17.9	20.7	18.76	19.1	2.83	14.8	2.77
66	Zn	141	156	145	152	151	11.0	7.3	7.20
71	Ga	25.3	20.4	21.4	20.3	20.7	1.24	5.97	-18.1
85	Rb	65.3	70.4	75.0	69.3	71.6	6.11	8.5	9.61
88	Sr	94.1	90.8	90.0	89.7	90.2	1.19	1.32	-4.19
89	Y	94.5	92.3	97.9	90.5	93.5	7.72	8.2	-1.01
90	Zr	512	505	538	477	507	61.6	12.2	-1.02
93	Nb	62.4	69.5	70.7	69.5	70	1.43	2.05	12.0
95	Mo	4.80	3.73	5.37	4.77	4.62	1.67	36.0	-3.68
133	Cs	1.08	0.943	1.05	0.925	0.97	0.137	14.1	-9.87
137	Ba	559	551	581	551	561	34.4	6.14	0.344
139	La	55.6	54.8	52.6	54.6	54.0	2.46	4.56	-2.91
140	Ce	121	125	125	124	125	1.73	1.39	3.09
141	Pr	14.6	14.8	14.4	14.5	14.6	0.405	2.78	-0.259
146	Nd	60.9	61.5	64.4	56.3	60.7	8.29	13.6	-0.283
147	Sm	14.2	14.8	15.5	12.4	14.3	3.24	22.7	0.460
153	Eu	2.76	2.58	2.65	2.59	2.61	0.078	3.01	-5.53
157	Gd	15.3	15.5	14.1	13.6	14.4	2.01	14.0	-5.94
163	Dy	16.2	17.4	16.4	14.5	16.1	2.96	18.4	-0.64
166	Er	10.3	10.5	9.9	9.69	10.0	0.802	7.99	-2.58
172	Yb	10.5	9.66	11.1	9.80	10.2	1.53	15.0	-3.12
175	Lu	1.54	1.46	1.49	1.51	1.49	0.047	3.14	-3.57
178	Hf	13.7	14.4	13.3	12.3	13.3	2.05	15.4	-2.71
181	Ta	3.90	4.20	4.46	3.60	4.09	0.88	21.6	4.82
182	W	9.30	9.74	10.4	9.81	10.0	0.777	7.77	7.50
208	Pb	5.67	5.55	5.77	5.17	5.50	0.612	11.1	-3.02
232	Th	7.40	7.64	7.89	7.00	7.51	0.919	12.2	1.52
238	U	2.37	2.74	2.89	2.39	2.67	0.515	19.3	12.8

Table A1.17. Analysis of ATHO-G and NIST 612 as the unknown and standard respectively. Elemental concentrations in ppm except CaO and TiO_2 in wt%.

	Ref values	50 µm	% 2 SD	35 µm	% 2 SD	20 µm	% 2 SD
		n = 5		n = 20		n = 3	
Mg	621	750	7.16	740	6.97	695	11.5
CaO	1.70	1.70		1.70		1.70	
Sc	7.00	9.13	7.43	15.1	63.1	11.7	24.1
TiO2	0.255	0.296	5.52	0.252	20.6	0.264	3.80
V	3.91	3.68	3.02	3.52	16.5	3.22	32.3
Cr	6.10	5.88	13.0	5.66	50.2	20.7	44.7
Mn	821	818	2.42	812	8.63	785	15.9
Co	2.13	1.36	19.5	1.37	18.4	1.73	21.5
Ni	13.0	6.91	16.8	6.30	21.3	7.74	38.6
Cu	18.6	17.7	8.28	16.1	9.32	16.2	16.2
Zn	141	149	5.81	145	14.4	144	2.35
Ga	25.3	22.3	6.75	21.5	9.43	19.6	10.8
Rb	65.3	69.8	7.84	63.7	6.94	59.9	8.52
Sr	94.1	91.9	5.27	92.4	3.38	89.8	10.3
Y	94.5	89.8	6.35	92.9	8.61	90.3	9.08
Zr	512	510	9.41	514	8.24	512	10.7
Nb	62.4	67.9	6.58	65.6	7.55	61.1	11.2
Mo	4.80	4.12	7.94	3.59	21.3	4.10	12.8
Cs	1.08	0.961	15.8	0.892	16.7	0.951	23.8
Ba	559	560	3.1	556	9.45	532	0.696
La	55.6	54.0	3.6	54.8	7.40	52.7	4.49
Ce	121	127	3.2	124	6.28	117	8.54
Pr	14.6	14.4	3.8	14.3	6.99	13.5	3.42
Nd	60.9	61.6	3.2	61.1	7.78	58.2	9.71
Sm	14.2	14.2	8.3	14.5	9.80	14.5	17.1
Eu	2.76	2.55	6.5	2.67	9.24	2.51	3.36
Gd	15.3	14.6	11.1	15.0	9.67	14.7	30.4
Dy	16.2	16.7	2.89	16.9	7.97	16.4	9.19
Er	10.3	10.2	6.21	10.5	7.46	9.51	14.5
Yb	10.5	10.3	7.77	10.8	8.35	10.8	10.4
Lu	1.54	1.49	6.72	1.54	10.4	1.50	20.0
Hf	13.7	13.3	9.73	13.3	12.1	12.7	7.63
Ta	3.90	4.08	4.97	4.05	8.24	3.91	5.50
W	9.30	9.85	3.47	8.95	11.4	8.38	14.4
Pb	5.67	5.67	4.76	5.29	13.6	4.99	4.69
Th	7.40	7.56	5.16	7.60	6.34	7.11	6.62
U	2.37	2.47	3.07	2.34	10.5	2.28	19.2

Table A1.18. Analysis of ATHO-G and NIST 612 as unknown and standard respectively at varying spot sizes. Elemental concentrations in ppm except CaO and TiO_2 in wt%.

		ref values STH-G	KSTHG6	KSTHG7	KSTHG8	KSTHG9	KSTHG10	Mean	2 SD	% 2 SD	% difference
24	Mg	11879	11643	11145	10935	12839.18	12763	11865	1786	15.0	-0.119
25	Mg	11879	11965	10717	11067	13055.62	13154	11992	2228	18.6	0.949
43	CaO	5.28	5.28	5.28	5.28	5.28	5.28	5.28			
88	Sr	482	517	479	482	562	521	512	67.3	13.1	6.29
137	Ba	298	329	279	335	331	342	323	50.0	15.5	8.48
139	La	12.0	10.5	12.5	12.9	13.7	9.59	11.8	3.46	29.2	-1.29
140	Ce	26.1	24.5	25.1	25.4	30.8	30.3	27.2	6.15	22.6	4.34
141	Pr	3.20	2.41	3.22	2.31	2.83	3.44	2.84	0.987	34.7	-11.2
146	Nd	13.0	11.5	11.4	10.9	12.9	12.3	11.8	1.59	13.5	-9.06
147	Sm	2.78	4.87	4.22	4.14	5.56	7.72	5.30	2.93	55.4	90.7
153	Eu	0.953	1.35	1.35	1.98	1.87	1.79	1.67	0.598	35.8	75.2
157	Gd	2.59	6.84	5.84	5.39	5.22	7.17	6.09	1.75	28.7	135
163	Dy	2.22	4.06	3.57	3.22	2.91	4.99	3.75	1.62	43.3	69.0
166	Er	1.18	3.03	2.27	3.06	2.08	2.37	2.56	0.912	35.6	117
172	Yb	1.13	3.17	2.69	3.94	3.03	4.84	3.54	1.73	48.8	212
175	Lu	0.168	0.797	0.751	0.575	0.706	1.03	0.773	0.335	43.4	359

Table A1.19 Analysis of STH-80G and NIST 610 as unknown and standard respectively at 10 µm spot size. Elemental concentrations in ppm except CaO and TiO_2 in wt%.

		ref values STH-G	KSTHG1	KSTHG2	KSTHG3	KSTHG4	KSTHG5	Mean	2 SD	% 2 SD	% difference
24	Mg	11879	12574	12676	12625	12578	12761	12643	155	1.23	6.43
25	Mg	11879	11082	11187	11393	11026	11481	11234	393	3.50	-5.43
43	CaO	5.280	5.28	5.28	5.28	5.28	5.28	5.28			
88	Sr	482	480	496	487	490	476	486	15.6	3.21	0.773
137	Ba	298	297	304	305	326	300	306	22.6	7.37	2.74
139	La	12.000	11.0	12.8	12.1	11.4	12.0	11.9	1.36	11.4	-1.20
140	Ce	26.100	26.7	24.8	27.1	24.9	25.9	25.9	1.99	7.70	-0.847
141	Pr	3.200	2.70	3.19	3.01	3.11	3.20	3.04	0.414	13.6	-4.98
146	Nd	13.000	11.9	13.4	13.6	11.8	10.6	12.3	2.48	20.2	-5.51
147	Sm	2.780	2.47	2.28	2.56	2.98	2.25	2.51	0.590	23.5	-9.81
153	Eu	0.953	0.714	0.872	0.737	0.987	0.786	0.819	0.224	27.3	-14.0
157	Gd	2.590	1.93	2.43	2.64	2.89	2.01	2.38	0.817	34.3	-8.16
163	Dy	2.220	1.96	1.87	1.83	2.23	1.92	1.96	0.313	15.9	-11.6
166	Er	1.180	1.34	0.865	1.33	1.02	1.22	1.16	0.415	35.9	-2.12
172	Yb	1.130	1.38	1.08	1.06	0.93	1.49	1.19	0.467	39.3	5.04
175	Lu	0.168	0.233	0.175	0.228	0.184	0.204	0.205	0.0517	25.2	21.9

Table A1.20. Analysis of STH-80G and NIST 610 as unknown and standard respectively at 20 μm spot size. Elemental concentrations in ppm except CaO and TiO_2 in wt%.

A1.4.6 References

Baker, J.A., Allan, A.S.R., Alloway, B.V., Carter, L., Stevens, M., Wilson, C.J.N., and Wysoczanski, R.J., 2008. Tephra geochemical studies in NZ – New opportunities and pitfalls. Geological Society of New Zealand, New Zealand Geophysical Society, New Zealand Geochemical and Mineralogical Society Joint Annual Conference, Geosciences 2008. Wellington New Zealand, 23rd-26th November 2008.

Bence, A.E., and Albee, A.L., 1968. Empirical correction factors for the electron microprobe analysis of silicates and oxides. Journal of Geology, 76: 382-403.

Brown, S.J.A., Wilson, C.J.N., Cole, J.W. and Wooden, J., 1998. The Whakamaru group ignimbrites, Taupo Volcanic Zone, New Zealand: evidence for reverse tapping of a zoned silicic magmatic system. Journal of Volcanology and Geothermal Research, 84(1-2): 1-37.

Devine, J.D., Gardner, J.E., Brack, H.P., Layne, G.D., and Rutherford, M.J., 1995. Comparison of microanalytical methods fro estimating H_2O contents of silicic volcanic glasses. American Mineralogist, 80:319-328.

Dixon, J.E., Stolper, E.M., and Delaney, J.R., 1988. Infrared spectroscopic measurements of CO_2 and H_2O in Juan de Fuca ridge basaltic glasses. Earth and Planetary Science Letters, 90: 87-104.

Durrant, S.F., 1999. Laser ablation inductively coupled plasma mass spectrometry: achievements, problems, prospects. Journal of Analytical Atomic Spectrometry, 14: 1385-1403.

Fine, G.J., and Stolper, E.M., 1985. The speciation of carbon dioxide in sodium aluminosilicate glasses. Contributions to Mineralogy and Petrology, 91: 105-121.

Günther, D., and Hattendorf, B., 2005. Solid sample analysis using laser ablation inductively coupled plasma mass spectrometry. Trends in Analytical Chemistry, 24: 255-265.

Hauri, E., Wang, J., Dixon, J.E., King, P.L., Mandeville, C., and Newman, S., 2002. SIMS analysis of volatiles in silicate glasses 1. Calibration, matrix effects and comparisons with FTIR. Chemical Geology, 183: 99-114.

Hildreth, W., 1981. Gradients in silicic magma chambers: implications for lithospheric magmatism. Journal of Geophysical Research, 86: 10153-10192.

Heinrich, C.A., Pettke, T., Halter, W.E., Aigner-Torres, M., Audétat, Günther, D., Hattendorf, B., Bleiner, D., Guillong, M., and Horn, I., 2003. Quantitative multi-element analysis of minerals, fluids and melt inclusions by laser-ablation inductively-coupled plasma mass-spectrometry. Geochimica et Cosmochimica Acta, 67: 3473-3496.

Horn, I. and Günther, D., 2003. The influence of ablation carrier gasses Ar, He and Ne on the particle size distribution and transport efficiencies of laser ablation-induced aerosols: implications for LA-ICP-MS. Applied Surface Science, 207(1-4): 144-157.

Ihinger, P.D., Hervig, R.L. and McMillan, P.F., 1994. Analytical methods for volatiles in glasses. In: M.R. Carroll and J.R. Holloway (Editors), Volatiles in magmas. Mineralogical Society of America, Washington, pp. 517.

Ihinger, P.D., Zhang, Y. and Stolper, E.M., 1999. The speciation of dissolved water in rhyolitic melt. Geochimica et Cosmochimica Acta, 63(21): 3567-3578.

Jackson, S.E., Longerich, H.P., Dunning, G.R., and Fryer, B.J., 1992. The application of laser-ablation microprobe-inductively coupled plasma-mass spectrometry (LAM-ICP-MS) to in situ trace-element determinations in minerals. Canadian Mineralogist, 30: 1049-1064.

Jochum, K. P., Stoll, B., Herwig, K., Willbold, M., Hofmann, A.W., Amini, M., Aarburg, S., Abouchami, W., Hellebrand, E., Mocek, B., Raczek, I., Stracke, A., Alard, O., Bouman, C., Becker, S., Dücking, M., Brätz, H., Klemd, R., de Bruin, D., Canil, D., Cornell, D., de Hoog, C-J., Dalpé, C., Danyushevsky, L., Eisenhauer, A., Gao, Y., Snow, J.E., Groschopf, N., Günther, D., Latkoczy, C., Guillong, M., Hauri, E.H., Höfer, H.E., Lahaye, Y., Horz, K., Jacob, D.E., Kasemann, S.A., Kent, A.J.R., Ludwig, T., Zack, T., Mason, P.R.D., Meixner, A., Rosner, M., Misawa, K., Nash, B.P., Pfänder, J., Premo, W.R., Sun, W.D., Tiepolo, M., Vannucci, R., Vennemann, T., Wayne, D., and Woodhead, J., 2006. MPI-DING reference glasses for in situ microanalysis: new reference values for element concentrations and isotope ratios. Geochemistry, Geophysics, Geosystems 7: Q02008, doi:10.1029/2005GC001060.

Kent, A.J.R. and Ungerer, C.A., 2005. Production of barium and light rare earth element oxides during LA-ICP-MS microanalysis. Journal of Analytical Atomic Spectrometry, 20: 1256-1262.

Košler, J. and Sylvester, P.J., 2003. Present Trends and the Future of Zircon in Geochronology: Laser Ablation ICPMS. Reviews in Mineralogy and Geochemistry, 53(1): 243-275.

Longerich, H.P., Günther, D., and Jackson, S.E., (1996). Laser ablation inductively coupled plasma mass spectrometric transient signal data acquisition and analyte concentration calculation. Journal of Analytical Atomic Spectrometry, 11: 899-904.

Luhr, J., 2001. Glass inclusions and melt volatile contents at Parícutin Volcano, Mexico. Contributions to Mineralogy and Petrology, 142(3): 261-283.

Lui, Y., Zhang, Y., and Behrens, H., 2005. Solubility of H_2O in rhyolitic melts at low pressures and a new empirical model for mixed H_2O-CO_2 solubility in rhyolitic melts. Journal of Volcanology and Geothermal Research, 143: 219-235.

Mason, P., 2001. Expanding the capabilities of laser-ablation ICP-MS with collision and reaction cells. In: Sylvester, P., (Editor), Laser-ablation ICPMS in the Earth Sciences: Principles and applications. Mineralogical Association of Canada, 29: 63-81.

Newman, S., Stolper, E.M. and Epstein, S., 1986. Measurement of water in rhyolitic glasses: calibration of an infrared spectroscopic technique. American Mineralogist, 71: 1527-1541.

Nichols, A.R.L., and Wysoczanski, R.J., 2007. Using micro-FTIR spectroscopy to measure volatile contents in small and unexposed inclusions hosted in olivine crystals. Chemical Geology, 242: 371-384.

Outridge, P.M., Doherty, W., and Gregoire, D.C., 1997. Ablative and transport fractionation of trace elements during laser sampling of glass and copper. Spectrochimica Acta, 52B: 2093-2101.

Smith, B.C., 1996. Fundamentals of Fourier Transform Infrared Spectrometry. CRC Press, Boca Raton, 224pp.

Sylvester, P., (editor), 2001. LA-ICPMS in the Earth Sciences: Principles and applications. Short Course Series 29. Mineralogy Association of Canada.

Turekian, K.K., and Holland, H.D (editors), 2003. Treatise on Geochemistry. Elsevier.

Wright, I.C. and Gamble, J.A., 1999. Southern Kermadec submarine caldera arc volcanoes (SW Pacific): caldera formation by effusive and pyroclastic eruption. Marine Geology, 161: 207-227.

Wysoczanski, R. and Tani, K., 2006. Spectroscopic FTIR imaging of water species in silicic volcanic glasses and melt inclusions: An example from the Izu-Bonin arc. Journal of Volcanology and Geothermal Research, 156(3-4): 302-314.

Zhang, Y., Belcher, R., Ihinger, P.D., Wang, L., Xu, Z., and Newman, S., 1997. New calibration of infrared measurement of dissolved water in rhyolitic glasses. Geochimica et Cosmochimica Acta, 61(15): 3089-3100.

GeoRem - http://georem.mpch-mainz.gwdg.de

NIST – www.nist.gov

Appendix 2

Diffusion

Diffusion is the relative movement of atoms or molecules that leads to the homogenisation of chemical constituents of a substance in response to chemical or temperature gradients (Brady, 1995; McDougall and Harrison, 1999; Glicksman, 2000; Watson and Baxter, 2007 and references therein). Diffusion occurs on the micro- to macroscopic scale affecting many different processes (Chakraborty, 2008). Diffusion processes of interest here are those that can be used to extract timescales of magmatic processes from chemically zoned crystals in igneous rocks.

A2.1 Diffusion in minerals

Minerals structures are composed of a fixed regular frameworks of atoms and ions that oscillate (ca. 10^{12} times a second) about a fixed position (Putnis, 1992; Watson and Baxter, 2007). Above temperatures of absolute zero, minerals possess point defects and atoms have the potential to obtain sufficient energy to jump and relocate a short distance away (Putnis, 1992; McDougall and Harrison, 1999; Watson and Baxter, 2007). The presence of point defects in the crystal lattice is important as it provides a potential conduit for atoms to diffuse through (Putnis, 1992). The movement of atoms through a crystal can occur by one of several mechanisms (Figure A2.1): (1) vacancy migration, whereby atoms jump into vacant sites in the crystal lattice; (2) interstitial migration, where atoms are sufficiently small and are able to jump and occupy interstitial sites; and (3) exchange of atoms (Putnis, 1992; Giletti and Shanahan, 1997; McDougall and

Harrison, 1999; Glicksman, 2000; Watson and Baxter, 2007 and references therein).

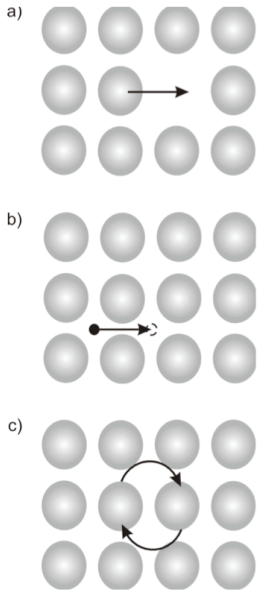

Figure A2.1. Diffusion mechanisms of atoms in solids; (a) vacancy mechanism; (b) interstitial mechanism; (c) exchange of atoms. Adapted from McDougall and Harrison (1999) and Watson and Baxter (2007).

In each instance an energy barrier (activation energy) of the migrating atom must be overcome in order for the atom to migrate (Gill, 1992; Putnis, 1992). Hence, the mechanism by which trace elements diffuse in crystals is dependent on the size and charge of the atom(s) involved and the properties of the host crystal lattice, which differs from mineral to mineral and element to element. For example in plagioclase, Sr, K and Rb diffuse through vacancies, Li by an interstitial mechanism and Na and Ca through a combination of vacancy and interstitial mechanisms (Giletti and Casserly, 1994; Giletti and Shanahan, 1997; Watson and Baxter, 2007). Both Na and Ca have the potential to jump into unoccupied interstitial sites, which creates a vacancy permitting for the subsequent diffusion of other elements through the vacancies (Giletti and

Casserly, 1994). However, Ca atoms require a greater amount of energy to instigate the jump into interstitial sites than Na atoms. Consequently, the diffusion of elements by the vacancy mechanism is slower in anorthite than in albite (Giletti and Casserly, 1994; Giletti and Shanahan, 1997).

A2.2 Fick's Laws

The mathematical relationships that describe molecular diffusion in a heterogeneous medium were formalised by Adolf Fick in 1855 who adapted Fourier's Law of Heat Conduction (Brady, 1995; McDougall and Harrision, 1999; Glicksman, 2000; Watson and Baxter, 2007 and references therein). The resulting laws are known as Fick's first and second laws. Fick's first law (Equation A2.1) describes the steady-state diffusion of a species, *i*, in one dimension assuming the concentration gradient in all other directions is zero;

$$J_i = -D_i \frac{\partial C_i}{\partial x} \qquad \text{(A2.1)}$$

where J_i is the flux of a species, *i*, through the medium of interest (in atoms per unit time, passing through unit volume), D_i is the diffusivity or diffusion coefficient (m^2s^{-1}), C_i is the concentration gradient of *i* in the *x* direction.

As timescales of diffusional processes are of relevance to this study, Fick's second law is of greater use as it describes the changing concentration of *i* with time, *t* (Equation A2.2);

$$\frac{\partial C_i}{\partial t} = D_i \frac{\partial^2 C_i}{\partial x} \qquad \text{(A2.2)}$$

Analytical solutions for Fick's laws for numerous geometries and boundary conditions have been obtained and can be found in works such as Carslaw and

Jaeger (1947) and Crank (1976). The appropriate solution to use in each instance depends on the system being modelled and the amount of diffusion that has occurred (D. Morgan, pers. comm.). For example, modelling of cathodoluminescence (CL) intensity as a proxy for Ti concentrations in quartz crystals (Chapter 3) uses a simple one dimensional diffusion model, as the extent of diffusion on either side of the modelled interface is small in comparison to the thickness of the regions (Doremus, 2002). In contrast, diffusion of Sr in plagioclase crystals affects a larger extent of the regions bordering the modelled interface (Chapter 4) and therefore a spherical model is more appropriate (see discussion below).

A2.3 Diffusivity of elements

Diffusion is a thermally activated process (e.g. Brady, 1995) and thus kinetic energy increases with temperature. Accordingly, the probability of an atom to obtain sufficient energy to overcome the energy barrier (activation energy of diffusion, Q) required for the atom to move from one site to another in the crystal lattice increases exponentially with temperature (Putnis, 1992; McDougall and Harrison, 1999; Watson and Baxter, 2007). This energy is provided from the thermal motion of atoms and the probability (p) of an atom in attaining sufficient energy to 'jump' can be expressed by the Boltzmann distribution expression;

$$p = e^{(-Q/kT)} \quad \text{(A2.3)}$$

where k is the Boltzmann's constant and T is the mean thermal energy (temperature) of the system (Putnis, 1992). When considering the mass transport of atoms this expression becomes;

$$p = e^{(-Q/RT)} \quad \text{(A2.4)}$$

where R is the gas constant (8.13451 J $mol^{-1}K^{-1}$) (Putnis, 1992). The diffusivity (D) of an element is proportional to the probability of an atom obtaining sufficient energy to 'jump', and the temperature (T in Kelvin) (Equation A2.4). Thus the above expression can be rewritten as the familiar Arrhenius equation (Equation A2.5);

$$D = D_0 e^{(-Q/RT)} \qquad \text{(A2.5)}$$

with the introduction of a rate constant, in this case the pre-exponential factor (D_0) (Putnis, 1992; McDougall and Harrison, 1999; Watson and Baxter, 2007). This pre-exponential factor (D_0) contains information about the specific medium such as the atomic vibrational frequency, the inter-atomic distance between atomic sites and the fraction of vacancies within the crystal lattice (Putnis, 1992; McDougall and Harrison, 1999; Watson and Baxter, 2007). The pre-exponential factor and activation energy must be determined for each medium and each element of interest before any diffusion modelling can be conducted. Numerous experiments have been conducted to determine the pre-exponential and activation energies of trace elements in plagioclase and those of interest to this study are shown in Table A2.1.

In addition, the diffusivity of trace elements in anisotropic crystals can vary with crystal orientation. Sr diffusion in plagioclase is slightly anisotropic with diffusion normal to the (001) cleavage plane faster than diffusion normal to the (010) cleavage plane by 0.7-1 log units (ca. factor of five to 10 faster) (Cherniak and Watson, 1994). This is close to the uncertainties on these measurements and therefore, Sr diffusion is assumed to be isotropic during diffusion modelling

(Giletti and Casserly, 1994; LaTourette and Wasserburg, 1998; Zellmer et al., 1999).

Element	X An	D_0 (m^2s^{-1})	Q ($kJmol^{-1}$)	Source
Sr	0-1	$Log_{10}D_0 = -4.08 – 4.1$ XAn	276	1
Ba	0.67	1.1×10^{-6}	341	2
Li	0-1	1.58×10^{-4}	146	3
K	0.23-0.67	4.46×10^{-6}	271	3
Pb	0.43-0.67	Log D = -6.94 – (266.5/2.303 RT)		4
Mg	0-1	$D = [2.92 \times 10^{(-4.1 \times XAn - 3.1)} \exp(-266000/RT)]$		5
OH	0-1	$5.7 \pm 2.5 \times 10^{-4}$ (for 800°C)	224	6

Table A2.1. Pre-exponential and activation energies for selected trace elements in plagioclase. Abbreviations: X An = plagioclase anorthite composition calculated on a mole fraction basis over which the D_0 and Q are applicable; D_0 = pre-exponential factor; Q = activation energy; D = diffusivity; R = gas constant; T = temperature. Sources: (1) Giletti and Casserly (1994); (2) Cherniak (2002); (3) Giletti and Shanahan (1997); (4) Cherniak (1995); (5) Costa et al. (2003); (6) Johnson (2003).

A2.4. Activity

Diffusion modelling across phase boundaries of a crystal, for example, between discrete zones of a crystal or the crystal and the external melt, requires consideration of the chemical thermodynamics of the system and the influence of other chemical components on the diffusion of the species of interest (Alberède, 1996; Costa et al., 2003; Zellmer et al., 2003; Watson and Baxter, 2007). Thus, perhaps counter-intuitively, it is not the concentration of the species of interest that diffuses but the species' activity (chemical potential) and this may result in 'uphill' diffusion (Alberède, 1996; Costa et al., 2003; Zellmer et al., 2003; Watson and Baxter, 2007). Activity of a species is the 'effective' concentration and is the energy gradient that drives the atoms in one direction or another during diffusion (Alberède, 1996; Housecroft and Constable, 1997).

Equilibrium is obtained when the chemical potential of the element of interest across the modelled interface is equal (Fletcher, 1993). This occurs when the thermodynamic quantity of Gibbs free energy (G) of the system is equal to zero (e.g. Gill, 1992; Putnis, 1992; Fletcher, 1993; Brady, 1995) and can be illustrated by considering two adjacent zones of a plagioclase crystal *A,* and *B,* that possess Sr concentrations of Sr_A and Sr_B respectively. If a small quantity of Sr in zone *A* (δSr_A) is transferred to zone *B* the change in Gibbs free can be written as;

$$dG = dG^A + dG^B = \delta Sr_A(\mu_{Sr}^B - \mu_{Sr}^A) \quad \text{(A2.6)}$$

where *dG* is the change of Gibbs free energy of the system, dG^A and dG^B are the change in Gibbs free energy in zones *A* and *B* respectively and μ_{Sr}^A and μ_{Sr}^B are the chemical potential of Sr in zones *A* and *B* respectively (Fletcher, 1993). If *d*G = 0 (i.e. at equilibrium) the Sr concentration between the two zones will not change as $\mu_{Sr}^A = \mu_{Sr}^B$ (Fletcher, 1993). However, if *dG* is less than zero a spontaneous reaction will occur between the two zones and Sr will be free to diffuse from zone *A* to zone *B* as $\mu_{Sr}^A > \mu_{Sr}^B$ (Fletcher, 1993). Therefore, it is the chemical potential of the substance of interest that governs the position of equilibrium of the system at a constant temperature and pressure and not the concentration (Fletcher, 1993).

Activity or a calculated fictional melt composition can be approximated if a standard state for the element of interest can be constrained (Fletcher, 1993). For modelling of elements in crystals this can be taken as the equilibration concentration (see section A2.5). The simplest method for approximating the calculated fictional melt composition of an element is to divide the measured concentration by the equilibrium concentration (Zellmer et al., 2003). This

allows identification of regions of a crystal that are in local equilibrium (calculated fictional melt composition ~ 1) and those that are not and display gradients in the calculated fictional melt composition to be recognised. Regions of the crystal that possess time information can be identified by gradients in the calculated fictional melt composition (Figure A2.2) (Zellmer et al., 2003).

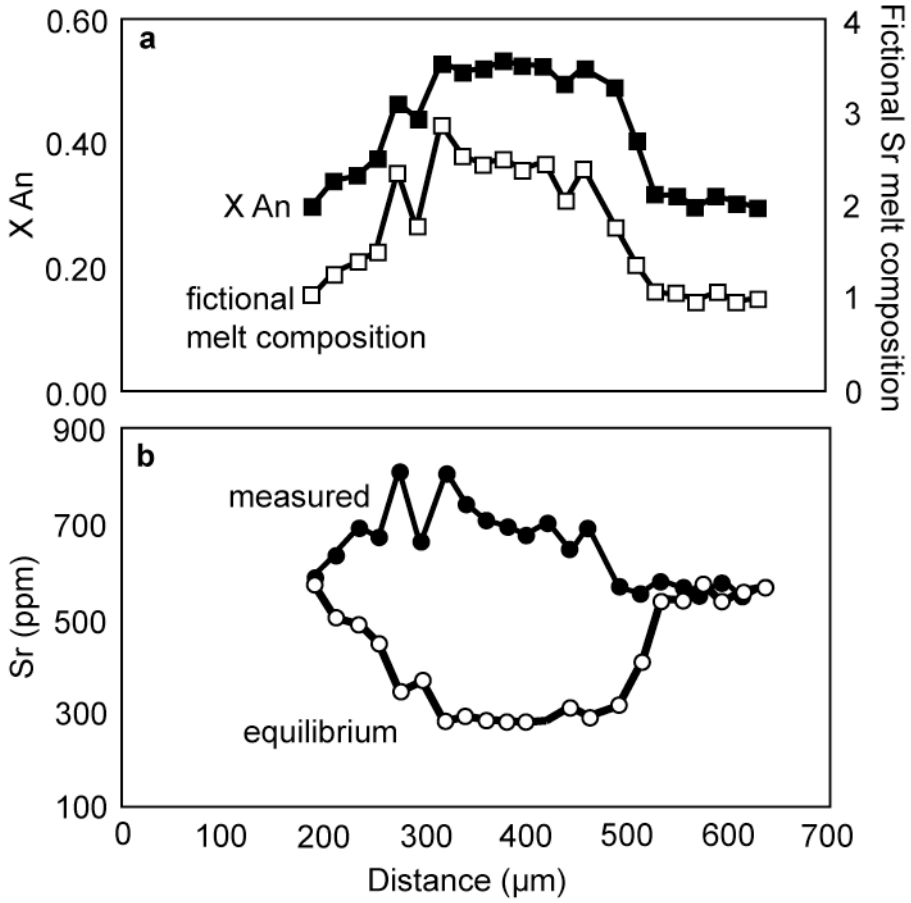

Figure A2.2. a) Measured *An* profile and fictional Sr melt composition of a plagioclase crystal from the Whakamaru ignimbrite (Chapter 4). Fictional Sr melt composition = measured Sr concentration/equilibrium concentration of Sr. The fictional melt compositon profile indicates the core (325-450 μm) and the rim (550-670 μm) of the crystal are in local equilibrium. The gradient in fictional melt composition (450-550 μm) indicates where time information is accessible in the profile; b) corresponding measured and equilibrium concentrations of Sr in the plagioclase crystal. Equilibrium concentrations of Sr are calculated from the partitioning relationship of Blundy and Wood (1991); $RTlnK_{Sr} = 26{,}800\text{-}26{,}700\ X_{An}$ and the calculated melt composition in equilibrium with the rim of the crystal (see section A2.5).

A2.5. Diffusion in plagioclase crystals

During crystallisation of plagioclase, the rim of the crystal is in local equilibrium with the surrounding melt and the plagioclase composition reflects that of the melt (Grove et al., 1984; Morse et al., 1984; Blundy and Shimizu, 1991). The original anorthite composition of the plagioclase is retained due to the very slow (ca. 10^{-28} m^2s^{-1} at 800°C) inter-diffusion of NaSi-CaAl (Grove et al., 1984; Morse et al., 1984; Blundy and Shimizu, 1991). However, partition coefficients govern the ease with which minor and trace elements are incorporated into plagioclase and these relationships are dominated by the anorthite composition (Blundy and Wood, 1991 and 1994; Bindeman et al., 1998). Conversely, the trace element concentrations of plagioclase crystals, although in equilibrium with the melt they crystallised from, may not be in equilibrium with the anorthite composition (e.g. Blundy and Wood, 1991). With time diffusion will serve to homogenise any compositional heterogeneities and only ceases on eruption when the compositional profile is 'frozen' into the crystal.

Three compositional profiles have been identified and defined in plagioclase crystals: (1) the initial concentration growth profile produced during the growth of the crystal; (2) the equilibrium profile that would result if the trace element concentrations were in equilibrium with the *An* content of the plagioclase crystal; and (3) the measured trace element concentration profile that is most likely intermediary between the initial and equilibrium profiles (Zellmer et al., 1999; Costa et al., 2003). The time that an interface within a crystal resided at magmatic temperature can be calculated from the time required for an element to

diffuse from the initial to the measured concentration profile (Zellmer et al., 1999).

The strong dependence of partition coefficients on the anorthite concentration of plagioclase crystals results in equilibrium profiles that are not flat but reflect the anorthite composition (Zellmer et al., 1999). Plagioclase crystals can be treated as either open or closed systems and this controls the calculated equilibrium concentrations (Zellmer et al., 1999; Costa et al., 2003). Equilibrium profiles in this study are calculated using the open system model of Costa et al. (2003).

Partition coefficients are determined by dividing the concentration of the element, *i*, in the mineral (C^{min}) by the concentration of the element in the liquid (C^{liq}) (Equation A2.7).

$$K_i = \frac{C^{\min}}{C^{liq}} \qquad \text{(A2.7)}$$

The difference in partition coefficients controls the equilibrium values of trace elements in each zone and with the external melt (Blundy and Wood, 1991; Zellmer et al., 1999). Thus by utilising the well-established trace element partitioning relationships on *An* content (Equation A2.8) and partition coefficient (Equation A2.7), the melt composition in equilibrium with the rim of the plagioclase crystal can be determined if the magmatic temperature (T in Kelvin) is known (Blundy and Wood, 1991; Bindeman et al., 1998).

$$\begin{aligned} RT\ln K_{Sr} &= 26{,}800 - 26{,}700X_{An} \\ RT\ln K_{Ba} &= 10{,}200 - 38{,}200X_{An} \\ RT\ln K_{Mg} &= -25{,}700 - 26{,}100X_{An} \end{aligned} \qquad \text{(A2.8a-c)}$$

This calculated melt composition can then be substituted as the melt composition into Equations A2.7 and A2.8 to determine the equilibrium concentration of the

element, *i*, throughout the crystal (Zellmer et al., 1999; Costa et al., 2003). This assumes the plagioclase crystal remained an open system post-crystallisation with the ability to exchange trace elements with the external melt (Costa et al., 2003). Thus, the entire crystal is attempting to achieve equilibrium with the final host melt (Costa et al., 2003), irrespective of the prior melt compositions in which the plagioclase resided in or crystallised from.

A2.6 Residence time of plagioclase crystals

The potential for plagioclase as an archive of magmatic processes has long been recognised and exploited. Residence times of plagioclase crystals have been documented from trace element diffusion employing both square wave (Zellmer et al., 1999; Costa et al., 2003) and spherical (Cherniak, 2002; Kent et al., 2007) solutions to Fick's second law. Here, both models are considered and the residence time of a Whakamaru plagioclase crystal is calculated and compared to establish the most applicable model for use in this study. The spatial resolution of analytical techniques restricts the size of plagioclase regions that are suitable for this type of modelling. Therefore, whilst timescales of magmatic events that result in large-scale chemical zonation of plagioclase crystals can be determined, the duration of processes responsible for the fine-scale oscillatory zonation of crystals cannot currently be resolved.

A2.6.1 Square-wave model

Zellmer et al. (1999) developed a one-dimensional diffusion model that simplifies the zonation of crystals, homogenising the elemental concentrations across each zone. The model considers the diffusional smoothing of Sr

concentrations between two adjacent zones *A* and *B* of equal widths (2*w*) with constant Sr diffusivity (D_{Sr}) and initial concentrations of $C^{A}_{Sr,0}$ and $C^{B}_{Sr,0}$ respectively (Zellmer et al., 1999) (Figure A2.3).

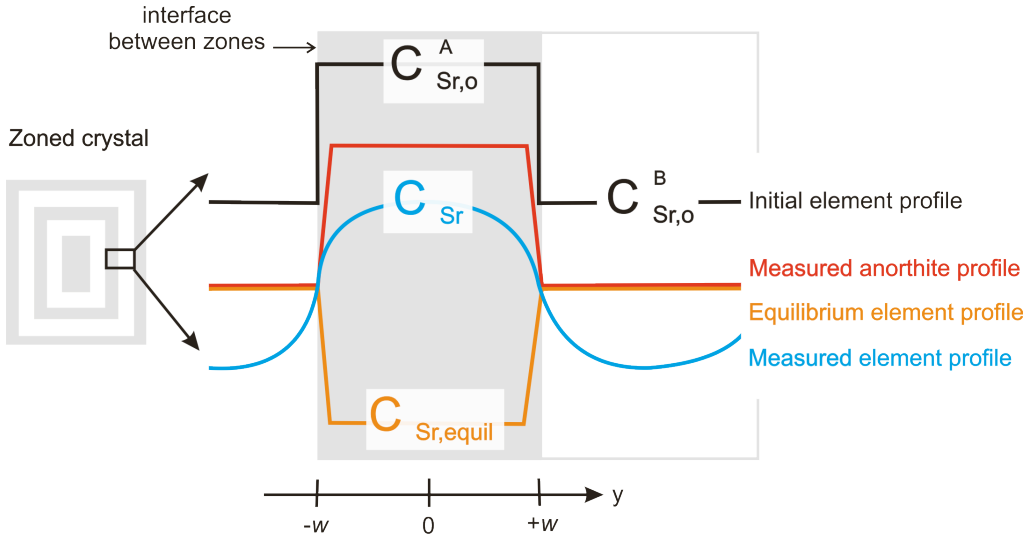

Figure A2.3. Square-wave diffusion model after Zellmer et al. (1999) with the three compositional zones highlighted. Two adjacent zones of equal width (2*w*) are modelled with different initial Sr concentrations. Abbreviations: $C^{A}_{Sr,0}$ and $C^{B}_{Sr,0}$ = initial Sr concentrations in zone *A* and *B* respectively; C_{Sr}= measured Sr concentration; $C_{Sr,\ equil}$ = equilibrium Sr concentration.

The estimation of the initial elemental concentrations is the largest source of error associated with this type of diffusion model. Zellmer et al. (1999) proposed that a petrological reasonable estimate of the initial maximum Sr concentrations could be calculated by a factor ~2.5 from the measured concentration of plagioclase crystals after examination of published Sr concentrations. The residence time (*t*) of crystals are calculated from Equation A2.9, the solution to Fick's second law in a layer of half width, *w,* where the edge of the model zone is equal to y = +*w* (Figure A2.3);

$$\frac{C_{Sr} - C_{Sr,equil}}{C_{Sr,0} - C_{Sr,equil}} = 2\sum_{n=0}^{\infty} \frac{(-n)^n}{\left(n+\frac{1}{2}\right)\pi} e^{-\left(n+\frac{1}{2}\right)^2 \pi^2 D_{Sr} t / w^2} \cos\left(\left(n+\frac{1}{2}\right)\frac{\pi y}{w}\right) \quad \text{(A2.9)}$$

where C_{Sr} is the measured Sr concentration, $C_{Sr,equil}$ is the equilibrium Sr concentration and $C_{Sr,0}$ is the initial Sr concentration (Zellmer et al., 1999). The left hand side of Equation A2.9 represents the percentage of the undiffused fraction of the initial concentration at the centre of the model zone and can be plotted against the right hand side of Equation A2.9 allowing the residence time of the crystal to be established (Figure A2.4) (Zellmer et al., 1999).

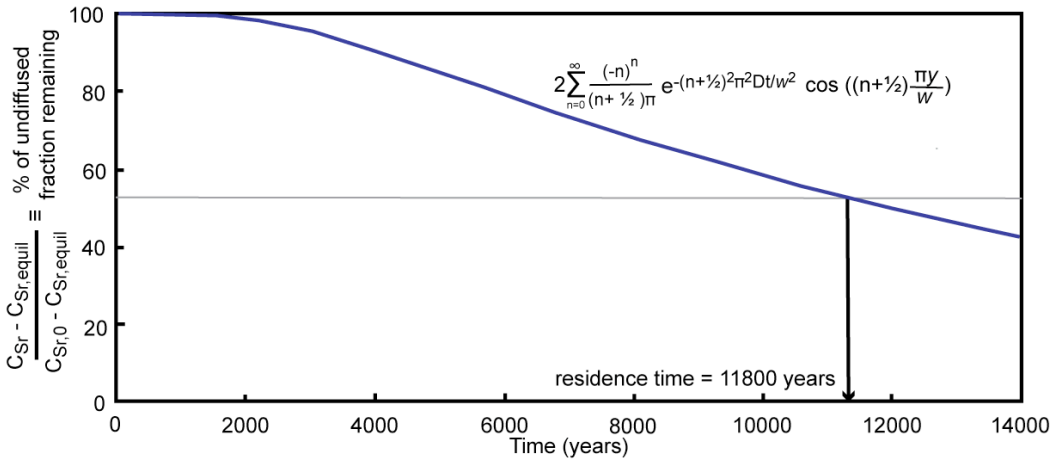

Figure A2.4 Calculation of the residence time of plagioclase crystals using the square-wave model as described by Zellmer et al. (1999). The model curve calculated form the right hand side of Equation A2.9 is shown in blue. A grey line denotes the percentage of the undiffused initial fraction remaining calculated from the measured (C_{Sr}), equilibrium ($C_{Sr,equil}$) and initial ($C_{Sr,0}$) concentrations of Sr (left hand side of Equation A2.9). The residence time is determined from the intersection of the blue and grey lines.

As discussed above, the diffusivity of elements that diffuse via a vacancy mechanism (e.g. Sr) is slowest at higher *An* compositions in plagioclase (Giletti and Casserly, 1994; Giletti and Shanahan, 1997; Zellmer et al., 1999; Watson and Baxter, 2007). Thus, the calculation of residence times at the highest

measured *An* content results in maximum estimates of timescales assisting in reducing the errors associated with this model (Zellmer et al., 1999).

A2.6.2. Spherical diffusion models

One of the simplest diffusion models are those constructed for spheres (Figure A2.5) with a radii of *a,* an initial trace element concentration of C_1, exposed to a medium with a constant surface concentration of C_0 (Crank, 1976; Lasaga, 1998; Cherniak, 2002).

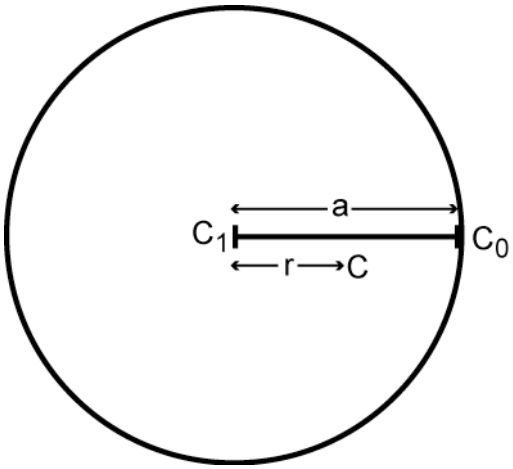

Figure A2.5. Spherical diffusion model. Sphere of radius, *a*, with an uniform initial species concentration of C_i, maintained in a magma of constant surface concentration C_0. A point a distance *r* from the centre of the circle has a species concentration of C at time *t*.

A point a distance *r* from the centre of the circle has a species concentration of C, at time *t* and can be modelled by the solution to Fick's second law shown in Equation A2.10.

$$\frac{C - C_1}{C_0 - C_1} = 1 + \frac{2a}{\pi r} \sum_{n=1}^{\infty} \frac{(-1)^n}{n} \sin \frac{n\pi r}{a} e^{-Dn^2 \pi^2 t / a^2} \qquad \text{(A2.10)}$$

The left hand side of the equation represents the percent of re-equilibration that has occurred and allows a graph similar to Figure A2.4 to be plotted and the residence time of crystals determined.

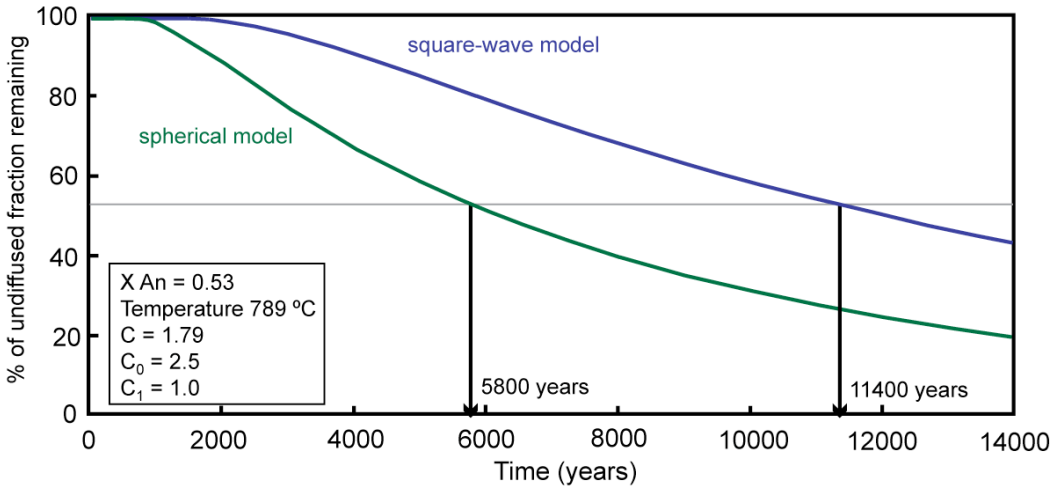

Figure A2.6. Diffusion curves for both the square-wave and spherical models and the residence times calculated from each model. Models assume a maximum *An* = 0.53 mol %, a diffusivity of 1.49 x10^{-20} m^2s^{-1}, an initial fictional Sr melt composition of 2.5, an equilibrium fictional melt composition of 1, a measured concentration of 1.79 and a radius of the sphere (r) or the diffusional half width (*w*) of 200 μm.

A2.6.3. Comparison of calculated residence times: square-wave versus spherical models

Both the square-wave model of Zellmer et al. (1999) and the spherical model have been used to calculate the residence time of a plagioclase crystal (WH1_h) from the Whakamaru ignimbrite (Chapter 4) (Figure A2.6). In both instances, the fictional Sr melt compositon has been substituted for concentration in Equations A2.9 and A2.10. It is clear that there is a discrepancy in residence times calculated from the two models (Figure A2.6), illustrating the importance of applying the most appropriate diffusion model for the problem. The rim-to-rim diffusion in a plane sheet overestimates the time required for diffusion to affect

the core of the region as the core of the plane sheet overestimates the volume of a crystal core. Crystal cores are volumetrically small in comparison to their surface area and, therefore, will reset significantly faster than the timescales estimated using a plane sheet model. In contrast, a spherical model possesses a large surface area and a volumetrically small core, which more adequately portrays a plagioclase crystal providing a more realistic timescale (D.Morgan, pers. comm.). A spherical model has been implemented to calculate residence times of plagioclase crystals from Sr diffusion from the Whakamaru Ignimbrite (Chapter 4).

A2.7 Source of errors

Several sources of error are associated with this type of model, but can be minimised with careful consideration. Errors can be introduced from: (1) the analytical errors of the chemical composition of plagioclase analysis; (2) the magmatic temperature and hence the diffusivity of elements (3) estimation of the initial elemental concentrations; (4) calculation of the equilibrium concentration; and (5) identification of the half width over which diffusion is modelled.

A2.7.1 Chemical composition of plagioclase

Errors for the composition of the major elements of plagioclase crystals are given in Chapter 4. CaO, Na_2O and K_2O have a two standard deviation (2σ) of 0.38, 0.19 and 0.07 wt% respectively, which results in negligible errors for the calculated *An* composition (± 0.008 mol %) of analyses. The variation in *An* concentration across a zone is not modelled, but is simplified to the highest measured *An* composition which will introduce additional uncertainties to the

calculated residence time (Zellmer et al., 1999). Errors for the trace element composition of plagioclase crystals are given in Chapter 4 and indicate Sr concentrations are precise to 3 % (2SD).

A2.7.2 Magmatic temperature and diffusivity

Magmatic temperatures for the Whakamaru ignimbrite are derived from Fe-Ti oxides and plagioclase-melt equilibria (Chapter 4). Errors on magmatic temperatures determined from Fe-Ti oxides are estimated ± 30 °C (Anderson et al., 1993) and from plagioclase-melt equilibria ± 23 °C (Putirka, 2005). This could potentially propagate into substantial errors for the calculated diffusivity. Therefore the diffusivity of a modelled element should always be quoted at the magmatic temperature it was derived from. Experimental data indicates an uncertainty of a factor of 2 may occur on the calculated diffusivity of Sr in plagioclase (Giletti and Casserly, 1994).

A2.7.3 Initial elemental concentrations

This is the largest source of error associated with these calculations (Zellmer et al., 1999). Zellmer et al. (1999) suggested a petrologically reasonable maximum estimate was a factor of 2.5 times the measured Sr concentration, whilst Costa et al. (2003) assumed the central proportions of large zones are unmodified by diffusion and represents a best estimate of the initial concentrations. The former method is likely to overestimate the original elemental concentrations miscalculating the residence times of crystal, with the latter method being more realistic and is the approach used in this study. Additionally, a step function is assumed, which may oversimplify the genuine initial concentrations and

overestimate the residence times of crystal by a maximum of 5-10 % (Zellmer et al., 1999).

A2.7.4 Equilibrium profiles

Equilibrium concentrations are calculated from Equations A2.7 and A2.8 and any error in the *An* concentration, magmatic temperature or constants will be propagated into the calculated equilibrium concentrations. As long as temperature estimates are known within ± 100 °C, Blundy and Wood (1991) estimated uncertainties of < 10% in RT ln K_i space. However, as the relative partition coefficients of adjacent zones of the crystal are of interest, it is likely that the errors on the calculated partition coefficients are minor (Zellmer et al., 1999).

Zellmer et al. (2003) derived equation A2.11 constraining the uncertainties on the calculated equilibrium concentrations where σC_{equil} is the error on the calculated equilibrium concentrations, w is a constant (w_{Sr} = -26 700 ± 1900 mol/J) and σAn is the error associated with the *An* concentration.

$$\sigma C_{equil} = C_{equil} \frac{w}{RT} \sigma An \quad \text{(A2.11)}$$

Assuming a magmatic temperature of 789 °C, an error of ± 0.008 on the *An* concentration and a calculated Sr equilibrium concentration of 600 ppm (Figure A2.2) this would equate to an σC_{equil} of < ± 15 ppm. Propagating these uncertainties through to the fictional Sr melt calculations indicates errors of ± 0.05, which yield negligible errors on the calculated timescales.

A2.7.5 Identification of diffusional half-width

Diffusion will homogenise smaller regions faster and therefore it is imperative to correctly identify the area over which diffusion is occurring. For example, increasing or decreasing the radius of the sphere used for modelling the residence time of WH1_h (section A2.6.3) by 10 μm results in ages of ± 1200 years.

A2.8. References

Albarède, F., 1996. Introduction to Geochemical Modeling. Cambridge University Press, 543 pp.

Anderson, D.J., Lindsley, D.H., and Davidson, P.M., 1993. QUILF: A pascal program to assess equilibria among Fe-Mg-Mn-Ti oxides, pyroxenes, olivine and quartz. Computers and Geoscience, 19: 1333-1350.

Bindeman, I.N., Davis, A.M. and Drake, M.J., 1998. Ion microprobe study of plagioclase-basalt partition experiments at natural concentration levels of trace elements. Geochimica et Cosmochimica Acta, 62(7): 1175-1193.

Blundy, J.D. and Shimizu, N., 1991. Trace-element evidence for plagioclase recycling in calc-alkaline magmas. Earth and Planetary Science Letters, 102(2): 178-197.

Blundy, J.D. and Wood, B.J., 1991. Crystal-chemical controls on the partitioning of Sr and Ba between plagioclase feldspar, silicate melts, and hydrothermal solutions. Geochimica et Cosmochimica Acta, 55(1): 193-209.

Blundy, J.D., and Wood, B.J., 1994. Prediction of crystal-melt partition coefficients from elastic moduli. Nature, 372: 452-454.

Brady, J.B., 1995. Diffusion data for silicate minerals, glasses and liquids., Mineral Physics and Crystallography, A Handbook of Physical Constants. AGU Reference Shelf 2, pp. 269-290.

Carslaw, H., S., and Jaeger, J., C., 1947. Conduction of heat in solids. Oxford, Clarendon Press, 515pp.

Chakraborty, S., 2008. Diffusion in Solid Silicates: A Toll to Track Timescales of Processes Comes of Age. Annual Reviews of Earth Science, 36: 153-190.

Cherniak, D.J., 1995. Diffusion of lead in plagioclase and K-feldspar: An investigation using Rutherford Backscattering and resonant nuclear reaction analysis. Contributions to Mineralogy and Petrology, 120: 358-371.

Cherniak, D.J., 2002. Ba diffusion in feldspar. Geochimica et Cosmochimica Acta, 66(9): 1641-1650.

Cherniak, D.J., and Watson, E.B., 1994. A study of strontium diffusion in plagioclase using Rutherford backscattering spectroscopy. Geochimica et Cosmochimica Acta, 58: 5179-5190.

Costa, F., Chakraborty, S. and Dohmen, R., 2003. Diffusion coupling between trace and major elements and a model for calculation of magma residence times using plagioclase. Geochimica et Cosmochimica Acta, 67(12): 2189-2200.

Crank, J., 1976. The mathematics of diffusion. Oxford University Press, 414pp.

Doremus, R.H., 2002. Diffusion of Reactive Molecules in Solids and Melts. A Wiley-Interscience Publication, New York, 293pp.

Fletcher, P., 1993. Chemical thermodynamics for earth scientists. Geochemistry series. Longman scientific and technical, London, 464 pp.

Giletti, B.J. and Casserly, J.E.D., 1994. Strontium diffusion kinetics in plagioclase feldspars. Geochimica et Cosmochimica Acta, 58(18): 3785-3793.

Giletti, B.J. and Shanahan, T.M., 1997. Alkali diffusion in plagioclase feldspar. Chemical Geology, 139(1-4): 3-20.

Gill, R., 1992. Chemical fundamentals of Geology. Unwin Hyman, London, 291pp.

Glicksmann, M.D., 2000. Diffusion in solids: Field theory, solid-state principles, and applications. A Wiley-Interscience Publication, 472 pp.

Grove, T.L., Baker, M.B. and Kinzler, R.J., 1984. Coupled CaAl-NaSi diffusion in plagioclase feldspar: Experiments and applications to cooling rate speedometry. Geochimica et Cosmochimica Acta, 48(10): 2113-2121.

Housecroft, C.E. and Constable, E.C., 1997. Chemistry: An integrated approach. Prentice Hall, 1032 pp.

Johnson, E.A., 2003. Hydrogen in nominally hydrous crustal minerals. PhD thesis, California Institute of Technology, Pasadena, California.

Kent, A.J.R., Blundy, J., Cashman, K.V., Cooper, K.M., Donnelly, C., Pallister, J.S., Reagan. M., Rowe, M.C., and Thornber, C.R.. 2007. Vapor transfer prior to the October 2004 eruption of Mount St. Helens, Washington. Geology, 35(3): 231-234.

Lasaga, A.C., 1998. Kinetic theory in Earth Sciences. Princeton Series in Geochemistry, Princeton University Press, pp.728

LaTourette, T., and Wasserburg, G.L., 1998. Mg diffusion in anorthite: implication for the formation of early solar system planetesimals. Earth and Planetary Science Letters, 158: 91-108.

McDougall, I. and Harrison, T.M., 1999. Geochronology and thermochronology by the $^{40}Ar/^{39}Ar$ method. Oxford University Press, New York.

Morse, S.A., 1984. Cation Diffusion in Plagioclase Feldspar. Science, 225(4661): 504-505.

Putnis, A., 1992. Introduction to Mineral Sciences. Cambridge University Press. 460 pp.

Putirka, K.D., 2005. Igneous thermometers and barometers based on plagioclase + liquid equilibria: Tests of some existing models and new calibrations. American Mineralogist, 90(2-3): 336-346.

Watson, E.B. and Baxter, E.F., 2007. Diffusion in solid-Earth systems. Earth and Planetary Science Letters, 253(3-4): 307-327.

Zellmer, G.F., Blake, S., Vance, D., Hawkesworth, C. and Turner, S., 1999. Plagioclase residence times at two island arc volcanoes (Kameni Islands, Santorini, and Soufriere, St. Vincent) determined by Sr diffusion systematics. Contributions to Mineralogy and Petrology, 136(4): 345-357.

Zellmer, G.F., Sparks, R.S.J., Hawkesworth, C.J. and Wiedenbeck, M., 2003. Magma emplacement and remobilization timescales beneath Montserrat: Insights from Sr and Ba zonation in plagioclase phenocrysts. Journal of Petrology, 44(8): 1413-1431.

Appendix 3

Table A3.1: Major and trace element compositions of melt inclusions

Major element concentrations are given in wt% and trace element concentrations are given in ppm.

Table A3.1

Sample	WH1_2	WH1_1	WH1_4	WH1_8	WH1_1	WH1_1	WH1_3	WH1_3
ID	6-1	-5	-1	-1	6-1	9-1	5-1	6-1
Host	opx	qtz	qtz	qtz	qtz	qtz	qtz	qtz
SiO_2	76.91	77.68	78.07	77.18	76.53	76.86	75.97	75.56
TiO_2	0.11	0.19	0.16	0.14	0.17	0.16	0.13	0.12
Al_2O_3	12.42	12.31	12.55	13.07	13.44	12.76	13.66	13.09
FeO	0.61	0.36	0.93	0.41	0.57	0.95	0.34	1.06
MnO	0.06	0.10	0.07	0.06	0.07	0.03	0.08	0.09
MgO	0.01	0.00	0.14	0.03	0.07	0.10	0.02	0.09
CaO	0.65	0.66	0.73	0.74	0.81	0.74	0.64	0.60
Na_2O	3.08	1.40	2.68	3.45	3.10	3.12	3.38	3.78
K_2O	3.52	7.17	4.49	4.75	5.07	4.96	5.46	5.25
Cl	2.62	0.11	0.19	0.17	0.17	0.24	0.12	0.20
SO_3	0.01	0.00	0.00	0.00	0.00	0.02	0.04	0.04
Total	100.00	100.00	100.00	100.00	100.00	100.00	100.00	100.00
Sc	7.96	7.58	18.0	9.60	11.63	10.56	8.27	8.77
V	1.67	1.60	9.91	4.25	2.00	3.33	1.94	2.10
Cr	7.99	3.35	16.0	57.0	5.64	8.48	16.1	32.6
Mn	186	323	744	584	452	402	127	1047
Co	0.206	0.843	2.73	1.23	1.38	0.621	1.78	3.25
Ni	1.27	1.86	4.54	14.0	2.00	1.38	3.64	5.31
Cu	b.d.	2.06	8.96	21.7	1.22	6.62	5.43	5.88
Zn	10.6	30.4	89.2	46.3	48.0	45.3	7.98	77.1
Ga	13.2	15.3	22.2	13.1	17.0	19.4	15.9	21.3
Rb	157	171	298	182	264	269	221	277
Sr	38.4	43.1	41.1	37.6	40.6	44.0	45.8	52.3
Y	13.0	13.4	30.7	15.8	21.6	15.9	17.4	25.8
Zr	80.7	102	71.5	63.4	119	80.8	99.0	124
Nb	8.93	6.61	18.9	9.35	8.67	12.1	9.90	12.7
Mo	1.06	0.769	5.39	11.29	1.38	1.80	3.79	4.54
Cs	8.21	8.66	12.3	5.1	11.5	11.9	11.7	13.2
Ba	686	605	756	1527	752	720	710	918
La	13.9	16.8	53.1	34.4	23.2	19.4	22.9	32.3
Ce	36.7	43.0	118	54.5	52.6	55.6	50.7	65.5
Pr	3.29	4.32	10.0	6.61	4.74	4.80	4.18	6.37
Nd	13.4	11.4	39.1	20.1	17.5	15.4	15.6	23.5
Sm	1.84	2.93	6.63	6.34	2.72	1.89	3.70	4.92
Eu	0.122	0.339	1.14	0.502	0.398	0.285	0.516	0.616
Gd	1.96	1.94	4.82	3.34	2.71	2.05	3.16	4.07
Tb							0.533	0.715
Dy	2.78	2.58	5.64	3.29	2.96	2.30	2.98	5.43
Ho							0.678	1.06
Er	1.63	1.64	3.46	1.83	2.36	1.35	2.08	2.94
Tm							0.373	0.588
Yb	2.14	1.60	2.78	1.46	1.79	1.53	3.59	4.16
Lu	0.218	0.378	0.502	0.293	0.368	0.236	0.539	0.695
Hf	3.29	3.13	3.08	2.47	3.87	2.15	3.90	4.98
Ta	0.679	0.762	1.23	0.929	1.04	0.864	1.35	1.58
W	1.97	2.14	4.51	7.05	1.81	2.67	3.40	4.27
Pb	5.13	16.3	50.5	20.0	25.4	21.2	9.76	34.1
Th	13.0	10.3	20.4	15.2	16.2	15.2	18.3	21.8
U	3.66	3.43	6.23	3.70	4.63	4.84	5.08	5.52

Table A3.1 continued

Sample	WH1_	WH1_	WH1_	WH1_	WH1_	OR1_	OR1_	OR1_	OR1_
ID	37-1	38-1	38-2	39-2	40-1	12-1.1	12-2.1	26-1	26-2
Host	qtz	qtz	qtz	qtz	qtz	opx	opx	opx	opx
SiO_2	75.75	76.48	75.46	75.96	76.20	78.62	79.02	78.74	78.10
TiO_2	0.21	0.20	0.24	0.10	0.16	0.21	0.21	0.13	0.17
Al_2O_3	13.02	13.06	13.68	13.46	12.88	12.25	12.18	11.97	12.57
FeO	0.99	0.19	0.25	0.26	0.25	1.67	1.62	1.64	1.60
MnO	0.13	0.16	0.07	0.15	0.02	0.07	0.03	0.09	0.09
MgO	0.13	0.01	0.00	0.06	0.04	0.17	0.10	0.10	0.11
CaO	0.71	0.67	0.75	0.60	0.68	0.86	0.85	0.88	1.16
Na_2O	3.78	3.49	3.87	3.77	1.86	2.50	2.40	2.88	3.07
K_2O	4.81	5.31	5.36	5.36	7.53	3.29	3.32	3.23	2.78
Cl	0.17	0.10	0.14	0.09	0.15	0.21	0.19	0.20	0.23
SO_3	0.03	0.20	0.04	0.04	0.07	0.05	0.08	0.12	0.12
Total	100.00	100.00	100.00	100.00	100.00	100.00	100.00	100.00	100.00
Sc	10.0	10.5	20.5	7.77	7.54	9.06	10.9	44.0	53.2
V	8.05	4.23	3.76	1.65	2.89	2.62	2.48	28.6	25.3
Cr	26.8	23.4	79.9	15.7	12.6	14.9	6.39	9.26	10.9
Mn	418	233	129	264	123	314	493	11854	15784
Co	3.42	2.09	4.33	1.59	1.46	0.572	1.87	51.6	58.3
Ni	4.61	7.46	19.7	3.02	2.55	b.d.	1.78	8.47	11.47
Cu	11.75	6.49	15.6	12.9	7.96	1.95	1.27	0.85	2.03
Zn	52.17	30.4	15.3	34.0	23.8	27.1	54.3	468	626
Ga	18.7	18.7	12.1	17.9	15.4	14.1	14.3	6.33	7.68
Rb	208	248	151	248	201	182	184	45.4	52.3
Sr	65.8	49.0	70.2	46.0	48.6	56.5	63.3	17.1	34.2
Y	27.8	20.4	18.0	19.8	22.0	17.8	18.2	12.2	16.2
Zr	190	116	119	96	119	90.7	101	32.1	50.4
Nb	10.7	10.5	10.7	10.0	9.58	8.13	8.51	1.92	2.91
Mo	4.71	3.17	4.08	2.52	3.02	2.06	1.54	0.973	1.37
Cs	10.1	11.8	5.4	11.9	10.0	8.97	10.5	2.26	2.57
Ba	493	874	894	653	899	766	874	225	288
La	30.2	25.5	25.2	24.1	27.3	26.1	25.1	6.82	8.89
Ce	65.4	60.8	53.4	53.4	55.7	48.3	52.2	14.8	20.0
Pr	6.39	5.41	5.48	4.95	5.24	4.36	4.75	1.36	2.00
Nd	24.7	19.2	19.0	16.8	19.5	17.7	17.2	5.41	7.06
Sm	5.60	4.24	4.51	3.03	3.77	3.88	2.74	1.09	1.71
Eu	0.982	0.741	0.766	0.524	0.469	0.440	0.358	0.201	0.220
Gd	4.69	4.32	3.36	2.99	3.24	2.81	2.86	1.18	1.74
Tb	0.822	0.513	0.501	0.450	0.516			0.206	0.280
Dy	4.96	3.92	3.43	3.45	3.72	3.07	2.59	1.65	2.41
Ho	1.18	0.821	0.686	0.667	0.728			0.453	0.608
Er	3.55	2.79	2.65	2.00	2.27	1.71	1.74	1.69	2.25
Tm	0.716	0.426	0.534	0.277	0.407			0.249	0.275
Yb	5.49	5.44	2.68	3.63	3.58	2.36	2.03	1.86	2.50
Lu	1.27	0.653	0.489	0.599	0.573	0.291	0.298	0.474	0.531
Hf	4.72	4.78	4.06	3.84	3.76	3.37	2.51	1.05	1.62
Ta	1.37	1.31	1.27	1.32	0.991	1.14	0.862	0.255	0.272
W	5.24	3.27	3.21	3.49	2.57	2.19	2.19	1.00	1.60
Pb	22.9	21.5	16.6	28.1	15.0	19.2	19.9	4.92	5.50
Th	17.3	18.5	14.6	18.3	17.7	18.9	19.4	4.13	4.46
U	5.15	5.22	4.62	5.40	4.33	4.54	4.75	1.05	1.14

Table A3.1 continued

Sample ID	OR1_ 14.1 plag	OR1_ 17-2 plag	OR1_ 16.2 qtz	OR1_ 16-3 qtz	OR2_ 24-1 opx	OR2_ 1-2.1 qtz	OR2_ 1-3.1 qtz	OR2_ 15-1 qtz	OR2_ 15-2 qtz
SiO_2	75.93	78.74	78.86	79.14	77.80	77.61	77.76	78.19	77.36
TiO_2	0.34	0.18	0.18	0.12	0.14	0.05	0.20	0.18	0.19
Al_2O_3	13.13	12.35	12.29	12.67	12.84	12.67	12.87	12.37	12.32
FeO	2.16	1.22	1.27	1.10	1.62	1.28	0.96	1.06	1.12
MnO	0.10	0.10	0.07	0.09	0.10	0.00	0.13	0.00	0.07
MgO	0.33	0.15	0.12	0.10	0.15	0.15	0.06	0.09	0.13
CaO	1.46	1.13	1.06	1.12	1.29	0.89	0.80	0.81	0.81
Na_2O	2.94	2.56	3.06	2.95	3.03	2.96	3.01	3.02	3.45
K_2O	2.76	2.62	2.72	2.53	2.74	3.78	3.69	3.83	3.75
Cl	0.31	0.26	0.21	0.19	0.24	0.34	0.23	0.29	0.36
SO_3	0.43	0.43	0.04	0.00	0.04	0.12	0.05	0.06	0.03
Total	100.00	100.00	100.00	100.00	100.00	100.00	100.00	100.00	100.00
Sc	17.0	9.1	10.1	10.3	8.92	27.5	7.59	9.69	10.1
V	7.57	3.49	1.14	1.23	1.91	7.04	1.87	3.06	3.32
Cr	6.68	8.26	4.23	6.94	5.37	51.6	12.8	10.0	9.26
Mn	606	387	354	385	407	401	338	292	280
Co	1.30	1.00	0.75	0.976	1.04	0.807	0.769	1.27	1.05
Ni	0.977	1.79	1.23	1.26	0.966	14.1	2.42	1.62	2.22
Cu	2.56	2.82	1.82	2.59	2.76	15.5	4.56	10.36	4.50
Zn	79.0	32.3	42.6	44.6	45.1	50.0	25.7	42.2	39.1
Ga	17.8	13.5	13.4	14.1	15.8	23.8	11.7	14.8	12.9
Rb	120	144	107	118	132	233	163	200	200
Sr	104	75.9	74.9	82.0	99.2	77.3	55.5	54.2	52.2
Y	26.1	21.8	19.7	23.3	21.0	22.8	15.0	21.5	19.9
Zr	245	134	107	122	157	127	85.5	127	120
Nb	10.3	7.30	7.03	7.55	7.85	12.4	7.16	10.3	9.78
Mo	1.65	1.44	1.07	1.23	1.45	8.05	1.87	2.01	2.13
Cs	5.90	7.80	5.46	6.15	6.45	8.14	7.59	9.37	8.81
Ba	598	960	619	656	761	1302	955	1023	971
La	21.4	27.9	19.9	22.6	22.6	22.0	24.0	25.8	25.2
Ce	52.8	58.7	43.8	47.5	50.3	73.1	46.9	58.1	53.2
Pr	5.15	5.17	4.24	4.84	5.13	7.37	4.26	4.80	5.00
Nd	20.8	18.3	16.9	17.8	19.9	19.6	14.2	19.4	17.4
Sm	4.57	3.27	3.32	3.63	4.03	3.57	2.44	3.54	3.96
Eu	0.641	0.443	0.642	0.616	0.667	0.643	0.343	0.408	0.380
Gd	4.46	3.20	3.33	3.86	3.48	4.41	2.23	3.74	3.06
Tb	0.684	0.512	0.503	0.573	0.559			0.533	0.534
Dy	4.80	3.61	3.38	4.34	3.78	3.45	2.39	3.53	3.23
Ho	0.993	0.715	0.718	0.843	0.763			0.804	0.613
Er	2.83	2.13	2.32	2.66	2.09	2.71	1.57	2.19	1.87
Tm	0.408	0.425	0.421	0.419	0.342			0.371	0.336
Yb	3.08	2.56	2.53	2.63	2.23	2.27	1.67	3.36	2.64
Lu	0.499	0.479	0.408	0.456	0.384	0.385	0.291	0.584	0.421
Hf	6.03	3.51	3.17	3.80	4.27	4.22	2.63	4.76	3.58
Ta	0.716	0.805	0.786	0.811	0.643	1.11	0.791	0.958	0.933
W	1.67	1.56	1.45	1.59	1.77	2.63	1.70	3.01	2.50
Pb	16.6	18.2	14.0	13.9	16.1	25.5	17.8	21.4	20.1
Th	10.4	16.2	11.8	12.6	11.5	19.2	14.2	17.4	18.2
U	3.16	3.68	2.73	2.63	2.87	5.37	3.51	4.95	4.75

Table A3.1 continued

Sample	RA1_	RA1_	RA1_	RA1_	RA2_	RA2_	RA2_	RA2_	RA3_
ID	5-1.1	5-3.1	7-1.1	7-2.1	4-1.1	7-1.1	11-2.1	13-3.1	8-1,1
Host	opx	opx	opx	opx	opx	opx	opx	plag	opx
SiO_2	77.24	78.62	78.67	78.16	78.17	77.06	77.91	77.41	77.30
TiO_2	0.29	0.44	0.27	0.28	0.24	0.13	0.46	0.19	0.30
Al_2O_3	13.91	12.97	13.20	13.25	12.25	13.19	12.36	13.51	13.12
FeO	1.89	1.60	1.54	1.69	2.19	1.99	1.85	1.39	2.31
MnO	0.13	0.07	0.11	0.06	0.00	0.44	0.50	0.12	0.08
MgO	0.25	0.21	0.24	0.24	0.30	0.29	0.18	0.24	0.17
CaO	1.38	1.25	1.02	1.38	1.35	1.31	1.43	1.33	1.60
Na_2O	2.51	1.84	2.22	2.01	2.80	2.83	2.69	2.81	2.46
K_2O	2.20	2.75	2.48	2.61	2.41	2.56	2.32	2.74	2.30
Cl	0.16	0.18	0.14	0.24	0.21	0.20	0.14	0.19	0.16
SO_3	0.04	0.07	0.12	0.07	0.07	b.d.	0.16	0.07	0.20
Total	100.00	100.00	100.00	100.00	100.00	100.00	100.00	100.00	100.00
Sc	11.2	17.2	7.5	11.5	7.56	13.2	4.85	9.50	4.40
V	3.94	7.69	4.84	4.82	4.48	2.55	6.87	4.55	3.82
Cr	11.4	57.7	7.9	18.5	21.8	12.3	10.0	7.54	0.0
Mn	475	472	423	469	333	486	657	443	418
Co	0.570	2.38	1.02	0.694	0.429	0.730	1.60	0.599	3.37
Ni	1.83	26.6	0.828	2.75	5.35	3.65	6.03	1.86	b.d.
Cu	2.04	8.34	2.06	3.58	3.71	b.d.	b.d.	2.21	b.d.
Zn	48.5	64.2	39.3	50.6	43.1	60.6	50.4	40.1	45.9
Ga	15.6	16.3	16.1	17.1	10.1	9.24	13.9	16.0	13.6
Rb	136	196	124	124	96.0	101	132	97	98.6
Sr	101	124	119	131	112	105	158	140	134
Y	22.2	27.8	18.2	20.1	20.2	23.9	23.9	19.9	23.1
Zr	130	246	205	172	211	179	251	153	209
Nb	5.39	13.0	9.10	7.58	6.89	11.14	10.2	7.84	10.2
Mo	1.24	3.89	0.912	1.38	1.52	1.34	2.69	1.59	0.00
Cs	5.12	6.73	5.18	4.91	3.50	3.81	4.63	4.47	3.17
Ba	1085	1145	856	894	717	843	896	802	783
La	23.6	27.3	18.9	19.5	18.4	25.8	23.0	19.2	17.6
Ce	47.3	61.9	44.4	44.3	44.3	51.9	53.1	44.4	44.4
Pr	4.53	6.27	4.20	4.47	4.78	4.96	4.72	4.36	4.88
Nd	18.3	20.6	18.9	17.8	18.6	18.9	22.3	15.3	24.0
Sm	3.94	6.26	3.22	3.35	3.36	3.47	3.92	2.74	1.91
Eu	0.908	1.02	0.556	0.873	0.879	0.641	0.972	0.770	1.18
Gd	2.54	5.43	2.40	3.27	4.60	3.55	4.98	2.68	2.89
Tb									
Dy	3.92	5.40	3.35	3.12	4.25	3.29	5.57	2.72	4.89
Ho									
Er	2.54	2.74	1.97	1.82	2.54	1.92	2.12	1.82	2.88
Tm									
Yb	2.88	3.51	1.98	2.21	2.34	1.78	2.33	2.05	2.29
Lu	0.372	0.683	0.233	0.422	0.118	0.285	0.414	0.429	0.367
Hf	4.07	6.95	4.78	4.48	5.44	3.70	4.69	4.17	3.69
Ta	0.521	0.985	0.613	0.901	0.485	0.492	0.765	0.394	0.272
W	1.66	2.01	1.13	1.31	2.12	1.77	1.67	1.07	1.13
Pb	18.0	16.2	16.3	17.6	11.4	14.5	12.8	14.5	13.5
Th	12.4	21.9	8.75	9.15	8.65	8.67	9.93	8.00	9.41
U	2.72	3.73	2.69	2.55	2.19	2.72	2.95	2.21	2.02

Table A3.1 continued

Sample	RA3_	TA1_3	TA1_3	TA1_3	TA1_3	TA1_3	TA1_3	TA1_3	TA1_4
ID	9-1.1	0-1.1	0-2	4-1	4-2	5-1	5-2	5-3	3-3.1
Host	opx	plag	plag	plag	plag	plag	plag	plag	plag
SiO_2	77.88	76.73	76.88	75.95	74.47	76.51	75.52	77.02	76.39
TiO_2	0.21	0.32	0.29	0.31	0.40	0.32	0.44	0.31	0.23
Al_2O_3	12.51	13.42	13.52	13.85	14.09	13.61	13.96	13.06	13.47
FeO	2.22	1.97	1.79	2.43	2.98	2.21	2.57	2.04	1.92
MnO	0.25	0.11	0.03	0.11	0.09	0.14	b.d.	0.14	0.08
MgO	0.16	0.30	0.24	0.37	0.53	0.33	0.40	0.27	0.22
CaO	1.47	1.68	1.55	1.77	1.88	1.62	1.89	1.42	1.53
Na_2O	2.62	2.94	2.89	3.08	3.23	3.20	3.23	3.34	3.20
K_2O	2.42	2.38	2.46	1.93	1.90	1.76	1.78	2.06	2.53
Cl	0.26	0.15	0.16	0.19	0.31	0.17	0.21	0.29	0.22
SO_3	b.d.	b.d.	0.19	b.d.	0.12	0.14	b.d.	0.05	0.20
Total	100.00	100.00	100.00	100.00	100.00	100.00	100.00	100.00	100.00
Sc	18.5	17.9	16.6	15.5	19.8	14.6	18.8	14.8	11.2
V	6.55	0.747	1.58	7.61	3.96	1.76	1.14	0.875	0.540
Cr	11.7	9.28	4.34	14.6	13.3	2.36	4.70	4.20	7.32
Mn	484	798	692						546
Co	1.85	0.541	0.578	1.06	0.691	0.420	0.744	0.457	0.466
Ni	5.69	1.94	1.74	2.48	5.32	0.365	1.30	0.57	1.01
Cu	0.00	3.61	1.87	6.65	3.29	1.89	3.53	2.13	2.51
Zn	48.1	119	93.3	89.4	98.9	66.0	102	72.3	49.0
Ga	14.2	20.2	16.7	17.1	17.1	15.4	23.7	16.8	11.2
Rb	97.1	119	114	80.7	125	96.6	144	104	82.2
Sr	121	140	127	172	182	168	183	131	105
Y	25.9	34.8	29.9	31.9	38.4	34.8	51.2	39.8	37.3
Zr	221	234	204	205	274	239	342	255	166
Nb	9.56	10.5	9.91	8.45	9.95	8.72	12.3	9.69	7.15
Mo	4.01	1.16	1.20						0.785
Cs	4.62	4.61	5.36	3.87	5.46	4.60	7.27	4.66	3.90
Ba	1023	659	610	461	563	540	821	608	466
La	23.0	22.7	23.7	21.5	24.0	23.3	35.5	27.2	24.7
Ce	50.0	53.5	51.3	49.0	59.8	51.1	75.2	56.2	65.6
Pr	5.13	5.93	5.94						7.96
Nd	22.3	25.9	22.6	22.4	24.4	23.9	34.3	27.2	32.7
Sm	3.37	5.36	4.97	5.43	5.71	4.74	7.76	5.95	8.89
Eu	1.22	1.17	1.31	0.829	1.32	0.904	1.56	1.26	1.26
Gd	2.53	4.71	5.44	4.88	4.78	5.53	8.23	6.36	7.60
Tb									
Dy	5.12	4.65	5.14	5.65	6.41	5.32	8.14	6.40	6.38
Ho									
Er	2.87	3.74	3.52	3.75	3.70	3.48	5.92	4.10	3.27
Tm									
Yb	2.29	3.29	3.17	2.52	4.21	3.51	5.34	3.81	3.76
Lu	0.647	0.519	0.574	0.519	0.563	0.569	0.939	0.659	0.467
Hf	5.21	5.46	5.56	5.47	8.56	5.45	9.38	6.91	5.39
Ta	0.881	0.88	0.740	0.585	0.632	0.645	0.809	0.667	0.462
W	1.50	2.00	1.74						0.87
Pb	14.9	21.6	22.0	18.0	19.2	17.4	28.3	22.2	12.4
Th	9.32	12.2	10.5	8.05	10.7	9.84	15.4	11.5	8.11
U	2.31	2.92	2.60	2.00	2.36	2.22	3.42	2.42	2.00

Table A3.1 continued

Sample	TA1_4	TA2_2	TA2_2	TA2_2	TA2_2	TA2_2	TA2_2	TA4_9	TA4_5
ID	4-2.1	0-1	0-2	2-1	7-1.2	7-2.2	7-3.1	-5.1	-7.1
Host	plag	plag	plag	plag	plag	plag	plag	opx	opx
SiO_2	75.81	75.67	73.62	76.14	76.27	76.72	76.36	75.53	76.77
TiO_2	0.26	0.30	0.35	0.26	0.31	0.31	0.24	0.17	0.16
Al_2O_3	13.75	13.80	13.51	13.48	12.90	12.79	13.27	13.38	13.02
FeO	1.96	2.05	1.76	2.06	2.05	2.02	1.99	2.57	2.50
MnO	0.12	0.06	0.05	0.12	0.03	0.08	0.09	0.99	0.39
MgO	0.22	0.32	0.24	0.23	0.23	0.30	0.25	0.33	0.34
CaO	1.61	1.45	1.48	1.45	1.59	1.51	1.29	1.49	1.39
Na_2O	3.38	3.58	3.23	3.29	3.76	3.44	3.59	2.98	2.88
K_2O	2.61	2.55	2.53	2.58	2.50	2.62	2.70	2.32	2.34
Cl	0.26	0.16	3.22	0.26	0.20	0.17	0.21	0.18	0.17
SO_3	0.01	0.06	0.01	0.13	0.16	0.05	b.d.	0.05	0.02
Total	100.00	100.00	100.00	100.00	100.00	100.00	100.00	100.00	100.00
Sc	8.6	13.9	4.55	15.0	15.3	15.5	15.0	25.9	16.8
V	0.917	0.812	0.239	1.29	0.908	1.04	0.673	1.75	0.650
Cr	7.95	4.65	0.535	8.24	5.33	7.50	6.49	7.67	6.42
Mn	449	770	254	741	743	659	728	2650	726
Co	0.165	0.323	0.100	0.738	0.469	0.470	0.575	2.44	0.511
Ni	1.01	1.32	0.632	1.75	0.572	1.43	0.676	1.53	1.35
Cu	2.04	3.08	1.14	1.47	1.69	2.75	2.18	1.56	1.80
Zn	53.2	81.8	25.3	111	68.9	80.6	112	202	67.7
Ga	11.4	14.1	3.9	17.2	15.3	15.9	18.4	15.9	13.4
Rb	70.4	105.0	32.2	143	98.3	115	135	104	92
Sr	144	120	42.7	126	136	125	119	126	114
Y	18.9	28.0	25.3	31.2	28.5	29.3	28.3	34.7	30.5
Zr	130	215	56.3	216	179	216	200	199	196
Nb	6.80	10.4	2.08	10.5	9.99	9.33	10.1	9.04	8.43
Mo	0.805	1.40	0.52	1.15	0.785	1.35	1.33	1.19	1.89
Cs	3.36	6.10	1.19	5.59	5.25	5.10	6.35	5.05	4.81
Ba	416	608	144	632	557	645	605	611	593
La	15.4	24.3	18.4	23.6	21.1	22.3	23.5	24.1	21.1
Ce	28.8	49.8	51.3	59.3	55.4	52.0	59.7	53.0	50.4
Pr	3.49	5.70	6.39	5.54	4.71	5.78	6.23	5.34	5.65
Nd	12.9	22.7	31.1	24.0	21.6	23.5	22.3	22.9	22.6
Sm	3.72	3.46	9.06	5.20	4.51	4.96	5.39	4.85	4.72
Eu	0.908	0.820	1.16	1.12	0.922	1.04	1.14	1.27	0.969
Gd	2.96	5.64	6.13	4.14	4.32	4.77	4.60	4.66	4.91
Tb									
Dy	2.43	5.35	4.60	5.14	5.12	5.17	5.49	5.90	5.88
Ho									
Er	1.68	2.99	2.48	2.97	2.93	3.00	2.91	3.98	3.24
Tm									
Yb	1.62	3.32	1.92	3.24	2.69	3.01	3.55	3.95	3.33
Lu	0.274	0.523	0.309	0.611	0.402	0.512	0.539	0.656	0.499
Hf	3.64	5.10	1.90	6.63	5.81	5.67	4.66	5.50	5.23
Ta	0.508	0.795	0.197	0.611	0.704	0.770	0.664	0.711	0.680
W	1.32	1.65	0.709	1.58	1.76	1.54	2.04	1.71	1.24
Pb	14.3	19.0	6.00	24.6	22.3	19.2	23.9	19.7	18.7
Th	7.28	10.0	3.16	11.4	9.22	9.68	10.07	9.55	9.17
U	1.90	2.41	0.81	2.93	2.33	2.27	2.68	2.49	2.36

Table A3.1 continued

Sample ID	X590/B_6-1.1	X590_2-1	X609_5-1.1	X609_8-1	X609_17-2.2	X609_17-3.1
Host	opx	opx	opx	opx	plag	plag
SiO_2	76.46	75.79	76.14	76.14	76.26	76.67
TiO_2	0.42	0.39	0.24	0.27	0.42	0.42
Al_2O_3	13.83	13.12	13.44	13.25	13.50	13.61
FeO	1.95	2.65	2.22	2.35	2.14	2.00
MnO	0.00	0.27	0.14	0.24	0.10	0.09
MgO	0.13	0.16	0.24	0.19	0.43	0.42
CaO	2.08	1.66	1.80	1.94	1.88	2.01
Na_2O	3.22	3.61	3.54	3.29	3.19	2.43
K_2O	1.35	1.89	1.78	1.85	1.57	1.75
Cl	0.50	0.37	0.47	0.47	0.49	0.45
SO_3	0.03	0.09	0.00	0.01	0.01	0.14
Total	100.00	100.00	100.00	100.00	100.00	100.00
Sc	27.5	19.4	11.9	9.93	12.0	16.7
V	19.5	9.88	9.75	4.11	14.0	9.51
Cr	36.7	2.92	4.85	26.3	4.23	5.59
Mn	5646	2434	832	583	857	970
Co	28.7	6.21	1.16	2.58	2.57	1.10
Ni	8.14	0.989	1.22	24.64	2.78	1.45
Cu	17.0	8.85	14.9	19.6	15.9	2.88
Zn	258	159	69.9	79.5	60.5	88.8
Ga	12.1	13.6	15.5	16.5	14.9	14.1
Rb	34.8	25.4	35.7	20.9	36.1	42.2
Sr	118	113	129	107	144	164
Y	38.7	37.5	38.3	41.1	46.2	66.1
Zr	121	142	209	156	222	339
Nb	3.85	3.24	4.29	4.95	4.10	6.12
Mo	4.70	2.13	2.45	2.00	1.99	3.05
Cs	1.18	0.77	1.02	0.732	0.895	1.21
Ba	677	811	976	777	1167	1255
La	11.4	11.3	13.9	9.53	16.0	18.3
Ce	40.4	31.0	33.2	25.6	37.9	43.7
Pr	4.22	3.89	4.26	2.31	4.77	6.10
Nd	18.4	16.4	18.6	22.3	23.2	29.8
Sm	5.35	4.42	4.30	6.85	6.46	6.30
Eu	1.43	1.06	0.945	1.34	1.23	2.04
Gd	6.28	4.86	5.13	5.43	6.56	8.91
Tb						
Dy	5.10	6.13	6.53	6.01	7.02	12.44
Ho						
Er	3.66	4.07	4.32	3.91	4.90	8.23
Tm						
Yb	4.39	4.39	4.05	6.21	5.38	8.21
Lu	0.848	0.739	0.759	0.572	0.912	1.33
Hf	3.03	3.24	5.20	3.55	5.66	9.98
Ta	0.300	0.258	0.246	0.316	0.289	0.373
W	0.896	0.287	0.459	0.798	0.395	0.462
Pb	3.22	4.45	5.40	3.80	5.04	6.07
Th	2.25	2.17	2.96	2.75	3.35	4.55
U	0.650	0.831	0.951	1.28	0.942	1.36

All sample data are recalculated on an anhydrous basis. Abbreviations: plag – plagioclase; opx – orthopyroxene; qtz – quartz; b.d. – below detection limits.

Appendix 3

Table A3.2: Major element compositions of melt inclusions where no trace element data is available. Major element concentrations are given in wt %.

Table A3.2

Sample ID	WH1_21-3	WH1_21-8.2	WH1_21-8.3	WH1_24-2	WH1_25-1	WH1_28-1	WH1_28_2.2	WH1_1-2	WH1_2-1	WH1_5-1	WH15_2-1	WH1_5-3	WH1_5-4
Host	opx	opx	opx	opx	opx	opx	opx	qtz	qtz	qtz	qtz	qtz	qtz
SiO_2	77.97	77.91	78.43	78.40	78.59	79.19	77.23	77.79	77.91	79.97	78.42	78.50	78.22
TiO_2	0.14	0.19	0.25	0.16	0.13	0.04	0.14	0.07	0.17	0.19	0.04	0.14	0.09
Al_2O_3	12.36	12.71	12.98	12.03	12.29	11.67	12.70	13.16	12.95	12.63	13.99	12.51	12.80
FeO	1.66	0.76	0.83	1.24	0.75	0.93	0.66	0.29	0.40	0.37	0.10	0.49	0.46
MnO	0.10	0.07	0.00	0.06	0.04	0.06	0.06	0.04	b.d.	0.02	0.02	0.05	0.06
MgO	0.63	0.10	0.05	0.37	0.07	0.25	0.01	0.03	0.01	0.05	0.01	0.07	b.d.
CaO	0.87	0.11	0.14	0.77	0.90	0.64	0.69	0.62	0.73	0.48	0.80	0.68	0.64
Na_2O	3.30	4.12	3.01	2.92	3.19	3.14	3.14	0.82	0.88	1.59	1.75	3.47	3.54
K_2O	2.80	3.79	3.79	3.52	3.39	3.24	3.76	6.87	6.85	4.56	4.73	3.77	3.90
Cl	0.18	0.24	0.49	0.45	0.60	0.85	1.59	0.15	0.10	0.11	0.14	0.23	0.19
SO_3	b.d.	b.d.	0.02	0.08	0.05	b.d.	0.01	0.16	b.d.	0.04	b.d.	0.09	0.10
Total	100.00	100.00	100.00	100.00	100.00	100.00	100.00	100.00	100.00	100.00	100.00	100.00	100.00

Table A3.2 continued

Sample ID	WH1_6-3.2	WH1_6-5.2	WH1_7-1	WH1_7-2.2	WH1_35-2	WH1_35_3	WH2_2-1.1	WH2_3-1.1	WH2_4-1.1	WH2_5-1.1	WH2_7-1.1	OR1_8-1.1	OR1_9-1.1	OR1_9-3.1
Host	qtz	qtz	qtz	qtz	qtz	qtz	qtz	qtz	qtz	qtz	qtz	opx	opx	opx
SiO_2	73.79	77.54	74.74	75.58	76.72	75.33	74.81	67.98	73.66	75.35	74.30	75.91	77.58	75.41
TiO_2	0.09	0.13	0.13	0.18	0.18	0.14	0.30	0.33	0.09	0.30	0.17	0.13	0.10	0.06
Al_2O_3	16.13	13.71	16.43	14.84	13.06	13.87	13.37	17.01	13.30	14.03	14.19	12.52	13.66	12.57
FeO	0.01	0.14	0.13	0.13	0.13	0.23	2.15	1.73	1.34	0.76	1.08	2.01	1.58	2.42
MnO	0.01	b.d.	0.03	0.03	0.05	b.d.	0.03	0.15	0.05	0.05	0.15	0.15	0.08	0.10
MgO	b.d.	0.11	b.d.	0.05	0.06	0.03	0.04	0.29	b.d.	b.d.	0.13	0.19	0.19	0.80
CaO	1.29	0.77	0.97	0.96	0.65	0.70	0.08	1.27	0.22	0.08	0.81	0.90	1.11	1.11
Na_2O	4.10	3.24	2.22	3.36	3.64	3.75	4.34	6.76	3.87	3.92	4.06	3.77	3.23	4.40
K_2O	4.32	4.25	5.05	4.55	5.11	5.40	4.44	4.32	4.56	5.00	4.68	3.65	2.24	2.18
Cl	0.20	0.09	0.15	0.22	0.12	0.11	0.30	0.14	2.66	0.31	0.29	0.61	0.17	0.74
SO_3	0.06	0.01	0.14	0.10	0.09	0.12	0.15	0.02	0.08	0.03	0.08	0.13	0.04	0.15
Total	100.00	100.00	100.00	100.00	100.00	100.00	100.00	100.00	100.00	100.00	100.00	100.00	100.00	100.00

Table A3.2 continued

Sample ID	OR1_11-1.1	OR1_11-2.1	OR1_11-3.1	OR1_12-3.1	OR1_13-1.1	OR1_30-1	OR1_30-2	OR1_30-3	OR1_2-1.1	OR1_2-2.1	OR1_2-3.1	OR1_2-4.1	OR1_2-5.1	OR1_5-1.1
Host	opx	opx	opx	opx	opx	opx	opx	opx	plag	plag	plag	plag	plag	plag
SiO_2	75.27	74.59	75.11	77.67	74.88	77.14	78.18	76.34	77.10	78.49	76.78	77.68	77.62	75.87
TiO_2	0.17	0.13	0.14	0.27	0.18	0.16	0.12	0.15	0.43	0.23	0.46	0.33	0.21	0.53
Al_2O_3	13.80	14.01	13.34	12.68	12.69	13.12	12.49	13.16	12.87	12.59	12.95	13.04	12.99	13.20
FeO	2.00	2.17	2.00	2.02	2.30	1.87	1.64	1.86	2.07	1.75	1.95	1.94	2.09	2.79
MnO	0.09	0.06	0.11	0.07	0.08	0.05	0.09	0.13	0.24	0.12	0.34	0.09	0.23	0.16
MgO	0.21	0.25	0.42	0.12	0.71	0.13	0.11	0.13	0.34	0.23	0.29	0.19	0.22	0.49
CaO	1.44	1.56	1.10	1.13	1.40	1.15	1.05	1.16	1.60	1.46	1.63	1.71	1.33	1.83
Na_2O	4.01	4.36	4.42	2.80	3.88	3.09	2.89	3.34	2.40	2.17	2.24	2.13	2.40	2.04
K_2O	2.58	2.56	2.83	2.92	2.70	2.88	3.22	3.42	2.34	2.23	2.71	2.53	2.33	2.52
Cl	0.30	b.d.	0.50	0.30	0.77	0.30	0.20	0.27	0.35	0.31	0.42	0.23	0.40	0.30
SO_3	0.02	0.09	0.02	0.01	b.d.	0.10	0.00	0.05	0.12	0.14	0.11	0.13	0.04	0.11
Total	100.00	100.00	100.00	100.00	100.00	100.00	100.00	100.00	100.00	100.00	100.00	100.00	100.00	100.00

Table A3.2

Sample ID	OR1_5-2.1	OR1_5-3.1	OR1_1-1.1	OR1_1-2.1	OR1_1-3.1	OR1_1-4.1	OR2_7-1.1	OR2_11-1.1	OR2_11-2.1	OR2_13-2.1	OR2_24-2	OR2_24-3	OR2_1-1.1	OR2_1-4.1
Host	plag	plag	qtz	qtz	qtz	qtz	opx	opx	opx	opx	opx	opx	qtz	qtz
SiO_2	73.85	76.45	79.95	79.46	79.25	79.31	76.43	76.20	76.68	78.05	78.06	76.60	78.63	78.26
TiO_2	0.37	0.34	0.17	0.11	0.12	0.17	0.20	0.26	0.25	0.31	0.15	0.12	0.10	0.14
Al_2O_3	15.15	13.24	12.61	12.69	12.67	12.90	13.34	13.75	13.30	12.27	12.27	13.20	12.28	12.82
FeO	2.19	2.64	0.93	0.92	1.10	0.89	1.82	2.30	1.92	1.89	1.80	2.02	1.00	0.73
MnO	0.09	0.15	0.15	0.29	0.04	0.11	0.11	0.30	0.37	0.05	0.06	0.11	0.35	0.10
MgO	0.39	0.39	0.11	0.11	0.16	0.11	0.18	0.15	0.14	0.14	0.13	0.18	0.14	0.06
CaO	2.99	1.54	0.69	0.96	0.98	0.95	1.49	1.53	1.38	1.21	0.92	1.26	0.96	0.89
Na_2O	2.60	2.13	2.52	2.66	2.55	2.78	3.45	2.92	2.82	2.61	2.93	3.40	2.71	2.95
K_2O	1.99	2.36	2.52	2.50	2.55	2.46	2.61	2.30	2.55	3.17	3.37	2.82	3.45	3.65
Cl	0.23	0.54	0.24	0.28	0.31	0.27	0.28	0.12	0.23	0.24	0.22	0.18	0.30	0.30
SO_3	0.02	0.07									0.10	0.11	0.06	0.09
Total	100.00	100.00	100.00	100.00	100.00	100.00	100.00	100.00	100.00	100.00	100.00	100.00	100.00	100.00

Table A3.2 continued

Sample ID	OR2_2-1.1	OR2_2-2.1	OR2_2-3.1	OR2_3-1.1	OR2_4-1.1	OR2_17-1	OR2_16-1	RA1_2-1.1	RA1_2-2.1	RA1_8-1.1	RA1_8-2.1	RA1_8-3.1	RA1_9-1.1	RA1_11-1.1
Host	qtz	qtz	qtz	qtz	qtz	qtz	qtz	opx	opx	opx	opx	opx	opx	opx
SiO_2	79.69	78.81	79.09	79.21	78.65	75.63	79.45	78.08	78.20	78.67	78.52	78.16	79.45	78.12
TiO_2	0.04	0.11	0.14	0.07	0.13	0.06	0.06	0.33	0.22	0.28	0.20	0.27	0.28	0.24
Al_2O_3	12.15	12.33	12.02	12.37	12.15	14.30	12.01	13.26	12.92	11.88	12.39	12.54	11.50	12.72
FeO	0.77	0.83	0.95	1.14	1.11	0.94	0.76	1.72	1.74	2.17	1.85	1.97	2.03	1.79
MnO	0.06	0.16	0.29	0.10	0.02	0.11	0.10	0.09	0.08	0.07	0.06	0.09	0.06	0.17
MgO	0.04	0.10	0.07	0.12	0.12	0.04	0.08	0.18	0.22	0.25	0.26	0.22	0.20	0.24
CaO	0.48	0.51	0.54	0.99	0.81	0.30	0.64	1.23	1.22	1.32	1.42	1.38	1.17	1.19
Na_2O	2.57	2.67	2.62	3.00	2.77	3.59	2.73	2.20	2.24	2.73	2.84	2.78	2.61	3.14
K_2O	4.06	4.18	3.86	2.65	3.75	4.74	3.53	2.73	2.88	2.46	2.26	2.40	2.38	2.19
Cl	0.14	0.19	0.12	0.21	0.26	0.21	0.19	0.18	0.27	0.17	0.18	0.19	0.14	0.15
SO_3			0.17	0.04	0.07	0.01	0.19	0.02	0.02	b.d.	0.01	0.01	0.18	0.06
Total	100.00	100.00	100.00	100.00	100.00	100.00	100.00	100.00	100.00	100.00	100.00	100.00	100.00	100.00

Table A3.2 continued

Sample ID	RA2_1.1	RA2_4-2.1	RA2_6-1.1	RA2_6-2.1	RA2_6-3.1	RA2_7-2.1	RA2_8-1.1	RA2_8-2.1	RA2_8-4.1	RA2_10-1.1	RA2_11-1.1	RA2_11-3.1	RA2_13-2.2	RA2_13-4.2
Host	opx	opx	opx	opx	opx	opx	opx	opx	opx	opx	opx	opx	plag	plag
SiO_2	76.19	76.87	77.45	77.58	77.04	78.18	77.63	76.53	77.37	77.79	76.77	77.63	77.46	76.74
TiO_2	0.35	0.26	0.42	0.45	0.42	0.17	0.15	0.32	0.21	0.64	0.38	0.48	0.20	0.38
Al_2O_3	13.49	12.97	13.03	12.61	12.79	12.32	12.74	12.91	12.90	12.47	12.72	12.85	13.15	13.49
FeO	2.55	2.12	1.89	1.71	2.13	2.01	2.16	2.55	2.12	1.27	2.02	1.83	1.58	1.33
MnO	0.05	0.24	0.43	0.58	0.36	0.19	0.21	0.25	0.19	0.13	0.99	0.27	0.15	0.09
MgO	0.40	0.38	0.30	0.32	0.36	0.25	0.39	0.44	0.32	0.16	0.18	0.17	0.26	0.25
CaO	1.60	1.59	1.27	1.25	1.43	1.28	1.41	1.46	1.55	1.37	1.24	1.55	1.19	1.34
Na_2O	2.76	2.98	2.36	2.30	2.68	2.78	2.89	2.83	2.83	3.46	2.49	2.57	2.77	3.45
K_2O	2.41	2.34	2.68	2.84	2.45	2.52	2.22	2.43	2.31	2.41	2.88	2.37	3.02	2.71
Cl	0.15	0.20	0.17	0.27	0.18	0.17	0.22	0.21	0.19	0.23	0.20	0.16	0.21	0.17
SO_3	0.05	0.04	b.d.	0.08	0.17	0.14	b.d.	0.07	0.02	0.06	0.12	0.11	0.02	0.05
Total	100.00	100.00	100.00	100.00	100.00	100.00	100.00	100.00	100.00	100.00	100.00	100.00	100.00	100.00

Table A3.2 continued

Sample	RA2_14	RA2_15	RA2_15	RA2_15	RA2_16	RA2_16	RA2_18	RA2_18	RA2_18	RA3_4-	RA3_8-	RA3_8-	RA3_9-	RA3_9-
ID	-1.1	-1.1	-2.1	-3.2	-1.2	-2.1	-1.2	-2.1	-3.2	1.1	2.1	4.1	2.1	3.1
Host	plag	plag	plag	plag	plag	plag	plag	plag	plag	opx	opx	opx	opx	opx
SiO_2	77.15	77.56	77.42	77.18	76.89	76.13	78.66	77.98	77.47	78.28	77.65	77.96	78.60	77.57
TiO_2	0.21	0.24	0.26	0.25	0.23	0.32	0.18	0.28	0.23	0.15	0.18	0.23	0.29	0.32
Al_2O_3	12.92	13.02	13.10	13.34	13.56	13.31	12.59	13.05	13.12	12.18	12.43	12.31	12.39	12.77
FeO	1.40	1.42	1.35	1.45	1.42	1.45	1.32	1.33	1.32	2.06	2.32	2.30	2.08	2.08
MnO	0.05	0.12	0.07	0.02	0.04	0.14	0.02	0.12	0.13	0.28	0.15	0.21	0.16	0.11
MgO	0.31	0.23	0.30	0.32	0.26	0.24	0.25	0.28	0.23	0.09	0.14	0.20	0.18	0.16
CaO	1.36	1.39	1.57	1.52	1.38	1.49	1.32	1.43	1.55	1.22	1.13	1.25	1.33	1.51
Na_2O	3.21	3.21	2.68	2.90	3.10	3.70	2.48	2.60	2.68	2.67	2.23	2.69	2.61	2.84
K_2O	3.11	2.64	3.06	2.79	2.82	2.92	2.93	2.76	3.01	2.82	3.57	2.58	2.13	2.36
Cl	0.22	0.14	0.19	0.23	0.30	0.25	0.19	0.17	0.20	0.20	0.19	0.22	0.20	0.22
SO_3	0.07	0.03	b.d.	b.d.	b.d.	0.05	0.06	0.00	0.07	0.05	b.d.	0.05	0.05	0.08
Total	100.00	100.00	100.00	100.00	100.00	100.00	100.00	100.00	100.00	100.00	100.00	100.00	100.00	100.00

Table A3.2 continued

Sample	TA1_7-	TA1_9-	TA1_10	TA1_10	TA1_13	TA1_13	TA1_14	TA1_14	TA1_14	TA1_14	TA1_15	TA1_18	TA1_18	TA1_30
ID	2.1	2.1	-1.1	-2.1	-2.1	-3.1	-1.1	-2.1	-4.1	-5.1	-1.1	-2.1	-3.1	-3
Host	opx	opx	opx	opx	opx	opx	opx	opx	opx	opx	opx	opx	opx	plag
SiO_2	75.64	76.05	75.85	76.71	75.40	75.68	75.18	74.99	75.83	75.56	76.78	75.25	76.18	76.58
TiO_2	0.30	0.29	0.32	0.30	0.33	0.28	0.36	0.40	0.36	0.29	0.41	0.73	0.37	0.27
Al_2O_3	13.43	12.74	12.96	12.70	12.84	13.41	13.14	13.65	13.02	13.09	12.69	13.73	13.21	13.45
FeO	2.69	2.89	2.98	2.85	3.09	2.61	3.01	2.37	2.51	2.94	2.64	2.47	2.51	2.10
MnO	0.23	0.28	0.25	0.17	0.07	0.13	0.08	0.16	0.11	0.15	0.06	0.03	0.08	0.09
MgO	0.23	0.28	0.32	0.27	0.34	0.30	0.34	0.30	0.30	0.31	0.20	0.33	0.34	0.27
CaO	1.69	1.52	1.62	1.50	1.63	1.55	1.64	1.60	1.60	1.61	1.41	1.69	1.48	1.69
Na_2O	3.33	3.46	3.09	3.08	3.48	3.25	3.34	3.73	3.46	3.28	3.16	3.19	3.25	2.95
K_2O	2.27	2.13	2.26	2.23	2.51	2.48	2.53	2.53	2.50	2.45	2.35	2.32	2.26	2.36
Cl	0.15	0.26	0.18	0.18	0.22	0.19	0.24	0.22	0.25	0.26	0.21	0.26	0.24	0.19
SO_3	0.04	0.11	0.17	0.01	0.08	0.12	0.13	0.04	0.07	0.07	0.10	b.d.	0.07	0.05
Total	100.00	100.00	100.00	100.00	100.00	100.00	100.00	100.00	100.00	100.00	100.00	100.00	100.00	100.00

Table A3.2 continued

Sample	TA1_31	TA1_31	TA1_43	TA1_43	TA1_38	TA1_38	TA2_1-	TA2_1-	TA2_1-	TA2_2-	TA2_2-	TA2_2-	TA2_2-	TA2_2-
ID	-1	-2	-1.1	-2.1	-1	-2	1.1	2.1	3.1	1.1	2.1	3.1	4.1	5.1
Host	plag	plag	plag	plag	qtz	qtz	opx	opx	opx	opx	opx	opx	opx	opx
SiO_2	77.03	76.85	76.36	76.01	79.52	79.37	76.02	76.22	75.70	76.36	75.76	76.65	76.59	76.33
TiO_2	0.23	0.27	0.24	0.30	0.13	0.13	0.30	0.24	0.45	0.28	0.32	0.36	0.38	0.27
Al_2O_3	13.85	13.68	13.66	13.58	12.72	12.86	13.23	13.05	12.80	12.60	13.25	12.76	12.55	12.95
FeO	1.77	1.73	1.89	1.98	1.14	1.16	2.62	2.54	2.81	2.52	2.34	2.45	2.57	2.36
MnO	0.15	0.05	0.09	0.13	b.d.	0.02	0.13	0.03	0.22	0.15	0.15	0.17	0.16	0.22
MgO	0.23	0.26	0.25	0.24	0.14	0.11	0.22	0.22	0.23	0.21	0.26	0.20	0.19	0.25
CaO	1.55	1.65	1.49	1.48	1.03	1.09	1.25	1.47	1.29	1.39	1.37	1.26	1.38	1.40
Na_2O	2.60	2.78	3.26	3.36	2.76	2.80	3.69	3.71	3.89	3.77	3.76	3.54	3.72	3.67
K_2O	2.39	2.51	2.43	2.56	2.28	2.28	2.30	2.24	2.40	2.44	2.50	2.37	2.28	2.35
Cl	0.20	0.14	0.22	0.26	0.20	0.19	0.22	0.24	0.21	0.24	0.18	0.19	0.15	0.20
SO_3	b.d.	0.08	0.10	0.10	0.09	b.d.	0.02	0.04	b.d.	0.02	0.11	0.06	0.02	b.d.
Total	100.00	100.00	100.00	100.00	100.00	100.00	100.00	100.00	100.00	100.00	100.00	100.00	100.00	100.00

Table A3.2 continued

Sample	TA2_4-	TA2_5-	TA2_6-	TA2_9-	TA2_11	TA2_11	TA2_12	TA2_15	KS_15-	TA2_15	TA2_16	TA2_16	TA2_16	TA2_24
ID	1.1	1.1	2.1	1.1	-1.2	-2.1	-1.1	-1.1	2.1	-3.1	-1.1	-2.1	-3.1	-1.1
Host	opx	opx	opx	opx	opx	opx	opx	opx	opx	opx	opx	opx	opx	plag
SiO_2	76.36	74.71	76.00	75.33	75.57	76.03	76.82	76.26	74.45	75.99	75.99	75.67	75.89	76.38
TiO_2	0.31	0.34	0.24	0.28	0.36	0.33	0.30	0.23	0.40	0.39	0.30	0.28	0.26	0.21
Al_2O_3	12.70	13.74	12.95	13.22	13.01	13.00	12.48	12.99	13.23	13.17	13.13	13.04	13.03	13.44
FeO	2.65	2.60	2.91	3.42	2.90	3.01	2.99	2.87	3.71	2.83	2.68	3.12	2.93	1.46
MnO	0.14	0.19	0.14	0.18	0.12	0.17	0.04	0.20	0.16	0.23	0.13	0.18	0.24	0.07
MgO	0.23	0.55	0.51	0.39	0.45	0.41	0.39	0.39	0.66	0.34	0.39	0.38	0.48	0.19
CaO	1.44	1.35	1.33	1.15	1.26	1.38	1.35	1.14	1.41	1.23	1.23	1.32	1.31	1.57
Na_2O	3.73	3.51	3.22	3.62	3.49	3.12	3.09	3.28	3.46	3.34	3.41	3.54	3.31	3.74
K_2O	2.20	2.71	2.28	2.14	2.55	2.29	2.33	2.27	2.29	2.22	2.46	2.29	2.29	2.73
Cl	0.15	0.23	0.21	0.22	0.23	0.18	0.21	0.36	0.20	0.17	0.27	0.18	0.25	0.20
SO_3	0.08	0.07	0.19	0.04	0.06	0.07	b.d.	0.01	0.04	0.08	0.01	0.02	0.02	b.d.
Total	100.00	100.00	100.00	100.00	100.00	100.00	100.00	100.00	100.00	100.00	100.00	100.00	100.00	100.00

Table A3.2 continued

Sample ID	TA2_26 -1.2	TA3_3- 1.1	TA3_3- 2.1	TA3_3- 3.1	TA3_4- 1.1	TA3_4- 2.1	TA3_5- 1.1	TA3_5- 2.1	TA3_9- 1.1	TA3_11 -1.1	TA3_11 -3.1	TA3_11 -4.1	TA3_11 -5.1	TA3_12 -1.1
Host	plag	opx	opx	opx	opx	opx	opx	opx	opx	opx	opx	opx	opx	opx
SiO_2	75.86	77.02	77.28	77.51	76.78	77.44	77.30	76.83	77.48	76.16	75.83	76.47	76.38	77.44
TiO_2	0.21	0.24	0.25	0.17	0.20	0.24	0.18	0.18	0.21	0.47	0.27	0.39	0.28	0.18
Al_2O_3	13.05	12.95	13.00	12.84	13.04	12.68	12.64	13.40	12.84	13.39	13.81	13.47	13.59	12.90
FeO	2.08	3.06	2.82	2.93	2.96	3.02	3.05	2.71	2.89	2.70	2.64	2.48	2.59	2.60
MnO	0.04	0.13	0.09	0.18	0.14	0.04	0.09	0.10	0.09	0.18	0.11	0.08	0.12	0.18
MgO	0.22	0.30	0.31	0.25	0.32	0.24	0.28	0.31	0.28	0.29	0.30	0.27	0.27	0.31
CaO	1.48	1.36	1.26	1.24	1.48	1.38	1.31	1.35	1.19	1.61	1.55	1.71	1.60	1.37
Na_2O	4.18	2.33	2.36	2.30	2.51	2.40	2.49	2.59	2.43	2.70	2.79	2.56	2.66	2.46
K_2O	2.63	2.27	2.43	2.41	2.33	2.21	2.37	2.35	2.23	2.18	2.51	2.32	2.31	2.33
Cl	0.20	0.19	0.17	0.15	0.19	0.20	0.19	0.13	0.19	0.23	0.18	0.21	0.20	0.20
SO_3	0.06	0.16	0.02	0.01	0.06	0.15	0.11	0.05	0.17	0.09	b.d.	0.06	b.d.	0.05
Total	100.00	100.00	100.00	100.00	100.00	100.00	100.00	100.00	100.00	100.00	100.00	100.00	100.00	100.00

Table A3.2 continued

Sample	TA3_12	TA3_13	TA3_15	TA3_15	TA3_16	TA3_16	TA3_19	TA4_5-	TA4_5-	TA4_5-	TA4_5-	TA4_5-	TA4_7-	TA4_7-
ID	-2.1	-2.1	-1	-2	-1	-2	-1	2.1	3.1	4.1	5.1	6.1	1.1	3.1
Host	opx	opx	plag	plag	plag	plag	plag	opx	opx	opx	opx	opx	opx	opx
SiO_2	77.68	77.16	75.67	76.68	77.28	76.39	75.94	76.14	76.77	76.64	75.67	76.59	76.87	76.18
TiO_2	0.23	0.22	0.32	0.33	0.18	0.21	0.24	0.31	0.20	0.17	0.18	0.12	0.23	0.49
Al_2O_3	12.88	12.97	12.94	13.72	13.12	14.06	13.58	13.21	12.90	12.95	13.16	12.80	12.66	13.37
FeO	2.42	2.86	2.36	1.81	1.84	1.83	2.23	2.72	2.40	2.83	2.74	2.74	2.89	2.95
MnO	0.09	0.17	0.15	0.15	0.13	0.17	0.13	0.46	0.50	0.55	0.63	0.70	0.10	0.07
MgO	0.35	0.28	0.39	0.23	0.20	0.23	0.26	0.31	0.32	0.30	0.35	0.26	0.23	0.25
CaO	1.26	1.50	1.63	1.57	1.47	1.66	1.50	1.38	1.42	1.46	1.62	1.39	1.23	1.34
Na_2O	2.58	2.43	3.04	3.15	3.30	3.25	3.59	3.01	2.94	2.74	3.03	3.05	3.26	2.53
K_2O	2.27	2.13	3.18	2.15	2.30	1.98	2.30	2.26	2.23	2.14	2.35	2.14	2.28	2.24
Cl	0.24	0.24	0.29	0.17	0.15	0.15	0.19	0.19	0.14	0.19	0.19	0.16	0.20	0.23
SO_3	0.01	0.05	0.02	0.04	0.01	0.07	0.05	0.00	0.18	0.02	0.08	0.04	0.05	0.34
Total	100.00	100.00	100.00	100.00	100.00	100.00	100.00	100.00	100.00	100.00	100.00	100.00	100.00	100.00

Table A3.2 continued

Sample ID	X590_1-1	X590_3-1.1	X590_3-3	X590_9-1.1	X590_9-2.2	X590_9-3.1	X590_11-1.1	X590_12-1.1	X590_12-2.2	590B-1i1	590B-3i1	590B-4i1	590B-5i1	590B-6i1
Host	opx	opx	opx	plag	plag	plag	plag	plag	plag	plag	plag	plag	plag	plag
SiO_2	76.55	76.60	77.67	75.56	75.91	75.46	75.83	75.07	76.64	77.50	76.87	76.63	75.54	76.63
TiO_2	0.37	0.31	0.22	0.30	0.37	0.36	0.27	0.46	0.37	0.34	0.32	0.33	0.38	0.30
Al_2O_3	13.22	13.35	12.76	13.85	13.56	13.64	14.11	14.00	13.48	14.09	13.56	13.71	13.82	13.78
FeO	2.11	2.38	2.15	2.02	2.02	2.06	1.90	2.50	1.95	2.29	2.11	2.14	2.37	1.86
MnO	0.39	0.14	0.12	0.15	0.13	0.16	0.07	0.11	0.11	0.15	0.13	0.15	0.13	0.07
MgO	0.14	0.06	0.10	0.43	0.39	0.58	0.41	0.44	0.34	0.23	0.16	0.12	0.48	0.34
CaO	1.58	2.04	1.33	2.04	2.00	2.03	2.11	2.18	1.88	1.97	1.81	1.83	1.92	1.86
Na_2O	3.40	3.02	3.36	3.19	3.18	3.15	2.90	2.88	2.83	1.53	3.08	2.97	3.06	3.09
K_2O	1.85	1.52	1.86	1.69	1.77	1.82	1.87	1.70	1.72	1.35	1.49	1.59	1.70	1.58
Cl	0.40	0.53	0.33	0.66	0.56	0.66	0.47	0.63	0.57	0.56	0.48	0.52	0.61	0.48
SO_3	b.d.	0.05	0.10	0.11	0.11	0.07	0.06	0.04	0.11					
Total	100.00	100.00	100.00	100.00	100.00	100.00	100.00	100.00	100.00	100.00	100.00	100.00	100.00	100.00

Table A3.2 continued

Sample	590B-7i1	590B-8i1	590B-8i2	X590/B_	X590/B_	X590/B_	X609_14	X609_16	X609_16	X609_18	X609_18
ID				10-1.1	11-1.2	13-1.1	-1.1	-1.1	-2.2	-1.1	-2.2
Host	plag	plag	plag	plag	plag	plag	plag	plag	plag	plag	plag
SiO_2	76.82	75.87	76.86	77.49	76.63	76.22	77.09	78.89	75.33	75.00	76.95
TiO_2	0.37	0.40	0.38	0.23	0.35	0.30	0.30	0.40	0.48	0.55	0.40
Al_2O_3	13.71	13.83	13.58	13.02	13.44	13.61	12.98	12.81	13.50	13.71	13.04
FeO	1.86	2.07	2.08	1.71	1.92	2.07	1.98	2.35	2.30	2.20	2.28
MnO	0.15	0.12	0.09	0.19	0.04	0.07	0.07	0.11	0.19	0.13	0.10
MgO	0.40	0.43	0.41	0.32	0.43	0.35	0.42	0.36	0.46	0.45	0.41
CaO	1.92	1.96	1.87	1.55	1.90	1.92	1.88	1.93	2.16	2.10	1.84
Na_2O	2.60	3.09	2.42	3.24	3.15	3.20	3.24	1.40	3.36	3.22	2.64
K_2O	1.66	1.65	1.73	1.89	1.65	1.77	1.54	1.13	1.64	1.90	1.75
Cl	0.50	0.59	0.59	0.37	0.45	0.46	0.46	0.57	0.51	0.64	0.49
SO_3				0.01	0.03	0.04	0.05	0.06	0.06	0.10	0.09
Total	100.00	100.00	100.00	100.00	100.00	100.00	100.00	100.00	100.00	100.00	100.00

All sample data are recalculated on an anhydrous basis. Abbreviations: b.d. – below detection limits; opx- orthopyroxene; plag – plagioclase; qtz - quartz

Appendix 3

Table A3.3: Major element compositions of groundmass glass adhered to crystals

Major element concentrations are given in wt%

Table A3.3

Sample ID	OR1_8g	RA1_8g	RA2_8g	TA1_9g	TA1_13g	TA1_14g	TA1_15g	TA2_1g	TA2_2g	TA2_5g	TA2_11g	TA3_13g	TA3_11g	TA4_5g
SiO_2	77.02	77.35	76.80	76.55	75.40	75.36	75.60	75.52	75.44	75.22	75.33	76.48	76.34	76.43
TiO_2	0.14	0.29	0.34	0.24	0.31	0.28	0.46	0.30	0.28	0.30	0.28	0.26	0.33	0.17
Al_2O_3	12.50	12.82	12.69	12.85	13.60	13.70	13.01	13.54	13.40	13.58	13.40	13.61	13.60	12.84
FeO	1.82	1.51	2.05	2.36	2.54	2.15	2.39	2.23	2.25	2.42	2.44	2.24	2.27	2.39
MnO	0.12	0.03	0.32	0.22	0.09	0.06	0.07	0.13	0.18	0.11	0.10	0.07	0.07	0.71
MgO	0.21	0.34	0.46	0.30	0.34	0.35	0.32	0.47	0.42	0.60	0.71	0.26	0.20	0.21
CaO	1.21	1.46	1.58	1.51	1.57	1.55	1.51	1.45	1.42	1.61	1.52	1.58	1.44	1.33
Na_2O	4.26	3.52	3.27	3.44	3.49	3.89	4.00	3.91	4.00	3.35	3.39	3.00	2.86	3.20
K_2O	2.61	2.43	2.26	2.19	2.35	2.35	2.41	2.38	2.44	2.53	2.54	2.22	2.35	2.44
Cl	b.d.	0.21	0.16	0.22	0.27	0.20	0.21	0.20	0.17	0.14	0.19	0.20	0.22	0.16
SO_3	0.11	0.04	0.08	0.10	0.02	0.10	0.03	0.05	b.d.	0.14	0.10	0.01	0.26	0.11
Total	100.00	100.00	100.00	100.00	100.00	100.00	100.00	100.19	100.00	100.00	100.00	100.00	100.00	100.00

All sample data are recalculated on an anhydrous basis. b.d. – below detection limits.

Appendix 3

Table A3.4: Trace element composition (in ppm) of orthopyroxene and plagioclase phenocrysts from the Healy and Oruanui samples.

Table A3.4

	Healy		Oruanui	
	opx	plag	opx	plag
n	5	1	2	1
Sc	52.8	5.53	55.6	3.95
Ti	0.16	0.02	577	88.1
V	20.2	0.27	31.18	0.44
Cr	6.29	10.1	7.80	6.08
Mn	19442	46.52	14294	30.61
Co	59.8	0.37	66.0	0.42
Ni	4.08	3.09	12.7	1.05
Cu	0.93	2.99	0.70	2.12
Zn	634	11.6	602	8.22
Ga	2.69	25.1	2.83	21.6
Rb	0.16	0.38	0.11	0.28
Sr	0.28	724	0.13	610
Y	11.06	0.37	8.46	0.34
Zr	1.60	0.00	1.08	0.44
Nb	0.22	0.00	0.00	0.00
Mo	0.89	0.00	0.61	0.00
Cs	0.03	0.10	0.03	0.06
Ba	5.18	248	0.87	139
La	0.09	2.78	0.13	3.35
Ce	0.15	5.13	0.15	5.46
Pr	0.07	0.45	0.11	0.52
Nd	0.30	1.71	0.36	1.23
Sm	0.33	0.57	0.52	0.56
Eu	0.08	1.68	0.08	1.45
Gd	0.53	0.66	0.58	0.55
Tb			0.12	0.08
Dy	1.39	0.38	1.05	0.35
Ho			0.32	0.09
Er	1.54	0.27	1.26	0.33
Tm			0.27	0.10
Yb	2.74	0.36	2.30	0.90
Lu	0.50	0.00	0.44	0.20
Hf	0.20	0.00	0.46	0.00
Ta	0.03	0.00	0.00	0.00
W	0.00	0.30	0.00	0.00
Pb	0.22	0.92	0.21	2.61
Th	0.04	0.00	0.17	0.25
U	0.03	0.00	0.13	0.00

Appendix 3

Table A3.5: Major element compositions of Taupo melt inclusions plagioclase hosts and representative analyses of Whakamaru plagioclase crystals.

Major element concentrations are given in wt%

Table A3.5

Sample	TA1_30host	TA1_31host	TA1_31host2	TA1_31host3	TA1_35host	TA1_35host3	TA1_34host2	TA1_34host3	TA2_24host1
SiO_2	58.99	58.62	60.50	59.40	58.23	58.07	55.31	59.66	58.91
Al_2O_3	26.50	26.62	25.78	26.17	26.98	26.99	29.22	25.90	25.31
FeO	0.24	0.35	0.27	0.37	0.28	0.51	0.35	0.35	0.27
CaO	9.56	9.08	7.95	8.32	9.44	9.72	11.96	8.49	7.80
Na_2O	6.23	6.24	6.47	6.32	5.72	5.93	4.78	6.47	6.83
K_2O	0.23	0.26	0.27	0.21	0.19	0.14	0.11	0.16	0.23
Total	101.75	101.18	101.23	100.79	100.83	101.36	101.73	101.04	99.36
X An	0.45	0.44	0.40	0.42	0.47	0.47	0.58	0.42	0.38
Temp (°C)	778	773	758	766	784	785	800	768	755
H_2O (wt%)	8.40	8.38	8.33	8.31	8.44	8.40	9.02	8.28	8.25

Table A3.5 continued

Sample	TA2_24host 2	TA2_27host	TA2_27host 21	TA2_26host. 1	TA2_29host	WHh_2	WH1h_3	WH1h_4	WH1h_34	WH1h_64
SiO_2	60.37	55.96	56.60	57.10	59.54	61.27	61.37	62.03	55.81	59.77
Al_2O_3	25.79	26.77	28.70	24.77	26.61	25.12	25.40	24.71	29.00	25.80
FeO	0.19	0.30	0.47	0.41	0.42	0.25	0.31	0.31	0.23	0.31
CaO	7.83	8.92	10.60	8.88	8.17	6.54	6.48	5.81	10.42	6.30
Na_2O	6.93	6.23	5.38	6.39	6.66	7.55	7.88	7.67	5.69	7.89
K_2O	0.23	0.18	0.16	0.22	0.22	0.78	0.68	0.82	0.29	0.72
Total	101.34	98.36	101.91	97.76	101.62	101.51	102.12	101.34	101.45	100.78
X An	0.38	0.44	0.52	0.43	0.40	0.31	0.30	0.28	0.49	0.29
Temp (°C)	752	774	793	771	760	752	749	735	836	744
H_2O (wt%)	8.30	8.33	8.64	8.33	8.30	8.14	8.10	8.22	8.46	8.13

Table A3.5 continued

Sample	WH1h_65	WH1h_66	WH1b_2	WH1b_3	WH1b_4	WH1b_5	WH1b_6
SiO_2	60.46	60.23	60.12	60.55	61.03	60.51	60.47
Al_2O_3	25.63	25.43	24.92	24.65	24.37	24.38	24.33
FeO	0.29	0.24	0.26	0.23	0.20	0.34	0.22
CaO	6.27	6.08	7.00	6.58	6.42	6.16	6.04
Na_2O	7.44	7.50	7.17	7.37	7.54	7.45	7.62
K_2O	0.69	0.72	0.66	0.68	0.67	0.62	0.71
Total	100.78	100.19	100.13	100.06	100.22	99.47	99.39
X An	0.31	0.30	0.34	0.32	0.31	0.30	0.29
Temp (°C)	751	745	769	758	753	750	743
H_2O (wt%)	8.11	8.14	8.08	8.09	8.10	8.09	8.14

X An calculated on a mole fraction basis (Ca/(Ca+Na+K). Temperature and water estimates were calculated using plagioclase-melt equilibria of Putirka, (2005) assuming a pressure of 100 MPa.

Appendix 3

Table A3.6: Major element compositions (are given in wt%) of Whakamaru plagioclase crystals Empty cells indicate no data collected.

Table A3.6

Sample	SiO_2	Al_2O_3	FeO	MgO	CaO	Na_2O	K_2O	Total	XAn	T (°C)	G	Dist. (μm)
WH1b_2	60.12	24.92	0.26		7.00	7.17	0.66	100.13	0.34	770	2	20
WH1b_3	60.55	24.65	0.23		6.58	7.37	0.68	100.06	0.32	759	2	30
WH1b_4	61.03	24.37	0.20		6.42	7.54	0.67	100.22	0.31	753	2	40
WH1b_5	60.51	24.38	0.34		6.16	7.45	0.62	99.47	0.30	751	2	50
WH1b_6	60.47	24.33	0.22		6.04	7.62	0.71	99.39	0.29	743	2	60
WH1b_7	60.36	24.46	0.30		6.13	7.85	0.75	99.85	0.29	741	2	70
WH1b_8	60.51	24.40	0.24		6.04	7.72	0.70	99.61	0.29	742	2	80
WH1b_9	60.17	24.30	0.14		6.16	7.63	0.70	99.10	0.30	746	2	90
WH1b_10	60.12	24.17	0.18		5.99	7.58	0.82	98.86	0.29	740	2	100
WH1b_12	60.50	24.33	0.22		6.24	7.52	0.63	99.43	0.30	751	2	120
WH1b_13	59.82	24.37	0.22		6.32	7.47	0.69	98.89	0.31	752	2	130
WH1b_14	61.27	24.70	0.26		6.25	7.89	0.81	101.17	0.29	742	2	140
WH1b_15	60.23	24.81	0.20		6.67	7.44	0.70	100.05	0.32	759	2	150
WH1b_18	60.77	24.98	0.25		6.44	7.65	0.75	100.84	0.30	750	2	180
WH1b_19	60.88	25.10	0.14		6.79	7.36	0.70	100.96	0.32	762	2	190
WH1b_21	59.80	24.83	0.25		6.30	7.58	0.77	99.53	0.30	748	2	210
WH1b_22	60.70	24.29	0.18		6.32	7.76	0.80	100.06	0.30	745	2	220
WH1b_23	60.66	24.20	0.23		6.16	7.72	0.80	99.77	0.29	742	2	230
WH1b_24	61.20	24.70	0.20		6.26	7.37	0.72	100.45	0.31	752	2	240
WH1b_25	60.71	24.58	0.31		6.48	7.42	0.72	100.22	0.31	755	2	250
WH1b_26	61.11	25.03	0.33		6.48	7.69	0.72	101.37	0.30	751	2	260
WH1b_27	60.53	24.61	0.25		6.12	7.45	0.71	99.67	0.30	748	2	270
WH1b_28	60.24	24.52	0.19		6.08	7.67	0.70	99.39	0.29	744	2	280
WH1b_30	59.98	24.61	0.18		6.52	7.48	0.68	99.44	0.31	756	2	300
WH1b_31	59.84	24.74	0.21		6.40	7.57	0.73	99.49	0.31	751	2	310
WH1b_33	60.59	24.28	0.21		6.13	7.63	0.71	99.55	0.29	745	2	330
WH1b_34	60.61	24.40	0.21		6.50	7.39	0.73	99.84	0.31	756	2	340
WH1b_35	60.23	24.52	0.13		6.47	7.48	0.77	99.59	0.31	753	2	350
WH1b_36	61.06	24.25	0.17		6.21	7.43	0.75	99.86	0.30	749	2	360
WH1b_37	60.71	24.54	0.23		6.52	7.59	0.70	100.29	0.31	754	2	370
WH1b_38	59.78	24.43	0.15		6.09	7.56	0.75	98.77	0.29	744	2	380
WH1b_39	59.12	24.61	0.17		6.31	7.51	0.73	98.45	0.30	750	2	390
WH1b_40	59.25	24.89	0.17		6.61	7.67	0.72	99.31	0.31	754	2	400
WH1b_41	59.40	24.45	0.22		6.50	7.45	0.73	98.75	0.31	755	2	410
WH1b_42	59.68	24.50	0.20		6.50	7.42	0.69	98.98	0.31	756	2	420
WH1b_43	59.52	24.40	0.32		6.25	7.50	0.64	98.64	0.30	751	2	430
WH1b_44	59.55	24.34	0.25		6.40	7.52	0.74	98.80	0.31	751	2	440
WH1b_45	59.97	24.37	0.16		6.40	7.65	0.75	99.29	0.30	749	2	450
WH1b_46	59.96	24.38	0.23		6.36	7.50	0.78	99.20	0.30	750	2	460
WH1b_47	59.38	24.59	0.24		6.53	7.49	0.74	98.96	0.31	755	2	470
WH1b_48	60.00	24.68	0.19		6.43	7.51	0.56	99.37	0.31	757	2	480
WH1b_49	59.63	24.49	0.22		6.40	7.25	0.72	98.71	0.31	756	2	490
WH1b_50	60.07	24.97	0.30		6.52	7.43	0.66	99.94	0.31	757	2	500
WH1b_51	60.19	24.81	0.17		6.83	7.48	0.68	100.15	0.32	762	2	510
WH1b_52	60.39	24.52	0.21		6.29	7.32	0.67	99.41	0.31	754	2	520
WH1b_53	59.80	24.58	0.21		6.24	7.70	0.74	99.27	0.30	746	2	530
WH1b_55	61.09	25.82	0.21		6.52	7.54	0.62	101.79	0.31	757	2	540
WH1b_56	60.23	25.62	0.28		6.53	7.65	0.73	101.03	0.31	752	2	550
WH1b_57	61.88	26.26	0.20		6.76	5.14	0.66	100.90	0.40	796	2	560
WH1b_58	60.57	26.18	0.30		6.57	7.63	0.66	101.91	0.31	755	2	570
WH1b_61	61.87	25.07	0.17		6.41	7.52	0.65	101.70	0.31	754	2	600
WH1b_62	60.65	25.17	0.29		6.47	7.59	0.73	100.89	0.31	752	2	610
WH1b_63	60.40	24.98	0.14		6.61	7.62	0.69	100.44	0.31	755	2	620
WH1b_64	60.30	25.10	0.26		6.28	7.76	0.77	100.46	0.30	745	2	630
WH1b_65	61.15	25.87	0.29		6.29	7.67	0.71	101.97	0.30	748	2	640
WH1b_68	59.56	24.62	0.16		6.39	7.30	0.68	98.69	0.31	756	2	670
WH1b_72	61.85	25.92	0.18		6.51	5.01	0.69	100.15	0.40	793	2	680

Table A3.6 continued

Sample	SiO_2	Al_2O_3	FeO	MgO	CaO	Na_2O	K_2O	Total	XAn	T (°C)	G	Dist. (μm)
WH1b_76	60.62	25.71	0.26		6.26	7.51	0.76	101.12	0.30	748	2	720
WH1b_77	60.14	26.11	0.25		6.40	7.29	0.72	100.90	0.31	755	2	730
WH1b_78	60.40	26.08	0.20		6.62	7.46	0.72	101.49	0.32	757	2	740
WH1b_79	60.52	26.07	0.19		6.45	7.47	0.77	101.46	0.31	753	2	750
WH1b_80	60.60	25.88	0.14		6.34	7.44	0.82	101.21	0.30	750	2	760
WH1b_81	61.18	25.42	0.22		6.23	7.52	0.69	101.25	0.30	749	2	770
WH1b_85	61.08	25.50	0.26		6.67	7.52	0.65	101.68	0.32	759	2	810
WH1b_86	60.83	25.60	0.22		6.39	7.71	0.72	101.47	0.30	749	2	820
WH1b_87	60.14	25.22	0.19		6.35	7.57	0.67	100.14	0.30	751	2	830
WH1b_89	60.40	24.97	0.25		6.31	7.59	0.72	100.24	0.30	749	2	850
WH1b_90	61.57	24.34	0.13		5.60	7.86	0.77	100.27	0.27	729	2	860
WH1b_91	63.68	25.86	0.17		5.69	4.73	0.69	100.81	0.38	784	2	870
WH1b_92	60.97	26.14	0.18		6.13	7.57	0.73	101.73	0.30	746	2	880
WH1b_93	61.34	25.61	0.26		5.86	7.85	0.77	101.69	0.28	735	2	890
WH1b_94	61.13	26.17	0.16		6.18	7.17	0.74	101.55	0.31	752	2	900
WH1b_95	63.65	26.52	0.25		6.31	7.83	0.68	105.23	0.30	747	2	910
WH1b_96	62.12	25.60	0.20		6.29	7.33	0.69	102.23	0.31	753	2	920
WH1b_97	61.93	25.31	0.27		5.91	7.35	0.79	101.56	0.29	743	2	930
WH1b_98	60.04	25.78	0.11		6.47	7.41	0.73	100.56	0.31	755	2	940
WH1b_100	60.87	25.04	0.19		5.97	7.87	0.74	100.67	0.28	738	2	950
WH1b_101	61.79	25.31	0.19		6.00	7.66	0.78	101.74	0.29	740	2	960
WH1b_102	62.03	25.19	0.23		6.02	7.77	0.73	101.97	0.29	740	2	970
WH1b_104	60.42	24.69	0.30		5.63	7.42	0.77	99.23	0.28	736	2	990
WH1b_106	60.35	24.94	0.23		6.35	7.33	0.69	99.89	0.31	755	2	1010
WH1b_110	61.02	25.73	0.24		6.53	7.70	0.65	101.86	0.31	754	2	1050
WH1b_113	60.70	25.82	0.24		6.71	7.25	0.59	101.31	0.33	765	2	1080
WH1b_114	60.69	26.06	0.37		6.50	7.52	0.69	101.84	0.31	755	2	1090
WH1b_115	60.07	25.70	0.27		6.97	7.57	0.61	101.18	0.33	765	2	1100
WH1h_2	61.27	25.12	0.25		6.54	7.55	0.78	101.51	0.31	756	1	20
WH1h_4	62.03	24.71	0.31		5.81	7.67	0.82	101.34	0.28	738	1	40
WH1h_7	61.20	25.27	0.27		6.15	7.75	0.73	101.38	0.29	746	1	70
WH1h_8	59.90	25.79	0.31		6.56	7.63	0.73	100.91	0.31	756	1	80
WH1h_10	61.49	25.31	0.35		6.03	7.85	0.80	101.83	0.28	740	1	100
WH1h_11	61.25	25.29	0.31		5.94	7.51	0.77	101.07	0.29	744	1	110
WH1h_12	61.43	25.70	0.24		5.97	7.68	0.77	101.79	0.29	742	1	120
WH1h_13	61.25	24.74	0.21		5.99	7.67	0.76	100.62	0.29	743	1	130
WH1h_14	60.95	25.19	0.26		6.26	7.65	0.76	101.06	0.30	749	1	140
WH1h_15	59.99	25.83	0.21		6.48	7.57	0.67	100.76	0.31	757	1	150
WH1h_16	60.33	25.81	0.29		6.39	7.87	0.79	101.47	0.30	748	1	160
WH1h_22	58.92	25.51	0.36		6.97	7.19	0.60	99.55	0.34	773	1	220
WH1h_23	58.21	26.08	0.25		7.39	7.31	0.56	99.80	0.35	780	1	230
WH1h_24	59.01	26.14	0.21		7.31	7.12	0.55	100.33	0.35	781	1	240
WH1h_25	59.35	26.87	0.25		7.43	7.31	0.53	101.73	0.35	781	1	250
WH1h_26	58.33	26.60	0.19		7.44	7.26	0.49	100.30	0.35	783	1	260
WH1h_27	57.23	27.65	0.23		8.59	6.72	0.42	100.84	0.40	809	1	270
WH1h_28	55.23	29.13	0.29		10.14	6.00	0.34	101.14	0.47	833	1	280
WH1h_29	55.20	29.21	0.23		9.82	6.13	0.36	100.95	0.46	829	1	290
WH1h_30	56.09	28.23	0.14		9.13	6.35	0.39	100.33	0.43	820	1	300
WH1h_31	56.76	28.32	0.29		9.41	6.06	0.37	101.21	0.45	826	1	310
WH1h_33	54.00	30.34	0.26		11.38	4.96	0.23	101.16	0.55	849	1	330
WH1h_34	55.81	29.00	0.23		10.42	5.69	0.29	101.45	0.49	839	1	340
WH1h_35	55.71	29.63	0.30		10.70	5.35	0.29	101.97	0.52	843	1	350
WH1h_36	54.40	30.11	0.26		11.51	5.15	0.26	101.70	0.54	848	1	360
WH1h_37	54.15	30.02	0.27		10.95	5.40	0.24	101.02	0.52	846	1	370
WH1h_39	53.88	29.83	0.33		11.32	5.18	0.27	100.82	0.54	847	1	390
WH1h_40	53.60	28.99	0.21		11.12	5.28	0.28	99.48	0.53	846	1	400

Table A3.6 continued

Sample	SiO_2	Al_2O_3	FeO	MgO	CaO	Na_2O	K_2O	Total	XAn	T (°C)	G	Dist. (μm)
WH1h_48	54.21	28.06	0.29		10.03	5.60	0.30	98.49	0.49	838	1	480
WH1h_49	54.11	29.67	0.26		10.95	5.47	0.27	100.73	0.52	844	1	490
WH1h_53	59.11	26.94	0.31		7.50	7.11	0.51	101.48	0.36	785	1	530
WH1h_54	60.74	26.01	0.25		6.65	6.99	0.66	101.30	0.33	769	1	540
WH1h_55	60.61	25.45	0.29		6.31	7.56	0.72	100.94	0.30	752	1	550
WH1h_56	59.71	25.95	0.21		6.61	7.59	0.68	100.75	0.31	759	1	560
WH1h_58	60.23	25.76	0.34		6.44	7.92	0.68	101.36	0.30	751	1	580
WH1h_60	60.72	26.07	0.30		6.68	7.40	0.71	101.88	0.32	762	1	600
WH1h_61	59.96	26.32	0.22		6.63	7.46	0.70	101.29	0.32	760	1	610
WH1h_62	60.63	25.30	0.26		6.13	7.55	0.72	100.59	0.30	749	1	620
WH1h_63	60.49	26.10	0.25		6.52	7.41	0.68	101.44	0.31	759	1	630
WH1h_64	59.77	25.80	0.31		6.30	7.89	0.72	100.78	0.29	747	1	640
WH1h_65	60.46	25.63	0.29		6.27	7.44	0.69	100.78	0.31	754	1	650
WH1h_66	60.23	25.43	0.24		6.08	7.50	0.72	100.19	0.30	748	1	660
WH2a_2	60.94	24.51	0.25		6.47	7.30	0.68	100.14	0.32	758	2	20
WH2a_3	61.06	24.20	0.31		6.30	7.44	0.72	100.02	0.31	751	2	30
WH2a_4	60.79	24.53	0.31		6.53	7.39	0.61	100.16	0.32	759	2	40
WH2a_5	60.29	24.56	0.27		6.87	7.15	0.63	99.77	0.33	768	2	50
WH2a_6	59.73	24.30	0.24		6.60	7.09	0.65	98.60	0.33	764	2	60
WH2a_7	59.58	24.21	0.40		7.16	6.99	0.67	99.01	0.35	775	2	70
WH2a_8	58.60	24.87	0.32		7.70	6.41	0.65	98.55	0.38	792	2	80
WH2a_9	58.98	24.90	0.19		7.75	6.76	0.49	99.07	0.38	792	2	90
WH2a_10	58.59	25.23	0.15		7.85	6.47	0.46	98.74	0.39	799	2	100
WH2a_11	59.46	25.27	0.20		7.69	6.48	0.55	99.64	0.38	794	2	110
WH2a_12	60.10	24.32	0.37		6.51	7.06	0.67	99.02	0.32	762	2	120
WH2a_13	60.61	24.05	0.33		6.66	7.06	0.57	99.27	0.33	768	2	130
WH2a_14	61.04	23.73	0.32		6.05	7.55	0.65	99.33	0.30	746	2	140
WH2a_15	59.99	23.94	0.28		6.43	7.29	0.62	98.56	0.32	759	2	150
WH2a_17	59.92	23.94	0.25		6.32	7.20	0.63	98.26	0.31	758	2	170
WH2a_18	59.47	23.90	0.36		6.38	7.30	0.73	98.13	0.31	755	2	180
WH2a_19	59.91	24.16	0.28		6.88	7.21	0.66	99.10	0.33	767	2	190
WH2a_20	59.58	24.41	0.31		6.88	7.04	0.61	98.83	0.34	771	2	200
WH2a_21	61.58	24.41	0.26		6.42	7.32	0.74	100.74	0.31	755	2	210
WH2a_22	61.00	25.14	0.29		7.12	7.19	0.64	101.37	0.34	772	2	220
WH2a_23	60.00	25.12	0.23		7.67	6.64	0.55	100.21	0.38	791	2	230
WH2a_25	60.26	25.06	0.24		7.18	7.17	0.58	100.50	0.34	775	2	250
WH2a_26	61.68	23.67	0.24		6.34	7.50	0.69	100.12	0.31	752	2	260
WH2a_27	61.45	23.82	0.19		6.18	7.37	0.72	99.72	0.30	750	2	270
WH2a_28	61.69	24.14	0.21		6.68	7.40	0.63	100.74	0.32	762	2	280
WH2a_30	61.74	24.85	0.26		6.70	7.38	0.66	101.57	0.32	761	2	300
WH2a_31	60.68	25.26	0.17		7.25	6.83	0.51	100.69	0.36	783	2	310
WH2a_32	60.77	25.20	0.19		7.40	7.09	0.56	101.21	0.35	780	2	320
WH2a_33	60.79	24.83	0.28		6.83	7.08	0.65	100.46	0.33	768	2	330
WH2a_34	60.71	24.19	0.20		6.64	7.28	0.67	99.69	0.32	761	2	340
WH2a_35	61.59	24.60	0.23		6.24	7.42	0.67	100.75	0.30	751	2	350
WH2a_36	60.63	24.81	0.15		6.30	7.39	0.69	99.97	0.31	753	2	360
WH2a_37	61.00	25.00	0.24		6.63	7.45	0.67	100.98	0.32	759	2	370
WH2a_38	59.96	25.19	0.22		6.45	7.22	0.66	99.69	0.32	759	2	380
WH2a_39	60.20	24.88	0.20		6.75	7.53	0.66	100.22	0.32	760	2	390
WH2a_40	61.58	24.62	0.21		6.34	7.44	0.77	100.96	0.31	751	2	400
WH2a_41	59.89	24.48	0.24		6.22	7.51	0.69	99.04	0.30	749	2	410
WH2a_42	59.82	25.44	0.30		7.29	6.87	0.58	100.30	0.36	781	2	420
WH2a_43	72.95	15.00	0.42		1.92	3.78	4.94	99.00	0.13		2	430
WH2a_44	59.00	24.28	0.33		6.03	7.22	0.73	97.59	0.30	749	2	440
WH2a_45	60.33	24.39	0.22		6.17	7.59	0.78	99.48	0.30	745	2	450
WH2a_46	60.70	24.41	0.35		5.97	7.65	0.76	99.84	0.29	740	2	460

Table A3.6 continued

Sample	SiO_2	Al_2O_3	FeO	MgO	CaO	Na_2O	K_2O	Total	XAn	T (°C)	G	Dist. (μm)
WH2a_50	60.04	25.34	0.29		6.96	6.96	0.52	100.12	0.35	776	2	500
WH2a_51	60.30	25.39	0.25		6.82	7.29	0.55	100.60	0.33	768	2	510
WH2a_52	60.11	24.74	0.18		6.45	7.41	0.66	99.54	0.31	756	2	520
WH2a_54	60.03	25.07	0.18		6.41	7.40	0.65	99.74	0.31	756	2	540
WH2a_55	59.84	24.89	0.30		6.52	7.45	0.67	99.67	0.31	757	2	550
WH2a_56	60.04	24.86	0.28		6.25	7.44	0.62	99.49	0.31	753	2	560
WH2a_57	60.11	24.76	0.26		6.38	7.34	0.66	99.51	0.31	756	2	570
WH2a_58	60.51	24.62	0.28		5.96	7.60	0.73	99.70	0.29	741	2	580
WH2a_59	60.87	24.36	0.28		6.05	7.46	0.71	99.72	0.30	746	2	590
WH2a_60	60.20	24.48	0.19		6.37	7.32	0.68	99.23	0.31	755	2	600
WH2a_61	60.60	24.60	0.18		6.28	7.48	0.75	99.90	0.30	749	2	610
WH2a_62	61.14	24.72	0.24		5.96	7.60	0.67	100.32	0.29	743	2	620
WH2a_68	59.70	25.04	0.23		6.46	7.34	0.62	99.39	0.32	759	2	680
WH2a_69	61.06	24.73	0.26		6.18	7.50	0.71	100.44	0.30	748	2	690
WH2a_70	59.52	25.13	0.31		7.02	6.92	0.59	99.49	0.35	776	2	700
WH2a_71	59.83	25.11	0.16		6.81	7.06	0.57	99.54	0.34	770	2	710
WH2a_73	59.72	24.68	0.25		6.41	7.48	0.72	99.25	0.31	753	2	730
WH2a_74	59.84	24.84	0.28		6.24	7.34	0.72	99.25	0.31	752	2	740
WH2a_75	57.80	23.95	0.29		5.98	7.12	0.72	95.85	0.30	749	2	750
WH2a_76	60.55	24.55	0.21		6.37	7.30	0.76	99.74	0.31	754	2	760
WH2a_77	60.57	24.71	0.18		6.36	7.10	0.67	99.59	0.32	759	2	770
WH2a_78	60.49	25.05	0.17		6.74	7.08	0.68	100.21	0.33	766	2	780
WH2a_79	59.93	25.57	0.31		6.78	7.18	0.58	100.34	0.33	768	2	790
WH2a_80	59.34	25.09	0.19		6.82	7.13	0.57	99.14	0.33	770	2	800
WH2a_81	59.50	25.62	0.20		7.07	7.05	0.57	100.01	0.34	775	2	810
WH2a_82	60.26	25.08	0.25		6.69	7.44	0.69	100.41	0.32	759	2	820
WH2a_83	61.12	24.88	0.21		6.35	7.31	0.71	100.57	0.31	754	2	830
WH2a_84	61.32	24.95	0.21		6.64	7.41	0.72	101.25	0.32	758	2	840
WH2a_85	60.65	25.23	0.26		6.58	7.42	0.72	100.85	0.32	757	2	850
WH2a_87	61.61	24.91	0.19		6.56	7.33	0.60	101.19	0.32	761	2	870
WH2a_89	60.87	24.39	0.24		6.05	7.66	0.79	100.01	0.29	741	2	890
WH2a_90	60.62	24.76	0.17		6.42	7.42	0.74	100.12	0.31	753	2	900
WH2a_91	60.38	24.90	0.19		6.34	7.54	0.73	100.08	0.30	750	2	910
WH2a_92	60.90	25.00	0.14		6.03	7.46	0.64	100.17	0.30	747	2	920
WH2a_93	60.58	24.65	0.29		5.96	7.55	0.71	99.72	0.29	743	2	930
WH2a_94	60.92	24.48	0.24		6.19	7.59	0.76	100.16	0.30	746	2	940
WH2a_95	61.08	24.52	0.25		6.17	7.57	0.76	100.35	0.30	746	2	950
WH2a_96	61.05	24.75	0.17		6.10	7.08	0.77	99.93	0.31	751	2	960
WH2a_97	60.89	24.84	0.27		6.00	7.45	0.75	100.21	0.29	744	2	970
WH2a_98	61.06	24.64	0.30		6.09	7.56	0.74	100.38	0.30	745	2	980
WH2a_99	59.14	25.93	0.27		7.32	6.93	0.61	100.21	0.36	780	2	990
WH2a_100	60.17	25.13	0.25		6.65	7.41	0.64	100.25	0.32	760	2	1000
WH2a_101	60.90	24.86	0.21		6.04	7.56	0.69	100.25	0.29	745	2	1010
WH2a_102	61.01	24.61	0.20		6.15	7.45	0.73	100.15	0.30	748	2	1020
WH2a_103	61.42	24.68	0.30		6.02	7.60	0.81	100.83	0.29	741	2	1030
WH2a_104	70.01	25.40	0.22		5.98	7.82	0.84	110.28	0.28	736	2	1040
WH2a_112	62.26	24.95	0.22		6.38	7.35	0.78	101.93	0.31	753	2	1120
WH2a_116	62.95	24.75	0.17		6.08	7.27	0.67	101.90	0.30	750	2	1160
WH2a_119	62.26	23.95	0.12		6.33	7.32	0.73	100.71	0.31	753	2	1190
WH2a_124	61.77	24.74	0.18		6.16	7.32	0.75	100.91	0.30	749	2	1250
WH2a_125	61.40	24.91	0.24		6.38	7.37	0.70	101.00	0.31	754	2	1260
WH2a_126	61.07	24.91	0.25		6.54	7.48	0.64	100.89	0.31	757	2	1270
WH2a_127	60.52	24.99	0.31		6.36	7.39	0.71	100.26	0.31	753	2	1280
WH2a_130	63.46	24.01	0.25		5.74	6.96	0.75	101.17	0.30	746	2	1320
WH2a_140	61.52	24.69	0.37		6.62	7.19	0.67	101.06	0.32	762	2	1420
WH2a_141	60.42	24.15	0.27		6.63	6.99	0.71	99.16	0.33	765	2	1430
WH2a_145	61.13	23.51	0.35		5.76	7.47	0.76	98.98	0.29	738	2	1470

Table A3.6 continued

Sample	SiO_2	Al_2O_3	FeO	MgO	CaO	Na_2O	K_2O	Total	XAn	T (°C)	G	Dist. (μm)
WH2b_4	61.43	25.04	0.31		6.91	7.41	0.72	101.83	0.33	763	1	40
WH2b_5	61.91	25.00	0.23		6.51	7.50	0.68	101.82	0.31	755	1	50
WH2b_6	61.69	25.15	0.24		6.74	7.43	0.68	101.93	0.32	761	1	60
WH2b_7	61.63	25.22	0.15		6.62	7.36	0.59	101.57	0.32	762	1	70
WH2b_8	61.68	24.80	0.24		6.26	7.50	0.74	101.21	0.30	749	1	80
WH2b_9	60.88	25.53	0.23		6.59	7.37	0.68	101.27	0.32	759	1	90
WH2b_10	60.44	25.22	0.27		6.73	7.37	0.67	100.70	0.32	762	1	100
WH2b_11	60.40	24.62	0.26		6.42	7.42	0.61	99.72	0.31	757	1	110
WH2b_12	60.81	24.91	0.25		6.58	7.65	0.61	100.81	0.31	756	1	120
WH2b_13	61.37	24.61	0.33		6.23	7.38	0.69	100.61	0.31	751	1	130
WH2b_14	60.77	24.20	0.24		6.42	7.26	0.70	99.58	0.31	757	1	140
WH2b_15	61.19	24.47	0.26		6.35	7.37	0.76	100.39	0.31	752	1	150
WH2b_17	61.60	24.92	0.20		6.67	7.41	0.70	101.49	0.32	759	1	170
WH2b_18	60.86	25.09	0.21		6.58	7.75	0.66	101.14	0.31	754	1	180
WH2b_19	61.08	25.14	0.24		6.76	7.60	0.68	101.50	0.32	759	1	190
WH2b_20	60.68	24.66	0.29		6.68	7.74	0.72	100.76	0.31	754	1	200
WH2b_21	61.61	24.47	0.26		6.35	7.48	0.66	100.83	0.31	753	1	210
WH2b_23	62.54	24.65	0.20		5.96	7.63	0.73	101.71	0.29	741	1	230
WH2b_26	62.86	24.15	0.25		5.71	7.81	0.88	101.67	0.27	730	1	260
WH2b_27	62.37	23.88	0.16		5.31	7.91	0.89	100.51	0.26	718	1	270
WH2b_28	61.36	24.60	0.24		6.37	7.69	0.75	101.01	0.30	748	1	280
WH2b_29	61.84	24.63	0.30		6.53	7.66	0.73	101.68	0.31	752	1	290
WH2b_30	61.62	24.53	0.25		6.40	7.60	0.76	101.16	0.30	750	1	300
WH2b_33	62.00	25.08	0.21		6.56	7.36	0.69	101.90	0.32	758	1	330
WH2b_36	60.85	25.30	0.30		6.86	7.51	0.65	101.48	0.32	763	1	360
WH2b_37	60.79	25.17	0.13		6.82	7.42	0.67	100.99	0.32	763	1	370
WH2b_38	60.79	25.17	0.13		6.82	7.42	0.67	100.99	0.32	763	1	380
WH2b_39	60.25	25.50	0.28		7.53	7.22	0.58	101.35	0.35	780	1	390
WH2b_40	59.56	25.49	0.23		7.08	7.32	0.57	100.24	0.34	771	1	400
WH2b_41	59.15	25.52	0.24		7.21	7.23	0.61	99.95	0.34	774	1	410
WH2b_42	60.29	25.20	0.27		7.17	7.35	0.61	100.90	0.34	771	1	420
WH2b_43	60.41	25.02	0.17		7.08	7.15	0.60	100.44	0.34	773	1	430
WH2b_44	60.69	25.51	0.22		6.97	7.35	0.67	101.40	0.33	767	1	440
WH2b_45	60.85	25.13	0.26		6.92	7.34	0.66	101.16	0.33	766	1	450
WH2b_46	60.34	25.44	0.26		7.50	7.08	0.62	101.24	0.36	780	1	460
WH2b_47	60.20	25.95	0.26		7.53	7.06	0.51	101.50	0.36	784	1	470
WH2b_48	59.36	26.00	0.24		7.69	6.97	0.60	100.86	0.37	785	1	480
WH2b_49	60.16	25.68	0.19		7.28	7.39	0.56	101.26	0.34	774	1	490
WH2b_51	59.06	25.48	0.24		7.30	7.41	0.61	100.10	0.34	773	1	510
WH2b_52	59.68	25.49	0.20		7.33	7.33	0.64	100.66	0.34	774	1	520
WH2b_53	58.10	25.29	0.18		7.66	7.12	0.54	98.89	0.36	785	1	530
WH2b_54	58.94	25.83	0.24		7.76	6.80	0.53	100.10	0.38	791	1	540
WH2b_55	59.58	25.85	0.24		7.89	6.89	0.56	101.00	0.38	790	1	550
WH2b_56	60.19	26.53	0.18		7.78	6.69	0.56	101.93	0.38	792	1	560
WH2b_57	59.12	26.67	0.19		7.69	6.81	0.56	101.04	0.37	789	1	570
WH2b_59	59.25	26.72	0.22		7.63	6.71	0.49	101.02	0.37	791	1	590
WH2b_60	59.09	26.87	0.20		7.97	6.70	0.48	101.30	0.39	796	1	600
WH2b_61	58.68	27.07	0.23		8.05	6.64	0.46	101.14	0.39	799	1	610
WH2b_62	57.76	27.07	0.28		8.50	6.28	0.46	100.34	0.42	809	1	620
WH2b_63	57.58	27.17	0.21		8.46	6.54	0.42	100.38	0.41	807	1	630
WH2b_64	57.70	26.91	0.21		8.46	6.51	0.41	100.20	0.41	807	1	640
WH2b_65	58.04	27.11	0.22		8.89	6.24	0.49	100.97	0.43	813	1	650
WH2b_66	57.33	27.17	0.18		8.99	6.29	0.40	100.35	0.43	816	1	660
WH2b_67	57.38	27.36	0.17		8.69	6.28	0.47	100.34	0.42	811	1	670
WH2b_68	56.98	27.04	0.17		8.78	6.43	0.42	99.82	0.42	812	1	680
WH2b_69	58.81	26.59	0.25		7.76	6.85	0.58	100.84	0.37	788	1	690
WH2b_70	58.56	26.74	0.18		8.04	6.66	0.45	100.62	0.39	799	1	700

Table A3.6 continued

Sample	SiO_2	Al_2O_3	FeO	MgO	CaO	Na_2O	K_2O	Total	XAn	T (°C)	G	Dist. (μm)
WH2b_75	57.21	27.40	0.24		9.10	6.23	0.45	100.63	0.44	816	1	750
WH2b_76	56.87	27.53	0.23		9.00	6.07	0.40	100.10	0.44	819	1	760
WH2b_77	57.44	27.07	0.21		8.48	6.53	0.42	100.14	0.41	807	1	770
WH2b_78	57.24	27.27	0.27		8.74	6.21	0.46	100.18	0.43	813	1	780
WH2b_79	57.13	26.99	0.34		8.46	6.31	0.46	99.70	0.41	808	1	790
WH2b_80	57.98	27.02	0.28		8.49	6.44	0.41	100.62	0.41	809	1	800
WH2b_81	57.27	27.57	0.18		8.93	6.22	0.41	100.57	0.43	816	1	810
WH2b_82	57.37	27.23	0.25		8.52	6.35	0.42	100.14	0.42	810	1	820
WH2b_83	57.03	27.80	0.18		9.03	6.04	0.44	100.52	0.44	818	1	830
WH2b_84	57.09	27.72	0.26		8.92	6.20	0.41	100.60	0.43	816	1	840
WH2b_85	55.89	28.28	0.23		9.55	5.74	0.38	100.07	0.47	828	1	850
WH2b_86	56.46	27.60	0.35		9.13	6.20	0.39	100.13	0.44	819	1	860
WH2b_87	56.02	27.54	0.26		9.09	6.12	0.39	99.42	0.44	819	1	870
WH2b_88	55.03	28.64	0.20		10.14	5.52	0.31	99.84	0.49	836	1	880
WH2b_89	56.02	28.17	0.19		9.66	5.66	0.39	100.09	0.47	829	1	890
WH2b_91	56.31	28.56	0.24		10.10	5.65	0.37	101.22	0.49	832	1	910
WH2b_92	58.04	27.70	0.19		8.78	6.32	0.45	101.48	0.42	812	1	920
WH2b_93	59.80	25.92	0.26		6.93	7.14	0.71	100.76	0.33	768	1	930
WH2b_96	56.84	28.04	0.18		9.70	6.10	0.37	101.24	0.46	825	1	960
WH2b_97	57.88	27.80	0.26		9.54	5.88	0.36	101.72	0.46	827	1	970
WH2b_100	56.68	27.91	0.30		9.54	5.88	0.40	100.72	0.46	825	1	1000
WH2b_101	57.43	27.26	0.16		9.05	6.35	0.45	100.69	0.43	814	1	1010
WH2b_103	58.11	27.37	0.29		8.94	6.28	0.40	101.39	0.43	816	1	1030
WH2b_104	58.71	27.18	0.20		8.43	6.73	0.51	101.76	0.40	801	1	1040
WH2b_105	59.45	26.87	0.28		8.11	6.57	0.47	101.75	0.39	800	1	1050
WH2b_110	56.96	26.49	0.24		8.74	6.09	0.47	98.99	0.43	814	1	1100
WH2b_111	58.26	26.72	0.18		8.36	6.73	0.51	100.76	0.40	800	1	1110
WH2b_112	58.69	26.43	0.23		7.92	6.86	0.56	100.70	0.38	791	1	1120
WH2b_113	59.23	26.26	0.24		7.42	6.97	0.58	100.70	0.36	782	1	1130
WH2b_114	58.91	26.16	0.23		7.32	7.13	0.58	100.32	0.35	778	1	1140
WH2b_115	59.60	26.01	0.21		7.19	7.06	0.59	100.66	0.35	776	1	1150
WH2b_116	60.69	25.44	0.19		6.65	7.37	0.68	101.02	0.32	760	1	1160
WH2b_117	61.35	25.05	0.22		6.43	7.41	0.65	101.10	0.31	756	1	1170
WH2b_118	60.48	25.22	0.17		6.59	7.27	0.65	100.38	0.32	761	1	1180
WH2b_119	60.89	24.74	0.28		5.92	7.53	0.78	100.13	0.29	741	1	1190
WH2b_120	59.79	25.73	0.24		7.23	7.20	0.58	100.77	0.34	775	1	1200
WH2b_121	59.91	25.81	0.21		6.82	7.27	0.64	100.66	0.33	766	1	1210
WH2b_122	60.66	24.88	0.19		6.06	7.65	0.70	100.14	0.29	744	1	1220
WH2b_123	60.06	24.76	0.20		6.17	7.51	0.82	99.52	0.30	745	1	1230
WH2b_124	61.33	24.75	0.23		5.89	7.76	0.83	100.79	0.28	735	1	1240
WH2b_126	60.55	25.01	0.23		6.17	7.42	0.66	100.04	0.30	750	1	1260
WH2b_127	59.70	25.13	0.22		6.59	7.33	0.72	99.69	0.32	759	1	1270
WH2b_128	59.87	25.29	0.31		6.39	7.28	0.73	99.87	0.31	755	1	1280
WH2b_129	60.74	25.03	0.23		6.25	7.48	0.71	100.43	0.30	750	1	1290
WH2b_130	60.38	25.23	0.23		6.50	7.43	0.75	100.51	0.31	755	1	1300
WH2b_131	60.16	25.47	0.26		6.74	7.32	0.66	100.60	0.32	763	1	1310
WH2b_132	60.22	25.49	0.30		6.60	7.22	0.71	100.54	0.32	760	1	1320
WH2b_133	60.46	25.10	0.15		6.40	7.40	0.72	100.22	0.31	754	1	1330
WH2b_135	61.29	25.54	0.24		6.69	7.41	0.78	101.95	0.32	758	1	1350
WH2b_136	60.31	25.66	0.27		6.78	7.47	0.71	101.20	0.32	760	1	1360
WH2d_1	58.74	25.04			6.50	7.03	0.64	97.95	0.33	763	1	20
WH2d_2	58.32	25.05			6.55	7.06	0.65	97.64	0.33	763	1	30
WH2d_3	57.24	25.37			7.10	6.83	0.54	97.07	0.35	780	1	40
WH2d_5	58.42	25.00			6.35	7.19	0.60	97.55	0.32	759	1	60
WH2d_6	58.54	24.96			6.25	7.25	0.64	97.63	0.31	755	1	70
WH2d_7	58.70	24.73			6.65	6.94	0.68	97.69	0.33	766	1	80

Table A3.6 continued

Sample	SiO_2	Al_2O_3	FeO	MgO	CaO	Na_2O	K_2O	Total	XAn	T (°C)	G	Dist. (μm)
WH2d_11	58.79	24.70			6.15	7.67	0.77	98.09	0.29	744	1	120
WH2d_12	58.70	24.91			6.25	7.20	0.67	97.73	0.31	755	1	130
WH2d_13	59.19	24.68			6.35	7.23	0.77	98.23	0.31	754	1	140
WH2d_14	59.34	25.01			6.05	7.37	0.64	98.41	0.30	749	1	150
WH2d_15	59.10	24.96			6.28	7.21	0.66	98.20	0.31	756	1	160
WH2d_16	59.01	24.84			6.37	7.24	0.74	98.20	0.31	755	1	170
WH2d_17	58.09	25.52			6.61	7.20	0.56	97.98	0.33	765	1	180
WH2d_18	58.08	24.90			6.53	7.41	0.72	97.63	0.31	756	1	190
WH2d_19	58.01	25.01			6.47	7.13	0.66	97.28	0.32	761	1	200
WH2d_20	58.60	24.84			6.45	7.30	0.70	97.88	0.31	757	1	210
WH2d_21	61.43	25.46	0.34		6.79	7.12	0.61	101.75	0.33	768	1	220
WH2d_22	60.10	25.01	0.18		6.32	7.50	0.71	99.82	0.30	751	1	230
WH2d_23	60.65	24.82	0.19		5.74	7.65	0.78	99.83	0.28	735	1	240
WH2d_24	60.09	25.24	0.27		6.19	7.51	0.74	100.03	0.30	747	1	250
WH2d_25	60.21	25.01	0.20		6.25	7.41	0.72	99.79	0.30	751	1	260
WH2d_26	59.94	24.98	0.25		6.44	7.62	0.67	99.89	0.31	753	1	270
WH2d_27	59.54	25.68	0.25		7.05	6.98	0.55	100.04	0.35	776	1	280
WH2d_28	53.99	29.72	0.28		11.68	4.80	0.26	100.73	0.57	846	1	290
WH2d_29	53.69	29.70	0.18		11.77	4.98	0.23	100.55	0.56	847	1	300
WH2d_30	54.07	29.65	0.25		11.51	4.91	0.22	100.62	0.56	847	1	310
WH2d_31	53.28	29.82	0.21		11.47	4.73	0.29	99.81	0.56	845	1	320
WH2d_32	54.73	29.27	0.20		10.70	5.09	0.28	100.27	0.53	842	1	330
WH2d_33	52.07	30.64	0.26		12.46	4.28	0.20	99.92	0.61	848	1	340
WH2d_34	55.48	28.70	0.26		10.30	5.45	0.34	100.52	0.50	836	1	350
WH2d_36	59.28	26.06	0.19		7.48	7.05	0.57	100.62	0.36	782	1	370
WH2d_38	57.67	25.16	0.53		6.38	6.96	0.47	97.17	0.33	767	1	390
WH2d_39	55.48	27.43	0.26		9.13	5.79	0.37	98.47	0.46	824	1	400
WH2d_44	58.57	26.23	0.25		7.33	6.84	0.49	99.70	0.36	785	1	450
WH2d_45	60.09	25.30	0.31		6.60	7.45	0.66	100.40	0.32	758	1	460
WH2d_46	58.52	24.84	0.35		6.28	7.26	0.63	97.87	0.31	756	1	470
WH2d_47	60.18	25.48	0.26		6.55	7.38	0.70	100.56	0.32	758	1	480
WH2d_48	60.55	25.28	0.26		6.55	7.19	0.72	100.54	0.32	760	1	490
WH2d_49	58.33	26.05	0.24		7.58	6.79	0.53	99.51	0.37	788	1	500
WH2d_50	55.44	28.53	0.24		10.87	4.93	0.28	100.29	0.54	844	1	510
WH2d_52	59.29	26.02	0.28		6.94	7.07	0.58	100.18	0.34	773	1	530
WH2d_53	58.73	26.66	0.22		7.79	6.79	0.51	100.70	0.38	792	1	540
WH2d_54	56.05	27.82	0.24		9.55	5.94	0.33	99.93	0.46	827	1	550
WH2d_55	53.99	29.96	0.21		11.43	4.74	0.27	100.59	0.56	846	1	560
WH2d_56	54.03	29.67	0.23		11.32	4.94	0.28	100.46	0.55	845	1	570
WH2d_57	53.62	29.92	0.22		11.89	4.80	0.24	100.69	0.57	847	1	580
WH2d_58	54.46	29.32	0.26		10.75	5.27	0.27	100.32	0.52	842	1	590
WH2d_59	60.77	24.92	0.24		5.87	7.63	0.71	100.14	0.29	740	1	600
WH2d_60	59.91	24.89	0.22		6.31	7.47	0.72	99.52	0.30	751	1	610
WH2d_61	60.25	25.28	0.26		6.35	7.34	0.60	100.08	0.31	757	1	620
WH2d_62	59.04	25.76	0.21		7.11	6.72	0.60	99.43	0.36	780	1	630
WH2d_63	60.53	25.49	0.28		6.86	7.26	0.56	100.98	0.33	769	1	640
WH2d_64	60.66	25.40	0.22		6.64	7.51	0.69	101.12	0.32	757	1	650
WH2d_65	61.08	25.02	0.28		6.31	7.10	0.71	100.50	0.32	757	1	660
WH2d_66	60.55	25.32	0.20		6.41	7.25	0.64	100.36	0.32	758	1	670
WH2d_67	60.71	25.05	0.29		6.24	7.43	0.73	100.45	0.30	750	1	680
WH2d_69	61.17	25.33	0.29		6.52	7.23	0.73	101.27	0.32	758	1	700
WH2d_70	61.69	25.42	0.28		6.51	7.21	0.63	101.74	0.32	761	1	710
WH2d_71	60.52	25.40	0.23		6.46	7.19	0.65	100.45	0.32	760	1	720
WH2d_72	59.97	25.04	0.31		6.41	7.41	0.69	99.82	0.31	755	1	730
WH2d_73	59.66	25.09	0.30		6.48	7.36	0.68	99.57	0.31	757	1	740
WH2d_74	59.25	25.19	0.20		6.70	7.21	0.70	99.24	0.33	763	1	750
WH2d_75	59.77	25.51	0.27		6.13	7.39	0.62	99.68	0.30	751	1	760

Table A3.6 continued

Sample	SiO_2	Al_2O_3	FeO	MgO	CaO	Na_2O	K_2O	Total	XAn	T (°C)	G	Dist. (μm)
WH2d_80	59.81	25.51	0.24		6.68	7.32	0.75	100.30	0.32	760	1	810
WH2d_81	59.65	25.45	0.25		6.77	7.29	0.68	100.08	0.33	763	1	820
WH2d_82	60.04	25.35	0.29		6.31	7.45	0.77	100.22	0.30	750	1	830
WH2d_83	59.69	25.91	0.26		6.62	7.19	0.65	100.33	0.32	763	1	840
WH2d_84	59.55	25.58	0.23		6.57	7.26	0.73	99.91	0.32	759	1	850
WH2f_30	57.51	26.99	0.21		8.00	6.86	0.52	100.08	0.38	794	2	20
WH2f_31	58.67	25.93	0.30		6.98	7.08	0.59	99.54	0.34	773	2	30
WH2f_32	58.36	26.47	0.20		7.98	6.70	0.47	100.17	0.39	797	2	40
WH2f_33	60.05	25.93	0.34		6.77	7.09	0.57	100.75	0.33	769	2	50
WH2f_34	60.17	25.90	0.24		6.94	7.21	0.56	101.01	0.34	771	2	60
WH2f_35	58.51	25.43	0.23		6.76	7.04	0.59	98.57	0.33	769	2	70
WH2f_36	59.88	25.65	0.26		6.42	7.06	0.69	99.96	0.32	760	2	80
WH2f_37	59.63	25.73	0.20		6.65	7.51	0.72	100.43	0.32	757	2	90
WH2f_38	59.36	25.64	0.24		6.70	7.47	0.70	100.11	0.32	759	2	100
WH2f_39	59.35	25.51	0.17		6.63	7.40	0.61	99.67	0.32	761	2	110
WH2f_40	59.71	25.57	0.30		6.50	7.43	0.67	100.17	0.31	757	2	120
WH2f_41	59.24	25.18	0.23		6.41	7.37	0.67	99.10	0.31	756	2	130
WH2f_42	59.75	25.71	0.19		6.66	7.36	0.64	100.31	0.32	762	2	140
WH2f_43	60.15	25.92	0.25		6.83	7.40	0.66	101.21	0.33	763	2	150
WH2f_46	59.21	25.59	0.24		6.67	7.44	0.66	99.82	0.32	760	2	180
WH2f_47	59.34	25.48	0.26		6.43	7.29	0.65	99.46	0.32	758	2	190
WH2f_48	59.11	25.31	0.25		6.28	7.69	0.70	99.34	0.30	748	2	200
WH2f_49	58.96	25.80	0.15		6.61	7.31	0.73	99.58	0.32	759	2	210
WH2f_50	59.99	25.37	0.24		6.22	7.26	0.68	99.75	0.31	753	2	220
WH2f_51	59.81	25.62	0.20		6.53	7.42	0.63	100.20	0.32	758	2	230
WH2f_52	58.98	25.79	0.25		7.10	6.99	0.53	99.64	0.35	778	2	240
WH2f_53	60.21	26.19	0.17		6.91	7.20	0.66	101.33	0.33	768	2	250
WH2f_54	59.77	26.12	0.31		6.80	7.28	0.66	100.93	0.33	765	2	260
WH2f_55	59.72	26.06	0.25		6.72	7.20	0.62	100.58	0.33	765	2	270
WH2f_56	59.06	25.91	0.33		6.58	7.34	0.63	99.85	0.32	760	2	280
WH2f_57	58.70	25.66	0.25		6.59	7.31	0.63	99.13	0.32	761	2	290
WH2f_58	58.86	25.86	0.22		7.01	7.24	0.59	99.78	0.34	771	2	300
WH2f_59	58.93	26.15	0.27		6.78	7.34	0.61	100.09	0.33	765	2	310
WH2f_60	58.22	25.72	0.32		6.77	7.30	0.61	98.94	0.33	765	2	320
WH2f_61	59.63	25.65	0.30		6.76	7.14	0.64	100.12	0.33	767	2	330
WH2f_62	60.09	25.91	0.30		6.75	7.31	0.70	101.05	0.32	762	2	340
WH2f_63	58.88	25.13	0.24		6.49	7.51	0.65	98.89	0.31	756	2	350
WH2f_64	59.85	25.97	0.26		6.56	7.47	0.61	100.73	0.32	759	2	360
WH2f_65	59.89	25.76	0.19		6.86	7.29	0.65	100.65	0.33	766	2	370
WH2f_66	59.90	25.72	0.28		6.74	7.47	0.58	100.68	0.32	763	2	380
WH2f_67	60.42	25.47	0.28		6.18	7.41	0.66	100.41	0.30	751	2	390
WH2f_68	59.70	25.69	0.23		6.31	7.37	0.66	99.96	0.31	754	2	400
WH2f_69	59.12	25.41	0.34		6.26	7.32	0.67	99.12	0.31	754	2	410
WH2f_70	59.10	25.26	0.26		5.94	7.40	0.72	98.67	0.29	744	2	420
WH2f_71	60.37	25.24	0.26		5.99	7.43	0.86	100.15	0.29	741	2	430
WH2f_72	60.48	25.13	0.22		6.08	7.44	0.76	100.11	0.30	746	2	440
WH2f_73	60.39	25.60	0.25		6.38	7.58	0.73	100.92	0.30	751	2	450
WH2f_74	60.01	25.47	0.28		6.41	7.47	0.71	100.35	0.31	753	2	460
WH2f_75	59.73	26.01	0.24		6.97	7.30	0.60	100.84	0.33	769	2	470
WH2f_76	60.01	25.80	0.21		6.53	7.45	0.74	100.73	0.31	755	2	480
WH2f_77	60.50	26.02	0.19		6.65	7.45	0.61	101.42	0.32	761	2	490
WH2f_78	58.65	25.54	0.30		6.59	7.11	0.67	98.86	0.33	763	2	500
WH2f_79	60.09	25.65	0.23		6.30	7.38	0.67	100.33	0.31	753	2	510
WH2f_80	59.42	25.78	0.24		6.50	7.30	0.68	99.91	0.32	758	2	520
WH2f_81	59.98	25.62	0.38		6.49	7.53	0.70	100.69	0.31	754	2	530
WH2f_82	60.69	25.73	0.25		6.26	7.42	0.71	101.06	0.30	751	2	540

Table A3.6 continued

Sample	SiO_2	Al_2O_3	FeO	MgO	CaO	Na_2O	K_2O	Total	Xan	T (°C)	G	Dist. (μm)
WH2f_88	59.95	26.11	0.30		6.85	7.03	0.59	100.82	0.34	771	2	600
WH2f_89	59.53	26.31	0.22		6.85	7.33	0.64	100.87	0.33	765	2	610
WH2f_90	60.86	25.76	0.27		6.56	7.45	0.63	101.53	0.32	758	2	620
WH2f_91	60.80	25.53	0.14		6.04	7.58	0.77	100.86	0.29	743	2	630
WH2f_92	59.69	26.41	0.25		6.78	7.35	0.60	101.08	0.33	765	2	640
WH2f_93	60.44	26.02	0.27		6.57	7.25	0.66	101.19	0.32	761	2	650
WH2f_94	60.90	25.67	0.24		6.38	7.42	0.59	101.20	0.31	756	2	660
WH2f_95	60.83	25.33	0.28		6.33	7.60	0.69	101.06	0.30	750	2	670
WH2f_96	59.52	24.99	0.39		6.14	7.20	0.68	98.93	0.31	753	2	680
WH2f_97	59.14	25.62	0.26		6.78	7.26	0.62	99.68	0.33	766	2	690
WH2f_99	59.74	26.06	0.26		6.60	7.22	0.68	100.55	0.32	761	2	710
WH2g_x2	63.43	24.21	0.24		5.62	7.53	0.72	101.74	0.28	735	3	30
WH2g_x3	61.90	24.74	0.17		5.96	7.48	0.75	100.99	0.29	743	3	40
WH2g_x4	60.04	24.85	0.15		6.52	6.98	0.48	99.03	0.33	769	3	50
WH2g_x5	62.56	24.66	0.21		6.20	7.54	0.66	101.83	0.30	749	3	60
WH2g_x7	62.05	24.77	0.16		6.28	7.41	0.67	101.33	0.31	753	3	80
WH2g_x8	63.12	24.79	0.33		6.28	6.81	0.65	101.97	0.32	762	3	90
WH2g_x9	62.54	24.74	0.13		6.01	7.51	0.62	101.55	0.30	747	3	100
WH2g_x10	62.45	24.62	0.29		5.97	7.36	0.66	101.35	0.30	747	3	110
WH2g_x11	61.67	24.73	0.29		5.98	7.31	0.60	100.59	0.30	749	3	120
WH2g_x13	62.50	24.53	0.19		6.26	7.32	0.64	101.44	0.31	754	3	140
WH2g_x14	59.75	24.38	0.22		6.13	7.36	0.61	98.44	0.30	752	3	150
WH2g_x15	62.98	24.43	0.27		5.88	7.56	0.71	101.83	0.29	741	3	160
WH2g_x16	61.84	25.31	0.21		6.62	6.99	0.62	101.58	0.33	767	3	170
WH2g_x17	61.59	26.18	0.19		6.86	6.59	0.51	101.93	0.35	780	3	180
WH2g_x19	60.36	24.17	0.17		6.13	7.19	0.64	98.65	0.31	754	3	200
WH2g_x20	61.58	24.95	0.20		6.35	7.08	0.57	100.72	0.32	762	3	210
WH2g_x30	61.89	25.16	0.15		6.58	7.06	0.57	101.41	0.33	766	3	320
WH3b_4	60.54	24.98	0.17		5.88	8.26	0.69	100.51	0.27	731	3	20
WH3b_5	60.22	25.02	0.18		6.02	8.09	0.72	100.25	0.28	736	3	30
WH3b_6	61.60	24.95	0.20		5.91	8.20	0.66	101.52	0.27	733	3	40
WH3b_7	60.89	24.92	0.17		5.93	8.25	0.73	100.88	0.27	731	3	50
WH3b_8	59.76	25.68	0.21		6.63	7.71	0.61	100.60	0.31	756	3	60
WH3b_9	59.72	25.56	0.19		6.50	7.72	0.65	100.34	0.31	753	3	70
WH3b_10	61.39	24.89	0.23		6.55	7.78	0.65	101.48	0.31	753	3	80
WH3b_11	61.22	25.14	0.22		6.39	7.89	0.60	101.46	0.30	749	3	90
WH3b_12	60.98	25.09	0.19		6.56	7.64	0.67	101.12	0.31	755	3	100
WH3b_13	60.97	25.24	0.20		6.43	7.57	0.62	101.04	0.31	754	3	110
WH3b_14	61.36	25.33	0.25		6.42	7.65	0.65	101.66	0.31	752	3	120
WH3b_15	61.41	25.21	0.24		6.27	7.79	0.73	101.66	0.30	745	3	130
WH3b_16	61.97	24.78	0.22		5.79	8.03	0.67	101.46	0.27	733	3	140
WH3b_17	62.10	24.78	0.21		6.16	8.00	0.66	101.89	0.29	741	3	150
WH3b_18	61.52	24.88	0.32		6.15	7.77	0.66	101.30	0.29	745	3	160
WH3b_19	61.60	24.67	0.30		6.00	7.92	0.72	101.21	0.28	738	3	170
WH3b_20	61.56	24.75	0.12		6.12	7.87	0.70	101.11	0.29	742	3	180
WH3b_21	61.66	24.93	0.22		6.16	7.59	0.65	101.20	0.30	748	3	190
WH3b_22	61.35	25.45	0.24		6.36	7.71	0.73	101.83	0.30	748	3	200
WH3b_26	61.82	24.99	0.18		6.11	7.89	0.67	101.65	0.29	742	3	240
WH3b_27	61.74	24.59	0.25		5.97	7.91	0.72	101.17	0.28	737	3	250
WH3b_30	61.37	25.21	0.21		6.52	7.82	0.63	101.77	0.30	752	3	280
WH3b_31	60.54	25.87	0.16		7.27	7.36	0.64	101.83	0.34	772	3	290
WH3b_34	59.98	25.87	0.19		7.06	7.54	0.49	101.14	0.33	770	3	320
WH3b_36	57.12	27.42	0.24		8.97	6.58	0.38	100.71	0.42	813	3	340
WH3b_37	58.86	26.79	0.22		8.32	6.76	0.42	101.36	0.40	802	3	350
WH3b_38	59.05	26.66	0.23		8.38	6.71	0.42	101.46	0.40	803	3	360

Table A3.6 continued

Sample	SiO_2	Al_2O_3	FeO	MgO	CaO	Na_2O	K_2O	Total	Xan	T (°C)	G	Dist. (μm)
WH3b_42	61.45	25.15	0.23		6.35	7.74	0.66	101.57	0.30	749	3	400
WH3b_43	61.58	25.13	0.23		6.21	7.87	0.64	101.65	0.29	745	3	410
WH3b_44	61.88	24.98	0.18		6.07	7.83	0.77	101.70	0.29	740	3	420
WH3b_45	62.42	24.75	0.22		5.93	8.04	0.62	101.96	0.28	737	3	430
WH3b_46	61.95	24.76	0.19		6.03	7.91	0.64	101.49	0.29	741	3	440
WH3b_47	60.72	25.70	0.18		6.83	7.54	0.53	101.50	0.32	765	3	450
WH3b_48	60.55	25.77	0.21		6.62	7.80	0.55	101.49	0.31	756	3	460
WH3b_49	60.97	24.60	0.17		6.07	7.71	0.59	100.12	0.29	746	3	470
WH3b_50	60.38	24.53	0.21		6.01	7.86	0.70	99.68	0.29	739	3	480
WH3b_51	60.71	24.43	0.25		5.83	7.73	0.68	99.62	0.28	738	3	490
WH3b_52	61.47	24.14	0.18		5.52	7.80	0.71	99.82	0.27	729	3	500
WH3b_53	61.88	23.50	0.21		4.80	8.15	0.83	99.37	0.23	703	3	510
WH3b_54	62.60	23.42	0.26		4.77	8.13	0.91	100.09	0.23	701	3	520
WH3b_55	63.10	23.36	0.14		4.74	7.96	0.95	100.25	0.23	702	3	530
WH3c_7	60.01	24.87	0.20		6.33	7.17	0.59	99.17	0.32	759	2	20
WH3c_8	60.53	24.99	0.23		6.40	7.31	0.64	100.09	0.31	757	2	30
WH3c_9	59.94	25.19	0.32		6.65	7.12	0.55	99.76	0.33	767	2	40
WH3c_10	60.56	24.39	0.29		6.23	7.29	0.68	99.43	0.31	753	2	50
WH3c_11	60.12	24.84	0.21		6.58	7.31	0.60	99.66	0.32	762	2	60
WH3c_12	59.21	24.92	0.19		6.27	7.21	0.61	98.41	0.31	757	2	70
WH3c_13	59.08	25.03	0.25		6.59	7.16	0.60	98.70	0.33	764	2	80
WH3c_14	59.40	25.02	0.25		6.51	7.32	0.60	99.11	0.32	760	2	90
WH3c_15	58.34	25.33	0.20		6.99	7.07	0.54	98.46	0.34	774	2	100
WH3c_16	59.12	24.61	0.25		6.41	7.14	0.65	98.18	0.32	760	2	110
WH3c_17	59.43	24.84	0.25		6.07	7.38	0.70	98.67	0.30	748	2	120
WH3c_18	57.91	24.29	0.19		6.22	7.15	0.68	96.45	0.31	755	2	130
WH3c_19	58.89	25.16	0.27		6.83	7.01	0.61	98.77	0.34	770	2	140
WH3c_20	59.17	24.57	0.36		6.07	7.24	0.66	98.07	0.30	751	2	150
WH3c_21	59.35	24.95	0.17		6.14	7.50	0.69	98.81	0.30	748	2	160
WH3c_22	59.06	24.87	0.23		6.47	7.39	0.65	98.68	0.31	757	2	170
WH3c_23	58.58	24.93	0.23		6.47	7.18	0.63	98.02	0.32	761	2	180
WH3c_24	58.74	25.03	0.21		6.84	6.98	0.55	98.35	0.34	773	2	190
WH3c_25	58.82	25.34	0.19		7.22	6.90	0.60	99.07	0.35	779	2	200
WH3c_26	58.21	25.74	0.34		7.56	6.71	0.49	99.04	0.37	790	2	210
WH3c_27	57.97	25.98	0.32		7.40	6.65	0.47	98.79	0.37	789	2	220
WH3c_28	57.75	25.82	0.30		7.46	6.70	0.50	98.53	0.37	788	2	230
WH3c_29	58.13	25.98	0.28		7.35	6.74	0.51	98.99	0.36	786	2	240
WH3c_30	58.23	25.71	0.18		7.15	6.82	0.58	98.68	0.35	780	2	250
WH3c_31	57.82	25.70	0.17		7.36	6.87	0.54	98.46	0.36	783	2	260
WH3c_32	57.72	25.69	0.32		7.26	6.82	0.50	98.32	0.36	783	2	270
WH3c_33	58.50	25.28	0.22		7.21	6.81	0.51	98.53	0.36	783	2	280
WH3c_34	59.94	25.10	0.19		6.67	7.24	0.57	99.71	0.33	765	2	290
WH3c_35	60.16	24.63	0.22		6.16	7.40	0.66	99.23	0.30	751	2	300
WH3c_36	60.42	24.79	0.37		6.17	7.28	0.69	99.72	0.31	752	2	310
WH3c_37	59.73	24.61	0.23		6.15	7.37	0.65	98.74	0.30	751	2	320
WH3c_38	59.95	24.63	0.17		6.16	7.42	0.68	99.01	0.30	750	2	330
WH3c_39	59.50	24.77	0.18		6.11	7.46	0.62	98.64	0.30	750	2	340
WH3c_41	58.99	24.61	0.21		6.33	7.12	0.68	97.93	0.32	758	2	360
WH3c_42	60.55	25.05	0.19		6.67	6.92	0.54	99.92	0.34	771	2	370
WH3c_43	60.59	25.07	0.21		6.57	7.01	0.60	100.04	0.33	766	2	380
WH3c_44	60.31	25.11	0.19		6.67	6.96	0.56	99.80	0.33	770	2	390
WH3c_45	60.48	25.13	0.29		7.00	7.07	0.58	100.54	0.34	773	2	400
WH3c_46	61.26	24.80	0.28		6.49	7.10	0.65	100.59	0.32	762	2	410
WH3c_47	60.74	24.55	0.31		6.44	7.12	0.53	99.69	0.32	763	2	420
WH3c_48	60.49	24.93	0.26		6.90	7.14	0.52	100.24	0.34	772	2	430
WH3c_49	60.20	25.01	0.16		6.96	7.04	0.53	99.91	0.34	774	2	440

Table A3.6 continued

Sample	SiO_2	Al_2O_3	FeO	MgO	CaO	Na_2O	K_2O	Total	Xan	T (°C)	G	Dist. (μm)
WH3c_53	60.29	24.86	0.25		6.40	7.37	0.57	99.74	0.31	758	2	480
WH3c_54	61.46	24.41	0.31		6.17	7.43	0.65	100.43	0.30	751	2	490
WH3c_55	61.70	24.20	0.25		5.88	7.32	0.71	100.05	0.29	744	2	500
WH3c_56	61.18	24.69	0.18		6.58	7.24	0.58	100.45	0.32	763	2	510
WH3c_57	61.58	24.46	0.26		6.34	7.28	0.59	100.51	0.31	758	2	520
WH3c_58	60.05	24.98	0.21		6.81	7.24	0.50	99.79	0.33	770	2	530
WH3d_1	58.75	25.11	0.28		6.59	7.66	0.57	98.96	0.31	757	2	20
WH3d_2	59.73	25.76	0.23		6.64	7.68	0.63	100.67	0.31	757	2	30
WH3d_3	61.02	24.66	0.29		5.73	8.34	0.80	100.84	0.26	724	2	40
WH3d_4	60.64	24.91	0.23		5.71	7.98	0.74	100.21	0.27	730	2	50
WH3d_5	59.69	25.39	0.20		6.52	7.66	0.63	100.09	0.31	754	2	60
WH3d_7	58.61	26.44	0.26		7.66	7.28	0.52	100.77	0.36	783	2	70
WH3d_8	58.23	26.75	0.23		7.97	7.12	0.56	100.85	0.37	788	2	80
WH3d_9	57.56	27.23	0.25		8.45	6.56	0.44	100.49	0.41	806	2	90
WH3d_10	58.03	26.93	0.24		8.33	6.78	0.47	100.76	0.39	800	2	100
WH3d_11	59.57	25.30	0.23		7.31	7.24	0.64	100.30	0.35	774	2	110
WH3d_12	60.04	25.62	0.27		6.84	7.46	0.63	100.86	0.32	764	2	120
WH3d_13	59.29	25.46	0.24		6.53	7.92	0.61	100.04	0.30	751	2	130
WH3d_14	59.52	25.49	0.28		6.43	7.67	0.63	100.03	0.31	753	2	140
WH3d_15	59.06	25.75	0.24		6.84	7.36	0.64	99.88	0.33	765	2	150
WH3d_16	59.75	25.60	0.31		6.92	7.58	0.62	100.78	0.32	764	2	160
WH3d_17	60.27	25.52	0.27		6.99	7.44	0.57	101.05	0.33	768	2	170
WH3d_18	59.82	25.55	0.31		6.89	7.33	0.61	100.51	0.33	767	2	180
WH3d_19	59.52	25.82	0.19		7.06	7.48	0.64	100.69	0.33	767	2	190
WH3d_20	59.76	26.19	0.22		7.12	7.42	0.56	101.28	0.34	771	2	200
WH3d_21	59.33	25.94	0.22		7.06	7.26	0.59	100.40	0.34	771	2	210
WH3d_22	58.51	26.43	0.24		7.68	7.03	0.59	100.48	0.36	785	2	220
WH3d_23	58.78	26.26	0.26		7.25	7.17	0.58	100.29	0.35	776	2	230
WH3d_24	58.29	26.52	0.14		7.61	7.19	0.51	100.24	0.36	784	2	240
WH3d_25	57.79	26.90	0.29		8.10	6.90	0.47	100.45	0.38	796	2	250
WH3d_26	57.62	26.89	0.19		7.93	7.06	0.53	100.22	0.37	790	2	260
WH3d_27	57.78	26.45	0.26		7.66	6.94	0.58	99.66	0.37	786	2	270
WH3d_28	59.15	26.38	0.26		7.66	7.05	0.57	101.07	0.36	785	2	280
WH3d_29	58.43	26.97	0.25		8.38	6.97	0.48	101.47	0.39	798	2	290
WH3d_30	60.01	25.77	0.25		7.04	7.54	0.64	101.24	0.33	766	2	300
WH3d_31	60.55	25.46	0.19		6.82	7.46	0.66	101.14	0.32	762	2	310
WH3d_32	59.63	25.64	0.19		6.67	7.66	0.66	100.44	0.31	757	2	320
WH3d_33	58.31	25.72	0.20		7.08	7.02	0.58	98.90	0.35	775	2	330
WH3d_34	58.61	26.08	0.29		7.32	7.39	0.58	100.26	0.34	774	2	340
WH3d_35	58.63	26.28	0.16		7.20	7.39	0.57	100.22	0.34	773	2	350
WH3d_36	58.24	26.32	0.18		7.23	7.21	0.56	99.74	0.35	776	2	360
WH3d_37	59.51	26.27	0.17		7.31	7.26	0.55	101.08	0.35	777	2	370
WH3d_38	59.12	26.10	0.26		7.62	7.20	0.54	100.83	0.36	783	2	380
WH3d_39	58.26	26.65	0.26		7.93	7.11	0.49	100.70	0.37	790	2	390
WH3d_40	58.04	26.93	0.14		8.05	6.85	0.49	100.50	0.38	795	2	400
WH3d_41	57.41	27.02	0.18		8.50	6.85	0.46	100.43	0.40	802	2	410
WH3d_42	57.48	26.63	0.23		7.91	6.72	0.48	99.44	0.38	795	2	420
WH3d_43	58.48	26.31	0.15		7.55	7.23	0.52	100.23	0.36	782	2	430
WH3d_44	57.78	26.14	0.25		7.62	7.16	0.53	99.49	0.36	784	2	440
WH3d_45	57.87	26.77	0.26		7.99	6.83	0.53	100.25	0.38	793	2	450
WH3d_46	57.45	26.72	0.23		8.04	6.97	0.42	99.84	0.38	795	2	460
WH3d_47	57.14	26.73	0.22		7.87	6.77	0.49	99.22	0.38	794	2	470
WH3d_48	57.30	26.90	0.19		8.45	6.89	0.46	100.19	0.39	801	2	480
WH3d_49	57.74	26.86	0.30		8.10	6.89	0.45	100.34	0.38	796	2	490
WH3d_50	57.43	26.69	0.31		8.34	7.03	0.46	100.27	0.39	797	2	500
WH3d_51	58.33	26.76	0.18		8.34	6.92	0.46	100.98	0.39	799	2	510

Table A3.6 continued

Sample	SiO_2	Al_2O_3	FeO	MgO	CaO	Na_2O	K_2O	Total	Xan	T (°C)	G	Dist. (μm)
WH3d_55	59.07	26.59	0.19		8.11	6.98	0.54	101.48	0.38	793	2	550
WH3d_56	59.99	25.87	0.21		7.23	7.25	0.59	101.14	0.34	774	2	560
WH3d_57	60.39	25.74	0.27		6.80	7.52	0.63	101.34	0.32	762	2	570
WH3d_58	59.79	25.83	0.28		7.01	7.26	0.60	100.77	0.34	770	2	580
WH3e_1	60.57	24.81	0.30	0.05	6.45	7.28	0.59	100.06	0.32	760	2	20
WH3e_2	60.08	25.03	0.22	0.01	6.82	7.12	0.69	99.97	0.33	766	2	30
WH3e_3	60.62	24.78	0.22	0.03	6.77	7.47	0.65	100.54	0.32	762	2	40
WH3e_4	60.56	24.71	0.28	0.03	6.65	7.35	0.65	100.23	0.32	761	2	50
WH3e_5	61.06	24.99	0.24	0.01	6.79	7.79	0.75	101.63	0.31	755	2	60
WH3e_6	61.11	24.97	0.24	0.03	6.75	7.43	0.68	101.21	0.32	761	2	70
WH3e_7	59.86	24.60	0.19	0.04	6.49	7.18	0.61	98.96	0.32	762	2	80
WH3e_8	60.88	24.90	0.19	0.01	6.54	7.39	0.69	100.59	0.32	757	2	90
WH3e_9	61.05	24.94	0.18	0.01	6.93	7.27	0.72	101.09	0.33	766	2	100
WH3e_10	61.03	25.11	0.17	0.01	6.78	7.39	0.62	101.10	0.32	764	2	110
WH3e_11	61.20	24.80	0.21	b.d	6.49	7.58	0.70	100.97	0.31	753	2	120
WH3e_12	60.12	24.65	0.17	b.d	6.46	7.56	0.68	99.64	0.31	753	2	130
WH3e_13	60.06	24.92	0.18	0.01	6.99	7.25	0.60	100.01	0.34	770	2	140
WH3e_14	60.38	24.80	0.22	0.01	6.82	7.22	0.66	100.11	0.33	766	2	150
WH3e_15	60.39	24.82	0.19	0.01	6.78	7.31	0.67	100.17	0.33	764	2	160
WH3e_16	60.38	25.03	0.24	0.00	6.77	7.24	0.62	100.28	0.33	766	2	170
WH3e_17	60.88	24.57	0.28	0.02	6.69	7.08	0.72	100.23	0.33	764	2	180
WH3e_18	60.56	24.48	0.20	0.01	6.21	7.54	0.73	99.73	0.30	748	2	190
WH3e_19	61.45	24.19	0.16	0.03	6.33	7.69	0.74	100.59	0.30	748	2	200
WH3e_20	61.06	24.20	0.17	0.01	6.21	7.79	0.71	100.14	0.29	745	2	210
WH3e_21	60.49	24.46	0.19	0.00	6.14	7.37	0.79	99.45	0.30	747	2	220
WH3e_22	59.65	23.96	0.99	1.12	6.92	7.08	0.80	100.52	0.33	766	2	230
WH3e_23	59.86	24.66	0.17	0.01	6.48	7.32	0.63	99.13	0.32	759	2	240
WH3e_24	60.19	24.63	0.23	0.04	6.65	7.42	0.68	99.84	0.32	759	2	250
WH3e_25	60.02	24.61	0.17	0.04	6.64	7.34	0.68	99.52	0.32	760	2	260
WH3e_26	60.37	24.54	0.21	0.01	6.49	7.57	0.66	99.85	0.31	755	2	270
WH3e_27	60.30	24.65	0.20	0.02	6.56	7.35	0.67	99.74	0.32	759	2	280
WH3e_28	61.24	24.43	0.25	0.04	6.50	7.26	0.70	100.41	0.32	758	2	290
WH3e_29	60.79	24.72	0.21	0.03	6.72	7.33	0.60	100.39	0.32	764	2	300
WH3e_30	61.12	24.40	0.22	0.01	6.46	7.44	0.66	100.31	0.31	756	2	310
WH3e_31	60.64	24.54	0.29	0.02	6.25	7.57	0.64	99.95	0.30	750	2	320
WH3e_32	61.48	24.45	0.24	0.05	6.30	7.41	0.68	100.62	0.31	753	2	330
WH3e_33	60.97	24.52	0.21	0.01	6.63	7.14	0.64	100.13	0.33	764	2	340
WH3e_34	60.59	24.47	0.22	0.05	6.67	7.29	0.65	99.96	0.32	762	2	350
WH3e_35	61.20	24.03	0.16	0.02	6.07	7.40	0.72	99.61	0.30	747	2	360
WH3e_38	61.52	24.54	0.19	0.01	6.52	7.21	0.70	100.70	0.32	759	2	390
WH3e_39	60.25	24.69	0.23	0.00	6.48	7.25	0.66	99.55	0.32	759	2	400
WH3e_40	60.91	24.76	0.20	0.01	6.53	7.39	0.61	100.41	0.32	759	2	410
WH3e_41	60.57	24.87	0.15	0.04	6.77	7.25	0.64	100.29	0.33	765	2	420
WH3e_42	61.44	24.85	0.27	0.04	6.88	7.03	0.60	101.11	0.34	771	2	430
WH3e_43	60.24	25.39	0.24	0.03	7.54	6.95	0.55	100.95	0.36	785	2	440
WH3e_44	59.94	25.64	0.22	b.d.	7.73	6.93	0.60	101.06	0.37	787	2	450
WH3e_45	59.72	25.22	0.21	0.02	7.22	6.88	0.58	99.84	0.35	780	2	460
WH3e_46	60.59	24.86	0.18	b.d.	6.52	7.18	0.67	100.01	0.32	761	2	470
WH3e_47	59.96	25.04	0.23	0.01	7.09	7.00	0.63	99.97	0.35	774	2	480
WH3e_48	59.46	25.34	0.20	0.05	7.34	7.05	0.58	100.02	0.35	779	2	490
WH3e_49	59.62	25.36	0.26	0.03	7.48	6.81	0.58	100.16	0.37	785	2	500
WH3e_50	59.13	25.95	0.19	0.05	8.11	6.84	0.52	100.80	0.38	795	2	510
WH3e_51	60.29	25.01	0.24	0.04	6.83	7.16	0.58	100.14	0.33	769	2	520
WH3e_52	62.01	23.95	0.22	0.01	5.91	7.71	0.82	100.62	0.28	737	2	530
WH3e_53	61.78	24.33	0.16	0.04	5.90	7.58	0.76	100.53	0.29	740	2	540
WH3e_54	61.39	24.53	0.25	0.03	6.42	7.48	0.70	100.79	0.31	753	2	550

Table A3.6 continued

Sample	SiO_2	Al_2O_3	FeO	MgO	CaO	Na_2O	K_2O	Total	Xan	T (°C)	G	Dist. (μm)
WH3e_58	61.81	23.96	0.17	0.04	5.55	7.66	0.85	100.03	0.27	729	2	590
WH3e_59	61.89	23.99	0.20	0.03	6.10	7.31	0.76	100.28	0.30	748	2	600
WH3e_60	62.38	24.10	0.17	0.02	6.01	7.66	0.75	101.11	0.29	741	2	610
WH3e_61	60.76	24.11	0.21	0.02	6.19	7.41	0.81	99.52	0.30	747	2	620
WH3e_62	61.62	24.36	0.23	0.01	5.80	7.63	0.76	100.41	0.28	737	2	630
WH3e_63	61.82	24.24	0.22	0.01	6.06	7.45	0.77	100.57	0.30	745	2	640
WH3e_64	61.21	24.83	0.25	0.01	6.42	7.57	0.68	100.98	0.31	753	2	650
WH3e_65	61.18	24.30	0.25	0.00	6.26	7.66	0.72	100.36	0.30	747	2	660
WH3e_66	60.24	24.51	0.18	0.03	6.44	7.50	0.74	99.64	0.31	753	2	670
WH3e_67	60.99	24.59	0.25	0.01	6.56	7.31	0.73	100.44	0.32	758	2	680
WH3e_68	60.95	24.56	0.26	0.01	6.46	7.55	0.67	100.45	0.31	754	2	690
WH3e_69	60.80	24.58	0.24	b.d.	6.66	7.26	0.62	100.17	0.32	764	2	700
WH3e_70	60.89	24.53	0.16	b.d.	6.33	7.29	0.68	99.89	0.31	755	2	710
WH3e_71	61.45	24.55	0.20	0.04	6.31	7.20	0.68	100.43	0.31	756	2	720
WH3e_72	61.47	24.38	0.27	0.01	6.17	7.49	0.78	100.57	0.30	746	2	730
WH3e_73	60.99	24.77	0.22	b.d.	6.67	7.32	0.73	100.71	0.32	760	2	740
WH3e_74	60.96	24.62	0.22	0.01	6.63	7.32	0.67	100.42	0.32	761	2	750
WH3e_75	60.93	24.82	0.20	0.03	6.75	7.17	0.66	100.55	0.33	765	2	760
WH3e_76	61.00	24.70	0.22	b.d.	6.62	7.45	0.77	100.75	0.31	756	2	770
WH3e_77	60.59	25.24	0.35	0.02	6.85	7.32	0.69	101.05	0.33	764	2	780
WH3e_78	60.22	24.87	0.26	0.05	7.15	7.06	0.64	100.25	0.35	774	2	790
WH3e_79	61.35	24.54	0.23	0.04	6.35	7.31	0.75	100.57	0.31	753	2	800
WH3e_80	62.68	23.56	0.22	b.d.	5.87	7.65	0.83	100.81	0.28	736	2	810
WH3e_81	62.26	23.85	0.30	0.01	5.90	7.71	0.80	100.84	0.28	737	2	820
WH3e_82	62.22	23.93	0.25	0.01	5.89	7.68	0.78	100.76	0.28	738	2	830
WH3e_83	62.07	24.11	0.19	0.03	6.01	7.58	0.81	100.79	0.29	741	2	840
WH3e_84	62.35	24.22	0.28	0.01	5.88	7.42	0.81	100.96	0.29	740	2	850
WH3e_85	61.16	23.92	0.31	0.04	5.98	7.56	0.75	99.73	0.29	742	2	860
WH3e_86	61.38	24.15	0.20	0.01	6.02	7.47	0.84	100.07	0.29	742	2	870
WH3e_87	61.49	24.34	0.28	0.01	5.98	7.77	0.83	100.70	0.28	737	2	880
WH5d_2	61.09	25.28	0.24		6.75	7.34	0.56	101.25	0.33	765	2	20
WH5d_3	60.54	25.54	0.28		6.85	7.41	0.58	101.21	0.33	766	2	30
WH5d_4	59.85	25.68	0.30		7.15	7.24	0.60	100.82	0.34	773	2	40
WH5d_5	60.22	25.59	0.22		7.22	6.88	0.50	100.63	0.36	782	2	50
WH5d_6	60.25	26.12	0.22		7.37	6.89	0.58	101.42	0.36	782	2	60
WH5d_15	60.43	26.25	0.30		7.30	7.06	0.57	101.92	0.35	779	2	150
WH5d_17	59.77	26.59	0.24		8.14	6.70	0.46	101.90	0.39	799	2	170
WH5d_21	59.84	26.49	0.29		7.86	6.92	0.52	101.92	0.37	791	2	210
WH5d_22	60.63	25.66	0.30		6.92	7.19	0.57	101.26	0.34	771	2	220
WH5d_23	59.99	26.29	0.17		7.64	6.79	0.44	101.32	0.37	792	2	230
WH5d_26	60.53	25.99	0.15		7.12	7.19	0.56	101.53	0.34	774	2	260
WH5d_27	59.59	26.61	0.16		7.86	6.60	0.52	101.35	0.38	795	2	270
WH5d_29	59.07	26.62	0.31		8.32	6.70	0.51	101.53	0.40	800	2	290
WH5d_30	58.96	26.60	0.18		8.10	6.71	0.47	101.02	0.39	798	2	300
WH5d_31	58.90	26.67	0.20		8.18	6.54	0.45	100.94	0.40	802	2	310
WH5d_34	58.66	27.00	0.20		8.36	6.55	0.44	101.22	0.40	805	2	340
WH5d_36	58.78	26.91	0.33		8.47	6.42	0.43	101.33	0.41	808	2	360
WH5d_37	59.75	25.98	0.19		7.35	6.97	0.51	100.74	0.36	783	2	370
WH5d_38	60.32	25.90	0.24		7.18	7.08	0.53	101.26	0.35	778	2	380
WH5d_39	59.55	25.47	0.19		6.62	7.38	0.59	99.80	0.32	762	2	390
WH5d_40	60.27	25.37	0.17		6.57	7.41	0.55	100.34	0.32	761	2	400
WH5d_42	60.34	26.11	0.26		7.14	7.29	0.53	101.67	0.34	774	2	420
WH5d_43	59.84	26.09	0.29		7.08	7.17	0.58	101.04	0.34	773	2	430
WH5d_44	60.37	26.11	0.21		7.29	7.34	0.48	101.80	0.34	777	2	440
WH5d_45	60.16	26.17	0.17		7.18	7.17	0.49	101.33	0.35	777	2	450
WH5d_49	59.31	25.97	0.26		7.06	6.86	0.50	99.96	0.35	780	2	490

Table A3.6 continued

Sample	SiO_2	Al_2O_3	FeO	MgO	CaO	Na_2O	K_2O	Total	Xan	T (°C)	G	Dist. (μm)
WH5d_53	59.73	26.15	0.25		7.47	6.88	0.47	100.97	0.36	787	2	530
WH5d_54	59.81	26.06	0.23		7.66	7.13	0.48	101.37	0.36	786	2	540
WH5d_55	59.54	26.04	0.31		7.09	7.16	0.52	100.65	0.34	775	2	550
WH5d_56	59.58	25.99	0.21		7.18	7.24	0.54	100.74	0.34	775	2	560
WH5d_57	58.91	25.98	0.17		6.96	7.22	0.55	99.78	0.34	771	2	570
WH5d_58	58.94	27.12	0.17		8.00	6.41	0.49	101.13	0.40	800	2	580
WH5d_59	58.27	27.83	0.19		8.84	6.20	0.37	101.70	0.43	817	2	590
WH5d_61	58.53	27.10	0.26		9.21	6.44	0.35	101.90	0.43	818	2	610
WH5d_62	60.63	25.99	0.35		7.01	7.32	0.54	101.84	0.34	771	2	620
WH5d_63	61.21	25.19	0.29		6.48	7.60	0.63	101.41	0.31	755	2	630
WH5d_64	60.74	25.07	0.24		5.94	7.19	0.65	99.83	0.30	749	2	640
WH5d_65	58.84	25.59	0.20		7.52	7.57	0.48	100.20	0.34	777	2	650
WH5d_66	58.89	25.59	0.19		7.19	6.72	0.58	99.15	0.36	782	2	660
WH5d_67	59.05	25.89	0.16		7.51	6.97	0.44	100.03	0.36	787	2	670
WH5d_68	60.54	25.95	0.23		7.17	7.25	0.51	101.66	0.34	775	2	680
WH5d_69	59.81	26.32	0.29		7.53	6.97	0.49	101.41	0.36	786	2	690
WH5d_70	58.86	24.76	0.18		6.72	7.01	0.57	98.10	0.33	770	2	700
WH5f_1	59.98	25.07	0.25		6.95	7.40	0.63	100.28	0.33	766	2	20
WH5f_2	60.16	25.60	0.29		7.03	7.29	0.67	101.05	0.33	768	2	30
WH5f_3	60.06	25.38	0.23		6.83	7.47	0.68	100.65	0.32	762	2	40
WH5f_4	59.62	25.38	0.22		6.79	7.47	0.65	100.14	0.32	762	2	50
WH5f_5	60.22	24.97	0.29		6.59	7.47	0.66	100.19	0.32	758	2	60
WH5f_6	59.70	25.09	0.29		6.39	7.35	0.60	99.43	0.31	757	2	70
WH5f_7	61.34	24.27	0.23		5.71	7.98	0.82	100.35	0.27	728	2	80
WH5f_8	59.67	25.02	0.25		6.72	7.38	0.68	99.72	0.32	761	2	90
WH5f_9	60.92	25.15	0.19		6.50	7.32	0.63	100.71	0.32	759	2	100
WH5f_10	59.90	25.22	0.31		6.74	7.29	0.65	100.11	0.33	764	2	110
WH5f_11	59.82	25.17	0.26		6.72	7.31	0.66	99.93	0.32	763	2	120
WH5f_12	59.86	25.19	0.25		6.66	7.32	0.72	100.01	0.32	760	2	130
WH5f_13	60.26	24.80	0.26		6.38	7.33	0.61	99.64	0.31	757	2	140
WH5f_14	60.71	24.97	0.25		6.30	7.38	0.67	100.28	0.31	753	2	150
WH5f_15	58.79	24.76	0.38		6.31	7.11	1.04	98.40	0.31	749	2	160
WH5f_16	60.84	25.00	0.27		6.49	7.39	0.63	100.62	0.31	758	2	170
WH5f_17	60.86	24.90	0.16		6.34	7.66	0.73	100.66	0.30	749	2	180
WH5f_18	62.16	24.87	0.28		6.38	7.48	0.64	101.79	0.31	754	2	190
WH5f_19	60.66	24.92	0.29		6.53	7.53	0.70	100.63	0.31	755	2	200
WH5f_20	61.20	25.09	0.28		6.48	7.50	0.65	101.20	0.31	756	2	210
WH5f_21	60.50	24.82	0.22		5.92	7.91	0.71	100.08	0.28	736	2	220
WH5f_22	60.74	24.59	0.19		6.13	7.44	0.75	99.83	0.30	747	2	230
WH5f_23	62.10	23.98	0.29		6.46	7.62	0.69	101.14	0.31	753	2	240
WH5f_26	61.13	24.42	0.28		5.88	7.57	0.80	100.07	0.29	739	2	270
WH5f_28	61.13	25.52	0.30		6.54	7.50	0.62	101.61	0.31	758	2	290
WH5f_29	61.20	25.74	0.19		6.67	7.25	0.71	101.77	0.32	761	2	300
WH5f_30	61.99	25.28	0.24		6.43	7.42	0.59	101.95	0.31	757	2	310
WH5f_31	62.59	24.74	0.24		5.70	7.69	0.76	101.72	0.28	734	2	320
WH5f_33	62.25	24.96	0.26		6.09	7.60	0.72	101.89	0.29	744	2	340
WH5f_36	62.59	24.94	0.21		5.81	7.65	0.73	101.93	0.28	738	2	370
WH5f_42	60.24	25.75	0.26		7.17	7.11	0.63	101.16	0.34	774	2	430
WH5f_43	60.51	25.78	0.20		7.46	7.13	0.60	101.68	0.35	779	2	440
WH5f_44	61.91	25.85	0.24		7.18	6.89	0.56	102.64	0.35	779	2	450
WH5f_45	58.61	25.06	0.15		7.01	6.65	0.51	97.99	0.36	782	2	460
WH5f_47	59.95	26.57	0.18		7.56	6.72	0.48	101.46	0.37	790	2	480
WH5f_48	60.32	26.64	0.15		7.63	6.69	0.46	101.88	0.38	792	2	490
WH5f_50	60.18	26.18	0.22		7.64	6.87	0.51	101.60	0.37	789	2	510
WH5f_51	59.96	26.57	0.23		7.76	6.85	0.49	101.86	0.37	791	2	520
WH5f_52	59.69	26.34	0.17		7.48	6.90	0.56	101.13	0.36	784	2	530

Table A3.6 continued

Sample	SiO_2	Al_2O_3	FeO	MgO	CaO	Na_2O	K_2O	Total	Xan	T (°C)	G	Dist. (μm)
WH6b_3	62.19	24.78	0.09		5.85	7.77	0.65	101.32	0.28	738	3	30
WH6b_4	62.19	24.67	0.27		5.94	7.85	0.78	101.69	0.28	736	3	40
WH6b_6	61.73	24.98	0.32		6.02	8.09	0.71	101.84	0.28	736	3	60
WH6b_7	61.60	25.52	0.22		5.74	7.70	0.70	101.49	0.28	736	3	70
WH6b_10	62.13	24.77	0.19		5.83	8.04	0.70	101.65	0.27	733	3	100
WH6b_12	62.71	24.49	0.24		5.34	8.11	0.73	101.62	0.26	720	3	120
WH6b_13	63.99	23.22	0.20		4.25	8.60	1.07	101.32	0.20	677	3	130
WH6b_14	60.46	22.97	0.22		4.15	8.54	0.97	97.30	0.20	677	3	140
WH6b_15	62.13	24.45	0.23		4.92	8.39	0.87	100.97	0.23	702	3	150
WH6b_16	63.23	24.62	0.23		5.40	7.67	0.73	101.88	0.27	727	3	160
WH6b_17	61.47	24.22	0.22		5.70	7.79	0.76	100.16	0.28	732	3	170
WH6b_18	62.32	24.78	0.29		5.68	7.84	0.76	101.66	0.27	731	3	180
WH6b_19	60.41	23.91	0.18		5.77	7.47	0.84	98.58	0.28	737	3	190
WH6b_21	60.98	24.36	0.13		5.30	8.04	0.84	99.65	0.25	717	3	210
WH6b_22	61.18	24.63	0.21		5.41	8.12	0.80	100.36	0.26	720	3	220
WH6b_23	60.67	24.88	0.14		5.56	7.86	0.72	99.82	0.27	729	3	230
WH6b_24	61.16	24.87	0.27		5.62	7.96	0.85	100.72	0.27	726	3	240
WH6b_25	61.77	24.22	0.14		5.19	8.07	0.85	100.23	0.25	714	3	250
WH6b_26	62.11	24.42	0.09		5.04	8.12	0.85	100.63	0.24	709	3	260
WH6b_27	61.88	24.04	0.19		5.22	7.99	0.75	100.08	0.25	718	3	270
WH6b_28	62.30	24.15	0.17		4.79	8.16	0.87	100.43	0.23	702	3	280
WH6b_29	62.33	24.32	0.21		5.02	7.87	0.85	100.60	0.25	713	3	290
WH6b_30	63.27	24.08	0.17		4.42	8.52	0.92	101.39	0.21	686	3	300
WH6b_31	63.33	23.38	0.17		4.37	8.58	0.99	100.81	0.21	683	3	310
WH6b_32	62.89	23.09	0.24		3.92	8.38	1.02	99.53	0.19	671	3	320
WH6b_34	62.40	24.26	0.19		4.35	8.45	1.05	100.70	0.21	682	3	340
WH6b_35	60.02	25.56	0.17		5.91	7.74	0.71	100.11	0.28	739	3	350
WH6b_36	61.01	24.06	0.17		4.79	8.10	0.80	98.94	0.23	704	3	360
WH6b_37	62.17	23.26	0.12		3.96	8.49	0.97	98.97	0.19	672	3	370
WH6b_38	61.98	24.08	0.16		4.20	8.28	0.92	99.61	0.21	682	3	380
WH6b_39	62.18	23.46	0.25		4.75	8.24	0.99	99.86	0.23	697	3	390
WH6b_40	62.45	23.75	0.12		4.25	8.13	0.97	99.68	0.21	685	3	400
WH6b_41	62.24	23.29	0.18		4.18	8.39	1.10	99.37	0.20	677	3	410
WH6b_42	62.63	23.55	0.26		4.10	8.58	1.03	100.15	0.20	674	3	420
WH6b_43	62.99	23.54	0.13		4.10	8.49	1.11	100.36	0.20	673	3	430
WH6b_44	62.82	23.70	0.11		4.32	8.24	1.11	100.30	0.21	683	3	440
WH6b_45	62.21	23.30	0.26		3.76	8.54	1.06	99.13	0.18	663	3	450
WH6b_46	61.62	23.88	0.16		4.44	8.35	1.03	99.47	0.21	686	3	460
WH6b_47	62.91	23.65	0.16		4.19	8.60	1.08	100.58	0.20	675	3	470
WH6b_48	62.52	23.93	0.20		4.49	8.30	1.05	100.49	0.22	689	3	480
WH6b_49	62.21	23.50	0.12		4.07	8.30	0.93	99.13	0.20	678	3	490
WH6c_2	64.02	23.49	0.14		4.67	8.51	0.86	101.71	0.22	694	3	20
WH6c_3	64.92	22.92	0.18		4.16	8.45	1.10	101.72	0.20	676	3	30
WH6c_4	63.95	23.54	0.24		4.74	8.32	0.95	101.74	0.23	697	3	40
WH6c_5	63.39	23.32	0.25		4.68	8.15	0.98	100.78	0.23	697	3	50
WH6c_6	63.82	23.55	0.09		4.66	8.48	1.04	101.64	0.22	691	3	60
WH6c_7	64.29	23.44	0.13		4.34	8.64	0.93	101.76	0.21	682	3	70
WH6c_9	64.22	23.22	0.11		4.65	8.24	0.95	101.38	0.22	696	3	90
WH6c_10	64.59	23.44	0.08		4.73	8.12	0.89	101.87	0.23	700	3	100
WH6c_14	63.84	23.46	0.18		4.64	8.20	0.84	101.17	0.23	698	3	140
WH6c_15	63.98	23.35	0.14		4.82	8.12	0.98	101.40	0.23	701	3	150
WH6c_16	64.31	23.19	0.19		4.67	8.32	0.98	101.68	0.22	694	3	160
WH6c_17	65.37	22.85	0.17		4.12	8.33	1.15	101.98	0.20	676	3	170
WH6c_18	64.92	22.98	0.23		4.05	8.52	1.04	101.74	0.20	673	3	180
WH6c_19	63.54	23.74	0.20		5.01	8.22	0.93	101.64	0.24	706	3	190
WH6c_20	64.01	23.34	0.34		4.75	8.37	0.93	101.75	0.23	697	3	200

Table A3.6 continued

Sample	SiO_2	Al_2O_3	FeO	MgO	CaO	Na_2O	K_2O	Total	Xan	T (°C)	G	Dist. (μm)
WH6c_30	62.95	24.14	0.19		5.32	8.11	0.94	101.65	0.25	715	3	300
WH6c_31	62.38	24.36	0.14		5.63	7.82	0.75	101.09	0.27	730	3	310
WH6c_32	62.74	24.53	0.25		5.88	7.68	0.81	101.89	0.28	737	3	320
WH6c_34	63.27	23.93	0.20		5.36	8.01	0.78	101.55	0.26	720	3	340
WH6c_35	63.51	23.91	0.17		5.31	8.20	0.82	101.94	0.25	716	3	350
WH6c_36	63.34	24.15	0.26		5.34	8.07	0.76	101.93	0.26	720	3	360
WH6c_38	62.74	24.37	0.24		5.70	7.95	0.82	101.82	0.27	728	3	380
WH6c_41	63.13	24.23	0.19		5.29	8.23	0.81	101.88	0.25	715	3	410
WH6c_42	63.47	23.91	0.13		5.16	8.10	0.80	101.56	0.25	714	3	420
WH6c_44	62.97	23.90	0.17		5.53	7.89	0.74	101.20	0.27	727	3	440
WH6c_48	62.37	24.30	0.19		5.43	8.04	0.75	101.08	0.26	722	3	480
WH6c_49	61.27	24.67	0.23		5.50	7.99	0.79	100.44	0.26	724	3	490
WH6c_50	62.05	24.63	0.19		5.72	8.08	0.74	101.40	0.27	729	3	500
WH6c_51	61.99	24.86	0.18		6.01	7.84	0.71	101.59	0.29	739	3	510
WH6c_52	61.39	25.37	0.19		6.57	7.67	0.69	101.88	0.31	754	3	520
WH6c_53	61.17	25.36	0.23		7.21	7.27	0.61	101.85	0.34	773	3	530
WH6c_54	60.21	25.68	0.22		7.39	7.45	0.56	101.51	0.34	775	3	540
WH6c_55	59.87	26.46	0.21		7.68	7.12	0.52	101.85	0.36	785	3	550
WH6c_56	59.51	26.05	0.26		7.69	7.08	0.62	101.21	0.36	783	3	560
WH6c_57	59.79	26.06	0.28		7.54	7.21	0.55	101.43	0.35	781	3	570
WH6c_58	59.88	25.64	0.12		7.30	7.10	0.53	100.57	0.35	779	3	580
WH6c_59	59.67	25.80	0.18		7.19	7.13	0.59	100.56	0.35	775	3	590
WH6c_60	60.08	25.35	0.24		7.15	7.26	0.63	100.71	0.34	772	3	600
WH6c_61	62.05	24.74	0.23		6.50	7.68	0.65	101.85	0.31	753	3	610
WH6c_62	61.87	25.00	0.26		6.20	7.67	0.72	101.73	0.30	746	3	620
WH6c_63	60.64	25.25	0.22		6.57	7.45	0.64	100.78	0.32	758	3	630
WH6c_64	60.95	25.20	0.29		6.51	7.63	0.71	101.30	0.31	753	3	640
WH6c_65	60.85	24.99	0.22		6.88	7.48	0.69	101.11	0.32	763	3	650
WH6c_66	61.35	24.72	0.11		5.85	7.86	0.70	100.59	0.28	736	3	660
WH6c_67	60.31	25.37	0.16		6.76	7.43	0.67	100.71	0.32	761	3	670
WH6c_68	60.38	25.57	0.20		6.94	7.38	0.62	101.07	0.33	767	3	680
WH6c_70	60.77	25.19	0.18		6.81	7.50	0.65	101.11	0.32	762	3	690
WH6c_71	60.86	25.06	0.24		6.38	7.44	0.67	100.65	0.31	754	3	700
WH6c_72	61.22	25.17	0.23		6.66	7.30	0.63	101.20	0.32	763	3	710
WH6c_73	60.48	25.07	0.18		6.79	7.16	0.56	100.24	0.33	769	3	720
WH6c_74	61.55	25.22	0.28		6.60	7.39	0.67	101.72	0.32	759	3	730
WH6c_75	61.05	25.20	0.16		6.78	7.70	0.66	101.55	0.32	758	3	740
WH6c_76	61.43	25.25	0.24		6.58	7.59	0.75	101.85	0.31	754	3	750
WH6c_77	61.16	25.21	0.24		6.59	7.47	0.65	101.32	0.32	758	3	760
WH6c_78	60.92	25.02	0.29		6.36	7.48	0.62	100.70	0.31	754	3	770
WH6c_79	61.20	25.12	0.18		6.49	7.55	0.64	101.19	0.31	755	3	780
WH6c_80	60.64	25.36	0.20		6.47	7.43	0.59	100.67	0.31	758	3	790
WH6c_81	60.14	25.20	0.24		6.48	7.56	0.63	100.26	0.31	755	3	800
WH6c_82	60.83	25.26	0.19		6.55	7.58	0.71	101.11	0.31	754	3	810
WH6c_83	60.80	25.12	0.27		6.48	7.45	0.61	100.73	0.31	757	3	820
WH6c_84	61.44	25.16	0.23		6.52	7.51	0.73	101.58	0.31	754	3	830
WH6c_85	61.21	24.89	0.21		6.26	7.80	0.70	101.06	0.30	746	3	840
WH6c_86	61.34	25.02	0.17		6.08	7.73	0.73	101.07	0.29	742	3	850
WH6c_87	61.78	25.20	0.16		6.34	7.74	0.66	101.88	0.30	749	3	860
WH6c_88	61.46	24.96	0.15		6.28	7.59	0.72	101.16	0.30	749	3	870
WH6c_89	61.43	24.80	0.18		6.20	7.64	0.64	100.88	0.30	748	3	880
WH6c_90	61.83	24.89	0.16		6.05	7.81	0.73	101.49	0.29	740	3	890
WH6c_91	62.14	24.28	0.32		6.06	7.52	0.72	101.03	0.30	745	3	900
WH6c_93	62.56	24.72	0.25		5.86	7.89	0.70	101.97	0.28	736	3	920
WH6da_1	60.24	25.22	0.33		6.58	7.39	0.58	100.35	0.32	761	1	20
WH6da_2	59.71	25.25	0.21		6.65	7.38	0.63	99.81	0.32	761	1	30

Table A3.6 continued

Sample	SiO_2	Al_2O_3	FeO	MgO	CaO	Na_2O	K_2O	Total	Xan	T (°C)	G	Dist. (μm)
WH6da_6	61.20	25.13	0.33		6.33	7.77	0.66	101.41	0.30	748	1	70
WH6da_9	60.31	25.08	0.24		6.66	7.53	0.65	100.46	0.32	759	1	100
WH6da_10	59.87	25.31	0.22		6.39	7.47	0.64	99.90	0.31	754	1	110
WH6da_11	60.31	26.06	0.22		6.78	7.40	0.66	101.43	0.32	762	1	120
WH6da_12	59.73	25.42	0.21		6.72	7.28	0.68	100.04	0.32	763	1	130
WH6da_13	60.70	25.56	0.25		6.37	7.42	0.78	101.07	0.31	751	1	140
WH6da_15	60.34	24.91	0.22		6.68	7.51	0.61	100.26	0.32	760	1	160
WH6da_16	59.43	25.35	0.20		6.83	7.40	0.63	99.84	0.33	764	1	170
WH6da_17	59.52	25.41	0.22		6.49	7.32	0.56	99.51	0.32	761	1	180
WH6da_18	59.73	25.01	0.39		6.13	7.44	0.60	99.31	0.30	751	1	190
WH6da_19	59.36	25.47	0.23		6.33	7.37	0.62	99.38	0.31	755	1	200
WH6da_27	55.37	29.53	0.27		10.55	5.44	0.32	101.47	0.51	838	1	280
WH6da_28	55.56	29.54	0.25		10.48	5.43	0.35	101.61	0.51	837	1	290
WH6da_29	55.65	29.33	0.18		10.27	5.56	0.32	101.30	0.50	836	1	300
WH6da_30	54.94	29.95	0.24		11.35	5.23	0.25	101.94	0.54	845	1	310
WH6da_31	53.84	29.42	0.27		10.98	5.25	0.25	100.01	0.53	843	1	320
WH6da_32	58.27	26.43	0.29		7.58	6.82	0.46	99.85	0.37	790	1	330
WH6da_33	58.05	26.68	0.27		7.69	6.77	0.53	99.99	0.37	790	1	340
WH6da_37	56.30	29.34	0.27		9.88	5.74	0.28	101.82	0.48	833	1	380
WH6da_39	56.09	29.14	0.22		9.94	5.62	0.32	101.33	0.49	833	1	400
WH6da_40	57.15	28.58	0.45		9.13	5.89	0.32	101.51	0.45	825	1	410
WH6da_41	58.25	27.83	0.31		8.72	6.44	0.43	101.97	0.42	811	1	420
WH6da_42	59.85	26.39	0.18		7.04	7.12	0.60	101.18	0.34	773	1	430
WH6da_43	59.95	26.10	0.27		6.84	7.08	0.62	100.86	0.34	769	1	440
WH6da_47	60.89	25.50	0.22		6.64	7.57	0.59	101.41	0.32	759	1	480
WH6da_48	60.59	26.05	0.24		6.66	7.39	0.65	101.58	0.32	761	1	490
WH6da_49	60.59	25.71	0.21		6.65	7.36	0.60	101.13	0.32	762	1	500
WH6da_50	60.49	26.10	0.19		6.90	7.38	0.62	101.67	0.33	766	1	510
WH6da_52	60.39	26.34	0.25		7.05	7.22	0.58	101.82	0.34	772	1	530
WH6da_55	61.11	25.51	0.30		6.43	7.69	0.66	101.69	0.30	752	1	560
WH6da_56	59.99	25.36	0.22		6.90	7.43	0.63	100.52	0.33	765	1	570
WH6da_57	59.08	25.93	0.29		6.94	7.38	0.64	100.26	0.33	766	1	580
WH6da_58	59.31	26.26	0.26		6.59	7.13	0.68	100.23	0.32	763	1	590
WH6da_59	60.32	26.30	0.28		6.84	7.40	0.61	101.75	0.33	765	1	600
WH6da_60	59.49	26.44	0.22		6.57	7.39	0.63	100.75	0.32	760	1	610
WH6db_2	60.18	25.93	0.29		7.04	7.29	0.52	101.26	0.34	772	1	30
WH6db_3	58.52	26.84	0.22		8.19	6.78	0.47	101.02	0.39	799	1	40
WH6db_4	57.52	27.13	0.24		8.45	6.45	0.42	100.20	0.41	808	1	50
WH6db_5	58.55	27.04	0.27		7.90	6.79	0.47	101.02	0.38	794	1	60
WH6db_6	58.57	26.13	0.31		7.32	6.77	0.56	99.66	0.36	784	1	70
WH6db_7	58.47	27.11	0.30		7.01	7.22	0.60	100.70	0.34	771	1	80
WH6db_8	58.64	27.34	0.18		7.84	6.79	0.51	101.31	0.38	793	1	90
WH6db_9	58.65	27.13	0.31		7.76	6.74	0.56	101.15	0.38	790	1	100
WH6db_11	58.67	26.95	0.25		7.90	6.90	0.53	101.19	0.38	791	1	120
WH6db_12	58.19	27.54	0.22		8.32	6.77	0.40	101.44	0.40	802	1	130
WH6db_13	58.43	27.10	0.28		7.88	6.91	0.49	101.09	0.38	792	1	140
WH6db_14	59.66	26.24	0.24		6.72	7.40	0.63	100.88	0.32	762	1	150
WH6db_15	58.45	27.23	0.24		7.47	7.16	0.50	101.05	0.36	782	1	160
WH6db_16	59.27	27.03	0.21		7.62	6.86	0.49	101.48	0.37	789	1	170
WH6db_17	60.79	26.33	0.18		6.45	7.49	0.69	101.93	0.31	754	1	180
WH6db_19	60.38	26.20	0.26		6.75	7.16	0.66	101.40	0.33	766	1	200
WH6db_20	56.08	28.89	0.20		10.29	5.71	0.34	101.51	0.49	834	1	210
WH6db_21	57.59	27.58	0.37		8.82	6.42	0.52	101.31	0.42	809	1	220
WH6db_22	53.36	31.38	0.24		12.23	4.37	0.25	101.82	0.60	847	1	230
WH6db_23	53.33	31.35	0.23		11.80	4.84	0.28	101.82	0.56	846	1	240
WH6db_24	54.14	30.30	0.34		10.81	5.14	0.30	101.02	0.53	842	1	250

Table A3.6 continued

Sample	SiO_2	Al_2O_3	FeO	MgO	CaO	Na_2O	K_2O	Total	Xan	T (°C)	G	Dist. (μm)
WH6db_28	60.41	26.30	0.20		6.61	7.41	0.63	101.55	0.32	760	1	290
WH6db_29	60.75	26.18	0.26		6.31	7.48	0.67	101.65	0.31	752	1	300
WH6db_31	60.70	25.99	0.24		6.40	7.62	0.62	101.57	0.31	753	1	320
WH6db_34	60.45	26.11	0.34		6.63	7.21	0.64	101.38	0.32	763	1	350
WH6db_35	60.50	26.13	0.25		6.57	7.53	0.66	101.63	0.31	757	1	360
WH6db_36	60.01	26.09	0.37		6.47	7.34	0.58	100.86	0.32	760	1	370
WH6db_37	60.14	25.90	0.19		6.40	7.38	0.75	100.75	0.31	753	1	380
WH6db_38	59.83	26.77	0.29		6.78	7.17	0.65	101.49	0.33	766	1	390
WH6db_39	59.96	26.75	0.34		7.00	7.20	0.49	101.74	0.34	774	1	400
WH6e_2	59.92	25.44	0.24		6.58	7.43	0.61	100.22	0.32	760	2	30
WH6e_3	60.13	25.46	0.30		6.52	7.33	0.64	100.39	0.32	759	2	40
WH6e_4	60.85	25.83	0.25		6.84	7.38	0.64	101.80	0.33	765	2	50
WH6e_5	61.64	24.42	0.27		6.79	7.05	0.55	100.72	0.34	771	2	60
WH6e_6	60.02	25.51	0.23		7.73	6.83	0.51	100.82	0.37	790	2	70
WH6e_7	60.72	24.75	0.18		6.60	7.17	0.62	100.04	0.32	764	2	80
WH6e_8	61.05	24.68	0.22		6.57	7.22	0.64	100.37	0.32	762	2	90
WH6e_9	60.89	24.49	0.25		6.65	7.30	0.57	100.14	0.32	764	2	100
WH6e_10	60.59	24.75	0.24		6.96	6.97	0.54	100.06	0.34	775	2	110
WH6e_11	60.46	24.66	0.19		6.65	7.32	0.65	99.92	0.32	762	2	120
WH6e_12	61.54	24.63	0.25		6.56	7.32	0.66	100.95	0.32	760	2	130
WH6e_13	61.75	24.80	0.16		6.45	7.27	0.58	101.01	0.32	760	2	140
WH6e_14	62.18	24.68	0.32		6.62	7.26	0.61	101.67	0.32	763	2	150
WH6e_15	61.28	24.73	0.27		6.62	7.27	0.66	100.83	0.32	761	2	160
WH6e_16	61.69	24.67	0.21		6.44	7.21	0.59	100.81	0.32	761	2	170
WH6e_17	61.39	24.67	0.19		6.86	7.49	0.64	101.25	0.32	763	2	180
WH6e_18	59.71	24.70	0.33		6.88	7.05	0.56	99.21	0.34	772	2	190
WH6e_19	60.65	24.29	0.26		6.32	7.52	0.61	99.64	0.31	753	2	200
WH6e_20	60.73	24.67	0.16		6.30	7.50	0.63	99.98	0.31	753	2	210
WH6e_21	62.23	24.00	0.22		6.16	7.50	0.68	100.80	0.30	749	2	220
WH6e_22	61.82	24.30	0.18		6.10	7.32	0.61	100.32	0.30	752	2	230
WH6e_23	62.11	24.02	0.31		6.03	7.33	0.67	100.46	0.30	749	2	240
WH6e_24	61.12	24.38	0.25		6.52	7.28	0.67	100.21	0.32	759	2	250
WH6e_25	61.61	24.54	0.24		6.09	7.34	0.68	100.50	0.30	749	2	260
WH6e_26	61.43	24.22	0.32		6.45	7.28	0.75	100.46	0.31	756	2	270
WH6e_27	61.20	24.90	0.32		7.03	7.03	0.61	101.09	0.34	774	2	280
WH6e_28	61.60	24.62	0.28		6.74	7.22	0.56	101.02	0.33	767	2	290
WH6e_29	60.66	24.90	0.26		7.20	6.79	0.51	100.31	0.36	783	2	300
WH6e_30	59.84	25.91	0.23		7.75	6.83	0.48	101.04	0.37	791	2	310
WH6e_31	60.83	25.56	0.30		7.36	7.00	0.50	101.55	0.36	782	2	320
WH6e_32	60.57	25.07	0.28		6.85	7.03	0.58	100.38	0.34	771	2	330
WH6e_33	61.02	24.43	0.22		6.62	7.28	0.62	100.19	0.32	762	2	340
WH6e_34	60.76	24.96	0.26		6.89	7.21	0.61	100.68	0.33	769	2	350
WH6e_35	60.84	24.91	0.26		6.76	7.24	0.52	100.53	0.33	768	2	360
WH6e_36	60.99	24.71	0.27		6.60	7.27	0.67	100.51	0.32	761	2	370
WH6e_37	61.00	24.33	0.29		6.22	7.39	0.69	99.91	0.30	751	2	380
WH6e_38	60.47	24.72	0.25		6.76	7.19	0.61	99.99	0.33	767	2	390
WH6e_39	60.67	24.85	0.26		6.80	7.26	0.60	100.42	0.33	767	2	400
WH6e_40	60.70	24.37	0.28		6.27	7.13	0.67	99.41	0.31	757	2	410
WH6e_41	60.90	24.46	0.28		6.67	7.24	0.67	100.20	0.32	763	2	420
WH6e_42	61.91	24.39	0.23		6.45	7.40	0.63	101.02	0.31	757	2	430
WH6e_43	61.67	24.45	0.19		6.34	7.50	0.62	100.77	0.31	754	2	440
WH6e_44	61.49	24.32	0.27		6.30	7.33	0.66	100.37	0.31	754	2	450
WH6e_45	61.45	24.47	0.27		6.20	7.33	0.66	100.36	0.31	752	2	460
WH6e_46	61.41	24.04	0.26		6.24	7.54	0.65	100.14	0.30	750	2	470
WH6e_47	61.44	24.45	0.32		6.47	7.21	0.59	100.48	0.32	761	2	480
WH6e_48	61.42	24.38	0.30		6.38	7.38	0.61	100.48	0.31	757	2	490

Table 3.6 continued

Sample	SiO_2	Al_2O_3	FeO	MgO	CaO	Na_2O	K_2O	Total	Xan	T (°C)	G	Dist. (μm)
WH6f_2	59.92	24.46	0.29		6.68	7.37	0.63	99.34	0.32	762	1	30
WH6f_3	60.20	24.50	0.26		6.61	7.08	0.65	99.30	0.33	764	1	40
WH6f_4	60.80	24.50	0.31		6.56	7.38	0.66	100.21	0.32	759	1	50
WH6f_5	61.45	24.48	0.27		6.47	7.12	0.59	100.38	0.32	763	1	60
WH6f_6	61.45	24.30	0.28		6.28	7.46	0.65	100.41	0.31	752	1	70
WH6f_7	61.50	24.25	0.31		6.26	7.36	0.68	100.35	0.31	753	1	80
WH6f_8	61.40	24.49	0.23		6.52	7.32	0.57	100.54	0.32	761	1	90
WH6f_9	60.42	24.92	0.23		6.83	7.03	0.57	99.99	0.34	771	1	100
WH6f_10	60.64	24.93	0.27		7.02	7.12	0.50	100.48	0.34	775	1	110
WH6f_11	59.89	25.37	0.31		7.23	6.92	0.55	100.26	0.35	780	1	120
WH6f_12	61.31	24.76	0.33		6.84	6.92	0.61	100.77	0.34	772	1	130
WH6f_13	61.62	24.22	0.15		6.53	7.26	0.56	100.35	0.32	762	1	140
WH6f_14	60.12	24.80	0.12		6.79	7.07	0.59	99.49	0.33	769	1	150
WH6f_15	60.81	24.63	0.28		6.67	7.23	0.60	100.20	0.33	765	1	160
WH6f_16	61.22	24.78	0.38		6.55	7.39	0.61	100.94	0.32	760	1	170
WH6f_17	60.97	24.72	0.29		6.69	7.23	0.55	100.43	0.33	766	1	180
WH6f_18	60.58	24.87	0.26		6.48	7.27	0.57	100.03	0.32	761	1	190
WH6f_19	61.64	24.47	0.30		6.69	7.16	0.62	100.88	0.33	765	1	200
WH6f_20	60.21	24.56	0.25		6.36	7.30	0.66	99.35	0.31	756	1	210
WH6f_21	60.52	24.88	0.20		6.57	7.31	0.62	100.09	0.32	761	1	220
WH6f_22	59.88	24.59	0.05		6.66	7.07	0.59	98.85	0.33	767	1	230
WH6f_23	60.45	24.77	0.25		6.37	7.26	0.68	99.77	0.31	756	1	240
WH6f_24	61.50	24.38	0.28		6.28	7.47	0.66	100.57	0.31	752	1	250
WH6f_25	60.85	24.59	0.27		6.61	7.17	0.61	100.09	0.33	764	1	260
WH6f_26	61.18	24.55	0.21		6.65	7.16	0.60	100.35	0.33	765	1	270
WH6f_27	60.95	24.70	0.30		6.81	6.92	0.76	100.44	0.34	767	1	280
WH6f_28	59.45	25.76	0.27		7.65	6.76	0.49	100.39	0.37	791	1	290
WH6f_32	60.41	25.54	0.26		7.67	6.90	0.59	101.37	0.37	786	1	330
WH6f_34	62.02	23.83	0.27		5.91	7.61	0.77	100.40	0.29	739	1	350
WH6f_35	61.73	24.14	0.20		5.97	7.22	0.75	100.01	0.30	747	1	360
WH6f_36	59.90	24.14	0.24		6.35	7.42	0.72	98.76	0.31	753	1	370
WH6f_37	59.81	24.68	0.23		6.41	7.33	0.70	99.15	0.31	756	1	380
WH6f_38	57.08	27.07	0.26		8.17	6.19	0.48	99.24	0.41	806	1	390
WH6f_39	53.68	29.62	0.27		11.62	4.57	0.26	100.02	0.58	846	1	400
WH6f_40	52.67	29.92	0.25		12.06	4.26	0.23	99.39	0.60	847	1	410
WH6f_41	54.87	27.83	0.58		10.48	5.13	0.36	99.23	0.52	839	1	420
WH6f_43	55.26	27.82	0.16		10.51	5.29	0.28	99.33	0.51	840	1	440
WH6f_44	53.11	29.63	0.23		12.14	4.53	0.19	99.83	0.59	849	1	450
WH6f_45	53.17	29.01	0.26		11.15	4.66	0.25	98.50	0.56	846	1	460
WH6f_46	54.10	27.47	0.53		10.16	5.55	0.30	98.10	0.49	836	1	470
WH6f_47	58.05	26.45	0.36		7.59	6.54	0.58	99.57	0.38	790	1	480
WH6f_48	60.54	24.63	0.34		6.29	7.30	0.74	99.83	0.31	753	1	490
WH6f_49	60.30	23.83	0.27		5.91	7.25	0.61	98.17	0.30	749	1	500
WH6f_50	62.34	24.14	0.28		5.86	7.49	0.78	100.90	0.29	740	1	510
WH6f_51	60.86	24.46	0.31		6.55	7.22	0.68	100.08	0.32	760	1	520
WH6f_52	60.44	24.75	0.40		6.71	7.10	0.65	100.06	0.33	766	1	530
WH6f_53	60.69	24.85	0.17		6.48	7.24	0.69	100.11	0.32	758	1	540
WH6f_54	59.60	24.90	0.23		6.87	7.18	0.62	99.40	0.33	768	1	550
WH6f_55	59.58	25.32	0.34		6.83	7.11	0.50	99.68	0.34	772	1	560
WH6f_57	61.42	25.62	0.20		6.82	6.90	0.61	101.57	0.34	772	1	580
WH6f_58	62.40	24.59	0.19		6.17	7.12	0.70	101.17	0.31	754	1	590
WH6f_59	61.36	24.02	0.26		6.12	7.44	0.74	99.95	0.30	747	1	600
WH6f_60	61.69	25.22	0.27		6.85	7.01	0.66	101.68	0.34	770	1	610
WH6f_61	61.75	25.16	0.28		6.66	7.17	0.54	101.56	0.33	767	1	620
WH6f_62	61.34	24.70	0.28		6.62	7.44	0.61	100.99	0.32	760	1	630
WH6f_63	61.20	24.60	0.21		6.83	7.24	0.64	100.71	0.33	766	1	640
WH6f_64	61.41	24.93	0.27		6.64	7.08	0.60	100.94	0.33	766	1	650

Table A3.6 continued

Sample	SiO_2	Al_2O_3	FeO	MgO	CaO	Na_2O	K_2O	Total	Xan	T (°C)	G	Dist. (μm)
WH6g_3	61.66	24.41	0.32		6.50	7.07	0.61	100.58	0.32	764	2	40
WH6g_4	60.82	24.67	0.35		6.97	7.14	0.60	100.55	0.34	771	2	50
WH6g_5	61.29	24.39	0.36		6.45	7.06	0.66	100.21	0.32	761	2	60
WH6g_6	61.91	24.39	0.25		6.85	7.11	0.60	101.10	0.34	769	2	70
WH6g_7	61.85	24.39	0.34		6.74	7.00	0.66	100.98	0.33	768	2	80
WH6g_8	61.52	24.45	0.24		6.57	7.02	0.67	100.46	0.33	764	2	90
WH6g_9	61.67	24.49	0.27		6.54	7.12	0.67	100.76	0.32	762	2	100
WH6g_10	62.06	24.29	0.27		6.32	7.52	0.75	101.22	0.30	750	2	110
WH6g_11	62.18	24.22	0.22		6.35	7.23	0.70	100.89	0.31	756	2	120
WH6g_12	61.43	24.54	0.22		6.76	7.00	0.61	100.56	0.34	769	2	130
WH6g_13	61.44	24.70	0.16		6.95	7.21	0.63	101.09	0.33	769	2	140
WH6g_14	61.31	24.46	0.21		6.78	7.01	0.56	100.33	0.34	771	2	150
WH6g_15	61.79	24.49	0.26		6.86	7.10	0.59	101.08	0.34	770	2	160
WH6g_16	60.61	25.18	0.19		7.71	6.73	0.54	100.96	0.38	791	2	170
WH6g_17	60.74	25.46	0.24		7.68	6.86	0.53	101.51	0.37	789	2	180
WH6g_18	61.71	24.51	0.24		6.61	7.03	0.67	100.77	0.33	765	2	190
WH6g_19	62.53	24.51	0.24		6.33	7.27	0.67	101.55	0.31	755	2	200
WH6g_20	62.30	24.33	0.30		6.48	7.33	0.74	101.47	0.31	756	2	210
WH6g_21	61.69	24.81	0.18		6.94	6.93	0.63	101.18	0.34	773	2	220
WH6g_22	62.56	24.55	0.24		6.38	7.19	0.71	101.63	0.32	757	2	230
WH6g_25	59.33	26.62	0.17		8.77	6.31	0.40	101.59	0.42	813	2	260
WH6g_26	61.12	25.58	0.18		7.45	6.85	0.56	101.74	0.36	784	2	270
WH6g_27	61.80	24.28	0.17		6.19	7.22	0.71	100.37	0.31	753	2	280
WH6g_28	61.55	24.61	0.19		6.70	7.35	0.67	101.05	0.32	762	2	290
WH6g_29	60.82	24.70	0.19		6.55	7.20	0.65	100.10	0.32	761	2	300
WH6g_30	61.57	24.55	0.30		6.37	7.27	0.66	100.71	0.31	757	2	310
WH6g_32	62.10	24.16	0.23		6.14	7.20	0.76	100.59	0.31	751	2	330
WH6g_33	61.70	24.42	0.16		6.51	7.13	0.69	100.61	0.32	761	2	340
WH6g_34	61.18	24.74	0.29		6.69	7.37	0.63	100.91	0.32	762	2	350
WH6g_35	61.36	24.58	0.17		6.77	7.26	0.69	100.83	0.33	764	2	360
WH6g_36	61.39	24.51	0.21		6.71	7.08	0.64	100.54	0.33	766	2	370
WH6g_37	60.74	24.60	0.18		6.75	7.17	0.73	100.17	0.33	764	2	380
WH6g_38	61.05	24.78	0.26		6.67	7.15	0.64	100.56	0.33	765	2	390
WH6g_39	61.47	23.56	0.30		6.21	7.35	0.66	99.55	0.31	752	2	400
WH6g_40	61.67	25.05	0.22		6.46	7.49	0.71	101.60	0.31	754	2	410
WH6g_41	61.96	23.98	0.18		6.32	7.42	0.73	100.58	0.31	752	2	420
WH6g_42	61.82	24.13	0.21		6.02	7.51	0.69	100.37	0.29	745	2	430
WH6g_43	62.73	24.24	0.25		5.97	7.38	0.66	101.23	0.30	747	2	440
WH6g_44	62.64	23.88	0.18		5.97	7.41	0.78	100.85	0.29	743	2	450
WH6g_45	62.75	23.54	0.21		5.73	7.50	0.82	100.55	0.28	736	2	460
WH6g_46	62.11	23.83	0.35		5.85	7.69	0.80	100.61	0.28	736	2	470
WH6g_47	62.74	23.72	0.21		5.97	7.45	0.68	100.76	0.29	745	2	480
WH6g_48	62.35	24.70	0.25		6.42	7.38	0.68	101.78	0.31	755	2	490
WH6g_49	61.84	24.56	0.25		6.30	7.54	0.69	101.18	0.30	751	2	500
WH6g_53	62.11	24.58	0.20		6.36	7.43	0.71	101.37	0.31	753	2	540
WH6g_54	62.87	24.65	0.18		6.19	7.32	0.66	101.86	0.31	752	2	550
WH6g_56	62.30	24.43	0.12		5.91	7.47	0.73	100.96	0.29	742	2	570
WH6g_57	62.92	24.39	0.19		5.85	7.56	0.75	101.66	0.29	739	2	580
WH6g_58	62.74	24.47	0.23		6.17	7.36	0.76	101.72	0.30	749	2	590
WH6g_59	62.10	24.24	0.23		6.09	7.44	0.74	100.84	0.30	747	2	600
WH6g_60	62.14	24.75	0.25		6.34	7.43	0.71	101.62	0.31	752	2	610
WH6g_61	61.13	24.72	0.20		6.45	7.19	0.71	100.40	0.32	758	2	620
WH6g_62	61.64	25.06	0.33		6.52	7.30	0.74	101.57	0.32	757	2	630
WH6g_63	61.68	24.98	0.16		6.71	7.40	0.59	101.52	0.32	763	2	640
WH6g_64	62.00	24.39	0.22		6.43	7.21	0.71	100.96	0.32	757	2	650
WH6g_65	62.15	24.81	0.22		6.51	7.32	0.71	101.71	0.32	758	2	660
WH6g_66	62.06	24.88	0.20		6.51	7.24	0.70	101.58	0.32	759	2	670

Table A3.6 continued

Sample	SiO_2	Al_2O_3	FeO	MgO	CaO	Na_2O	K_2O	Total	XAn	T (°C)	G	Dist. (μm)
WH6g_69	61.92	24.32	0.22		6.18	7.68	0.61	100.93	0.30	748	2	700

Major elements are given in wt%, *X An* are calculated on a mole fraction basis and temperatures (T) are calculated using the Plagioclase-melt equilibria of Putirka (2005) and a pressure of 60 MPa.

Appendix 3

Table A3.7: Major element compositions (given in wt%) of core and rim analyses of Whakamaru plagioclase crystals

Table A3.7

Sample	SiO_2	Al_2O_3	FeO	CaO	Na_2O	K_2O	TOTAL	X An	Position
WH2K_1	60.37	24.71	0.24	7.18	8.28	0.54	101.31	0.31	Rim
WH2R_1	61.36	24.71	0.27	6.97	8.21	0.61	102.13	0.31	Rim
WH2S_1	60.99	24.18	0.24	6.72	8.63	0.69	101.45	0.29	Rim
WH2V_1	60.35	24.46	0.26	6.49	8.51	0.73	100.80	0.29	Rim
WH2AA_1	59.30	24.60	0.25	6.96	8.30	0.63	100.05	0.31	Rim
WH2ACa_1	61.42	24.54	0.26	6.56	8.44	0.62	101.85	0.29	Rim
WH2AD_1	60.30	24.26	0.25	6.66	8.23	0.62	100.32	0.30	Rim
WH2AE_1	60.11	24.21	0.31	6.94	8.20	0.57	100.34	0.31	Rim
WH2AG_1	60.36	24.24	0.31	6.89	8.30	0.60	100.71	0.30	Rim
WH3i_3	59.53	25.54	0.19	7.97	7.59	0.56	101.38	0.36	Middle
WH3i_4	61.77	23.70	0.36	6.19	8.58	0.68	101.29	0.28	Middle
WH3K_2	61.14	24.31	0.33	6.54	8.18	0.57	101.08	0.30	Rim
WH3_P1	61.69	23.32	0.29	5.99	7.95	0.72	99.97	0.28	Core
WH3_P2	61.97	23.34	0.30	6.24	8.08	0.66	100.59	0.29	Rim
WH3_Q1	59.13	24.01	0.27	7.00	7.34	0.63	98.38	0.33	Core
WH3_Q3	61.22	24.14	0.21	6.60	7.65	0.68	100.49	0.31	Middle
WH3_Q5	59.14	24.72	0.39	8.13	7.19	0.45	100.02	0.37	Rim
WH3R_1	61.98	23.96	0.16	6.55	8.27	0.69	101.61	0.29	Rim
WH3T_1	57.80	26.20	0.27	9.33	6.77	0.34	100.70	0.42	Core
WH3T_2	61.21	24.37	0.28	6.91	8.23	0.65	101.66	0.31	Rim
WH3_W1	59.78	24.11	0.15	7.53	7.12	0.45	99.15	0.36	Core
WH3_W3	64.16	21.81	0.19	4.44	8.92	1.04	100.55	0.20	Rim
WH3_AI1	61.31	23.38	0.20	6.23	8.04	0.71	99.86	0.29	Middle
WH3_AI2	59.99	22.85	0.30	6.29	7.28	0.57	97.28	0.31	Core
WH4A_1	61.12	23.98	0.22	6.68	8.20	0.57	100.78	0.30	Rim
WH4B_1	60.16	24.46	0.29	7.08	8.15	0.59	100.74	0.31	Rim
WH4B_2	58.26	24.88	0.20	7.63	7.47	0.50	98.94	0.35	Core
WH4E_1	60.46	24.30	0.24	6.78	8.40	0.64	100.82	0.30	Core
WH4E_2	59.79	23.64	0.34	6.55	8.27	0.67	99.25	0.29	Rim
WH4F_1	60.95	23.85	0.26	6.50	8.38	0.62	100.55	0.29	Core
WH4F_2	60.73	23.98	0.15	6.72	8.32	0.61	100.51	0.30	Rim
WH4G_1	59.46	25.09	0.22	6.87	8.19	0.52	100.35	0.31	Core
WH4G_2	63.25	22.06	0.14	4.16	9.40	1.08	100.09	0.19	Rim
WH4H_1	60.62	24.14	0.23	6.65	8.45	0.61	100.69	0.29	Rim
WH4H_2	59.40	24.51	0.24	7.15	7.89	0.52	99.71	0.32	Core
WH4i_1	59.79	23.88	0.25	6.62	7.94	0.65	99.14	0.30	Core
WH4i_2	61.05	24.07	0.25	7.09	8.09	0.59	101.13	0.32	Rim
WH4J_1	61.15	24.29	0.26	6.72	8.33	0.66	101.41	0.30	Core
WH4J_2	61.52	24.30	0.26	7.01	8.29	0.62	102.00	0.31	Rim
WH4K_1	61.69	23.80	0.27	6.20	8.58	0.65	101.19	0.28	Rim
WH4L_1	60.71	24.46	0.19	6.89	8.12	0.55	100.92	0.31	Rim
WH4M_1	59.41	25.07	0.23	7.85	7.83	0.50	100.90	0.35	Core
WH4M_2	60.72	24.74	0.17	7.24	7.91	0.56	101.34	0.33	Rim
WH4N_1	60.20	23.99	0.27	6.70	8.07	0.65	99.87	0.30	Rim
WH4O_1	60.99	23.96	0.22	6.42	8.21	0.65	100.44	0.29	Rim
WH4P_1	59.68	25.28	0.29	8.15	7.69	0.48	101.58	0.36	Core
WH4P_2	58.87	26.05	0.29	8.68	7.26	0.44	101.58	0.39	Middle
WH4P_3	60.42	24.15	0.30	6.57	8.39	0.63	100.45	0.29	Rim
WH4Q_1	58.36	27.20	0.38	9.02	6.70	0.31	101.97	0.42	Core
WH4S_1	59.64	23.82	0.21	6.46	8.53	0.67	99.33	0.28	Rim
WH4T_1	60.16	24.10	0.20	6.80	8.12	0.63	100.01	0.31	Core
WH4T_2	60.62	23.67	0.20	6.47	8.50	0.68	100.14	0.29	Rim
WH4Y_1	60.94	24.69	0.20	7.01	8.12	0.67	101.64	0.31	Rim
WH4Z_1	61.67	24.50	0.31	6.80	8.46	0.64	102.37	0.30	Rim
WH4AA_1	61.50	23.94	0.33	6.53	8.50	0.74	101.53	0.29	Core
WH4AA_2	58.23	25.90	0.30	8.69	7.07	0.43	100.62	0.39	Middle
WH4AA_3	61.05	24.60	0.29	7.22	8.08	0.56	101.81	0.32	Rim
WH4AB_1	60.65	25.16	0.22	7.09	8.03	0.55	101.69	0.32	Core
WH4AB_2	59.48	24.73	0.29	7.00	8.24	0.58	100.33	0.31	Rim
WH4AE_1	60.54	24.69	0.29	6.95	8.27	0.60	101.33	0.31	Rim
WH4AF_1	60.79	24.83	0.25	6.99	8.18	0.59	101.64	0.31	Rim
WH4AF_2	59.18	26.06	0.36	8.41	7.44	0.45	101.90	0.38	Core

Table A3.7 continued

WH4AJ_1	60.61	24.40	0.19	6.89	8.47	0.65	101.21	0.30	Rim
WH4AK_1	61.55	24.26	0.23	6.57	8.79	0.70	102.10	0.28	Core
WH4AK_2	60.73	24.56	0.27	7.07	8.23	0.65	101.51	0.31	Rim
WH4AL_1	60.55	25.31	0.22	7.24	8.01	0.60	101.93	0.32	Core
WH4AL_2	60.48	24.44	0.34	6.93	8.39	0.61	101.20	0.30	Rim
WH4AN_1	60.46	24.18	0.21	6.34	8.44	0.69	100.32	0.28	Rim
WH4AO_1	61.37	24.31	0.28	6.50	8.60	0.69	101.75	0.28	Core
WH4AO_2	55.97	26.65	0.30	9.86	6.74	0.41	99.94	0.44	Rim
WH6H_1	59.73	24.16	0.19	6.81	8.36	0.57	99.82	0.30	Rim
WH6K_1	60.04	24.43	0.17	6.95	8.32	0.70	100.60	0.30	Rim
WH6M_1	60.53	24.53	0.28	7.54	8.08	0.63	101.59	0.33	Rim
WH6N_2	60.34	23.95	0.27	6.52	8.50	0.65	100.22	0.29	Rim
WH6O_1	60.78	24.51	0.30	7.06	8.35	0.62	101.62	0.31	Rim
WH6Q_1	59.33	24.00	0.27	6.73	8.29	0.60	99.21	0.30	Rim
WH6S_1	59.84	24.02	0.18	6.42	8.13	0.64	99.24	0.29	Rim
WH6T_1	64.50	22.22	0.15	4.25	9.80	1.15	102.07	0.18	Rim
WH6T_2	60.93	23.71	0.19	5.61	8.89	0.73	100.06	0.25	Core
WH6AA_1	62.70	23.86	0.23	6.52	8.30	0.66	102.27	0.29	Middle
WH6AD_1	59.71	24.60	0.18	6.89	8.39	0.66	100.42	0.30	Rim
WH6AF_1	59.58	24.16	0.31	6.83	8.30	0.64	99.80	0.30	Rim
WH6AG_1	61.33	24.41	0.22	6.47	8.56	0.62	101.62	0.28	Rim
WH6AH_1	60.23	24.30	0.33	6.85	8.39	0.69	100.79	0.30	Rim
WH6AH_2	56.15	26.50	0.27	9.56	6.92	0.34	99.73	0.43	Core
WH6AI_1	60.45	23.99	0.19	6.71	8.38	0.58	100.29	0.30	Core
WH6AI_2	63.96	22.39	0.18	4.72	9.38	0.88	101.51	0.21	Rim
WH6AJ_1	60.68	23.95	0.33	6.77	8.22	0.68	100.64	0.30	Rim
WH6AP_1	54.88	28.16	0.23	12.12	5.41	0.25	101.05	0.55	Core
WH6AP_2	63.14	23.72	0.30	7.00	7.92	0.62	102.71	0.32	Rim

Core and rim analyses of Whakamaru plagioclase crystals, position of analyses are illustrated in Appendix A4.2. Major elements are given in wt% with X_{An} calculated on a mole fraction basis.

Appendix 3

Table A3.8: Sr, Ba and Mg profiles of Whakamaru plagioclase crystals

CaO concentrations are given in Wt%

Sr, Ba, Mg concentrations are given in ppm

Table A3.8

Sample	Group	Distance (μm)	X An	CaO (wt%)	Mg (ppm)	Sr (ppm)	Ba (ppm)
WH1h_L22	1	189	0.30	6.35	74	589	852
WH1h_L21	1	211	0.34	7.18	79	634	875
WH1h_L20	1	234	0.35	7.37	85	693	982
WH1h_L19	1	254	0.38	8.01	88	674	635
WH1h_L18	1	275	0.47	9.98	103	811	617
WH1h_L17	1	295	0.44	9.27	86	663	367
WH1h_L16	1	320	0.53	10.90	92	806	364
WH1h_L15	1	340	0.52	11.10	83	746	277
WH1h_L14	1	361	0.52	10.98	82	710	210
WH1h_L13	1	381	0.53	11.22	77	698	175
WH1h_L12	1	398	0.53	11.21	79	680	191
WH1h_L11	1	421	0.53	11.13	78	705	247
WH1h_L10	1	442	0.49	9.98	77	647	111
WH1h_L9	1	461	0.52	10.82	96	692	144
WH1h_L8	1	492	0.49	8.57	75	567	139
WH1h_L7	1	513	0.41	8.67	62	555	115
WH1h_L6	1	533	0.32	6.48	76	581	716
WH1h_L5	1	554	0.32	6.65	71	565	671
WH1h_L4	1	573	0.30	6.39	69	554	655
WH1h_L3	1	594	0.32	6.65	72	577	681
WH1h_L2	1	614	0.30	6.32	74	547	732
WH1h_L1	1	634	0.30	6.29	78	569	738
WH2b_L68	1	9	0.30	6.23	65	511	604
WH2b_L67	1	41	0.31	6.52	73	533	717
WH2b_L66	1	64	0.31	6.45	69	543	700
WH2b_L65	1	80	0.32	6.60	67	564	685
WH2b_L64	1	104	0.31	6.51	65	577	687
WH2b_L63	1	120	0.31	6.24	67	555	659
WH2b_L62	1	139	0.31	6.36	69	572	620
WH2b_L61	1	159	0.32	6.68	73	615	698
WH2b_L60	1	179	0.32	6.77	78	613	699
WH2b_L59	1	199	0.31	6.36	66	561	620
WH2b_L58	1	218	0.29	6.05	72	560	616
WH2b_L57	1	238	0.33	6.91	75	591	573
WH2b_L56	1	254	0.27	5.52	70	540	681
WH2b_L55	1	274	0.31	6.46	62	555	602
WH2b_L54	1	294	0.31	6.41	62	550	614
WH2b_L53	1	317	0.32	6.59	61	560	590
WH2b_L52	1	337	0.32	6.64	58	553	563
WH2b_L51	1	373	0.34	7.18	64	600	582
WH2b_L50	1	396	0.34	7.15	62	591	504
WH2b_L49	1	412	0.34	7.14	61	591	521
WH2b_L48	1	432	0.33	6.96	73	581	513
WH2b_L47	1	452	0.36	7.53	68	621	573
WH2b_L46	1	471	0.37	7.70	63	610	510
WH2b_L45	1	483	0.34	7.29	70	616	503
WH2b_L44	1	515	0.34	7.50	67	599	513
WH2b_L43	1	534	0.38	7.84	66	621	494
WH2b_L42	1	554	0.37	7.69	68	601	453
WH2b_L41	1	578	0.37	7.75	66	601	410
WH2b_L40	1	594	0.38	7.97	69	593	376
WH2b_L39	1	625	0.40	8.42	66	622	346
WH2b_L38	1	649	0.42	8.94	70	645	354
WH2b_L37	1	665	0.41	8.68	74	659	419
WH2b_L36	1	689	0.38	8.00	68	605	353

Table A3.8 continued

Sample	Group	Distance (μm)	X An	CaO (wt%)	Mg (ppm)	Sr (ppm)	Ba (ppm)
WH2b_L34	1	732	0.40	8.52	71	563	332
WH2b_L33	1	752	0.41	8.69	72	601	393
WH2b_L32	1	772	0.41	8.55	69	593	342
WH2b_L31	1	791	0.40	8.44	78	555	290
WH2b_L30	1	815	0.41	8.68	67	583	302
WH2b_L29	1	835	0.44	9.18	70	602	288
WH2b_L28	1	854	0.43	9.06	67	572	252
WH2b_L27	1	874	0.47	9.85	79	676	336
WH2b_L26	1	902	0.48	10.04	85	698	388
WH2b_L25	1	922	0.36	7.77	82	622	450
WH2b_L24	1	937	0.42	9.25	78	635	338
WH2b_L23	1	961	0.45	9.49	76	626	309
WH2b_L22	1	981	0.44	8.82	72	580	270
WH2b_L21	1	1001	0.42	9.00	73	644	341
WH2b_L20	1	1020	0.42	8.89	74	636	353
WH2b_L19	1	1040	0.38	8.06	70	637	414
WH2b_L18	1	1060	0.41	8.65	74	667	412
WH2b_L12	1	1084	0.41	8.50	69	648	398
WH2b_L11	1	1107	0.38	8.10	77	654	534
WH2b_L10	1	1127	0.34	7.33	69	589	529
WH2b_L9	1	1147	0.32	6.88	72	599	602
WH2b_L8	1	1170	0.31	6.56	79	587	648
WH2b_L7	1	1190	0.34	7.19	75	585	561
WH2b_L6	1	1210	0.28	6.03	66	537	592
WH2b_L5	1	1230	0.27	5.83	77	499	580
WH2b_L4	1	1257	0.30	6.35	70	548	595
WH2b_L3	1	1277	0.30	6.28	71	521	569
WH2b_L4	1	1297	0.31	6.58	75	536	639
WH2d_L57	1	25	0.32	6.32	72	506	631
WH2d_L56	1	48	0.31	6.32	72	546	678
WH2d_L55	1	66	0.32	6.63	74	558	659
WH2d_L54	1	84	0.31	6.51	70	548	641
WH2d_L53	1	102	0.30	6.23	71	534	684
WH2d_L52	1	117	0.30	6.33	72	537	710
WH2d_L51	1	137	0.30	6.19	73	544	695
WH2d_L50	1	155	0.31	6.52	76	548	667
WH2d_L49	1	173	0.31	6.53	71	553	649
WH2d_L48	1	188	0.31	6.48	69	539	622
WH2d_L47	1	214	0.30	6.42	70	565	658
WH2d_L46	1	234	0.31	6.42	67	556	611
WH2d_L45	1	249	0.31	6.65	73	619	550
WH2d_L44	1	272	0.57	12.10	73	761	218
WH2d_L43	1	290	0.56	11.88	75	777	177
WH2d_L42	1	310	0.53	11.04	78	797	233
WH2d_L14	1	586	0.30	11.32	74	729	242
WH2d_L13	1	595	0.31	6.09	74	607	671
WH2d_L12	1	612	0.35	6.73	80	585	688
WH2d_L11	1	631	0.32	6.75	78	610	726
WH2d_L10	1	649	0.32	6.36	83	551	642
WH2d_L9	1	668	0.30	5.84	68	502	633
WH2d_L8	1	688	0.32	6.52	79	549	675
WH2d_L7	1	707	0.32	6.43	81	551	717
WH2d_L6	1	727	0.33	6.59	81	571	755
WH2d_L5	1	747	0.33	6.22	83	575	831
WH2d_L4	1	764	0.37	7.58	84	646	550

Table A3.8 continued

Sample	Group	Distance (μm)	X An	CaO (wt%)	Mg (ppm)	Sr (ppm)	Ba (ppm)
WH2d_L2	1	800	0.32	6.54	74	565	678
WH2d_L1	1	820	0.33	6.59	77	590	842
WH6da_L2	1	10	0.32	6.65	73	554	689
WH6da_L3	1	31	0.30	6.24	68	557	741
WH6da_L4	1	53	0.31	6.42	71	568	740
WH6da_L5	1	73	0.32	6.57	69	553	650
WH6da_L6	1	92	0.32	6.62	67	539	617
WH6da_L7	1	111	0.32	6.58	71	569	652
WH6da_L8	1	136	0.32	6.15	63	517	558
WH6da_L9	1	150	0.33	6.87	74	589	627
WH6da_L10	1	169	0.31	6.35	68	571	541
WH6da_L11	1	189	0.31	6.52	63	504	349
WH6da_L12	1	208	0.41	8.38	58	541	245
WH6da_L13	1	227	0.44	9.12	58	562	205
WH6da_L14	1	251	0.51	10.50	79	652	257
WH6da_L15	1	271	0.50	10.43	76	669	228
WH6da_L16	1	285	0.52	10.87	75	710	232
WH6da_L17	1	305	0.45	9.33	80	708	340
WH6da_L18	1	324	0.42	8.68	75	609	296
WH6da_L19	1	343	0.47	8.65	64	574	260
WH6da_L20	1	365	0.49	10.20	73	643	312
WH6da_L21	1	387	0.47	9.59	88	714	493
WH6da_L22	1	406	0.38	7.92	85	692	653
WH6da_L23	1	428	0.33	6.72	70	563	595
WH6da_L24	1	450	0.31	6.58	67	538	617
WH6da_L25	1	466	0.32	6.69	71	561	660
WH6da_L26	1	493	0.33	6.95	69	562	641
WH6da_L27	1	508	0.34	7.03	72	567	673
WH6da_L28	1	532	0.30	6.28	74	557	821
WH6da_L29	1	551	0.33	6.96	74	554	682
WH6da_L30	1	571	0.33	6.75	68	545	635
WH6db_L2	1	11	0.33	6.94	73	548	612
WH6db_L3	1	33	0.40	8.22	75	569	502
WH6db_L4	1	56	0.35	7.21	70	541	499
WH6db_L5	1	78	0.38	7.85	82	605	556
WH6db_L6	1	98	0.37	7.84	73	546	444
WH6db_L7	1	120	0.38	7.93	77	587	457
WH6db_L8	1	142	0.37	7.59	75	558	445
WH6db_L9	1	162	0.34	7.13	74	553	470
WH6db_L10	1	184	0.41	8.57	71	546	386
WH6db_L11	1	206	0.51	10.58	66	498	242
WH6db_L12	1	228	0.55	11.37	78	601	350
WH6db_L13	1	262	0.33	6.88	71	536	548
WH6db_L14	1	290	0.31	6.39	64	478	487
WH6db_L15	1	309	0.32	6.61	79	571	663
WH6db_L16	1	329	0.33	6.67	73	546	633
WH6db_L17	1	351	0.32	6.47	71	533	631
WH6db_L18	1	370	0.33	6.82	75	580	713
WH6f_L1	1	10	0.33	6.83	75	560	810
WH6f_L2	1	30	0.33	6.70	78	548	725
WH6f_L3	1	52	0.32	6.41	76	545	762
WH6f_L4	1	71	0.32	6.83	77	549	653
WH6f_L5	1	91	0.35	7.28	85	588	708

Table A3.8 continued

Sample	Group	Distance (μm)	X An	CaO (wt%)	Mg (ppm)	Sr (ppm)	Ba (ppm)
WH6f_L7	1	153	0.33	6.88	78	554	636
WH6f_L8	1	153	0.33	6.77	76	549	632
WH6f_L9	1	172	0.33	6.73	75	552	623
WH6f_L10	1	190	0.32	6.51	73	534	580
WH6f_L11	1	207	0.33	6.77	75	549	597
WH6f_L12	1	231	0.31	6.59	76	472	898
WH6f_L13	1	296	0.36	7.83	80	598	643
WH6f_L14	1	315	0.33	6.82	86	630	775
WH6f_L15	1	340	0.30	6.19	72	551	583
WH6f_L16	1	379	0.36	8.21	71	576	367
WH6f_L17	1	384	0.59	11.89	109	694	247
WH6f_L18	1	406	0.52	9.12	73	636	280
WH6f_L19	1	428	0.55	11.38	82	688	238
WH6f_L20	1	448	0.57	10.71	84	727	352
WH6f_L21	1	473	0.34	6.63	81	609	617
WH6f_L22	1	495	0.29	6.14	83	576	702
WH6f_L23	1	517	0.32	6.63	78	581	662
WH6f_L24	1	532	0.32	6.88	95	555	655
WH6f_L25	1	552	0.32	6.58	104	558	760
WH6f_L26	1	576	0.32	6.18	68	476	668
WH6f_L27	1	596	0.32	6.79	80	564	708
WH6f_L28	1	616	0.32	6.76	79	547	660
WH6f_L29	1	640	0.33	7.00	80	562	675
WH3e_L1	2	34	0.32	6.56	68	625	661
WH3e_L2	2	49	0.32	6.46	55	586	594
WH3e_L3	2	68	0.32	6.35	56	569	627
WH3e_L4	2	83	0.33	6.68	66	574	576
WH3e_L5	2	108	0.31	6.31	57	574	584
WH3e_L6	2	127	0.33	6.73	51	560	590
WH3e_L7	2	147	0.33	6.60	55	566	603
WH3e_L8	2	162	0.31	6.29	55	567	638
WH3e_L9	2	184	0.30	6.12	76	607	715
WH3e_L10	2	203	0.30	6.37	71	609	716
WH3e_L11	2	220	0.32	6.31	64	583	577
WH3e_L12	2	240	0.32	6.47	66	567	592
WH3e_L13	2	259	0.31	6.36	63	552	594
WH3e_L14	2	279	0.32	6.44	62	558	562
WH3e_L15	2	299	0.31	6.20	66	559	582
WH3e_L16	2	319	0.31	6.30	60	549	535
WH3e_L21	2	421	0.36	7.45	71	593	483
WH3e_L22	2	441	0.35	6.70	69	549	436
WH3e_L23	2	463	0.35	7.04	72	618	532
WH3e_L24	2	483	0.37	7.60	79	637	530
WH3e_L25	2	505	0.33	6.21	62	525	456
WH3e_L26	2	524	0.29	6.00	72	623	623
WH3e_L27	2	544	0.31	6.15	73	570	569
WH3e_L28	2	564	0.29	5.55	66	550	576
WH3e_L30	2	613	0.28	5.78	48	592	660
WH3e_L31	2	632	0.31	6.18	59	585	570
WH3e_L32	2	657	0.31	6.33	54	627	618
WH3e_L33	2	671	0.31	6.39	62	590	633
WH3e_L34	2	691	0.31	6.16	60	574	624
WH3e_L35	2	708	0.31	6.08	58	536	634
WH3e_L36	2	728	0.32	6.49	57	612	713
WH3e_L37	2	747	0.33	6.51	61	629	732

Table A3.8 continued

Sample	Group	Distance (μm)	X An	CaO (wt%)	Mg (ppm)	Sr (ppm)	Ba (ppm)
WH3e_L39	2	784	0.31	7.47	84	813	1323
WH3e_L40	2	804	0.28	5.74	64	625	1017
WH3e_L41	2	823	0.29	5.80	58	651	1091
WH6b_L1	3	20	0.29	5.80	28	434	458
WH6b_L2	3	41	0.28	5.89	29	456	505
WH6b_L3	3	62	0.28	5.83	28	465	510
WH6b_L4	3	83	0.28	5.74	27	440	478
WH6b_L5	3	103	0.26	5.78	31	432	483
WH6b_L8	3	166	0.28	5.53	32	466	708
WH6b_L9	3	187	0.29	5.77	31	440	565
WH6b_L10	3	208	0.26	5.38	26	416	562
WH6b_L11	3	229	0.27	5.54	27	481	633
WH6b_L12	3	249	0.25	5.44	28	478	633
WH6b_L13	3	270	0.25	5.17	27	445	656
WH6b_L14	3	291	0.20	4.93	25	433	712
WH6b_L15	3	312	0.21	4.39	24	407	789
WH6b_L16	3	333	0.26	3.98	20	355	559
WH6b_L17	3	354	0.20	5.17	26	464	839
WH6b_L18	3	375	0.21	4.47	22	367	632
WH6b_L19	3	395	0.22	4.53	22	385	725
WH6b_L20	3	416	0.20	4.28	22	343	632
WH6b_L21	3	437	0.21	4.14	20	286	455
WH6b_L22	3	458	0.22	4.10	19	307	527

Appendix 3

Table A3.9: Rare earth elements, Sr, Yb and Pb analyses of Whakamaru plagioclase crystals

CaO concentrations are given in wt%

Trace element concentrations are given in ppm

Table A3.9

Sample	Position	Spot	Group	X An	CaO	Sr	Y	La	Ce	Pr	Nd	Sm	Eu	Gd	Tb	Dy	Ho	Er	Tm	Yb	Lu	Pb
WH1h_32	rim	35	1	0.30	6.28	537	0.2	9.0	10.1	0.79	2.4	0.34	1.59	0.10	b.d.	0.11	b.d.	b.d.	b.d.	b.d.	b.d.	6.28
WH1h_33	rim	35	1	0.41	8.45	556	0.2	5.6	7.50	0.70	2.4	0.23	1.57	0.14	0.01	b.d.	b.d.	0.04	0.01	b.d.	b.d.	5.18
WH1h_34	core	35	1	0.54	10.9	697	0.7	4.0	6.20	0.63	2.4	0.47	1.74	0.43	0.02	0.27	0.02	0.03	b.d.	0.09	0.01	4.40
WH1h_35	core	35	1	0.56	11.4	768	0.2	3.4	4.80	0.45	1.5	0.27	1.94	0.26	b.d.	0.09	0.01	0.04	b.d.	0.11	0.01	4.89
WH1h_36	rim	35	1	0.30	6.34	540	0.2	9.1	10.5	0.83	2.2	0.07	1.55	0.07	b.d.	0.03	0.02	b.d.	0.01	0.02	b.d.	5.97
WH2b_66a	rim	50	1	0.31	6.39	546	0.1	8.8	10.2	0.78	2.2	0.09	1.53	0.07	b.d.	0.05	b.d.	0.03	0.01	0.05	b.d.	6.75
WH2b_67a	rim	50	1	0.37	7.69	583	0.2	9.0	11.8	0.93	2.5	0.23	1.65	0.20	b.d.	0.02	b.d.	0.04	0.01	b.d.	b.d.	5.79
WH2b_68a	core	50	1	0.41	8.68	588	0.3	7.2	9.70	0.81	2.5	0.26	1.39	0.15	0.02	0.02	0.01	0.02	b.d.	0.01	b.d.	4.93
WH2b_69	core	50	1	0.47	9.83	632	1.1	8.3	12.4	1.11	3.6	0.5	1.51	0.38	0.04	0.22	0.03	0.06	0.02	0.02	b.d.	5.95
WH2b_70	rim	50	1	0.40	8.50	611	0.3	7.7	10.5	0.78	2.2	0.34	1.50	0.11	0.02	0.05	b.d.	0.01	b.d.	0.03	0.01	5.67
WH2b_71	rim	50	1	0.31	6.74	528	0.2	9.1	11.0	0.79	2.5	0.26	1.62	0.12	0.03	0.03	0.02	b.d.	0.01	b.d.	0.01	6.02
WH2d_58	rim	50	1	0.32	6.32	516	0.2	8.6	9.70	0.74	2.2	0.17	1.49	0.13	0.01	0.02	0.01	b.d.	b.d.	b.d.	b.d.	5.41
WH2d_59	rim	50	1	0.30	6.33	519	0.2	9.2	10.7	0.80	2.4	0.21	1.40	0.14	0.01	0.08	b.d.	0.05	0.01	0.01	0.01	6.12
WH2d_60	core	50	1	0.56	11.8	975	0.5	8.6	10.8	0.90	2.8	0.27	2.15	0.25	0.02	0.09	b.d.	b.d.	0.01	b.d.	b.d.	6.59
WH2d_61	core	50	1	0.58	12.3	734	0.6	5.2	7.50	0.73	2.3	0.44	1.73	0.08	0.03	0.13	b.d.	0.07	0.01	0.09	b.d.	5.99
WH2d_62	rim	50	1	0.34	7.08	567	0.2	9.8	11.1	0.83	2.4	0.14	1.55	0.10	0.02	0.03	0.01	0.01	0.01	0.03	b.d.	6.69
WH2d_63	rim	50	1	0.33	6.98	585	0.2	9.5	11.1	0.76	2.3	0.39	1.65	0.06	0.01	0.07	b.d.	0.03	0.02	0.01	b.d.	6.24
WH6da_23a	rim	35	1	0.32	6.75	582	0.1	9.8	12.5	0.85	2.4	0.28	1.65	0.13	0.01	0.10	b.d.	b.d.	b.d.	b.d.	b.d.	7.34

Table A3.9 continued

Sample	Position	Spot	Group	X An	CaO	Sr	Y	La	Ce	Pr	Nd	Sm	Eu	Gd	Tb	Dy	Ho	Er	Tm	Yb	Lu	Pb
WH6da_24a	core	35	1	0.52	10.9	727	0.4	7.5	11.8	1.05	3.2	0.43	2.11	0.12	0.03	0.15	b.d.	0.04	b.d.	b.d.	0.02	6.78
WH6da_25a	rim	35	1	0.33	6.65	564	0.2	9.3	11.8	0.83	2.5	0.31	1.60	0.16	0.01	0.02	0.01	0.03	0.01	0.03	0.01	7.19
WH6db_20	rim	35	1	0.33	6.65	478	0.2	7.5	10.4	0.71	2.1	0.16	1.30	0.11	0.02	0.06	b.d.	b.d.	b.d.	b.d.	b.d.	5.82
WH6db_21	core	35	1	0.46	9.61	506	0.5	4.7	7.80	0.64	2.2	0.24	1.30	0.20	0.02	0.11	0.02	0.04	0.01	0.05	b.d.	5.93
WH6db_22	rim	35	1	0.32	6.94	501	0.2	8.1	11.0	0.80	2.5	0.22	1.41	0.16	0.01	0.05	0.01	0.05	0.01	b.d.	0.01	5.95
WH6f_31	rim	35	1	0.32	6.76	547	0.3	7.9	11.3	0.77	2.6	0.9	1.53	0.10	b.d.	b.d.	b.d.	b.d.	b.d.	b.d.	b.d.	6.75
WH6f_32	rim	35	1	0.32	6.18	520	0.1	8.5	11.2	0.74	2.3	0.22	1.46	0.16	b.d.	0.05	b.d.	b.d.	b.d.	b.d.	b.d.	6.63
WH6f_33	rim	35	1	0.30	5.91	562	0.1	8.5	11.2	0.76	1.8	0.12	1.46	0.04	b.d.	b.d.	b.d.	b.d.	b.d.	0.07	b.d.	6.49
WH6f_34	rim	35	1	0.34	5.91	556	0.2	7.2	9.40	0.61	1.7	0.23	1.51	0.02	0.03	0.06	b.d.	0.06	b.d.	b.d.	0.01	7.08
WH6f_35	core	35	1	0.59	11.9	741	0.4	4.8	7.90	0.67	2.0	0.26	1.99	0.16	0.02	0.10	b.d.	0.04	b.d.	b.d.	0.01	7.25
WH6f_36	core	35	1	0.52	9.12	554	0.3	3.2	5.50	0.40	1.5	0.21	1.41	0.06	0.01	0.08	0.01	b.d.	b.d.	0.02	0.01	5.62
WH6f_37	rim	35	1	0.33	6.66	603	0.2	8.7	11.2	0.72	1.7	0.21	1.63	0.18	0.01	0.08	0.01	b.d.	b.d.	0.02	0.01	7.66
WH6f_38	rim	35	1	0.32	6.41	533	0.2	7.9	10.8	0.72	2.3	0.24	1.42	0.10	0.00	b.d.	0.01	0.08	b.d.	b.d.	0.01	6.47
WH6f_39	rim	35	1	0.32	6.52	549	0.2	8.1	10.8	0.79	2.5	0.13	1.61	0.05	b.d.	0.03	0.02	b.d.	b.d.	b.d.	0.01	6.88
WH3e_45	rim	50	2	0.32	6.51	547	0.1	9.6	10.7	0.79	2.3	0.23	1.51	0.06	b.d.	b.d.	b.d.	b.d.	b.d.	b.d.	b.d.	6.31
WH3e_46	rim	50	2	0.32	6.48	554	0.2	9.6	10.7	0.79	2.4	0.12	1.48	0.11	0.01	b.d.	0.02	0.01	b.d.	0.03	0.01	6.15
WH3e_47	rim	50	2	0.36	7.47	606	0.2	8.5	9.70	0.80	2.3	0.36	1.53	0.13	0.01	0.10	0.02	b.d.	b.d.	0.06	0.01	6.55
WH3e_48	rim	50	2	0.32	6.56	575	0.1	8.8	10.3	0.74	2.1	0.12	1.57	b.d.	b.d.	0.06	0.01	b.d.	b.d.	0.03	b.d.	6.16
WH3e_49	core	50	2	0.29	5.94	590	0.1	9.2	9.40	0.61	1.7	0.15	1.4	0.15	0.02	0.04	b.d.	b.d.	b.d.	b.d.	0.01	6.42

Table A3.9 continued

Sample	Position	Spot	Group	X An	CaO	Sr	Y	La	Ce	Pr	Nd	Sm	Eu	Gd	Tb	Dy	Ho	Er	Tm	Yb	Lu	Pb
WH6b_50	core	50	3	0.28	5.86	485	0.2	12.5	12.8	0.91	2.6	0.15	2.65	b.d.	0.01	b.d.	0.01	b.d.	b.d.	b.d.	b.d.	11.0
WH6b_51	rim	50	3	0.27	5.69	479	0.1	8.9	9.50	0.75	2.3	0.14	1.99	b.d.	0.02	0.08	0.02	0.01	0.01	b.d.	b.d.	7.91
WH6b_52	rim	50	3	0.21	4.27	332	0.1	7.7	8.80	0.63	2.2	0.16	1.43	0.02	0.01	0.03	0.01	0.02	0.01	0.06	0.01	6.56

Position relates to location of the analysis in either the core or the rim.
Spot – denotes spot size diameter used in analysis in μm
X An – calculated on a mole fraction basis
CaO in wt% all other elements in ppm.

Appendix 3

Table A3.10: Major element compositions (are given in wt%) of Healy plagioclase crystals

Table A3.10

Sample	SiO_2	Al_2O_3	FeO	CaO	Na_2O	K_2O	Total	Dist (μm)	X An	Temp °C	H_2O wt%
X590b_2	58.40	27.30	0.39	9.36	6.18	0.19	101.81	0	0.45	733	8.84
X590b_4	58.22	27.46	0.39	9.05	6.12	0.11	101.35	20	0.45	733	8.79
X590b_5	57.86	27.39	0.51	9.34	6.06	0.15	101.32	30	0.46	735	8.83
X590b_6	57.59	27.44	0.52	9.20	6.18	0.17	101.10	40	0.45	732	8.82
X590b_7	57.90	27.40	0.48	9.56	6.14	0.16	101.64	50	0.46	735	8.83
X590b_8	57.90	27.46	0.44	9.30	5.95	0.17	101.22	60	0.46	735	8.85
X590b_9	58.35	27.61	0.49	9.49	5.99	0.12	102.06	70	0.46	737	8.82
X590b_10	57.93	27.33	0.42	9.43	6.11	0.15	101.38	80	0.46	735	8.83
X590b_11	58.68	27.66	0.51	9.48	6.19	0.13	102.65	90	0.45	735	8.81
X590b_20	58.75	27.88	0.49	9.42	6.15	0.14	102.83	180	0.45	735	8.82
X590b_21	58.24	27.73	0.40	9.20	6.13	0.09	101.80	190	0.45	735	8.78
X590b_22	58.26	27.66	0.40	9.38	6.18	0.13	102.01	200	0.45	734	8.81
X590b_23	58.37	27.74	0.45	9.47	6.33	0.13	102.49	210	0.45	734	8.80
X590b_24	58.10	27.85	0.41	9.41	6.22	0.17	102.16	220	0.45	733	8.83
X590b_25	58.45	27.75	0.43	9.19	6.09	0.15	102.04	230	0.45	733	8.82
X590b_26	57.87	27.64	0.43	9.47	5.98	0.13	101.52	240	0.46	737	8.83
X590b_27	58.11	27.55	0.37	9.57	6.07	0.13	101.80	250	0.46	737	8.83
X590b_28	58.06	27.15	0.43	9.06	6.31	0.16	101.17	260	0.44	730	8.81
X590b_30	58.43	27.25	0.48	9.13	6.21	0.15	101.66	280	0.44	732	8.81
X590b_31	58.76	27.18	0.46	9.15	6.22	0.12	101.89	290	0.45	733	8.79
X590b_32	58.40	27.61	0.45	9.25	6.16	0.16	102.03	300	0.45	733	8.82
X590b_33	58.39	27.67	0.46	9.87	6.06	0.12	102.57	310	0.47	739	8.84
X590b_34	57.76	27.75	0.55	9.49	5.86	0.11	101.53	320	0.47	739	8.83
X590b_35	58.03	27.78	0.39	9.33	6.04	0.12	101.68	330	0.46	736	8.81
X590b_36	57.73	27.75	0.44	9.47	6.07	0.10	101.55	340	0.46	737	8.80
X590b_37	57.26	27.49	0.48	9.54	5.97	0.13	100.86	350	0.47	738	8.83
X590b_39	57.96	27.77	0.45	9.63	5.86	0.11	101.78	370	0.47	740	8.84
X590b_40	58.19	27.54	0.52	9.57	5.93	0.12	101.87	380	0.47	738	8.83
X590b_41	58.18	27.71	0.35	9.34	6.17	0.14	101.88	390	0.45	734	8.81
X590b_42	58.17	27.78	0.49	9.52	6.00	0.12	102.08	400	0.46	737	8.83
X590b_43	57.98	27.93	0.38	9.57	5.85	0.20	101.92	410	0.47	737	8.89
X590b_44	57.76	27.48	0.39	9.65	6.07	0.12	101.47	420	0.46	738	8.83
X590b_45	58.15	27.43	0.40	9.70	6.11	0.12	101.91	430	0.46	738	8.82
X590b_46	58.65	27.50	0.52	9.25	6.09	0.13	102.13	440	0.45	734	8.81
X590b_47	58.74	27.52	0.45	9.25	6.33	0.14	102.43	450	0.44	732	8.80
X590b_48	58.70	27.62	0.43	9.15	6.11	0.15	102.17	460	0.45	733	8.81
X590b_49	58.30	27.43	0.42	9.30	6.04	0.10	101.58	470	0.46	736	8.80
X590b_50	57.69	27.33	0.47	9.17	6.04	0.16	100.87	480	0.45	733	8.83
X590b_51	58.11	27.27	0.44	9.32	6.19	0.16	101.48	490	0.45	733	8.82
X590b_52	58.14	27.22	0.41	8.91	6.20	0.09	100.97	500	0.44	732	8.77
X590b_53	58.23	27.42	0.49	9.14	6.22	0.12	101.61	510	0.45	732	8.79
X590b_54	58.24	27.46	0.43	9.39	6.09	0.11	101.72	520	0.46	736	8.80
X590b_55	57.81	27.60	0.50	9.35	6.09	0.12	101.47	530	0.46	735	8.81
X590b_56	57.98	27.56	0.35	9.39	6.10	0.15	101.53	540	0.46	735	8.83
X590b_57	57.92	27.41	0.45	8.84	6.05	0.15	100.83	550	0.44	731	8.81
X590b_58	58.21	27.30	0.38	9.19	6.18	0.14	101.39	560	0.45	733	8.81
X590b_59	58.12	27.37	0.43	9.04	6.29	0.13	101.37	570	0.44	731	8.79
X590b_60	58.32	27.54	0.40	9.07	6.17	0.13	101.63	580	0.44	732	8.80
X590b_61	60.00	27.09	0.41	9.13	6.24	0.13	102.99	590	0.44	732	8.80
X590b_62	59.67	27.37	0.42	8.69	6.26	0.12	102.53	600	0.43	728	8.78
X590b_63	59.79	26.74	0.34	8.56	6.67	0.13	102.22	610	0.41	722	8.77
X590b_64	59.22	26.59	0.39	8.09	6.84	0.17	101.29	620	0.39	714	8.80
X590b_65	59.84	26.63	0.32	8.23	6.72	0.17	101.90	630	0.40	717	8.80
X590b_66	59.61	26.77	0.31	8.30	6.74	0.15	101.88	640	0.40	718	8.79
X590b_67	60.39	26.43	0.41	8.27	6.73	0.16	102.39	650	0.40	718	8.79
X590b_68	59.93	26.35	0.33	8.13	6.73	0.15	101.61	660	0.40	716	8.79
X590b_69	60.31	26.47	0.36	8.05	6.70	0.19	102.09	670	0.39	715	8.81
X590b_70	60.51	26.43	0.36	7.85	6.83	0.17	102.16	680	0.38	711	8.81
X590b_71	60.91	25.84	0.43	7.46	6.77	0.16	101.56	690	0.38	708	8.82
X590b_72	60.61	25.84	0.22	7.10	7.31	0.22	101.30	700	0.34	694	8.91
X590b_73	61.01	25.60	0.32	7.10	7.07	0.17	101.27	710	0.35	698	8.87
X590b_74	60.40	25.60	0.36	7.55	7.15	0.17	101.23	720	0.36	704	8.84
X590b_75	60.82	26.13	0.36	7.92	6.84	0.15	102.23	730	0.39	713	8.80
X590b_76	60.17	26.47	0.43	8.20	6.56	0.14	101.96	740	0.41	720	8.78
X590b_77	58.82	27.07	0.35	8.44	6.19	0.17	101.03	750	0.43	726	8.80
X590b_78	58.97	27.06	0.34	8.90	6.49	0.12	101.88	760	0.43	727	8.78
X590b_79	59.02	26.64	0.34	8.39	6.60	0.18	101.18	770	0.41	720	8.80
X590b_80	56.19	28.44	0.47	10.34	5.62	0.15	101.21	780	0.50	744	8.95
X590b_81	57.13	28.15	0.30	9.95	5.69	0.11	101.34	790	0.49	743	8.88
X590b_83	58.06	27.36	0.41	9.37	6.15	0.11	101.46	810	0.45	735	8.80

Table A3.10 continued

Sample	SiO_2	Al_2O_3	FeO	CaO	Na_2O	K_2O	Total	Dist (μm)	X An	Temp °C	H_2O wt%
X590b_85	58.66	27.63	0.47	8.97	6.08	0.12	101.94	830	0.45	733	8.80
X590b_86	59.88	26.40	0.41	8.31	6.68	0.12	101.80	840	0.40	720	8.77
X590b_87	58.92	27.28	0.44	8.35	6.36	0.12	101.47	850	0.42	724	8.77
X590b_88	59.03	27.05	0.32	8.70	6.55	0.12	101.78	860	0.42	725	8.77
X590b_89	59.44	27.07	0.30	8.10	6.58	0.15	101.65	870	0.40	718	8.79
X590b_90	59.26	26.85	0.33	8.66	6.56	0.19	101.85	880	0.42	723	8.81
X590b_91	59.26	26.05	0.29	8.26	6.77	0.15	100.78	890	0.40	717	8.79
X590b_92	59.92	26.14	0.39	7.73	6.70	0.14	101.01	900	0.39	712	8.79
X590b_93	60.19	26.32	0.46	7.93	7.10	0.12	102.12	910	0.38	710	8.79
X590b_94	59.63	26.57	0.40	8.00	6.74	0.20	101.54	920	0.39	714	8.82
X590b_95	58.78	26.82	0.38	8.67	6.29	0.15	101.09	930	0.43	727	8.80
X590b_96	58.26	27.13	0.36	8.90	6.32	0.14	101.11	940	0.43	729	8.79
X590b_97	58.48	27.61	0.43	9.45	6.04	0.11	102.11	950	0.46	737	8.81
X590b_98	58.13	27.33	0.37	9.32	6.04	0.16	101.35	960	0.46	734	8.83
X590b_99	57.89	27.55	0.39	9.39	6.10	0.14	101.45	970	0.46	735	8.82
X590b_100	57.76	27.34	0.40	9.05	6.15	0.13	100.82	980	0.45	732	8.80
X590d_2	58.14	27.03	0.35	9.36	5.88	0.12	100.88	0	0.46	738	8.82
X590d_3	57.36	27.23	0.39	9.77	5.74	0.09	100.58	10	0.48	742	8.85
X590d_4	57.30	27.35	0.47	9.35	5.84	0.13	100.44	20	0.47	737	8.84
X590d_5	59.31	26.36	0.36	8.31	6.41	0.14	100.89	30	0.41	722	8.78
X590d_6	58.95	26.28	0.45	8.26	6.45	0.15	100.53	40	0.41	721	8.79
X590d_7	58.53	26.38	0.44	8.19	6.32	0.15	100.00	50	0.41	722	8.79
X590d_8	59.49	26.93	0.36	8.54	6.34	0.14	101.81	60	0.42	725	8.79
X590d_9	60.29	26.96	0.36	8.67	6.45	0.13	102.85	70	0.42	726	8.78
X590d_10	59.29	26.67	0.31	8.54	6.08	0.11	101.01	80	0.43	729	8.78
X590d_11	59.23	26.53	0.30	8.06	6.51	0.13	100.77	90	0.40	719	8.78
X590d_12	58.25	26.12	0.32	8.05	6.27	0.15	99.16	100	0.41	721	8.79
X590d_13	57.60	26.27	0.38	8.23	6.43	0.14	99.06	110	0.41	721	8.78
X590d_15	58.07	25.78	0.47	8.06	6.36	0.17	98.90	130	0.41	720	8.80
X590d_16	57.44	25.96	0.29	7.99	6.30	0.16	98.13	140	0.41	720	8.79
X590d_17	57.71	25.83	0.38	8.32	6.24	0.14	98.62	150	0.42	725	8.79
X590d_18	57.91	25.68	0.41	8.07	6.30	0.16	98.52	160	0.41	721	8.79
X590d_19	57.79	25.90	0.38	8.18	6.35	0.13	98.74	170	0.41	722	8.78
X590d_20	57.81	25.66	0.42	7.72	6.56	0.18	98.35	180	0.39	713	8.81
X590d_21	58.77	26.79	0.38	8.43	6.65	0.13	101.15	190	0.41	721	8.77
X590d_22	59.14	26.83	0.42	8.54	6.69	0.15	101.78	200	0.41	721	8.79
X590d_23	58.86	26.90	0.37	8.35	6.53	0.18	101.18	210	0.41	721	8.80
X590d_24	59.70	27.10	0.37	8.52	6.51	0.18	102.38	220	0.42	722	8.80
X590d_25	59.12	27.12	0.41	8.83	6.60	0.17	102.24	230	0.42	724	8.80
X590d_26	59.23	26.86	0.35	8.63	6.57	0.14	101.78	240	0.42	724	8.78
X590d_27	58.87	26.86	0.41	8.44	6.63	0.13	101.35	250	0.41	721	8.78
X590d_28	57.76	27.10	0.39	8.61	6.47	0.13	100.46	260	0.42	725	8.78
X590d_30	55.95	27.21	0.44	8.98	6.33	0.16	99.06	280	0.44	729	8.80
X590d_32	55.42	27.86	0.30	9.97	5.85	0.14	99.54	300	0.48	741	8.88
X590d_33	55.53	27.83	0.37	9.74	5.84	0.12	99.43	310	0.48	740	8.85
X590d_34	55.63	27.77	0.39	10.11	5.80	0.09	99.80	320	0.49	743	8.87
X590d_35	56.93	27.43	0.30	9.29	6.25	0.15	100.35	330	0.45	733	8.81
X590d_36	57.85	26.50	0.31	8.38	6.62	0.18	99.85	340	0.41	720	8.80
X590d_37	58.54	26.31	0.32	7.89	6.92	0.16	100.13	350	0.38	711	8.80
X590d_38	58.20	26.12	0.31	8.02	6.58	0.16	99.39	360	0.40	717	8.80
X590d_39	56.83	26.40	0.33	8.12	6.54	0.16	98.38	370	0.40	718	8.79
X590d_40	57.01	26.88	0.42	8.81	6.48	0.15	99.75	380	0.43	726	8.79
X590d_41	58.78	27.21	0.32	8.63	6.63	0.12	101.69	390	0.42	723	8.77
X590d_42	59.16	26.96	0.53	8.61	6.66	0.14	102.06	400	0.41	722	8.78
X590d_43	58.97	26.87	0.36	8.97	6.35	0.14	101.67	410	0.43	729	8.79
X590d_44	59.43	26.97	0.42	8.49	6.46	0.18	101.93	420	0.42	723	8.80
X590d_45	59.60	26.85	0.47	8.41	6.69	0.16	102.18	430	0.41	720	8.79
X590d_46	59.26	26.79	0.47	8.55	6.62	0.10	101.79	440	0.41	723	8.76
X590d_47	58.22	26.74	0.46	8.41	6.68	0.14	100.64	450	0.41	720	8.78
X590d_48	58.87	26.66	0.37	8.37	6.64	0.15	101.05	460	0.41	720	8.78
X590d_49	59.67	26.41	0.38	8.36	6.76	0.16	101.74	470	0.40	718	8.79
X590d_50	59.30	27.01	0.43	8.48	6.68	0.14	102.04	480	0.41	721	8.78
X590d_51	58.69	27.33	0.44	8.78	6.19	0.14	101.58	490	0.44	729	8.79
X590d_52	59.65	26.67	0.40	8.34	6.57	0.16	101.79	500	0.41	720	8.79
X590d_53	60.29	26.71	0.42	8.29	6.89	0.15	102.74	510	0.40	716	8.79
X590d_54	58.38	26.69	0.32	8.48	6.59	0.17	100.64	520	0.41	721	8.80
X590d_55	57.31	27.69	0.30	9.11	6.02	0.12	100.55	530	0.45	734	8.80
X590d_56	56.84	28.33	0.41	10.06	5.66	0.09	101.40	540	0.49	744	8.88
X590d_57	56.75	28.24	0.50	9.85	5.71	0.12	101.18	550	0.48	742	8.88

Table A3.10 continued

Sample	SiO_2	Al_2O_3	FeO	CaO	Na_2O	K_2O	Total	Dist (μm)	X An	Temp °C	H_2O wt%
X590d_59	57.00	28.12	0.44	9.66	5.86	0.12	101.19	570	0.47	740	8.85
X590d_60	56.60	27.97	0.47	9.66	5.83	0.11	100.64	580	0.47	740	8.85
X590d_61	57.25	28.10	0.36	9.76	5.95	0.11	101.54	590	0.47	739	8.84
X590d_62	57.04	28.17	0.44	9.69	6.00	0.13	101.48	600	0.47	738	8.84
X590d_63	57.15	28.16	0.51	9.77	6.00	0.14	101.73	610	0.47	738	8.85
X590d_64	57.25	27.74	0.40	9.60	6.18	0.10	101.27	620	0.46	737	8.80
X590d_65	57.83	27.47	0.33	9.36	6.26	0.12	101.36	630	0.45	734	8.80
X590d_66	57.68	27.49	0.45	9.17	6.36	0.10	101.26	640	0.44	732	8.78
X590d_67	57.72	28.02	0.49	9.45	6.00	0.13	101.80	650	0.46	737	8.83
X590d_68	57.45	27.97	0.47	9.73	6.08	0.14	101.85	660	0.47	737	8.84
X590d_69	57.89	27.34	0.48	9.10	6.29	0.16	101.26	670	0.44	730	8.81
X590d_70	57.66	27.66	0.46	9.10	6.43	0.11	101.42	680	0.44	730	8.78
X590d_71	57.41	27.30	0.48	9.00	6.39	0.14	100.72	690	0.43	729	8.79
X590d_72	57.29	27.38	0.47	9.53	6.11	0.11	100.89	700	0.46	737	8.81
X590d_73	59.21	27.25	0.40	9.40	6.13	0.13	102.52	710	0.45	735	8.81
X590d_74	58.99	27.36	0.31	9.48	6.18	0.14	102.46	720	0.46	735	8.82
X590d_75	58.93	27.08	0.37	8.82	6.41	0.15	101.75	730	0.43	727	8.79
X590d_76	57.11	27.90	0.38	9.27	6.07	0.11	100.85	740	0.45	735	8.80
X590d_77	57.63	27.86	0.31	8.90	6.50	0.16	101.36	750	0.43	726	8.80
X590d_78	58.09	27.45	0.50	8.94	6.30	0.19	101.47	760	0.43	728	8.82
X590d_79	57.97	26.67	0.40	8.83	6.60	0.15	100.62	770	0.42	725	8.79
X590d_80	58.29	26.69	0.41	8.32	6.63	0.16	100.50	780	0.41	719	8.79
X590d_81	59.42	26.57	0.34	8.19	6.70	0.16	101.39	790	0.40	717	8.80
X590d_82	60.09	26.70	0.39	8.19	6.75	0.13	102.25	800	0.40	717	8.78
X590d_83	59.65	26.54	0.43	8.24	6.89	0.18	101.93	810	0.39	715	8.80
X590d_84	60.19	26.59	0.44	7.92	6.73	0.15	102.02	820	0.39	714	8.80
X590d_85	60.16	25.97	0.30	7.29	7.04	0.15	100.91	830	0.36	702	8.84
X590d_86	59.92	26.03	0.37	7.35	7.11	0.19	100.98	840	0.36	701	8.86
X590d_87	59.34	25.90	0.28	7.56	7.07	0.14	100.29	850	0.37	705	8.82
X590d_88	58.94	26.34	0.33	7.77	6.72	0.18	100.28	860	0.39	712	8.82
X590d_89	59.42	26.19	0.32	7.77	6.89	0.17	100.75	870	0.38	710	8.82
X590d_90	59.72	26.18	0.34	7.78	6.93	0.17	101.13	880	0.38	709	8.82
X590d_91	59.53	26.82	0.36	7.94	6.86	0.15	101.66	890	0.39	712	8.80
X590d_92	57.52	27.78	0.46	9.12	6.34	0.13	101.35	900	0.44	731	8.79
X590d_93	57.04	27.18	0.36	9.03	6.44	0.13	100.19	910	0.43	729	8.79
X590d_94	56.76	27.22	0.29	8.74	6.41	0.14	99.56	920	0.43	726	8.79
X590d_95	56.65	27.12	0.33	9.01	6.25	0.17	99.51	930	0.44	730	8.81
X590d_96	57.12	26.76	0.37	8.81	6.32	0.13	99.51	940	0.43	728	8.79
X590d_97	57.13	26.87	0.33	8.94	6.35	0.15	99.77	950	0.43	729	8.79
X590d_98	57.50	26.93	0.36	8.88	6.33	0.14	100.13	960	0.43	729	8.79
X590d_99	58.12	26.38	0.29	8.24	6.71	0.17	99.92	970	0.40	717	8.80
X590d_100	59.13	26.41	0.43	8.13	6.75	0.15	101.00	980	0.40	716	8.79
X590d_101	58.12	26.79	0.35	8.51	6.45	0.14	100.36	990	0.42	724	8.78
X590d_102	58.54	26.70	0.42	8.31	6.75	0.15	100.87	1000	0.40	718	8.79
X590d_103	58.99	26.27	0.29	8.07	6.92	0.14	100.68	1010	0.39	713	8.79
X590d_104	59.65	26.16	0.44	8.06	6.82	0.20	101.34	1020	0.39	713	8.82
X590d_105	60.07	26.08	0.38	7.78	7.08	0.14	101.54	1030	0.37	708	8.81
X590d_106	59.80	25.86	0.32	7.44	6.95	0.16	100.52	1040	0.37	705	8.83
X590d_107	60.12	25.91	0.35	7.41	7.00	0.19	100.98	1050	0.37	703	8.85
X590d_108	59.74	25.96	0.36	7.55	7.15	0.13	100.88	1060	0.37	705	8.82
X590d_109	57.23	26.88	0.38	8.50	6.45	0.14	99.58	1070	0.42	724	8.78
X590d_110	55.12	27.92	0.50	10.13	5.61	0.11	99.39	1080	0.50	744	8.91
X590d_111	55.81	27.49	0.45	9.98	5.66	0.12	99.50	1090	0.49	743	8.89
X590d_112	56.18	27.23	0.53	9.70	5.89	0.09	99.62	1100	0.47	740	8.83
X590d_113	57.78	27.43	0.42	9.64	5.80	0.13	101.21	1110	0.48	740	8.86
X590d_114	58.07	26.97	0.33	9.04	6.22	0.10	100.73	1120	0.44	732	8.78
X590d_115	57.15	27.46	0.38	9.44	5.90	0.12	100.44	1130	0.47	738	8.83
X590d_116	56.38	27.55	0.37	9.13	6.02	0.15	99.60	1140	0.45	734	8.82
X590d_117	56.12	27.32	0.39	9.04	5.94	0.12	98.93	1150	0.45	735	8.81
X590d_118	56.42	26.82	0.42	8.98	6.21	0.14	98.98	1160	0.44	731	8.80
X590d_119	56.80	26.49	0.33	8.73	6.39	0.15	98.89	1170	0.43	726	8.79
X590d_120	57.03	27.07	0.29	9.40	6.12	0.12	100.03	1180	0.46	735	8.81
X590e_3	59.65	26.83	0.50	8.85	6.60	0.13	102.57	20	0.42	726	8.78
X590e_4	58.26	26.45	0.42	8.86	6.38	0.18	100.54	30	0.43	727	8.81
X590e_5	59.26	26.74	0.46	8.70	6.67	0.17	102.00	40	0.41	722	8.80
X590e_6	59.91	26.82	0.41	8.91	6.66	0.14	102.84	50	0.42	725	8.78
X590e_7	60.24	26.70	0.41	8.81	6.52	0.15	102.82	60	0.42	725	8.79
X590e_8	59.83	26.91	0.38	8.38	6.62	0.13	102.24	70	0.41	721	8.78
X590e_9	59.48	26.88	0.35	8.52	6.65	0.13	102.01	80	0.41	722	8.77

Table A3.10 continued

Sample	SiO_2	Al_2O_3	FeO	CaO	Na_2O	K_2O	Total	Dist (μm)	X An	Temp °C	H_2O wt%
X590e_11	59.94	26.38	0.39	8.33	6.87	0.16	102.07	100	0.40	716	8.80
X590e_12	59.74	26.55	0.36	8.48	6.75	0.15	102.02	110	0.41	720	8.78
X590e_13	59.57	26.71	0.41	8.62	6.69	0.15	102.15	120	0.41	722	8.78
X590e_14	59.09	26.87	0.45	8.55	6.54	0.15	101.66	130	0.42	723	8.79
X590e_15	59.18	26.90	0.41	8.76	6.39	0.16	101.80	140	0.43	726	8.80
X590e_16	60.24	26.66	0.32	8.66	6.61	0.11	102.60	150	0.42	724	8.76
X590e_17	59.62	27.18	0.39	9.03	6.43	0.10	102.74	160	0.43	730	8.77
X590e_18	58.64	27.07	0.32	8.93	6.39	0.12	101.48	170	0.43	729	8.78
X590e_19	58.60	27.02	0.45	8.80	6.36	0.12	101.35	180	0.43	728	8.78
X590e_20	59.23	26.71	0.43	8.81	6.06	0.12	101.36	190	0.44	732	8.79
X590e_21	59.18	26.73	0.37	8.60	6.73	0.12	101.73	200	0.41	722	8.77
X590e_22	59.38	26.63	0.39	8.48	6.78	0.12	101.78	210	0.41	720	8.77
X590e_23	59.82	26.77	0.35	8.61	6.53	0.17	102.25	220	0.42	723	8.80
X590e_24	59.65	27.00	0.39	9.22	6.43	0.13	102.82	230	0.44	731	8.79
X590e_25	58.10	27.23	0.34	9.37	6.35	0.14	101.54	240	0.45	732	8.80
X590e_26	59.49	26.78	0.38	8.67	6.77	0.18	102.27	250	0.41	721	8.80
X590e_27	58.12	27.33	0.39	9.52	6.11	0.09	101.55	260	0.46	737	8.80
X590e_30	57.91	27.73	0.44	9.41	6.15	0.10	101.73	290	0.46	736	8.80
X590e_32	58.50	27.59	0.39	9.32	6.28	0.11	102.19	310	0.45	733	8.79
X590e_33	58.82	27.68	0.44	9.61	6.05	0.14	102.74	320	0.46	737	8.83
X590e_34	59.19	27.27	0.32	8.97	6.52	0.13	102.40	330	0.43	728	8.78
X590e_35	59.51	27.11	0.31	8.42	6.42	0.12	101.88	340	0.42	724	8.77
X590e_36	59.34	27.02	0.32	8.64	6.47	0.10	101.89	350	0.42	726	8.76
X590e_37	59.10	27.31	0.38	8.73	6.58	0.18	102.28	360	0.42	723	8.80
X590e_38	59.04	26.89	0.47	8.66	6.55	0.14	101.74	370	0.42	724	8.78
X590e_39	59.85	27.15	0.36	8.68	6.51	0.12	102.68	380	0.42	725	8.77
X590e_40	59.63	27.19	0.32	8.46	6.46	0.14	102.19	390	0.42	723	8.78
X590e_41	59.74	27.09	0.41	8.66	6.55	0.18	102.62	400	0.42	723	8.80
X590e_42	59.77	26.84	0.37	8.61	6.43	0.12	102.13	410	0.42	726	8.77
X590e_43	59.81	26.99	0.40	8.46	6.67	0.19	102.51	420	0.41	720	8.81
X590e_45	60.11	27.21	0.32	8.64	6.46	0.18	102.92	440	0.42	724	8.80
X590e_50	59.45	26.95	0.28	8.58	6.58	0.16	101.99	490	0.42	723	8.79
X590e_51	58.29	27.04	0.35	8.35	6.39	0.15	100.57	500	0.42	723	8.79
X590e_52	58.44	26.98	0.37	8.35	6.48	0.12	100.74	510	0.41	722	8.77
X590e_53	59.10	27.29	0.29	8.52	6.75	0.12	102.09	520	0.41	721	8.77
X590e_54	59.23	27.00	0.45	8.49	6.52	0.15	101.84	530	0.42	723	8.78
X590e_55	59.22	27.18	0.41	8.46	6.63	0.14	102.04	540	0.41	721	8.78
X590e_56	59.29	26.90	0.40	8.44	6.62	0.14	101.80	550	0.41	721	8.78
X590e_57	58.63	26.97	0.41	8.54	6.49	0.19	101.23	560	0.42	722	8.81
X590e_58	58.72	27.11	0.49	8.48	6.58	0.19	101.56	570	0.41	721	8.81
X590e_59	58.05	26.90	0.52	8.50	6.46	0.14	100.57	580	0.42	724	8.78
X590e_60	58.42	26.99	0.35	8.39	6.72	0.15	101.01	590	0.40	719	8.78
X590e_61	57.56	26.89	0.46	8.59	6.54	0.12	100.15	600	0.42	724	8.77
X590e_62	59.46	27.08	0.46	8.51	6.71	0.15	102.37	610	0.41	720	8.79
X590e_63	59.65	27.02	0.40	8.51	6.55	0.12	102.25	620	0.41	723	8.77
X590e_64	59.43	26.99	0.46	8.39	6.59	0.15	102.01	630	0.41	721	8.79
X590e_65	59.18	26.96	0.37	8.29	6.49	0.18	101.47	640	0.41	720	8.80
X590e_66	59.18	26.94	0.37	8.64	6.66	0.14	101.92	650	0.41	722	8.78
X590e_67	59.13	27.32	0.38	8.56	6.67	0.14	102.21	660	0.41	722	8.78
X590e_68	57.80	27.54	0.42	8.62	6.35	0.14	100.87	670	0.43	726	8.79
X590e_69	58.45	27.39	0.37	9.10	6.44	0.13	101.89	680	0.44	729	8.79
X590e_70	58.75	27.42	0.43	8.89	6.25	0.13	101.88	690	0.44	730	8.79
X590e_71	59.04	27.32	0.40	8.81	6.57	0.15	102.29	700	0.42	725	8.79
X590e_72	59.01	27.58	0.37	8.46	6.51	0.16	102.09	710	0.41	722	8.79
X590e_73	59.16	27.24	0.39	8.50	6.58	0.18	102.04	720	0.41	721	8.80
X590e_74	59.31	27.12	0.32	8.32	6.82	0.13	102.02	730	0.40	718	8.78
X590e_75	58.82	26.64	0.31	8.15	6.68	0.13	100.74	740	0.40	718	8.78
X590e_76	58.04	27.07	0.33	8.61	6.44	0.10	100.59	750	0.42	726	8.76
X590e_77	58.21	27.05	0.28	8.83	6.43	0.15	100.95	760	0.43	727	8.79
X590e_78	58.30	27.02	0.37	8.34	6.61	0.16	100.79	770	0.41	720	8.79
X590e_79	58.67	27.26	0.36	8.48	6.54	0.15	101.47	780	0.41	722	8.78
X590e_80	58.81	27.11	0.48	8.43	6.50	0.11	101.44	790	0.41	723	8.77
X590e_81	58.79	27.04	0.33	8.24	6.39	0.14	100.93	800	0.41	722	8.78
X590e_82	58.41	27.25	0.37	8.70	6.45	0.16	101.34	810	0.42	725	8.79
X590e_83	58.76	26.68	0.29	7.92	6.77	0.13	100.55	820	0.39	714	8.78
X590e_84	58.57	26.55	0.39	8.00	6.93	0.15	100.59	830	0.39	712	8.80
X590e_85	58.95	26.68	0.43	8.19	6.74	0.14	101.13	840	0.40	717	8.79
X590e_86	59.37	26.43	0.47	8.04	6.64	0.17	101.13	850	0.40	716	8.80
X590e_87	59.95	26.41	0.50	7.72	6.82	0.17	101.56	860	0.38	710	8.82
X590e_88	57.96	27.35	0.44	8.83	6.33	0.14	101.05	870	0.43	728	8.79

Table A3.10 continued

Sample	SiO_2	Al_2O_3	FeO	CaO	Na_2O	K_2O	Total	Dist (μm)	X An	Temp °C	H_2O wt%
X590e_90	58.34	26.92	0.42	8.71	6.55	0.15	101.09	890	0.42	724	8.79
X590e_91	58.02	26.83	0.43	8.28	6.51	0.17	100.23	900	0.41	720	8.80
X590e_92	58.39	26.68	0.35	8.10	6.52	0.13	100.16	910	0.40	719	8.78
X590e_93	59.14	26.09	0.40	7.65	6.86	0.20	100.35	920	0.38	708	8.84
X590e_94	60.27	26.32	0.31	7.79	6.83	0.17	101.68	930	0.38	711	8.81
X590e_95	60.43	26.47	0.40	7.44	7.00	0.19	101.93	940	0.37	703	8.85
X590e_96	59.52	26.41	0.34	7.85	6.72	0.16	100.99	950	0.39	713	8.80
X590e_97	57.88	27.23	0.38	8.68	6.37	0.10	100.64	960	0.43	727	8.77
X590g_1	58.61	27.43	0.43	9.00	6.01	0.15	101.62	0	0.45	733	8.81
X590g_2	59.36	27.29	0.33	8.73	6.20	0.09	101.99	10	0.44	730	8.76
X590g_3	58.99	27.51	0.41	9.26	6.10	0.15	102.41	20	0.45	734	8.82
X590g_4	59.08	27.01	0.42	8.76	5.96	0.12	101.34	30	0.45	732	8.80
X590g_5	59.13	27.51	0.33	9.30	5.97	0.15	102.40	40	0.46	735	8.83
X590g_6	59.28	27.45	0.45	9.01	5.97	0.16	102.32	50	0.45	733	8.82
X590g_7	59.33	27.13	0.45	8.66	6.22	0.15	101.93	60	0.43	728	8.79
X590g_8	58.75	27.14	0.35	8.73	6.23	0.15	101.35	70	0.43	728	8.80
X590g_9	58.54	27.17	0.50	8.75	6.18	0.13	101.27	80	0.44	730	8.79
X590g_10	59.55	26.77	0.38	8.23	6.08	0.11	101.12	90	0.43	727	8.77
X590g_11	60.57	26.66	0.30	8.48	6.21	0.16	102.38	100	0.43	726	8.80
X590g_12	60.29	27.09	0.39	8.70	6.05	0.11	102.63	110	0.44	731	8.78
X590g_13	59.72	26.90	0.39	8.81	6.11	0.09	102.03	120	0.44	732	8.77
X590g_14	59.45	27.44	0.39	9.19	5.83	0.12	102.41	130	0.46	737	8.82
X590g_15	58.70	27.33	0.44	8.98	5.98	0.17	101.59	140	0.45	732	8.83
X590g_16	58.27	27.34	0.46	9.27	5.94	0.16	101.44	150	0.46	735	8.84
X590g_17	57.92	27.63	0.46	9.24	5.77	0.13	101.15	160	0.47	738	8.84
X590g_18	57.55	27.37	0.35	9.41	5.84	0.11	100.65	170	0.47	738	8.83
X590g_19	57.63	27.74	0.49	9.75	5.81	0.12	101.54	180	0.48	740	8.86
X590g_20	58.44	27.27	0.38	9.32	5.75	0.13	101.28	190	0.47	738	8.84
X590g_21	58.51	27.74	0.37	9.47	5.75	0.13	101.98	200	0.47	739	8.85
X590g_22	58.56	27.79	0.42	9.48	5.76	0.12	102.12	210	0.47	740	8.84
X590g_23	58.43	28.12	0.42	9.81	5.77	0.13	102.67	220	0.48	741	8.87
X590g_24	53.07	25.94	0.32	13.83	5.23	0.14	98.53	230	0.59	752	9.41
X590g_25	56.47	28.27	0.34	10.45	5.30	0.12	100.95	240	0.52	748	8.99
X590g_26	56.78	28.18	0.33	10.05	5.57	0.12	101.03	250	0.50	744	8.91
X590g_27	57.15	27.71	0.49	9.37	5.90	0.14	100.76	260	0.46	737	8.84
X590g_28	57.92	26.92	0.29	8.60	6.44	0.11	100.28	270	0.42	726	8.77
X590g_29	57.85	26.82	0.45	8.74	6.26	0.14	100.27	280	0.43	728	8.79
X590g_30	58.04	26.82	0.35	8.84	6.50	0.14	100.68	290	0.43	726	8.78
X590g_31	58.10	26.98	0.40	8.67	6.18	0.17	100.50	300	0.43	728	8.81
X590g_32	58.10	26.59	0.31	8.63	6.16	0.11	99.90	310	0.43	729	8.77
X590g_33	58.02	26.51	0.37	8.70	6.32	0.15	100.07	320	0.43	727	8.79
X590g_34	57.54	26.40	0.39	8.59	6.34	0.14	99.40	330	0.42	726	8.79
X590g_35	58.82	26.47	0.34	8.32	6.01	0.13	100.09	340	0.43	728	8.79
X590g_36	60.11	26.45	0.35	8.32	6.69	0.17	102.09	350	0.40	718	8.80
X590g_37	60.31	26.31	0.31	8.01	6.56	0.14	101.63	360	0.40	718	8.79
X590g_38	59.99	26.21	0.43	7.90	6.72	0.13	101.38	370	0.39	714	8.79
X590g_39	58.41	26.04	0.44	8.17	6.84	0.16	100.05	380	0.39	715	8.80
X590g_40	58.52	25.86	0.34	7.77	6.57	0.14	99.20	390	0.39	715	8.79
X590g_41	59.00	25.63	0.39	7.71	6.62	0.11	99.46	400	0.39	714	8.78
X590g_42	59.46	25.57	0.34	7.51	6.72	0.14	99.75	410	0.38	709	8.81
X590g_43	59.77	25.93	0.33	7.62	6.77	0.12	100.53	420	0.38	711	8.79
X590g_44	59.06	25.84	0.35	7.52	6.82	0.15	99.75	430	0.38	708	8.82
X590g_45	59.21	25.75	0.36	7.54	6.97	0.21	100.04	440	0.37	705	8.85
X590g_46	59.21	25.75	0.36	7.54	6.97	0.21	100.04	450	0.37	705	8.85
X590g_47	59.75	25.81	0.42	7.58	6.97	0.16	100.68	460	0.37	707	8.82
X590g_48	59.89	25.46	0.38	7.44	6.86	0.16	100.19	470	0.37	706	8.83
X590g_49	59.96	25.46	0.31	7.20	6.92	0.21	100.07	480	0.36	701	8.87
X590g_50	60.14	25.21	0.48	7.42	6.92	0.19	100.36	490	0.37	704	8.84
X590g_51	59.28	25.57	0.38	7.24	7.03	0.14	99.63	500	0.36	702	8.84
X590g_52	60.29	25.11	0.37	7.24	7.01	0.13	100.15	510	0.36	702	8.83
X590g_53	59.59	25.25	0.31	7.30	7.00	0.21	99.68	520	0.36	701	8.87
X590g_54	59.68	25.10	0.37	7.22	6.86	0.16	99.39	530	0.36	703	8.84
X590g_55	59.69	25.67	0.37	7.52	6.96	0.18	100.39	540	0.37	705	8.84
X590g_56	60.00	25.67	0.29	7.87	6.77	0.20	100.79	550	0.39	712	8.83
X590g_57	60.18	26.18	0.32	7.85	6.75	0.18	101.46	560	0.39	712	8.81
X590g_58	59.18	26.21	0.29	8.18	6.57	0.13	100.57	570	0.40	719	8.78
X590g_59	59.08	26.47	0.37	7.94	6.69	0.18	100.73	580	0.39	714	8.81
X590g_60	59.32	26.23	0.32	8.02	6.67	0.16	100.71	590	0.40	715	8.80
X590g_61	60.43	26.15	0.32	7.98	6.41	0.14	101.43	600	0.40	719	8.79

Table A3.10 continued

Sample	SiO_2	Al_2O_3	FeO	CaO	Na_2O	K_2O	Total	Dist (μm)	X An	Temp °C	H_2O wt%
X590g_63	60.68	26.24	0.34	8.22	6.38	0.14	101.99	620	0.41	722	8.78
X590g_64	60.20	26.40	0.36	8.30	6.55	0.13	101.95	630	0.41	721	8.78
X590g_65	59.77	26.41	0.43	8.08	6.53	0.17	101.39	640	0.40	718	8.80
X590g_66	59.97	26.40	0.30	8.19	6.62	0.13	101.62	650	0.40	719	8.78
X590g_67	58.73	25.96	0.39	8.31	6.32	0.22	99.93	660	0.42	721	8.83
X590g_68	58.61	25.83	0.32	8.03	6.34	0.14	99.27	670	0.41	721	8.78
X590g_69	59.83	26.44	0.33	8.28	6.26	0.13	101.27	680	0.42	724	8.78
X590g_70	59.97	26.38	0.44	8.30	6.36	0.16	101.61	690	0.42	723	8.79
X590g_71	59.82	26.72	0.40	8.42	6.41	0.15	101.93	700	0.42	723	8.79
X590g_72	59.68	26.62	0.50	8.24	6.45	0.15	101.64	710	0.41	721	8.79
X590g_73	59.62	26.38	0.41	8.17	6.31	0.14	101.03	720	0.41	722	8.78
X590g_74	59.33	27.22	0.33	8.64	6.27	0.15	101.93	730	0.43	727	8.79
X590g_75	58.73	26.91	0.27	8.78	6.20	0.17	101.07	740	0.43	728	8.81
X590g_76	58.94	27.11	0.36	8.77	6.28	0.17	101.64	750	0.43	727	8.81
X590g_77	58.30	27.12	0.45	8.95	6.07	0.17	101.06	760	0.44	731	8.82
X590g_78	58.10	27.28	0.48	8.99	6.12	0.15	101.12	770	0.44	731	8.81
X590g_79	58.01	26.95	0.31	8.91	6.31	0.16	100.65	780	0.43	728	8.80
X590g_80	58.75	27.06	0.36	8.77	6.29	0.15	101.38	790	0.43	728	8.79
X590g_81	58.54	26.83	0.42	8.94	6.28	0.17	101.17	800	0.44	729	8.81
X590g_82	59.08	27.12	0.38	8.73	6.36	0.16	101.84	810	0.43	726	8.80
X590g_83	59.74	26.94	0.34	8.91	6.37	0.17	102.46	820	0.43	728	8.80
X590g_84	59.48	27.23	0.41	8.78	6.36	0.17	102.44	830	0.43	727	8.80
X590g_85	59.36	27.02	0.40	8.50	6.41	0.11	101.80	840	0.42	725	8.77
X590g_89	58.99	26.35	0.36	8.19	6.44	0.17	100.50	850	0.41	720	8.80
X590g_90	58.88	26.47	0.33	8.43	6.39	0.12	100.63	860	0.42	724	8.77
X590g_91	58.51	26.59	0.43	8.66	6.28	0.10	100.58	870	0.43	728	8.77
X590g_93	57.55	27.29	0.33	8.61	6.04	0.12	99.93	890	0.44	730	8.78
X590g_94	57.31	27.18	0.39	9.16	6.20	0.11	100.35	900	0.45	733	8.79
X590g_95	57.25	27.17	0.30	9.23	6.25	0.10	100.30	910	0.45	734	8.78
X590g_96	57.99	27.31	0.42	9.19	6.00	0.11	101.03	920	0.46	735	8.81
X590g_97	58.19	26.99	0.37	9.01	5.94	0.15	100.65	930	0.45	734	8.82
X590g_98	58.31	26.90	0.31	9.19	6.02	0.16	100.88	940	0.45	734	8.83
X590g_99	58.17	27.05	0.34	9.00	6.20	0.13	100.89	950	0.44	731	8.79
X590g_100	57.85	27.15	0.40	8.88	6.10	0.11	100.49	960	0.44	732	8.79
X590g_101	56.95	27.10	0.36	9.03	5.96	0.14	99.54	970	0.45	734	8.82
X590g_102	57.47	26.90	0.38	8.93	6.11	0.16	99.95	980	0.44	731	8.81
X590g_103	58.07	26.86	0.41	9.04	6.09	0.13	100.60	990	0.45	733	8.80
X590g_104	57.51	26.90	0.44	8.85	6.09	0.12	99.90	1000	0.44	731	8.79
X590g_105	57.67	27.08	0.41	9.09	6.01	0.13	100.39	1010	0.45	734	8.81
X590g_106	57.05	27.39	0.53	9.25	5.93	0.15	100.29	1020	0.46	736	8.83
X590g_107	56.89	27.28	0.39	9.35	5.91	0.15	99.97	1030	0.46	736	8.84
X590g_108	56.29	27.25	0.48	9.22	5.97	0.13	99.34	1040	0.46	735	8.82
X590g_109	54.98	26.32	0.50	8.70	5.61	0.12	96.22	1050	0.46	736	8.82
X590g_110	57.47	27.18	0.42	9.02	6.29	0.12	100.50	1060	0.44	731	8.78
X590g_111	57.72	27.05	0.35	9.11	6.06	0.14	100.44	1070	0.45	733	8.81
X590Ba_2	59.52	26.41	0.43	8.25	6.43	0.15	101.18	0	0.41	721	8.79
X590Ba_3	59.95	26.75	0.44	8.32	6.22	0.15	101.83	10	0.42	724	8.79
X590Ba_4	59.14	27.49	0.40	9.35	6.05	0.14	102.57	20	0.46	735	8.82
X590Ba_5	58.77	28.12	0.32	9.86	5.55	0.13	102.75	30	0.49	743	8.91
X590Ba_6	59.04	27.22	0.37	8.51	6.17	0.14	101.44	40	0.43	727	8.79
X590Ba_7	57.10	27.93	0.40	9.91	5.48	0.12	100.94	50	0.50	744	8.91
X590Ba_8	57.16	28.52	0.40	10.07	5.39	0.11	101.66	60	0.50	746	8.94
X590Ba_9	57.12	27.96	0.45	9.85	5.57	0.12	101.08	70	0.49	743	8.90
X590Ba_10	58.63	27.62	0.37	9.46	5.87	0.14	102.09	80	0.47	738	8.84
X590Ba_11	58.91	27.44	0.42	9.03	6.18	0.16	102.13	90	0.44	731	8.81
X590Ba_12	59.25	27.14	0.37	8.84	5.97	0.12	101.70	100	0.45	733	8.80
X590Ba_13	58.56	27.40	0.40	9.05	5.89	0.14	101.42	110	0.46	735	8.82
X590Ba_14	60.53	26.61	0.43	8.18	6.23	0.17	102.15	120	0.42	722	8.80
X590Ba_15	60.63	26.17	0.30	7.75	6.43	0.15	101.44	130	0.40	716	8.79
X590Ba_16	60.13	26.32	0.35	8.00	6.57	0.16	101.54	140	0.40	717	8.80
X590Ba_17	57.67	27.32	0.39	9.31	5.86	0.11	100.66	150	0.46	738	8.82
X590Ba_18	57.92	27.05	0.33	8.91	5.96	0.11	100.29	160	0.45	734	8.80
X590Ba_19	58.15	27.00	0.48	8.72	5.95	0.12	100.42	170	0.44	732	8.79
X590Ba_20	59.77	26.97	0.43	8.35	6.41	0.17	102.12	180	0.41	722	8.80
X590Ba_21	60.48	26.40	0.36	7.98	6.48	0.12	101.83	190	0.40	719	8.77
X590Ba_22	59.58	26.62	0.42	7.93	6.31	0.15	101.00	200	0.41	720	8.79
X590Ba_23	59.89	26.78	0.43	8.16	6.25	0.14	101.65	210	0.42	723	8.79
X590Ba_24	60.11	26.92	0.44	8.28	6.44	0.18	102.37	220	0.41	721	8.80
X590Ba_25	59.35	26.44	0.42	7.71	6.33	0.15	100.41	230	0.40	717	8.79

Table A3.10 continued

Sample	SiO_2	Al_2O_3	FeO	CaO	Na_2O	K_2O	Total	Dist (μm)	X An	Temp °C	H_2O wt%
X590Ba_27	56.88	27.95	0.39	9.73	5.71	0.14	100.79	250	0.48	741	8.88
X590Ba_28	57.78	28.16	0.39	10.09	5.55	0.13	102.11	260	0.50	744	8.93
X590Ba_29	55.27	29.83	0.40	12.08	4.52	0.08	102.18	270	0.59	754	9.41
X590Ba_30	54.36	30.26	0.40	12.54	4.38	0.07	102.02	280	0.61	753	9.53
X590Ba_31	54.52	30.46	0.52	12.40	4.14	0.07	102.10	290	0.62	753	9.62
X590Ba_32	53.74	30.91	0.42	12.86	4.02	0.09	102.03	300	0.64	751	9.76
X590Ba_33	54.65	29.97	0.49	12.02	4.49	0.08	101.69	310	0.59	754	9.42
X590Ba_34	53.51	30.54	0.49	12.78	4.50	0.11	101.91	320	0.61	753	9.53
X590Ba_35	54.18	30.10	0.48	12.45	4.28	0.10	101.59	330	0.61	753	9.58
X590Ba_36	53.40	30.64	0.42	12.83	4.09	0.08	101.47	340	0.63	752	9.72
X590Ba_37	53.75	30.35	0.36	12.74	4.27	0.07	101.55	350	0.62	753	9.61
X590Ba_38	53.82	30.64	0.46	12.92	4.00	0.10	101.93	360	0.64	751	9.78
X590Ba_39	53.95	30.23	0.44	12.53	4.12	0.06	101.34	370	0.62	753	9.65
X590Ba_40	55.67	29.62	0.39	11.58	4.57	0.11	101.94	380	0.58	753	9.34
X590Ba_41	57.99	27.95	0.48	9.60	5.74	0.13	101.88	390	0.48	740	8.86
X590Ba_42	59.00	27.52	0.41	9.13	5.77	0.13	101.95	400	0.46	737	8.83
X590Ba_43	59.45	26.73	0.37	8.07	6.28	0.17	101.07	410	0.41	721	8.80
X590Ba_44	58.76	26.83	0.42	8.62	6.09	0.15	100.88	420	0.44	729	8.80
X590Ba_46	58.02	27.57	0.36	9.49	5.81	0.12	101.37	430	0.47	739	8.84
X590Ba_47	58.86	27.02	0.44	8.78	6.16	0.11	101.37	440	0.44	731	8.78
X590Ba_48	59.72	26.58	0.41	8.63	6.26	0.15	101.76	450	0.43	727	8.79
X590Ba_49	60.44	26.48	0.38	8.16	6.18	0.12	101.76	460	0.42	724	8.77
X590Ba_50	59.97	26.77	0.44	8.74	5.88	0.14	101.94	470	0.45	732	8.81
X590Bb_1	57.78	27.29	0.38	9.25	5.76	0.13	100.58	0	0.47	738	8.84
X590Bb_3	58.53	27.55	0.46	9.42	5.73	0.17	101.86	10	0.47	738	8.87
X590Bb_4	59.64	27.18	0.34	9.27	5.83	0.14	102.39	20	0.46	737	8.84
X590Bb_5	59.22	26.34	0.29	8.38	6.31	0.15	100.69	30	0.42	724	8.79
X590Bb_6	60.72	26.57	0.41	7.96	6.61	0.14	102.41	40	0.40	716	8.78
X590Bb_7	60.01	26.66	0.41	8.17	6.52	0.15	101.91	50	0.41	719	8.79
X590Bb_8	59.78	26.64	0.45	8.46	6.48	0.16	101.97	60	0.42	723	8.79
X590Bb_9	61.01	26.73	0.37	8.11	6.45	0.17	102.84	70	0.41	719	8.80
X590Bb_12	61.72	25.98	0.36	7.58	6.67	0.18	102.49	100	0.38	710	8.82
X590Bb_13	61.29	25.79	0.29	7.55	6.77	0.14	101.82	110	0.38	709	8.80
X590Bb_14	62.15	25.73	0.36	7.50	6.87	0.20	102.81	120	0.37	706	8.84
X590Bb_15	61.76	25.74	0.43	7.23	6.81	0.20	102.19	130	0.37	703	8.86
X590Bb_16	60.98	25.37	0.35	7.43	7.07	0.19	101.40	140	0.36	702	8.85
X590Bb_17	61.83	25.88	0.30	7.26	6.83	0.22	102.32	150	0.37	703	8.87
X590Bb_18	61.12	25.72	0.40	7.55	6.72	0.24	101.75	160	0.38	707	8.86
X590Bb_19	60.60	25.25	0.43	7.14	6.82	0.21	100.44	170	0.36	701	8.87
X590Bb_20	62.65	25.59	0.29	7.25	6.89	0.21	102.88	180	0.36	702	8.86
X590Bb_21	63.12	25.17	0.30	6.91	7.15	0.24	102.89	190	0.34	693	8.92
X590Bb_22	63.12	25.17	0.30	6.91	7.15	0.24	102.89	200	0.34	693	8.92
X590Bb_23	61.24	26.09	0.41	7.67	6.67	0.21	102.30	210	0.38	710	8.83
X590Bb_24	60.11	27.05	0.33	8.69	6.27	0.12	102.58	220	0.43	728	8.78
X590Bb_25	59.72	27.24	0.35	8.91	6.14	0.14	102.50	230	0.44	731	8.80
X590Bb_26	59.72	27.35	0.44	9.23	6.05	0.14	102.91	240	0.45	735	8.81
X590Bb_27	59.47	26.67	0.35	8.86	6.10	0.15	101.61	250	0.44	731	8.81
X590Bb_28	58.25	27.41	0.39	9.36	6.02	0.15	101.58	260	0.46	735	8.83
X590Bb_29	58.56	27.49	0.36	8.97	5.99	0.12	101.50	270	0.45	733	8.80
X590Bb_30	59.74	26.80	0.37	8.88	6.15	0.15	102.08	280	0.44	730	8.80
X590Bb_31	59.25	27.09	0.35	8.72	6.24	0.14	101.79	290	0.43	728	8.79
X590Bb_32	59.73	27.13	0.41	9.00	6.26	0.19	102.72	300	0.44	729	8.82
X590Bb_33	60.06	26.80	0.35	8.66	6.34	0.15	102.36	310	0.43	726	8.79
X590Bb_35	58.61	27.61	0.52	9.55	5.88	0.16	102.33	330	0.47	737	8.86
X590Bb_36	58.62	27.36	0.38	8.75	6.21	0.14	101.46	340	0.43	729	8.79
X590Bb_37	60.11	25.96	0.44	7.94	6.54	0.17	101.16	350	0.40	716	8.80
X590Bb_38	59.21	27.00	0.35	9.04	6.10	0.14	101.85	360	0.45	732	8.81
X590Bb_39	58.38	27.50	0.38	9.53	5.87	0.13	101.79	370	0.47	738	8.84
X590Bb_40	58.54	27.64	0.44	9.71	5.82	0.15	102.30	380	0.48	739	8.87
X590Bb_41	58.48	27.33	0.40	9.23	6.08	0.13	101.65	390	0.45	734	8.81
X590Bb_42	58.65	27.54	0.40	9.35	6.06	0.11	102.11	400	0.46	736	8.81
X590Bb_43	58.54	27.52	0.39	9.15	5.87	0.12	101.60	410	0.46	736	8.82
X590Bb_44	58.21	26.53	0.51	8.65	5.98	0.17	100.05	420	0.44	730	8.82
X590Bb2_2	58.55	26.32	0.31	7.95	6.17	0.16	99.45	10	0.41	721	8.80
X590Bb2_3	59.37	26.13	0.35	8.13	6.28	0.14	100.39	20	0.41	722	8.78
X590Bb2_4	59.45	26.30	0.41	7.96	6.28	0.14	100.54	30	0.41	720	8.79
X590Bb2_5	61.25	26.35	0.31	7.88	6.73	0.15	102.67	40	0.39	713	8.80
X590Bb2_6	60.71	26.47	0.44	7.89	6.44	0.15	102.11	50	0.40	717	8.79

Table A3.10 continued

Sample	SiO_2	Al_2O_3	FeO	CaO	Na_2O	K_2O	Total	Dist (μm)	X An	Temp °C	H_2O wt%
X590Bb2_8	60.74	26.58	0.38	7.81	6.57	0.17	102.26	70	0.39	714	8.81
X590Bb2_9	61.02	26.30	0.38	7.96	6.64	0.17	102.47	80	0.39	715	8.80
X590Bb2_10	58.31	27.31	0.36	8.96	5.99	0.17	101.09	90	0.45	732	8.83
X590Bb2_12	60.07	27.20	0.30	8.27	6.08	0.17	102.09	110	0.42	725	8.80
X590Bb2_13	61.01	26.62	0.34	7.74	6.47	0.19	102.38	120	0.39	714	8.82
X590Bb2_14	59.58	26.48	0.35	8.17	6.26	0.13	100.97	130	0.42	723	8.78
X590Bb2_16	60.23	26.66	0.38	8.58	6.00	0.20	102.06	150	0.44	728	8.83
X590Bb2_19	60.35	26.43	0.34	7.98	6.44	0.14	101.66	180	0.40	719	8.78
X590Bb2_21	59.34	27.38	0.42	8.96	5.91	0.15	102.14	200	0.45	734	8.82
X590Bb2_22	59.76	27.23	0.37	8.89	6.30	0.13	102.67	210	0.43	729	8.78
X590Bb2_23	60.24	27.08	0.38	8.77	6.06	0.10	102.64	220	0.44	732	8.78
X590Bb2_24	58.24	26.97	0.28	8.95	6.24	0.15	100.84	230	0.44	730	8.80
X590Bb2_25	59.65	26.69	0.32	8.25	6.52	0.14	101.56	240	0.41	721	8.78
X590Bb2_26	57.92	27.60	0.39	9.19	6.03	0.09	101.21	250	0.45	736	8.79
X590Bb2_27	60.54	26.05	0.35	7.63	6.79	0.18	101.54	260	0.38	709	8.82
X590Bb2_28	60.50	26.62	0.36	8.29	6.60	0.17	102.53	270	0.41	719	8.80
X590Bb2_30	58.91	27.61	0.40	9.56	5.52	0.21	102.22	290	0.48	739	8.93
X590Bb2_31	56.39	29.34	0.45	11.00	5.03	0.11	102.31	300	0.54	751	9.12
X590Bb2_32	57.23	27.49	0.38	9.32	5.91	0.15	100.49	310	0.46	736	8.84
X590Bb2_33	58.01	27.69	0.35	9.47	5.86	0.13	101.51	320	0.47	738	8.84
X590Bb2_34	58.11	27.63	0.46	9.31	5.82	0.13	101.46	330	0.47	738	8.83
X590Bb2_35	59.41	27.32	0.35	9.00	6.05	0.12	102.25	340	0.45	733	8.80
X590Bb2_36	59.40	27.40	0.35	9.01	6.00	0.14	102.31	350	0.45	733	8.81
X590Bb2_37	59.81	27.50	0.38	8.89	6.01	0.20	102.79	360	0.44	731	8.84
X590Be_2	57.61	26.80	0.41	8.97	6.43	0.15	100.36	0	0.43	728	8.79
X590Be_3	57.45	26.89	0.39	8.70	6.45	0.10	99.98	10	0.42	727	8.76
X590Be_4	57.42	26.62	0.42	9.36	6.25	0.12	100.18	20	0.45	734	8.80
X590Be_5	58.23	26.57	0.37	8.43	6.56	0.16	100.32	30	0.41	721	8.79
X590Be_6	59.30	25.97	0.39	8.15	6.69	0.18	100.69	40	0.40	716	8.81
X590Be_7	59.79	26.06	0.43	8.05	6.91	0.14	101.38	50	0.39	713	8.79
X590Be_8	57.91	25.46	0.37	7.89	6.61	0.14	98.39	60	0.39	716	8.79
X590Be_9	58.38	26.17	0.39	8.04	6.87	0.19	100.03	70	0.39	713	8.82
X590Be_10	57.80	26.77	0.39	9.24	6.20	0.15	100.55	80	0.45	733	8.81
X590Be_11	56.70	27.40	0.37	9.80	5.85	0.13	100.26	90	0.48	740	8.86
X590Be_12	57.05	27.49	0.39	9.67	5.80	0.13	100.52	100	0.48	740	8.86
X590Be_13	56.99	27.38	0.48	10.01	5.76	0.12	100.74	110	0.49	742	8.88
X590Be_14	55.93	27.30	0.31	10.28	5.63	0.12	99.56	120	0.50	745	8.92
X590Be_15	58.60	26.86	0.46	9.08	6.34	0.15	101.48	130	0.44	730	8.80
X590Be_16	58.99	26.70	0.44	8.83	6.38	0.14	101.47	140	0.43	728	8.79
X590Be_17	57.68	26.73	0.41	8.88	6.31	0.10	100.11	150	0.43	730	8.77
X590Be_18	57.39	27.04	0.43	9.19	6.20	0.14	100.40	160	0.45	732	8.81
X590Be_19	58.05	26.40	0.47	8.28	6.50	0.18	99.88	170	0.41	720	8.81
X590Be_20	59.96	26.41	0.49	8.44	6.63	0.12	102.06	180	0.41	722	8.77
X590Be_21	60.54	26.56	0.49	8.15	6.74	0.19	102.66	190	0.40	715	8.81
X590Be_22	58.86	26.56	0.55	8.78	6.32	0.16	101.23	200	0.43	727	8.80
X590Bl_1	58.55	27.52	0.46	9.36	5.65	0.15	101.68	0	0.47	739	8.87
X590Bl_3	59.17	26.61	0.31	8.76	6.13	0.15	101.14	20	0.44	730	8.80
X590Bl_4	59.67	26.98	0.40	9.12	6.13	0.13	102.43	30	0.45	733	8.80
X590Bl_5	59.27	27.18	0.35	9.28	6.12	0.17	102.37	40	0.45	733	8.83
X590Bl_6	59.00	27.53	0.48	9.14	6.14	0.13	102.41	50	0.45	733	8.80
X590Bl_7	56.58	28.39	0.42	10.70	5.36	0.08	101.52	60	0.52	749	8.99
X590Bl_8	55.81	29.05	0.44	11.31	5.11	0.11	101.83	70	0.55	751	9.13
X590Bl_9	55.87	29.29	0.45	11.18	5.15	0.07	101.99	80	0.54	752	9.08
X590Bl_10	55.76	29.31	0.40	11.55	4.83	0.10	101.95	90	0.57	753	9.24
X590Bl_11	56.06	29.48	0.43	11.64	4.70	0.10	102.41	100	0.57	753	9.29
X590Bl_12	56.06	29.52	0.38	11.42	5.00	0.13	102.52	110	0.55	751	9.19
X590Bl_13	55.76	29.11	0.40	11.01	5.10	0.10	101.48	120	0.54	751	9.09
X590Bl_14	58.76	27.27	0.52	9.10	6.11	0.15	101.90	130	0.45	732	8.81
X590Bl_15	59.90	26.96	0.38	8.27	6.21	0.13	101.85	140	0.42	725	8.78
X590Bl_16	58.47	27.60	0.34	8.87	6.17	0.20	101.65	150	0.44	729	8.83
X590Bl_19	59.99	26.98	0.48	8.86	6.31	0.19	102.81	180	0.43	727	8.82
X590Bl_20	59.79	27.28	0.45	9.05	6.14	0.13	102.84	190	0.45	732	8.80
X590Bl_21	58.84	26.55	0.43	8.82	6.28	0.18	101.10	200	0.43	728	8.81
X590Bl_22	59.55	26.95	0.49	8.56	6.45	0.17	102.18	210	0.42	724	8.80
X590Bl_23	59.73	26.95	0.33	8.57	6.46	0.15	102.20	220	0.42	724	8.79
X590Bl_24	58.86	27.02	0.42	8.85	6.14	0.18	101.47	230	0.44	729	8.82
X590Bl_25	58.11	28.22	0.36	10.07	5.77	0.12	102.66	240	0.49	742	8.89
X590Bl_32	59.46	26.99	0.34	8.76	6.35	0.15	102.06	310	0.43	727	8.79

Table A3.10 continued

Sample	SiO_2	Al_2O_3	FeO	CaO	Na_2O	K_2O	Total	Dist (μm)	X An	Temp °C	H_2O wt%
X590Bl_34	59.27	27.51	0.40	8.89	6.25	0.11	102.44	330	0.44	731	8.78
X590Bl_35	59.42	27.18	0.44	9.08	6.19	0.14	102.44	340	0.44	732	8.80
X590Bl_36	61.14	26.14	0.35	8.06	6.79	0.21	102.69	350	0.39	713	8.82
X590Bl_37	60.44	26.78	0.41	8.44	6.41	0.16	102.64	360	0.42	723	8.79
X590Bl_38	59.39	27.25	0.39	9.01	6.18	0.19	102.42	370	0.44	730	8.83
X609j_11	60.11	26.65	0.46	9.00	5.97	0.19	102.39	100	0.45	732	8.84
X609j_12	59.27	26.72	0.37	8.87	6.29	0.17	101.70	110	0.43	728	8.81
X609j_13	58.93	26.30	0.40	8.46	6.00	0.23	100.33	120	0.43	726	8.85
X609j_14	59.27	27.03	0.39	8.85	6.08	0.17	101.80	130	0.44	730	8.82
X609j_15	58.87	26.74	0.36	9.19	6.09	0.11	101.37	140	0.45	734	8.80
X609j_16	59.30	26.79	0.42	9.38	6.16	0.16	102.21	150	0.45	734	8.83
X609j_17	59.79	26.99	0.41	8.78	6.20	0.15	102.32	160	0.44	729	8.80
X609j_18	59.46	27.07	0.37	8.75	6.27	0.19	102.10	170	0.43	727	8.81
X609j_19	60.31	26.00	0.28	8.22	6.54	0.15	101.51	180	0.41	720	8.79
X609j_20	60.92	26.20	0.33	8.00	6.62	0.17	102.22	190	0.40	716	8.80
X609j_21	60.03	26.56	0.34	8.67	6.51	0.16	102.28	200	0.42	724	8.79
X609j_22	60.13	26.54	0.33	8.50	6.25	0.16	101.91	210	0.42	726	8.80
X609j_24	59.75	26.96	0.36	9.03	6.27	0.14	102.52	230	0.44	730	8.80
X609j_25	59.90	26.66	0.42	8.69	6.26	0.16	102.09	240	0.43	727	8.80
X609j_28	58.69	27.45	0.45	8.95	6.21	0.15	101.90	270	0.44	730	8.80
X609j_29	58.53	27.78	0.37	9.41	6.18	0.10	102.37	280	0.45	735	8.80
X609j_30	60.05	27.03	0.49	8.64	6.53	0.15	102.88	290	0.42	724	8.79
X609j_31	59.36	27.34	0.41	8.75	6.23	0.12	102.21	300	0.43	729	8.78
X609j_32	57.80	27.46	0.41	9.22	6.22	0.13	101.24	310	0.45	733	8.80
X609j_33	58.81	27.49	0.48	8.80	6.34	0.17	102.10	320	0.43	727	8.80
X609j_34	59.15	27.15	0.54	8.87	6.37	0.15	102.22	330	0.43	728	8.79
X609j_35	58.84	27.30	0.29	9.31	6.33	0.13	102.19	340	0.45	732	8.79
X609j_36	60.74	25.94	0.36	7.56	6.83	0.21	101.64	350	0.37	707	8.85
X609j_37	60.66	26.16	0.36	7.68	6.91	0.17	101.95	360	0.38	708	8.82
X609j_38	60.36	26.04	0.28	7.75	6.99	0.21	101.63	370	0.38	707	8.84
X609j_39	59.85	26.22	0.38	7.64	6.88	0.17	101.14	380	0.38	708	8.82
X609j_40	59.95	26.97	0.35	8.00	6.60	0.19	102.06	390	0.40	715	8.81
X609j_41	61.00	25.95	0.42	7.61	6.80	0.13	101.91	400	0.38	710	8.80
X609j_42	61.21	25.96	0.45	7.46	6.92	0.14	102.14	410	0.37	706	8.81
X609j_43	60.81	26.14	0.39	7.69	6.91	0.15	102.09	420	0.38	709	8.81
X609j_44	60.89	26.21	0.40	7.63	6.62	0.16	101.91	430	0.39	712	8.81
X609j_45	60.23	25.83	0.44	7.60	6.89	0.13	101.12	440	0.38	709	8.80
X609j_46	60.73	25.55	0.40	7.61	6.91	0.22	101.42	450	0.37	706	8.85
X609j_47	61.40	25.74	0.35	7.83	6.97	0.15	102.44	460	0.38	710	8.81
X609j_48	61.08	26.09	0.40	7.86	6.86	0.18	102.47	470	0.38	711	8.81
X609j_49	59.57	26.07	0.39	8.27	6.85	0.21	101.35	480	0.40	715	8.82
X609j_50	59.46	26.11	0.36	8.07	6.73	0.17	100.90	490	0.39	715	8.80
X609j_51	59.33	26.19	0.52	8.39	6.71	0.17	101.30	500	0.40	719	8.80
X609j_52	57.79	27.20	0.40	9.56	6.45	0.13	101.54	510	0.45	733	8.80
X609j_53	57.56	27.01	0.35	9.53	5.89	0.15	100.49	520	0.47	738	8.85
X609j_54	58.35	27.27	0.28	9.27	6.23	0.21	101.60	530	0.45	731	8.84
X609j_55	58.09	27.24	0.39	9.62	5.98	0.11	101.44	540	0.47	739	8.82
X609j_56	57.53	27.73	0.38	9.93	5.84	0.15	101.56	550	0.48	740	8.88
X609j_57	57.17	27.77	0.33	9.69	5.89	0.12	100.97	560	0.47	739	8.85
X609j_58	56.93	27.68	0.42	9.98	5.94	0.12	101.07	570	0.48	741	8.86
X609j_59	57.02	27.43	0.32	9.92	5.82	0.12	100.63	580	0.48	741	8.87
X609j_60	56.97	27.74	0.38	9.78	5.96	0.13	100.95	590	0.47	739	8.84
X609j_61	57.35	27.57	0.30	9.89	5.79	0.10	101.00	600	0.48	742	8.86
X609j_62	57.70	27.40	0.40	10.16	6.02	0.14	101.82	610	0.48	740	8.87
X609j_63	57.80	27.65	0.46	9.80	5.79	0.14	101.64	620	0.48	741	8.87
X609j_64	57.62	28.04	0.39	9.71	5.97	0.11	101.85	630	0.47	739	8.83
X609j_65	57.32	27.88	0.36	10.00	5.97	0.10	101.64	640	0.48	741	8.85
X609j_66	56.34	27.58	0.39	9.84	5.92	0.13	100.20	650	0.48	740	8.85
X609j_67	56.76	27.49	0.38	9.81	5.80	0.11	100.36	660	0.48	741	8.86
X609j_68	56.78	27.23	0.42	9.50	5.94	0.13	100.00	670	0.47	738	8.83
X609j_69	57.11	27.48	0.38	9.89	5.81	0.10	100.76	680	0.48	742	8.86
X609j_70	57.02	27.83	0.32	10.08	5.92	0.10	101.27	690	0.48	742	8.85
X609j_71	57.18	28.06	0.30	10.10	5.52	0.12	101.28	700	0.50	745	8.93
X609j_72	57.12	28.03	0.40	10.12	5.51	0.09	101.27	710	0.50	746	8.91
X609j_74	56.24	28.54	0.36	10.60	5.53	0.11	101.39	730	0.51	747	8.96
X609j_75	55.78	28.47	0.35	10.79	5.33	0.09	100.81	740	0.53	749	9.01
X609j_76	55.30	28.34	0.39	10.86	5.35	0.15	100.39	750	0.52	748	9.05
X609j_77	55.58	28.37	0.49	10.86	5.25	0.10	100.65	760	0.53	750	9.04
X609j_78	56.28	28.13	0.35	10.49	5.49	0.11	100.85	770	0.51	747	8.96

Table A3.10 continued

Sample	SiO_2	Al_2O_3	FeO	CaO	Na_2O	K_2O	Total	Dist (μm)	X An	Temp °C	H_2O wt%
X609j_80	56.19	28.30	0.38	10.57	5.44	0.11	100.98	790	0.51	748	8.97
X609j_81	55.93	28.54	0.34	10.67	5.35	0.08	100.92	800	0.52	749	8.99
X609j_82	55.55	28.23	0.38	10.41	5.55	0.12	100.24	810	0.51	746	8.95
X609j_83	58.25	26.60	0.44	8.73	6.38	0.17	100.56	820	0.43	726	8.80
X609j_84	58.36	26.64	0.42	8.52	6.52	0.13	100.60	830	0.42	723	8.78
X609j_85	58.55	26.58	0.43	8.79	6.47	0.11	100.93	840	0.43	727	8.77
X609j_86	58.41	26.88	0.38	8.89	6.28	0.16	100.99	850	0.43	729	8.80
X609j_87	57.45	27.17	0.32	9.30	5.94	0.11	100.29	860	0.46	737	8.81
X609j_88	57.22	27.08	0.40	9.04	6.12	0.15	100.02	870	0.45	732	8.81
X609j_89	57.37	27.29	0.41	9.27	6.09	0.11	100.54	880	0.45	735	8.80
X609j_90	56.00	27.83	0.41	10.32	5.75	0.12	100.43	890	0.49	744	8.91
X609k_1	67.13	21.85	0.92	6.21	5.33	0.83	102.27	0	0.37	691	9.25
X609k_2	58.12	27.44	0.44	9.00	5.98	0.14	101.12	10	0.45	733	8.81
X609k_3	58.73	27.34	0.32	9.18	6.32	0.17	102.05	20	0.44	730	8.81
X609k_4	59.46	27.00	0.46	8.98	6.43	0.15	102.48	30	0.43	728	8.79
X609k_5	57.19	27.29	0.27	9.17	5.84	0.15	99.93	40	0.46	736	8.84
X609k_6	57.57	27.59	0.47	9.38	5.71	0.19	100.90	50	0.47	737	8.88
X609k_7	58.57	27.69	0.41	9.45	5.72	0.13	101.97	60	0.47	739	8.86
X609k_9	58.95	27.28	0.36	9.10	6.08	0.20	101.96	80	0.45	731	8.84
X609k_10	59.71	27.11	0.48	8.69	6.64	0.18	102.81	90	0.42	722	8.80
X609k_11	59.49	27.01	0.47	9.21	5.68	0.16	102.02	100	0.47	737	8.86
X609k_12	58.18	27.24	0.42	9.00	5.56	0.11	100.51	110	0.47	739	8.83
X609k_13	58.58	27.30	0.40	9.10	6.25	0.12	101.74	120	0.44	732	8.79
X609k_14	59.60	26.56	0.34	8.33	6.47	0.17	101.48	130	0.41	721	8.80
X609k_15	60.71	25.95	0.35	7.57	6.77	0.21	101.57	140	0.38	708	8.84
X609k_16	60.67	26.21	0.35	7.92	6.65	0.20	102.00	150	0.39	714	8.82
X609k_17	61.08	26.02	0.31	7.43	6.76	0.20	101.79	160	0.37	706	8.84
X609k_18	60.33	26.64	0.34	8.03	6.58	0.13	102.04	170	0.40	718	8.78
X609k_19	59.85	26.97	0.36	8.65	6.35	0.16	102.33	180	0.43	726	8.80
X609k_20	59.40	27.05	0.38	8.82	6.08	0.14	101.87	190	0.44	731	8.80
X609k_21	59.71	26.87	0.36	8.78	6.14	0.17	102.03	200	0.44	729	8.81
X609k_22	58.84	27.25	0.36	9.14	6.02	0.15	101.76	210	0.45	734	8.82
X609k_23	58.64	27.77	0.37	9.42	5.88	0.16	102.24	220	0.47	737	8.85
X609k_24	60.64	26.70	0.47	8.41	6.41	0.14	102.77	230	0.42	723	8.78
X609k_25	60.89	26.49	0.39	8.30	6.29	0.17	102.54	240	0.42	723	8.80
X609k_26	59.90	26.99	0.30	8.81	6.11	0.16	102.27	250	0.44	730	8.81
X609k_27	59.27	27.34	0.31	8.89	6.01	0.14	101.96	260	0.45	732	8.81
X609k_28	61.23	25.73	0.32	7.32	6.94	0.17	101.70	270	0.36	703	8.84
X609k_29	61.21	26.03	0.39	7.34	6.93	0.19	102.09	280	0.36	703	8.85
X609k_30	60.86	26.30	0.27	7.88	6.57	0.17	102.05	290	0.39	715	8.81
X609k_31	59.89	25.90	0.41	7.60	6.68	0.16	100.64	300	0.38	711	8.81
X609k_32	61.09	26.34	0.38	7.92	6.72	0.14	102.60	310	0.39	714	8.79
X609k_33	60.16	26.54	0.44	8.32	6.58	0.17	102.21	320	0.41	720	8.80
X609k_34	60.67	26.33	0.44	7.84	6.94	0.17	102.38	330	0.38	710	8.82
X609k_35	59.75	26.43	0.42	8.16	6.43	0.19	101.38	340	0.41	719	8.81
X609k_36	58.71	27.38	0.44	9.04	6.27	0.12	101.97	350	0.44	731	8.79
X609k_37	58.85	27.61	0.33	8.98	6.10	0.13	102.02	360	0.44	732	8.80
X609k_38	59.20	26.45	0.36	7.83	6.39	0.18	100.42	370	0.40	716	8.81
X609k_39	60.91	26.10	0.35	7.75	6.82	0.16	102.10	380	0.38	710	8.81
X609k_40	60.79	26.13	0.41	7.69	6.66	0.17	101.85	390	0.39	712	8.81
X609k_41	61.42	26.13	0.39	7.42	6.99	0.20	102.56	400	0.37	703	8.86
X609k_42	61.29	26.15	0.39	7.30	6.67	0.19	102.00	410	0.37	706	8.84
X609k_43	60.23	26.09	0.38	7.82	6.68	0.19	101.40	420	0.39	712	8.82
X609k_44	58.69	27.45	0.39	9.28	6.17	0.15	102.14	430	0.45	733	8.81
X609k_45	59.15	26.21	0.45	7.76	6.57	0.18	100.31	440	0.39	713	8.81
X609k_46	58.75	26.04	0.42	8.21	6.59	0.19	100.21	450	0.40	718	8.81
X609k_51	58.99	26.95	0.47	8.70	6.32	0.18	101.61	500	0.43	726	8.81
X609k_52	59.32	27.31	0.35	8.76	6.19	0.11	102.05	510	0.44	730	8.78
X609k_53	59.59	27.02	0.38	8.81	6.40	0.16	102.35	520	0.43	727	8.80
X609k_54	59.17	27.30	0.35	8.79	6.19	0.17	101.97	530	0.44	729	8.81
X609k_55	58.84	27.02	0.23	8.69	6.40	0.18	101.37	540	0.42	725	8.81
X609k_56	59.48	26.89	0.38	8.55	6.42	0.15	101.87	550	0.42	724	8.79
X609k_57	59.77	26.69	0.41	8.38	6.29	0.14	101.67	560	0.42	725	8.78
X609k_58	59.55	26.30	0.40	8.22	6.59	0.18	101.24	570	0.40	718	8.80
X609k_59	58.87	26.07	0.39	8.15	6.19	0.20	99.87	580	0.42	722	8.82
X609k_60	60.68	26.34	0.38	7.85	6.86	0.21	102.31	590	0.38	710	8.83
X609k_61	60.40	25.91	0.46	7.60	6.99	0.16	101.53	600	0.37	706	8.82
X609k_62	59.78	26.31	0.35	8.19	6.63	0.22	101.49	610	0.40	717	8.83
X609k_63	60.53	26.13	0.36	7.81	6.82	0.17	101.81	620	0.38	711	8.81

Table A3.10 continued

Sample	SiO_2	Al_2O_3	FeO	CaO	Na_2O	K_2O	Total	Dist (μm)	X An	Temp °C	H_2O wt%
X609k_66	59.02	27.78	0.46	9.47	5.91	0.12	102.77	650	0.47	738	8.83
X609k_67	57.83	27.97	0.52	9.67	6.02	0.12	102.12	660	0.47	738	8.83
X609k_68	58.10	27.64	0.40	9.14	6.33	0.13	101.74	670	0.44	731	8.79
X609k_69	58.91	27.25	0.27	8.81	6.23	0.15	101.62	680	0.43	729	8.80
X609k_70	58.55	27.35	0.42	9.08	6.07	0.13	101.60	690	0.45	733	8.80
X609k_71	65.30	21.63	0.91	6.10	5.43	0.65	100.02	700	0.37	694	9.14
X609l_1	60.94	25.38	0.40	6.88	7.27	0.16	101.03	0	0.34	692	8.90
X609l_2	61.10	25.29	0.31	6.75	7.24	0.22	100.91	10	0.34	690	8.94
X609l_3	61.60	25.49	0.30	7.01	7.17	0.16	101.73	20	0.35	696	8.87
X609l_4	61.39	25.36	0.38	6.94	7.11	0.19	101.37	30	0.35	695	8.89
X609l_5	62.48	25.15	0.36	6.43	7.35	0.22	101.98	40	0.32	683	8.98
X609l_6	62.62	25.07	0.32	6.44	7.34	0.22	102.01	50	0.32	683	8.98
X609l_7	62.09	24.33	0.33	6.15	7.52	0.24	100.66	60	0.31	675	9.05
X609l_8	61.92	24.98	0.30	6.33	7.20	0.23	100.97	70	0.32	683	8.99
X609l_9	61.67	24.88	0.32	6.62	6.94	0.27	100.70	80	0.34	690	8.95
X609l_10	62.01	24.86	0.35	6.71	7.30	0.23	101.45	90	0.33	688	8.95
X609l_11	61.92	25.00	0.25	6.56	7.44	0.19	101.37	100	0.32	684	8.96
X609l_12	62.62	24.87	0.39	6.43	7.30	0.23	101.84	110	0.32	683	8.99
X609l_14	61.34	25.70	0.39	7.05	7.13	0.20	101.80	130	0.35	696	8.89
X609l_15	60.03	26.58	0.33	8.11	6.76	0.16	101.96	140	0.39	716	8.79
X609l_16	60.32	26.03	0.37	7.85	6.74	0.17	101.49	150	0.39	713	8.81
X609l_17	59.55	26.19	0.37	7.49	6.79	0.13	100.53	160	0.38	708	8.81
X609l_18	61.19	25.66	0.37	7.23	6.89	0.20	101.54	170	0.36	702	8.86
X609l_19	62.30	25.42	0.42	7.08	7.11	0.19	102.51	180	0.35	697	8.88
X609l_20	62.49	25.76	0.33	7.10	6.94	0.23	102.85	190	0.36	699	8.89
X609l_21	61.73	25.54	0.35	6.75	7.05	0.20	101.62	200	0.34	693	8.91
X609l_22	61.37	25.90	0.38	7.22	7.12	0.15	102.15	210	0.36	700	8.85
X609l_23	61.20	26.09	0.42	7.21	7.00	0.15	102.08	220	0.36	702	8.84
X609l_24	61.05	25.85	0.34	7.15	7.15	0.17	101.70	230	0.35	698	8.86
X609l_25	61.04	25.68	0.28	7.14	7.21	0.20	101.56	240	0.35	696	8.89
X609l_26	60.69	25.86	0.34	7.49	7.15	0.17	101.70	250	0.36	703	8.84
X609l_27	60.85	25.89	0.25	7.25	7.01	0.19	101.46	260	0.36	701	8.86
X609l_28	59.47	26.31	0.37	8.31	6.42	0.18	101.07	270	0.41	721	8.81
X609l_30	59.88	26.45	0.30	7.77	6.55	0.16	101.11	290	0.39	714	8.80
X609l_31	60.00	26.60	0.40	8.00	6.52	0.16	101.68	300	0.40	717	8.80
X609l_32	58.91	27.05	0.41	8.33	6.44	0.14	101.29	310	0.41	722	8.78
X609l_33	60.11	26.61	0.33	7.97	6.69	0.17	101.88	320	0.39	715	8.80
X609l_34	60.30	26.17	0.29	7.65	6.78	0.16	101.35	330	0.38	710	8.81
X609l_35	61.08	25.99	0.30	7.25	6.96	0.18	101.76	340	0.36	702	8.85
X609l_36	61.08	25.83	0.34	7.43	7.02	0.17	101.88	350	0.37	704	8.84
X609l_37	60.92	26.41	0.40	7.89	6.80	0.16	102.58	360	0.39	713	8.80
X609l_38	60.95	26.57	0.27	7.79	6.94	0.17	102.70	370	0.38	709	8.82
X609l_39	60.69	26.32	0.40	7.85	6.77	0.20	102.22	380	0.39	711	8.82
X609l_40	59.94	26.55	0.40	7.71	6.56	0.13	101.28	390	0.39	714	8.79
X609l_41	59.36	27.18	0.39	8.43	6.67	0.16	102.18	400	0.41	720	8.79
X609l_42	59.64	26.64	0.29	8.42	6.64	0.14	101.76	410	0.41	721	8.78
X609l_43	60.50	26.40	0.33	8.06	6.77	0.17	102.23	420	0.39	715	8.80
X609l_44	59.92	26.64	0.44	8.29	6.64	0.17	102.12	430	0.40	719	8.80
X609l_45	59.08	27.11	0.41	8.65	6.36	0.19	101.80	440	0.42	725	8.81
X609l_46	60.03	27.00	0.32	8.75	6.35	0.13	102.58	450	0.43	728	8.78
X609l_47	60.00	26.93	0.40	8.59	6.38	0.17	102.47	460	0.42	725	8.80
X609l_50	60.02	26.94	0.37	8.77	6.10	0.15	102.35	490	0.44	730	8.80
X609l_51	60.09	26.87	0.33	8.73	6.29	0.16	102.48	500	0.43	727	8.80
X609l_52	59.39	26.98	0.40	9.02	6.12	0.14	102.05	510	0.44	732	8.80
X609l_53	58.81	27.31	0.39	8.93	6.17	0.16	101.76	520	0.44	730	8.81
X609l_54	58.53	27.25	0.32	8.65	6.23	0.18	101.16	530	0.43	727	8.81
X609l_55	58.79	26.88	0.38	8.93	6.16	0.12	101.27	540	0.44	732	8.79
X609l_56	59.46	26.97	0.36	8.54	6.19	0.12	101.64	550	0.43	728	8.78
X609l_57	59.96	26.63	0.42	8.29	6.56	0.13	101.99	560	0.41	721	8.77
X609l_58	59.84	26.68	0.28	8.46	6.39	0.16	101.82	570	0.42	724	8.79
X609l_59	59.48	26.52	0.33	8.42	6.39	0.15	101.29	580	0.42	723	8.79
X609l_60	59.49	26.64	0.43	8.19	6.58	0.15	101.48	590	0.40	719	8.79
X609l_61	58.76	26.71	0.34	8.15	6.41	0.17	100.54	600	0.41	720	8.80
X609l_62	59.87	26.77	0.32	8.03	6.35	0.16	101.50	610	0.41	720	8.80
X609l_63	60.12	26.51	0.40	8.16	6.59	0.16	101.94	620	0.40	718	8.79
X609l_64	60.48	26.08	0.39	7.94	6.65	0.12	101.65	630	0.39	716	8.78
X609l_65	60.33	26.16	0.39	8.02	6.75	0.18	101.83	640	0.39	714	8.81
X609l_66	60.14	24.74	0.30	6.85	7.16	0.16	99.35	650	0.34	694	8.89
X609l_67	59.67	25.77	0.37	7.69	6.60	0.22	100.32	660	0.39	711	8.84

Table A3.10 continued

Sample	SiO_2	Al_2O_3	FeO	CaO	Na_2O	K_2O	Total	Dist (μm)	X An	Temp °C	H_2O wt%
X609l_69	60.04	26.29	0.35	7.65	6.65	0.21	101.18	680	0.38	711	8.83
X609l_70	60.20	26.23	0.36	7.82	6.96	0.20	101.77	690	0.38	709	8.83
X609l_71	60.53	26.41	0.36	7.79	6.59	0.21	101.89	700	0.39	713	8.83
X609l_72	58.61	26.67	0.30	8.55	6.30	0.18	100.60	710	0.42	725	8.81
X609l_73	59.32	27.12	0.44	8.90	6.48	0.18	102.44	720	0.43	726	8.81
X609l_74	58.65	27.32	0.42	9.16	5.97	0.14	101.67	730	0.45	735	8.82
X609l_75	57.23	27.37	0.46	9.12	5.89	0.15	100.23	740	0.46	735	8.83
X609l_76	58.07	27.39	0.55	9.15	6.05	0.16	101.36	750	0.45	733	8.82
X609l_77	59.21	27.29	0.48	8.73	6.30	0.14	102.16	760	0.43	728	8.79
X609l_78	58.29	27.33	0.37	8.98	6.18	0.17	101.31	770	0.44	730	8.81
X609l_79	57.90	27.03	0.43	9.06	6.10	0.15	100.66	780	0.45	732	8.81
X609l_80	58.37	26.94	0.39	8.85	6.32	0.15	101.03	790	0.43	728	8.80
X609p_81	60.01	26.13	0.41	7.62	6.94	0.17	101.28	800	0.37	707	8.83
X609p_82	59.28	26.57	0.31	8.47	6.61	0.12	101.37	810	0.41	722	8.77
X609p_83	58.63	27.03	0.38	8.87	6.27	0.12	101.31	820	0.44	730	8.78
X609p_84	58.40	27.47	0.33	9.29	6.13	0.12	101.74	830	0.45	734	8.80
X609p_85	58.55	27.53	0.42	9.44	6.06	0.18	102.17	840	0.46	735	8.85
X609p_86	58.57	27.79	0.42	9.03	6.13	0.13	102.07	850	0.45	732	8.80
X609p_87	58.67	27.15	0.34	8.42	6.26	0.14	100.97	860	0.42	725	8.78
X609p_88	60.94	25.60	0.34	7.33	6.98	0.20	101.39	870	0.36	702	8.86
X609p_89	60.15	25.84	0.33	7.57	6.89	0.18	100.95	880	0.37	707	8.83
X609p_90	64.70	22.20	0.75	5.83	6.10	0.61	100.19	890	0.33	681	9.17
X609p_4	60.49	26.53	0.35	8.00	6.88	0.14	102.41	30	0.39	713	8.79
X609p_5	59.15	27.70	0.45	9.23	6.10	0.10	102.74	40	0.45	735	8.79
X609p_6	58.65	27.93	0.45	9.34	5.95	0.12	102.44	50	0.46	737	8.82
X609p_7	58.68	28.10	0.49	9.73	5.82	0.13	102.95	60	0.48	740	8.86
X609p_8	58.94	27.70	0.40	9.13	5.90	0.15	102.22	70	0.46	735	8.83
X609p_9	59.29	27.73	0.48	9.09	5.98	0.11	102.68	80	0.45	735	8.80
X609p_10	60.45	26.75	0.34	7.94	6.79	0.16	102.43	90	0.39	713	8.80
X609p_11	60.30	27.09	0.32	8.59	6.43	0.16	102.88	100	0.42	724	8.79
X609p_12	59.26	27.39	0.34	8.59	6.44	0.16	102.19	110	0.42	724	8.80
X609p_13	59.10	27.33	0.40	8.95	6.16	0.13	102.06	120	0.44	731	8.79
X609p_14	58.92	27.42	0.41	9.22	6.09	0.12	102.18	130	0.45	734	8.80
X609p_15	58.90	27.77	0.36	9.35	6.12	0.13	102.63	140	0.45	735	8.81
X609p_16	59.15	27.71	0.34	8.89	6.14	0.14	102.37	150	0.44	731	8.80
X609p_18	59.61	27.32	0.39	8.90	6.23	0.12	102.58	170	0.44	730	8.78
X609p_19	59.16	27.69	0.38	8.86	6.23	0.15	102.48	180	0.44	729	8.80
X609p_20	58.82	26.64	0.31	8.52	6.30	0.12	100.72	190	0.42	726	8.77
X609p_21	58.27	26.55	0.39	8.48	6.23	0.16	100.09	200	0.43	726	8.80
X609p_22	58.82	27.36	0.35	8.94	6.18	0.16	101.80	210	0.44	730	8.81
X609p_23	59.98	26.76	0.37	8.20	6.42	0.12	101.85	220	0.41	722	8.77
X609p_24	60.93	26.38	0.36	7.94	6.69	0.21	102.52	230	0.39	713	8.83
X609p_25	69.46	17.78	1.15	4.30	4.16	1.15	98.00	240	0.33	664	9.66
X609p_26	57.81	28.06	0.38	9.62	5.72	0.11	101.69	250	0.48	741	8.86
X609p_27	58.21	27.30	0.42	8.82	6.21	0.14	101.10	260	0.44	729	8.80
X609p_28	59.54	26.26	0.29	8.48	6.22	0.12	100.91	270	0.43	727	8.78
X609p_29	57.75	26.47	0.31	8.65	6.37	0.15	99.69	280	0.43	726	8.79
X609p_30	58.98	27.05	0.39	8.66	6.37	0.14	101.58	290	0.43	726	8.78
X609p_31	59.35	27.09	0.35	8.56	6.30	0.16	101.81	300	0.42	726	8.80
X609p_32	58.62	27.05	0.41	8.29	6.37	0.16	100.89	310	0.41	722	8.79
X609p_33	58.07	26.58	0.39	8.35	6.47	0.12	99.99	320	0.41	723	8.77
X609p_34	58.13	26.58	0.37	8.18	6.39	0.14	99.79	330	0.41	721	8.79
X609p_35	57.86	26.25	0.32	7.87	6.34	0.17	98.81	340	0.40	718	8.80
X609p_36	58.17	26.51	0.34	8.43	6.38	0.17	100.00	350	0.42	723	8.80
X609p_37	59.41	26.39	0.28	8.33	6.40	0.13	100.95	360	0.41	723	8.78
X609p_38	58.37	26.24	0.30	8.09	6.25	0.09	99.34	370	0.41	724	8.76
X609p_39	58.15	26.72	0.31	8.49	6.28	0.13	100.08	380	0.42	726	8.78
X609p_40	58.04	26.63	0.33	8.36	6.28	0.12	99.77	390	0.42	725	8.78
X609p_41	59.40	26.81	0.39	8.01	6.82	0.15	101.57	400	0.39	714	8.79
X609p_42	59.44	26.85	0.43	8.33	6.61	0.17	101.83	410	0.41	719	8.80
X609p_43	59.61	26.71	0.33	8.14	6.72	0.16	101.65	420	0.40	716	8.79
X609p_44	60.63	26.61	0.39	8.17	6.72	0.17	102.69	430	0.40	716	8.80
X609p_45	59.70	26.65	0.46	8.34	6.36	0.14	101.66	440	0.42	723	8.78
X609p_46	60.30	27.02	0.36	8.51	6.50	0.12	102.81	450	0.42	724	8.77
X609p_47	59.99	27.33	0.43	8.67	6.32	0.16	102.90	460	0.43	727	8.79
X609p_48	59.29	27.05	0.43	8.49	6.61	0.15	102.02	470	0.41	722	8.78
X609p_49	59.03	26.99	0.50	8.72	6.41	0.13	101.78	480	0.43	727	8.78
X609p_50	58.79	27.37	0.40	8.72	6.29	0.14	101.70	490	0.43	728	8.79
X609p_51	58.78	27.24	0.48	8.75	6.38	0.13	101.76	500	0.43	727	8.78

Table A3.10 continued

Sample	SiO_2	Al_2O_3	FeO	CaO	Na_2O	K_2O	Total	Dist (μm)	X An	Temp °C	H_2O wt%
X609p_53	58.98	26.69	0.53	8.32	6.41	0.17	101.09	520	0.41	722	8.80
X609p_54	59.72	27.09	0.43	8.61	6.60	0.15	102.60	530	0.42	723	8.79
X609p_55	60.58	26.63	0.45	7.81	6.77	0.14	102.38	540	0.39	713	8.79
X609p_56	60.27	26.44	0.38	7.73	6.67	0.18	101.67	550	0.39	712	8.82
X609p_57	60.16	26.65	0.31	7.94	6.85	0.17	102.08	560	0.39	712	8.81
X609p_58	59.00	26.80	0.33	8.34	6.29	0.14	100.90	570	0.42	724	8.78
X609p_59	58.51	26.89	0.50	8.49	6.16	0.16	100.71	580	0.43	727	8.80
X609p_60	59.34	26.92	0.46	8.49	6.49	0.15	101.85	590	0.42	723	8.79
X609p_61	59.93	26.88	0.32	8.39	6.54	0.17	102.22	600	0.41	721	8.80
X609p_62	59.77	26.70	0.40	8.31	6.41	0.13	101.71	610	0.41	723	8.78
X609p_63	60.41	26.63	0.46	7.99	6.90	0.13	102.52	620	0.39	713	8.79
X609p_64	59.77	26.75	0.35	8.41	6.43	0.18	101.90	630	0.42	722	8.80
X609p_65	58.58	27.56	0.33	9.08	6.08	0.13	101.76	640	0.45	733	8.81
X609p_66	58.79	27.22	0.31	8.58	6.36	0.13	101.40	650	0.42	726	8.78
X609p_67	59.62	26.79	0.33	8.30	6.73	0.12	101.89	660	0.40	719	8.77
X609p_68	59.01	27.11	0.42	8.45	6.44	0.13	101.57	670	0.42	724	8.78
X609p_69	59.54	27.11	0.48	8.70	6.34	0.15	102.32	680	0.43	727	8.79
X609p_70	59.11	27.65	0.34	8.98	6.25	0.11	102.42	690	0.44	731	8.78
X609p_71	59.00	27.11	0.35	8.61	6.52	0.11	101.70	700	0.42	725	8.77
X609p_72	59.44	27.17	0.40	8.94	6.22	0.14	102.31	710	0.44	730	8.79
X609p_73	58.96	27.15	0.46	8.85	6.39	0.16	101.97	720	0.43	727	8.80
X609p_74	58.71	27.41	0.41	8.76	6.15	0.15	101.59	730	0.44	729	8.80
X609p_75	59.25	26.96	0.31	8.47	6.34	0.14	101.48	740	0.42	725	8.79
X609p_76	58.94	26.87	0.40	8.36	6.52	0.23	101.32	750	0.41	719	8.83
X609p_77	59.24	27.07	0.30	8.67	6.49	0.13	101.90	760	0.42	725	8.78
X609p_78	59.61	26.67	0.33	8.28	6.55	0.17	101.61	770	0.41	720	8.80
X609p_79	60.36	26.56	0.38	7.91	6.88	0.18	102.28	780	0.38	711	8.82
X609p_80	60.33	26.65	0.38	7.95	6.63	0.16	102.11	790	0.39	715	8.80
X609p_81	60.01	26.13	0.41	7.62	6.94	0.17	101.28	800	0.37	707	8.83
X609p_82	59.28	26.57	0.31	8.47	6.61	0.12	101.37	810	0.41	722	8.77
X609p_83	58.63	27.03	0.38	8.87	6.27	0.12	101.31	820	0.44	730	8.78
X609p_84	58.40	27.47	0.33	9.29	6.13	0.12	101.74	830	0.45	734	8.80
X609p_85	58.55	27.53	0.42	9.44	6.06	0.18	102.17	840	0.46	735	8.85
X609p_86	58.57	27.79	0.42	9.03	6.13	0.13	102.07	850	0.45	732	8.80
X609p_87	58.67	27.15	0.34	8.42	6.26	0.14	100.97	860	0.42	725	8.78
X609p_88	60.94	25.60	0.34	7.33	6.98	0.20	101.39	870	0.36	702	8.86
X609p_89	60.15	25.84	0.33	7.57	6.89	0.18	100.95	880	0.37	707	8.83
X609p_90	64.70	22.20	0.75	5.83	6.10	0.61	100.19	890	0.33	681	9.17

Major elements are given in wt%, *X An* are calculated on a mole fraction basis and temperatures (temp) and H_2O concentration (are given in wt%) are calculated using the Plagioclase-melt equilibria of Putirka (2005) and a pressure of 60 MPa. Distance represents the distance from the start of the profile and correlates with 'S' on the relevant backscattered electron image

Appendix 3

Table A3.11: Major element compositions (given in wt%) of Taupo plagioclase crystals

Table A3.11

Sample	SiO_2	Al_2O_3	FeO	CaO	Na_2O	K_2O	Total	Dist (μm)	X An	Temp (°C)	H_2O (wt%)
TA1a_2	58.23	25.74	0.33	8.50	6.82	0.27	99.89	20	0.40	762	8.27
TA1a 3	60.13	25.45	0.34	8.18	6.88	0.26	101.23	30	0.39	758	8.27
TA1a 4	58.95	25.99	0.39	8.72	6.59	0.31	100.94	40	0.42	766	8.31
TA1a 5	58.14	26.09	0.35	8.56	6.84	0.25	100.24	50	0.40	763	8.27
TA1a 6	58.66	25.65	0.31	8.44	6.69	0.29	100.04	60	0.40	763	8.29
TA1a 7	57.59	25.54	0.31	8.48	6.62	0.27	98.81	70	0.41	765	8.28
TA1a 8	58.57	26.81	0.33	9.03	6.51	0.23	101.48	80	0.43	773	8.28
TA1a 9	58.24	26.64	0.33	9.00	6.49	0.23	100.92	90	0.43	773	8.28
TA1a 10	58.61	26.36	0.30	8.94	6.41	0.25	100.85	100	0.43	772	8.30
TA1a 11	58.32	26.47	0.33	8.84	6.52	0.26	100.73	110	0.42	770	8.29
TA1a 12	59.48	25.91	0.31	8.54	6.89	0.31	101.44	120	0.40	761	8.29
TA1a 13	57.89	25.96	0.28	8.84	6.71	0.26	99.94	130	0.42	768	8.28
TA1a 14	57.87	26.27	0.31	9.03	6.53	0.23	100.24	140	0.43	772	8.28
TA1a 15	57.71	26.60	0.27	8.75	6.36	0.26	99.94	150	0.43	771	8.30
TA1a 16	58.07	26.73	0.41	9.03	6.55	0.28	101.06	160	0.43	771	8.31
TA1a 17	58.74	26.31	0.28	9.00	6.53	0.26	101.11	170	0.43	771	8.30
TA1a 18	58.90	26.14	0.44	8.95	6.60	0.24	101.27	180	0.42	770	8.28
TA1a 19	57.62	25.48	0.32	8.64	6.50	0.27	98.83	190	0.42	768	8.29
TA1a 20	58.71	26.20	0.36	8.87	6.41	0.28	100.84	200	0.43	771	8.31
TA1a_21	58.23	25.81	0.33	8.64	6.68	0.30	99.98	210	0.41	765	8.30
TA1a 22	58.32	26.06	0.27	8.70	6.60	0.24	100.18	220	0.42	768	8.27
TA1a 23	58.96	26.86	0.25	8.63	6.56	0.26	101.51	230	0.41	767	8.28
TA1a 24	58.19	26.47	0.44	8.55	6.62	0.25	100.52	240	0.41	766	8.27
TA1a 25	59.15	26.29	0.33	8.45	6.79	0.23	101.23	250	0.40	763	8.26
TA1a 26	60.05	25.75	0.34	8.33	6.88	0.25	101.59	260	0.40	760	8.26
TA1a 27	59.52	25.51	0.28	7.89	6.90	0.28	100.37	270	0.38	754	8.28
TA1a 28	59.66	25.39	0.32	7.74	6.93	0.30	100.34	280	0.37	750	8.29
TA1a 29	59.71	25.41	0.30	7.86	6.93	0.28	100.48	290	0.38	753	8.28
TA1a 30	59.56	25.50	0.25	7.74	7.15	0.28	100.47	300	0.37	748	8.28
TA1a 31	59.29	25.29	0.22	7.61	7.14	0.34	99.89	310	0.36	745	8.32
TA1a 32	59.53	25.44	0.30	7.83	7.03	0.33	100.45	320	0.37	750	8.30
TA1a 33	60.50	25.27	0.31	7.88	7.07	0.33	101.34	330	0.37	750	8.30
TA1a 34	60.26	25.17	0.26	7.67	6.92	0.31	100.59	340	0.37	749	8.30
TA1a 35	59.54	24.79	0.28	7.73	7.02	0.29	99.65	350	0.37	749	8.29
TA1a 36	59.44	25.24	0.22	7.60	7.06	0.33	99.90	360	0.37	746	8.31
TA1a_37	59.05	25.00	0.24	7.53	7.08	0.41	99.31	370	0.36	743	8.36
TA1a_38	58.93	25.77	0.47	8.13	7.06	0.30	100.66	380	0.38	754	8.28
TA1a 39	58.29	25.54	0.26	8.01	6.74	0.31	99.15	390	0.39	756	8.30
TA1a 41	60.65	25.49	0.24	7.89	6.96	0.34	101.58	410	0.38	751	8.31
TA1a 42	59.83	25.39	0.21	7.72	7.21	0.32	100.68	420	0.37	746	8.31
TA1a 43	59.74	25.72	0.26	7.77	6.82	0.33	100.63	430	0.38	752	8.31
TA1a 44	59.20	25.63	0.20	8.12	6.96	0.30	100.40	440	0.39	755	8.29
TA1a 45	59.20	25.53	0.29	8.06	6.94	0.30	100.32	450	0.38	755	8.29
TA1a 46	58.91	25.33	0.36	7.71	6.98	0.34	99.63	460	0.37	749	8.31
TA1a 47	59.45	25.29	0.29	7.65	7.11	0.31	100.10	470	0.37	747	8.30
TA1a 48	58.65	25.86	0.34	7.89	6.77	0.27	99.77	480	0.39	755	8.28
TA1a 49	59.11	25.78	0.34	7.92	7.00	0.32	100.45	490	0.38	751	8.30
TA1a 50	58.17	25.36	0.31	7.69	6.81	0.29	98.63	500	0.38	752	8.29
TA1a 51	59.15	25.99	0.31	8.10	6.94	0.27	100.76	510	0.39	756	8.27
TA1a 52	60.12	25.29	0.27	7.73	6.88	0.32	100.61	520	0.38	751	8.30
TA1a 53	59.96	25.59	0.30	7.95	6.58	0.28	100.66	530	0.39	759	8.29
TA1a 54	60.40	25.53	0.16	7.89	6.97	0.32	101.27	540	0.38	752	8.30
TA1a 55	60.16	25.36	0.23	7.84	6.87	0.30	100.77	550	0.38	753	8.29
TA1a 56	58.88	25.78	0.26	8.19	6.88	0.30	100.28	560	0.39	757	8.28
TA1a 57	59.24	25.79	0.23	7.98	6.96	0.25	100.45	570	0.38	755	8.26
TA1a 58	59.55	26.45	0.28	7.97	7.04	0.29	101.58	580	0.38	752	8.28
TA1a 59	58.94	25.86	0.27	8.05	7.00	0.32	100.44	590	0.38	753	8.30
TA1a 60	59.65	25.57	0.24	8.31	6.82	0.27	100.86	600	0.40	760	8.27
TA1a 61	59.30	26.07	0.25	7.79	6.91	0.27	100.59	610	0.38	752	8.28
TA1a 63	58.12	26.08	0.40	7.96	6.79	0.28	99.61	630	0.39	756	8.28
TA1a 64	59.39	26.65	0.27	7.96	6.75	0.28	101.30	640	0.39	756	8.28
TA1a 65	58.61	26.50	0.36	8.06	7.12	0.27	100.91	650	0.38	753	8.27
TA1a_66	59.95	26.28	0.28	8.00	7.10	0.29	101.90	660	0.38	752	8.28
TA1a 67	59.99	26.08	0.32	7.70	7.05	0.27	101.41	670	0.37	749	8.28
TA1a 68	58.32	26.23	0.28	7.91	7.00	0.28	100.02	680	0.38	752	8.28
TA1a 69	59.97	26.27	0.28	7.68	7.17	0.32	101.68	690	0.37	746	8.30
TA1a 70	59.82	26.10	0.28	7.69	7.29	0.33	101.50	700	0.36	744	8.31
TA1a 71	59.88	25.94	0.26	7.34	7.39	0.30	101.11	710	0.35	738	8.32
TA1a 72	59.79	26.22	0.20	7.27	7.40	0.35	101.23	720	0.34	736	8.35
TA1a 73	59.88	25.95	0.28	7.51	7.32	0.33	101.27	730	0.36	741	8.32
TA1a 74	60.53	25.74	0.30	7.31	7.55	0.32	101.73	740	0.34	735	8.33
TA1a 78	58.79	25.59	0.25	7.25	7.35	0.31	99.53	780	0.35	737	8.32
TA1a 79	60.22	25.99	0.32	7.62	7.39	0.38	101.92	790	0.36	741	8.34
TA1a 80	59.64	25.85	0.23	7.44	7.52	0.34	101.01	800	0.35	737	8.34
TA1a 84	60.19	25.59	0.39	7.48	7.37	0.33	101.34	840	0.35	740	8.33
TA1a 85	59.98	25.77	0.31	7.57	7.45	0.33	101.41	850	0.35	740	8.32

Table A3.11 continued

Sample	SiO_2	Al_2O_3	FeO	CaO	Na_2O	K_2O	Total	Dist (μm)	X An	Temp (°C)	H_2O (wt%)
TA1a 86	59.38	26.01	0.19	7.60	7.17	0.31	100.65	860	0.36	745	8.31
TA1a 87	59.05	25.88	0.37	7.77	7.41	0.27	100.75	870	0.36	745	8.28
TA1a 88	59.55	26.10	0.33	7.46	7.25	0.35	101.04	880	0.36	741	8.33
TA1a 89	59.55	25.84	0.27	7.68	7.34	0.30	100.98	890	0.36	744	8.30
TA1a 90	59.73	26.17	0.31	7.58	7.24	0.29	101.32	900	0.36	744	8.30
TA1a 91	59.78	25.98	0.26	7.95	7.08	0.34	101.39	910	0.38	750	8.31
TA1a 93	60.33	25.68	0.30	7.32	7.17	0.36	101.16	930	0.35	740	8.34
TA1a 94	59.59	25.86	0.39	7.48	7.26	0.33	100.91	940	0.36	741	8.32
TA1a 96	59.49	25.51	0.21	7.35	7.40	0.32	100.28	960	0.35	738	8.33
TA1a 97	60.31	26.11	0.25	7.39	7.42	0.36	101.83	970	0.35	737	8.35
TA1a 98	59.22	26.19	0.32	7.30	7.25	0.31	100.58	980	0.35	739	8.32
TA1a 99	59.27	26.22	0.30	7.48	7.31	0.32	100.89	990	0.35	741	8.32
TA1a 100	60.35	25.66	0.19	7.60	7.41	0.29	101.50	1000	0.36	742	8.30
TA1a 101	60.22	25.67	0.30	7.52	7.42	0.35	101.47	1010	0.35	739	8.33
TA1a 103	60.02	25.87	0.33	7.41	7.40	0.29	101.33	1030	0.35	740	8.31
TA1a 104	60.20	25.98	0.31	7.41	7.35	0.35	101.60	1040	0.35	739	8.34
TA1a 105	59.40	25.82	0.24	7.37	7.28	0.34	100.44	1050	0.35	740	8.33
TA1a 106	59.71	25.92	0.27	7.40	7.53	0.30	101.12	1060	0.35	737	8.32
TA1a 107	59.63	26.02	0.30	7.32	7.58	0.38	101.22	1070	0.34	734	8.37
TA1a 108	59.53	25.13	0.34	7.10	7.15	0.28	99.53	1080	0.35	739	8.31
TA1a 110	60.33	25.64	0.24	7.51	7.55	0.35	101.62	1100	0.35	737	8.34
TA1a 112	60.71	25.46	0.25	7.29	7.60	0.34	101.65	1120	0.34	734	8.35
TA1a 114	60.65	25.79	0.34	7.26	7.54	0.37	101.95	1140	0.34	733	8.36
TA1a 118	59.94	25.41	0.25	7.24	7.26	0.33	100.42	1180	0.35	738	8.33
TA1a 119	57.97	24.95	0.35	6.67	7.27	0.40	97.59	1190	0.33	727	8.41
TA1a 121	60.80	25.69	0.26	7.16	7.56	0.37	101.84	1210	0.34	731	8.37
TA1c 3	58.65	26.88	0.35	9.02	6.47	0.29	101.65	20	0.43	771	8.32
TA1c 4	58.42	26.78	0.34	8.81	6.39	0.28	101.03	30	0.43	770	8.31
TA1c 5	58.84	26.82	0.33	8.94	6.64	0.24	101.82	40	0.42	770	8.28
TA1c 6	58.87	26.84	0.30	8.97	6.41	0.21	101.60	50	0.43	774	8.28
TA1c 7	58.93	27.02	0.28	8.90	6.42	0.25	101.80	60	0.43	772	8.30
TA1c 8	58.57	26.83	0.33	8.56	6.59	0.29	101.16	70	0.41	765	8.30
TA1c 9	59.80	26.21	0.33	8.08	6.74	0.24	101.41	80	0.39	759	8.26
TA1c 10	60.38	25.54	0.27	7.39	7.03	0.32	100.93	90	0.36	744	8.31
TA1c 11	60.47	25.47	0.38	7.48	7.08	0.33	101.21	100	0.36	744	8.32
TA1c 12	59.29	26.00	0.34	8.36	6.62	0.29	100.91	110	0.40	762	8.29
TA1c 13	59.17	26.29	0.40	8.20	6.54	0.30	100.90	120	0.40	761	8.30
TA1c 14	58.91	26.23	0.40	8.62	6.71	0.28	101.15	130	0.41	764	8.29
TA1c 15	58.93	26.15	0.26	8.44	6.72	0.32	100.83	140	0.40	761	8.31
TA1c 16	58.57	25.90	0.36	8.20	6.61	0.31	99.96	150	0.40	760	8.30
TA1c 17	59.53	25.33	0.27	7.67	6.90	0.33	100.02	160	0.37	749	8.31
TA1c_18	60.67	25.73	0.36	7.36	7.04	0.32	101.48	170	0.36	743	8.31
TA1c 19	60.10	25.52	0.37	7.47	7.05	0.30	100.81	180	0.36	745	8.30
TA1c 20	59.82	25.64	0.37	7.76	7.13	0.37	101.09	190	0.37	746	8.33
TA1c 21	59.63	25.94	0.36	7.73	6.98	0.31	100.95	200	0.37	750	8.30
TA1c 22	57.83	25.19	0.31	7.80	6.82	0.32	98.27	210	0.38	752	8.30
TA1c 23	59.55	25.27	0.17	7.55	7.09	0.36	99.98	220	0.36	744	8.33
TA1c 24	60.04	25.96	0.38	7.90	6.77	0.32	101.36	230	0.38	754	8.30
TA1c 25	59.46	26.10	0.18	7.88	6.94	0.27	100.82	240	0.38	753	8.27
TA1c 26	59.26	25.83	0.34	8.15	6.81	0.32	100.71	250	0.39	757	8.30
TA1c 27	59.14	26.34	0.37	8.45	6.68	0.26	101.24	260	0.41	764	8.27
TA1c 28	59.54	26.00	0.30	8.24	6.86	0.26	101.20	270	0.39	759	8.27
TA1c_29	59.66	26.14	0.28	8.29	6.72	0.29	101.37	280	0.40	761	8.29
TA1c 30	59.53	26.08	0.35	8.15	6.85	0.27	101.23	290	0.39	758	8.27
TA1c 31	60.11	26.03	0.21	7.93	7.03	0.28	101.60	300	0.38	752	8.28
TA1c 32	60.42	25.77	0.33	7.87	7.06	0.32	101.78	310	0.37	750	8.30
TA1c 33	59.56	25.93	0.26	7.94	7.03	0.30	101.03	320	0.38	752	8.29
TA1c_34	59.53	26.45	0.24	8.36	7.08	0.28	101.93	330	0.39	757	8.27
TA1c 36	59.64	25.91	0.39	8.19	6.77	0.30	101.19	350	0.39	758	8.29
TA1c 37	59.33	25.79	0.35	8.01	6.83	0.31	100.62	360	0.39	755	8.30
TA1c 38	59.86	26.32	0.24	8.10	6.98	0.28	101.77	370	0.38	755	8.27
TA1c 39	59.99	26.17	0.23	7.96	6.98	0.30	101.63	380	0.38	753	8.29
TA1c 41	59.64	26.31	0.23	8.10	6.93	0.29	101.50	400	0.39	755	8.28
TA1c 42	59.85	26.10	0.31	8.04	6.74	0.26	101.29	410	0.39	758	8.27
TA1c 43	59.33	26.26	0.29	8.14	6.63	0.31	100.96	420	0.40	759	8.30
TA1c 44	58.65	26.62	0.30	8.80	6.44	0.25	101.08	430	0.42	770	8.29
TA1c 45	59.23	26.48	0.32	8.52	6.65	0.29	101.49	440	0.41	764	8.29
TA1c 46	59.17	26.24	0.29	8.62	6.71	0.33	101.35	450	0.41	763	8.32
TA1c_47	59.46	26.50	0.31	8.46	6.70	0.24	101.66	460	0.41	764	8.26
TA1c 48	59.44	26.51	0.36	8.56	6.50	0.26	101.64	470	0.41	767	8.29
TA1c 49	58.99	26.30	0.33	8.18	6.69	0.27	100.76	480	0.40	760	8.27
TA1c 51	58.74	26.86	0.26	8.89	6.43	0.22	101.40	500	0.43	773	8.28
TA1c 52	58.58	27.14	0.35	9.17	6.48	0.28	101.99	510	0.43	773	8.32
TA1c 53	58.16	26.67	0.36	8.99	6.52	0.26	100.96	520	0.43	771	8.30
TA1c_57	60.54	25.79	0.27	7.75	6.99	0.32	101.66	560	0.37	749	8.30

Table A3.11 continued

Sample	SiO_2	Al_2O_3	FeO	CaO	Na_2O	K_2O	Total	Dist (μm)	X An	Temp (°C)	H_2O (wt%)
TA1c 58	59.84	25.92	0.32	7.93	6.83	0.32	101.17	570	0.38	754	8.30
TA1c 59	59.99	26.21	0.29	8.15	7.01	0.33	101.98	580	0.38	754	8.30
TA1c 60	59.72	26.32	0.24	8.12	6.84	0.30	101.54	590	0.39	757	8.29
TA1c 61	59.79	26.49	0.15	8.10	7.06	0.32	101.91	600	0.38	753	8.30
TA1c 62	59.28	26.44	0.33	7.86	6.90	0.30	101.11	610	0.38	753	8.29
TA1c 63	58.83	26.44	0.25	8.14	6.80	0.28	100.74	620	0.39	758	8.28
TA1c 64	59.16	26.23	0.20	7.91	6.85	0.32	100.67	630	0.38	753	8.30
TA1c 65	59.28	26.51	0.24	7.84	7.14	0.29	101.30	640	0.37	749	8.29
TA1c 66	59.86	26.35	0.27	8.16	6.92	0.31	101.86	650	0.39	756	8.29
TA1c 68	59.90	26.55	0.28	7.80	7.05	0.33	101.91	670	0.37	749	8.31
TA1c 69	58.84	26.05	0.29	7.76	6.76	0.35	100.04	680	0.38	752	8.32
TA1c 70	59.60	26.34	0.23	7.81	7.19	0.31	101.47	690	0.37	748	8.30
TA1c 71	59.11	26.21	0.24	7.91	6.98	0.30	100.76	700	0.38	752	8.29
TA1c 72	58.67	26.61	0.33	8.09	6.98	0.27	100.95	710	0.38	755	8.27
TA1c 73	59.53	26.27	0.25	7.91	7.21	0.27	101.44	720	0.37	750	8.27
TA1c 75	59.81	26.13	0.26	7.82	7.15	0.32	101.50	740	0.37	748	8.30
TA1c 77	58.95	27.28	0.22	8.69	6.55	0.27	101.97	760	0.42	767	8.29
TA1c 78	57.14	27.64	0.24	9.62	6.40	0.20	101.24	770	0.45	780	8.31
TA1c 79	57.73	27.73	0.33	9.14	6.35	0.25	101.52	780	0.44	775	8.32
TA1c 80	57.47	27.53	0.25	9.14	6.43	0.23	101.05	790	0.43	774	8.30
TA1c 81	57.47	27.53	0.26	9.26	6.25	0.23	100.98	800	0.44	778	8.32
TA1c 82	57.70	27.84	0.20	9.22	6.44	0.19	101.59	810	0.44	776	8.28
TA1c 83	57.79	27.61	0.22	9.16	6.12	0.23	101.13	820	0.45	778	8.33
TA1c 84	58.00	27.75	0.18	9.41	6.12	0.21	101.68	830	0.45	780	8.34
TA1c 86	57.65	28.04	0.19	9.63	6.14	0.18	101.83	850	0.46	783	8.34
TA1c 87	56.77	27.87	0.28	9.67	6.02	0.23	100.83	860	0.46	783	8.38
TA1c_88	56.09	28.18	0.20	9.79	6.24	0.21	100.70	870	0.46	782	8.35
TA1c 89	55.95	27.55	0.14	9.50	6.03	0.22	99.38	880	0.46	782	8.36
TA1c 90	57.03	28.05	0.19	9.74	6.06	0.19	101.24	890	0.47	784	8.36
TA1c 91	56.94	28.18	0.30	10.10	5.86	0.17	101.54	900	0.48	789	8.42
TA1c 92	56.67	28.20	0.24	10.19	6.11	0.23	101.62	910	0.47	786	8.41
TA1c 95	56.55	28.38	0.17	10.43	5.71	0.19	101.42	940	0.50	791	8.49
TA1c 99	56.86	28.45	0.21	10.39	5.71	0.16	101.78	980	0.50	792	8.47
TA1c 100	56.79	28.15	0.29	10.05	5.88	0.18	101.34	990	0.48	788	8.41
TA1c 101	55.56	27.76	0.36	9.52	5.90	0.23	99.34	1000	0.46	783	8.39
TA1c 102	56.50	28.04	0.31	9.90	6.15	0.22	101.12	1010	0.46	784	8.37
TA1c 103	56.63	27.82	0.28	9.61	6.07	0.21	100.63	1020	0.46	782	8.36
TA1c 104	56.63	28.06	0.24	9.63	6.14	0.23	100.93	1030	0.46	781	8.36
TA1c 105	56.79	27.92	0.38	9.61	6.04	0.26	100.99	1040	0.46	782	8.39
TA1c 106	57.52	27.99	0.21	9.82	6.20	0.20	101.94	1050	0.46	783	8.35
TA1c 107	56.78	28.18	0.24	9.97	5.96	0.26	101.39	1060	0.47	785	8.43
TA1c 108	56.27	28.81	0.21	10.90	5.40	0.19	101.77	1070	0.52	796	8.62
TA1c_110	59.12	27.02	0.25	8.57	6.58	0.26	101.80	1090	0.41	766	8.28
TA1c 111	55.83	27.52	0.31	9.80	5.84	0.20	99.50	1100	0.48	787	8.40
TA1c 112	56.68	27.40	0.31	9.51	5.93	0.22	100.04	1110	0.46	783	8.37
TA1c 113	56.42	27.48	0.23	9.72	5.97	0.19	100.01	1120	0.47	785	8.37
TA1c 114	55.62	27.59	0.22	9.21	5.98	0.23	98.86	1130	0.45	780	8.35
TA1c 115	55.49	27.32	0.22	9.40	6.00	0.20	98.63	1140	0.46	782	8.35
TA1c 116	55.68	27.12	0.18	9.20	6.08	0.27	98.53	1150	0.45	778	8.36
TA1c 117	55.94	27.21	0.21	9.23	6.15	0.24	98.98	1160	0.45	778	8.34
TA1c 118	56.18	27.10	0.29	9.24	6.39	0.22	99.42	1170	0.44	776	8.30
TA1c 119	56.49	26.99	0.23	8.99	6.12	0.29	99.11	1180	0.44	775	8.35
TA1c 120	56.90	26.92	0.29	9.18	6.22	0.25	99.75	1190	0.44	777	8.33
TA1c_121	57.94	26.78	0.28	8.91	6.44	0.25	100.60	1200	0.43	771	8.30
TA1c 122	57.73	26.20	0.42	8.09	6.56	0.26	99.26	1210	0.40	761	8.27
TA1c 123	57.88	26.09	0.20	7.72	7.01	0.29	99.17	1220	0.37	750	8.29
TA1c 127	58.57	26.07	0.24	8.45	6.62	0.29	100.25	1260	0.41	764	8.29
TA1c 128	58.24	26.08	0.19	8.60	6.58	0.28	99.98	1270	0.41	766	8.30
TA1c_129	58.41	25.95	0.28	8.18	6.57	0.21	99.60	1280	0.40	763	8.25
TA1c 130	59.12	25.60	0.20	7.99	6.61	0.27	99.78	1290	0.39	759	8.28
TA1c 131	58.38	25.60	0.35	8.06	6.53	0.27	99.19	1300	0.40	761	8.28
TA1c 132	59.20	25.76	0.29	7.95	6.80	0.28	100.28	1310	0.39	756	8.28
TA1c 133	59.32	25.84	0.28	7.84	6.92	0.25	100.46	1320	0.38	753	8.27
TA1c 134	58.91	25.71	0.27	7.76	6.80	0.25	99.70	1330	0.38	754	8.26
TA1c 135	58.83	25.22	0.32	7.86	6.82	0.28	99.33	1340	0.38	754	8.28
TA1c 136	59.11	25.34	0.25	7.44	7.05	0.28	99.46	1350	0.36	745	8.29
TA1c 137	58.69	25.42	0.36	7.94	6.82	0.26	99.50	1360	0.39	756	8.27
TA1c 138	58.51	25.83	0.31	7.89	6.76	0.30	99.60	1370	0.39	755	8.29
TA1c 139	58.71	25.75	0.31	8.03	6.70	0.32	99.82	1380	0.39	757	8.30
TA1c_140	58.60	25.71	0.28	7.79	7.01	0.30	99.68	1390	0.37	750	8.29
TA1c 141	58.57	25.86	0.28	8.15	6.79	0.27	99.91	1400	0.39	759	8.27
TA1c 142	57.60	25.39	0.28	7.85	6.77	0.28	98.18	1410	0.38	755	8.28
TA1d 1	56.76	26.40	0.43	8.66	6.42	0.23	98.89	20	0.42	770	8.28
TA1d 2	57.03	26.33	0.31	8.36	6.07	0.29	98.39	30	0.42	769	8.33
TA1d 3	56.84	26.00	0.33	8.59	6.44	0.28	98.47	40	0.42	768	8.30

Table A3.11 continued

Sample	SiO_2	Al_2O_3	FeO	CaO	Na_2O	K_2O	Total	Dist (μm)	X An	Temp (°C)	H_2O (wt%)
TA1d 4	57.28	26.10	0.36	8.39	6.49	0.26	98.87	50	0.41	765	8.28
TA1d 5	57.90	25.32	0.27	7.64	6.87	0.30	98.30	60	0.37	750	8.29
TA1d 6	58.43	25.38	0.33	7.43	6.90	0.27	98.74	70	0.37	748	8.28
TA1d 7	58.30	25.78	0.34	7.99	6.55	0.33	99.28	80	0.40	758	8.31
TA1d 8	57.99	25.44	0.24	7.52	6.75	0.27	98.20	90	0.37	751	8.28
TA1d 9	59.18	25.12	0.34	7.93	6.60	0.24	99.42	100	0.39	759	8.26
TA1d 10	58.95	25.61	0.29	7.90	6.63	0.29	99.68	110	0.39	757	8.29
TA1d 11	58.72	25.09	0.36	7.31	6.72	0.27	98.46	120	0.37	749	8.28
TA1d 12	58.16	25.09	0.25	7.75	6.53	0.35	98.13	130	0.39	755	8.32
TA1d 13	57.30	25.49	0.33	7.94	6.63	0.30	97.98	140	0.39	757	8.30
TA1d 14	58.62	25.42	0.32	7.73	6.76	0.28	99.11	150	0.38	753	8.28
TA1d 15	58.50	25.36	0.26	7.65	6.52	0.30	98.59	160	0.39	755	8.30
TA1d 16	57.38	25.53	0.29	7.79	6.83	0.25	98.07	170	0.38	754	8.26
TA1d 17	57.58	24.81	0.31	7.32	6.77	0.28	97.07	180	0.37	748	8.29
TA1d 18	57.37	25.13	0.43	7.37	6.99	0.30	97.59	190	0.36	745	8.31
TA1d 21	58.98	25.78	0.36	7.84	6.80	0.27	100.02	200	0.38	755	8.27
TA1d 22	59.27	25.80	0.38	7.63	7.01	0.33	100.41	210	0.37	747	8.31
TA1d 23	59.75	25.93	0.34	7.81	6.99	0.28	101.09	220	0.38	751	8.28
TA1d 24	59.26	26.11	0.36	7.95	6.96	0.30	100.92	230	0.38	753	8.29
TA1d 25	59.08	25.66	0.30	7.64	6.94	0.29	99.90	240	0.37	749	8.29
TA1d 26	58.88	25.98	0.28	7.58	6.69	0.30	99.70	250	0.38	752	8.29
TA1d 27	60.07	25.58	0.40	7.53	6.51	0.31	100.39	260	0.38	753	8.30
TA1d 28	60.75	25.78	0.38	7.77	6.98	0.27	101.94	270	0.37	751	8.28
TA1d 29	60.54	25.93	0.35	7.97	6.66	0.28	101.74	280	0.39	758	8.28
TA1d 30	60.51	25.39	0.27	7.44	7.12	0.33	101.05	290	0.36	743	8.32
TA1d 31	59.94	25.58	0.29	7.76	6.93	0.33	100.82	300	0.37	750	8.31
TA1d_32	61.05	25.62	0.35	7.46	6.88	0.26	101.61	310	0.37	749	8.28
TA1d 33	58.77	25.99	0.29	7.67	6.67	0.30	99.68	320	0.38	753	8.29
TA1d 34	60.20	26.05	0.29	7.68	6.92	0.30	101.44	330	0.37	750	8.29
TA1d 35	60.15	26.30	0.31	7.81	6.93	0.27	101.77	340	0.38	752	8.28
TA1d 36	61.22	25.22	0.43	6.74	7.22	0.41	101.24	350	0.33	728	8.41
TA1d 37	58.34	25.31	0.36	7.59	6.73	0.32	98.64	360	0.38	751	8.30
TA1d 38	58.86	25.12	0.32	7.52	6.81	0.29	98.92	370	0.37	749	8.29
TA1d 39	59.08	25.53	0.32	7.56	7.10	0.30	99.90	380	0.36	746	8.30
TA1d 40	60.06	24.87	0.35	6.80	7.20	0.32	99.60	390	0.34	732	8.36
TA1d 41	59.36	25.15	0.33	7.18	7.08	0.31	99.41	400	0.35	740	8.32
TA1d 42	58.66	24.64	0.37	6.90	7.37	0.33	98.27	410	0.33	731	8.36
TA1d 43	59.83	24.26	0.30	6.20	7.13	0.36	98.07	420	0.32	721	8.43
TA1d 44	60.98	24.48	0.28	6.70	7.08	0.36	99.87	430	0.34	731	8.38
TA1d 45	60.55	24.36	0.31	6.80	6.85	0.31	99.18	440	0.35	737	8.34
TA1d 46	61.14	24.98	0.29	6.98	7.13	0.40	100.92	450	0.34	734	8.38
TA1d 47	61.02	24.78	0.31	7.00	7.25	0.33	100.69	460	0.34	734	8.35
TA1d_48	60.18	25.29	0.40	7.15	7.23	0.35	100.61	470	0.35	737	8.35
TA1d 50	58.09	24.60	0.34	6.86	6.90	0.35	97.14	490	0.35	737	8.36
TA1d 51	59.94	25.04	0.23	7.02	7.51	0.36	100.09	500	0.33	730	8.37
TA1d 52	59.01	25.86	0.26	7.84	7.19	0.29	100.45	510	0.37	749	8.28
TA1d 53	59.08	26.51	0.26	8.46	7.30	0.33	101.94	520	0.38	754	8.29
TA1d 54	58.98	25.79	0.34	7.92	6.68	0.33	100.04	530	0.39	756	8.31
TA1d 55	59.07	25.69	0.41	8.08	7.40	0.32	100.96	540	0.37	748	8.30
TA1d 56	60.02	24.79	0.25	6.78	7.32	0.40	99.55	550	0.33	728	8.41
TA1d 57	59.77	25.44	0.25	7.50	6.49	0.29	99.73	560	0.38	754	8.29
TA1d 58	59.07	25.78	0.27	7.90	7.08	0.27	100.38	570	0.38	752	8.27
TA1d 59	59.35	25.79	0.26	7.61	6.87	0.31	100.18	580	0.37	749	8.30
TA1d_60	59.13	25.30	0.34	7.11	7.47	0.32	99.67	590	0.34	733	8.34
TA1d 61	58.98	25.54	0.25	7.60	7.20	0.31	99.87	600	0.36	745	8.30
TA1d 62	58.85	26.01	0.20	7.75	6.99	0.31	100.11	610	0.37	750	8.30
TA1d 63	59.97	25.70	0.25	7.63	7.03	0.36	100.94	620	0.37	746	8.33
TA1d 64	59.67	25.56	0.25	7.63	6.84	0.23	100.18	630	0.38	752	8.26
TA1d_65	59.58	25.44	0.31	7.44	7.24	0.28	100.29	640	0.36	742	8.30
TA1d 66	58.62	25.79	0.16	7.58	6.85	0.31	99.31	650	0.37	749	8.30
TA1d 67	59.90	25.57	0.28	7.43	6.92	0.29	100.39	660	0.37	747	8.29
TA1d 68	60.21	25.58	0.25	7.73	6.84	0.31	100.92	670	0.38	751	8.30
TA1d 69	58.71	25.49	0.22	7.57	6.88	0.25	99.12	680	0.37	750	8.27
TA1d 70	58.78	25.44	0.35	7.28	7.01	0.32	99.16	690	0.36	743	8.32
TA1d 71	57.89	25.37	0.24	7.65	6.93	0.27	98.35	700	0.37	750	8.28
TA1d 72	58.38	25.75	0.31	7.68	6.71	0.30	99.12	710	0.38	753	8.29
TA1d 73	58.29	25.64	0.23	7.78	6.82	0.26	99.02	720	0.38	754	8.27
TA1d 74	58.07	25.51	0.29	7.63	6.95	0.36	98.82	730	0.37	747	8.33
TA1d 75	59.47	25.21	0.25	7.67	6.99	0.31	99.91	740	0.37	748	8.30
TA1d_76	59.80	26.02	0.17	7.93	6.94	0.27	101.13	750	0.38	754	8.27
TA1d 77	60.44	25.63	0.37	7.32	7.20	0.29	101.25	760	0.35	741	8.31
TA1d 78	60.02	25.80	0.23	7.97	7.03	0.28	101.32	770	0.38	753	8.28
TA1d 79	59.72	25.95	0.35	7.82	6.90	0.32	101.05	780	0.38	752	8.30
TA1d 80	59.31	25.97	0.30	7.72	6.98	0.30	100.57	790	0.37	750	8.29
TA1d 81	59.35	25.67	0.28	7.39	7.32	0.28	100.28	800	0.35	741	8.30
TA1d_82	58.35	26.12	0.23	8.02	6.79	0.32	99.84	810	0.39	755	8.30

Table A3.11 continued

Sample	SiO_2	Al_2O_3	FeO	CaO	Na_2O	K_2O	Total	Dist (μm)	X An	Temp (°C)	H_2O (wt%)
TA1d 83	59.18	25.90	0.39	8.01	7.03	0.28	100.79	820	0.38	753	8.28
TA1d 84	59.77	25.57	0.21	7.36	7.02	0.30	100.23	830	0.36	744	8.30
TA1d 85	59.13	25.79	0.29	7.79	7.11	0.40	100.50	840	0.37	746	8.34
TA1d 86	60.63	25.88	0.31	7.73	6.88	0.32	101.75	850	0.38	751	8.30
TA1d 88	60.40	25.78	0.28	7.63	7.03	0.33	101.45	870	0.37	747	8.31
TA1d 89	59.10	25.97	0.29	7.91	7.00	0.30	100.56	880	0.38	752	8.29
TA1d 90	58.47	25.94	0.28	7.69	7.09	0.27	99.74	890	0.37	749	8.28
TA1d 91	59.85	25.82	0.29	7.50	7.20	0.30	100.95	900	0.36	744	8.30
TA1d 92	60.64	25.50	0.25	7.40	7.20	0.29	101.29	910	0.36	742	8.30
TA1d 93	60.16	25.76	0.25	7.99	6.87	0.35	101.38	920	0.38	753	8.31
TA1d 94	60.21	25.86	0.33	7.93	7.07	0.33	101.72	930	0.38	750	8.30
TA1d 95	60.49	25.29	0.29	7.43	7.30	0.31	101.11	940	0.35	741	8.32
TA1d 96	59.59	25.51	0.28	7.40	7.33	0.35	100.45	950	0.35	739	8.34
TA1d 97	59.14	25.55	0.29	7.56	7.23	0.29	100.07	960	0.36	744	8.29
TA1d 98	59.11	25.71	0.26	7.52	7.21	0.29	100.10	970	0.36	744	8.30
TA1d 99	59.55	25.53	0.32	7.66	7.03	0.34	100.42	980	0.37	747	8.31
TA1d 100	59.07	25.80	0.28	8.07	6.80	0.28	100.30	990	0.39	757	8.28
TA1d 101	58.62	26.31	0.35	8.88	6.77	0.29	101.22	1000	0.41	766	8.29
TA1d 103	59.06	26.91	0.30	8.85	6.42	0.25	101.80	1020	0.43	771	8.29
TA1d 104	58.15	26.73	0.40	9.07	6.58	0.24	101.16	1030	0.43	772	8.29
TA1j 1	58.99	26.55	0.35	8.37	6.38	0.27	100.91	20	0.41	766	8.29
TA1j 2	58.25	26.16	0.34	8.66	6.27	0.23	99.91	30	0.43	772	8.29
TA1j 3	57.84	26.80	0.41	8.69	6.29	0.26	100.29	40	0.43	771	8.31
TA1j 4	59.94	25.39	0.30	7.22	7.14	0.36	100.34	50	0.35	739	8.34
TA1j 5	60.23	25.37	0.33	6.96	7.17	0.31	100.36	60	0.34	735	8.34
TA1j_6	59.94	25.53	0.25	7.24	7.10	0.36	100.41	70	0.35	739	8.35
TA1j 7	59.75	25.34	0.29	7.55	7.15	0.33	100.42	80	0.36	744	8.32
TA1j 8	59.52	25.56	0.28	7.79	6.81	0.31	100.28	90	0.38	752	8.30
TA1j 9	59.42	25.88	0.20	7.71	6.96	0.27	100.43	100	0.37	751	8.28
TA1j 10	59.47	25.65	0.33	7.52	7.05	0.28	100.31	110	0.36	746	8.29
TA1j 11	60.03	25.49	0.29	7.70	6.99	0.35	100.85	120	0.37	748	8.32
TA1j 12	59.45	25.21	0.28	7.60	7.03	0.30	99.87	130	0.37	747	8.30
TA1j 13	59.42	25.72	0.29	7.59	7.06	0.37	100.45	140	0.36	745	8.33
TA1j 14	59.03	25.98	0.30	7.61	7.10	0.27	100.29	150	0.37	747	8.28
TA1j 15	58.94	25.91	0.29	7.84	6.69	0.30	99.98	160	0.39	755	8.29
TA1j 16	59.55	25.96	0.23	7.80	6.78	0.24	100.56	170	0.38	755	8.26
TA1j 17	58.95	25.91	0.36	7.69	6.82	0.30	100.02	180	0.38	752	8.29
TA1j 18	59.90	25.73	0.27	7.35	6.99	0.29	100.51	190	0.36	745	8.30
TA1j 19	59.08	25.52	0.23	7.62	6.90	0.33	99.67	200	0.37	749	8.31
TA1j 20	59.54	25.68	0.30	7.82	6.83	0.31	100.47	210	0.38	753	8.29
TA1j 21	59.31	26.12	0.25	7.69	6.93	0.28	100.57	220	0.37	750	8.28
TA1j_22	59.34	25.79	0.33	7.73	6.78	0.29	100.25	230	0.38	753	8.29
TA1j 23	59.28	25.95	0.24	7.80	6.87	0.28	100.43	240	0.38	753	8.28
TA1j 24	59.11	26.09	0.25	7.92	6.86	0.24	100.47	250	0.38	756	8.26
TA1j 25	59.63	25.60	0.34	7.79	6.97	0.26	100.57	260	0.38	752	8.27
TA1j 26	58.98	25.83	0.20	7.76	6.78	0.29	99.84	270	0.38	753	8.29
TA1j 27	59.26	25.64	0.26	7.62	6.89	0.27	99.93	280	0.37	750	8.28
TA1j 28	58.99	25.80	0.30	7.89	6.87	0.30	100.15	290	0.38	753	8.29
TA1j 29	58.88	25.82	0.32	7.69	7.00	0.31	100.01	300	0.37	749	8.30
TA1j 30	59.21	25.82	0.22	7.60	6.94	0.27	100.05	310	0.37	749	8.28
TA1j 31	59.42	25.62	0.25	7.37	6.86	0.32	99.84	320	0.37	746	8.31
TA1j 32	60.05	25.67	0.25	7.36	7.14	0.31	100.79	330	0.36	742	8.32
TA1j_33	59.59	25.56	0.28	7.30	6.77	0.32	99.82	340	0.37	746	8.31
TA1j 34	59.53	25.44	0.22	7.46	6.84	0.30	99.79	350	0.37	748	8.30
TA1j 35	59.39	25.75	0.28	7.67	7.00	0.28	100.36	360	0.37	749	8.28
TA1j 36	58.96	25.65	0.29	7.79	6.72	0.31	99.72	370	0.38	754	8.30
TA1j 37	59.26	25.92	0.25	7.95	6.88	0.27	100.52	380	0.38	755	8.27
TA1j_38	60.00	25.85	0.29	7.72	7.10	0.27	101.22	390	0.37	749	8.28
TA1j 39	59.39	26.06	0.25	7.77	6.92	0.34	100.73	400	0.38	750	8.31
TA1j 40	59.41	25.80	0.34	7.82	7.00	0.27	100.63	410	0.38	752	8.27
TA1j 41	58.87	25.58	0.25	8.14	6.81	0.28	99.93	420	0.39	758	8.28
TA1j 42	58.98	25.68	0.30	8.00	6.89	0.25	100.10	430	0.39	756	8.26
TA1j 43	59.28	25.77	0.30	7.86	7.07	0.33	100.61	440	0.37	749	8.31
TA1j 45	58.01	26.04	0.25	7.61	6.88	0.28	99.07	460	0.37	750	8.29
TA1j 46	59.17	25.74	0.23	7.87	6.79	0.29	100.09	470	0.38	754	8.29
TA1j 47	59.81	25.84	0.23	8.03	6.82	0.26	100.99	480	0.39	757	8.27
TA1j 48	58.88	26.11	0.29	7.99	6.70	0.29	100.27	490	0.39	757	8.29
TA1j 49	57.57	25.69	0.31	8.01	6.47	0.29	98.32	500	0.40	761	8.29
TA1j_50	57.85	26.13	0.22	7.95	6.68	0.27	99.10	510	0.39	757	8.28
TA1j 51	57.49	25.74	0.20	7.93	6.74	0.27	98.36	520	0.39	757	8.27
TA1j 52	57.17	25.48	0.33	7.85	6.61	0.30	97.73	530	0.39	757	8.29
TA1j 54	57.93	26.01	0.29	7.92	6.77	0.31	99.22	550	0.39	755	8.29
TA1j 55	57.66	25.89	0.27	7.92	6.80	0.32	98.85	560	0.38	754	8.30
TA1j 56	58.60	25.84	0.27	7.56	7.04	0.31	99.62	570	0.37	746	8.30
TA1j 57	58.66	25.81	0.29	7.83	6.98	0.34	99.91	580	0.38	750	8.31

Table A3.11 continued

Sample	SiO_2	Al_2O_3	FeO	CaO	Na_2O	K_2O	Total	Dist (μm)	X An	Temp (°C)	H_2O (wt%)
TA1j_58	59.23	25.68	0.22	7.77	6.91	0.27	100.08	590	0.38	752	8.27
TA1j_59	58.37	25.85	0.16	7.74	6.98	0.33	99.44	600	0.37	749	8.31
TA1j_60	59.03	25.84	0.29	7.84	6.76	0.34	100.09	610	0.38	753	8.31
TA1j_61	59.28	25.98	0.30	7.78	6.97	0.29	100.59	620	0.38	751	8.28
TA1j_62	58.83	26.24	0.25	7.97	6.89	0.31	100.49	630	0.38	754	8.29
TA1j_63	58.47	26.28	0.25	7.92	6.87	0.31	100.10	640	0.38	754	8.29
TA1j_64	58.46	26.23	0.24	7.84	6.85	0.26	99.86	650	0.38	754	8.27
TA1j_65	58.47	26.14	0.22	7.69	6.87	0.26	99.64	660	0.38	752	8.27
TA1j_66	57.99	26.00	0.29	8.01	6.92	0.31	99.53	670	0.38	754	8.29
TA1j_67	58.43	25.75	0.33	7.94	6.85	0.25	99.56	680	0.38	756	8.26
TA1j_68	57.98	25.31	0.28	7.83	7.00	0.26	98.65	690	0.38	752	8.27
TA1j_69	58.74	25.66	0.21	7.74	6.91	0.30	99.55	700	0.38	751	8.29
TA1j_70	59.06	25.56	0.24	7.71	6.92	0.30	99.79	710	0.37	750	8.30
TA1j_71	59.49	26.04	0.19	7.86	6.95	0.30	100.83	720	0.38	752	8.29
TA1j_72	57.96	25.72	0.28	7.66	6.77	0.28	98.67	730	0.38	752	8.28
TA1j_73	58.25	26.05	0.36	7.81	6.96	0.38	99.82	740	0.37	749	8.33
TA1j_74	58.59	25.98	0.26	7.52	6.98	0.29	99.61	750	0.37	747	8.30
TA1j_75	58.66	26.06	0.33	7.75	6.95	0.30	100.06	760	0.37	751	8.29
TA1j_76	58.40	25.84	0.34	7.76	7.12	0.30	99.76	770	0.37	748	8.29
TA1j_77	59.32	25.92	0.29	7.47	6.95	0.31	100.25	780	0.37	747	8.30
TA1j_78	59.84	25.54	0.40	7.77	7.13	0.29	100.96	790	0.37	748	8.29
TA1j_79	59.35	26.32	0.25	7.59	6.81	0.30	100.62	800	0.37	750	8.29
TA1j_80	58.93	26.06	0.30	7.81	6.85	0.34	100.28	810	0.38	752	8.31
TA1j_81	57.89	26.14	0.31	7.91	6.98	0.31	99.54	820	0.38	752	8.30
TA1j_82	58.44	26.03	0.30	7.83	6.81	0.33	99.72	830	0.38	753	8.30
TA1j_83	59.79	26.18	0.29	8.05	6.64	0.25	101.19	840	0.40	760	8.26
TA1j_84	59.92	25.89	0.32	7.86	6.77	0.27	101.03	850	0.38	755	8.28
TA1j_85	58.37	26.25	0.30	8.00	6.83	0.27	100.01	860	0.39	756	8.27
TA1j_86	58.01	26.24	0.27	7.83	6.84	0.25	99.44	870	0.38	754	8.27
TA1j_87	57.87	26.34	0.22	7.91	6.79	0.30	99.42	880	0.38	755	8.29
TA1j_88	57.76	25.93	0.38	7.80	6.72	0.32	98.91	890	0.38	754	8.30
TA1j_89	58.89	25.96	0.18	7.74	7.06	0.30	100.14	900	0.37	749	8.29
TA1j_90	59.79	25.94	0.32	7.64	6.93	0.31	100.94	910	0.37	749	8.30
TA1j_91	59.48	25.65	0.25	7.83	6.29	0.29	99.78	920	0.40	761	8.30
TA1j_92	59.47	26.32	0.19	7.80	6.91	0.27	100.96	930	0.38	753	8.27
TA1j_93	59.01	26.03	0.28	7.66	6.77	0.27	100.02	940	0.38	753	8.28
TA1j_94	59.01	25.88	0.33	7.77	6.83	0.26	100.08	950	0.38	753	8.27
TA1j_95	57.42	25.17	0.23	7.45	6.78	0.30	97.35	960	0.37	749	8.30
TA1j_96	58.71	25.63	0.32	7.35	7.25	0.30	99.56	970	0.35	741	8.31
TA1j_97	58.67	25.91	0.24	7.28	7.01	0.33	99.44	980	0.36	742	8.33
TA1j_98	59.46	26.13	0.27	7.81	6.77	0.37	100.81	990	0.38	752	8.33
TA1j_99	59.16	26.30	0.34	8.04	6.75	0.31	100.90	1000	0.39	757	8.29
TA1j_100	59.11	25.97	0.34	8.04	6.68	0.30	100.45	1010	0.39	758	8.29
TA1j_101	58.63	26.26	0.26	7.98	6.82	0.28	100.24	1020	0.39	756	8.28
TA1j_102	59.16	26.33	0.24	7.96	6.67	0.28	100.64	1030	0.39	758	8.28
TA1j_103	58.28	26.18	0.22	7.73	6.81	0.29	99.51	1040	0.38	752	8.29
TA1j_104	58.32	26.13	0.24	7.88	6.84	0.25	99.66	1050	0.38	755	8.27
TA1j_105	58.18	26.16	0.29	7.82	6.86	0.22	99.53	1060	0.38	755	8.25
TA1j_106	57.98	26.23	0.28	7.87	6.71	0.35	99.42	1070	0.39	754	8.32
TA1j_107	58.19	26.15	0.30	7.99	6.77	0.27	99.66	1080	0.39	757	8.27
TA1j_108	59.34	26.03	0.39	8.00	6.57	0.34	100.67	1090	0.39	758	8.31
TA1j_109	59.22	26.04	0.26	7.88	6.59	0.32	100.31	1100	0.39	757	8.30
TA1j_110	58.97	26.24	0.30	8.01	6.69	0.27	100.48	1110	0.39	758	8.28
TA1j_111	58.73	26.31	0.30	7.91	6.68	0.28	100.20	1120	0.39	757	8.28
TA1j_112	57.60	26.36	0.24	8.02	6.87	0.31	99.40	1130	0.39	755	8.29
TA1j_113	58.05	26.12	0.29	8.06	6.91	0.29	99.73	1140	0.39	755	8.28
TA1j_114	59.06	26.19	0.30	7.99	6.89	0.33	100.76	1150	0.38	754	8.30
TA1j_115	59.65	25.98	0.30	7.86	6.83	0.31	100.93	1160	0.38	753	8.30
TA1j_116	59.28	25.92	0.27	8.10	6.68	0.31	100.56	1170	0.39	758	8.30
TA1j_117	59.07	25.95	0.24	8.06	6.88	0.28	100.47	1180	0.39	756	8.28
TA1j_118	58.11	26.34	0.35	8.23	6.60	0.26	99.89	1190	0.40	762	8.27
TA1j_119	59.51	26.09	0.32	7.94	7.03	0.30	101.20	1200	0.38	752	8.29
TA1j_120	60.15	25.96	0.38	7.75	6.89	0.34	101.47	1210	0.38	750	8.31
TA1j_121	59.21	26.24	0.19	7.89	6.99	0.33	100.84	1220	0.38	751	8.30
TA1j_122	58.73	26.03	0.33	7.66	6.97	0.31	100.02	1230	0.37	749	8.30
TA1j_123	58.06	25.93	0.36	7.80	6.91	0.30	99.36	1240	0.38	752	8.29
TA1j_124	57.20	25.87	0.29	7.59	6.67	0.36	97.97	1250	0.38	751	8.33
TA1j_125	57.49	25.93	0.23	7.84	6.66	0.28	98.43	1260	0.39	756	8.28
TA1j_126	58.59	26.10	0.30	7.61	6.85	0.29	99.74	1270	0.37	750	8.29
TA1j_127	59.16	25.59	0.22	7.47	7.01	0.32	99.76	1280	0.36	745	8.31
TA1j_128	59.77	25.55	0.33	7.21	7.37	0.33	100.56	1290	0.34	736	8.34
TA1j_129	60.55	25.65	0.38	7.67	6.99	0.30	101.53	1300	0.37	749	8.29
TA1j_130	59.78	25.69	0.29	7.65	7.14	0.33	100.89	1310	0.36	746	8.31
TA1j_131	60.77	25.36	0.33	7.06	7.23	0.36	101.11	1320	0.34	735	8.36
TA1j_132	60.65	25.23	0.28	6.77	7.21	0.36	100.50	1330	0.33	730	8.38
TA1j_133	59.23	25.74	0.36	7.40	7.15	0.33	100.22	1340	0.36	742	8.32

Table A3.11 continued

Sample	SiO_2	Al_2O_3	FeO	CaO	Na_2O	K_2O	Total	Dist (μm)	X An	Temp (°C)	H_2O (wt%)
TA1j_134	59.14	25.64	0.29	7.49	7.05	0.30	99.91	1350	0.36	745	8.30
TA2b 2	75.29	14.09	1.94	1.69	3.90	2.76	99.66	20	0.14		
TA2b 3	58.96	26.99	0.34	8.97	6.20	0.21	101.65	30	0.44	776	8.30
TA2b 4	59.36	26.96	0.33	8.51	6.34	0.28	101.77	40	0.42	768	8.31
TA2b 5	59.35	26.90	0.37	8.52	6.28	0.24	101.66	50	0.42	770	8.29
TA2b 6	58.95	26.77	0.42	8.59	6.46	0.30	101.49	60	0.42	767	8.31
TA2b 7	56.89	27.97	0.34	9.79	5.83	0.24	101.06	70	0.47	785	8.43
TA2b 8	57.06	27.85	0.35	9.51	5.78	0.26	100.80	80	0.47	783	8.42
TA2b 9	60.07	25.86	0.22	7.09	7.00	0.30	100.54	90	0.35	740	8.32
TA2b 10	60.42	25.78	0.19	7.28	6.91	0.30	100.89	100	0.36	744	8.31
TA2b 12	60.70	26.06	0.26	7.82	6.78	0.33	101.95	120	0.38	753	8.31
TA2b 13	60.22	26.22	0.30	7.69	6.83	0.29	101.56	130	0.38	751	8.29
TA2b 15	60.06	26.37	0.32	7.80	6.97	0.38	101.90	150	0.37	749	8.33
TA2b 17	60.36	26.20	0.24	7.88	6.79	0.29	101.76	170	0.38	755	8.28
TA2b 20	59.80	26.15	0.25	7.99	6.71	0.33	101.23	200	0.39	756	8.31
TA2b 21	59.35	26.71	0.29	7.92	6.68	0.31	101.26	210	0.39	756	8.30
TA2b 22	59.05	26.13	0.25	7.68	6.50	0.25	99.85	220	0.39	757	8.27
TA2b 23	58.32	26.27	0.26	8.27	6.56	0.28	99.96	230	0.40	763	8.29
TA2b_24	57.77	26.66	0.32	8.80	6.25	0.25	100.04	240	0.43	773	8.31
TA2b 25	58.12	26.62	0.32	8.63	6.12	0.22	100.04	250	0.43	774	8.30
TA2b 26	58.68	26.59	0.31	8.39	6.36	0.28	100.60	260	0.41	767	8.30
TA2b 27	58.24	26.32	0.32	8.23	6.32	0.27	99.70	270	0.41	766	8.29
TA2b 28	58.22	26.61	0.36	8.56	6.18	0.24	100.17	280	0.43	772	8.30
TA2b 29	57.83	26.91	0.27	8.65	6.17	0.25	100.07	290	0.43	772	8.31
TA2b 30	58.17	26.61	0.33	8.78	6.23	0.24	100.36	300	0.43	773	8.30
TA2b 31	57.63	27.05	0.34	8.70	6.25	0.20	100.17	310	0.43	773	8.27
TA2b 32	57.30	27.64	0.31	9.00	6.12	0.26	100.64	320	0.44	776	8.34
TA2b 33	56.08	27.32	0.37	9.61	5.81	0.21	99.40	330	0.47	785	8.40
TA2b 35	56.84	27.08	0.26	8.99	5.90	0.20	99.27	350	0.45	780	8.33
TA2b 36	55.33	27.61	0.28	9.45	5.72	0.21	98.59	360	0.47	785	8.40
TA2b 37	54.20	27.66	0.36	9.49	5.55	0.23	97.49	370	0.48	786	8.45
TA2b 49	58.02	27.71	0.36	8.96	6.31	0.24	101.59	490	0.43	774	8.30
TA2b 50	57.73	27.06	0.35	9.04	6.17	0.23	100.59	500	0.44	776	8.32
TA2b 51	57.11	27.61	0.30	9.15	5.56	0.21	99.94	510	0.47	785	8.40
TA2b_52	58.53	27.32	0.29	8.62	6.36	0.21	101.34	520	0.42	771	8.27
TA2b_53	57.66	27.76	0.61	9.24	5.78	0.23	101.29	530	0.46	782	8.38
TA2b 54	57.66	27.39	0.37	8.89	6.34	0.24	100.88	540	0.43	773	8.30
TA2b 55	58.08	27.28	0.25	8.82	6.08	0.24	100.74	550	0.44	775	8.32
TA2b 56	58.40	27.17	0.29	8.66	6.37	0.27	101.17	560	0.42	769	8.30
TA2b 57	58.56	27.03	0.37	8.50	6.44	0.33	101.24	570	0.41	765	8.33
TA2b 58	58.29	26.85	0.45	8.13	6.58	0.28	100.59	580	0.40	761	8.29
TA2b 59	57.28	27.16	0.29	8.59	6.28	0.25	99.84	590	0.42	771	8.30
TA2b 60	56.73	27.21	0.36	8.78	6.10	0.25	99.42	600	0.44	774	8.32
TA2b 61	57.34	26.71	0.33	8.66	6.20	0.26	99.50	610	0.43	772	8.31
TA2b 62	54.39	26.02	0.29	11.32	6.04	0.26	98.33	620	0.50	791	8.55
TA2b 63	57.58	27.42	0.23	9.12	5.82	0.25	100.42	630	0.46	780	8.38
TA2b 64	57.86	28.14	0.26	9.45	5.85	0.26	101.81	640	0.46	782	8.40
TA2b 65	56.92	27.95	0.29	9.28	6.00	0.22	100.65	650	0.45	781	8.35
TA2b 66	57.25	27.52	0.22	9.30	5.92	0.23	100.45	660	0.46	781	8.37
TA2b 67	56.39	28.02	0.28	9.50	5.81	0.22	100.22	670	0.47	784	8.40
TA2b 68	56.14	27.96	0.30	9.63	5.73	0.23	99.99	680	0.47	785	8.43
TA2b 69	56.27	27.73	0.29	9.36	5.91	0.22	99.78	690	0.46	782	8.37
TA2b 70	56.51	27.14	0.29	8.96	6.16	0.27	99.34	700	0.44	775	8.34
TA2b 71	58.21	27.45	0.30	9.01	6.24	0.24	101.46	710	0.44	775	8.31
TA2b 72	58.41	27.35	0.31	8.84	6.26	0.22	101.40	720	0.43	774	8.29
TA2b 73	58.14	27.53	0.35	8.62	6.12	0.25	101.02	730	0.43	773	8.31
TA2b 74	58.46	27.31	0.26	8.49	6.43	0.26	101.21	740	0.42	767	8.29
TA2b 75	57.70	27.02	0.27	8.38	6.39	0.27	100.03	750	0.41	766	8.30
TA2b 76	57.85	27.18	0.34	8.51	6.38	0.20	100.47	760	0.42	770	8.26
TA2b 77	57.67	27.17	0.33	8.36	6.34	0.27	100.15	770	0.41	767	8.30
TA2b 78	58.07	26.88	0.36	8.50	6.48	0.25	100.54	780	0.41	767	8.28
TA2b_79	59.26	26.37	0.18	7.74	6.75	0.29	100.58	790	0.38	753	8.29
TA2b 81	59.00	26.39	0.25	7.74	6.79	0.30	100.47	810	0.38	753	8.29
TA2b 82	58.88	26.37	0.27	7.89	6.78	0.27	100.47	820	0.39	755	8.27
TA2b 83	58.71	26.72	0.27	7.90	6.63	0.28	100.51	830	0.39	757	8.28
TA2b 84	58.80	26.32	0.29	8.22	6.45	0.24	100.32	840	0.41	765	8.27
TA2b 85	59.08	26.34	0.29	7.73	6.78	0.31	100.53	850	0.38	752	8.30
TA2b 86	59.32	26.42	0.25	8.18	6.63	0.33	101.13	860	0.40	759	8.31
TA2b 87	59.07	26.07	0.31	7.56	6.72	0.35	100.09	870	0.38	750	8.33
TA2b 88	57.74	25.88	0.24	7.64	6.55	0.27	98.31	880	0.39	756	8.28
TA2b 89	58.18	26.30	0.24	8.21	6.48	0.28	99.69	890	0.41	763	8.29
TA2b 90	58.53	26.06	0.31	7.81	6.73	0.26	99.70	900	0.38	755	8.27
TA2b 91	59.03	26.39	0.25	7.88	6.55	0.28	100.39	910	0.39	758	8.29
TA2b 92	58.94	25.87	0.20	7.58	6.58	0.37	99.55	920	0.38	751	8.34

Table A3.11 continued

Sample	SiO_2	Al_2O_3	FeO	CaO	Na_2O	K_2O	Total	Dist (μm)	X An	Temp (°C)	H_2O (wt%)
TA2d_1	59.14	26.67	0.29	8.09	6.75	0.28	101.22	20	0.39		
TA2d_2	59.60	26.24	0.33	7.41	7.06	0.31	100.95	30	0.36	744	8.31
TA2d_3	60.09	26.26	0.30	7.62	6.86	0.30	101.42	40	0.37	750	8.30
TA2d_6	59.77	26.80	0.30	7.96	6.80	0.26	101.88	70	0.39	756	8.27
TA2d_8	59.14	27.06	0.23	8.23	6.62	0.29	101.56	90	0.40	761	8.29
TA2d_9	58.81	27.18	0.27	8.28	6.72	0.26	101.51	100	0.40	761	8.27
TA2d_16	59.57	26.38	0.30	7.75	6.81	0.31	101.13	170	0.38	752	8.30
TA2d_17	59.32	26.57	0.34	7.57	6.92	0.23	100.96	180	0.37	750	8.26
TA2d_18	59.17	27.13	0.33	8.24	6.52	0.28	101.67	190	0.40	763	8.29
TA2d_19	59.26	26.60	0.31	7.92	6.82	0.26	101.17	200	0.38	755	8.27
TA2d_20	59.11	26.20	0.57	7.80	6.57	0.31	100.55	210	0.39	756	8.30
TA2d_21	58.95	26.51	0.20	7.95	6.93	0.32	100.85	220	0.38	753	8.30
TA2d_22	59.17	26.40	0.31	7.93	6.81	0.29	100.92	230	0.39	755	8.28
TA2d_23	59.12	26.24	0.27	7.95	6.88	0.29	100.74	240	0.38	754	8.28
TA2d_24	58.83	26.47	0.26	8.12	6.63	0.28	100.59	250	0.40	760	8.28
TA2d_25	59.40	26.64	0.28	7.83	6.67	0.25	101.08	260	0.39	757	8.26
TA2d_26	58.76	26.47	0.33	8.13	6.67	0.29	100.65	270	0.40	759	8.29
TA2d_27	59.25	26.26	0.25	7.70	6.59	0.25	100.30	280	0.39	756	8.27
TA2d_28	58.80	26.50	0.35	8.17	6.80	0.33	100.95	290	0.39	757	8.31
TA2d_29	59.82	26.19	0.30	8.24	6.73	0.29	101.57	300	0.40	760	8.29
TA2d_33	59.21	26.92	0.36	8.46	6.63	0.25	101.83	340	0.41	765	8.27
TA2d_34	58.51	27.00	0.24	8.37	6.58	0.26	100.96	350	0.41	764	8.28
TA2d_35	58.62	26.87	0.30	8.67	6.48	0.21	101.15	360	0.42	770	8.26
TA2d_36	58.04	27.06	0.41	8.50	6.53	0.25	100.79	370	0.41	766	8.28
TA2d_37	58.68	26.99	0.33	8.37	6.47	0.29	101.13	380	0.41	765	8.30
TA2d_38	58.76	26.98	0.40	8.42	6.45	0.26	101.27	390	0.41	766	8.28
TA2d_39	58.71	26.86	0.31	8.80	6.25	0.23	101.16	400	0.43	773	8.30
TA2d_40	58.31	27.08	0.31	9.20	6.30	0.27	101.46	410	0.44	775	8.33
TA2d_41	58.52	27.24	0.20	8.89	6.42	0.28	101.55	420	0.43	771	8.31
TA2d_42	58.58	27.00	0.23	8.62	6.47	0.31	101.21	430	0.42	767	8.32
TA2d_43	58.34	27.11	0.35	8.57	6.54	0.25	101.16	440	0.41	767	8.28
TA2d_44	58.30	26.87	0.26	8.38	6.60	0.21	100.61	450	0.41	765	8.25
TA2d_45	59.06	26.35	0.27	8.09	6.69	0.32	100.78	460	0.39	758	8.30
TA2d_46	59.02	26.89	0.28	8.28	6.60	0.30	101.37	470	0.40	762	8.29
TA2d_47	59.72	26.65	0.39	8.26	6.59	0.25	101.86	480	0.40	763	8.27
TA2d_48	59.48	26.77	0.29	8.33	6.33	0.28	101.48	490	0.41	766	8.30
TA2d_49	59.63	26.49	0.33	7.85	6.88	0.28	101.46	500	0.38	753	8.28
TA2d_50	59.23	26.43	0.26	7.92	6.76	0.28	100.89	510	0.39	756	8.28
TA2d_51	58.96	26.40	0.35	7.94	6.80	0.31	100.77	520	0.39	755	8.29
TA2d_52	59.12	26.05	0.38	8.14	6.70	0.28	100.67	530	0.40	759	8.28
TA2d_53	59.52	26.10	0.28	7.89	6.70	0.33	100.82	540	0.39	755	8.31
TA2d_54	60.10	26.30	0.34	8.08	6.68	0.27	101.78	550	0.39	759	8.28
TA2d_57	59.35	26.34	0.34	7.89	6.96	0.33	101.21	580	0.38	752	8.30
TA2d_58	58.85	26.44	0.40	8.02	6.62	0.30	100.63	590	0.39	758	8.29
TA2d_59	58.86	26.57	0.28	7.97	6.68	0.25	100.61	600	0.39	758	8.27
TA2d_60	58.54	26.29	0.34	8.32	6.77	0.25	100.51	610	0.40	761	8.27
TA2d_61	59.34	26.69	0.37	8.07	6.73	0.29	101.50	620	0.39	758	8.29
TA2d_62	59.35	26.19	0.35	8.14	6.65	0.31	100.98	630	0.40	759	8.30
TA2d_63	59.38	26.47	0.30	8.24	6.73	0.29	101.40	640	0.40	760	8.29
TA2d_64	59.31	26.55	0.46	8.02	6.88	0.26	101.49	650	0.39	756	8.27
TA2d_65	58.52	26.71	0.37	8.44	6.65	0.28	100.97	660	0.41	763	8.29
TA2d_66	58.63	26.96	0.33	8.34	6.71	0.23	101.21	670	0.40	763	8.26
TA2d_67	59.19	26.65	0.29	8.13	6.70	0.27	101.23	680	0.40	759	8.28
TA2d_68	59.36	26.46	0.34	8.57	6.57	0.31	101.61	690	0.41	765	8.31
TA2d_69	59.12	26.61	0.49	8.51	6.29	0.24	101.26	700	0.42	770	8.29
TA2d_70	59.00	26.51	0.32	8.31	6.60	0.27	101.02	710	0.40	763	8.28
TA2d_71	59.57	26.83	0.42	8.25	6.53	0.30	101.90	720	0.40	762	8.30
TA2i_2	57.11	25.86	0.27	7.94	6.74	0.28	98.19	30	0.39	756	8.28
TA2i_3	57.69	26.88	0.26	8.85	6.50	0.28	100.45	40	0.42	770	8.31
TA2i_4	57.48	26.92	0.33	8.63	6.47	0.24	100.07	50	0.42	769	8.28
TA2i_5	57.08	26.73	0.26	8.87	6.38	0.24	99.56	60	0.43	772	8.29
TA2i_6	57.94	26.48	0.36	8.46	6.59	0.25	100.09	70	0.41	765	8.27
TA2i_7	57.32	26.82	0.41	8.66	6.65	0.24	100.11	80	0.41	767	8.27
TA2i_8	57.07	27.04	0.26	8.63	6.69	0.24	99.93	90	0.41	766	8.27
TA2i_9	57.03	26.90	0.32	8.90	4.60	0.24	97.99	100	0.51	791	8.62
TA2i_10	56.68	27.11	0.25	8.79	6.32	0.22	99.38	110	0.43	773	8.29
TA2i_11	56.76	27.11	0.23	8.91	6.37	0.26	99.64	120	0.43	772	8.31
TA2i_12	57.25	27.14	0.34	8.80	6.27	0.24	100.03	130	0.43	773	8.30
TA2i_13	57.43	26.26	0.29	7.80	6.77	0.24	98.79	140	0.38	755	8.26
TA2i_14	57.88	26.32	0.27	8.12	6.59	0.25	99.43	150	0.40	761	8.27
TA2i_15	57.10	26.18	0.43	8.03	6.72	0.30	98.77	160	0.39	757	8.29
TA2i_16	57.17	26.29	0.29	7.93	6.78	0.26	98.72	170	0.39	756	8.27
TA2i_17	58.07	26.45	0.38	8.03	6.71	0.28	99.91	180	0.39	758	8.28
TA2i_18	58.48	26.64	0.31	8.23	6.74	0.33	100.73	190	0.40	758	8.31
TA2i_19	59.03	26.61	0.35	8.39	6.62	0.32	101.32	200	0.40	762	8.31

Table A3.11 continued

Sample	SiO_2	Al_2O_3	FeO	CaO	Na_2O	K_2O	Total	Dist (μm)	X An	Temp (°C)	H_2O (wt%)
TA2i 20	58.52	26.39	0.31	8.18	6.59	0.25	100.24	210	0.40	762	8.27
TA2i 21	58.18	26.47	0.38	8.11	6.73	0.28	100.15	220	0.39	759	8.28
TA2i 22	57.37	26.40	0.30	8.27	6.55	0.24	99.13	230	0.40	764	8.27
TA2i 23	57.56	26.14	0.31	8.04	6.47	0.26	98.78	240	0.40	762	8.28
TA2i 24	57.33	26.16	0.35	7.71	6.77	0.29	98.61	250	0.38	753	8.29
TA2i 25	58.54	26.66	0.34	8.27	6.70	0.31	100.81	260	0.40	760	8.30
TA2i 26	57.87	26.41	0.23	7.96	6.85	0.32	99.63	270	0.38	754	8.30
TA2i 27	57.72	26.57	0.28	8.19	6.43	0.28	99.46	280	0.41	763	8.29
TA2i 28	57.13	26.59	0.24	8.20	6.38	0.27	98.80	290	0.41	765	8.29
TA2i 29	56.40	26.52	0.25	8.38	6.58	0.25	98.38	300	0.41	764	8.27
TA2i 30	56.54	26.55	0.31	8.57	6.49	0.22	98.68	310	0.42	768	8.27
TA2i 31	57.17	26.77	0.27	8.70	6.43	0.23	99.57	320	0.42	770	8.28
TA2i 32	57.13	26.68	0.26	8.52	6.31	0.28	99.17	330	0.42	768	8.31
TA2i 33	58.02	26.15	0.20	8.16	6.67	0.32	99.52	340	0.40	759	8.30
TA2i 40	57.41	26.17	0.31	7.85	6.59	0.25	98.58	410	0.39	758	8.27
TA2i 41	58.41	26.44	0.33	8.00	6.79	0.30	100.27	420	0.39	756	8.29
TA2i 42	59.27	26.58	0.30	8.30	6.87	0.27	101.60	430	0.39	759	8.27
TA2i 46	59.49	26.69	0.35	8.14	6.80	0.30	101.77	470	0.39	757	8.29
TA2i 47	58.99	26.79	0.42	8.01	6.93	0.30	101.43	480	0.38	754	8.29
TA2i 48	58.76	26.88	0.33	8.24	6.89	0.28	101.39	490	0.39	758	8.28
TA2i 49	59.03	26.60	0.35	8.33	6.87	0.32	101.50	500	0.39	758	8.30
TA2i 50	57.85	26.33	0.30	7.83	6.85	0.28	99.43	510	0.38	753	8.28
TA2i 51	58.94	26.68	0.41	7.91	6.68	0.30	100.91	520	0.39	756	8.29
TA2i 52	58.91	26.41	0.30	8.08	6.78	0.30	100.77	530	0.39	757	8.29
TA2i 53	58.32	26.33	0.33	7.82	6.67	0.28	99.74	540	0.39	756	8.28
TA2i 54	58.58	26.55	0.37	8.01	6.74	0.30	100.56	550	0.39	757	8.29
TA2i_55	58.58	26.57	0.44	8.09	6.70	0.29	100.66	560	0.39	758	8.28
TA2i 56	57.89	26.63	0.35	8.03	6.78	0.34	100.01	570	0.39	755	8.31
TA2i 57	57.65	26.29	0.30	8.01	6.75	0.30	99.30	580	0.39	757	8.29
TA2i 58	57.47	26.55	0.39	8.41	6.72	0.31	99.84	590	0.40	762	8.30
TA2i 59	57.83	26.40	0.20	8.30	6.71	0.25	99.69	600	0.40	762	8.27
TA2i 60	57.65	26.22	0.36	8.51	6.55	0.23	99.52	610	0.41	767	8.27
TA2i 62	58.39	27.13	0.34	8.82	6.53	0.24	101.44	630	0.42	770	8.28
TA2i 63	57.20	27.37	0.29	9.12	6.33	0.25	100.56	640	0.44	775	8.32
TA2i 64	56.42	27.35	0.33	9.30	5.99	0.23	99.62	650	0.46	781	8.36
TA2i 65	56.56	27.32	0.27	8.78	6.38	0.24	99.55	660	0.43	771	8.29
TA2i 66	56.66	27.06	0.33	8.88	6.24	0.27	99.44	670	0.43	773	8.32
TA2i 67	58.36	26.61	0.41	8.55	6.26	0.31	100.51	680	0.42	768	8.33
TA3a 9	55.66	27.70	0.46	9.78	5.79	0.19	99.57	20	0.48	787	8.41
TA3a 10	58.03	27.45	0.43	9.16	6.33	0.24	101.64	30	0.44	775	8.32
TA3a 11	57.51	27.59	0.47	9.59	6.13	0.21	101.50	40	0.46	782	8.35
TA3a_12	57.13	27.91	0.43	9.88	5.80	0.18	101.33	50	0.48	788	8.41
TA3a 13	56.44	28.33	0.43	10.50	5.69	0.18	101.57	60	0.50	792	8.50
TA3a 14	54.75	28.32	0.34	10.23	5.57	0.20	99.40	70	0.50	791	8.51
TA3a 15	54.48	28.85	0.52	11.03	5.30	0.17	100.35	80	0.53	797	8.66
TA3a 20	56.35	27.94	0.24	9.89	5.81	0.22	100.46	130	0.48	787	8.43
TA3a 21	56.22	28.46	0.30	10.26	5.48	0.15	100.87	140	0.50	794	8.51
TA3a 22	56.16	28.90	0.26	10.52	5.35	0.15	101.34	150	0.52	796	8.57
TA3a 23	56.44	28.46	0.41	10.00	5.87	0.21	101.39	160	0.48	787	8.42
TA3a 24	56.79	28.43	0.42	9.86	5.77	0.25	101.51	170	0.48	786	8.45
TA3a 25	56.92	27.83	0.40	9.56	5.90	0.21	100.81	180	0.47	784	8.38
TA3a 26	57.20	28.09	0.42	9.82	5.83	0.21	101.57	190	0.48	787	8.41
TA3a_27	57.82	27.87	0.43	9.42	5.98	0.19	101.71	200	0.46	783	8.35
TA3a 28	58.22	27.17	0.40	9.02	6.24	0.25	101.29	210	0.44	775	8.32
TA3a 29	57.34	28.04	0.38	9.66	6.16	0.22	101.80	220	0.46	782	8.36
TA3a 30	57.20	28.14	0.35	10.19	5.74	0.23	101.86	230	0.49	789	8.48
TA3a 31	57.07	27.66	0.45	9.29	6.11	0.23	100.80	240	0.45	779	8.34
TA3a_32	58.21	26.85	0.26	8.73	6.32	0.25	100.61	250	0.43	771	8.30
TA3a 33	56.94	27.35	0.32	9.17	6.33	0.25	100.36	260	0.44	775	8.32
TA3a 34	57.64	27.21	0.34	9.03	6.47	0.26	100.96	270	0.43	772	8.30
TA3a 35	57.15	27.11	0.35	8.89	6.34	0.26	100.10	280	0.43	772	8.31
TA3a 36	57.85	26.86	0.38	9.02	6.04	0.25	100.39	290	0.45	777	8.34
TA3a 37	57.54	27.19	0.25	9.12	6.05	0.23	100.37	300	0.45	779	8.34
TA3a 38	57.29	27.35	0.30	9.13	6.40	0.23	100.68	310	0.44	775	8.30
TA3a 39	57.28	27.42	0.36	9.17	6.33	0.25	100.81	320	0.44	775	8.32
TA3a 40	57.30	26.87	0.33	8.83	5.43	0.23	98.99	330	0.47	783	8.40
TA3a 41	57.63	26.99	0.40	8.85	6.35	0.27	100.49	340	0.43	772	8.31
TA3a 43	57.67	26.76	0.53	9.02	6.21	0.23	100.42	360	0.44	776	8.31
TA3a_44	57.62	27.50	0.36	9.24	6.08	0.24	101.04	370	0.45	779	8.35
TA3a 45	57.70	27.39	0.29	9.00	6.29	0.20	100.87	380	0.44	776	8.28
TA3a 46	57.89	26.71	0.39	8.48	6.53	0.27	100.28	390	0.41	766	8.29
TA3a 47	57.99	26.71	0.43	8.57	6.63	0.28	100.61	400	0.41	765	8.29
TA3a 48	58.01	26.43	0.38	8.11	6.65	0.27	99.85	410	0.40	760	8.28
TA3a 49	57.98	26.18	0.30	8.44	6.45	0.29	99.64	420	0.41	765	8.30
TA3a_50	57.69	26.25	0.24	8.34	6.80	0.28	99.59	430	0.40	760	8.28

Table A3.11 continued

Sample	SiO_2	Al_2O_3	FeO	CaO	Na_2O	K_2O	Total	Dist (μm)	X An	Temp (°C)	H_2O (wt%)
TA3a 51	57.89	26.28	0.27	8.07	6.72	0.26	99.49	440	0.39	759	8.27
TA3a 52	59.60	26.00	0.36	8.00	6.67	0.25	100.86	450	0.39	759	8.27
TA3a 53	58.92	25.89	0.37	7.97	6.76	0.30	100.20	460	0.39	756	8.29
TA3a 54	59.12	26.01	0.32	7.77	6.97	0.31	100.50	470	0.37	750	8.29
TA3a 56	58.76	26.44	0.33	7.89	6.82	0.31	100.55	490	0.38	754	8.30
TA3a 57	58.56	26.69	0.33	8.13	6.68	0.28	100.66	500	0.40	760	8.28
TA3a 58	59.12	26.67	0.27	8.28	6.73	0.29	101.35	510	0.40	760	8.29
TA3a 59	59.87	25.91	0.31	7.75	7.08	0.27	101.20	520	0.37	749	8.28
TA3a 60	60.32	24.97	0.24	6.84	7.25	0.36	99.99	530	0.34	731	8.38
TA3a 61	60.75	25.51	0.24	6.98	7.28	0.35	101.11	540	0.34	733	8.36
TA3a 62	59.95	25.63	0.44	7.59	7.03	0.34	100.98	550	0.37	746	8.32
TA3a 63	59.11	26.20	0.19	7.74	6.99	0.30	100.53	560	0.37	750	8.29
TA3a 65	58.43	26.74	0.29	8.39	6.73	0.28	100.85	580	0.40	762	8.28
TA3a 66	58.52	26.49	0.27	8.16	6.78	0.27	100.48	590	0.39	759	8.27
TA3a 67	58.03	26.81	0.36	8.47	6.25	0.29	100.20	600	0.42	768	8.32
TA3a 68	58.72	26.54	0.28	8.53	6.37	0.26	100.71	610	0.42	769	8.29
TA3a 69	58.55	26.84	0.30	8.62	6.34	0.24	100.89	620	0.42	770	8.29
TA3a 70	58.59	26.89	0.37	8.61	6.37	0.26	101.09	630	0.42	769	8.29
TA3a 71	57.80	26.93	0.38	8.47	6.46	0.23	100.26	640	0.41	768	8.27
TA3a 72	58.27	26.55	0.30	8.60	6.35	0.27	100.35	650	0.42	769	8.30
TA3a 73	58.00	26.68	0.34	8.78	6.47	0.23	100.50	660	0.42	771	8.28
TA3f 1	60.16	23.81	0.24	5.39	8.18	0.61	98.39	20	0.26	684	8.78
TA3f 2	61.74	24.72	0.33	5.72	7.97	0.57	101.05	30	0.27	694	8.68
TA3f 3	61.16	24.48	0.27	5.70	8.00	0.61	100.22	40	0.27	693	8.70
TA3f 4	59.48	24.38	0.30	5.73	8.01	0.57	98.47	50	0.27	694	8.67
TA3f_5	59.87	24.33	0.25	5.82	8.21	0.63	99.11	60	0.27	692	8.71
TA3f 7	60.45	24.62	0.23	5.99	8.00	0.61	99.90	80	0.28	699	8.65
TA3f 8	59.30	25.48	0.23	7.25	7.53	0.53	100.31	90	0.34	729	8.44
TA3f 9	58.38	25.78	0.15	7.35	7.13	0.44	99.22	100	0.35	739	8.38
TA3f 10	56.83	26.32	0.20	7.87	7.01	0.38	98.62	110	0.37	749	8.33
TA3f 11	58.31	26.08	0.27	7.83	7.09	0.39	99.97	120	0.37	747	8.34
TA3f 12	57.17	25.46	0.23	7.26	7.42	0.42	97.96	130	0.34	734	8.39
TA3f 13	57.08	26.01	0.17	7.77	7.11	0.41	98.54	140	0.37	746	8.35
TA3f 14	58.06	26.08	0.33	7.32	7.32	0.38	99.49	150	0.35	737	8.36
TA3f 15	59.21	24.62	0.26	6.35	7.58	0.58	98.60	160	0.31	713	8.55
TA3f 16	58.65	25.42	0.36	7.39	7.41	0.42	99.65	170	0.35	736	8.38
TA3f 17	58.66	26.70	0.18	7.74	6.86	0.40	100.54	180	0.38	749	8.34
TA3f 18	57.46	25.95	0.21	8.11	7.03	0.39	99.13	190	0.38	752	8.33
TA3f 19	58.99	25.72	0.19	7.43	7.33	0.45	100.10	200	0.35	737	8.39
TA3f 20	58.08	25.15	0.20	6.87	7.39	0.48	98.17	210	0.33	726	8.44
TA3f 21	57.01	26.61	0.23	8.06	6.98	0.46	99.35	220	0.38	750	8.37
TA3f_22	57.32	25.93	0.22	7.37	7.41	0.41	98.65	230	0.35	736	8.37
TA3f 23	58.75	25.67	0.24	7.31	7.32	0.40	99.68	240	0.35	736	8.37
TA3f 24	58.74	25.70	0.26	7.31	7.39	0.47	99.86	250	0.34	734	8.41
TA3f 25	60.31	24.68	0.32	6.05	7.84	0.52	99.71	260	0.29	704	8.59
TA3f 26	60.77	24.15	0.25	5.93	8.00	0.64	99.73	270	0.28	697	8.68
TA3f 27	59.62	24.93	0.17	6.04	7.95	0.51	99.21	280	0.29	703	8.59
TA3f 28	59.11	24.95	0.10	6.17	7.90	0.62	98.85	290	0.29	704	8.62
TA3f 29	49.83	20.96	0.41	5.04	6.54	0.55	83.34	300	0.29	701	8.65
TA3f 30	59.31	24.57	0.25	6.14	7.85	0.64	98.77	310	0.29	703	8.63
TA3f 31	60.50	24.86	0.27	5.90	7.88	0.59	100.00	320	0.28	699	8.65
TA3f 32	60.45	24.80	0.20	6.02	8.04	0.61	100.11	330	0.28	699	8.65
TA3f_33	60.42	24.84	0.25	6.12	7.89	0.57	100.09	340	0.29	704	8.60
TA3f 34	59.30	24.62	0.34	6.28	7.85	0.61	98.99	350	0.30	707	8.60
TA3f 35	60.30	24.15	0.30	5.71	8.00	0.59	99.05	360	0.27	694	8.69
TA3f 36	61.14	24.16	0.20	5.29	8.19	0.71	99.69	370	0.25	679	8.85
TA3f 37	61.52	24.19	0.16	5.26	8.32	0.66	100.11	380	0.25	678	8.85
TA3f_38	60.90	24.17	0.15	5.24	8.34	0.64	99.43	390	0.25	677	8.84
TA3f 39	61.13	23.67	0.17	4.98	8.23	0.77	98.96	400	0.24	670	8.95
TA3f 40	61.30	23.34	0.22	4.70	8.45	0.79	98.79	410	0.22	660	9.06
TA3f 41	62.39	23.41	0.19	4.68	8.47	0.74	99.87	420	0.22	660	9.04
TA3f 42	62.15	23.25	0.19	4.64	8.57	0.80	99.59	430	0.22	657	9.09
TA3f 43	62.78	23.24	0.20	4.36	8.97	0.80	100.35	440	0.20	645	9.23
TA3f 46	64.76	22.43	0.60	3.85	6.82	2.79	101.24	470	0.20	625	10.01
TA3f 50	63.71	23.94	0.16	4.73	8.04	0.75	101.32	510	0.23	667	8.98
TA3h 1a	56.69	27.36	0.36	8.79	6.35	0.25	99.80	20	0.43	771	8.30
TA3h 1	57.41	26.46	0.38	7.91	6.90	0.31	99.37	30	0.38	753	8.29
TA3h_2	56.81	26.70	0.34	8.22	6.66	0.25	98.98	40	0.40	762	8.27
TA3h 3	57.16	26.91	0.34	8.68	6.43	0.27	99.79	50	0.42	769	8.30
TA3h 4	58.19	26.66	0.44	8.24	6.50	0.24	100.26	60	0.41	764	8.27
TA3h 5	57.81	26.80	0.37	8.66	6.34	0.30	100.29	70	0.42	769	8.32
TA3h 6	57.89	27.08	0.37	8.44	6.47	0.26	100.50	80	0.41	766	8.28
TA3h 7	57.84	26.95	0.36	8.64	6.55	0.25	100.57	90	0.42	768	8.28
TA3h 8	58.17	26.69	0.19	8.32	6.59	0.23	100.19	100	0.41	764	8.26

Table A3.11 continued

Sample	SiO_2	Al_2O_3	FeO	CaO	Na_2O	K_2O	Total	Dist (μm)	X An	Temp (°C)	H_2O (wt%)
TA3h 9	57.59	26.91	0.29	8.44	6.61	0.24	100.09	110	0.41	765	8.27
TA3h 10	57.04	27.26	0.34	8.52	6.58	0.24	99.98	120	0.41	766	8.27
TA3h 11	58.29	25.81	0.27	7.25	7.05	0.26	98.92	130	0.36	743	8.29
TA3h 12	59.38	25.31	0.27	7.17	7.30	0.36	99.79	140	0.34	736	8.36
TA3h 13	58.78	26.08	0.27	7.69	6.92	0.29	100.03	150	0.37	750	8.29
TA3h 14	58.54	25.92	0.34	7.59	6.87	0.30	99.56	160	0.37	749	8.30
TA3h 15	58.74	25.87	0.23	7.22	7.11	0.27	99.44	170	0.35	741	8.30
TA3h 16	58.72	25.67	0.20	7.40	7.18	0.27	99.44	180	0.36	743	8.29
TA3h 17	59.45	25.78	0.37	7.48	6.97	0.30	100.34	190	0.37	747	8.30
TA3h 18	60.65	25.66	0.22	7.15	7.19	0.33	101.19	200	0.35	738	8.34
TA3h 19	61.28	25.41	0.25	6.93	7.43	0.36	101.65	210	0.33	730	8.38
TA3h 20	61.21	25.31	0.30	6.66	7.57	0.37	101.42	220	0.32	723	8.42
TA3h 21	60.16	25.71	0.30	7.10	7.39	0.27	100.93	230	0.34	735	8.32
TA3h 22	58.82	26.78	0.34	8.17	6.78	0.27	101.16	240	0.39	759	8.27
TA3h 23	57.85	26.37	0.36	7.95	6.61	0.25	99.38	250	0.39	759	8.26
TA3h 24	57.14	26.69	0.27	8.30	6.59	0.27	99.26	260	0.40	763	8.28
TA3h 25	58.84	26.86	0.35	8.55	6.65	0.21	101.46	270	0.41	767	8.25
TA3h 28	59.16	27.17	0.28	8.30	6.69	0.30	101.90	300	0.40	761	8.29
TA3h 29	58.71	27.76	0.29	8.86	6.27	0.24	102.13	310	0.43	773	8.31
TA3h 30	57.87	27.97	0.35	9.08	6.17	0.18	101.61	320	0.44	778	8.29
TA3h 32	58.08	27.54	0.31	9.13	6.15	0.20	101.42	340	0.45	778	8.31
TA3h 33	58.74	27.41	0.29	8.93	6.33	0.17	101.86	350	0.43	775	8.26
TA3h 35	58.53	27.40	0.34	9.02	6.29	0.25	101.82	370	0.44	774	8.31
TA3h 36	57.94	28.21	0.45	8.98	6.05	0.20	101.82	380	0.45	778	8.31
TA3h 39	57.19	27.85	0.34	9.32	6.20	0.21	101.12	410	0.45	779	8.32
TA3h 40	57.65	27.81	0.31	9.32	6.08	0.22	101.37	420	0.45	780	8.34
TA3h_41	57.80	27.81	0.33	9.55	6.01	0.23	101.72	430	0.46	782	8.37
TA3h 42	57.78	27.82	0.31	9.24	6.14	0.21	101.51	440	0.45	779	8.32
TA3h 43	57.82	27.71	0.29	9.18	6.23	0.18	101.41	450	0.44	778	8.29
TA3h 45	57.80	27.80	0.43	9.15	6.21	0.23	101.61	470	0.44	777	8.32
TA3h 46	57.65	27.64	0.34	9.05	6.18	0.22	101.06	480	0.44	777	8.31
TA3h 47	57.31	27.71	0.27	9.12	6.05	0.22	100.68	490	0.45	779	8.33
TA3h 48	56.93	27.89	0.36	9.45	6.06	0.21	100.89	500	0.46	782	8.35
TA3q 2	57.93	26.49	0.36	8.10	6.77	0.31	99.95	20	0.39	757	8.29
TA3q 3	58.20	26.04	0.37	7.84	6.70	0.29	99.44	30	0.39	755	8.29
TA3q 4	57.83	26.91	0.28	8.80	6.30	0.30	100.42	40	0.43	771	8.33
TA3q 5	58.32	26.87	0.30	9.16	6.30	0.23	101.18	50	0.44	776	8.31
TA3q 6	57.29	27.13	0.26	9.20	6.20	0.26	100.34	60	0.44	777	8.34
TA3q 7	57.41	27.98	0.30	9.80	5.98	0.22	101.69	70	0.47	784	8.40
TA3q 8	56.99	28.00	0.30	10.12	5.57	0.20	101.18	80	0.50	791	8.49
TA3q 9	56.90	27.18	0.33	9.11	6.08	0.24	99.84	90	0.45	778	8.34
TA3q_10	57.31	26.83	0.29	8.57	6.39	0.24	99.63	100	0.42	769	8.28
TA3q 11	59.15	26.12	0.31	7.50	6.68	0.31	100.07	110	0.38	751	8.30
TA3q 12	59.69	26.04	0.30	7.91	6.70	0.31	100.94	120	0.39	756	8.30
TA3q 13	59.50	26.05	0.33	7.45	7.06	0.31	100.71	130	0.36	744	8.31
TA3q 14	60.81	25.56	0.28	7.47	6.99	0.29	101.41	140	0.37	746	8.30
TA3q 15	58.68	26.02	0.24	7.72	6.78	0.30	99.74	150	0.38	752	8.29
TA3q 16	59.73	25.77	0.33	7.56	6.86	0.26	100.50	160	0.37	750	8.27
TA3q 17	58.26	25.27	0.25	7.40	6.86	0.30	98.34	170	0.37	747	8.30
TA3q 18	59.99	25.90	0.22	7.44	6.98	0.35	100.88	180	0.36	744	8.33
TA3q 19	59.20	26.10	0.28	7.64	7.16	0.29	100.66	190	0.36	746	8.29
TA3q 20	59.28	26.28	0.22	7.66	7.10	0.34	100.87	200	0.37	746	8.31
TA3q_21	58.33	25.74	0.29	7.26	7.01	0.31	98.93	210	0.36	742	8.31
TA3q 22	58.31	25.96	0.35	7.61	7.08	0.33	99.64	220	0.37	746	8.31
TA3q 23	58.42	25.86	0.21	7.23	6.88	0.30	98.90	230	0.36	744	8.31
TA3q 24	58.84	25.67	0.31	7.49	6.88	0.28	99.48	240	0.37	748	8.29
TA3q 25	59.72	25.55	0.30	7.34	7.02	0.39	100.31	250	0.36	741	8.35
TA3q_26	59.89	26.21	0.28	7.60	6.74	0.35	101.08	260	0.38	750	8.32
TA3q 27	59.60	26.13	0.34	7.70	6.93	0.31	101.02	270	0.37	750	8.30
TA3q 28	58.04	25.55	0.31	7.28	6.68	0.33	98.19	280	0.37	747	8.32
TA3q 29	57.17	24.99	0.32	7.32	6.99	0.29	97.08	290	0.36	744	8.30
TA3q 34	57.14	26.98	0.27	8.89	6.41	0.24	99.94	340	0.43	772	8.29
TA3q 35	56.23	27.98	0.44	9.88	5.76	0.22	100.50	350	0.48	787	8.44
TA3q 36	55.74	28.23	0.35	10.51	5.49	0.21	100.53	360	0.51	793	8.56
TA3q 37	55.49	27.96	0.33	10.15	5.75	0.21	99.88	370	0.49	789	8.46
TA3q 38	55.73	27.98	0.31	10.30	5.67	0.20	100.19	380	0.50	791	8.49
TA3q 39	56.13	27.38	0.33	9.08	6.34	0.23	99.48	390	0.44	775	8.30
TA3q 40	56.13	27.15	0.27	8.46	6.19	0.28	98.47	400	0.42	769	8.32
TA3q_41	56.28	27.00	0.32	8.65	6.30	0.21	98.76	410	0.43	772	8.28
TA3q 42	56.85	27.01	0.41	8.76	6.27	0.25	99.55	420	0.43	772	8.30
TA3q 43	57.37	26.80	0.29	8.55	6.17	0.23	99.42	430	0.43	772	8.29
TA3q 44	58.62	26.77	0.39	8.91	6.47	0.24	101.41	440	0.43	772	8.29
TA3q 45	58.66	26.92	0.28	8.79	6.33	0.26	101.24	450	0.43	771	8.31
TA3q 46	58.02	26.92	0.31	8.59	6.21	0.23	100.28	460	0.43	772	8.29
TA3q 47	57.61	26.92	0.29	8.94	6.37	0.24	100.38	470	0.43	773	8.30

Table A3.11 continued

Sample	SiO_2	Al_2O_3	FeO	CaO	Na_2O	K_2O	Total	Dist (μm)	X An	Temp (°C)	H_2O (wt%)
TA3q 48	57.38	26.76	0.36	8.53	6.57	0.28	99.89	480	0.41	765	8.29
TA3q 49	56.75	26.92	0.36	9.01	6.49	0.22	99.74	490	0.43	773	8.28
TA3q 50	57.16	27.05	0.35	8.62	6.46	0.25	99.89	500	0.42	768	8.29
TA3q 51	57.14	27.25	0.27	8.88	6.18	0.22	99.94	510	0.44	775	8.30
TA3q 52	57.22	26.79	0.37	8.85	6.34	0.23	99.79	520	0.43	773	8.29
TA3q 53	57.42	27.34	0.26	9.20	6.41	0.26	100.88	530	0.44	774	8.32
TA3q 54	56.95	27.34	0.43	9.32	6.27	0.25	100.55	540	0.44	777	8.33
TA3q 55	56.38	27.31	0.32	9.15	6.13	0.24	99.52	550	0.45	778	8.33
TA3q 56	57.58	26.54	0.39	8.16	6.82	0.30	99.78	560	0.39	757	8.29
TA3q 57	58.13	26.01	0.26	7.98	6.75	0.28	99.40	570	0.39	757	8.28
TA3q 58	61.23	24.13	0.61	6.78	6.17	0.71	99.62	580	0.36	736	8.55
TA4a 2	59.86	26.14	0.32	7.64	7.13	0.33	101.42	20	0.36	746	8.31
TA4a 3	60.15	25.71	0.23	7.35	7.46	0.32	101.21	30	0.35	737	8.33
TA4a 4	59.34	26.53	0.32	8.29	6.98	0.33	101.77	40	0.39	756	8.30
TA4a 5	58.55	25.73	0.30	7.57	7.17	0.37	99.70	50	0.36	743	8.34
TA4a 7	59.52	26.16	0.32	7.65	7.45	0.31	101.41	70	0.36	742	8.31
TA4a 8	58.18	26.06	0.24	7.42	7.22	0.28	99.40	80	0.36	742	8.30
TA4a 9	58.45	25.78	0.34	7.45	7.32	0.34	99.67	90	0.35	740	8.33
TA4a 10	59.33	25.34	0.32	7.33	7.24	0.35	99.92	100	0.35	739	8.34
TA4a 11	59.38	25.42	0.21	7.46	7.14	0.30	99.91	110	0.36	744	8.30
TA4a 12	58.77	25.52	0.31	7.25	6.98	0.29	99.11	120	0.36	743	8.30
TA4a 13	58.17	25.60	0.31	7.47	7.18	0.27	99.00	130	0.36	744	8.29
TA4a 14	57.81	25.40	0.36	7.14	7.03	0.31	98.06	140	0.35	740	8.32
TA4a 15	56.62	25.77	0.27	7.71	6.71	0.30	97.38	150	0.38	753	8.29
TA4a 17	57.81	26.31	0.26	8.12	6.82	0.31	99.63	170	0.39	757	8.29
TA4a_18	59.84	26.41	0.24	8.15	6.83	0.32	101.78	180	0.39	757	8.30
TA4a 21	59.86	26.00	0.27	7.85	7.27	0.33	101.57	210	0.37	747	8.31
TA4a 22	58.45	25.78	0.21	8.07	6.82	0.31	99.63	220	0.39	756	8.29
TA4a 23	59.72	26.49	0.31	7.83	7.36	0.28	101.98	230	0.36	746	8.28
TA4a 30	60.54	25.85	0.30	7.56	7.19	0.34	101.78	300	0.36	743	8.32
TA4a 31	60.06	25.84	0.35	7.31	7.47	0.29	101.32	310	0.35	737	8.32
TA4a 32	58.66	25.53	0.24	7.16	7.02	0.28	98.87	320	0.35	742	8.30
TA4a 34	58.37	26.88	0.27	8.61	6.43	0.20	100.77	340	0.42	770	8.26
TA4a 36	59.43	26.81	0.29	8.16	7.02	0.29	101.98	360	0.38	755	8.28
TA4a 38	58.43	26.92	0.28	8.65	6.61	0.22	101.10	380	0.41	768	8.26
TA4a 39	57.42	26.73	0.37	8.64	6.71	0.24	100.11	390	0.41	766	8.27
TA4a 41	59.45	26.42	0.31	8.56	6.64	0.27	101.64	410	0.41	765	8.29
TA4a 42	58.48	26.40	0.34	8.34	6.59	0.24	100.38	420	0.41	764	8.26
TA4a 43	59.27	26.76	0.30	8.50	6.75	0.27	101.84	430	0.40	763	8.28
TA4a 45	56.21	26.37	0.24	8.76	6.33	0.26	98.16	450	0.43	771	8.31
TA4a 48	59.38	26.89	0.35	8.38	6.59	0.30	101.88	480	0.41	763	8.30
TA4a_52	57.94	26.99	0.31	8.97	6.70	0.28	101.18	520	0.42	768	8.29
TA4a 53	57.04	26.44	0.33	8.60	6.53	0.27	99.19	530	0.41	767	8.29
TA4a 59	59.28	26.49	0.38	8.06	6.82	0.26	101.30	590	0.39	757	8.27
TA4a 60	58.57	26.84	0.17	8.54	6.63	0.27	101.01	600	0.41	765	8.28
TA4a 61	58.88	27.10	0.21	8.59	6.66	0.28	101.72	610	0.41	765	8.29
TA4a 62	58.27	27.18	0.36	8.87	6.68	0.28	101.62	620	0.42	768	8.29
TA4a 68	58.22	26.74	0.27	8.78	6.72	0.29	101.02	680	0.41	766	8.30
TA4a 69	58.15	27.16	0.30	8.52	6.58	0.26	100.98	690	0.41	766	8.28
TA4a 70	58.27	27.37	0.31	8.94	6.66	0.24	101.78	700	0.42	770	8.28
TA4a 71	58.04	26.63	0.32	8.46	6.83	0.26	100.53	710	0.40	762	8.27
TA4c_3	57.96	26.80	0.34	8.59	6.78	0.28	100.73	20	0.41	763	8.28
TA4c 4	58.43	27.01	0.40	8.38	7.00	0.30	101.51	30	0.39	758	8.28
TA4c 5	58.48	27.32	0.33	8.93	6.56	0.30	101.91	40	0.42	769	8.31
TA4c 6	58.60	26.77	0.37	8.46	6.94	0.26	101.40	50	0.40	760	8.27
TA4c 10	60.79	25.79	0.31	7.12	7.63	0.30	101.94	90	0.33	732	8.35
TA4c_11	59.54	26.17	0.22	7.76	7.47	0.28	101.44	100	0.36	744	8.29
TA4c 12	59.83	26.01	0.21	7.50	7.40	0.33	101.28	110	0.35	740	8.32
TA4c 13	59.79	26.43	0.30	7.95	7.19	0.23	101.89	120	0.37	752	8.25
TA4c 17	57.11	27.93	0.38	9.81	6.21	0.19	101.63	160	0.46	783	8.35
TA4c 18	56.69	28.42	0.43	10.14	5.88	0.21	101.77	170	0.48	788	8.44
TA4c 19	56.32	28.59	0.33	10.31	5.93	0.19	101.66	180	0.49	789	8.43
TA4c 25	56.55	28.64	0.42	10.14	5.92	0.21	101.89	240	0.48	787	8.43
TA4c 31	56.57	28.58	0.37	10.47	5.75	0.25	101.99	300	0.49	789	8.52
TA4c 33	56.42	28.41	0.33	10.23	5.96	0.20	101.55	320	0.48	788	8.43
TA4c 40	58.11	27.83	0.26	9.09	6.38	0.23	101.91	390	0.43	775	8.30
TA4c 45	59.57	26.57	0.33	7.75	7.15	0.31	101.69	440	0.37	747	8.30
TA4c_46	59.75	26.43	0.31	7.80	7.31	0.33	101.92	450	0.36	745	8.31
TA4c 47	60.06	25.96	0.26	7.47	7.29	0.29	101.33	460	0.36	742	8.30
TA4c 53	58.99	26.88	0.28	7.88	7.26	0.31	101.59	520	0.37	748	8.29
TA4c 54	59.21	26.74	0.28	8.19	6.56	0.23	101.20	530	0.40	763	8.26
TA4c 62	58.00	27.58	0.29	9.07	6.59	0.25	101.79	610	0.43	771	8.29
TA4c 63	57.99	27.23	0.33	8.92	6.69	0.23	101.39	620	0.42	769	8.27
TA4c 64	58.19	27.18	0.39	8.91	6.63	0.24	101.55	630	0.42	770	8.28

Table A3.11 continued

Sample	SiO_2	Al_2O_3	FeO	CaO	Na_2O	K_2O	Total	Dist (μm)	X An	Temp (°C)	H_2O (wt%)
TA4c 65	58.72	27.61	0.24	9.17	6.42	0.25	102.41	640	0.43	774	8.31
TA4c 66	58.88	27.71	0.30	9.25	6.52	0.20	102.86	650	0.43	775	8.28
TA4c 67	58.71	27.73	0.38	8.94	6.48	0.25	102.50	660	0.43	771	8.29
TA4c 68	58.51	27.52	0.24	9.11	6.78	0.24	102.41	670	0.42	770	8.27
TA4c 69	58.32	27.44	0.33	8.67	6.71	0.25	101.73	680	0.41	766	8.27
TA4c 70	58.20	27.32	0.38	8.85	6.63	0.29	101.67	690	0.42	768	8.30
TA4f 1	66.55	21.62	0.90	5.82	5.71	1.19	101.78	20	0.33	713	8.88
TA4f 2	55.20	27.38	0.33	8.71	6.83	0.22	98.66	30	0.41	765	8.25
TA4f 6	59.05	26.37	0.29	8.69	6.72	0.23	101.35	70	0.41	766	8.26
TA4f 7	59.66	26.47	0.32	8.30	6.95	0.29	101.99	80	0.39	757	8.28
TA4f 8	58.85	26.58	0.29	8.51	6.69	0.28	101.19	90	0.41	763	8.28
TA4f 9	59.35	26.51	0.25	8.61	6.84	0.29	101.84	100	0.40	762	8.28
TA4f 11	58.22	26.47	0.19	8.91	6.56	0.26	100.60	120	0.42	769	8.29
TA4f 13	58.76	26.99	0.29	9.14	6.38	0.29	101.85	140	0.43	773	8.33
TA4f 14	58.70	27.17	0.30	9.14	6.30	0.31	101.92	150	0.44	773	8.35
TA4f 15	57.82	27.20	0.40	9.37	6.32	0.21	101.32	160	0.45	778	8.31
TA4f 16	58.36	26.74	0.27	8.91	6.43	0.24	100.94	170	0.43	772	8.29
TA4f 17	58.49	26.92	0.31	8.79	6.58	0.23	101.33	180	0.42	769	8.27
TA4f 18	58.81	26.78	0.30	8.80	6.67	0.23	101.58	190	0.42	768	8.27
TA4f 21	58.07	27.48	0.35	8.94	6.00	0.25	101.10	220	0.44	776	8.34
TA4f 25	57.16	27.75	0.34	9.49	6.28	0.24	101.26	260	0.45	778	8.34
TA4f 26	57.02	27.94	0.32	9.63	6.22	0.23	101.35	270	0.46	780	8.35
TA4f 27	57.17	27.90	0.42	9.40	6.37	0.26	101.52	280	0.44	776	8.34
TA4f 28	57.31	27.41	0.24	9.40	6.09	0.27	100.73	290	0.45	779	8.37
TA4f 31	58.12	27.61	0.35	9.20	6.26	0.29	101.82	320	0.44	775	8.35
TA4f_33	57.05	28.28	0.41	9.75	6.18	0.22	101.89	340	0.46	782	8.36
TA4f 34	56.15	28.61	0.33	10.13	5.88	0.18	101.27	350	0.48	788	8.42
TA4f 35	55.94	28.59	0.44	10.50	5.69	0.18	101.34	360	0.50	792	8.50
TA4f 36	57.23	27.48	0.36	9.47	6.39	0.24	101.17	370	0.44	777	8.33
TA4f 37	57.63	27.14	0.37	9.08	6.56	0.26	101.04	380	0.43	771	8.30
TA4f 38	57.94	27.26	0.37	9.32	6.39	0.20	101.47	390	0.44	777	8.30
TA4f 40	58.11	27.34	0.32	8.82	6.34	0.28	101.19	410	0.43	771	8.32
TA4f 42	57.73	27.40	0.31	9.02	6.57	0.32	101.33	430	0.42	769	8.33
TA4f 43	56.94	27.66	0.29	9.28	6.52	0.23	100.91	440	0.43	774	8.30
TA4f 44	57.13	27.36	0.32	9.18	6.54	0.26	100.79	450	0.43	772	8.30
TA4f 45	57.42	27.20	0.38	9.15	6.30	0.26	100.70	460	0.44	775	8.33
TA4f 46	57.73	27.26	0.41	9.38	6.43	0.23	101.42	470	0.44	776	8.31
TA4f 47	57.77	27.57	0.38	9.18	6.31	0.24	101.45	480	0.44	775	8.32
TA4f 48	57.49	27.50	0.36	9.50	6.51	0.28	101.64	490	0.44	775	8.34
TA4f 49	57.43	27.72	0.40	9.14	6.40	0.26	101.34	500	0.43	774	8.31
TA4f 50	57.36	27.60	0.40	9.42	6.57	0.20	101.56	510	0.44	776	8.28
TA4f_51	56.94	27.63	0.30	9.56	6.36	0.24	101.03	520	0.45	778	8.33
TA4f 52	57.08	27.73	0.32	9.61	6.18	0.23	101.15	530	0.46	780	8.36
TA4f 53	56.44	28.20	0.34	9.92	6.10	0.24	101.24	540	0.47	783	8.40
TA4f 54	56.63	28.24	0.34	10.14	5.87	0.19	101.41	550	0.48	788	8.43
TA4f 55	56.46	28.30	0.30	10.29	6.03	0.18	101.56	560	0.48	788	8.41
TA4f 56	55.92	28.51	0.32	10.45	5.97	0.18	101.34	570	0.49	789	8.44
TA4f 57	55.92	28.81	0.41	10.40	5.84	0.20	101.58	580	0.49	790	8.46
TA4f 58	56.14	28.23	0.42	10.32	6.00	0.20	101.29	590	0.48	788	8.42
TA4f 59	56.33	28.30	0.35	10.14	5.98	0.23	101.32	600	0.48	786	8.43
TA4f 60	56.26	28.07	0.33	9.97	5.96	0.17	100.76	610	0.48	787	8.39
TA4f 61	56.35	28.29	0.37	10.33	5.92	0.17	101.43	620	0.49	789	8.43
TA4f_62	56.50	28.41	0.44	10.27	5.75	0.23	101.61	630	0.49	789	8.49
TA4f 64	56.14	28.66	0.37	10.25	5.99	0.19	101.59	650	0.48	788	8.42
TA4f 65	55.99	28.23	0.32	10.21	5.78	0.22	100.75	660	0.49	788	8.47
TA4f 66	55.85	28.30	0.35	10.33	5.86	0.24	100.92	670	0.49	788	8.47
TA4f 67	55.81	28.48	0.40	10.15	5.81	0.18	100.82	680	0.49	789	8.44
TA4f_68	56.12	27.75	0.37	9.96	6.07	0.20	100.47	690	0.47	785	8.38
TA4f 69	56.72	27.70	0.38	9.47	6.09	0.22	100.58	700	0.46	781	8.35
TA4f 70	56.72	27.82	0.37	9.49	6.16	0.21	100.76	710	0.45	780	8.34
TA4f 71	57.26	27.46	0.52	9.58	6.41	0.23	101.46	720	0.45	778	8.32
TA4f 72	57.29	27.57	0.34	9.31	6.24	0.23	100.98	730	0.45	777	8.32
TA4f 73	56.90	27.69	0.32	9.38	6.33	0.26	100.88	740	0.44	776	8.34
TA4f 74	56.77	27.47	0.46	9.51	6.37	0.23	100.80	750	0.45	778	8.32
TA4f 75	56.58	27.45	0.37	9.36	6.13	0.26	100.15	760	0.45	778	8.36
TA4f 76	56.84	27.48	0.35	9.45	6.46	0.22	100.81	770	0.44	777	8.31
TA4f 77	56.89	27.82	0.33	9.64	6.21	0.26	101.14	780	0.45	779	8.37
TA4f 78	56.81	27.66	0.32	9.56	6.31	0.24	100.89	790	0.45	779	8.34
TA4f_79	57.09	27.55	0.38	9.41	6.18	0.20	100.81	800	0.45	780	8.32
TA4f 80	57.11	27.76	0.37	9.50	6.11	0.23	101.08	810	0.46	780	8.36
TA4f 81	56.84	27.68	0.41	9.38	6.37	0.24	100.91	820	0.44	776	8.32
TA4f 82	56.92	27.92	0.34	9.62	6.08	0.20	101.08	830	0.46	783	8.35
TA4f 83	56.54	27.29	0.32	9.35	6.37	0.28	100.15	840	0.44	775	8.34
TA4f 84	56.33	27.85	0.38	9.36	6.28	0.20	100.39	850	0.45	779	8.31
TA4f_85	56.70	27.69	0.37	9.52	6.29	0.24	100.81	860	0.45	778	8.34

Table A3.11 continued

Sample	SiO_2	Al_2O_3	FeO	CaO	Na_2O	K_2O	Total	Dist (μm)	X An	Temp (°C)	H_2O (wt%)
TA4f 86	56.80	27.67	0.29	9.70	6.26	0.24	100.96	870	0.46	780	8.36
TA4f 87	57.17	27.77	0.41	9.42	6.21	0.23	101.21	880	0.45	779	8.34
TA4f 88	56.95	27.67	0.38	9.70	6.60	0.27	101.56	890	0.44	776	8.33
TA4f 89	57.27	27.61	0.23	9.90	6.20	0.25	101.46	900	0.46	782	8.39
TA4f 90	57.25	27.10	0.46	9.21	6.45	0.24	100.70	910	0.44	774	8.30
TA4f 91	57.22	27.21	0.34	8.93	6.54	0.26	100.50	920	0.42	770	8.29
TA4f 92	57.58	27.27	0.29	9.11	6.54	0.26	101.05	930	0.43	772	8.30
TA4f 93	58.06	27.15	0.36	9.17	6.85	0.26	101.85	940	0.42	769	8.28
TA4f 94	56.88	27.65	0.28	9.30	6.46	0.23	100.79	950	0.44	775	8.30
TA4f 95	57.18	27.63	0.37	9.32	6.33	0.25	101.07	960	0.44	776	8.33
TA4f 96	57.24	27.45	0.33	8.87	6.64	0.27	100.80	970	0.42	768	8.29
TA4f 97	58.11	26.97	0.30	8.54	6.71	0.27	100.91	980	0.41	764	8.28
TA4f 98	57.38	26.62	0.25	8.41	6.60	0.25	99.51	990	0.41	764	8.27
TA4f 99	57.77	26.68	0.29	8.69	6.78	0.28	100.49	1000	0.41	764	8.29
TA4f 100	57.77	26.88	0.24	8.81	6.74	0.26	100.71	1010	0.41	766	8.28
TA4f 101	57.78	26.86	0.28	8.75	6.79	0.28	100.74	1020	0.41	765	8.28
TA4f 102	58.23	26.64	0.32	8.54	6.88	0.26	100.87	1030	0.40	762	8.27
TA4f 103	57.94	27.18	0.41	8.72	6.55	0.25	101.05	1040	0.42	768	8.28
TA4f 104	57.78	26.68	0.45	8.83	6.84	0.29	100.86	1050	0.41	764	8.29

Major elements are given in wt%, *X An* are calculated on a mole fraction basis and temperatures (temp) and H_2O concentration (wt%) are calculated using the Plagioclase-melt equilibria of Putirka (2005) and a pressure of 100 MPa. Distance represents the distance from the start of the profile and correlates with 'S' on the relevant backscatter image

Appendix 4

Figure A4.1: Backscattered electron images and X_{An} profiles of Whakamaru plagioclase crystals. Vertical dash lines represent the crystal core.

Figure A4.1

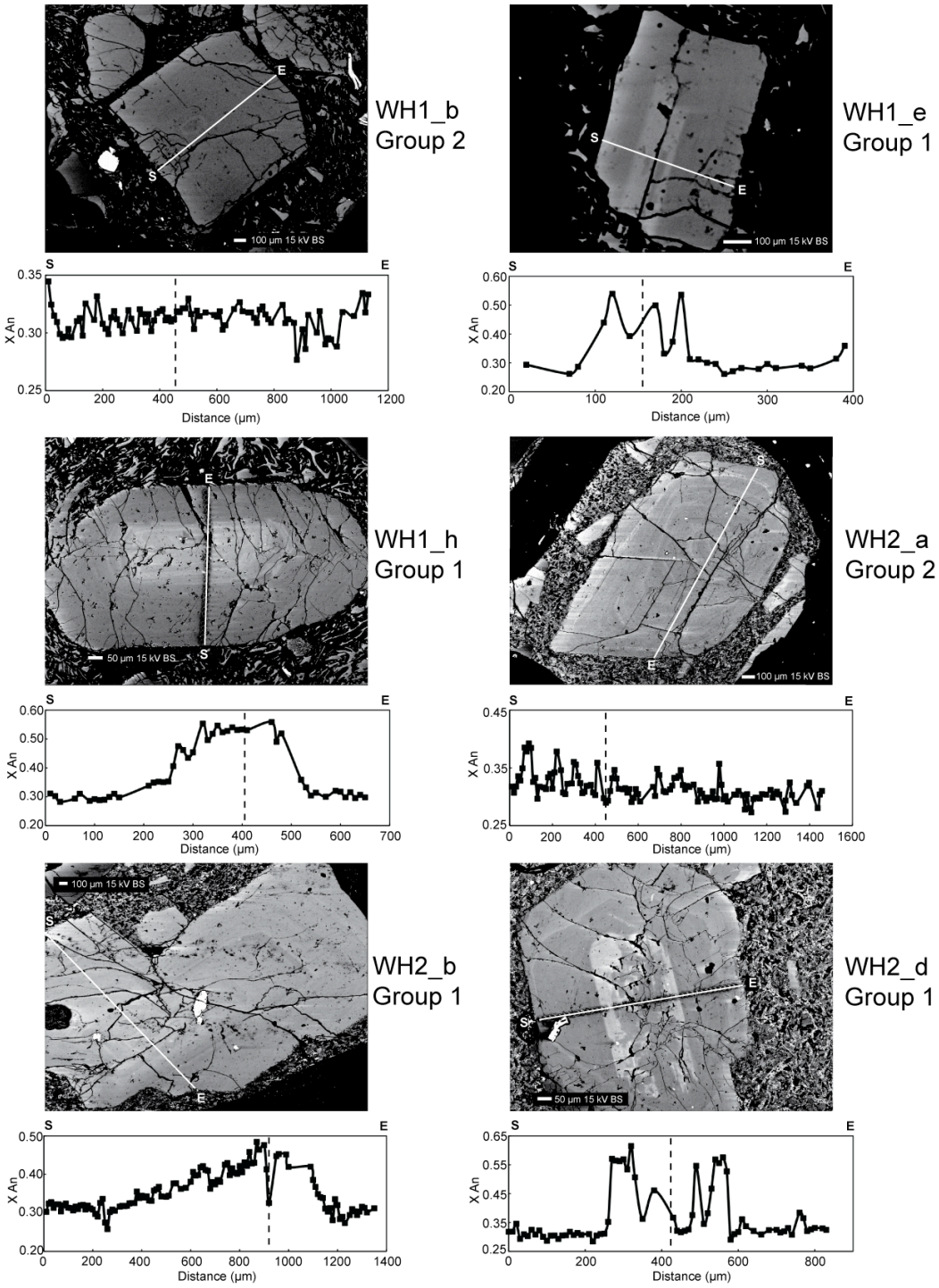
WH1_b
Group 2
WH1_e
Group 1
WH1_h
Group 1
WH2_a
Group 2
WH2_b
Group 1
WH2_d
Group 1
Distance (μm)
X An

Figure A4.1 continued

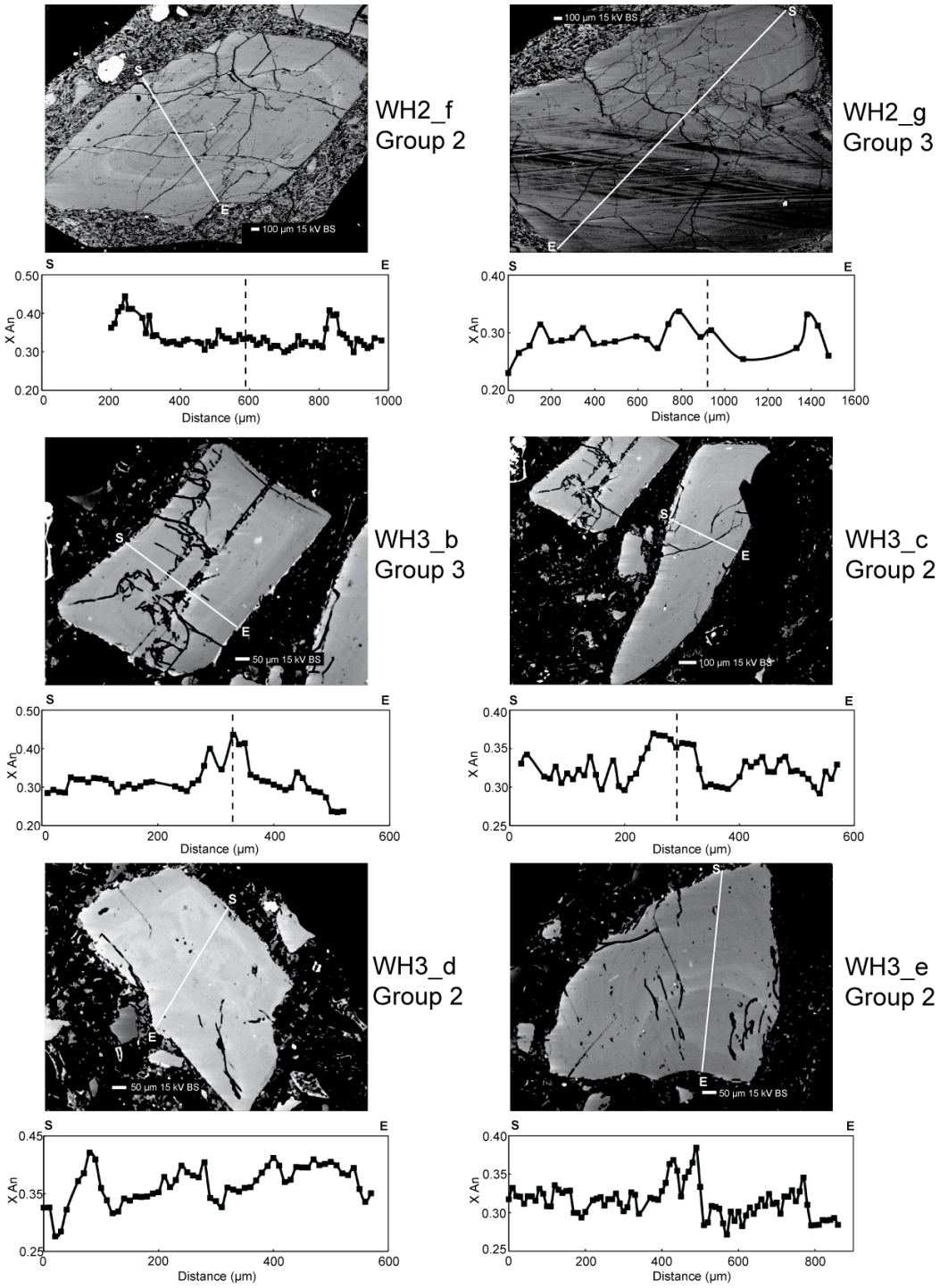

Figure A4.1 continued

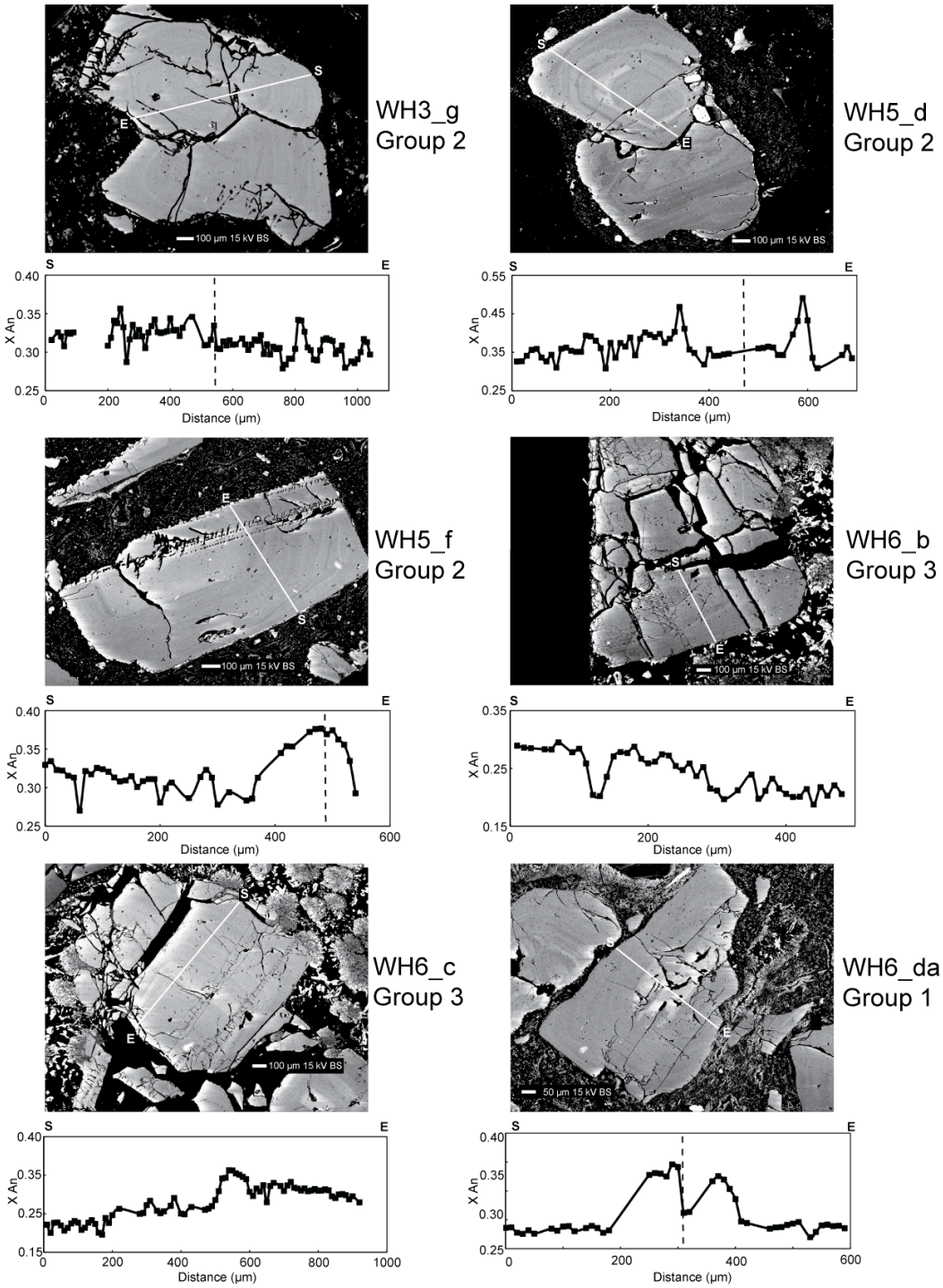

Figure A4.1 continued

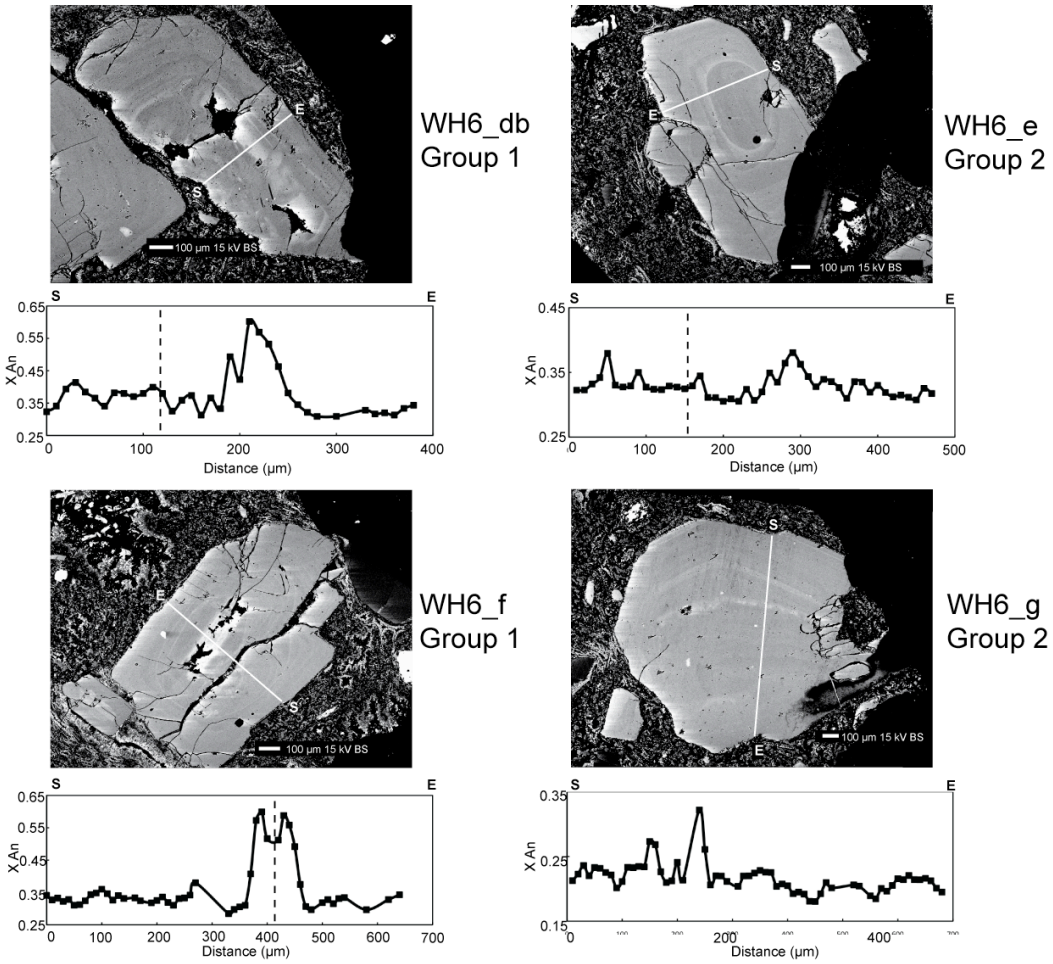

Appendix 4

Figure A4.2: Backscattered electron mages of Whakamaru plagioclase crystals.

Spot analyses of *An* concentration are given in mol%

Figure A4.2

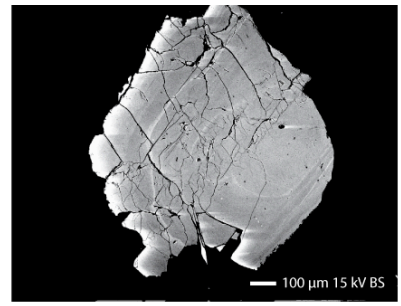

WH1_t
Group 2

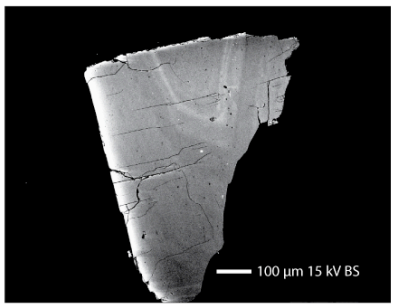

WH1_u
Group 2

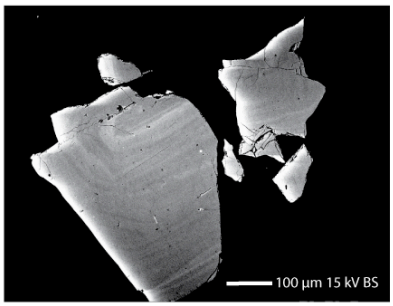

WH1_w
Group 2

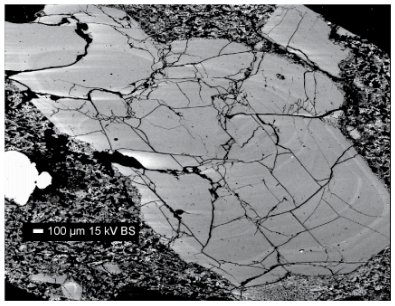

WH2_c
Group 2

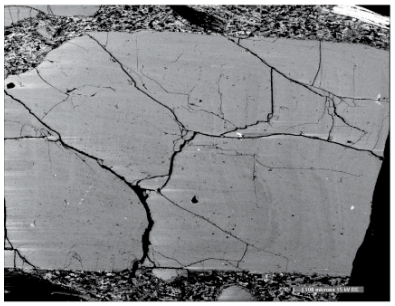

WH2_e
Group 2

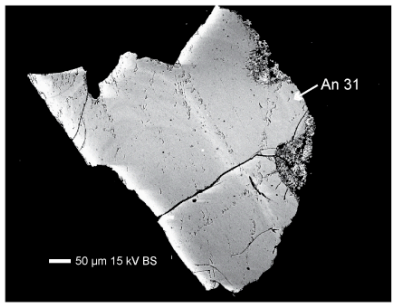

WH2_k
Group 2

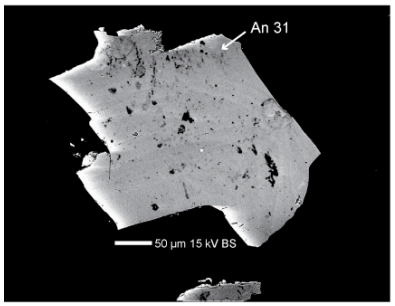

WH2_r
Group 2

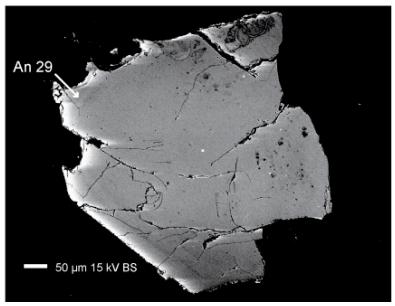

WH2_s
Group 2

Figure A4.2 continued

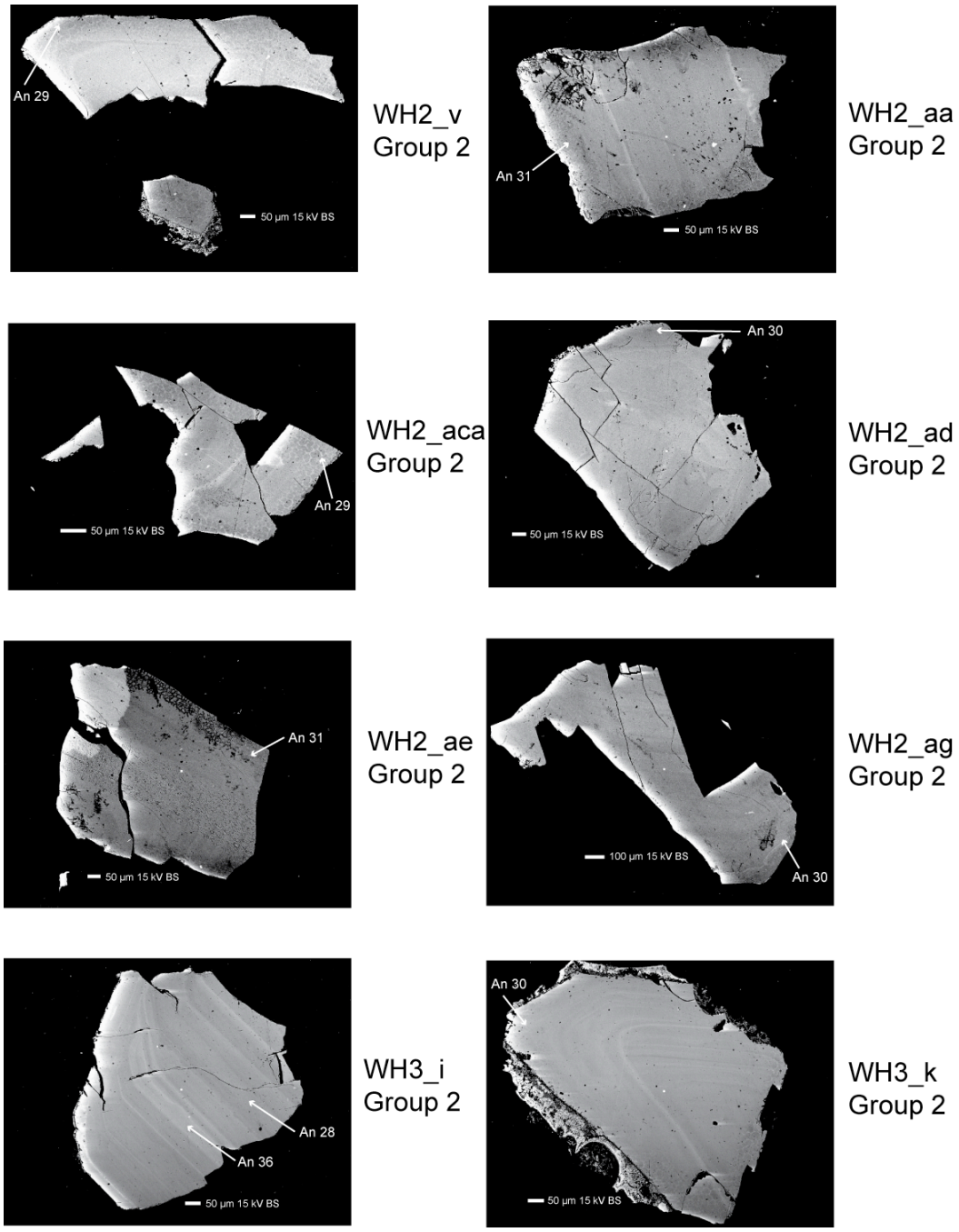

Figure A4.2 continued

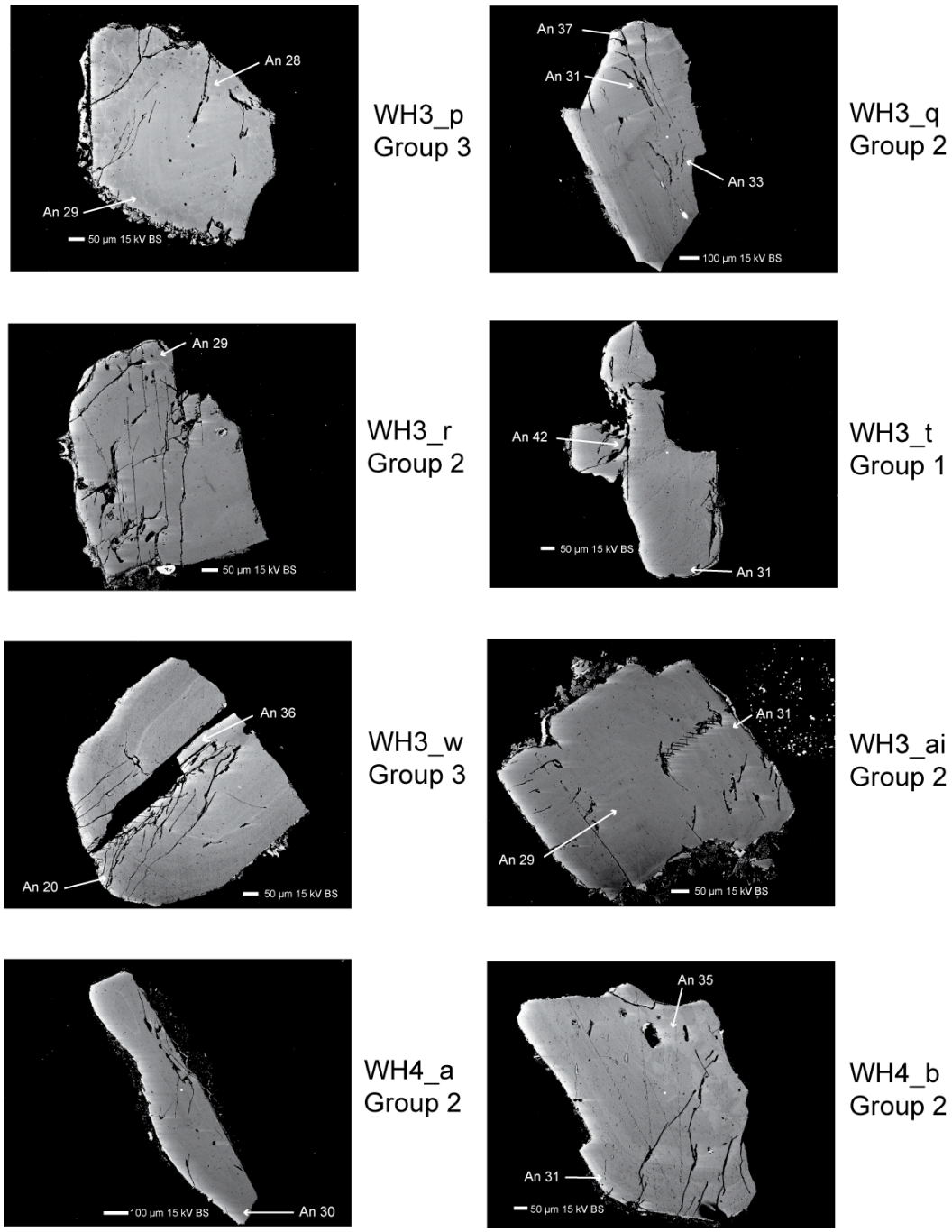

Figure A4.2 continued

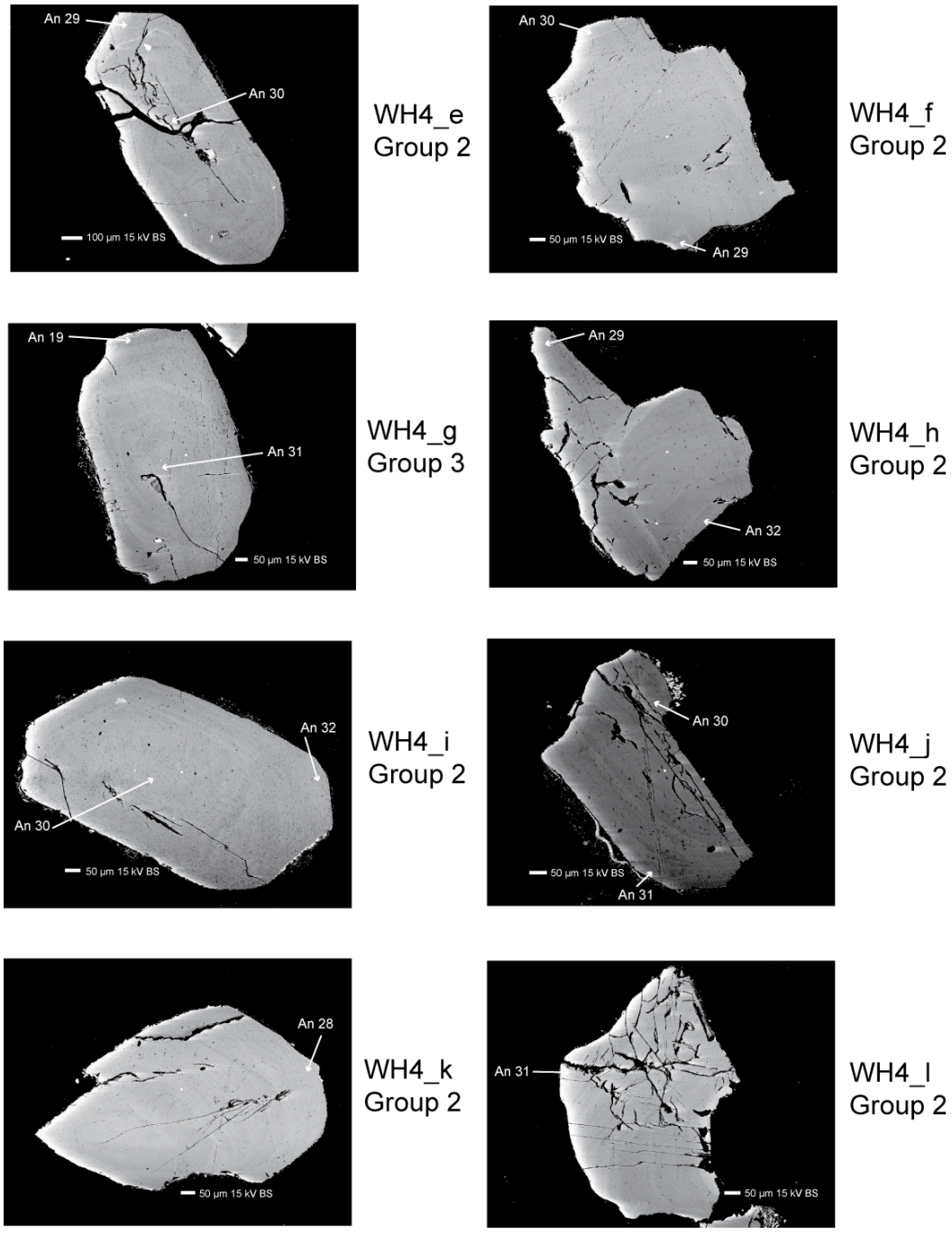

Figure A4.2 continued

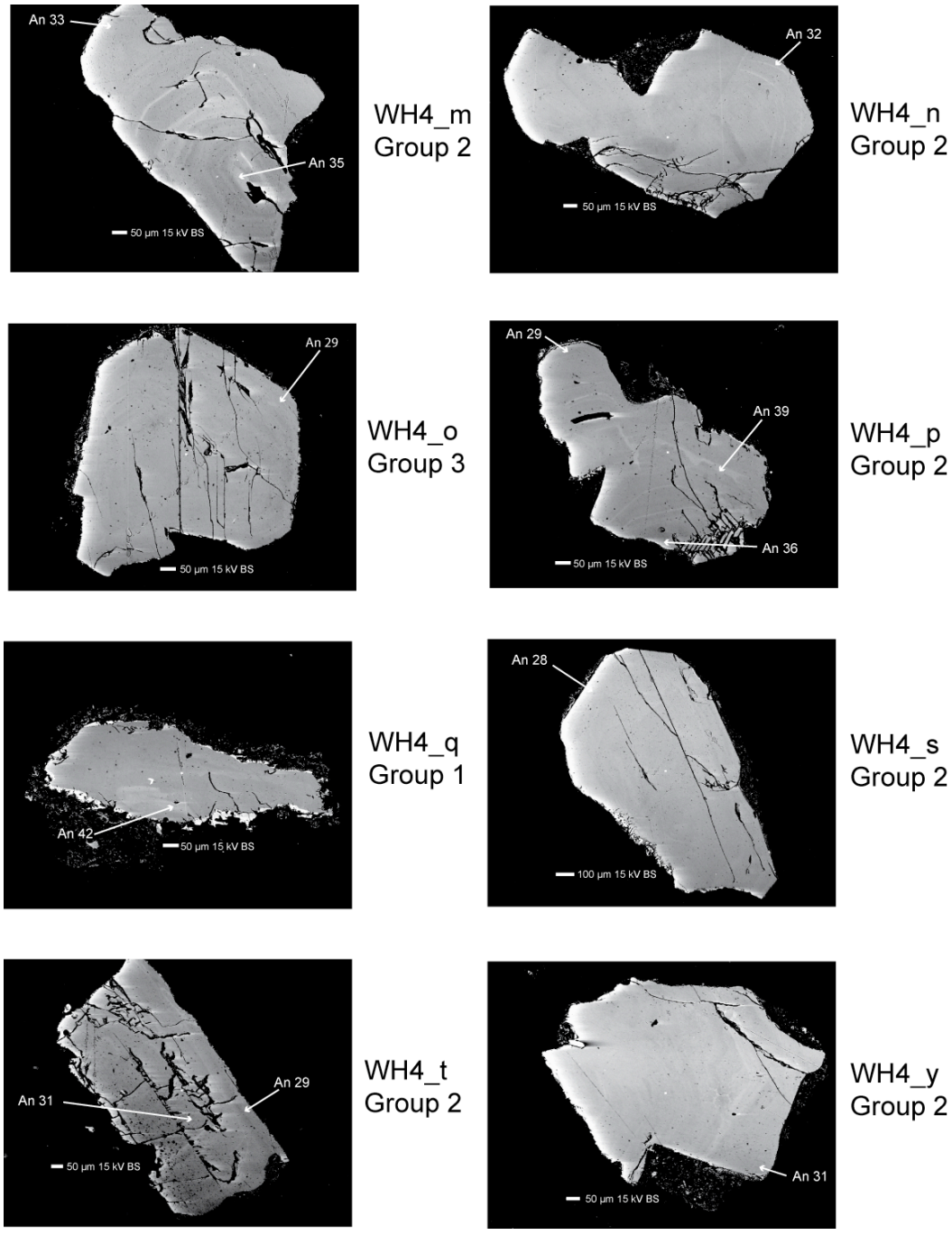

Figure A4.2 continued

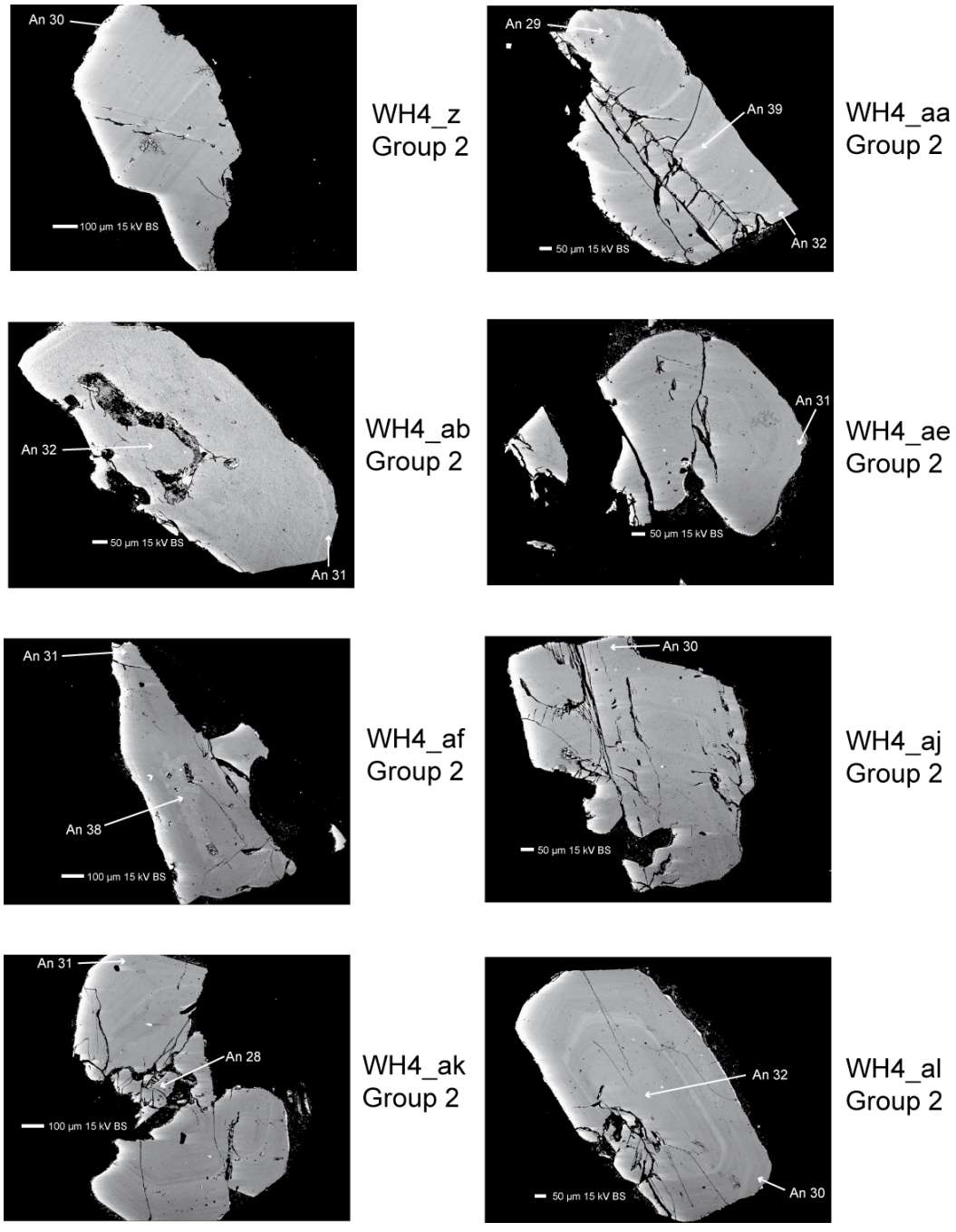

Figure A4.2 continued

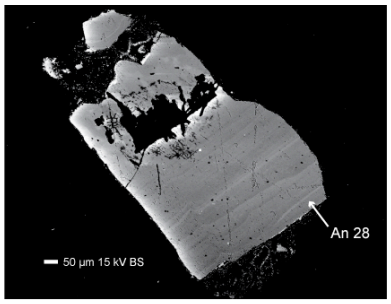

WH4_an
Group 2

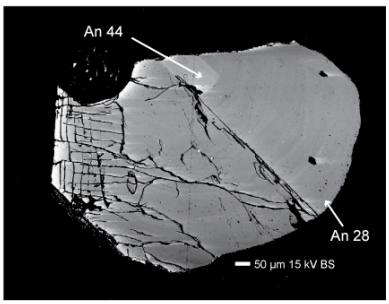

WH4_ao
Group 1

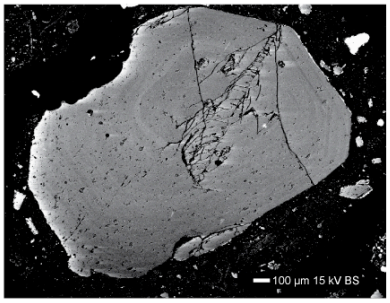

WH5_b
Group 2

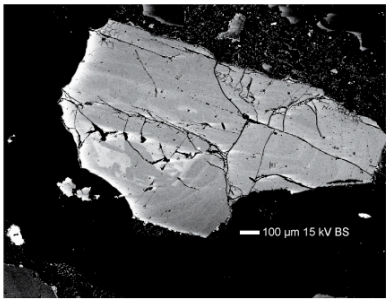

WH5_c
Group 1

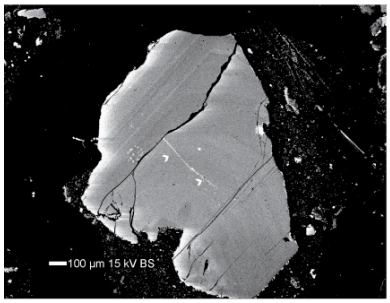

WH5_e
Group 2

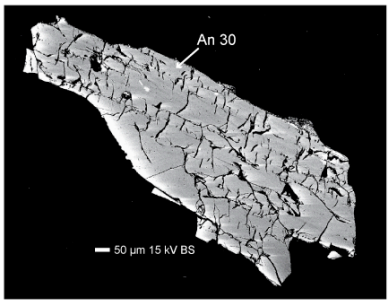

WH6_h
Group 2

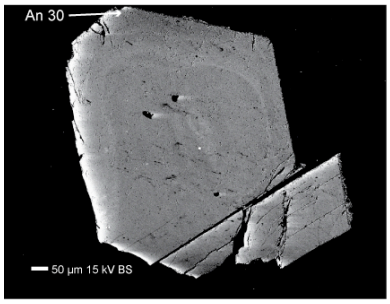

WH6_k
Group 2

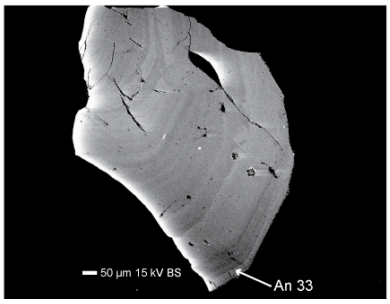

WH6_m
Group 2

Figure A4.2 continued

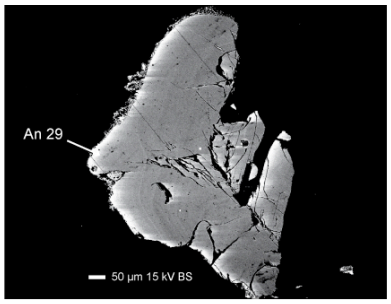

WH6_n
Group 2

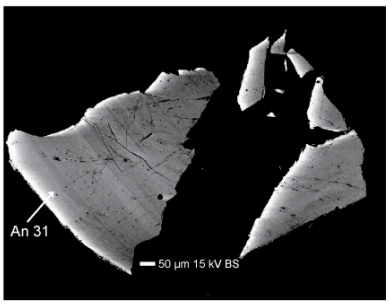

WH6_o
Group 2

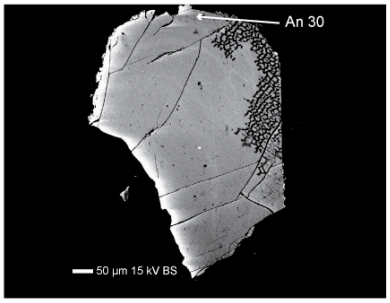

WH6_q
Group 2

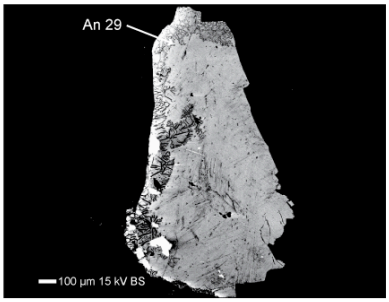

WH6_s
Group 2

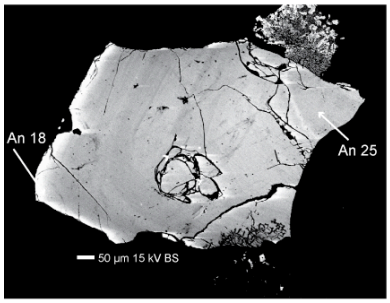

WH6_t
Group 3

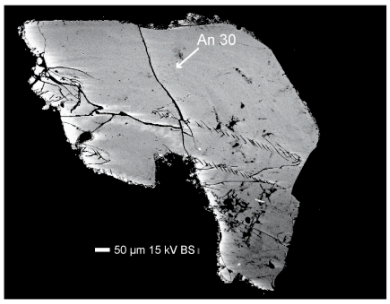

WH6_aa
Group 2

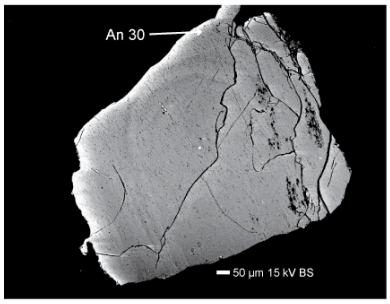

WH6_ad
Group 2

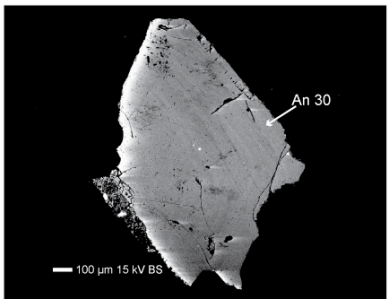

WH6_af
Group 2

Figure A4.2 continued

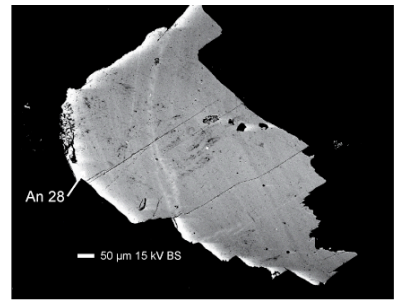

WH6_ag
Group 2

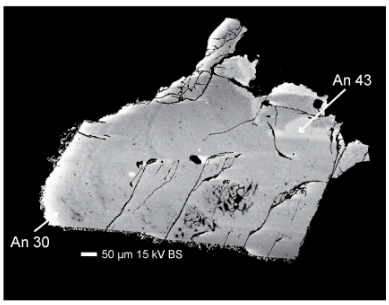

WH6_ah
Group 1

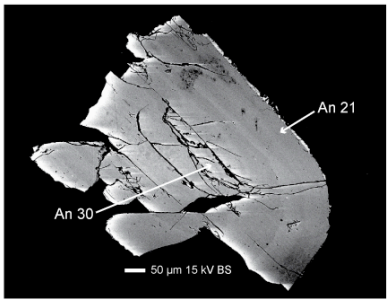

WH6_ai
Group 3

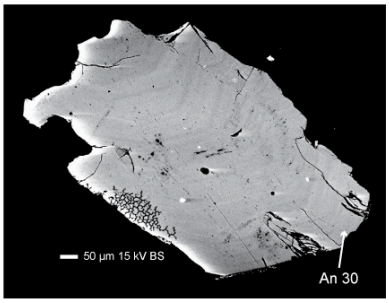

WH6_aj
Group 2

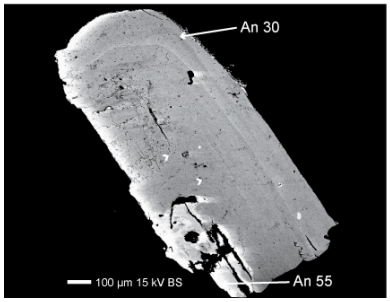

WH6_ap
Group 3

Appendix 4

Figure A4.3: Cathodoluminescence images of Whakamaru quartz crystals

Figure A4.3

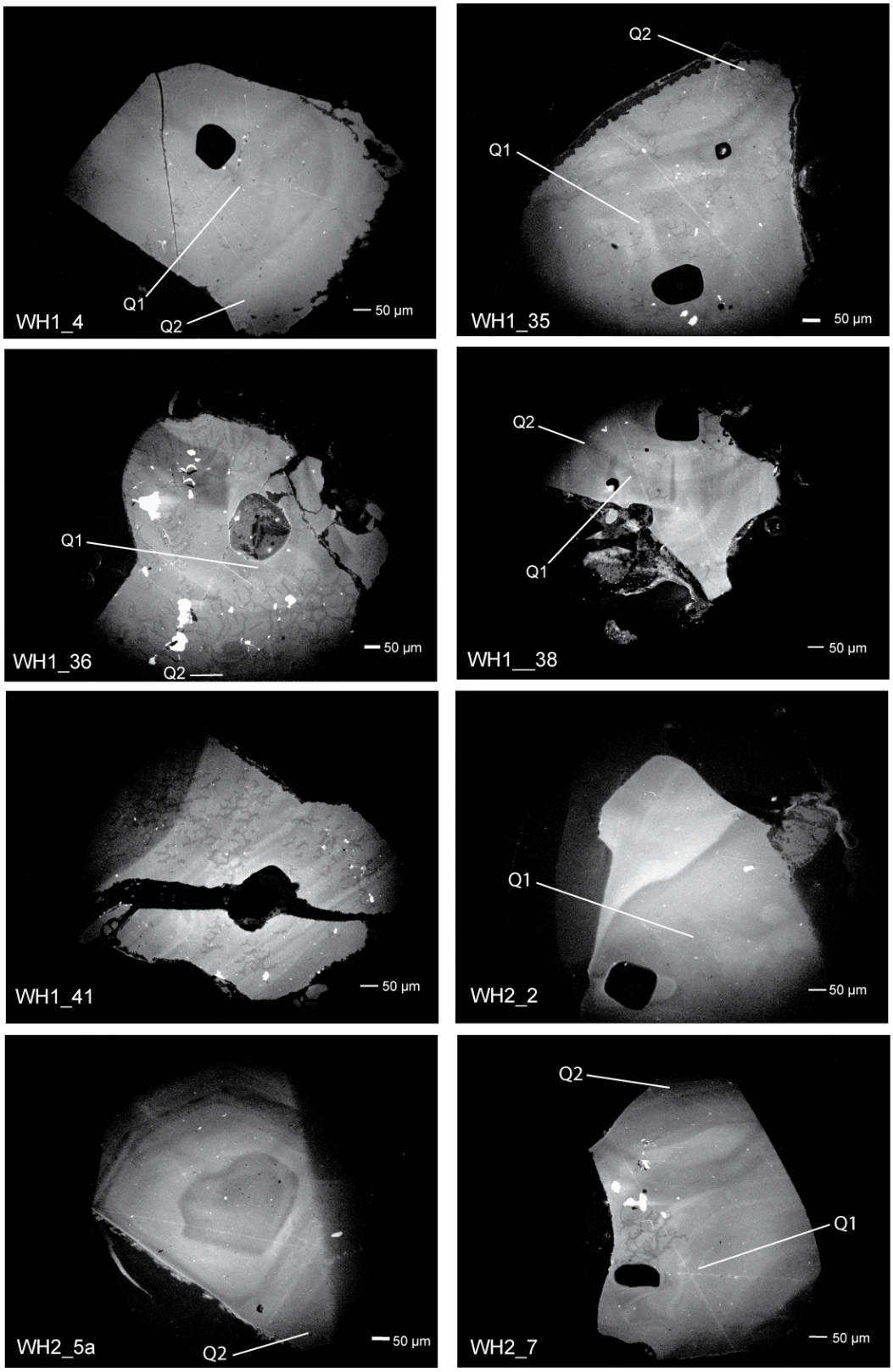
WH1_4
Q1
Q2
50 µm
WH1_35
Q2
Q1
50 µm
WH1_36
Q1
Q2
50 µm
WH1__38
Q2
Q1
50 µm
WH1_41
50 µm
WH2_2
Q1
50 µm
WH2_5a
Q2
50 µm
WH2_7
Q2
Q1
50 µm

Appendix 4

Figure A4.4: Backscattered electron images of Healy plagioclase crystals

Figure A4.4

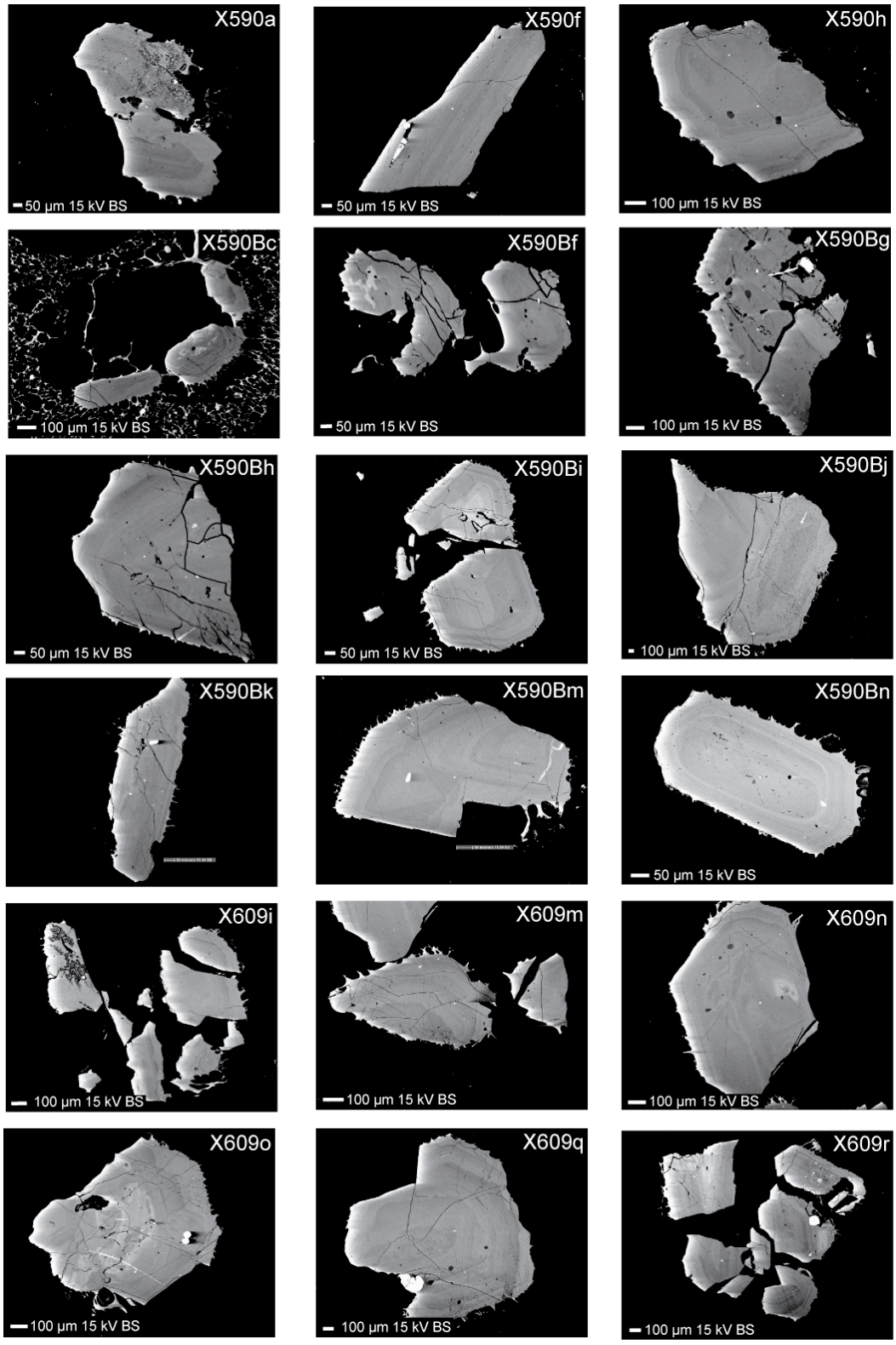
X590a
50 µm 15 kV BS
X590f
50 µm 15 kV BS
X590h
100 µm 15 kV BS
X590Bc
100 µm 15 kV BS
X590Bf
50 µm 15 kV BS
X590Bg
100 µm 15 kV BS
X590Bh
50 µm 15 kV BS
X590Bi
50 µm 15 kV BS
X590Bj
100 µm 15 kV BS
X590Bk
X590Bm
X590Bn
50 µm 15 kV BS
X609i
100 µm 15 kV BS
X609m
100 µm 15 kV BS
X609n
100 µm 15 kV BS
X609o
100 µm 15 kV BS
X609q
100 µm 15 kV BS
X609r
100 µm 15 kV BS

Appendix 4

Figure A4.5: Backscattered electron images of Taupo plagioclase crystals

Figure A4.5

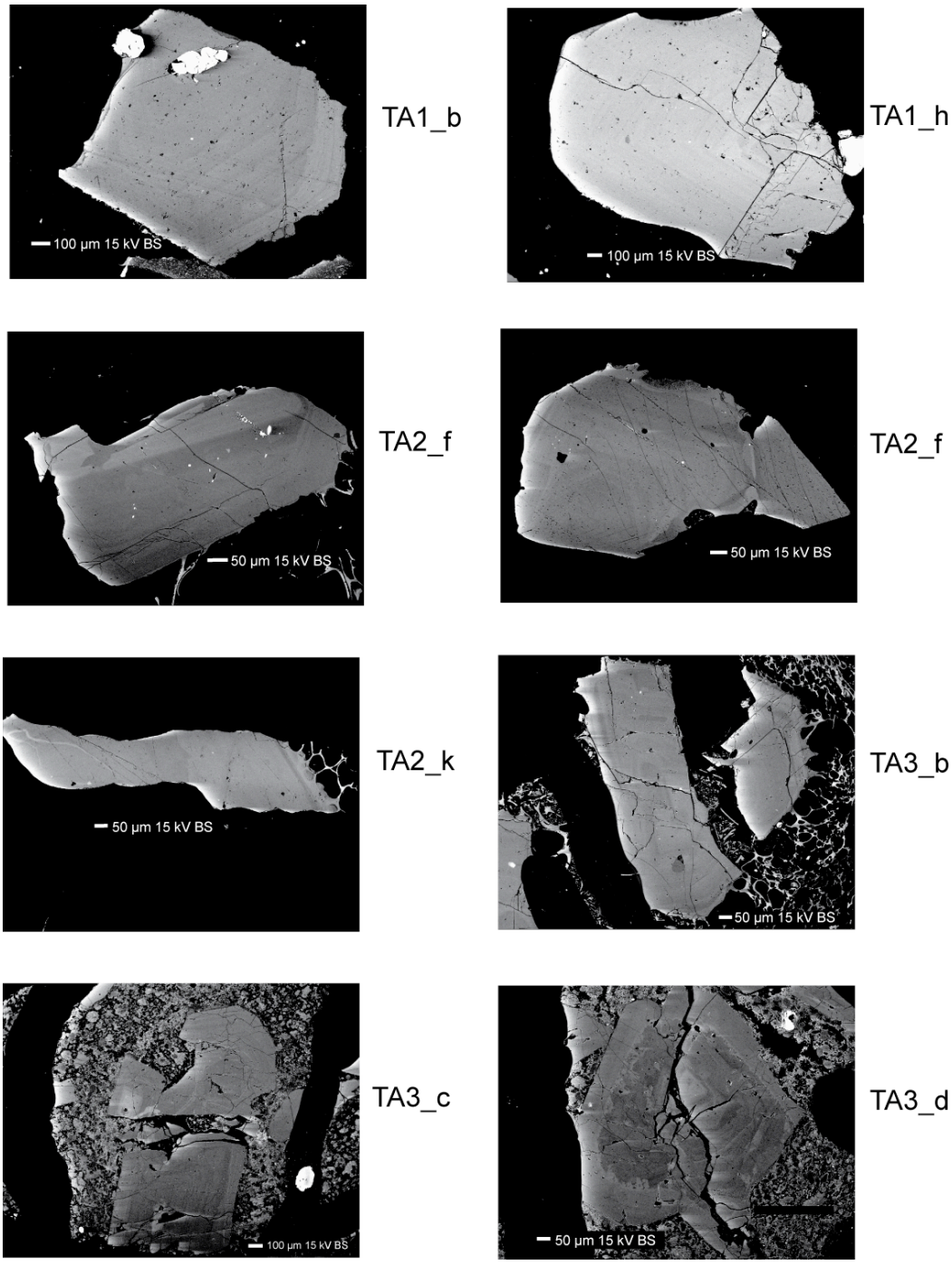
100 µm 15 kV BS
TA1_b
100 µm 15 kV BS
TA1_h
50 µm 15 kV BS
TA2_f
50 µm 15 kV BS
TA2_f
50 µm 15 kV BS
TA2_k
50 µm 15 kV BS
TA3_b
100 µm 15 kV BS
TA3_c
50 µm 15 kV BS
TA3_d

Figure A4.5 continued

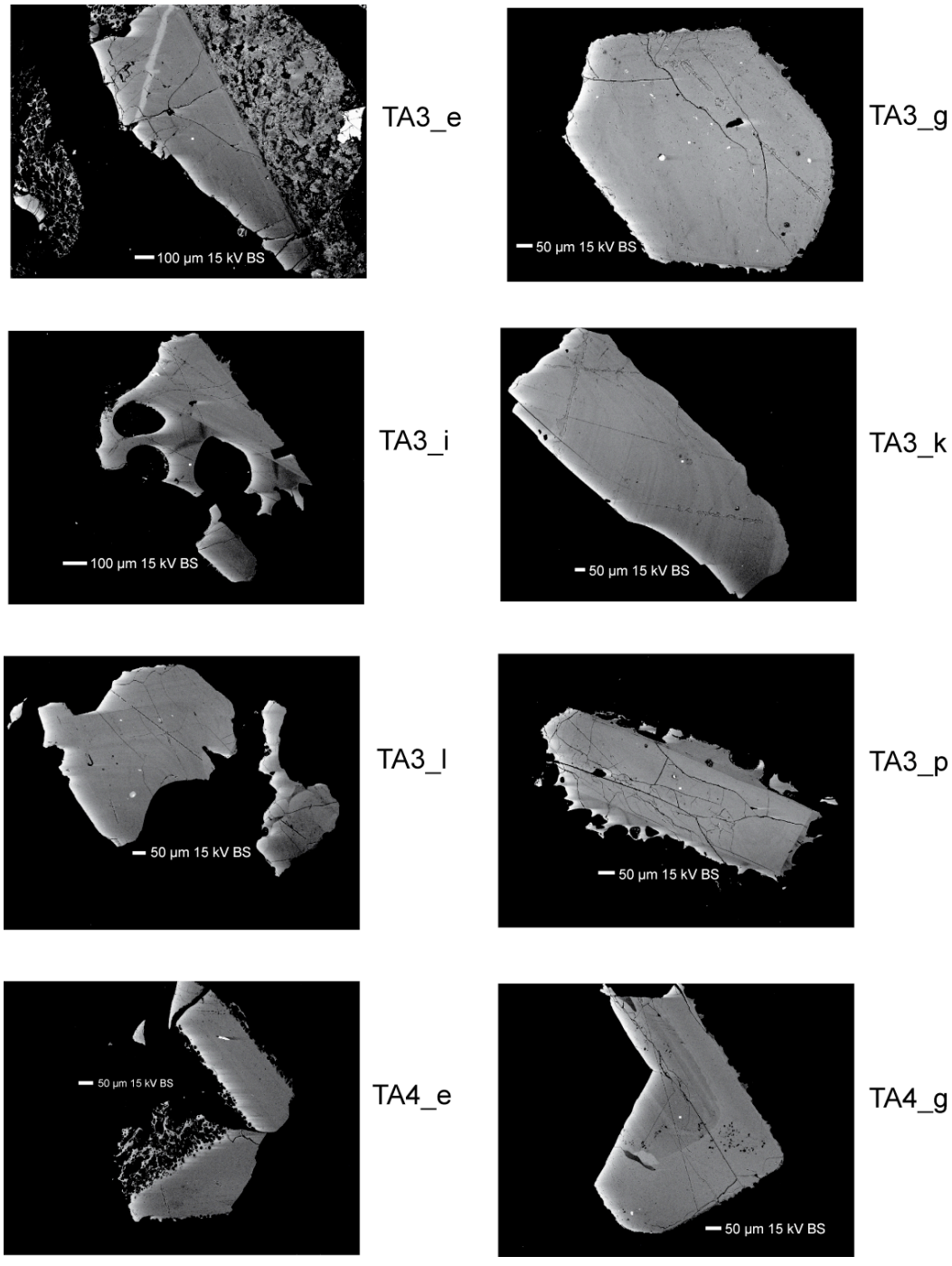

Figure A4.5 continued

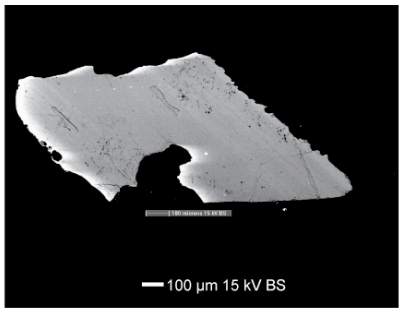

TA4_h

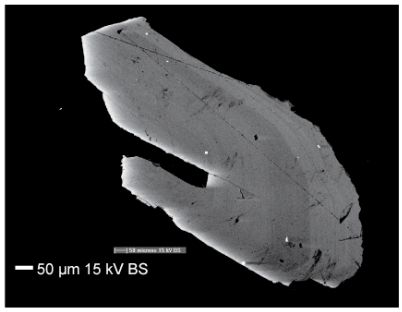

TA4_i

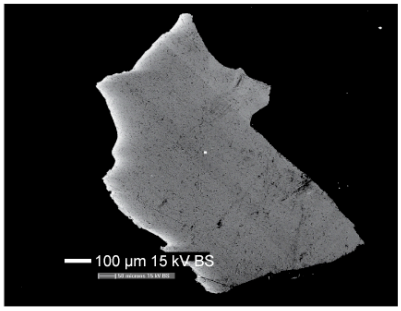

TA4_j

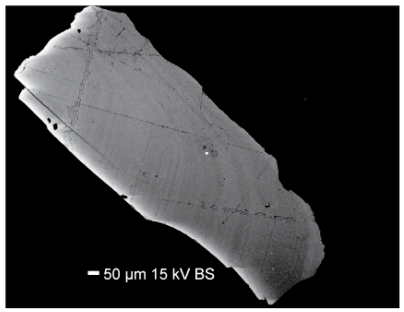

TA3_k

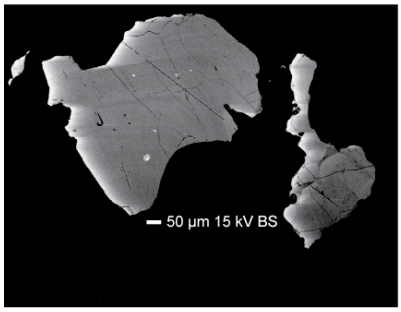

TA3_l

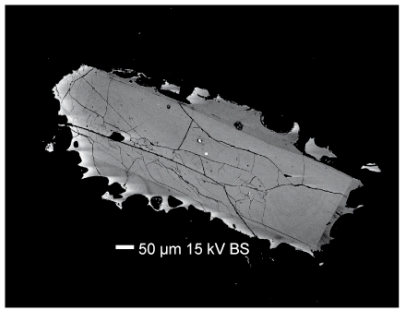

TA3_p

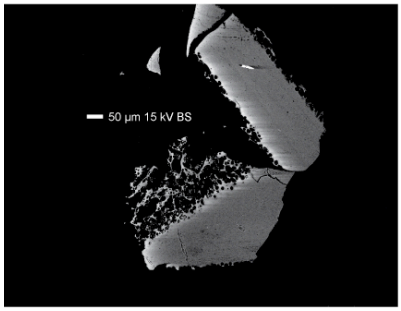

TA4_e

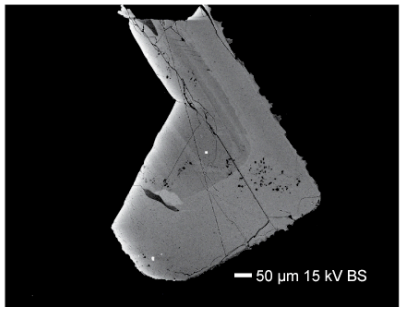

TA4_g